Experimental and numerical investigation of noise generation from the expansion of high velocity HVAC flows on board ocean going fast ferries

Author:
Neale, James Richard

Publication Date:
2006

DOI:
https://doi.org/10.26190/unsworks/17316

Experimental And Numerical Investigation Of Noise Generation From The Expansion Of High Velocity HVAC Flows On Board Ocean Going Fast Ferries

James Richard Neale

A thesis

submitted in fulfilment

of the requirements for the degree of

Doctor of Philosophy

School of Mechanical & Manufacturing Engineering

The University of New South Wales

Sydney

Australia

June 2006

Abstract

This thesis details a study of strategies used to limit the flow generated noise encountered in the outlet diffusers of high velocity heating, ventilation and air conditioning (HVAC) duct systems. The underlying noise rating criterion is drawn from the specifications covering ocean going aluminium fast ferries. Although directed primarily towards the fast ferry industry the results presented herein are applicable to other niche high velocity HVAC applications.

Experimental tests have been conducted to prove the viability of a high velocity HVAC duct system in meeting airflow requirements whilst maintaining acceptable passenger cabin noise levels. A 50 mm diameter circular jet of air was expanded using a primary conical diffuser with a variety of secondary outlet configurations. Noise measurements were taken across a velocity range of 15 to 60 m/s. An optimum outlet design has been experimentally identified by varying the diffuser angle, outlet duct length and the termination grill. A 4 to 5 fold reduction in required duct area was achieved with the use of a distribution velocity of 20 to 30 ms^{-1}, without exceeding the prescribed passenger cabin noise criteria. The geometric configuration of the diffuser outlet assembly was found to have a pronounced effect on the noise spectrum radiating from the duct outlet.

The development of a numerical model capable of predicting the flow induced noise generated by airflow exiting a ventilation duct is also documented. The model employs a Large Eddy Simulation (LES) CFD model to calculate the turbulent flow field through the duct diffuser section and outlet. The flow-generated noise is then calculated using a far field acoustic postprocessor based on the Ffowcs-Williams and Hawkings integral based formulation of Lighthill's acoustic analogy. Time varying flow field variables are used to calculate the fluctuating noise sources located at the duct outlet and the resulting far field sound pressure levels. This result is then used to

calculate the corresponding far field sound intensity and sound power levels. The numerical acoustic model has been verified and validated against the measured experimental results for multiple outlet diffuser configurations.

Executive Summary

The following summary has been prepared for the benefit of Austal Ships Ltd:

This research project has resulted in some useful findings that represent both immediate and longer term commercial opportunities for Austal Ships in relation to the design and construction of HVAC systems for ocean going fast ferries. The immediate opportunities can be summarised as follows:

1) The distribution velocity currently employed (5 to 7 ms^{-1}) can be increased significantly (10 to 12 ms^{-1}) without exceeding current passenger cabin noise limits. This is best achieved through use of flow control guide vanes to limit the generation of flow induced noise. This will result in significant space savings and overall reduced manufacturing and assembly costs.

2) Modern computational design tools such as CFD can be applied to the detailed design of the airflow and pressure balancing of the ducts, including the minimisation of unsteady turbulent flow conditions.

The following longer term opportunities have also been identified:

1) With further work the distribution velocity can potentially be increased significantly to around 20 to 30 ms^{-1} without exceeding the current passenger cabin noise limits. This will require a rigorous investigation into the development of specialised air handling and treatment equipment that can be integrated into a fully functioning high velocity HVAC distribution system. To minimise the net increase in power consumption it is strongly recommended that low velocity centralised air treatment systems are retained wherever possible.

2) There is also the potential to share the developmental costs of a high velocity system across other niche markets that can also benefit from space savings that can more than offset the increase in fan power required.

The implementation of the above two options would require the following recommendations for future research:

1) The development of an outlet grill model that can be used to predict their acoustic performance so that the current numerical model can be extended to include a more complete HVAC distribution system.

2) The application of advances in turbulent flow modelling capability, such as the newly immerging Scale Adaptive Simulation (SAS) models in reducing the computational cost of the numerical modelling approached used in this research. Rapid improvements in computational efficiency will no doubt be made in the coming years and this represents a commercial opportunity that could be exploited.

3) Flow control guide vanes are currently underutilised in the HVAC industry and in particular by Austal Ships. Significant gains can be made by customising the design of fast ferry HVAC systems to application specific design constraints, rather than established land based building services methodologies. The long term costs savings in both direct upfront costs and ongoing operational costs will only increase in an energy constrained global market place.

Dedication

To my eternal companion

Tania,

Thank you,

for your patience, understanding, love and support.

Acknowledgements

First and foremost, I would like to thank my supervisors Professor Eddie Leonardi and Dr Seng Leong for your many kind words and patience in humouring my many questions and ideas. To Professor Kerry Byrne, I thank you for your work in initiating the project with Austal Ships and your many comments on the acoustic components for this work. To Dr Tracie Barber I thank you for taking the time to discuss the many computer related issues that were encountered along the way and the many e-mails to Fluent on why the software wouldn't do what was always promised! A special mention also needs to be given to Professor Bob Randall, who despite not being linked with this project gave countless hours of his time to an enquiring mind and dare I say a pestering student.

I also need to offer my heartfelt thanks to the school administrative staff for their tireless efforts in assisting a new student to the campus despite the many other tasks that were always at hand. So to Mary, Cynthia, Pat, Blanche, Sharon, Loyce and others a very big and in many ways understated, thank you.

The assistance of the many laboratory staff should also be recognised, including Russell Overhaul for the many hours spent fine tuning the reverberation suite and the acoustic instrumentation employed. To Grahame Louke I thank for humouring my need to make clear conical diffusers and duct sections to my exacting specifications instead of using off the shelf pipe sections - it was worth the extra trouble. To Terry Flynn and Alex Litvak thank you for the little things that were never too difficult and help in smoothing the way ahead.

To my office companions Jason and Lehan I thank you for your patience, humour and most importantly the mental stimulation that was provided. It is always so easy to underestimate the value of a brief conversation in shaping the direction of ones research and the vision to look beyond the horizon of the day. I will always cherish our time together and the memories of keeping the office open three shifts per day! To Tim and my fellow formula SAE team members, thank you for the many memories gathered along the way, of loss and of victory.

I would also like to acknowledge the financial support of the Australian Research Council and Austal Ships Limited, and the School of Mechanical and Manufacturing Engineering.

To my loving parents, thank you for having faith in me and supporting me every step of the way. The odd prayer, friendly word and most of all a kind ear to listen will always be honoured and respected. Dad your voice of reason is one I will always treasure.

Finally, and most of all I wish to thank my loving wife Tania for all of her love and support. To Christina who was with us when we got started, Richard, Sydney and Hemi who have joined us along the way your daddy loves you and thanks you for always adding a little ray of sunshine to each day along the way. You have all sacrificed so much while this work was completed, and now thanks to you it has! Words can't express how grateful I am.

Thank you!

Table of Contents

List of Figures

List of Tables

Symbols & Abbreviations

Symbols

A	Duct cross sectional area	m^2
c	Speed of sound	ms^{-1}
c_o	Free-field speed of sound	ms^{-1}
D, D_i	Diameter of the circular duct	m
D_h	Hydraulic Diamter	m
D_{max}	Maximum width of a rectangular duct	m
δ_{ij}	Kronecker delta, $\delta_{ij} = 1$ for i = j otherwise $\delta_{ij} = 0$	
f	Frequency (sound)	Hz
f_{co}	Cut on frequency	Hz.
k	Wave number	m^{-1}
I_A	Acoustic Intensity	Wm^{-2}
I_T	Turbulence intensity	-
L	Length of muffler expansion chamber	m
L_A	A-weighted sound pressure level	dB (A)
L_p	Sound pressure level	dB
L_w	Sound power level	dB
M	Mach number	-
n_l	Normal vector	
p	Acoustic pressure	Pa
p'	Fluctuating pressure	Pa
Re_{Dh}	Reynolds number (based on hydraulic diameter)	-
r	Scalar distance between source and receiver	m
$\vec{r}$	Acoustic radiation vector (source to receiver)	m
S	Arbitrary surface (surface integral)	m^2
T_{ij}	Lighthill stress tensor	-
T_t	Transmission loss coefficient	-
TL	Sound power transmission loss	dB

t	Time	s
u_n	Normal velocity component (defined by n_l)	ms^{-1}
u_{ave}	Average velocity	ms^{-1}
u'	Fluctuating velocity	ms^{-1}
V	Arbitrary volume (volume integral)	m^3
v	Fluid velocity	ms^{-1}
v'	Fluctuating velocity	ms^{-1}
v_i, v_j	Vector component of fluid velocity	ms^{-1}
W	Acoustic Power (sound power)	W
x_i,x_j	Vector components of spatial displacement	m
$\boldsymbol{x}$, $\boldsymbol{y}$	Position vectors	m

Greek Symbols

α	Diffuser angle	degrees (º)
ρ	Density of fluid medium	kgm^{-3}
ρ_o	Free-field density of fluid medium	kgm^{-3}
θ	Angle between integral surface and normal vector	degrees (º)

Abbreviations

AIRAH	Australian Institute of Refrigeration, Air Conditioning and Heating
APE	Acoustic Perturbation Equations
ASHRAE	American Society of Heating, Refrigeration and Air-Conditioning Engineers
BEM	Boundary Element Method
CAA	Computational Aero-Acoustics
CAE	Computer Aided Engineering
CH	Cushion Head - fitted to square outlet diffuser grill
CFD	Computational Fluid Dynamics
CFL	Courant, Freidricks, Levy number
DG	Discontinuous Galerkin
DNC	Direct Noise Computation
DNS	Direct Numerical Simulation
DES	Detached Eddy Simulation
ELCH	Elbow (90˚) fitted to the Cushion Head box mounted square outlet grill
FEM	Finite Element Method
FFT	Fast Fourier Transform
FWH	Ffowcs-Williams & Hawkings
HVAC	Heating, Ventilating and Air Conditioning
IL	Insertion Loss
k-ε	k-ε Turbulence model for CFD
k-ω	k-ω Turbulence model for CFD
LAA	Lighthill Acoustic Analogy
LDV	Laser Doppler Velocimetry
LEE	Linearised Euler Equations
LES	Large Eddy Simulation
MAF	Minimum Audible Field
NC	Noise Criteria
NCB	Balanced Noise Criteria
NS	Navier Stokes
PISO	Pressure Implicit with Splitting of Operators (numerical P-V coupling)

RANS	Reynolds Averaged Navier Stokes
RC	Room Criteria
RJ	Round Jet outlet diffuser grill
RMS	Root Mean Squared
RNC	Room Noise Criteria
SAS	Scale Adaptive Simulation
SD	Square 4-way outlet diffuser grill
SGS	Sub Grid Scale
SPL	Sound Pressure Level
SWL	Sound Power Level
TL	Sound Power Transmission loss
USD	United States of America Dollar (US dollars)
ZES	Zonal Eddy Simulation

Chapter 1

Introduction

Ocean going fast ferries are required to operate in all of the different marine climates around the world, which places severe demands on the vessel air conditioning system. The available space for air conditioning ducts in these vessels is also very limited. The aim of this research is to investigate numerically and experimentally the feasibility of compressing the conditioned air and distributing it through a compact ducting system. Smaller air conditioning duct networks will enable size and weight savings, which can be used to improve vessel speed and cost.

Controlling the noise levels that are associated with high pressure and high velocity airflow is critical to the successful application of such a system. Minimum passenger comfort standards dictate a maximum A-weighted sound pressure level, air flow rates and maximum air velocities within the cabin space. Alternative outlet diffusers are required to provide additional expansion of the compressed air flows and noise attenuation. These outlet diffusers (if used at all) are custom designed for application specific requirements, resulting in significant cost increases over standard HVAC systems. The availability of ancillary HVAC plant and equipment to interface with a high velocity distribution system in an economically viable solution is an added design constraint.

1.1 Project Rationale

The feasibility of a high velocity HVAC system in ocean going fast ferry application hinges on the expansion (and deceleration) of a high velocity jet of air to an acceptable exit velocity. The exit velocity into the cabin space must satisfy both passenger comfort and noise levels. The primary purpose of this research is to first

prove such a system is viable and then develop a suitable design tool that can be used to predict the passenger cabin sound pressure levels for any given air velocity and HVAC air distribution system. It is anticipated that by addressing these priorities any remaining technical challenges relating to a commercial installation can be overcome with additional research or the application of current alternative technologies.

The viability of a high velocity air distribution network for an ocean going fast ferry was evaluated experimentally by determining the sound pressure levels generated by expanding a jet of air across a range of velocities. These initial tests provided a basis from which the comprehensive experimental program presented in this thesis was established. These results were then used to develop and validate a numerical based model to predict the sound power generated by the expansion of a high velocity jet of air. The results from these models will be used to provide the justification for the development of a complete high velocity HVAC system for installation on ocean going fast ferries. A numerical modelling tool will allow the optimum system velocity and pressures to be established across the wide range of customized passenger cabin sizes produced by Austal Ships. The assessment of a proposed design will provide a critical evaluation tool where increased system costs can be balanced against HVAC installation costs and overall vessel running costs.

Based on the above assumptions the primary research focus will be the expansion of a high velocity jet into a low velocity flow. Containing the flow-induced noise at this point is critical to the successful operation of a compact air distribution network. Upstream factors such as noise from any air handling equipment and from the high velocity ducts themselves have not been seriously addressed at this time. Once the viable velocity range has been identified these additional factors can then be considered for each individual design case and factored into the final system operational envelope. The author envisages future research will address these factors across air velocity ranges where there is an economic justification to do so.

1.2 Austal Ships

Austal Ships is an Australian public listed company based in Henderson, Western Australia. Their primary business interest is the manufacture of welded aluminium passenger and vehicle ferries for both domestic and international markets. The size of these vessels range from 20 m in length up to 126 m in length – being the largest aluminium vessels built anywhere in the world. The application of high velocity HVAC systems is most suited to the larger multi-level passenger and vehicle ocean going fast ferries. The running cost of these larger vessels is tightly related to the weight of the vessel, whereby the maximum payload (potential income) and speed are both adversely impacted by any increase in total vessel weight. The deck to deck height of these vessels is determined by the space required to house various utility services in the ceiling cavity where the primary determination of this height is the size of the HVAC duct system. The installation cost in terms of both materials and labour are also of major consideration.

Austal Ships, a Perth based fast ferry manufacturer, is supporting this project under an Australian Research Council SPIRT grant.

1.3 HVAC Ducting Designs

Fast ferry manufacturers adopt several different HVAC design philosophies depending on the targeted market for their respective vessels. The main drivers of this design decision are primarily the system installation, operating and maintenance costs. The fundamental designs used on vessels can be categorised as either a centrally run integrated HVAC system or a distributed system of individual small size reverse cycle air conditioning units. An example of an Austal designed centralised system is shown in Figure 1.1 and a distributed roof mounted system used by Northwest Bay Ships is shown in Figure 1.2.

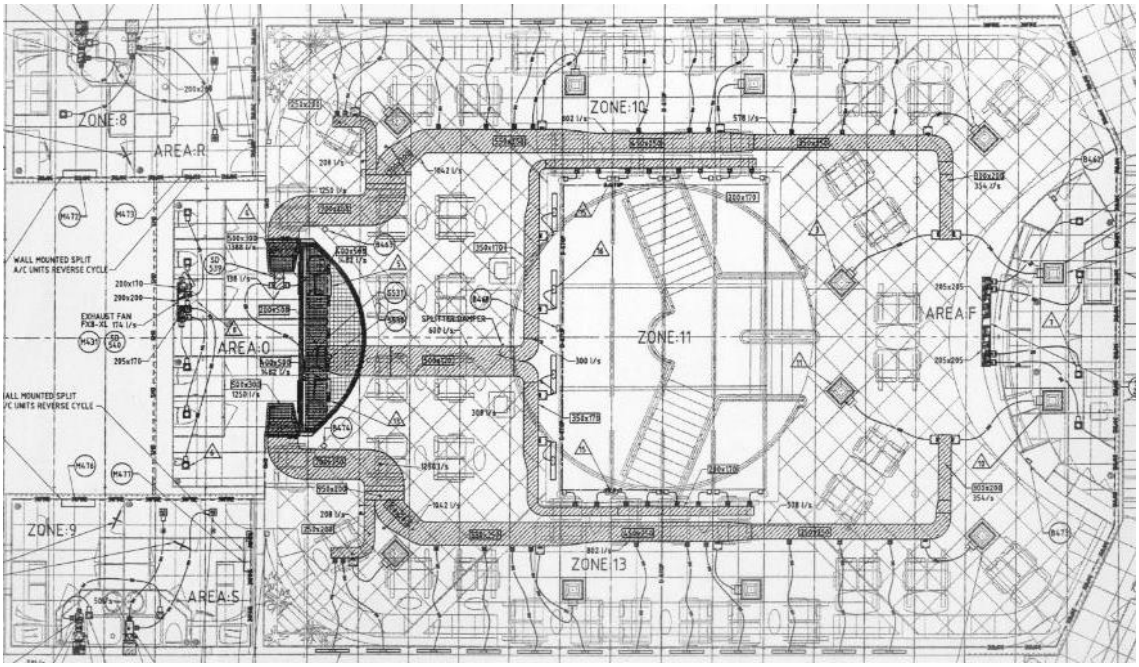

Figure 1.1: Centralised HVAC system as used by Austal Ships.

Figure 1.2: A Roof mounted distributed HVAC system as used by Northwest Bay Ships.

The centralised systems come at a distinctly higher installation cost but also have long term benefits in the form of improved system integration and control. A centralised system can take advantage of the greater efficiency of larger refrigeration and heating units to manage the desired heating and cooling loads. Any improvement in operating efficiency must however be balanced against the added cost of distributing the conditioned air from the centralised location(s). The distribution costs have two aspects, firstly the installation cost of fitting ducting into tight ceiling spaces and secondly the ongoing operational costs of air movement. In the case of a high velocity distribution system this cost can be quite substantial.

Aside from the operational cost issue the location of the centralised systems also presents a trade off between space requirements and protection from external environmental conditions. Having a large centralised HVAC system requires a significant space to be provided to house the respective units whilst also needing to isolate the passenger cabin areas from the noise associated with a centralised plant room. With passenger numbers directly linked to cabin area there is a quantifiable cost associated with HVAC space provisions. Having a plant room in a centralised location does however provide for easy access for servicing and provides the system with protection from the harsh external marine environment. The benefits of the system being wholly protected in this way are in no way insignificant.

The distributed system approach comes at a much cheaper installation cost in terms of both financial and logistical terms. There is minimal ducting associated with a roof mounted batch of individual reverse cycle units, however they have distinct long term disadvantages when operated in harsh marine environments. The standard commercial grade reverse cycle units are based around a land based fixed installation with little consideration of exposure to the salting atmosphere associated with a life span based on the open ocean. From a maintenance perspective there are considerable long term costs for the owner of such vessels. The hidden costs associated with down time required to fix and replace faulty units can prove far more costly than the actual replacement cost of the air conditioning units themselves.

On a large vessel the number of individual reverse cycle units mounted on the roof can be substantial, resulting in a significant drop off in the thermal performance of the external half of the systems. This drop off in performance has been well documented for fixed building applications as reported by Xue et al. [1]. In certain circumstances this drop in performance can be negated by the amount of airflow across the roof of the vessels when moving at high speed. Similarly the drop off in performance can be accounted for in the specification of the units to provide the required HVAC loads. The aesthetic appeal of such installations is an additional factor that may need to be considered in limiting the location of the roof mounted units. Based on all of the above mentioned factors the location of the roof mounted systems will be restricted to certain vessel configurations and design specifications.

The final design decision as to what type of HVAC system is installed on a fast ferry is primarily customer driven. Based on this underlying premise the author recognises that both type of systems will continue to be used unless standards are changed in regards to the use of land based systems on ocean going vessels. It is anticipated that the work relating to high velocity HVAC systems for fast ferry applications covered by this thesis will shape a viable design tool for the development of an optimised design solution tailored to the needs of individual customers.

1.4 Research Goals and Objectives

The aim of this research is to investigate numerically and experimentally the feasibility of compressing conditioned air and distributing it through a compact ducting system. Smaller air conditioning duct networks will enable size and weight savings, which can be used to improve vessel speed and cost. This will require both the acoustic modelling of the air distribution system and the development of the necessary duct silencers. The primary research focus is the expansion of a high velocity jet into a low velocity flow and containing the flow-induced noise at this point. Solving these two critical problems will help facilitate the compacting of the air distribution network.

This complex task has been broken down into several key objectives outlined below.

1. Numerical modelling of the airflow through the duct system will be used to model the expansion of a high velocity jet and the associated retardation of the jet velocity. Computational Fluid Dynamics (CFD) based models will be used to predict the airflow performance of potential design solutions to identify the optimum diffuser angle and outlet configuration for experimental evaluation. The outcome of this phase will be a documented CFD based modelling methodology applicable to high velocity HVAC outlet designs.

2. Experimental work will then be used to validate the numerical models, with the intent to develop a commercially viable duct system design strategy. This will ensure the integrity of the proposed modelling approach from the first objective.

3. A numerical acoustic model will be developed to predict the flow induced noise at the duct outlet based on the CFD based flow model from the first objective. The main outcome from this task will be a documented solution methodology to predict the total sound power spectra radiating from a given duct configuration.

4. Acoustic experiments will be conducted to validate the numerical acoustic model and assess potential outlet duct configurations. Sound power measurements will be recorded in both octave and ⅓ octave frequency bands.

5. The final objective of this thesis is to link all of the modelling and experimental work together to demonstrate the potential of high velocity HVAC systems in a fast ferry application.

1.5 Thesis Structure

This thesis has been organised in a manner consistent with the previously stated objectives. As such the thesis can be separated into four main sections covering the project background and the three main research areas already outlined. The first section, comprising Chapters 1 to 3, contains the introduction and a review of current theory relating to high velocity HVAC duct systems. The second section covers the experimental investigations into the noise generated by expanding a high velocity air supply. The third section details the numerical models developed to simulate the turbulent flow fields associated with an expanding air jet and the flow induced sound power generated. The thesis concludes with a discussion of the experimental and numerical results, with comments on the potential applications of the methodology thus employed. Applications beyond the fast ferry industry are also briefly explored.

The current theory covering the design and operation of high velocity HVAC duct systems is outlined in Chapter 2. The economic rational is also discussed, including the proposed fast ferry system. Particular attention has been given to the underlying design criteria relating to passenger comfort and noise levels in a fast ferry application. The following chapter details the current literature covering both the experimental and numerical modelling of high velocity HVAC systems. The literature review was focused on the expansion of a high velocity jet of air and the subsequent release of that air into a passenger cabin space.

The design specifications for the test apparatus and the details of its construction are contained in Chapter 4. This is followed by the experimental procedures and a discussion of the experimental error in the measurement of the sound pressure, sound power and the air jet velocity. The experimental results, presented in Chapters 5 and 6, have been separated into two main sections; the first dealing with the sound power generated by different duct outlet configurations and the second a detailed application to a fast ferry cabin space.

The CFD model used to simulate the expansion of the high velocity airflow is detailed in Chapter 7. The LES turbulence model is described including the initial starting condition, discretisation schemes and boundary conditions. The verification and validation of the model is also discussed. The results from the CFD model are contained in Chapter 8, with a wide variety of jet velocities and outlet configurations presented. The acoustic model, based on Lighthill's acoustic analogy [2, 3] is outlined in Chapter 9 with the numerical acoustic results presented in the following chapter. Finally, the thesis concludes with a review of the original research objectives and details of how they have been exceeded. Recommendations for future research are also laid down for the benefit of Austal Ships Limited.

Chapter 2

Design of High Velocity HVAC Duct Systems

2.1 High Velocity Duct Flows

High Velocity HVAC ducts have been used in specific applications for more than 50 years with detailed design guidance provided in HVAC handbooks as far back as 1959 [4]. For the purposes of this investigation high velocity is assumed to be an air distribution velocity above the limits stated in the ASHRAE standards [5] established for a standard building based HVAC system. These standards are written to ensure adequate system operation and the delivery of minimum environmental conditions such as temperature, humidity, air movement and noise levels. Collectively these conditions determine the overall comfort level for occupants of the space served by the given HVAC system. The current accepted velocity limits are 7 ms^{-1} for rectangular ducts and 12 ms^{-1} for circular ducts.

The 1959 HVAC design handbook mentioned above provides guidelines for the maximum air velocities in high velocity duct systems. The maximum prescribed velocity is defined as a function of the overall duct flow rate as illustrated in Table 2.1. For the flow rates used in the HVAC ducts on most ocean going fast ferries (highlighted in yellow) this translates to a maximum velocity of 12 to 18 ms^{-1}.

Table 2.1: Maximum prescribed air velocities for high velocity HVAC ducts.

Duct Flow (cfm)	Duct Flow (ls^{-1})	Max. Velocity (fpm)	Max. Velocity (ms^{-1})
40,000 to 60,000	18,892 to 28,339	6000	30.5
25,000 to 40,000	11,808 to 18,892	5000	25.4
15,000 to 25,000	7,085 to 11,808	4500	22.9
10,000 to 15,000	4,723 to 7,085	4000	20.3
6,000 to 10,000	2,834 to 4,723	3500	17.8
3,000 to 6,000	1,417 to 2,834	3000	15.2
1,000 to 3,000	472 to 1,417	2500	12.7

Habjan [6] revised these suggested flow rates and high velocity guidelines (suggested limits) in lieu of energy and design considerations. These guidelines were referred to as “medium pressure” duct designs for use in buildings with short floor to floor heights. The static pressure loss per unit of duct length in a medium pressure duct system is approximately 250 % greater than for an equivalent low pressure duct system. The lower maximum velocity limits were determined based on energy cost and noise restrictions. The revised velocity limits are provided in Table 2.2. Based on these revised guidelines the maximum velocity for the fast ferry HVAC system is only 6 ms^{-1} to 12 ms^{-1}.

Table 2.2: Revised maximum air velocities for medium pressure HVAC ducts.

Duct Flow (cfm)	Duct Flow (ls^{-1})	Max. Velocity (fpm)	Max. Velocity (ms^{-1})
100,000	47,231	3500	17.8
75,000	35,423	3500	17.8
50,000	23,616	3500	17.8
40,000	18,892	3370	17.1
35,000	16,531	3250	16.5
30,000	14,169	3150	16
25,000	11,808	2980	15.1
20,000	9,446	2820	14.3
15,000	7,085	2650	13.5
10,000	4,723	2400	12.2
8,000	3,778	2260	11.5
6,000	2,834	2120	10.8
4,000	1,889	1920	9.8
2,000	945	1620	8.2
1,000	472	1370	7.0
400	189	1090	5.5

Mason [7] provides a detailed design guide for HVAC ducting systems with mention of low, medium and high pressure systems. However, no specific guidelines or limits are noted for high pressure systems. The primary aim of the guide is to enable the minimisation of the energy consumption and capital cost of building based HVAC systems. The default recommendation for air duct velocity in all cases is the minimisation of the flow velocity and corresponding pressure drop as much as possible.

High velocity HVAC duct systems are typically used in applications where space for building (or vessel) services is limited or otherwise comes at a premium capital cost. The significant increases in running costs associated with moving conditioned air at high velocity through small ducts is offset against the capital cost of the initial installation. The use of high velocity systems in buildings has largely been eliminated due to increased awareness of operational expenses and the general push for sustainable and energy efficient building designs. The distribution velocity inside HVAC ducts is generally kept in the low velocity region of 3 ms^{-1} to 7 ms^{-1} and this is reflected in the focus of the design guides published by ASHRAE [5] and AIRAH [7]. Revised upper limits for the air velocity inside ducts are provided in the ASHRAE Applications Handbook [8] with an absolute maximum velocity of 17 ms^{-1} and 25 ms^{-1} in rectangular and circular ducts respectively. These relatively high limits are restricted to isolated ducts in isolated service shafts and in rigid ceiling spaces. For applications involving lightweight ceilings and walls these limits are lowered to only 10 ms^{-1} for rectangular ducts and 19 ms^{-1} for circular ducts.

The duct air velocity range from 15 ms^{-1} to 30 ms^{-1} considered in this work is therefore clearly within the prevailing definition of a high velocity HVAC system. The velocity range used in the experimental component of this thesis has been extended up to 60 ms^{-1} to improve the accuracy of the measured sound pressure level to air velocity relationship.

The current ASHRAE standards outline some generic guidelines for high velocity distribution systems and some limited suggestions for applications in the marine environment [9]. These high velocity guidelines do not currently provide any mechanism for specific noise level prediction or control; issuing a caution on exceeding desired noise levels instead. There are no specific guidelines on maximum velocities or pressure drops. There is limited generic advice on minimising head losses across a high velocity distribution system but once again limited guidance on how to predict or control flow generated noise is provided.

Increasing the air velocity inside HVAC ducts significantly increases the pressure drop across the length of the duct and compounds the losses incurred at each corner, side branch and any ancillary flow control or damping fixtures. Turbulence in the air flow and the onset of flow separation around corners and other such obstacles become significant as the air velocity is increased.

Strock and Koral [4] recommend the use of extended elbows and/or guide vanes to limit the onset of separation and the corresponding increase in pressure drop, as illustrated in Figure 2.1. The use of guide vanes in duct corners and splitters is also widely recommended to minimise these flow separation effects. A minimum spacing of 5 duct diameters between fittings is also recommended in the interest of minimising flow induced noise levels. All of these techniques will contribute to reducing the level of upstream flow generated noise inside the duct network through reducing the level of turbulence within the duct.

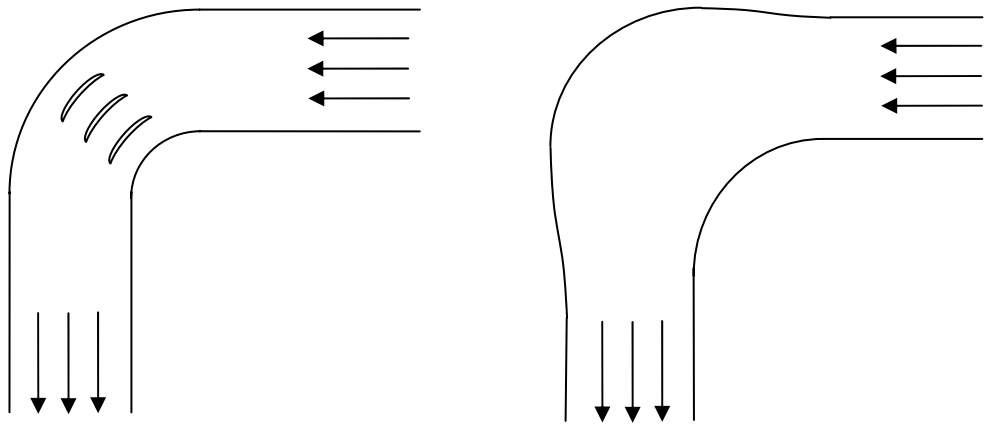

Figure 2.1: Expanded elbows and guide vanes used in high velocity HVAC duct corners.

2.2 Energy and Cost Optimisation

The recent shift in the global energy market and the increasing international pressures to reduce greenhouse gas emissions has generated renewed interest in the optimisation of the energy used in HVAC systems and other building services. These same pressures have also become more relevant in the application of ship based HVAC systems and more importantly the overall operational energy efficiency of the vessel as a whole.

There is little published material covering the optimisation of ship based HVAC designs, however there are several works relating to fixed building installations in commercial, industrial and residential settings. Soylemez [10] provides an economics based optimisation method for sizing HVAC ducts for minimum system energy. The primary dependent variable used is the pressure drop across the selected duct lengths. Lu et al. [11-13] developed a detailed optimisation method for the HVAC system as a whole; encompassing air, water and refrigerant loops as well as all of the utility streams employed. This method could be readily applied to a ship based system, provided all of the relevant input data was available.

Scheuer et al. [14] derived a life cycle energy and environmental analysis algorithm to enable an energy and cost optimisation to be made across the total life span of a fixed building. Based on a 75 year building life the HVAC and electricity demand accounted for 94.4 % of the total life cycle energy consumption. These Figures included the energy used to make the building materials themselves, during construction and the final demolition. Under such a scenario a high velocity HVAC system would clearly not be viable. However, if the same level of analysis is applied to an ocean going fast ferry quite the opposite could be expected. The HVAC system running costs make up only several percentage points of total system costs. With the possibility of reducing the deck to deck height and the subsequent weight of the superstructure the resultant weight savings and therefore increased payload capacity/reduced fuel consumption becomes significant. In effect the end result is a net reduction in the fuel consumption per passenger/freight mile.

2.3 Outlet Diffuser Grill Design and Selection

The actual exit velocity of the HVAC air into the conditioned space is governed by the selected outlet grill used to diffuse the air into the relevant occupied space. Where ceiling heights are low or the occurrence of drafts is undesirable, the exit velocities from the outlet grills are kept at or below 1 ms^{-1} [15]. If neither of these requirements is critical the exit velocities from the outlet grill can be significantly higher, provided that there are no noise related limitations [16]. In either case the distribution velocity through the main HVAC air ducts is usually maintained in the low velocity range outlined above, for energy minimisation purposes.

2.4 Design of HVAC Systems for Non-Stationary Applications

The use of standard HVAC designs developed for stationary buildings in non-stationary applications is a common occurrence with little published work on more case specific guidelines. Of the few publications covering alternate HVAC installations in non-stationary environments, most are preoccupied with air quality and to a lesser extent the level of noise produced. Noise treatment strategies are generally case specific, with a heavy dependence on empirical data and extrapolation thereof.

Pierce et al. [17]and Janczewski [18] provide a detailed analysis of the air quality on board a wide bodied commercial passenger aircraft, with air flow rates of 9.4 ls^{-1} per passenger. This flow rate was a 50-50 split between filtered re-circulated air and outside air. In both cases the remainder of the published investigation deals with the measurement and analysis of contaminants and the subsequent observed air quality. Given the expected number of passengers in the passenger cabin the HVAC ducts in this application are assumed to be of a medium to low velocity system.

Tokarev et al. [19] developed an empirical based model for predicting the contribution of HVAC systems to the overall internal cabin SPL. The ability to make noise reduction recommendations for specific aircraft cabin spaces based on their model is useful but of limited assistance to an engineer designing a system for a completely different application. A modelling technique that allowed any system to be evaluated including the prediction of the flow induced noise would provide a valuable step forward over the current status quo.

Warner et al. [20] presented a useful case study involving the experimental optimisation of the acoustic performance of an automotive HVAC system. Their experimental methods enabled the isolation of the flow generated noise from the blower noise (total) and a dominance of the blower noise was clearly identified. Across their tests the blower was found to increase the total sound spectra by 4 to 5 dB, with a particularly large gain in the low frequency bands below 1 kHz. A generic relationship was derived linking the SPL with the given air flow rates and corresponding pressure drop. The intention of this process was to provide a simple method of extrapolating new flow rates and pressure drops from CFD and CAE analyses to predict the new SPL. The SPL was found to vary with flow velocity to the power of 5.75. An accuracy of ± 5 dB was reported. Although useful for specific automotive design applications on an in-house basis, a widespread application of this method would be questionable. The ability of this method to handle significant variations in the flow field for radical HVAC design changes may well be compromised.

Botros et al. [21] provides a detailed description of an experimental programme used to reduce the SPL produced by another automotive HVAC system. Laser Doppler velocimetry (LDV) and SPL measurements were used to identify regions of turbulence within the flow ducts and the subsequent contribution to the overall SPL. Flow velocities of 7 ms^{-1} to 12 ms^{-1} were reported. This experimental approach resulted in a 1.5 to 2.5 dB reduction on the SPL and 7 to 15 % power saving from the air blower. The value of conducting detailed experimental investigations into reducing flow induced noise in HVAC systems is clearly demonstrated. The ability to simulate these system modifications would have the potential to reduce the design time taken and cost of experimental optimisation work.

Trent [22] provides a very generic discussion on the design considerations involved with HVAC systems in military submarines, however no actual data is provided. Clearly noise minimisation requirements are paramount and past experience is relied on heavily when developing a new system. Yankaskas [23] provides a similar discussion in relation to surface military vessels with a clear emphasis on attention to detail during the early design process. The construction of the USNS Waters (T-AGS 45) is sited where strict noise control specifications were met with the use of “low air velocities, duct turning vanes and duct linings”. For the case of a small, high speed craft the use of active noise control was found to be most effective in the low frequency bands, where traditional noise treatment strategies were not viable. Case specific solutions were developed with a sound pressure level reduction of 15 dB for tones and 7 to 10 dB for broadband noise at low frequencies.

When each of the above sources is related back to the ASHRAE handbooks [5, 8, 9, 15, 24, 25] a common theme of general advice, light on actual analytical design tools is found. The development of application specific empirical design rules has been the dominating design approach in recent times. The prediction and optimisation of airflow in ducts with the use of commercially available CFD packages provides a useful first step in the minimisation of the flow induced noise in any custom HVAC system. Clearly the ability to also predict the SPL for a given duct design would provide a valuable design tool for an engineer designing a customised high velocity HVAC system outside the specifications currently provided in the ASHRAE handbooks.

2.5 Fast Ferry Applications

The ocean going fast ferry market has rapidly grown over the past 10 to 20 years with little attention paid to optimising the design of the HVAC system. As mentioned previously the traditional centralised systems used by Austal Ships in their fast ferry designs are based on the standard ASHRAE guidelines used for regular building (land) based HVAC systems. The one major variation between the standard Austal designs and those outlined by the ASHRAE standards is the lack of any guide vanes in any duct corners and splitters. These fittings are generally omitted in the interest on reducing the weight and installation cost for the system. The consequence of this design compromise is an increase in the flow generated noise from the system and corresponding increases in the system pressure drop associated with the increase in turbulence present in the ducts.

Given the small fraction of the overall electrical loading used by the air handling fans, the increased fan power is of questionable relevance. The current acceptable sound pressure level reading of 65 dB (A) also negates the impact of any potential increase in the flow generated noise levels. The increase in sound pressure levels are also curtailed due to the relatively low distribution velocities employed.

The scope to increase the distribution velocity of the HVAC air is intrinsically linked to the above two observations. By restricting the increase in pressure drop due to increased air velocity to the distribution sides of the HVAC system the total impact on the system running costs can be minimised. The main airflow from the HVAC system enters the passenger cabins through ceiling mounted diffusers with some additional flow delivered to vents mounted along the windows. In both applications the velocity of the air entering the passenger cabins must be restricted to prevent any directional drafts and excessive local temperature gradients.

To satisfy this fundamental passenger comfort requirement the low exit velocity of the conditioned air from the HVAC system must be maintained as the internal distribution velocity is increased. The deceleration of the HVAC air from the distribution velocity down to the desired cabin entry velocity forms a fundamental and critical hurdle to the eventual commercial application of such a system.

Additional issues such as how to condition and distribute the air at higher velocities present additional challenges that will not be specifically addressed within the scope of this work. Further research into how to improve the design of the outlet diffusers used to deliver the conditioned air into the passenger space may also be required. The primary focus of this research will be on the junction between the high velocity air distribution ducts and the final outlet diffuser in the passenger cabins themselves.

For the purposes of this work the proposed high velocity HVAC system has been divided into four key zones for individual analysis and discussion in relation to the commercial reality of a fast ferry application. The first zone covers the conditioning of the air upstream of the adjoining second zone covering the high velocity air distribution network. The third zone is the major focus of this work and relates to the deceleration and expansion of the high velocity duct flow followed by the final zone covering the injection of the HVAC airflow into the cabin space. A block diagram representation of these HVAC system zones is illustrated in Figure 2.2.

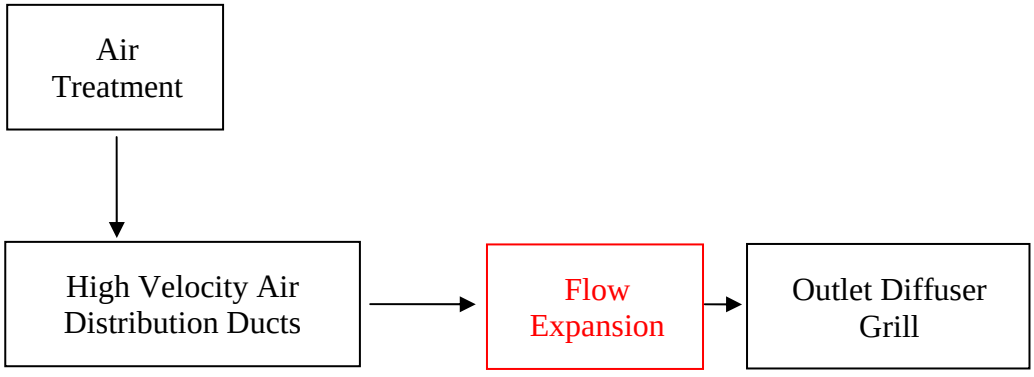

Figure 2.2: Block diagram representation of the HVAC system.

This same analogy can also be applied in reverse to the corresponding exhaust air side of the HVAC system, but without the need for the air treatment zone. This zone can be replaced with a much simpler recycling and exhaust air zone that can be modelled based on the desired mixture of fresh and recycled air. The number of exhaust points in the passenger space will be significantly less than the corresponding number of supply air diffusers.

For the purposes of refining the direction of this research the exhaust side of the proposed high velocity HVAC system will be assumed to be a mirror of the supply side of the system. In reality the impact on passenger comfort levels in terms of noise levels and air velocities in the exhaust system are assumed to be less significant, but not altogether trivial. Breakout noise from the walls of the exhaust ducts and excessive velocities at the exhaust grills inside the passenger space will present design challenges that will need to be addressed for a successful commercial installation.

By addressing the expansion zone of the distribution system the feasibility of a high velocity HVAC system can be demonstrated and the required numerical design tools can be developed and validated. On the completion of this foundation work a complete system design and analysis can be initiated where each of these additional aspects can be fully evaluated and optimised.

2.6 Economic Evaluation

The economic evaluation of the merits of installing a high velocity HVAC system on board an ocean going fast ferry is a complex optimisation problem based on multiple inter-dependent variables. The actual construction cost of the vessel in both time and money must be weighed against the operational costs of the vessel itself and the various on board systems such as the HVAC installation. In addition to this design compromise there are the added indirect costs and benefits to actual performance of the vessel in terms of maximum payload, speed and passenger comfort levels. These key cost considerations are illustrated in Figure 2.3.

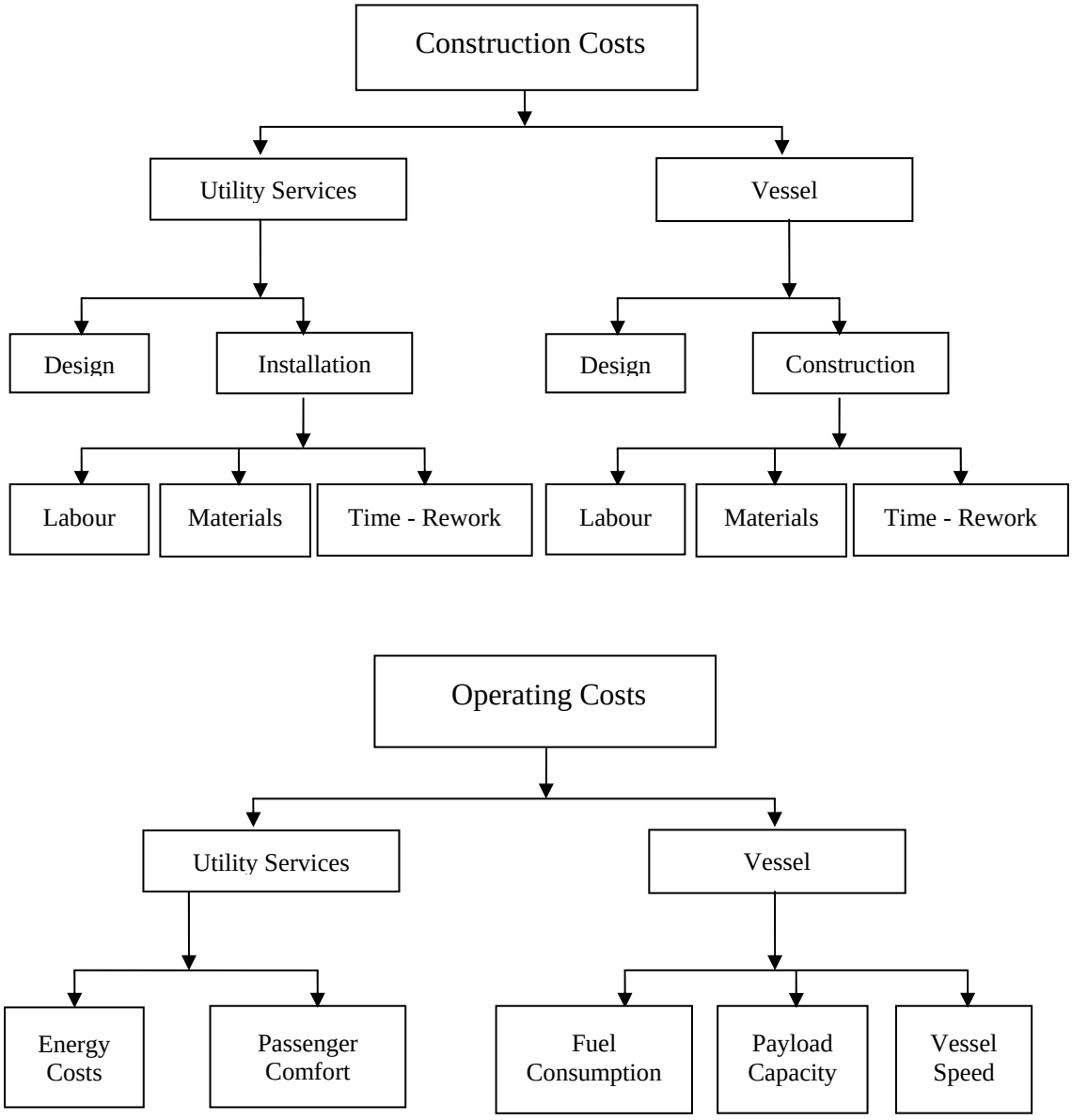

Figure 2.3: Cost – Benefit Analysis tree for high velocity HVAC system on an ocean going fast ferry.

Increasing the distribution velocity within the HVAC system will lead to an immediate increase in the electrical power required to move the air through the duct network. Switching from rectangular duct work to round pipes will provide minor reductions to the head loss associated with corners and other related duct fittings; however an initial estimate of a quadratic relationship between the increase in air velocity and total pressure loss across the duct network is realistic. This cost increase affects both the ongoing operational costs and the initial construction cost of the vessel due to the increased size of the onboard electrical generators used to power the system.

On a standard installation on a large vehicle and passenger ferry approximately 80 % of the electrical load on board the vessel is used to run the HVAC system, with the remaining 20 % being used for the remaining electrical systems. At the standard low air velocities typically only 12.5 % of the HVAC electrical load is used to move the conditioned air, with the remaining 87.5 % used to run the refrigeration and heating plants. The total pressure drop across the HVAC system can be apportioned to the various treatment, distribution, delivery and exhaust air zones with individual characteristic pressure-velocity system curves. The composite system curve for the complete HVAC installation is thus determined on the specific characteristics of each of these sub-systems for any given selected air flow rates. By maintaining the existing low velocity air treatment and delivery systems, the impact of the increased air distribution velocities on the total system curve can be minimised.

The ratio of fan power used in the treatment and delivery zones against the power used in the distribution zone will vary for different installations, depending on the length and complexity of the duct system employed. Damping individual outlets to balance air flow delivery rates can add considerable fan power demands which will be magnified with any increase in the distribution velocity. The increase in pressure drop (and fan power) from increasing the distribution velocity can be partially offset by reducing the number of outlet diffusers fitted to a given distribution duct. The reduction in outlets will lead to lower damping requirements for flow rate balancing and also reduce the size of the corresponding ducts further.

Smaller duct sizes lead to a reduction in the deck to deck height requirement and substantial material and structural savings for the vessel. The added benefits of reducing the size of the ducts used will also lead to easier installation procedures which will in part offset the cost of increasing the equivalent length of installed ducting. The additional ducts and the associated material and installation costs can be offset against the smaller ceiling space requirements and the reduction in pressure loss from damping the flow. The absolute increase in fan power required for a given air flow rate will be determined by the final balance between the increase in air velocity and the design of the distribution ducts.

For illustration purposes several potential deign configurations have been simulated to provide an indication of the likely range of composite system curves for a high velocity air distribution based HVAC system. A low velocity air distribution fan power loading of 30 to 60 % was considered, with the remaining fan power attributed to low velocity air treatment and delivery requirements. For the purposes of this example low velocity air treatment and air delivery zones were maintained with the only increase in velocity limited to the air distribution zones. Reduction in the pressure loss associated with flow damping and balancing has the potential to reduce the impact of this rise in fan power; however this will be offset against the increase in friction associated with a smaller pipe diameter.

A comparison between the total electrical power consumption based on the current system and a range of higher air distribution velocities is shown in Figure 2.4. This calculation is based on a standard air distribution velocity of 7 ms^{-1} and the remaining electrical demand onboard the vessel remaining unchanged. Based on the approximate calculations illustrated in this Figure, a target air distribution velocity of 20 to 25 ms^{-1} can potentially be met with only a 20 to 40 percent increase in the overall installed capacity of the on-board generator(s). This range of increase in air velocity translates to a 3 to 4 fold reduction in the total duct cross section required. The advantages of making a reduction of this size can potentially be significant in terms of reduced bulkhead openings and the absolute height of the ceiling cavity across the vessel.

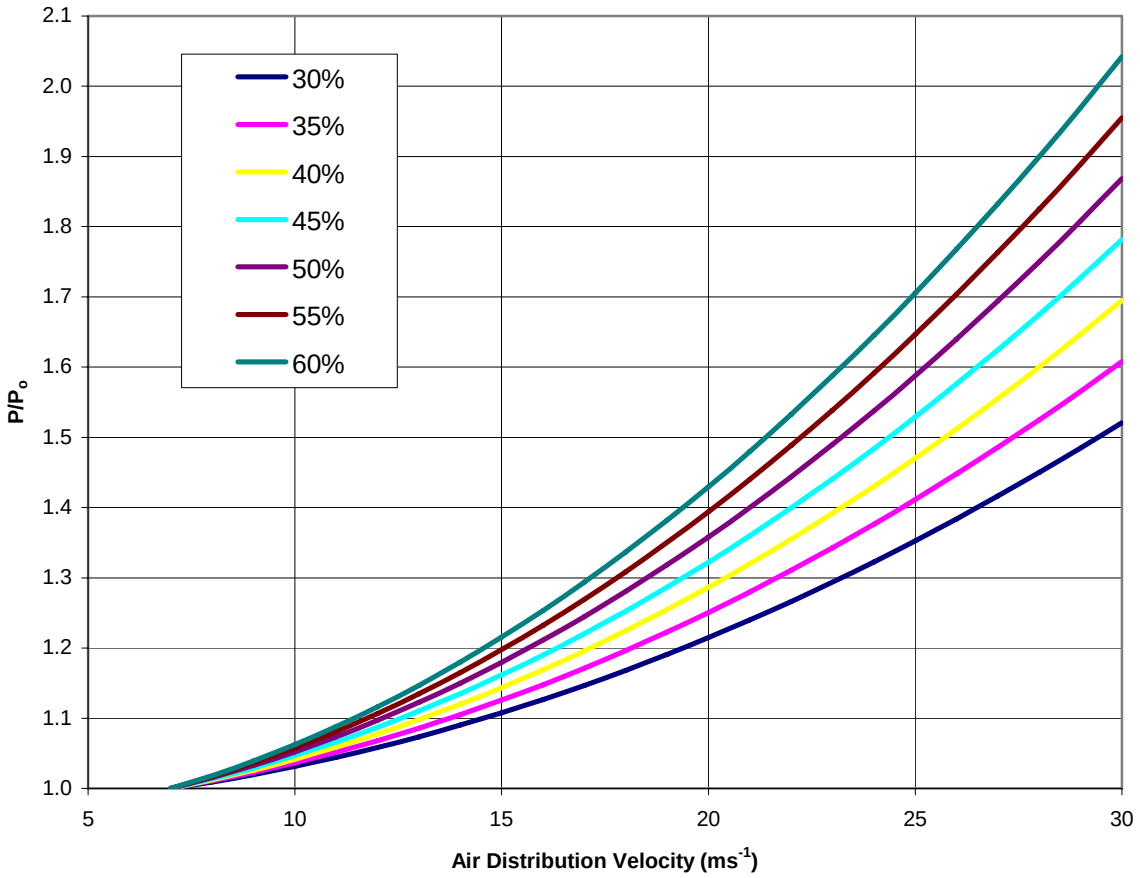

Figure 2.4: Projected total power consumption increases for a HVAC system with an air distribution head loss of 30 to 60 % of the total system head loss with a baseline distribution velocity of 7 ms^{-1} and a maximum velocity of 30 ms^{-1}.

.

If multiple small diameter ducts were used in lieu of a single compacted duct the absolute reduction in ceiling height and the size of the bulkhead access holes can be significantly reduced again. The exact savings from this design shift would have to be calculated in precise detail on a case by case basis. With these savings in mind the aim of this research is to establish that an air distribution velocity of 20 to 25 ms^{-1} can be successively decelerated and expanded into a simulated passenger cabin space and meet the required sound pressure levels. The culmination of this research will then focus on the development of a viable design methodology for assessing the performance of the proposed high velocity multi-stage diffuser used to slow the distribution air stream. This approach will cover both the fluid dynamics of the flow stream itself and the ability to predict the flow induced sound associated with the expansion and release of the high velocity HVAC air stream.

2.7 Diffuser Design and Head Loss Minimisation

Extensive research has been conducted in relation to the design of the diffuser outlet grills and their corresponding velocity profiles inside the conditioned space. The primary focus of this research has been centred on low velocity HVAC systems used in commercial land based installations. The noise levels, outlet velocity profiles and air diffusion rates for this type of diffuser have all been carefully studied and documented in the ASHRAE standards [15]. The application of these same outlet grills to a high velocity air distribution system is sparsely documented with typical installations being limited to high ceiling based applications and more lenient noise level criterion.

Given the low ceiling heights utilised on board ocean going fast ferries, the use of high velocity outlet diffusers is impractical on the basis of exit velocity of the conditioned air. The relaxed acoustic standards may be satisfied with a higher exit velocity; however the higher exit velocities will have a pronounced effect on the localised rates of cooling or heating. These localised temperature gradients and the corresponding drafts will lead to significant degradation in the localised passenger comfort levels and a compromised HVAC installation. Based on these limitations the outlet diffuser fitted to the passenger cabins must be configured with a standardised low velocity exit grill.

In order to meet the above requirements a primary diffuser must be developed to decelerate the high velocity air from the distribution ducts upstream of the outlet diffuser. The primary diffuser acts to decelerate the airflow, recover part of the dynamic head from the air flow and also contain any flow generated noise within acceptable limits. A schematical representation of the proposed high velocity diffuser is shown in Figure 2.5. The partial recovery of the dynamic head also helps to offset a small portion of the increase in pressure drop associated with the increased distribution velocities. Reducing the number of outlets per duct run will also lead to a reduction in the damping of the flow at the outlets, leading to additional fan power savings.

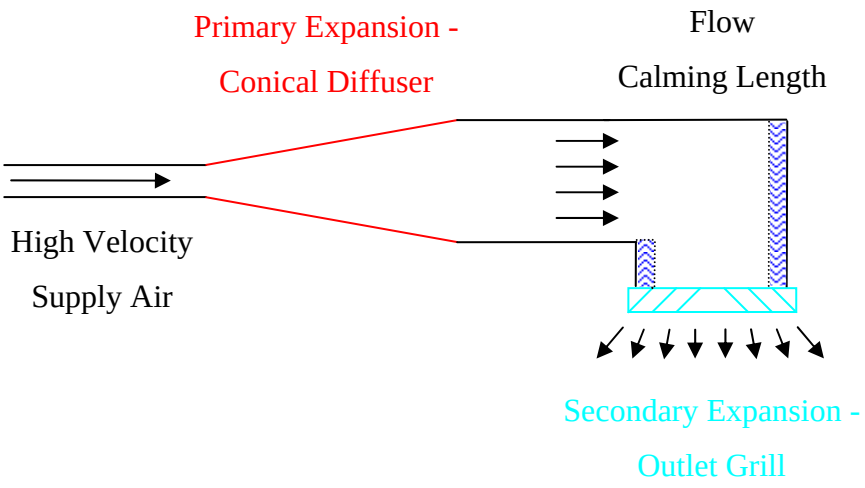

Figure 2.5: Schematic of the high velocity diffuser used to decelerate the HVAC air stream prior to the final outlet grill (diffuser).

The minimisation of the head loss across the whole air distribution system forms a critical component of the total optimisation calculations relating to the sizing of each distribution duct and the selection of the air distribution velocity. The use of round pipes, guide vanes and expanded corner fittings will all lead to reduced head loss for a given air velocity, with a corresponding reduction in the required fan power.

The use of multiple smaller round HVAC ducts (replacing the large rectangular ducts) will also lead to significant installation savings. The current rectangular sheet metal ducts are easily damaged and must be installed as multiple short sections – resulting in significant installation costs. Shifting to smaller round pipe based ducts will result in far less damage to the ducts and increased rigidity, thereby allowing longer individual sections and reduced labour costs. The time taken to fit the HVAC ducts is also a significant cost factor in itself due to the capital value of the assembly facilities used. Every day saved in the fit out of a vessel will also result in significant indirect cost savings to the manufacturer.

2.8 High Velocity HVAC Diffuser Duct Design

The control of the flow induced noise level is directly linked to the level of turbulence within the flow stream. As such the control of the onset of turbulence within the duct system and especially at the outlet diffuser is of up most importance. Clearly the worst case scenario would be associated with a high discharge velocity entering the passenger cabin space. This is considered an unviable design option due not only to noise constraints but also limitations on the generation of directional drafts [15, 26] within the cabin space. With these constraints in place the desired diffuser must release the conditioned air at a prescribed low level dictated by a variety of passenger comfort levels. Therefore the expansion of the high velocity HVAC air into a low velocity flow through the final outlet diffuser grill is a crucial element in the final system design. The specific details of the limitations on the final outlet velocity will be discussed in the coming section.

The fundamental mechanism of expanding a high velocity flow inside a closed duct must be considered with the aim of limiting the turbulence intensity of the flow. The turbulence present in the flow will not be eliminated and as such the aim of the outlet diffuser is to minimise the onset of flow separation and the size of any recirculation zone within the diffuser itself. A considerable amount of published work exists on the generic design of a diffuser meeting the above criteria. The diffuser angle and the shape of the duct are both critical design variables which have been investigated at length [27], particularly in relation to the design of wind tunnels. These works focused on the nature of the flow through the diffuser rather than the associated flow generated noise. These works will be used as a starting point for establishing the range of diffuser angles considered and the type of diffuser configuration selected.

The initial expansion of the high velocity supply inside the HVAC duct also requires a secondary redirection and expansion into the passenger cabin/space at an even lower velocity of 1 to 2 ms^{-1} as outlined above. The airflow through this section of outlet duct is highly turbulent and requires careful consideration. Further complexity is added with the back pressure associated with the final cabin grill and the impingement of flow on the support struts used to mount the grill itself. While the impact on the total

head loss in the system may be negligible the effect on the flow generated noise is of some significance. Due to the limited space in which additional attenuation can be added immediately adjacent to the duct outlet the airflow through this part of the distribution system is critical to meeting the desired acoustic standards.

The design of the actual cabin diffuser itself has been the subject of considerable study with detailed data available in the ASHRAE handbooks [15] and other HVAC texts [26]. For the purposes of this research the actual design of this outlet grill has been restricted to several existing standard HVAC grills readily available from current suppliers. The primary goal of this research was to focus on how to optimise the link between high speed airflow and the cabin outlet grill. There is considerable potential to pursue this research further by applying the numerical models discussed in this thesis to optimise the diffuser designs current used in the HVAC industry. A high velocity round jet diffuser and a standard square diffuser were used, as shown in Appendix A. An additional cushion head box was also incorporated into the experimental program to simulate the impact of a realistic installation.

Chapter 3

Literature Review

The foundation of this research is spread across the fields of both acoustics and fluid mechanics. Traditionally work in this area (aero-acoustics) has focused on the sound generated by external air flows over bluff bodies at high velocity (compressible flow regimes), with initial research spawning from the development of jet powered air travel. The turbulent flow regimes encountered in the proposed high velocity HVAC designs considered herein can be classified as incompressible flows and as such the validity of directly applying traditional compressible flow aero-acoustic methods will be reviewed. Alternate methods of analysis will be explored based on traditional fluid mechanics and fundamental acoustic principles.

In recognition of the broad spectrum of theory and applications used in this research the summary of the relevant current literature has been separated into the main distinct fields of interest. This review is followed by a summary of how all of the theories considered combine to form the fundamental justification of the work herein presented.

3.1 HVAC Noise Ratings

There has been considerable debate over the most suitable noise rating method for the assessment of HVAC systems. The ASHRAE [8, 24] standards outline three main noise rating criterion currently used commercially in rating the acoustic comfort level of enclosed spaces. They are as follows:

1. A-Weighted sound pressure level
2. Noise Criterion (NC) Curves
3. Room Criterion (RC) Curves

The A-weighted sound pressure level (L_A) is widely used, due to the simplicity of the equipment needed and the time required for data collection and analysis. A simple hand held sound pressure meter can be configured to electronically weight the measured sound spectrum and report a single weighted total sound pressure level. The A-weighting curve is designed to approximate the response of the human ear at low sound pressure levels (Bies and Hansen, [28]). The major disadvantage of this noise rating method is the lack of assessment of the spectral components of the overall sound pressure level. Where there are pronounced peaks in particular frequency bands the perceived annoyance level of a given spectra may be considerably higher than the overall A-weighted sound pressure level would indicate. The A-weighted weighting levels used are shown in Figure 3.1.

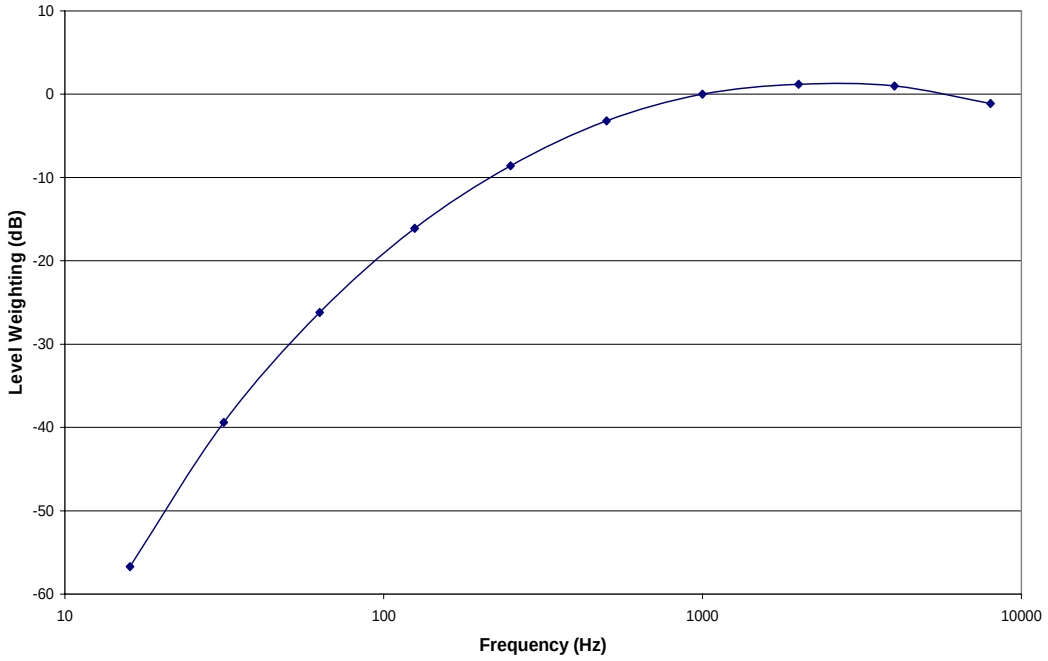

Figure 3.1: A-weighting sound pressure levels in octave frequency bands.

The NC curve method dates back to Beranek in 1957 [29], with an improved Balanced Noise Criterion (NCB) method proposed by the same author in 1989 [30, 31]. The NC curves define the limits that must not be exceeded by the measured octave band sound spectrum, as shown in Figure 3.2. This type of method is commonly described as a tangent method, with the highest peak with respect to the prescribed NC curve used to determine the NC rating of the measured noise spectrum. Kingsbury [32] rightly points out the major shortfall of the NC method being the inability to rate the quality of the

noise spectrum. The presence of particular peaks, especially in the lower frequency bands can lead to an unsatisfactory sound spectra being deemed acceptable.

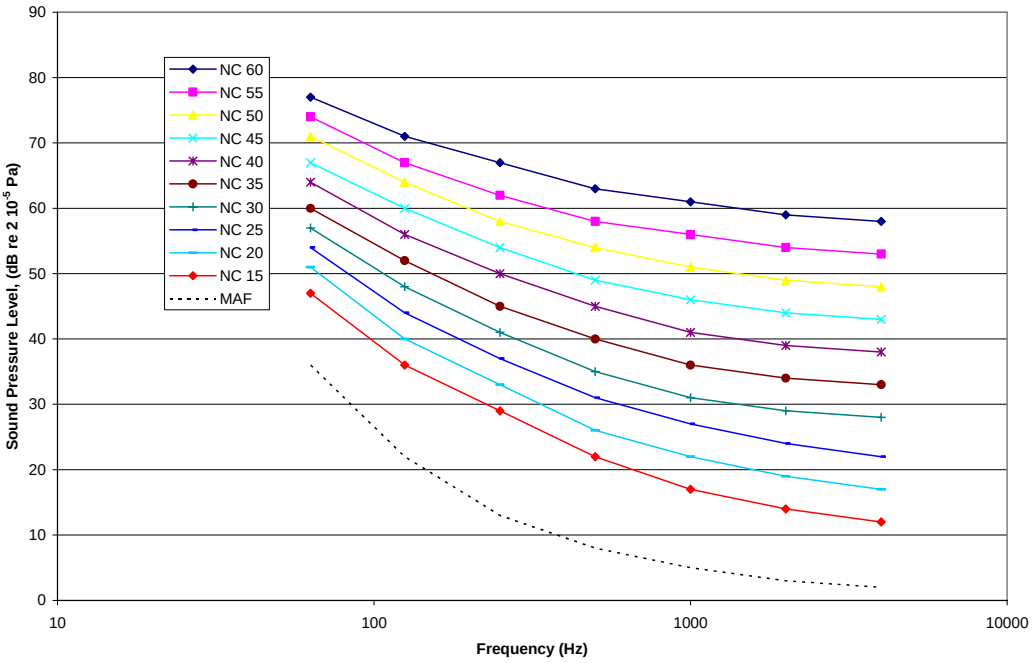

Figure 3.2: NC curves for octave band noise assessment.

The NCB method adjusted the allowable low frequency sound pressure levels to more accurately match the audible response of the human ear. Blazier [33] and Kingsbury [32] both argue that the increased low frequency limits of the revised NCB method are too lenient. The increased annoyance levels due to low frequency rumble using this criteria was investigated by Bradley [34], leading to a recommendation to incorporate an additional measure of the amplitude variation across the sound spectrum. Subsequent ASHRAE handbooks have therefore largely ignored the revised NCB method and provide the original NC method as one of the acceptable noise rating criterion.

The Room Criterion (RC) curves were specifically developed for assessing the acoustic performance of HVAC systems by Blazier [35] and have been subsequently refined [36] to account for low frequency annoyance limits. The RC curves are based on empirical data and were developed to approximate a well balanced, neutral acoustic

HVAC spectrum. The slope of the RC curves varies from the NC curves at both the low and high frequency ends of the spectrum. The NC curves have a steeper slope in the low frequency octave bands (16 to 250 Hz) and a flatter slope across the high frequency (2 to 8 kHz) bands. The RC curves have a constant slope of -5 dB per octave band across the whole spectrum, as seen in Figure 3.3.

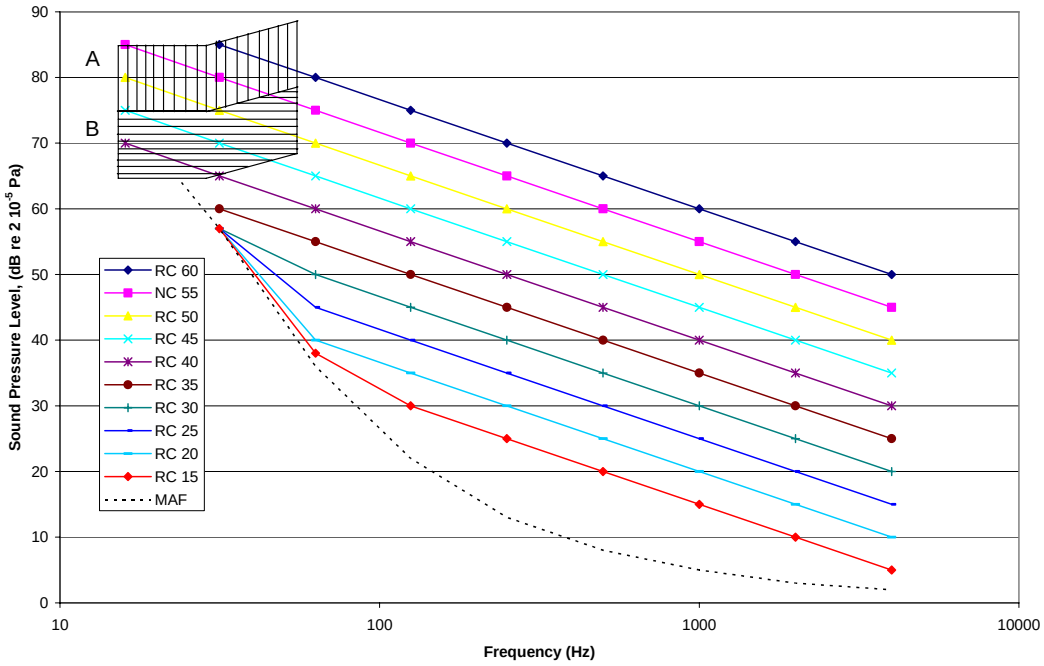

Figure 3.3: RC curves for octave band noise assessment.

The refined RC method (RC Mark II) makes minor adjustments to the slope in the low frequency bands to better match the minimum audible field (MAF) range of the human ear. The qualitative measure of the sound spectrum is also incorporated into the revised RC method, with one of the following terms:

1. N – Neutral sound spectrum
2. LF – Low frequency dominant (rumble) spectrum
    A. LF_A – Substantial sound induced vibration in light structures
    B. LF_B – Moderate, but clearly perceptible sound induced vibration
3. MF – Mid frequency dominant (roar) spectrum
4. HF – high frequency dominant (hiss) spectrum

The low frequency (LF) subcategories are determined by the shaded sections on the RC curve chart in Figure 3.3, labelled A and B respectively.

An additional noise rating criteria has subsequently been proposed by Schomer [37] that combines aspects of both the refined RC and NC methods and is called the room noise criteria (RNC) method. Although not yet fully adopted by the wider HVAC community this new criteria has the potential to rationalise the future characterisation of HVAC system noise spectra. The major change from the standard RC curves is a greater acceptable low frequency limit for the same rating level. The qualitative reference term is also dropped and replaced with a simple report of the limiting octave band that determines the rating level using the tangent method outlined previously.

3.2 Fast Ferry Passenger Comfort and Noise Ratings

The passenger comforts levels on ocean going fast ferries form an important aspect of the final sea trials prior to the delivery of the vessel, with severe penalties incurred in the event of any failure. The financial costs of any failure can be considerable when the payment of the full cost of the vessel of up to $100 million USD can be delayed while any such errors are rectified. The current passenger comfort levels for an ocean going fast ferry are summarised in Table 3.1. The maximum air velocity and the sound pressure level are of most interest to this particular study as these are the limiting design specifications for the air distribution system under investigation. The number of air changes per hour also affects the final air volume flow rates which will have an impact on the sizing on the final ducts used.

Table 3.1: Fast Ferry Passenger Comfort Requirements.

Climate	Air Temperature	18 to 25 ˚ C
	Relative Humidity	65 %
Air Movement	Air Changes	4 per hour
	Ventilation	9.4 Ls^{-1} per passenger.
Acoustics	Sound Pressure Level	65 dB A (re $2e^{-5}$ Pa)

The temperature of the delivered air and the relative humidity are additional factors that are important from a thermodynamic design point of view, but these have been removed from this work to reduce the number of variables under consideration. This omission is based on the assumption that the high velocity air distribution system being developed is for upgrading existing designs that have been used to date. The design methodology thus developed can be applied thereafter to other system specifications where additional thermodynamic considerations can be included.

The sound pressure level rating of 65 dB (A) refers to measurements throughout the passenger space on board each vessel. Bies & Hansen [28] note that an A-weighted sound pressure level of 65 is approximately equivalent to an RC or NC rating of 55 to 60. On initial inspection the sound generated in the HVAC system will be substantially under this level, giving rise to the suggestion that the noise rating of a HVAC system in a fast ferry application is superfluous. However, due to the vessels being a solid welded aluminium construction the engine and hydro-dynamically induced sound levels are quite close to this limit without the HVAC system running. These high levels of background noise therefore require a closer scrutiny of the HVAC system noise levels as these may be enough to exceed the overall sound pressure level of 65 dB (A). The sound pressure level commissioning test requires a hand-held sound pressure level meter being placed in multiple locations inside the empty cabin space during initial sea trials (Armstrong [38]).

The lack of published information specifically orientated at marine based applications is cited by Goujard et al. [39], who conducted a questionnaire based evaluation of passenger comfort levels on low speed passenger vessels. Thirty-nine percent of all respondents named acoustics as one of their top two priorities and forty-four percent of respondents mentioned a need to improve the acoustics on the vessels in question. In both of these cases the next highest response was for temperature at 24 and 25 percent respectively. Given that this investigation was targeted specifically at the acoustic conform of passengers on these vessels one must question the independence of this study.

In the past the bulk of this type of work has predominantly been based on passenger comfort in rail carriages [40-42], with particular attention paid to high speed rail applications. A more general assessment of ship based noise levels was made by Tamura [43], but specifically focused on the ability of passengers to sleep. There is a scarce supply of published literature on specific ship based HVAC noise standards.

Given the imprecise nature of the evaluation tests there is some question as to the accuracy to which the A-weighted rating of 65 dB must be satisfied. One could also argue that the cabin space filled with several hundred people would have a far greater acoustic absorption than the as tested empty cabin space. Therefore the full cabin space would have a lower ambient sound pressure level than otherwise tested under sea trial conditions.

3.3 Calculating Sound Power Levels from Sound Pressure Levels

All of the noise rating methods mentioned previously are based on sound pressure levels inside the passenger cabin space. The sound pressure level is directly related to the total acoustic power being radiated into the cabin space. The correlation between the two is determined by the acoustic properties of the passenger cabin itself and the distribution of the individual acoustic sources. The relationship between the acoustic power (W), acoustic intensity (I) and the acoustic pressure (p) are defined in most fundamental acoustics texts [28, 44] and will be discussed in further detail in Chapter 8. A distinction will be made between these relationships for free field acoustics (as used in most numerical models) and diffuse field acoustics - conditions encountered both experimentally and in typical passenger cabin installations.

As a secondary note there is also the potential that the current noise level standards may be reviewed in the future with tighter restrictions imposed. The design methodology developed as part of this research will provide a valuable resource in the event of this change being made at some future time.

3.4 Numerical Simulation of Flow Induced Noise

The numerical simulation of flow induced noise has been studied at great length over the past 50 years with a variety of modelling approaches developed to suit specific applications. The majority of these methods use either direct calculation of the sound pressure (computational aero-acoustics – CAA) or a solution derived using Lighthill's [2, 3, 45] far-field acoustic analogy. Each approach has both advantages and limitations that aid in the selection of the most appropriate and efficient approach for any given application. In both cases the modelling techniques have been derived for the prediction of noise generated by external flows around bluff bodies as opposed to internal flow inside ducts and cavities. The main subsets of both the CAA and far field methods will be reviewed with the intent to identify the most suitable modelling approach for this research.

3.4.1 Computational Aero-Acoustics – Numerical Methods

The field of computational aero-acoustics (CAA) first developed out of the aerospace industry in conjunction with the development of jet engine powered flight. The significant increase in engine power and flight speed resulted in significant increases in the noise generated by the engine itself [46-50] and the airflow around the external aircraft surfaces [51, 52]. Considerable research and experimental collaboration led to the development of numerical models capable of modelling the noise generated by high velocity air flows over external surfaces at both high subsonic and supersonic velocities. Recent improvements in these models have taken advantage of modern computing capabilities and the application of very high order numerical schemes [48, 53-59] for solving the complex governing equations.

CAA models are typically optimised to run for problem specific boundary conditions and flow parameters. The flow domain must include both the source of the flow generated noise and the required observer (acoustic receiver) locations of interest. Models of this nature simulate the direct propagation of the sound pressures generated and the interaction of any multiple sources with the model domain. This is particularly useful for analysing the acoustics of the near-field (close to the source points), yet

presents onerous demands on computing power for any extended acoustic analysis. In either case the application of CAA methods has been predominantly restricted to cases of external flows only.

CAA models such as those outlined above require a solution of the compressible Navier Stokes equations to fully simulate the propagation of sound through the fluid domain. The fluctuations in the flow field are typically several orders of magnitude greater than the corresponding acoustic field, leading to a disparity in length scales between the two respective fields [60]. Standard CFD based numerical schemes lead to the flow field fluctuations contaminating or otherwise masking the true acoustic field being modelled. Various customised numerical schemes have been developed specifically for CAA based problems to overcome the limitations of traditional finite volume based CFD numerical schemes.

Tam and Webb's [57] Dispersion-Relation-Preserving method was developed to improve the accuracy of the resolution of the high wave numbers within the model at the expense of the numerical scheme itself. Similar reductions in the dispersion error can also be made with the use of the compact difference scheme proposed by Lele [58], Kim and Lee [59] and subsequently Zhauang and Chen [61]. In each of these cases the models were developed for use on uniform mesh domains. Consequently the need to extend the flow domain to include far-field observer locations results in either a large number of grid points or a severe constraint on the mesh density used. In either case the accuracy of the model is balanced against the cost and availability of computational resources.

The need to optimise the use of limited computational resources has led to the development of dual mesh based models [62], with a small confined CFD based mesh surrounding the sources of the flow induced noise and an overlapping larger (and coarser) acoustic mesh for the acoustic calculations. B-spline methods have been successfully applied by several researchers to a variety of applications [63, 64] that have led to significant reductions in the total number of mesh points needed to successfully resolve the dual mesh simulation. Widjaja et al. [65] have recently achieved a mesh reduction of 26 %. They have concluded that the application of the B-spline collocation

to be superior to both the finite difference and compact difference methods mentioned previously.

The immaturity of these methods and the corresponding lack of integration with existing commercial modelling packages (at this early stage of their development) limit their application to this particular research project. Current published results are limited to the successful simulation of spinning co-rotating vortices. The potential application of this modelling technique to more complex flow phenomenon will be of some interest if and when this occurs. The future potential of this approach is worth noting in relation to future research opportunities.

An alternative solution to the dispersion and dissipation errors (outlined above) in CAA models is the use of a Discontinuous Galerkin (DG) method. High order discretisation schemes are used to solve the Linearised Euler Equations (LEE); normally in preference to the Navier Stokes equations. Hu et al. [53] developed a low dispersion and low dissipation Runge-Kutta scheme for application to CAA simulations. The stability of this model allowed far greater time steps than would otherwise be possible using standard high order schemes. However preventing the reflection of acoustic waves at the model boundaries requires the use of specialised non-reflecting boundary conditions.

The development of CAA models in general and specifically non-reflecting boundary conditions has gained significant momentum in the past couple of years [55, 56, 66-77] with notable contributions from Guenanff and Terracol [78] and Ozdemir et al. [79]. Delorme et al. [80] also developed a LEE based DG model with rigid wall, non-reflecting and imposed value boundary conditions. This model was then applied to a short section of 0.5 m square (constant cross section) lined duct with no mean flow. The attenuation of a 3.4 kHz tone was successfully modelled with a non-reflecting outlet boundary. The results were in good agreement with 1-dimensional (1-D) analytical solutions. Interestingly there is no mention of a mean flow model with flow induced noise generation inside the above duct.

The computation of acoustic diffraction around an aircraft wing has been studied (external flow simulation), but once again without any consideration of the generation of flow induced noise. Longatte et al. [81] present results for a LEE model for acoustic reflection, diffraction and propagation in the presence of mean flow; however they too omit the effects of flow induced noise. The extension of this model to the non-trivial inclusion of flow induced noise generation and propagation will be of some interest in the years to come.

Dumbser and Munz [54] recently developed the DG LEE aero-acoustic model further with a high order single-step discretisation scheme with significantly lower memory demands than the established Runge-Kutta based schemes. By improving the computational efficiency of the numerical schemes employed it is hoped that the simulation of more complex geometries will soon become a realistic possibility. The key development of this work is the capability of the model to run on unstructured meshes. Although in the early stages of development this presents a useful modelling option heading into the future, but not for the immediate needs of this research.

Bogey and Bailly [48] have recently adapted the more computationally efficient high order schemes outlined previously to both flow and acoustic computations. The method was first applied to the 1-D propagation of a noise governed by the convective wave equation. The results proved the improvements in both computational efficiency and accuracy of the numerical solution. The same discretisation schemes were then applied to LES models of 3-D turbulent flows. The flows considered included flows past open cavities and circular jets at a mach number of 0.9. At these air velocities the flow field is highly compressible. The LES model gave good agreement with existing published turbulent jet results with significant computational savings. Numerical stability at a CFL number of 1.98 was achieved, whereas existing modelling methods would otherwise demand a CFL number less than 1. This alone represents a 100 % increase in the size of the time step used in the LES model - assuming a constant mesh size. Once again however, there is no attempt to extend this model to include the actual prediction of the flow induced noise associated with the jet. The future integration of these improved discretisation schemes into commercially available CFD codes will no doubt be of significant value as they are developed further.

In the past year hybrid numerical methods for the prediction of aero-acoustic sound generation and propagation have been introduced by Nordstrom and Gong [82]. They adapted high order CAA numerical schemes to handle complex geometries defined with unstructured finite volume grids. Initial test cases have been solved, but the stability of the solution is strongly linked to the interface treatment for the hybrid meshes used.

When the CAA models are applied to flows with high subsonic mach numbers the convective velocities of the turbulent structures within the flow field are of a similar magnitude to the velocity of the acoustic waves induced by the flow field. With similar convective fields they can be resolved over the same mesh without compromising the numerical discretisation of both the acoustic and flow fields. However, when these same methods are applied to low mach number flows the convective flow field velocities tend to be an order of magnitude or more smaller than the acoustic propagation velocity. The divergence in the propagation velocity gives rise to a distinct variation in the wavelength of the acoustic and turbulent flow based fluctuations. Munz et al. [83] developed a multi-scale model for use in this type of application, where the flow is resolved over a very fine grid that is then embedded into a larger and coarser mesh used to resolve the acoustic domain. The transition from the fine CFD grid required a multi-scale expansion with one time scale and two space scales. This type of method is referred to as an acoustic perturbation method.

The acoustic perturbation equation (APE) method outlined above was also used by Ewert and Schroder [84, 85] for a number of test cases of a monopole source in sheared mean flow, a spinning vortex pair, a cylinder in cross flow and trailing edge noise. It is worth noting that the turbulent flow field in these cases were all solved using a compressible LES turbulence model solved over the localised fine flow domain. As the APE method directly simulates the propagation of the acoustic waves through the model a compressible flow field is required, even for flows that are essentially incompressible. Consequently compressible flow boundary conditions are required to eliminate unwanted reflections from the model boundaries. The multi-scale methods outlined above help to alleviate this issue; however one must question if this is the preferred method for calculating the noise generated by low subsonic flows.

The rapid rise of CFD based numerical flow models has precipitated renewed interest in the direct noise computation (DNC) methods, where the acoustic flow field is derived directly from the Navier-Stokes equations. This method requires a true transient solution such as an LES turbulence model or a DNS simulation. Computational limitations restrict the size of current DNS simulations leaving the LES method as the preferred modelling solution. The LES model allows the main turbulent flow structures to be modelled, while the filtered small scale components are incorporated into a sub-grid model of some kind.

Bogey and Bailly [86] applied a LES model based on explicit filtering to simulate the flow induced noise produced by a circular jet with a mach number of 0.9. A compressible CFD based model was required given the high mach number of the flow, which also facilitated the direct computation of the subsequent flow generated acoustic field. As the convective velocities of the flow field and the acoustic field were of similar size there is a reasonable correlation between the time scales of the respective propagations through the numerical domain. Bogey and Bailly conclude that the LES model provides a suitable representation of the turbulent flow field and length scales.

A similar DNC modelling approach was adopted by Marsden et al. [87] to flow over a cavity and the potential to apply an adaptive flow control mechanism. A mach number of 0.6 was used with a closed loop flow control using a synthetic jet located at the upstream edge of the cavity as the primary actuator and the feedback reference taken from the static pressure inside the cavity. Once again the compressible LES turbulence modelling approach was found to be effective for flows in this velocity range. Although this same method may be used to simulate jets/flows with considerably lower mach numbers (incompressible flows, $M<0.1$), an incompressible LES model would no doubt come at a much lower computational cost.

CAA models have also been developed to incorporate the effects of the flow induced noise on the flow field itself. Where the flow generated noise impacts on the flow field itself the standard modelling approach of decoupling the flow field from the acoustic field calculations is no longer valid and a more complex coupled solution process must be used. Clearly the added computational complexity of a directly coupled

solution process is best avoided unless absolutely necessary. The level of coupling between the local sound and flow fields is generally found to be closely related to flow velocity. For high subsonic and supersonic velocities a coupled analysis is required, however for low subsonic flow fields these effects are very weak and in most cases may be ignored.

3.4.2 Far-field Acoustic Analogies – Numerical Methods

Lilley [88] notes that the generation of noise by turbulent flows became a significant obstacle to the application of jet engines into the civilian air transport sector in the late 1940's and early 1950's. Professor E. J. Richards of Southampton University is acknowledged as one of the key people responsible for the establishment of the early experimental work conducted during this period to document the characteristics of jet noise and how best to control it. The theoretical understanding of flow generated noise can be traced back to the work of Lighthill [2, 3, 45] and his founding lectures "On sound generated aerodynamically". This theory is based on an acoustic analogy that exactly links the fluctuating fluid density to the resulting induced sound. The governing equation for this analogy is as follows:

$$\frac{\partial^2 \rho}{\partial t^2} - c_0^2 \frac{\partial^2 \rho}{\partial x_i^2} = \frac{\partial^2 T_{ij}}{\partial x_i \partial x_j} \tag{3.1}$$

where ρ is the fluid density, c_o is the free field speed of sound and T_{ij} is Lighthill's stress tensor, defined as follows:

$$T_{ij} = \rho v_i v_j + p_{ij} - c_0^2 \rho \delta_{ij} \tag{3.2}$$

where the first term, $\rho v_i v_j$ represents the direct convection of the momentum component ρv_i by the velocity component v_j and p_{ij} is the stress between adjacent elements of fluid. The final term includes the kronecker delta function, δ_{ij}, which has value of unity when $i = j$ and is otherwise zero.

Proudman [89] who was acknowledged by Lighthill in the aforementioned work applied this analogy to noise radiating from decaying isotropic turbulence at low mach numbers. This work identified the proportionality between the radiated sound power

(per unit volume of turbulence) to the eighth power of the flow velocity. Difficulties applying this relationship to real world applications such as the jet engines at this time arose due to the anisotropic nature of the turbulence encountered. True prediction of radiated sound would require accurate models of the true characteristics of the turbulent flow field.

With the modern advances in computing power at reasonable cost and the parallel development of efficient numerical schemes and algorithms accurate models of practical anisotropic turbulent flow fields are now possible. The initial work of Lighthill has subsequently spawned numerous numerical methods that implement the acoustic analogy in either an integral or derivative based formulation. The mainstream formulations cited in the majority of the published literature in the field of computational aero-acoustics are summarised in Figure 3.4.

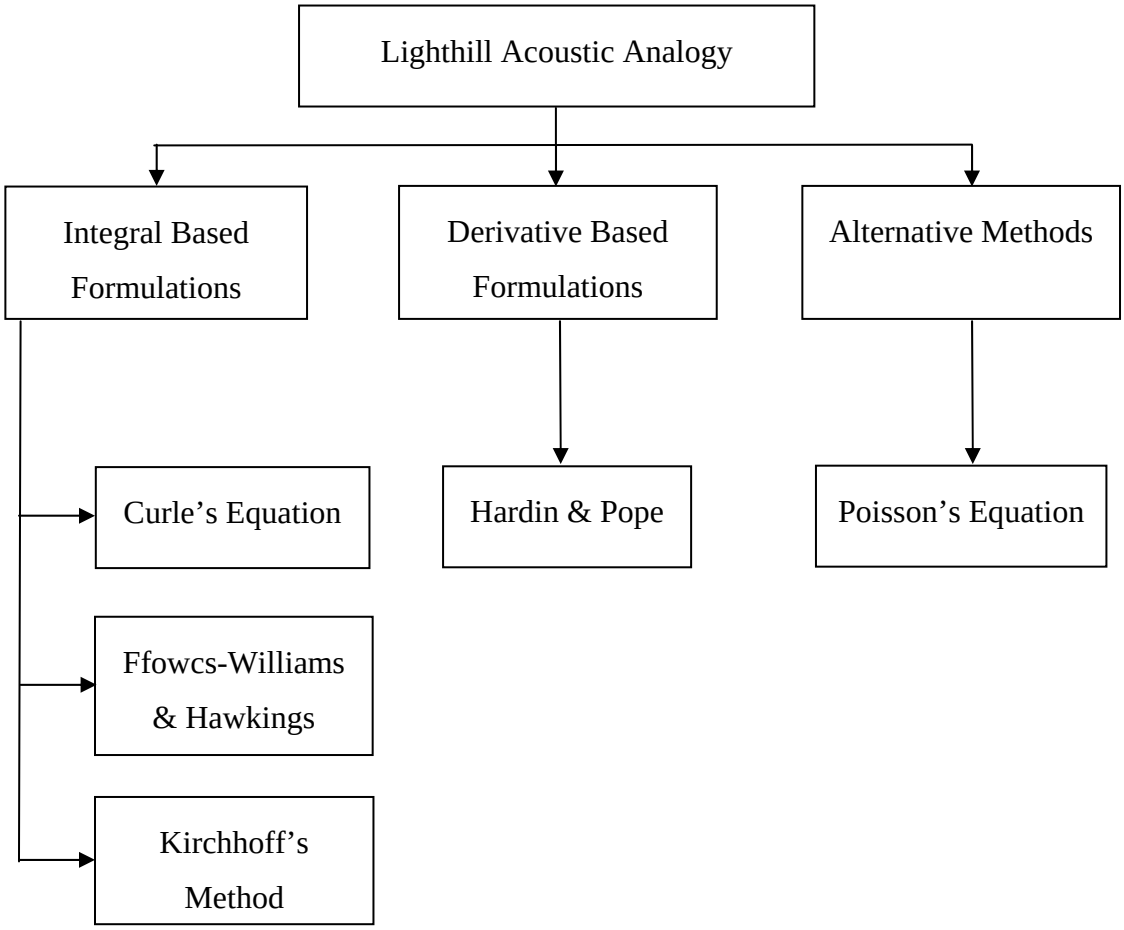

Figure 3.4: The evolution of acoustic analogy formulations based on Lighthill's theory on sound generated aerodynamically.

The development of these formulations will be summarised below with the intent to identify the most suitable acoustic analogy formulation for modelling the noise generated in high velocity HVAC systems.

Both the integral and derivative methods call for the time varying turbulent flow field to be resolved using numerical means (such as CFD) with the resulting data used to determine the location, type and strength of equivalent acoustic source terms. The acoustic source data is then used to calculate the corresponding sound pressure levels at the desired observer (receiver) locations that may be located at positions either inside or more commonly outside the existing flow field domain.

The majority of the formulations of Lighthill's acoustic analogy use an integral based method, whereby the acoustic sources are enclosed within a surface, S. The way in which the integration is performed varies slightly for each of the formulations identified above. Curle's equation [90] was the first acoustic formulation to incorporate the influence of solid boundaries on the flow generated noise. The equation for the acoustic pressure, $p'(\boldsymbol{x},t)$, for an observer at a location defined by a position vector, $\boldsymbol{x}$, and an acoustic point source located by a position vector, $\boldsymbol{y}$, is defined as follows:

$$p'(x,t) = \frac{1}{4\pi}\frac{\partial^2}{\partial x_i \partial x_j}\left[\int_V \frac{T_{ij}\left(y, t-\frac{r}{c_0}\right)}{r} dV(y)\right] - \frac{1}{4\pi}\frac{\partial}{\partial x_i}\left[\int_S \frac{F_{ij}\left(y, t-\frac{r}{c_0}\right)}{r} dS(y)\right] \qquad (3.3)$$

where T_{ij} is Lighthill's stress tensor as defined previously, F_{ij} is the fluctuating force associated with the fluctuating density field (source of sound) and r is the distance between the observer ($\boldsymbol{x}$) and the acoustic source ($\boldsymbol{y}$):

$$r = |x - y| \qquad (3.4)$$

The first term in Curle's equation (volume integral) calculates the far-field acoustic pressure produced by quadrupole acoustic sources while the second term incorporates the effects of the solid boundaries (dipole acoustic sources). The

$t - \frac{r}{c_0}$ term allows the acoustic calculation to be calculated at the retarded time that is seen by an observer located at $\boldsymbol{x}$.

There are several recent examples in current literature where Curle's equation [91] has been used to predict the flow induced noise for a variety of industrial applications. Kim et al. [92] investigated the unsteady flow over a NACA 0018 airfoil using Curle's equation coupled with a LES CFD model of the flow field. This work was motivated by the need to understand the fundamental flow mechanisms that generate noise in turbo-machinery (specifically jet engines). Both the LES flow model and the numerical prediction of the frequencies of the vortices along the trailing edge of the airfoil had good agreement with established experimental results. The predicted sound pressure level spectra predicted the correct discrete peak at 2.03 kHz, but no direct comparison is made with the magnitude of the sound pressure levels.

Curle's equation coupled with a LES CFD solver has also been used by Kato et al. [93] to predict the sound generated from a number of low mach number flows. Results are presented for flow at 50 ms^{-1} around an automobile side mirror, with reasonable agreement between the numerical predictions and corresponding experimental results. The predicted frequency spectra were heavily dependent on the quality of the mesh used in the LES flow model. The grid resolution surrounding the flow separation point was one of the key determining factors affecting the accuracy of the predicted far-field sound spectra.

Additional results were also presented for flow over a NACA 0012 airfoil and inside a multistage centrifugal pump. These two test cases made use of additional customised finite element (FEM) and boundary element methods (BEM) in order to complete the analysis. The results for these two test cases tended to over predict the amplitude of the far-field sound pressures, but provided a reasonable match in the shape of the frequency spectra. The over prediction in magnitude is attributed to the inability at this point in time to fully account for the scattering effects associated with solid surface interfaces and the need to have a fine enough mesh in these areas. The tendency to use high CFL numbers (between 5 and 10) may also contribute to these errors.

The 2-D case of low subsonic flow over an open rectangular cavity was completed by Ask and Davidson [94] using an incompressible CFD flow model coupled with Curle's formulation of the acoustic analogy. A laminar flow at a mach number of 0.15 and a Reynolds number of 1500 based on the cavity depth was used. Once again the sound pressure levels (amplitude) were over predicted slightly by 1 to 4 dB depending on the grid resolution used and the extent of the acoustic source surface used in the surface integral (dipole sources only). Rather than validating the results against experimental results a reference case using a compressible flow model is used instead. The variation between the compressible and incompressible models is very small (1 to 2 dB) which suggests that the added computational costs for low mach number flows is unnecessary. However it is important that this modelling approach is validated against real physical data and not just another numerical model (with an unknown validation status of its own).

The Ffowcs-Williams and Hawkings [95] formulation of Lighthill's acoustic analogy was developed to incorporate the effects of solid surfaces in the overall prediction of flow induced noise spectra. Any flow induced noise spectra is a composition of quadrupole, dipole and monopole acoustic sources. Dowling and Ffowcs-Williams [96] derive the proportionality between the flow velocity and the resulting flow generated sound power for each of these sources, as summarised in Table 3.2. At low mach numbers the strength of the quadrupole sources (free shear flows) is very weak and tends to be heavily masked by any dipole and monopole sources. The strength of the quadrupole sources become increasingly significant as the flow velocity is increased.

Table 3.2: Acoustic source property summary

Source	Sound Power	Examples
Monopole	αU^4	Point sources (single vortex)
Dipole	αU^6	Interactions with surfaces/walls
Quadrupole	αU^8	Free shear flows

The Ffowcs-Williams and Hawkings (FWH) formulation extends the Curle formulation of the dipole sources to also include the effects of monopole sources. For continuity the FWH equation is defined using the same location vectors (***x***) and (***y***) for the acoustic source and observer respectively:

$$p'(x,t) = \frac{1}{4\pi|x|}\left\{\frac{x_i x_j}{|x|^2 c_0^2}\frac{\partial^2}{\partial t^2}\left[\int_V T_{ij}\,dV\right] + \frac{x_i}{|x|c_0}\frac{\partial}{\partial t}\left[\int_S \left(pn_l + \rho u_i u_n\right)dS\right] + \frac{\partial}{\partial t}\left[\int_S \rho u_n\,dS\right]\right\} \tag{3.5}$$

where n_l is the normal vector to the integral surface (S) and u_n is the velocity normal to the same surface. The volume integral is computed over an arbitrarily defined volume (V) selected to contain all of the relevant quadrupole sources. The first term (containing the volume integral) calculates the noise generated by the quadrupole sources, with the second and third terms calculating the noise generated by the dipole and monopole sources respectively.

Two approximations can also be made to the FWH equation to simplify the analysis. Firstly the most common simplification is to drop the volume integral term for any model containing low mach number flows that are highly incompressible. This assumption is quite valid provided the strength of any quadrupole source is significantly less than the dipole and monopole sources present in the flow. This step is strongly recommended [97] due to the significant computational efficiencies gained from removing the volume integral.

In cases where there are potential quadrupole sources present that need to be included an alternative simplification may be made to negate the need to include the volume integral term. By carefully defining the surface integral (S) to encompass the quadrupole sources of interest their contribution to the overall flow induced noise gets included in the calculation of the surface integral along with the dipole and monopole sources [45, 97, 98]. In the case of expanding low velocity circular jets this is clearly the preferred modelling option to enable the contribution of the weak quadrupole sources to be included in the calculation of the flow induced noise spectra.

The FWH equation outlined above has been used extensively to calculate the far field flow induced sound spectra for a wide range of applications. All of these models have been based around external flows around/over bluff bodies (aircraft/turbo-machinery [97, 99-108], helicopter rotors [109-113] and others [114-116]). The closest application that is relevant to this particular work is the application of the FWH equation to predict the flow induced noise from jet engine exhausts. The primary focus of this work is on the minimisation of jet noise on modern commercial aircraft, with typical mach numbers of 0.7 to 0.9. Shur et al. [97] simulated a mach 0.9 jet with no surrounding mean flow and Tucker [108] extended this work further to include the effects of secondary flow (co flow) surrounding the primary jet. This example was designed to more closely match the physical mechanisms encountered in a modern jet engine fitted with a bypass fan. Tucker also investigated the effects of using alternative numerical schemes and sub-grid models in the LES based CFD flow model. The effects of swirl on the flow structures themselves and the resulting sound field were also investigated.

The bypass air (co flow) effectively reduced the total induced sound power spectra though reducing the extent of the shear layers in the expansion region of the flow. Similarly the swirl in the flow reduced the length and size of the primary jet core; however the rate of expansion of the jet was significantly increased. The results were inconclusive as to whether the addition of the swirl provided a net reduction in the overall sound power spectra. Although the size of the jet core is reduced there is a greater region of turbulent flow that also produces a broad spectrum of noise. Both of the aforementioned publications demonstrate that the noise generated by the expansion

of a round jet can be predicted using the FWH equation to a reasonable level of accuracy for a high mach number subsonic flow.

Chen et al. [117] coupled a LEE based CAA model with a FWH far field model to calculate the sound radiation from an un-flanged duct, however there was no attempt made to include any effects of flow induced noise. The simulation was based on predicting the effects of the duct on the radiation of an acoustic source upstream inside the duct (with no mean flow). Good agreement with experimental measurements was found, and interestingly the placement of the FWH integration surface (S) had only a marginal effect on the accuracy of the far-field predictions.

The theoretical development of the FWH model has been discussed at some length [118-122] and in 2003 was included as a post processing tool in the commercial CFD code Fluent 6.1.02. The wider acceptance of this modelling technique has increased further as validated modelling results are published in peer reviewed literature as cited above. The crucial step in the application of these modelling techniques to new problems such as HVAC noise predictions is ensuring that the chosen modelling approach is adequately validated against experimental data. The model should also be verified to ensure that the correct equations are being solved in accordance with the physical system being modelled. The AIAA guide to verification and validation [123] provides a detailed description on how to fulfil these requirements. These will be discussed in tandem with the development of the numerical model used in this research detailed in Chapter 7.

The third integral based formulation of Lighthill's acoustic analogy is the Kirchhoff method, based on an integral equation first derived in 1882 by Kirchhoff and then later named after him. Farassat [124] classifies the FWH method outlined above as one form of the Kirchhoff method. Both methods describe the solution of the wave equation in the exterior regions surrounding a surface (S) but using slightly different modes of derivation. The Kirchhoff method makes use of Green's identity in four dimensions [125] and uses this as a fundamental solution to the wave equation. In comparison the FWH equation is derived using mass and momentum conservation laws to then obtain a wave equation (to then solve for the given boundary conditions). The

Kirchhoff method itself has been used extensively in the study of helicopter rotor tip noise [104, 109, 110, 113, 121, 126-128] and high velocity jet engine/aircraft noise [101, 104, 124, 129-131]. More recently this method has also been applied by Yoon et al. [132] to predict the noise generated by flow surrounding high speed trains.

The main advantage of the Kirchhoff method [133] is the ability to use a linear formulation, such as the one derived by Lee et al. [126], instead of the more complex non-linear FWH equation that is more widely used. This assumption is made possible provided that there are no significant effects on the propagation of sound due to the non-linear flow field. In the event that this assumption is not valid, an alternative non-linear formulation is used. The linear formulation, as used by Lee is shown in equation 3.6 below:

$$p(\vec{x},t) = \frac{1}{4\pi}\iint_S \left[\frac{\cos\theta}{r^2}\, p - \frac{1}{r}\frac{\partial p}{\partial n} + \frac{\cos\theta}{c_0 r}\frac{\partial p}{\partial \tau} \right] dS(\vec{y},\tau) \qquad (3.6)$$

where θ is the angle between the normal vector ($\vec{n}$) on the integral surface (S) and the radiation vector ($\vec{r}$), with $\vec{r} = \vec{x} - \vec{y}$ as defined previously. The term, (r), in the above integral denotes the distance (scalar quantity) between the observer and the source as defined in the previously defined acoustic analogy formulations. The integral is also calculated at the retarded time, (τ).

The Kirchhoff equation has also been coupled with 3-D boundary element methods (BEM) for determining the radiation and reflection of sound around vibrating and moving surfaces [113, 134]. This work holds potential for application to the modelling of HVAC systems given the propensity of ducts to vibrate. However, the added degree of complexity that this additional analysis would add to the current field of work is deemed excessive at this point in time. As the existing method developed herein matures it may be timely to reconsider the inclusion of a secondary analysis that also incorporates the effects of vibration and reflection of the flow induced sound. The existing BEM method provided by Antes and Baaran [134] does not currently include the full effects of flow induced noise surrounding the moving objects, perhaps indicative of the extensive work that would be involved.

The Kirchhoff method is favoured for many high velocity flows, particularly when employed with rotating reference planes. The linear formulation of the acoustic source terms, particularly the quadrupole source terms, provides distinct numerical advantage over other the other more complex integral based solution methods. The quadrupole terms in the Ffowcs-Williams & Hawkings (FWH) equation uses a volume integral, whereas the Kirchhoff formulation contains only surface integrals. The major disadvantage of this method however, is the need to contain the whole non-linear flow field inside the integral surface.

Dowling and Hynes [135] conclude that the Kirchhoff method predicts the far-field sound, but provides little insight into the nature of the sources of sound. Other formulations, such as the FWH method can be better used to investigate the contributions of individual regions of the flow. These features will be of particular value to an engineer aiming to identify primary sources of noise to better facilitate the minimisation of theses sources during the design phase of a project. Therefore for low subsonic velocities where the quadrupole term in the FWH equation can be dropped and the subsequent integral calculation simplified the Kirchhoff equation is not required.

Of all of the integral based formulations of Lighthill's acoustic analogy presented above the FWH method provides the best overall solution for predicting the noise generated by low subsonic flows. The flexibility in defining the integral surface and the ability to also incorporate the effects of volume based quadrupole sources provides a distinct advantage over the other alternatives. The integration of this solution method with commercially available CFD codes also presents a compelling argument for the selection of this method over the alternatives considered.

An alternative CFD acoustics post processor was derived by Hardin and Pope [136] and further developed by Ekaterinaris et al. [137]. This approach employed a derivative based formulation of Lighthill's acoustic analogy. This method was developed heuristically to provide a simplified acoustic prediction technique that could be implemented with standard CFD based numerical schemes. Given the relative large latitude in accuracy demanded in most acoustic applications there is some merit in such an approach that comes at significantly less computational cost. The major downside to

this method however is the need for two computational grids – one for the initial CFD flow model and another more coarse mesh for the acoustic post processing calculations. The need to store significant quantities of flow field data to complete the post processing acoustic calculations also limits the size and resolution of potential models.

Grace and Curtis [138] applied the Hardin and Pope formulation to the test case of 2-D flow over a rectangular cavity. After linearising the equations about the non-uniform flow quantities the following free-field acoustic equation was derived:

$$\frac{D_0^2}{Dt^2}\left(\frac{p'}{c_0^2}\right) - \nabla^2 p' = \rho_0 \nabla \cdot (\vec{v} \cdot \nabla)\vec{v} \qquad (3.7)$$

where $\vec{v}$ and p' are the fluctuating components of the flow velocity and pressure respectively. The subscript (*0*) denotes the free-field or mean flow quantity as used in the formulations outlined previously. With the formulation in this form the acoustic calculation was able to be encoded as a subroutine within the CFD code itself. Significant computational performance gains were reported by Grace and Curtis. The results presented demonstrated the potential to provide an approximate prediction of the flow induced noise and identify the location of the major contributing acoustic sources. The accuracy of the CFD model employed and the size of the model were both limiting factors to the overall performance of the model. The selection of the CFD model used to solve the transient flow field was also found to be crucial to the accuracy of the final solution. Clearly the need to use a fully transient turbulence model is crucial to accurately predict the flow induced noise spectra.

Another similar simplified formulation was used by Su et al. [139] to approximate the flow induced noise from axis-symmetric jets. A CFD flow simulation based on a standard k-ε turbulence model was used, coupled with a simplified form of Lighthill's acoustic analogy. A jet velocity of 100 ms^{-1} and diameter of 5.53 mm was used. Once again the reported results demonstrated that this method provides a "satisfactory" match to experimental results. Unfortunately the lack of grid refinement in the jet region was insufficient and the subsequent turbulent flow field compromised. The authors themselves conclude that a full LES turbulence model is required for a complete and

accurate solution. However in the absence of more substantial computational resources these results suggest that simplified analyses using this technique may be used to provide approximate design solutions to external flow problems.

This general consensus is echoed by numerous other authors [140-144] who have also used similar k-ε turbulence models coupled with various forms of Lighthill's acoustic analogy. Given these conclusions a more accurate transient turbulence model should be used, which is capable of simulating the non-isentropic turbulence present in an expanding round jet.

Senthooran et al. [145] used an alternative acoustic modelling technique to predict the flow induced pressure fluctuations on buildings based on Poisson's equation. The accuracy of the overall solution was found to heavily depend on the resolution of the mean flow quantities derived from the CFD flow model using (k-ε). The turbulent kinetic energy tended to be over predicted by the CFD model, leading to variations in the resolution of the re-circulation zones surrounding the buildings in question. The critical shortcoming in this model was once again the inability of the CFD model to accurately simulate the true turbulent flow field inducing the pressure fluctuations.

All of the far field models cited here make use of Lighthill's acoustic analogy, linking the sound generated by the flow field to the strength of local acoustic sources. The need to validate each of these methods against real experimental data is clearly evident from the diverse range of applications and the respective solution methods employed and cited above.

Bailly et al. [146] make a direct comparison between acoustic analogy based hybrid methods and direct noise computation (DNC) CAA based models. Two tests cases were considered for flow over a rectangular cavity and flow around a cylinder (in cross flow). A Ffowcs-Williams and Hawkings integral based formulation of Lighthill's acoustic analogy was used for both cases, with both compressible and incompressible solutions to the Navier-Stokes equations. A corresponding CAA based solution was also generated using a solution for the compressible Linearised Euler Equations (LEE). The results demonstrated that the most suitable approach for low mach number flows and

complex geometries is the incompressible Navier-Stokes solver combined with the Ffowcs-Williams and Hawkings formulation of Lighthill's acoustic analogy. For cases involving compressible flows or critical high frequency spectra the same approach is recommended but with the use of a compressible Navier-Stokes solver.

The current literature contains a multitude of variations of computational methods that have been developed and employed in the prediction of flow induced noise. The common requirement of all of these methods is a suitable method of solving the turbulent flow field containing the acoustic sources of interest. In the case of the expansions of a high velocity HVAC flow and the subsequent noise generation a CFD model is clearly the preferred modelling option. Although 25 to 35 ms^{-1} is a high velocity in terms of HVAC applications it is a very low velocity in terms of standard aero-acoustic applications such as jet engines, helicopter rotors and other aerospace orientated flows. This velocity range corresponds to a mach number of 0.07 to 0.1, well inside the threshold of incompressible subsonic flow regimes. The numerical models of this flow will therefore have a disparity in time and length scales of more than a full order of magnitude. Therefore careful treatment of the fluid-acoustic wave field interactions is required.

Based on the current literature at the commencement of this project a CFD based flow modelling method was selected using an incompressible LES turbulence model. Subsequent literature published [146] during the duration of this project has reinforced the validity of this underlying assumption and modelling approach.

3.5 CFD Turbulent Flow Models – Numerical Methods

Computational Fluid Dynamics has developed rapidly in recent times to the present level now where commercial codes are available which are capable of solving complex industrial style problems. This advance has been possible due to the rapid increase in computer processing power - at a reasonable cost. These advances have helped facilitate an increase in the complexity of the available codes and the level of detail available. This research has been conducted using Fluent – a commercially available CFD package - with versions 6.0, 6.1 and 6.2 being used over the three year period of numerical simulations.

The selection and formulation of the CFD model used to simulate the noise producing flow field can be broken down to the following five main steps:

1. Turbulence model selection
2. Selecting physical model parameters
3. Establishing boundary and initial conditions
4. Construction and validation of the mesh
5. Numerical solver and discretisation scheme selection

The selections made for the numerical models developed during the completion of this thesis are detailed in Chapter 7. A review of the current literature pertinent to this research project for each of these key areas is summarised in the following pages.

3.5.1 Turbulence Models

There is a wide variety of turbulence models available for the numerical simulation of industrial turbulent flows, the most commonly used being the various forms of the Reynolds Averaged Navier Stokes models (RANS) [147]. Of these models, the predominant number of the published work in this area makes use of the two equation k-ε turbulence model [138, 141-144, 148, 149]. Wilcox [150] however presents results that demonstrate that the two equation k-ω model is considerably more accurate for a range of turbulent cases involving jets, mixing layers and wakes.

Surprisingly there is no mention in any of the aero-acoustics based literature covering the use of the k-ω model. Irrespective of this result, all of these models are time-averaged based models. Therefore an alternative unsteady transient turbulence model is needed to ensure quality input data for the desired acoustic calculations.

The use of large eddy simulation (LES) turbulence models has become increasingly predominant with the ever increasing availability of cost effective computing resources. There are many examples [151-155] in recent literature of LES turbulence models being applied to a wide cross section of complex flow regimes. The main advantage of the LES codes is the ability to directly simulate the large transient turbulent flow structures present in the flow (eddies), while using a filter to remove the sub grid scale (SGS) eddies [156]. The cascade of turbulent energy from the large eddies down to the smaller eddies is conserved with the use of a sub grid model that approximates the smaller eddies without requiring the fine mesh that would otherwise be needed to resolve them adequately [157].

A direct numerical simulation (DNS) of all turbulence scales can be used, however this comes at significant computational cost. There are some examples in the literature [64] where such models have been used, but these have been limited to small scale research level investigations. For the foreseeable future at least LES remains the more viable turbulence model for application to commercially focused design methodologies.

Variations of the LES model such as the detached eddy simulation (DES) method used by Slimon [158] may provide a long term solution to the ever present dilemma of limited computing resources. The DES model beneficially limits the application of the LES turbulence model to the portions of the flow domain that contain the major sources of turbulence and applies a RANS based turbulence model across the remainder of the flow domain. With this approach, the finer mesh required by the LES model is minimised while the remainder of the mesh can be considerably coarser for the RANS calculations. Structuring a model in this way can provide significant computational savings, however there can be some difficulties in integrating the two different mesh

scales. As these issues are resolved this may provide a future alternative that will further enhance the commercial viability of LES based design methodologies.

The turbulence model required for this research needed to successfully simulate the complex interaction of a primary and secondary expansion of a three dimensional flow structure in an enclosed duct. For the acoustic simulation to be successful the fluctuating velocity and pressure profiles at the external outlet of the model need to accurately capture the true turbulent flow profile. The Alessia project [159] solved similar problems with slightly simpler geometry using a large eddy simulation (LES) turbulence model. Both of the cases they presented used an unsteady LES simulation with an incompressible flow model.

3.5.2 Physical properties

A typical computational aero-acoustics (CAA) modelling approach makes use of a compressible flow model so as to enable the propagation of sound waves within the model itself. As the acoustic receivers are located inside the flow domain and the acoustic analysis is coupled to the flow simulation a fully compressible flow model must be used. One of the advantages of this approach is that the acoustic velocities and pressures are transmitted through the whole model allowing reflections and refraction of the sound waves to be incorporated into the analysis. However to include the acoustic receiver locations within the flow domain requires a considerably larger flow domain and therefore adds significant computational costs.

The far-field acoustic analogy approach allows the flow domain to be de-coupled from the acoustic domain, meaning the finer CFD based flow domain can be maintained around the area of interest (acoustic sources) whilst the acoustic receiver locations can be located outside the flow domain entirely. Grace and Curtis [138] used a decoupled acoustic solver that used a much coarser acoustic grid that overlaid the finer CFD based grid. This approach allowed the acoustic solution times to be significantly reduced whilst still maintaining the integrity of the actual flow solution.

In summary, the compressible flow model must be enabled whenever a near field acoustic analysis is required, while a far-field or decoupled analysis can make use of an incompressible flow model. The use of the incompressible model is also based on the assumption of an incompressible flow.

3.5.3 Boundary Conditions and Initial Conditions

The definition of boundary conditions is critical to the accuracy of the final outcome of any CFD based flow model, in terms of both the stability of the calculation and the accuracy of the final solution. For compressible flow cases care must be taken to ensure that any pressure fluctuations do not get reflected back into the flow domain, particularly at artificial far field boundaries. Reflected waves can introduce artificial instabilities into the flow that in some cases [160] overwhelmed the true flow field being modelled. These fluctuations can be avoided by using non reflective boundary conditions, however the implementation of these boundary conditions adds to the computational cost of the solution. Therefore a compressible flow model should be avoided wherever possible.

The initial condition used at the beginning of any simulation can also have an effect on the final outcome achieved. As with the definition of boundary conditions outlined above this is particularly critical for compressible flow situations. In the case of incompressible flow models the selection of a good initial condition can provide computational savings through minimising the time to achieve statistically steady flow. The Alessia report [159] recommends the use of a steady k-ε turbulence model to generate an approximation of the time averaged turbulent flow field and to use this as the initial solution to the unsteady LES calculations.

3.5.4 Mesh Generation

The mesh used to run the LES calculations must be fine enough to ensure an adequate resolution of the turbulent boundary layer and any subsequent flow separation. The Alessia report [159] suggests a target wall y^+ of around 1 for accurate resolution of the boundary layer. Recent developments [153] have led to LES numerical schemes being compatible with unstructured grids that are typically used with the complex geometries found in commercial cases. However the numerical efficiency of using a structured grid wherever possible still remains.

3.5.5 CFD Solvers and Discretisation Schemes

Segregated solvers should be used wherever possible so as to maximise the computational efficiency of the solution process. Therefore, a decoupled acoustic calculation such as the FWH method recommended by Bailly et al. [146] is preferred.

For any turbulent model the use of central differencing advection schemes is preferred over upwind schemes of the same order to minimise the effects of any artificial dissipation of the turbulence in the flow. The Alessia report [159] provides several comparisons where the use of second order upwind schemes was found to under predict the true level of turbulence in the flow. Repeating the simulation with central differencing schemes corrected this short coming.

3.6 Noise Generated by an Axial Jet

Predicting the noise generated from a circular axial jet has been considered extensively by numerous authors. The majority of this work related to the noise generated by aircraft jet engines [161-164] in general, the effects of the jet nozzle [49, 165, 166] and more theoretical axis-symmetric jet cases [167-170]. These studies were based on a mach number of 0.4 to 0.9. Investigations into low subsonic velocity jets of 15 to 30 ms^{-1} has been limited to a few select investigations, such as those completed by Picard and Deville [171] and Fleury et al. [172, 173]. Lower velocity jets, such as those encountered in standard HVAC systems have been investigated extensively, with an broad range of design data compiled into the ASHRAE handbooks [5, 15]. The velocity range of interest to this research investigation is therefore considered high by HVAC standards, yet extremely low by ordinary aero-acoustic standards. As such the behaviour of axial jet turbulence and the subsequent induced noise falls in between the two established fields of interest documented in available literature.

The use of a two stage expansion process to slow the expansion of the circular jet is relatively unique, with little similar work found in current literature. The purpose of a two stage expansion process is to minimise the effects of a sudden expansion and the correspondingly high levels of turbulence this creates. Based on Lighthill's theory of flow induced noise a successful high velocity HVAC diffuser will limit the generation of turbulence and the onset of flow separation. Assuming that this is the major source of any flow induced noise any numerical model must contain this primary expansion region inside the acoustic source region. The effects of the secondary expansion in the outlet diffuser itself (as the flow enters the passenger cabin) are assumed to be significantly lower and therefore less critical to the initial prediction of the total flow induced noise for a given diffuser design.

3.6.1 Experimental Studies

Picard and Deville [171] experimentally investigated the flow induced noise produced by a 50 mm diameter round jet at a velocity of 15.6 ms^{-1}. A rake of 16 condenser microphones and a similar rake of 12 hot wire anemometers were used to

measure the fluctuating pressure and velocity fields in the turbulent shear layer around the expanding jet. The jet considered in this work was allowed to expand freely in open space; however the rake of microphones and hot wire probes will no doubt have had some limited impact on the expansion of the jet. These effects were accounted for by comparing the results measured with and without the presence of each of the respective instrumentation rakes. This work focused on the near acoustic field, rather than the far field and was therefore not pursued further.

The work conducted by Fleury et al. [172, 173] focused on the acoustic radiation from an excited 50 mm diameter free circular jet with a jet velocity of 20 and 40 ms^{-1}. In this case the jet was generated using a contracting nozzle with an area ratio of 46:1 and the acoustic measurements were focused on the near field surrounding the jet. Acoustic pressures and jet velocities were both measured using similar experimental measurement techniques to those used by Picard and Deville (outlined above). Similar work has also been completed by Guj et al. [174], but at a higher jet velocity of 80 ms^{-1}.

The effects of scattering due to reflections has been investigated by Morfey and Joseph [175], however this work related to the high velocity flows encountered around jet powered civilian aircraft. The scattering effects studied here were based around external flow conditions rather than the internal reflections found inside a HVAC duct. Verma and Rathakrishnan investigated the effects of notched circular slot jets [176] and elliptical slot jets [177] on the acoustic characteristics of the subsequent flow induced noise. For the high mach number flows (1 to 1.5) considered the notched jets and the elliptical jets were both found to provide meaningful reductions in the resulting flow induced noise levels. The applicability of this technique to the relatively low velocity jets considered in this thesis is questionable.

All of the experimental studies cited above were based on the simple expansion of a free jet, with the major focus on the near acoustic field. Although not directly related to the two stage expansion of a confined jet of air, located inside a closed duct, they provide a useful guide for the experimental work required for this project.

3.6.2 Numerical Models - Benchmark CFD Analysis

Vast amounts of literature can be found regarding noise generation due to flow around bluff bodies such as aircraft, vehicles and buildings. However, there has been little published work on the generation of noise due to internal flows in cavities or ducts. Benchmark test cases from literature were sought to validate the Fluent 6.1 acoustic model before applying it to the current research application. Two cases were found, both in the Alessia report [159] that were loosely similar to the current research objective.

The first case modelled the expansion of a high velocity jet (10 mm square) in a closed rectangular box containing a square 20 mm outlet in the far end. Limited results are presented for the primary expansion of the jet inside the enclosed 300 mm long 100 mm square box; however no attempt was made at simulating the effect of the secondary contraction at the far 20 mm outlet. The geometry of the model is shown in Figure 3.5. The flow field was calculated using a CFD simulation using an LES turbulence model.

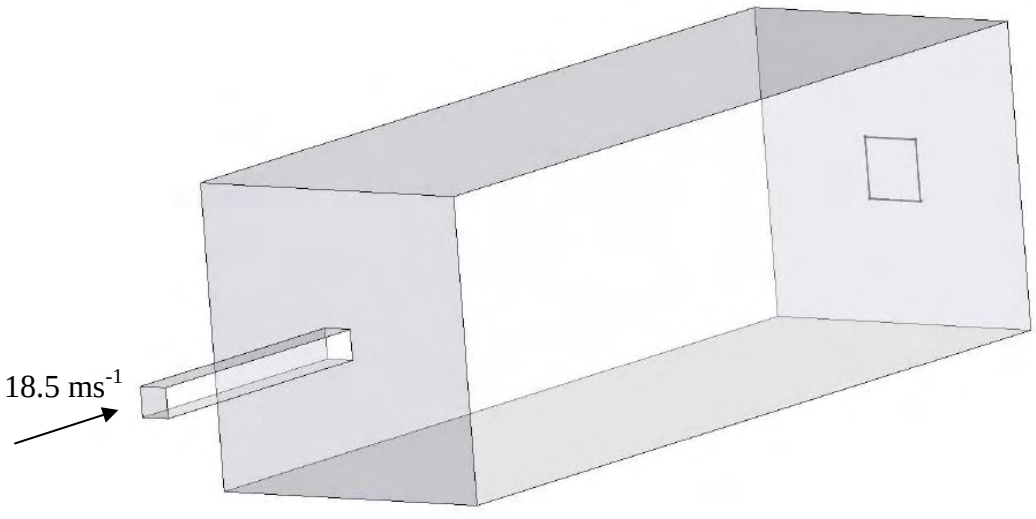

Figure 3.5: Model geometry of the Alessia report square jet expansion case study.

Comparisons were made to experimental results and with a standard k-ε turbulence model. Fluent results were able to match both of the published results (using CFX and experimental measurements), with only minor variances recorded. The primary purpose of this test case was to validate the use of the LES turbulence model and its stability on both structured and unstructured grids. It was found that the turbulent jet develops properly when a central differencing scheme is used while the turbulence tended to be artificially dissipated slightly when using a second order upwind scheme.

Limited acoustic data was presented for this test case, but given that the turbulent jet was predominantly contained inside a closed box, little value was placed on the published acoustic data. Interestingly, this report contained a plot of the predicted flow induced noise resulting from the primary expansion of the jet, but made no mention of a comparison to any experimental acoustic results. Disappointingly, there is only a brief explanation of the acoustic analogy based prediction method employed.

Although this test case was not useful in validating the acoustic model in Fluent 6.1 and 6.2, it was beneficial in determining the correct LES model parameters to use in subsequent turbulent jet problems. Initial simulations were run using Fluent 6.0, where the central differencing discretisation scheme was unavailable. These models resulted in an artificially high level of dissipation of the turbulence in the expansion box. When the simulation was repeated using the updated versions of Fluent (6.1 and 6.2) that allowed the use of a central differencing discretisation scheme this effect was eliminated. Good agreement in both the mean and fluctuating velocity field was found across the entire length of the expansion box.

The second test case investigated the noise generated by a 90 ms^{-1} jet of air passing over a longitudinal strut. For simplicity the strut was modelled inside a box with walls on both the floor and ceiling. A periodic boundary condition was applied along the walls of the box to limit the size of the flow domain. A side view of the flow domain is illustrated in Figure 3.6. This case provides a simple application in which to validate the FWH acoustic analogy used in Fluent 6.1. The time varying flow domain is resolved using a LES turbulence model – incorporating a central differencing advection scheme – and the local pressure and velocity fluctuations on the surface of the strut are saved over

a number of time steps. The FWH acoustic analogy is applied whereby the fluctuating pressure and velocity data is used to calculate the equivalent strength dipole acoustic sources across the surface of the strut. The FWH integrals are then resolved to determine the corresponding noise field at specified locations. Numerical acoustic data is compared against experimental results with very good agreement in all directions.

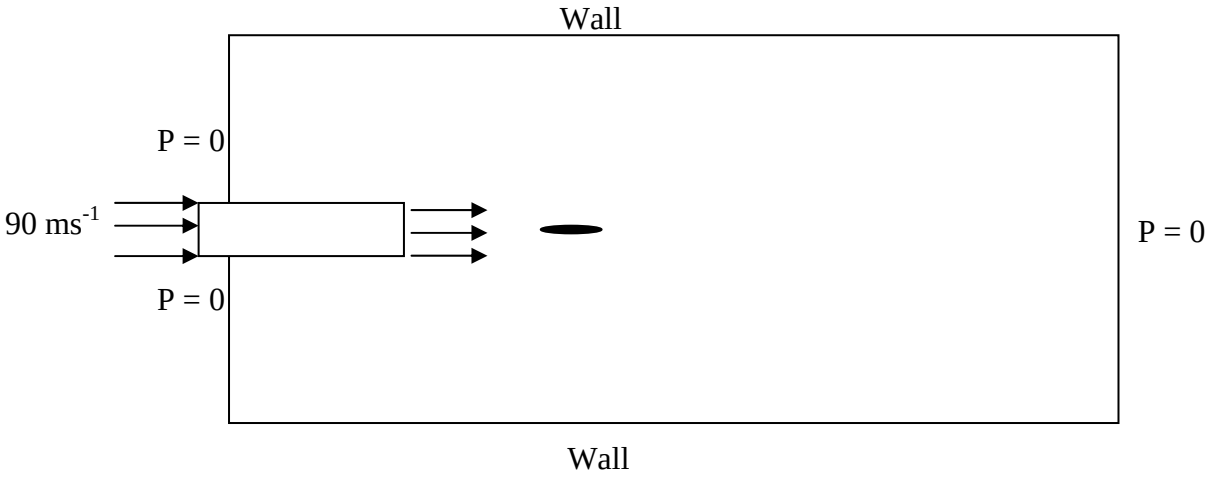

Figure 3.6: Side view of flow domain around the longitudinal strut (into the page).

3.7 Noise Attenuation in Ducts

The attenuation of noise inside ducts has been closely investigated from a multitude of perspectives and a diverse number of applications in mind. There is an extensive library of empirical data and simple analytical modelling tools available for predicting the attenuation of sound inside enclosed ducts and pipes. Attenuation occurs naturally within the duct itself and also with the insertion of mufflers or silencers. The amount of attenuation (reduction in sound pressure level) across a duct or silencer is defined as the transmission loss (TL). In case of silencers this term should not be confused with the insertion loss (IL), which is defined as the difference between the attenuation achieved with and without the insertion of the given silencer. To avoid confusion all subsequent references to acoustic attenuation will be in terms of the overall transmission loss (TL) – unless otherwise stated.

Acoustic attenuation requires the absorption of acoustic energy through dissipation (passive) or the reflection (reactive) of the acoustic energy away from a given location. Any silencer will make use of at least one of these methods, with many modern silencers designed to make optimum use of both forms of attenuation simultaneously. The characteristics of each form of attenuation require attention to maximise the overall transmission loss.

3.7.1 Reactive Dissipation

Reactive attenuation elements require a change in duct cross sectional area or other such means of reflecting acoustic energy. The most common form of reactive silencer is the cylindrical muffler used on internal combustion engine exhausts. A simple (single stage) expansion chamber muffler is shown in Figure 3.7, with the corresponding transmission loss curve shown in Figure 3.8. Byrne and Challen [44] derive the transmission loss coefficient, T_t, for this muffler from first principles and arrive at the following equation:

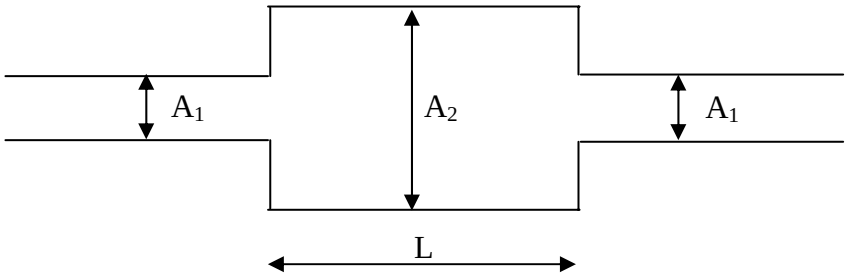

Figure 3.7: Single stage expansion silencer (reactive muffler).

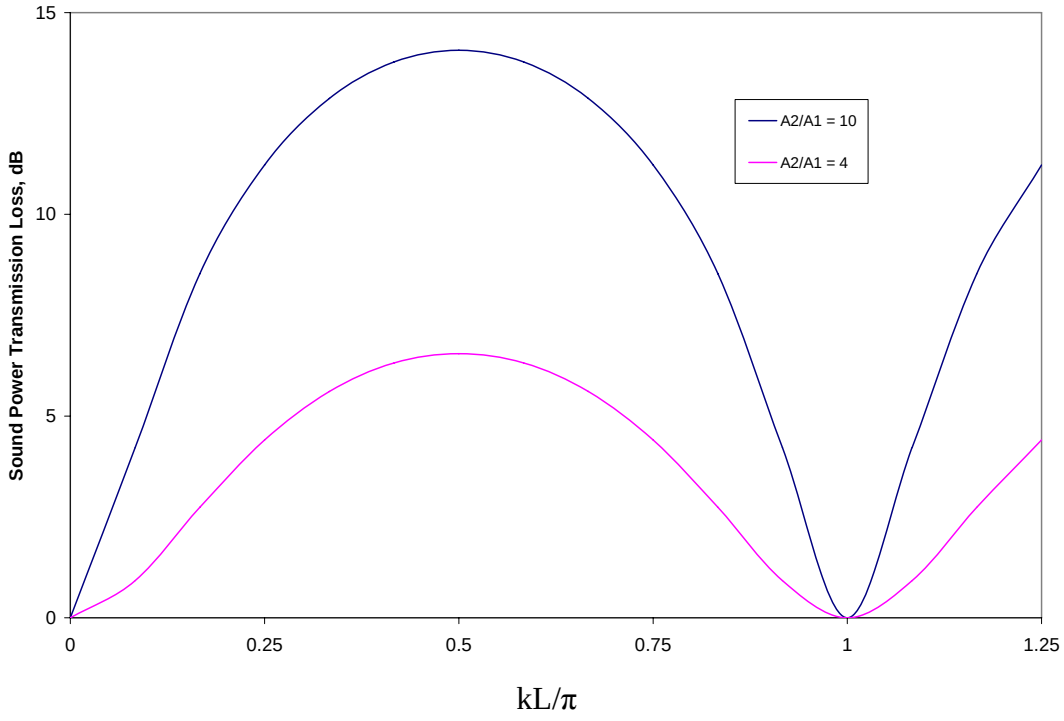

Figure 3.8: TL for the single stage expansion chamber silencer (reactive muffler).

$$T_t = \frac{4}{4\cos^2 kL + \left[\frac{A_2}{A_1} + \frac{A_1}{A_2}\right]\sin^2 kL} \qquad (3.8)$$

and

$$k = \frac{2\pi f}{c} \qquad (3.9)$$

The cross sectional area of the inlet and outlet ducts is the same (A_1) and the expansion chamber has a cross sectional area (A_2) and length (L). The expression is written in a non-dimensional form with the use of the wave number, k. The sound power transmission loss, TL, is then calculated from the transmission loss coefficient, T_t:

$$TL = -10\log_{10}(T_t) \tag{3.10}$$

The sound power transmission loss varies with frequency, with the length of the expansion chamber determining the specific frequencies of maximum and minimum TL. The peaks correspond to a kL product of $(2n-1)\pi/2$ (for n = 1,2,3, …n) and the minimum TL (of 0) occurs with a kL product of $n\pi$ (for n = 1,2,3, …n). The amplitude of the TL is determined by the area ratio between the inlet/outlet duct and the expansion chamber (A_2/A_1). The length of the expansion chamber may be tuned to target specific frequencies; however this will also provide zero attenuation at other specific frequencies that may be undesirable. The geometry and number of expansion chambers can be varied to generate a more evenly distributed transmission loss across the required frequency spectrum. Munjal [178] provides an extensive guide to designing reactive silencers with numerous analytical models available to acoustic engineers. This theory is based on the propagation of plane waves down the duct, with all higher order modes of propagation ignored. With this assumption in mind the application of this theory is limited to frequency bands below the cut on frequency of the duct. The cut on frequency (f_{co}) of the duct is defined by Morse [179] for circular and rectangular ducts respectively:

$$f_{co}(circ) = 0.586\frac{c}{D_i} \tag{3.11}$$

$$f_{co}(rect) = 0.5\frac{c}{D_{\max}} \tag{3.12}$$

where c is the speed of sound (ms^{-1}), D_i is the diameter of the circular duct and D_{max} is the largest width of a rectangular duct. The cut on frequency for a range of duct diameters is shown in Table 3.3.

Table 3.3: Cut on frequencies for circular and rectangular ducts

D (m)	0.050	0.075	0.100	0.150	0.200	0.250	0.300	0.400	0.500
F_{co}(circ) (Hz)	4032	2688	2016	1344	1008	806	672	504	403
F_{co}(rect) (Hz)	3440	2293	1720	1147	860	688	573	430	344

Therefore, using circular ducts of 200 to 100 mm (target range of this research) in diameter, plane wave theory can be used for frequencies above 1 to 2 kHz respectively.

Middelberg et al. [180] demonstrated the use of a commercial CFD code to predict the transmission loss for an expansion chamber muffler with a range of geometrical configurations. A compressible k-ε turbulence model was used to simulate the response of the muffler to a sinusoidal impulse input signal; with the transmission loss calculated using a frequency domain analysis of the resulting pressure waves at the outlet of the muffler. The CFD based predictions for the transmission loss closely match published experimental results with no mean flow. However the current simulation method breaks down under the presence of mean flow. The CFD model is able to predict with good levels of accuracy the pressure drop of the muffler under mean flow conditions, but the transmission loss is far more complex to calculate.

3.7.2 Passive Dissipation

Sound waves consist of oscillations of small amplitude propagating through a given medium, such as air. The fluctuating acoustic pressure is a direct function of the particle velocity and frequency of these oscillations. The amplitude of the acoustic pressure can be reduced by absorbing some of the energy from the oscillatory motion and dissipating it through momentum transfer or friction. Passive attenuation elements are designed to dampen the acoustic oscillations without adversely affecting the flow of air through the duct.

The acoustic properties of fibrous materials used to passively attenuate sound in ducts has been investigated extensively by Delaney and Bazley [181]. The design curves of silencers fitted with this type of material has been developed for both circular

and rectangular ducts by Ramakrishnan and Watson [182, 183]. This work was centred on low velocity HVAC system applications, with negligible flow induced noise. As such these design curves are prepared under the assumption of zero mean flow.

Numerous numerical methods have been employed to determine the sound power transmission loss curve for a variety of silencer geometries and acoustic lagging material. Finite element methods [184-187], boundary element methods [187-189] and direct analytical models [190-199] have been used with good correlation to experimental data. The large variety of geometrical configurations and acoustically absorptive materials available has led to a diverse range of reference literature for acoustic design engineers.

Numerical simulation methods have been developed for jet engine inlets [200], and various internal combustion engine exhausts [197, 201-210], most of which are based on the assumption of no mean flow. This assumption leads to any flow induced noise effects inside the muffler being ignored. Where mean flow has been included in the numerical analysis the resulting flow induced noise components are not directly computed but rather approximated, based on empirical relationships drawn from experimental comparison [187, 211-214]. Endo et al. [215] and Davies [216] both present results for high mach number flows based on aircraft engine exhaust noise applications, however both are heavily reliant on experimental data and neither present a model capable of modelling the flow induced noise of low velocity duct based flows.

3.7.3 Noise Treatment of HVAC Ducts

The attenuation of noise inside HVAC ducts with the use of acoustic lining is well known and clearly documented in the ASHRAE handbooks [8, 15, 24]. Data is available for both rectangular ducts [199, 217] and circular ducts as well [218, 219]. Cummings et al. [218] also identified the importance of aligning seams in the duct wall to prevent a reduction in the duct transmission loss of up to 6 dB. This effect was attributed to increased levels of acoustic scattering due to geometrical mismatches at joins between duct sections, leading to high levels of acoustic radiation. Any

misalignment in a high velocity duct would compound this affect further with significant increases in the level of flow induced noise expected.

The selection of HVAC equipment and duct design can make a significant difference to the final acoustic performance of the system as a whole. Cerami [220] provides a useful guide for low velocity building based HVAC systems covering all of the key components of the complete system and the impact each has on the final acoustic rating level. Ebbing and Blazier [221], Smith [222], Schaffer [223], Watson [224] and Jeng et al. [225] provide valuable guides to the practical use of acoustic data supplied by HVAC equipment suppliers and how these relate to the final noise rating. The variation between lab conditions and those experienced in the field coupled with the cumulative summation of multiple noise sources can lead to significantly higher localised sound levels than those predicted by equipment suppliers. It is this variation that must be carefully considered when assessing the contribution by the HVAC system on board an ocean going fast ferry to the overall passenger sound pressure level of 65 dB(A).

Dean [226] documents a useful case study in the treatment of excessive noise in a low velocity building based HVAC system. Thin layers of glass fibre (acoustic lining) are placed inside the duct system and terminal boxes effectively reduce the high frequency components of the excessive noise spectrum. This attenuation is valuable given that the upper frequency octave bands of 500 Hz and above is important for speech recognition and person to person communication. Dean records that the above treatment with acoustic lining leaves a prominent roar in the 90 to 360 Hz frequency range. Noise in these bands is commonly transmitted through rectangular duct walls, while circular ducts have a far lower rate of transmission. The use of circular ducts is therefore recommended wherever possible.

The use of circular ducts reduces the level of duct break out noise but does not eliminate the acoustic energy as it is retained within the duct itself. Additional in-duct sound absorbers are required to reduce the excess noise to an acceptable level. Lining material can be used with the additional of reactive elements tuned to the particular frequency ranges of concern. Dean [226] found that the use of a lined mitre bend and

open end reflections provided additional attenuation of 5^{+} dB. Further attenuation of 10 dB was also gained with the use of a tuned low frequency air cushion absorber. In summary the low frequency components of the unwanted noise inside the HVAC ducts is treatable using established HVAC components that are tuned to the desired frequency bands.

3.7.4 Active Noise Control

The mid to high frequency components of any sound generated can be attenuated to reasonable levels with the installation of a suitably designed combination of reactive and passive elements. However, the level of attenuation on the low frequency components of the same noise source is considerably smaller. Wise [227] demonstrated the success of applying active noise control strategies to effectively reduce the low frequency noise inside fixed building HVAC ducts. The method proved very effective in treating duct borne noise (inside the HVAC ducts). Multiple references [Eghtesadi, Tanaka] [228-231] are available that provide detailed case studies of successful applications of active noise control methods to enclosed ducts and tubes. The success of the active noise control was however limited to flow velocities up to 7 ms^{-1}[24]. Although this technique may have limited value in treating cabin based noise levels eliminating duct borne noise can also reduce the size (and associated pressure drop) of other noise treatment methods.

Powell and Sullivan [232] had some considerable success in applying active noise control inside a small aircraft passenger cabin. The tests included both subjective hearing tests and actual sound pressure measurements with a distinct drop in ambient noise levels achieved. Wright and Vuksanovic [233] devised a method to produce acoustic shadows in larger unconfined spaces using active noise control equipment. This work was primarily based on simulations of proving the concept rather than applying it to a real world application. It is unclear if this would be a viable solution to passenger cabin noise in an ocean going fast ferry given the multiple transmission paths available (air & structural). There may be some scope to apply active noise control methods to the noise problem in ocean going fast ferries, but the flow velocities in the HVAC ducts at the outlets would still need to be reduced considerably.

3.7.5 Predicting the Acoustic Performance for a Passenger Cabin Space

The acoustic performance of the passenger space on board an ocean going fast ferry is determined by a number of key variables. The sources of noise radiating into and around the cabin can be classified as either generated locally (passengers) or externally (engines, hydrodynamics, HVAC). Each of the respective sources will have a given acoustic power (watts) and frequency spectrum. The effects of any additional attenuation can be accounted for and the resultant total acoustic power in the cabin space can be calculated.

The effective acoustic performance of the cabin space can be simulated using existing room acoustic modelling methods like those used by Vorlander [234], Maluski and Bougdah [235] or Wentzel and Saha [236]. The purpose of this research is to identify and develop the missing tools required to predict the sound power radiated by a high velocity HVAC system into a cabin space. This information will then enable an acoustical analysis of the passenger cabin itself to be completed. The acoustic properties of the passenger cabin such as the size, shape and acoustical absorption of the cabin surfaces can also be incorporated into this modelling process.

Chapter 4

Experimental Test Rig Design and Operation

An experimental program was prepared with the aims of firstly verifying the potential application of high velocity HVAC duct systems to ocean going fast ferries and then identifying the viable range of air distribution velocities. Initial tests were successful, proving that air distribution velocities in excess of 20 ms^{-1} were possible without violating the required cabin sound pressure levels. Air distribution velocities in this range would represent a reduction in duct area of 67 percent and provide significant space savings in the ceiling cavities on board ocean going fast ferries. On completion of these tests a detailed design specification for a suitable experimental test rig was developed. Once the design specification was finalised the test rig was assembled and commissioned with careful attention to the accuracy of the instrumentation employed.

4.1 Test Rig Design Specification

The proposed test rig was required to meet both the needs of this research program and if feasible to allow for future research into high velocity HVAC systems. The design specification was separated into the three core components of airflow capacity, duct geometry variation and sound level measurement. Background noise levels were also considered as part of this process. The airflow capacity in terms of both static pressure and volumetric flow rate required to produce the air jet were identified as the critical link in the development of this test rig. The regulation and control of this flow was considered an integral part of the total system where sound level measurements could be taken across a wide statistical bandwidth in both time and space. The remaining specifications were also assigned an appropriate order of priority to prepare a detailed timeline for the design and construction of the test rig facility. This timeline was instrumental in identifying potential problems and avoiding unnecessary delays in the development of the test apparatus.

4.1.1 Airflow Requirements

The fundamental nature of this research led to the selection of a single jet diameter of 50 mm with a jet velocity range of 10 to 60 ms^{-1}. For air under standard atmospheric conditions this correlates to a jet Reynolds number of 25,000 to 160,000. In addition to the above airflow specifications the source of air also had to provide a static head sufficient to overcome the losses within the proposed test apparatus. The low background noise levels required to enable accurate measurement of the flow generated noise levels dictated that the air handling unit be placed sufficiently upstream of the test section. Consequently the total pressure drop required from the air handling unit was beyond the range of a standard fan or blower. A total flow rate of 20 to 100 litres per second was proposed with a corresponding static pressure range of 1 to 25 kPa. With this range of available air flow the test apparatus would also be suitable to test larger diameter flows across the anticipated velocity bands from practical high velocity HVAC systems.

The control of the airflow outlined above was equally important to ensuring that the desired airflow could be maintained and regulated while statistical sound pressure measurements were completed. The level of turbulence with the jet of air also needed to be carefully controlled to provide accurate and repeatable experimental conditions.

4.1.2 Duct Geometry and Diffuser Outlet Orientation

The duct geometry for the test section and the upstream components of the test apparatus required a smooth internal surface to minimise any flow disturbance and associated flow induced noise. The internal diameter of 50 mm was fixed to simplify the apparatus and reduce the cost of having multiple test sections and corresponding upstream ducts and fittings. The use of non-dimensional analyses will enable the experimental results to be used to predict the noise generated across a range of duct sizes and flow rates. The primary consideration when selecting the duct material is the ability to interconnect different outlet configurations easily and simultaneously minimise the generation of additional flow induced noise.

Three diffuser angles of 7˚, 10˚ and 14˚ were specified with a common outlet diameter of 150 mm. This size was set based on a compromise between minimising the space required in the ceiling cavities for the HVAC installations and also maximising the increase in duct area. The area ratio between the inlet and outlet pipes was kept constant to keep the total number of experimental tests to a reasonable level. Additional tests could be conducted in the future to extend this work across multiple expansion ratios as required. Alternately, the proposed numerical models can be used to limit the amount of experimental work as further high velocity HVAC system designs are developed. The primary focus of this research has been aimed at understanding the impact on flow induced noise due to variations in the length, shape and type of outlet fitted to the three conical diffusers outlined above.

The duct upstream from the test section also needed to be controlled so that a uniform level of turbulence could be generated to allow stable and repeatable turbulence levels. Although requiring a greater static head from the air supply an extended upstream pipe with a minimum length of 50 diameters was specified to ensure fully developed turbulent pipe flow.

4.1.3 Background Noise Levels

The sound power generated by the expansion of the HVAC air jet at lower jet velocities was expected to be relatively small and increase exponentially with increasing jet velocity. With this in mind the background noise levels around the test facility and the noise generated upstream of the main test section were considered critical design constraints. Isolation from the air handling unit and other external noise sources was a priority, as well as minimising the noise generated by sub-standard ducting and the onset of localised turbulence of any kind. Background noise levels also needed to be consistent to ensure repeatability of experiments, particularly where the flow induced sound pressure levels were close to the background ambient conditions.

The acoustic properties of the space containing the main test section had to be quantifiable and consistent in terms of reverberation time, room volume and room surface area. With careful characterisation of the acoustic space surrounding the test

section the sound pressure levels could be converted to an equivalent sound power reading to enable direct and fair comparison with the numerical models developed as a part of this research (outlined in Chapters 10 and 11). Given that the numerical models are based on an anechoic outlet condition all comparisons will be made in terms of sound power levels.

4.2 Test Rig Design and Construction

The dual room reverberation suite at the School of Mechanical & Manufacturing Engineering at the University of New South Wales was used to house the test apparatus. The need for a quantifiable and repeatable acoustic environment for the measurement of the flow induced sound pressures was the primary basis for this decision. The layout of the suite is shown in Figure 4.1. The main high velocity duct test section and variable geometry outlet diffuser were located in the receiver room; with a small exhaust vent to maintain a steady air flow rate. Additional acoustic lagging was applied to the exhaust vent to minimise the effect of external noise sources and flanking noise from the surrounding environment.

The source room was used to provide a steady air flow rate into the test section by way of a standardised bell-mouth fitted to an exit leading directly to the test section inside the receiver room. Initial tests were conducted using a high volume blower located inside the source room, with inlet air drawn externally to the reverberation suite. Locating the blower outside the source room lowered the sound pressure level inside the source room and the corresponding flanking noise levels measured inside the receiver room. Sealing the source room created a pressurised secondary plenum chamber with a single bell mouth outlet to form the air jet into the adjoining receiver room (test area).

All pipe work was lined with high-density lead impregnated acoustic lagging material to minimise the radiation of noise into the room. The flow control valves were also located externally to maximize the upstream distance from the source room inlet. The air inlet to the source room was also fitted with a two stage inline muffler (A) and dampened plenum box (B) to minimise the transmission of upstream noise into the room.

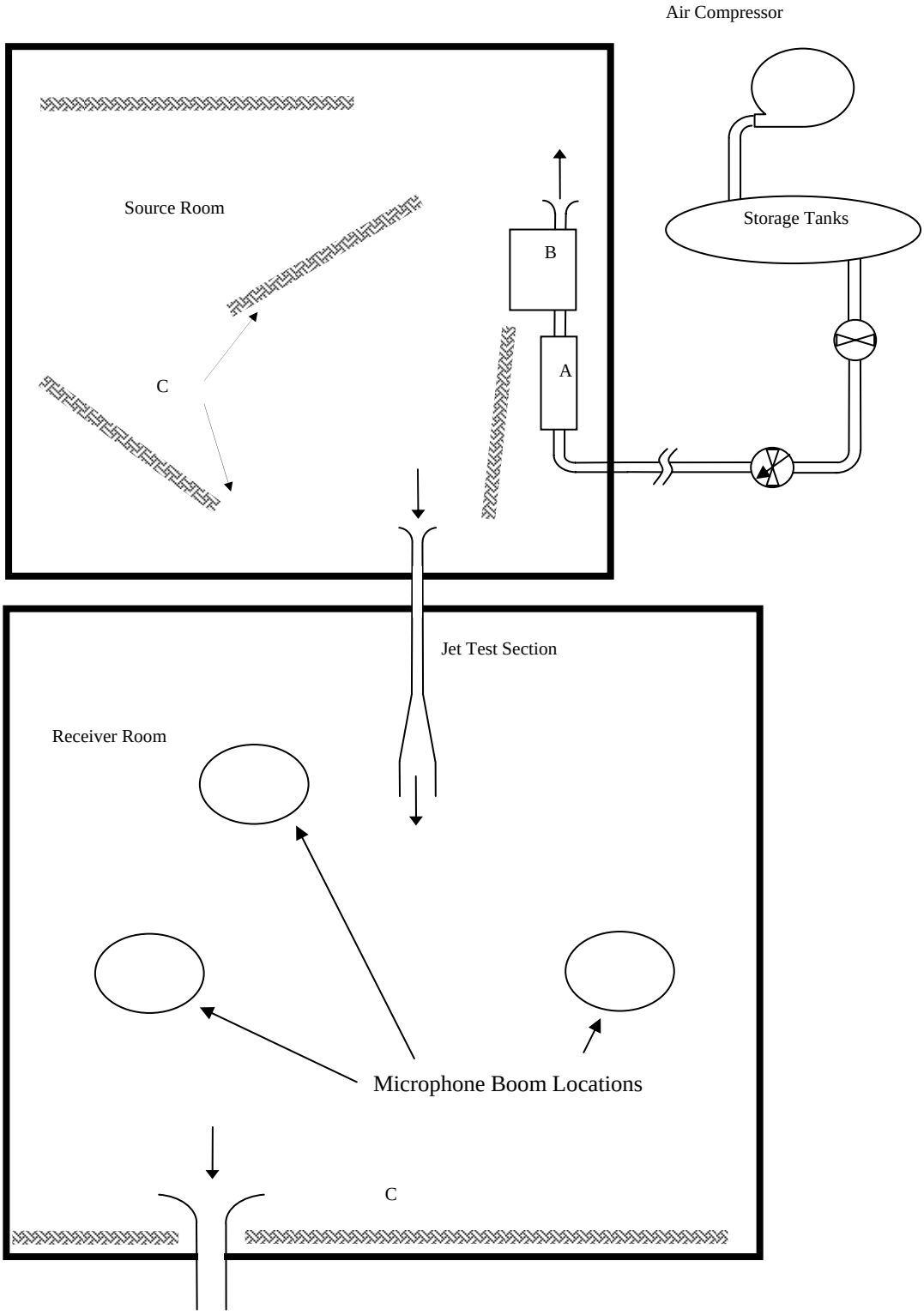

Figure 4.1: Floor plan of the reverberation suite used for jet noise measurements.

The ambient noise level in the source room was lowered further with the addition of acoustic lagging material (C) placed irregularly to maximize their effectiveness. The same material was used to improve the low frequency response [237] of the receiver room used for the flow induced noise measurements. An inline composite reactive/dissipative silencer was fitted upstream of the jet test section to minimise the level of transmitted noise from the source room. The flanking noise levels were also checked to ensure accurate sound pressure level measurements were possible. Figure 4.1 also illustrates the three locations of the microphone boom used to determine the time averaged sound power levels for each experimental test case.

4.2.1 High Pressure Air Supply

An external high pressure air supply was selected to maximise the upstream distance between the air supply and the reverberation room containing the main test section and microphone boom. A large centrifugal high flow oil-free (300 ls^{-1}) air compressor was used to supply a regulated flow of high pressure air to three storage tanks with a combined volume of 6 m^3, at a maximum pressure of 800 kPa. The air was also passed through a single stage desiccant dryer to remove most of the water content in the inlet air and provide air at a consistent temperature and relative humidity. Final calculations for any installed HVAC system would need to incorporate compensation factors for the desired humidity and supply air temperature.

A modulated control algorithm was used to maintain a constant outlet pressure from the compressor which in turn regulated the pressure in the storage tanks. Any excess air was vented through a variable position relief valve to ensure a constant flow rate into the test section located inside the reverberation suite. The storage tanks also served a secondary role of further isolating the reverberation suite from the upstream compressor noise with an increase in the supply line attenuation. This also enabled the main flow control valve to be located away from the reverberation suite and limit the impact of the noise generated through the control valve aperture.

4.2.2 Air Flow Rate Control

The airflow into the source room was controlled by way of a main throttling valve and a secondary flow control valve. A secondary emergency shut off ball valve was also located inside the receiver room to provide a fail safe means of escape in the event of accidental confinement inside the room whilst under pressure. During normal operation this valve remained 100 percent open to negate any ancillary noise generation. Real time monitoring of the air velocity inside the main jet test section was used to adjust the external flow control valve to generate the desired centreline velocity for each of the 1500 test cases.

The total flow rate inside the test section was calculated based on the time averaged centreline velocity inside the upstream 50 mm diameter pipe. The flow rate was monitored and controlled volumetrically with any minor variation due to changing atmospheric conditions negated. The air supply derived from the multi-stage centrifugal compressor fitted with an output air drier ensured consistent supply air properties with negligible variation across the test days used.

4.2.3 Air Duct Design

The main test section was designed to provide a consistent level of turbulence in the test section and incorporate variable outlet duct geometry. A standard bell-mouth (AS/NZS 3823.1.2.2001) was fitted to the outlet from the source room to provide a standardised inlet flow for the test section. The 50 mm diameter pipe upstream from the test section was 60 diameters in length (3 m). Coupling this with the standardised bell-mouth ensured fully developed turbulent flow was generated upstream from the various diffuser outlet geometries tested. Part of this entrance pipe passed through an inline muffler used to further isolate the test section from the upstream sound levels contained in the receiver room. The transmission loss curve for the muffler used is shown in Figure 4.2.

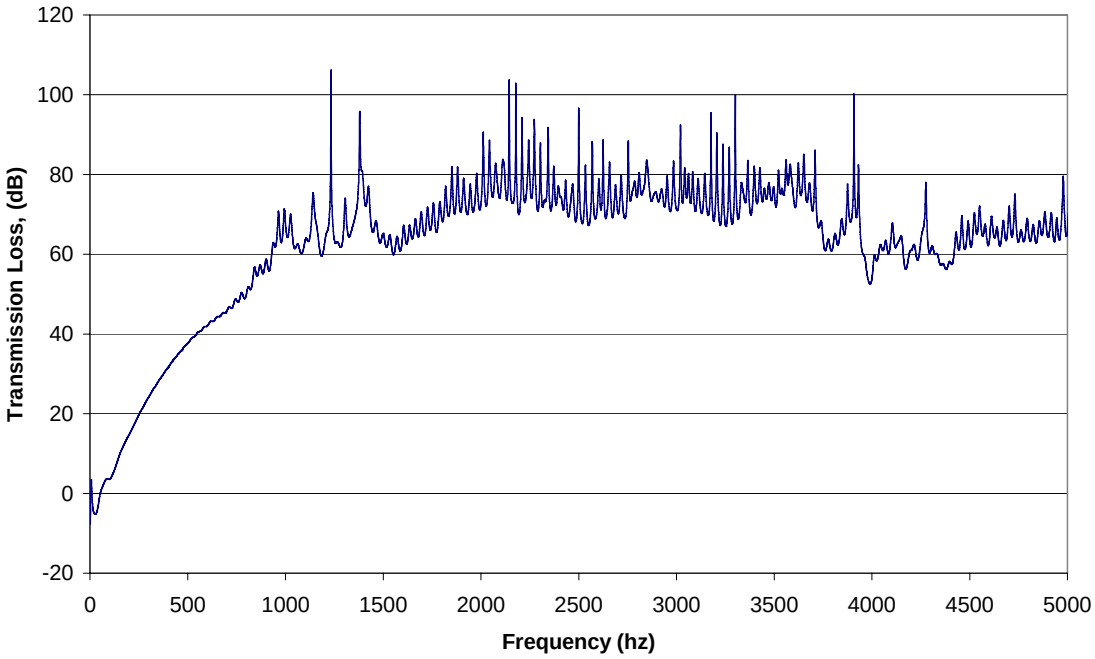

Figure 4.2: Transmission loss curve for the upstream inline muffler.

The inline muffler ensured that a minimum transmission loss of 40 dB was achieved across all frequencies above 500 Hz, and at least 20 dB down to 250 Hz. At 100 Hz however the transmission loss was only 4 dB. To ensure that the sound recordings made in the receiver room were not adversely contaminated by any upstream noise (from the source room) care was taken to ensure a minimum 10 dB difference between the sound pressure levels in the source and receiver rooms. The isolated walls of the respective reverberation rooms coupled with the length and size of the inlet pipe containing the air jet provided a very good transmission loss between the two rooms.

The ambient sound pressure level in the source room was lowered with the use of acoustic lagging material placed strategically around the room and heavy treatment of the supply line feeding air into the source room. This treatment included the installation of a large low frequency reactive muffler as shown in Figure 4.3 and the gradual expansion of the supply air entering the source room. The supply duct entering the source room was sized such that the outlet was more than an order of magnitude greater than the supply pipe feeding the test section leading into the receiver room. This decision was critical to controlling the low frequency noise generated inside the source room and therefore the potential acoustic propagation into the receiver room.

Figure 4.3: Inline muffler used to attenuate the air supply line feeding the source room.

4.2.4 Outlet Diffuser Design

The primary purpose of this study was to demonstrate the viability of using a high distribution air velocity in the HVAC system and to quantify the noise generated by a variety of outlet diffuser configurations. This study was separated into two key phases, firstly dealing with the expansion of a round jet of air inside a circular duct network (diffuser) and then the coupling of the diffuser to an outlet grill. The purpose in separating the study into these two areas was to isolate the fundamental flow phenomenon in the diffuser section from the complex vagaries of an outlet grill and the added noise generated by directing the airflow into cabin spaces. This approach was well suited to the concurrent development of the numerical CFD and acoustic models. Computational resource limitations dictated that the complex outlet grill geometry and room space was beyond the resource capabilities available at the time of this research. It is envisaged that this work could be extended as the speed and availability of such resources improves.

4.2.4.1. Diffuser Design

A parametric matrix was proposed to identify the most suitable outlet diffuser geometry that satisfied both airflow dispersion and minimised flow generated noise levels. A control test was conducted with a straight 50 mm diameter circular jet. Flow diffusers designed to limit the development of any large recirculation zones within the duct and therefore minimise the generation of flow induced noise were proposed. With the limitation on ceiling space stipulated by the original project brief a conical diffuser design was selected with a range of diffuser angles, (α), of 7, 10 and 14˚ used. To allow for an interchangeable outlet pipe structure downstream from the diffuser a set exit diameter of 150 mm was selected. The nine fold increase in pipe cross-sectional area provided a useful drop in overall air velocity without overly extending the required ceiling height. Consequently the length of each conical diffuser varied in length according to the respective diffuser angle employed. The three conical diffusers used are shown in Figure 4.4 below.

Figure 4.4: The three conical diffusers with an angle of 7˚, 10˚ and 14˚ (left to right).

The second aspect of the diffuser section was the length of 150 mm diameter outlet duct used to allow the expanded flow to disperse and for any large scale turbulent eddies to be dissipated. Four outlet duct lengths, (L), of 0, 300, 600 and 900 mm were selected to provide a wide coverage of potential outlet diffuser configurations without overly extending the number of experimental tests to be conducted. These combinations were facilitated with the 300 and 600 mm long duct sections shown in Figure 4.5. Combining the variable diffuser angle and outlet duct lengths outlined above provided 12 individual diffuser geometries to test for a range of jet velocities. The geometry specifications of the primary outlet diffuser are defined in Figure 4.6.

Figure 4.5: The 300 and 600 mm long 150 mm diameter outlet ducts.

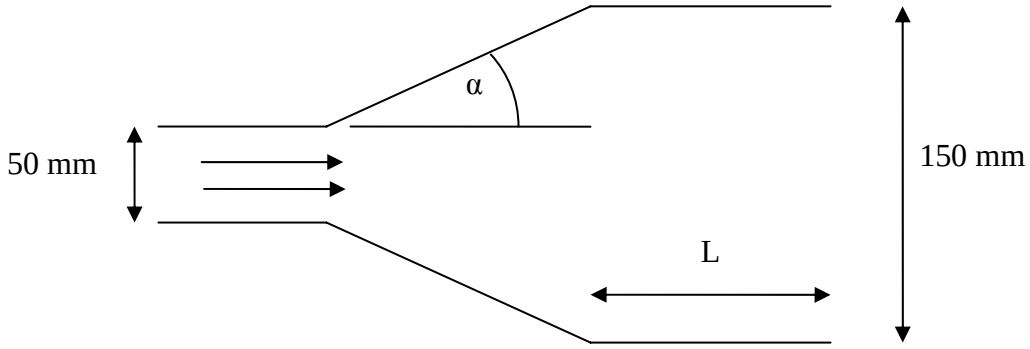

Figure 4.6: Primary outlet diffuser geometry specifications.

4.2.4.2. Diffuser Outlet Design

The parametric matrix covering the diffuser design was extended to include five different outlet grill options. The two dimensional 4x3 diffuser design matrix was extended into a third dimensional 4x3x5 matrix with a total of 60 individual design options for experimental evaluation across a range of centreline jet velocities. The five outlet options considered are listed below:

1. No outlet grill (Control)
2. Round conical grill
3. Standard square 4-way grill
4. Standard square 4-way grill fitted to a dampened cushion head
5. Standard square 4-way grill fitted to an upstream 90˚ elbow and cushion head

The round and square outlet grills are shown in Figure 4.7 and the geometry of each respective grill is detailed in Appendix A. The cushion head fitted to the square diffuser grill was lined with 12 mm acoustic lagging material. The attenuation of thicker material was not included in this trial in the interests of containing the variables under consideration. Where additional attenuation is required the thickness of lagging material can be increased.

Figure 4.7: Outlet diffuser grills - Square diffuser shown fitted to the cushion head box.

The location of the duct exit into the receiver room (in the reverberation suite) was maintained at the same geometric point to enable standardised acoustic measurements to be taken for each duct length without compromising the consistent location of the microphone booms. The change in total duct and upstream pipe length was accommodated by adjusting the length of upstream pipe located inside the receiver room. The surplus pipe length was pushed out into the source room where the pipe inlet was shifted away from the adjoining walls between the two rooms. Each movement of this pipe required the flange plate on the adjoining wall to be resealed to minimise the paths of any flanking noise between the two rooms.

The number of velocity set points for each diffuser configuration added a fourth dimension to the design matrix, resulting in a 3x4x5x15 matrix with a total of 900 individual experimental test cases. Every velocity reading for each diffuser outlet configuration in the design matrix required three separate statistically averaged sound pressure measurements. Consequently, the proposed experimental test cases outlined thus far would have required 2700 individual sound spectra measurements. In the interest of streamlining the experimental work, a few selected cases were omitted from the final experimental program. This assessment was based on progressive experimental results that indicated such a course of action would not compromise the integrity of the overall parametric study.

4.3 Instrumentation

4.3.1 Airflow Measurement

The air flow through the test duct was measured using a fine point pitot tube located along the centreline of the 50 mm diameter duct upstream from the main test section. All flow rate comparisons and references in this thesis will be based on the mean centreline velocity of the upstream air jet, as measured experimentally. The Pitot tube was located 40 diameters downstream from the bell-mouth inlet inside the source room to minimise any entrance effects at the point of measurement. The Pitot tube was connected via long run tubes to a Furness differential pressure anemometer. The long connection tubes served a dual purpose of firstly allowing the location of the anemometer box outside of the receiver room and secondly increasing the time constant of the differential pressure recording.

Having the anemometer box in the control space outside the reverberation suite enabled real time feedback for the control of the airflow through the test section without disturbing the reverberation suite. This set up also removed the need for any direct AC powered devices inside the reverberation suite and any subsequent electrical interference with the acoustic instrumentation employed. The turbulent nature of the air flow through the test section produced a statistically steady time varying centreline jet velocity. The mean centreline velocity was recorded across a 2 minute and 8 second window (128 seconds) to ensure synchronisation with the acoustic measurements from the rotating boom microphones.

4.3.2 Sound Pressure Level Measurement

All sound pressure readings were taken using Bruel & Kjaer type 4189 (½ inch) Falcon microphones connected to Bruel & Kjaer type 2699 microphone preamplifiers. The raw acoustic signals were analyzed with a Bruel & Kjaer Type 2133 Dual Channel Digital Frequency Analyzer. Spatially averaged sound pressure levels were measured with the use of Bruel & Kjaer type 3923 Rotating Microphone Booms. The rotating booms were powered by a DC battery pack to eliminate any electrically generated

harmonic noise and were rotated 360˚ every 64 seconds. The boom was moved to three asymmetric locations within the receiver room to increase the accuracy of the spatial averaging sound pressure measurements for each outlet diffuser configuration.

4.3.3 Background Noise Calibration

The ambient sound pressure levels for both reverberation rooms were recorded across the range of expected external environmental conditions. In each case the background noise level inside the receiver room was slightly higher than the source room. This result was expected given the external opening in the receiver room for venting the airflow from the test section. There was no significant variation in the background noise levels during the day and during the evening, however individual occurrences of a vehicle moving past the test facility had a minor effect on the noise level inside the receiver room. The ambient noise levels are shown in Figure 4.8

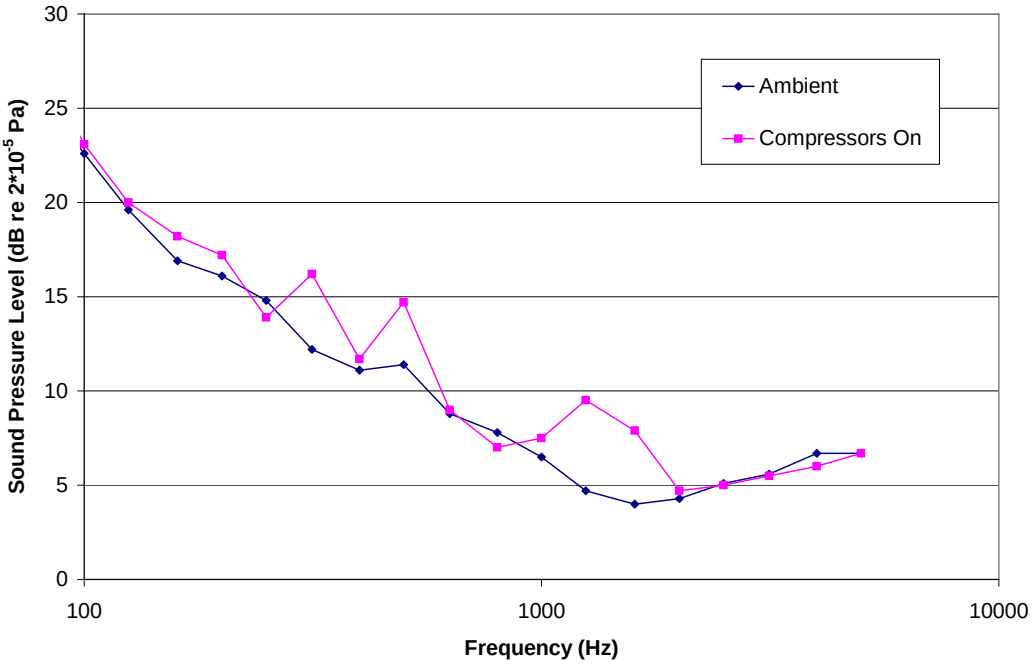

Figure 4.8: Ambient sound pressure levels in the reverberation suite.

The effect of starting the air compressors on the background noise levels is also shown, with a higher increase once again observed in the receiver room. The increase in sound pressure level was minimised by adding additional acoustic lagging material to the exhaust vent and by partially closing the external doors surrounding the receiver room access panel containing the vent.

4.3.4 Flanking Noise Calibration

The level of the flanking noise between the two reverberation rooms was closely scrutinised to ensure the integrity of the flow induced sound pressure measurements; particularly at the lower flow velocities. Potential flanking noise sources and their corresponding transmission paths were identified and addressed in a systematic manner. The following major sources were identified:

1. External air compressor (air supply)
2. Flow control valve noise
3. Flow generated noise inside the source room
4. Incidental external noise sources (intermittent)

The location of each of these sources in relation to the reverberation suite is shown in Figure 4.9 along with the flanking path to the receiver room. The effect of the external air compressor was minimised by isolating the plant room from the reverberation suite as much as was possible. The access points surrounding the pipe work from the plant room into the reverberation suite control room were plugged using high density modelling clay. This provided a two stage barrier between the reverberation rooms themselves and the compressor plant room. The indirect transmission path via the external access lane could not be avoided, however the access panel used to vent the receiver room was specifically configured to minimise this effect.

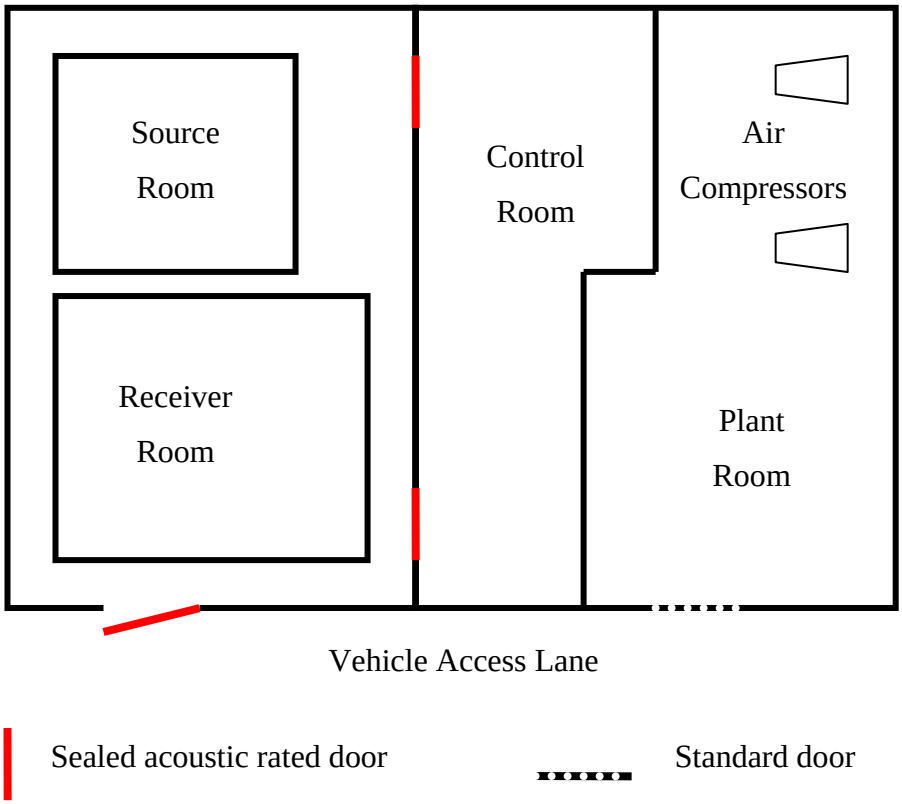

Figure 4.9: External noise sources and transmission paths surrounding the UNSW reverberation suite.

The flow control valve noise was treated by lagging the airline into the source room with high density lead impregnated lagging material and tuning the inlet muffler and plenum box inside the source room. Additional acoustic lagging material was added to the source room to increase the acoustic absorption and further lower the local sound pressure level. This measure also aided in the reduction of the sound pressure level inside the source room due to the inlet air flow. The transmission of the source room sound pressure into the receiver room was minimised with the addition of an inline muffler fitted to the air line feeding into the receiver room.

Intermittent external noise sources such as trucks moving down the access lane adjacent to the reverberation suite were monitored to ensure any necessary tests could be repeated after the noise source was removed. The timing of experimental tests was coordinated to minimise the interruptions due to external traffic movements.

4.3.5 Electronic Noise Considerations

The major contribution to electronic noise inside the reverberation suite was attributed to the use of 50 Hz AC power used to run the lighting inside the rooms and data acquisition equipment. The bulk of this noise was registered in the 50 Hz frequency range and was readily isolated and treated. The lights were switched off for all experimental work and all electrically (AC) powered data acquisition equipment was located outside both reverberation rooms. Additional equipment used for flow visualisation and measurement was either removed or switched off during all acoustic measurements. The electrical noise from the cables connecting the microphones to the frequency analyser was also checked regularly to eliminate any other indirect background noise.

4.4 Outlet Diffuser Preparation

The conical diffuser sections and outlet ducts were constructed from rolled clear polycarbonate sheet to allow for future flow visualisation. Test sections were made interchangeable to minimise changeover times. Combining a 300 mm and 600 mm length of outlet duct to produce a 900 mm section reduced the cost and time required to make the ducts. The integrity of the 0.5 mm thick polycarbonate sheet duct was maintained with clear interlocking acrylic flanges at both ends. The resulting ducts were light, transparent and most importantly rigid.

The conical diffusers and straight duct sections each contained a longitudinal lap joint with a localised 0.5 mm step along the seam. With a step size of only 0.003 D the impact on the airflow and turbulence levels in the duct was limited. In a practical installation seams such as these would not be considered unusual and any additional noise generation would generally be encountered. Care was taken to ensure that the seams along each duct section were aligned to minimise any flow disturbance.

The joints between each section of duct were clamped together with four orthogonal clamps to ensure accurate alignment. The rigid flanges in the duct sections were used to mount the test section while maintaining the outlet of the duct in the same geometrical location inside the receiver room. The total length of upstream pipe used in the test section remained constant, resulting in the outlet from the source room moving with respect to the source room walls. This was preferred over a variable location of the main acoustic source of interest, namely the outlet plane of the test section inside the receiver room.

4.5 Sound Pressure Level Measurement

Sound pressures were recorded across a velocity range of 10 to 60 ms^{-1} based on the time averaged centreline jet velocity for the 50 mm jet with and without the 7˚ diffuser. Additional tests were also conducted with a variety of outlet duct configurations fitted downstream from the diffuser. After careful calibration of the microphones and data acquisition equipment ambient and flanking noise levels were recorded for future reference. All noise measurements taken were at least 20 dB (re $2e^{-5}$ Pa) higher than the ambient and flanking noise measurements taken.

4.5.1 Microphone Boom Operating Procedures

The rotating microphone booms were configured to rotate in a plane at an angle of approximately 30˚ to the floor of the reverberation suite, as illustrated in Figure 4.10. The period of rotation was fixed at 64 seconds, allowing two full rotations inside the 128 second sampling window used to record the sound pressure level inside the reverberation rooms. The rotating boom was set at an angle of 30° to the floor plane to minimise any modal effects that are produced in planes perpendicular or parallel to the floor, walls and ceiling of the room. This is critical to the minimisation of modal resonance within the acoustic measurements – particularly in the low frequency bands.

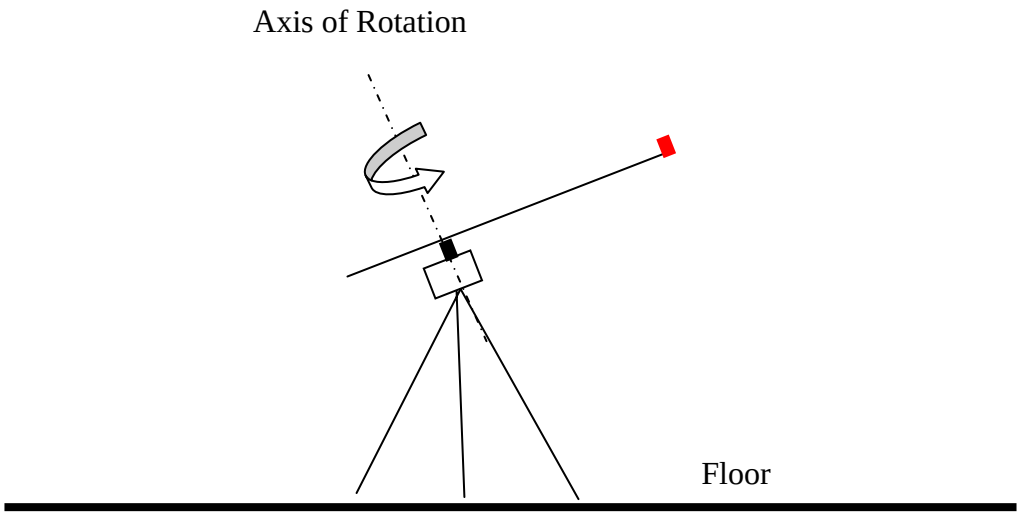

Figure 4.10: Rotating microphone boom configuration.

The booms were located in 3 different locations for each experimental test and the resulting sound pressure levels were spatially averaged. Each location was spaced at a different distance from the outlet of the duct, whilst maintaining a minimum separation of 1 m between the walls and the circular path of the boom. The variation in sound pressure level in ⅓ octave bands between the three boom locations is shown in Figure 4.11. The low frequency bands exhibit slightly higher levels of variation that are indicative of the size and acoustic properties of the receiver room used. By comparison the variation in the higher frequency bands was very minor.

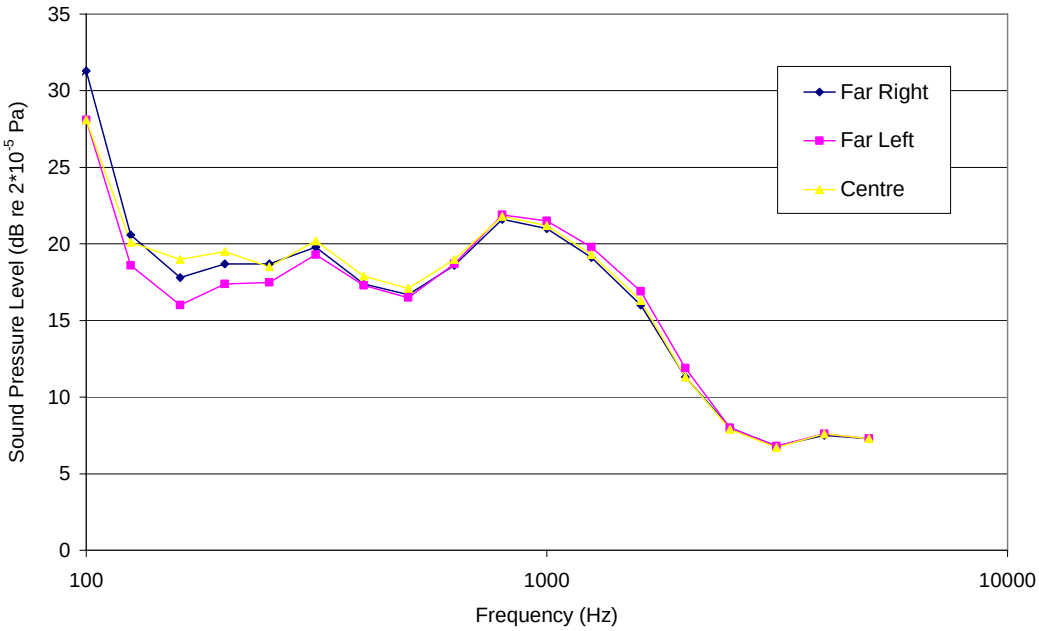

Figure 4.11: Variation in measured sound pressure levels for the three microphone boom locations inside the receiver room.

4.5.2 Frequency Analyser Operation

The Bruel & Kjaer Type 2133 Dual Channel Digital Frequency Analyser was used to process the raw acoustic data from both reverberation rooms. The source room sound pressure level was recorded to provide continual feedback on the potential background noise transmitted downstream into the receiver room. Monitoring the difference in sound pressure levels between the two rooms and comparing this back to the transmission loss of the muffled upstream pipe section meant the fidelity of the flow induced noise measurements in the receiver room was maintained. The multiple sound pressure measurements for each duct configuration were combined to provide a spatially averaged sound pressure level in ⅓ octave bands.

The calibration of the frequency analyser was checked regularly and the corresponding preamplifiers for each channel were adjusted to match the measured sound pressure levels recorded. The preamplifiers were continually adjusted to maximise the resolution of the frequency analyser whilst also preventing the system from being overloaded. In the cases where the sound pressure level exceeded the limits of the selected preamplifiers the experimental test was repeated with the appropriate adjustment to the preamplifier settings.

4.6 Safe Operation of the Reverberation Room

The use of the source room as a pressurised plenum chamber presented several safety concerns that had to be addressed. Given the large surface area of the walls, floor and ceiling in the room the structural integrity of the room was evaluated to ensure that the room would not be damaged when placed under pressure. In the event of the outlet pipe or the receiver room being blocked an emergency shut off valve was fitted to restrict the flow of pressurised air into the reverberation suite. Although low pressures were used in the general operation of the test facility, care was taken to prevent the large scale pressurisation of the source room in the unlikely event of a blockage occurring.

Even at low operating pressures the internally swinging door used to seal the source room could not be opened from the inside. To provide a means of escape in the event of an accidental pressurisation of the room an internal ball valve was fitted to the inlet pipe feeding the source room. The valve was fixed in the fully open position to minimise the generation of any noise during the regular operation of the room. The valve was sized to provide minimal obstruction to the airflow under normal operational conditions.

The risk assessment and standard operating procedure for the reverberation suite is recorded in Appendix B and risk assessment and standard operating procedure for the research air compressor used to generate the air jet is included in Appendix C.

4.7 Test Schedules

The first series of experimental tests were dedicated to the characterisation of the sound generated from the plain circular jet with no additional diffuser ducting. Sound pressure level recordings in ⅓ octave bands were taken for centreline jet velocities of 10 to 60 ms^{-1}. Once these initial benchmark tests were completed a single 7˚ conical diffuser was fitted to the circular jet and the sound pressure level measurements repeated for the same centreline jet velocity range. Additional outlet ducts were fitted downstream from the 7˚ diffuser and the acoustic measurement process repeated. These initial results were used to demonstrate the viability of increasing the air distribution velocity from 5 ms^{-1} up to 20 to 25 ms^{-1}.

With the success of the initial tests the detailed experimental program was organised with an increased focus on the accuracy of the sound pressure level measurements and maximising the spatial averaging of the sound pressure across the reverberation rooms. Each duct configuration was tested across a velocity range of 10 to 50 ms^{-1}, where the microphone booms were shifted to the three designated locations before adjusting the volume flow rate of air feeding the test section. The air flow rate was increased in regular intervals to provide the desired centreline jet velocity and the process repeated for each outlet duct configuration. Limitations in the manual actuation of the flow resulted in the mean centreline jet velocity for each test being slightly offset either side of the desired set points.

The analysis of the experimental results has been based on the exact values for the jet velocities as recorded rather than the prescribed set points. However, for graphing purposes the velocities have been rounded to simplify the labelling and orientation of the respective data streams.

4.8 Error Analysis

All of the instrumentation used in the experimental study was carefully checked and calibrated during the commissioning of the test facility. Over the course of the experimental work the equipment was regularly checked to ensure continued accuracy of the data recorded.

4.8.1 Air Velocity

The centreline jet velocity was time averaged across the duration of the acoustic measurement cycle to provide an accurate recording of the statistically steady jet. The combined error in the velocity reading was ± 2 %. The 6000 litre storage tanks fitted to the outlet of the air compressor used to supply air to the test section was equivalent to 7 to 35 minutes of flow at a velocity of 50 to 10 ms^{-1} respectively. By running the compressor in a modulating mode (constant pressure) the storage tanks were purely a buffering device to smooth any individual fluctuations in the system. This approach provided a very stable air flow that gave a consistent mean centreline jet velocity. The instantaneous velocity fluctuated in accordance with the turbulent flow regime inside the test section; while the time averaged mean velocity was stable.

4.8.2 Sound Pressure Measurements

The accuracy of the microphone and frequency analyser used to record the sound pressure levels inside the reverberation suite were calibrated using a standard encapsulated 94 dB source at 1 k Hz. The frequency analyser was adjusted to output the sound pressure level to ± 0.1 dB. Additional tests were conducted to evaluate the repeatability of the system with a true accuracy of ± 0.2 dB over the course of a days testing. Based on these parameters the microphones and frequency analyser were checked on a daily basis and adjusted where necessary.

The accuracy of the microphones and frequency analyser may well be less than the Figures outlined above across frequency bands either side of the 1 k Hz band used in the calibration process. This could not be quantified without additional calibrated sources at multiple frequencies; however the overall error in these bands is not expected to be significantly greater than that observed in the 1 k Hz band. An assumed error of ± 0.5 dB should suffice for the purposes of this analysis.

4.8.3 Reverberation Room Properties

The reverberation time for both the source and receiver rooms was measured with the same revolving microphone booms used for the experimental sound pressure level measurements. A white noise source was generated in each room and the resulting decay in the sound pressure level was recorded. Analysis of this decay across each individual ⅓ octave frequency band provided a calculated reverberation time that was averaged in both time and space. Repeating the above test 20 times at random time intervals for each microphone location resulted in a uniform representation of the reverberation time. This was done to ensure independence from both time and spatial location. The calculated sound power results presented in the following chapters have been based on the respective reverberation times for each individual microphone boom location.

Chapter 5

Experimental Results

There were 60 possible outlet configurations based on the three diffuser angles (7˚, 10˚ and 14˚), the four outlet duct lengths (0, 300, 600 & 900 mm) and the five outlet grills used in this fundamental analysis. Of these combinations 45 were fully evaluated, while the remaining 15 were found to be either trivial design options or of limited value to the final analysis. This decision was made on the basis of keeping the total number of flow and acoustic measurements to a manageable level. The additional 15 configurations would have required an additional 1000^{+} individual tests when allowing for multiple microphone locations and jet velocities. Therefore results will be presented for a total of 46 outlet configurations, being the 45 combinations mentioned above and the additional case of a straight jet with no outlet diffuser fitted.

This chapter will outline how the raw sound pressure and velocity data from each test was processed and the underlying performance of each outlet duct configuration. The influence of the jet velocity, diffuser angle, outlet duct length and the outlet grill on the flow generated noise will each be discussed. The following acoustic variables have been used to complete this analysis:

1. ⅓ Octave Sound Pressure Levels
2. Octave Sound Pressure Levels
3. Total Linear Sound Pressure Level
4. ⅓ Octave Sound Power Levels
5. Octave Sound Power Levels
6. Total Linear Sound Power Level

5.1 Raw Data Processing

5.1.1 Raw Data

The raw data for each outlet diffuser combination contained a 128 second ⅓ octave band sound pressure reading recorded across six microphone locations for each jet velocity. The instantaneous centreline jet velocity was simultaneously recorded producing an average jet velocity across each acoustic sample window. The final sound pressure levels (⅓ octave and octave) and corresponding jet velocities were averaged across all of the microphone locations leaving a spatially averaged sound pressure level and an average jet velocity.

Comprehensive measurement of the flow field through the diffuser and outlet duct was not possible due to experimental equipment limitations. No visualisation techniques capable of the flow velocities encountered were available to the researcher. Therefore all validation of the numerical models has been based on the resolution of the acoustic field generated by the flow expansion in terms of absolute sound power and the sound power spectra.

The individual result files were downloaded for further analysis, including the conversion to sound power levels in both ⅓ octaves and octave bands. The performance of each individual outlet configuration was prepared, followed by a cross matrix analysis of the various variables considered in this analysis. The logarithmic relationship between the jet velocity and the resulting sound power generated by the jet was also explored. This relationship provides a valuable indication to the underlying effectiveness of each respective outlet design and the nature of the individual sound source components.

5.1.2 Reverberation Time Measurements

The reverberation time of the receiver room was measured in ⅓ octave bands to enable the conversion of the measured sound pressure levels into the equivalent sound power levels. The T_{60} method was used, where a broad band sound pulse was generated and then switched off and the resulting sound pressure levels recorded (in time) across the ⅓ octave band frequency range of interest. The time required for the sound pressure level in each ⅓ octave frequency band to drop 60 dB was recorded and then used to determine the reverberation time for each individual frequency band.

Statistical accuracy was achieved by making multiple measurements in both time and space. Each test was randomly timed to provide maximum statistical variance from the rotating microphone boom. Multiple boom locations were also used to further improve the statistical averaging of the reverberation time. The time and space averaged reverberation time for the receiver room is shown in Figure 5.1 below. Care must be taken in interpreting any sound measurements below the 100 Hz band as the effectiveness of the reverberation room is limited by its size. At frequencies below this level the acoustic field inside the room is not fully diffuse and therefore modal resonances may occur.

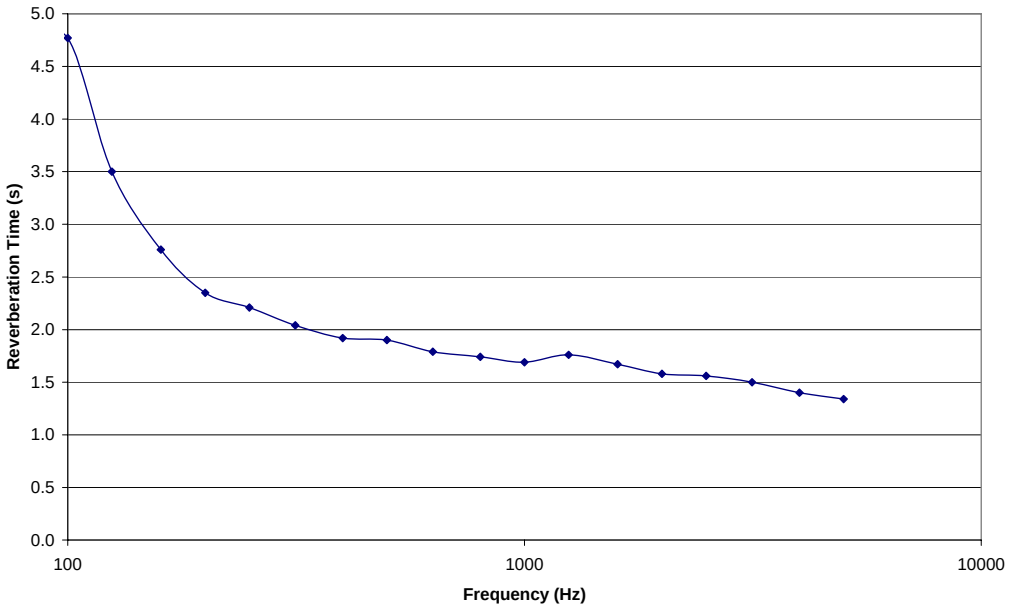

Figure 5.1: Statistically averaged reverberation times for the receiver room.

5.2 Preliminary Sound Pressure Level Measurements

Noise readings were recorded across a limited range of jet centreline velocities for a 50 mm jet with no diffuser, a 7° diffuser with no added ducting and the same 7° diffuser with an added 400 mm section of 150 mm diameter outlet pipe. Basic analysis of these results gave rise to some very interesting observations. Firstly it was found that the 7° diffuser significantly reduced the flow-generated noise at the duct outlet, despite the jet core being only partially dispersed. The addition of the extra outlet section of 150 mm diameter pipe (exit diameter of the diffuser) reduced the noise level even further and also increased the dispersion of the jet core (lower outlet velocity). A direct comparison between the three tests can be clearly seen in Figures 5.2 (50 ms^{-1} jet velocity) and 5.3 (59 ms^{-1} jet velocity).

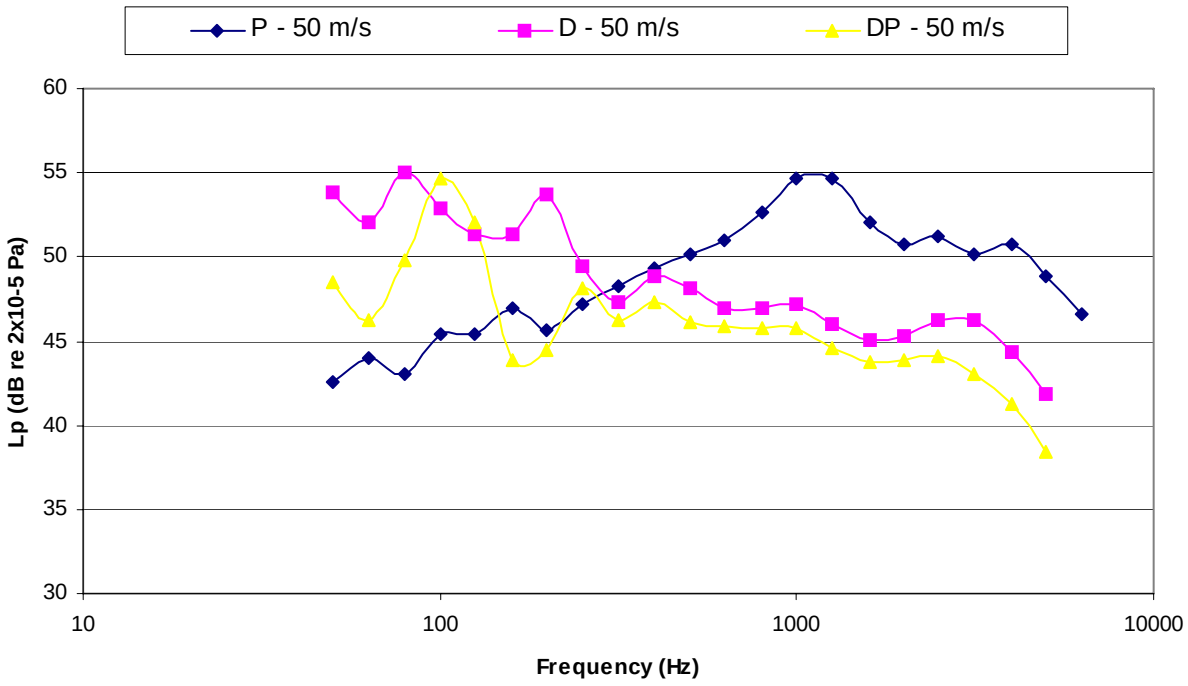

Figure 5.2: Jet noise spectrum comparison - 50 ms^{-1} jet velocity

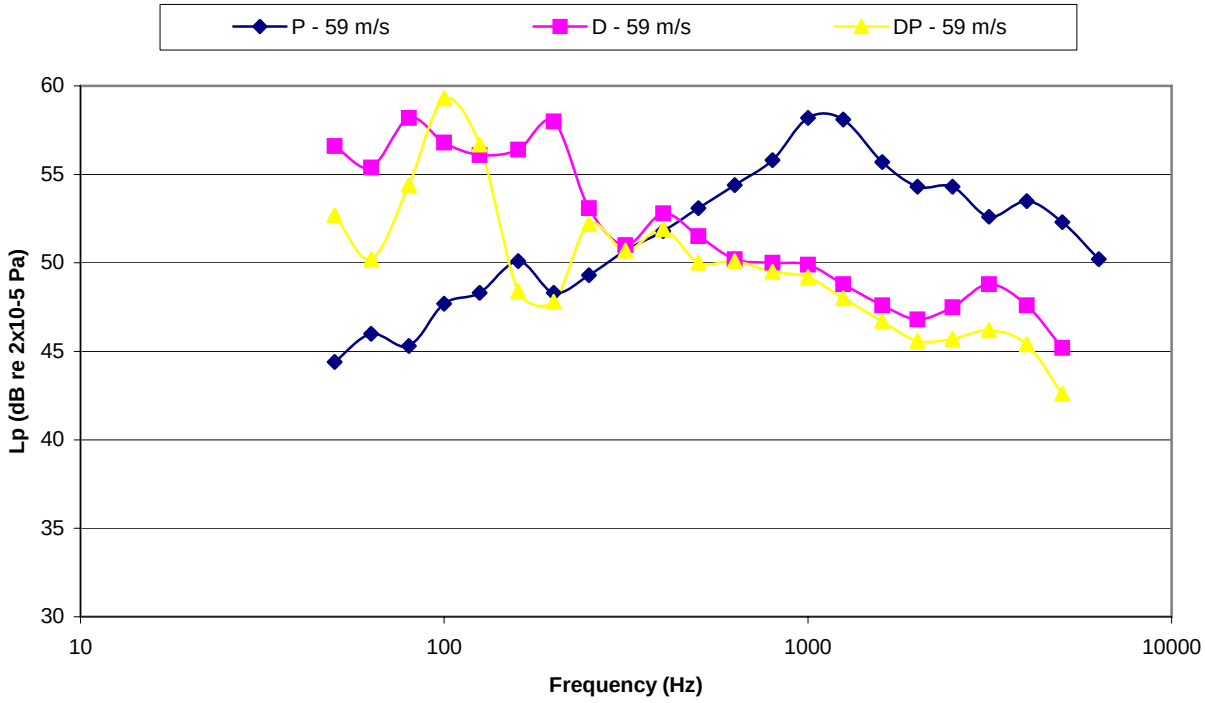

Figure 5.3: Jet noise spectrum comparison - 59 ms^{-1} jet velocity

In the case presented above the maximum sound pressure level in a given ⅓ octave band for all three outlet conditions are of a similar magnitude. However, the straight 50 mm pipe case has the peak noise levels occurring in the 1 kHz frequency range (voice recognition frequency range); while the two diffuser based outlet conditions have a peak around the 100 Hz frequency range (much less significant on an A-weighted or speech recognition basis). There is an additional point of interest raised by the above results in comparing the plain diffuser (D) to the diffuser with the added 150 mm section of outlet duct. The plain diffuser has a much broader peak in the sound pressure level, while both the diffuser and pipe (DP) and the plain 50 mm pipe (P) cases show a much more distinct peak. This indicates a pronounced fundamental frequency associated with the jet flow and the ducted diffuser case where the peak frequency is somewhat comparable to the ratio between jet speed and the duct diameter. Meanwhile the plain diffuser indicates that the variable cross sectional area of the diffuser broadens the bandwidth of the peak sound pressure level. These results will be more closely investigated to clarify this effect and how it can be best utilized in controlling the composition of the noise propagating from a duct outlet.

As expected the sound pressure level increased with velocity across all frequency bands considered. The relationship between the noise level (acoustic pressure) and the velocity will be evaluated in more detail in the subsequent sections. The preliminary results for the ducted diffuser (diffuser with 400 mm long 150 mm diameter pipe outlet) are shown in Figure 5.4. There is a clear, yet broad low frequency peak in the 125 Hz ⅓ octave band and two adjacent bands (100 and 160 Hz) that will be discussed in more detail in the following sections.

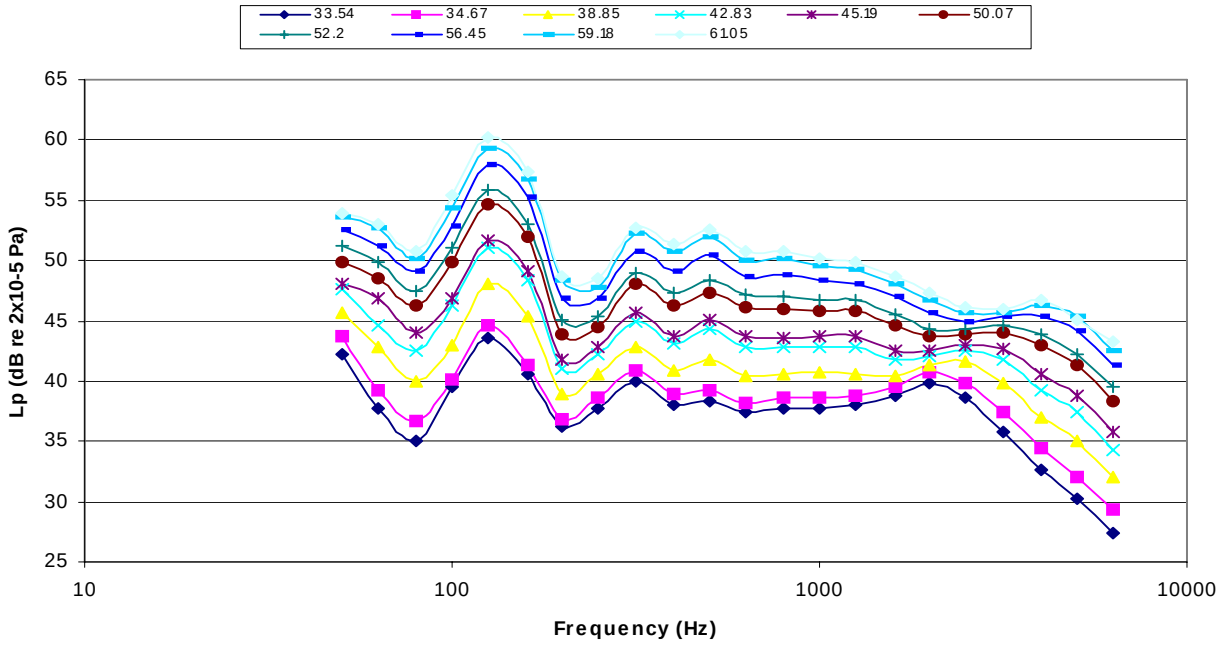

Figure 5.4: ⅓ Octave band sound pressure levels – 150 mm diffuser & outlet duct.

The ability to reduce the A-weighted sound pressure level of the flow generated noise from the expanding jet was the most significant outcome from these preliminary tests. This result was used to further refine the experimental procedure and more fully explore the relationship between the sound pressure levels generated by the expanding jet with a variation in the diffuser angle, length of outlet ducting fitted to the diffuser and several modifications to the final stage of the duct outlet.

5.3 Free Axial Jet

A 50 mm diameter free axial jet was first used to establish a clear baseline for both the experimental study and the corresponding numerical modelling investigation. The selection of this diameter was based on the availability of experimental airflow data published by Picard and Deville [171] and the capacity of the air compressor used to generate the experimental airflow. Distribution velocities of 40 to 60 ms^{-1} are typically going to be infeasible for most commercial applications due to significant increases in the fan power required, however these velocity ranges were used in the interest of minimising experimental errors. The sound generated through these higher velocity ranges is substantially greater and as such the differentiation between the background noise levels and the sound pressures inside the reverberation suite are maximised.

The sound pressure levels were recorded inside the receiver room (surrounding the jet outlet) in ⅓ octave frequency bands for a jet velocity up to 55 ms^{-1}, as shown in Figure 5.5. The first major observation to be made from these results is the distinct relationship between the rate of change in the sound pressure level with increasing jet velocity and the band frequency. In absolute terms the sound pressure in the higher frequency bands increases at a far greater rate than in the low frequency bands, however the low frequency sound pressure levels are initially higher than the corresponding readings in the high frequency bands.

This relationship is better seen when the results are re-plotted in terms of octave sound pressure level, as shown in Figure 5.6. There is a major change in the shape of the sound spectrum from a jet velocity of 15 ms^{-1} to the 22 ms^{-1} result and then the 28 ms^{-1} case. Much of this transition is attributed to the contribution of background noise levels, particularly in the low frequency bands. Once the sound pressure levels are converted to sound power levels the effects of the reverberation suite on the frequency spectrum are also corrected, leaving a much more accurate reflection of the flow generated acoustic sources.

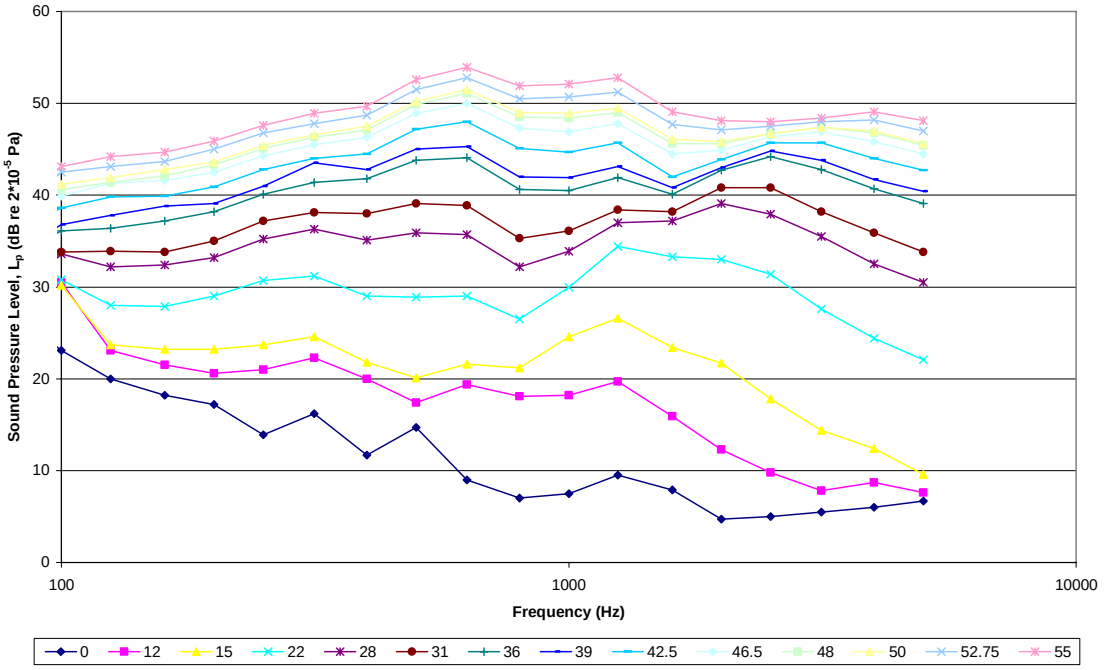

Figure 5.5: Calculated sound pressure levels for a 50 mm diameter free axial jet in ⅓ octave bands.

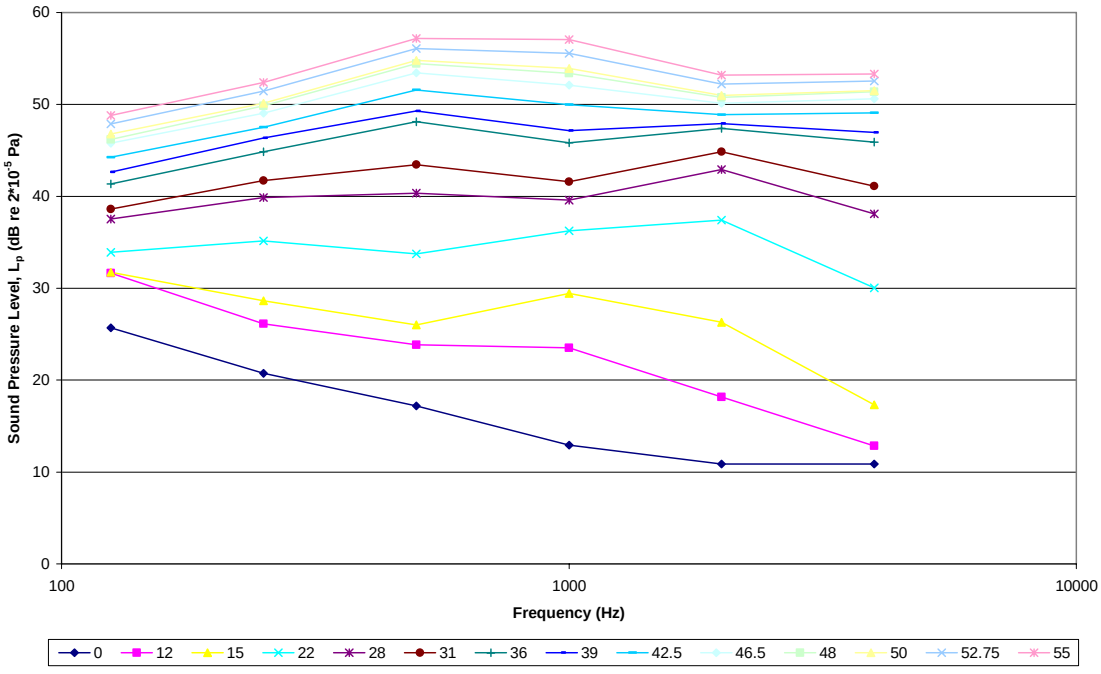

Figure 5.6: Calculated octave band SPL for a 50 mm diameter free axial jet.

The relationship between the sound power level and the jet velocity is best illustrated using a plot of the individual ⅓ octave band sound power levels against the jet velocity based on a log scale. Isolating the data for each individual ⅓ octave band provides a clear indication of the individual contribution to the overall sound power level and how this changes in relation to the jet velocity. This relationship also provides a good indication of the nature of the acoustic sources in each frequency band, and therefore how best to attenuate it. To simplify this process the ⅓ octave band data has been separated into low and high frequency components and plotted in Figures 5.7 and 5.8 respectively.

At jet velocities above 35 ms^{-1} the low frequency plot in Figure 5.7 shows a distinct 50logV relationship between the sound power level and the jet velocity, representative of a dipole dominated sound source. At frequencies above the 400 Hz band the slope of this relationship tends to increase towards the 60logV line, indicative of the presence of weak quadrupole sources. At jet velocities below 30 ms^{-1} the slope of each of the curves drops off slightly below the 50logV line, suggesting the dominance of dipole based acoustic sources. Based on this result it can be concluded that the contribution of surface (pipe wall) based acoustic sources dominate at jet velocities below 30 ms^{-1} and at jet velocities above this level the contribution from shear flow based sources (quadrupoles) progressively increases.

The corresponding results for the high frequency bands present a markedly different perspective to those seen in the low frequency plots. Firstly, in the 3150, 4000 and 5000 Hz bands the low velocity results demonstrate a clear 80logV relationship between the sound pressure and the jet velocity; indicating the presence of a dominant quadrupole sound source. As the jet velocity increases the slope drops off slightly, corresponding to the transfer of the peak sound power level from these bands into the lower 1600 to 2500 Hz bands. This trend is reversed in the 1600, 2000 and 2500 Hz bands with an initial 40logV to 60logV relationship that transitions into a 70logV to 80logV relationship at jet velocities above 40 ms^{-1}. This is the cause of the peak sound power level shifting into a lower frequency band as the jet velocity is increased. Therefore the quadrupole noise sources dominate in the high frequency bands and while the low frequency bands are dominated by dipole sources.

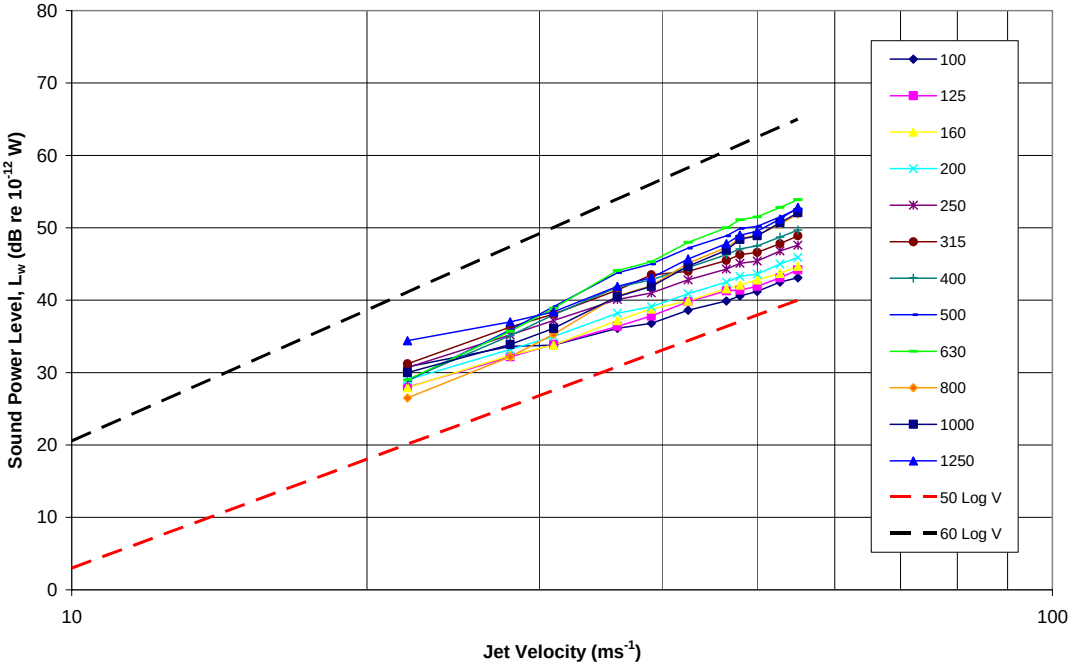

Figure 5.7: ⅓ Octave sound power levels for a 50 mm diameter free axial jet as a function of jet velocity – mid to low frequency bands.

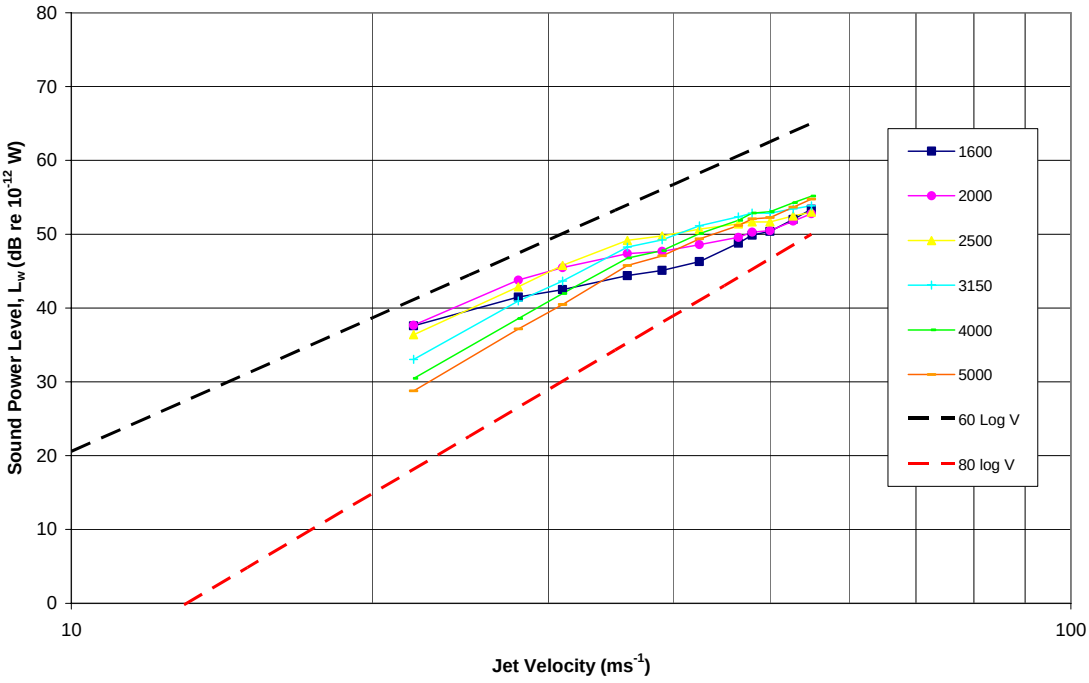

Figure 5.8: ⅓ Octave sound power levels for a 50 mm diameter free axial jet as a function of jet velocity – high frequency ⅓ octave bands.

5.4 ⅓ Octave Band Sound Pressure Level Measurements

The experimental ⅓ octave sound pressure levels corresponding to each of the 45 individual outlet diffuser configurations investigated were recorded using three separate microphone boom locations. Each reading was spatially averaged across the three microphone boom locations to minimise any experimental errors and modal fluctuations within the reverberation suite. An initial analysis of the data was performed based on the measured sound pressure levels in ⅓ octave bands in relation to both the individual centreline jet velocity and the configuration of the diffuser itself.

In the interest of economising on space and doubling up on the reporting of data the actual plots of the ⅓ octave sound pressure level data has been omitted. The ⅓ octave sound power level data is derived directly from the sound pressure level data using correction factors based on the acoustic properties of the reverberation suite. Therefore it was deemed unnecessary to essentially duplicate the same experimental data in two series of analyses.

5.5 Total Sound Pressure Level Analysis

The ⅓ octave band sound pressure level data was combined into octave bands and then total linear sound pressure level for each of the outlet configurations tested. The linear sound pressure data provides a good indication of the effectiveness of each of the individual outlet configurations under investigation and the data is in a form that allows easy comparison between multiple outlets across the desired jet velocity range. This level of analysis was useful in eliminating non-essential outlet configurations – saving valuable experimental resources without compromising the integrity of the overall research program.

As an initial first step the reverberation room based SPL will exceed the equivalent SPL observed in a real passenger cabin space due to an increase in the level of acoustic absorption. More detailed analysis of the sound spectrum for each outlet configuration will be more closely scrutinised in the subsequent sections using both total sound power level and ⅓ octave band sound power levels.

Three conical diffusers at angles of 7˚, 10˚ and 14˚ were tested with a variety of outlet fittings and duct configurations. The first series of tests used 11 diffuser configurations for each diffuser angle, with a combination of 2 outlet fittings and four outlet duct lengths of 0, 300, 600 and 900 mm. Three additional tests were derived from using no outlet fitting with each of the selected outlet duct lengths of 300, 600 and 900 mm. The trivial case of no outlet fitting and no outlet duct was ignored. The two outlet fittings used were a standard square 4-way HVAC diffuser (150 x 150) and a three vane round jet diffuser, as illustrated earlier in Figure 4.7 (page 85).

Once the results from this series of tests were evaluated two additional outlet duct geometries were also selected, incorporating a 90˚ elbow in the outlet duct and a standard HVAC cushion head box positioned between the outlet duct and the 4-way HVAC diffuser grill. Based on the earlier results these configurations were limited to the outlet duct lengths of 300 and 600 mm only. In total 45 of the possible 60 geometric configurations were investigated, with sound pressure levels recorded in ⅓ octave bands over a frequency range of 50 to 5000 Hz. (The results in the 50, 63 and 80 Hz bands are questionable given the size of the reverberation room used.) The combination of all the outlet configurations tested is shown in Table 5.1.

Table 5.1: Experimental diffuser outlet configurations investigated for the three diffuser angles of 7˚, 10˚ and 14˚.

	Outlet Duct Length (mm)			
Outlet Fitting	0	300	600	900
Nothing (0)	-	●	●	●
4-way square diffuser (SD)	●	●	●	●
Round jet diffuser (RJ)	●	●	●	●
Cushion head fitted to the square diffuser (CH)	-	●	●	-
Elbow fitted between the outlet duct and the cushion head (ELCH)	-	●	●	-

5.5.1 Conical Outlet Diffuser Angle Variation

The onset of flow separation inside the conical diffuser section and the location of the separation point for any given jet velocity is directly related to the angle of the diffuser. Increasing the diffuser angle was found to increase the chance of flow separation and move the subsequent separation point upstream towards the throat of the diffuser. Both of these effects were found to accelerate as the velocity of the jet was increased. Increased flow separation also correlated with an increase in the generation of flow induced noise. The length of the outlet duct section also provided some attenuation effects within particular frequency bands corresponding to the harmonic resonance frequencies associated with the given duct geometry. To better understand the complex interaction of all of these effects, multiple comparisons have been drawn between the three diffuser angles used. Variations in outlet duct length and the outlet grill termination have been used to better identify the underlying relationship between the diffuser angle used and the resulting level of flow induced noise.

The first comparison is made based on a straight 300 mm long open ended outlet duct fitted to each of the conical diffusers. This provides a direct comparison between the diffuser angles without the added complexity of the outlet termination grill. It should be noted however that lengths of the 7˚, 10˚ and 14˚ diffusers are 407, 285 and 200 mm respectively. Therefore the open ended outlet exit plane for each of the configurations was respectively located 707, 585 and 500 mm downstream from the diffuser throat. The same variation in total length also applied to the 600 and 900 mm long outlet duct cases, but with a progressively smaller percentage wise variation in the length of the duct geometry. The total linear sound pressure level for the 300, 600 and 900 mm long outlet ducts (open ended) for a selected jet velocity range are shown in Figures 5.9, 5.10 and 5.11 respectively.

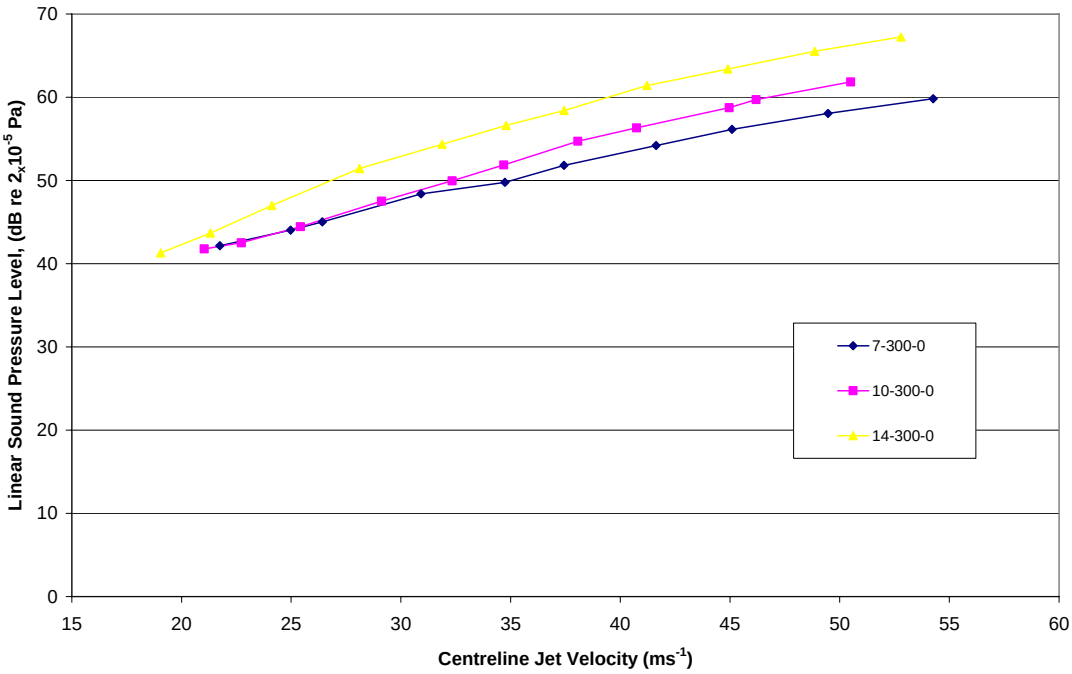

Figure 5.9: Linear SPL comparison for conical diffuser angles of 7˚, 10˚ and 14˚ – fitted with an open ended 300 mm long outlet duct.

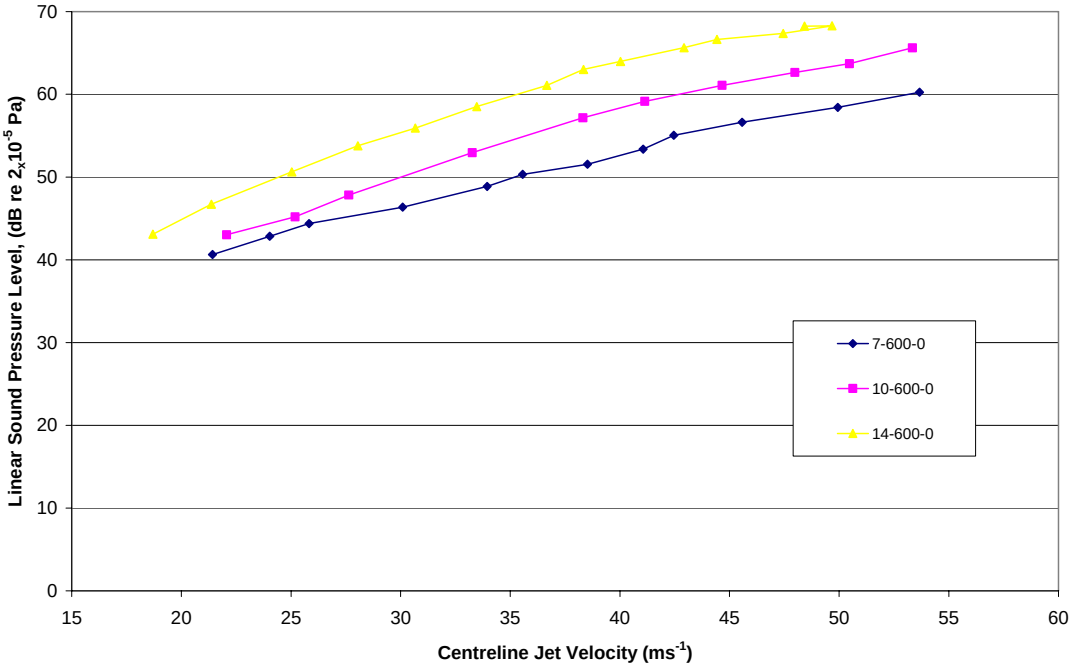

Figure 5.10: Linear SPL comparison for conical diffuser angles of 7˚, 10˚ and 14˚ – fitted with an open ended 600 mm long outlet duct.

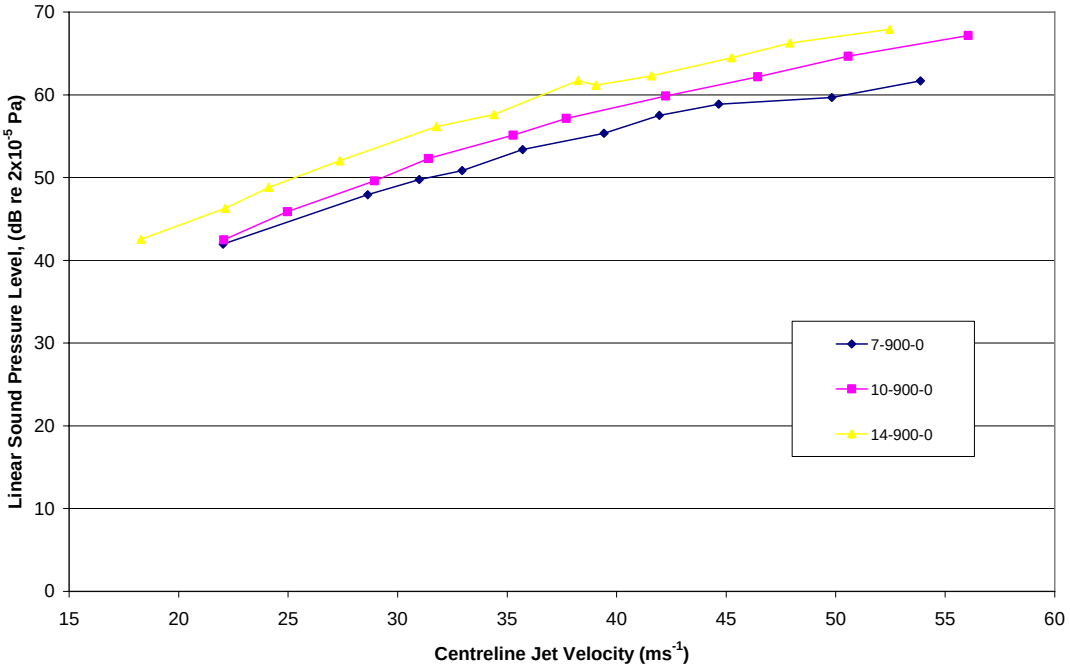

Figure 5.11: Linear SPL comparison for conical diffuser angles of 7˚, 10˚ and 14˚ – fitted with an open ended 900 mm long outlet duct.

The first observation from the above results was the increase in the sound pressure level for each outlet duct length as the angle of the conical diffuser was increased from 7˚ to 10˚ and then to 14˚. This variation was most pronounced for the 600 mm outlet duct and less so for a length of 300 and 900 mm. Interestingly, the variation between the 7˚ and 10˚ diffusers fitted with the 300 mm long outlet duct was negligible in the lower velocity range of 20 to 30 ms^{-1}. The divergence between the two for jet velocities above 30 ms^{-1} is most likely attributed to increased flow separation occurring as a result of the higher diffuser angle. A similar conclusion can be drawn at lower velocities for both the 600 and 900 mm long duct cases, however the increase in the overall length of the outlet duct appears to somewhat decouple this relationship, particularly in the case of the 14˚ diffuser. This effect is attributed to the onset of flow separation at velocities below 20 ms^{-1} for the 14˚ diffuser. The effects of the flow separation then appear to be compensated by increasing the length of the outlet duct further (to 900 mm) where the flow has more time to expand and the flow turbulence begins to dissipate through viscous effects.

To further reinforce the above observations similar comparisons were made between the three diffuser angles for the 300 and 600 mm long outlet ducts fitted with each of the four outlet grill terminations investigated. The first outlet termination grill tested was the round jet outlet (RJ), with the linear SPL for the 300 and 600 mm long outlet ducts shown in Figures 5.12 and 5.13 respectively. For the 300 mm long outlet duct in the lower velocity range of 20 to 25 ms^{-1} there was a limited increase in the linear SPL as the diffuser angle was increased. This matched the observations made with the open duct cases but over a smaller velocity range. As with the open ended duct models the gap between the 7˚ and 10˚ diffusers widened when the outlet duct length was increased from 300 to 600 mm. Meanwhile the difference between the 7˚ and 14˚ diffusers was relatively consistent across the velocity range considered. Extending the length of the outlet duct from 300 to 600 mm also produced a small reduction in the overall linear SPL of 2 to 3 dB. This effect will be further discussed in the subsequent sections.

The linear SPL for the square diffuser (SD) outlet termination grill fitted with a 300 and 600 mm long outlet duct across a range of jet velocities are shown in Figures 5.14 and 5.15 respectively. The general trend of increasing SPL as the diffuser angle is increased is maintained, however the previously observed convergence of the SPL at low jet velocities (20 to 25 ms^{-1}) is no longer present. The 10˚ and 14˚ diffusers are more closely aligned for the 300 mm outlet duct case, while the variation between the three diffuser angles used is relatively uniform in the case of the 600 mm outlet duct. The 600 mm outlet duct also appears to marginally reduce the SPL in the lower velocity ranges considered.

The same results for the cushion head mounted SD grill (CH) fitted to the 300 and 600 mm long outlet ducts are shown in Figures 5.16 and 5.17 respectively. The corresponding results for the same configurations with the addition of a 90˚ elbow between the outlet ducts and the cushion head (ELCH) are shown in Figures 5.18 and 5.19. The 7˚ diffuser was consistently the best performed configuration with a SPL 4 to 5 dB lower than each corresponding 10˚ configuration. The variation between these models and those using the 14˚ diffuser ranged from 2 to 4 dB, depending on the configuration considered.

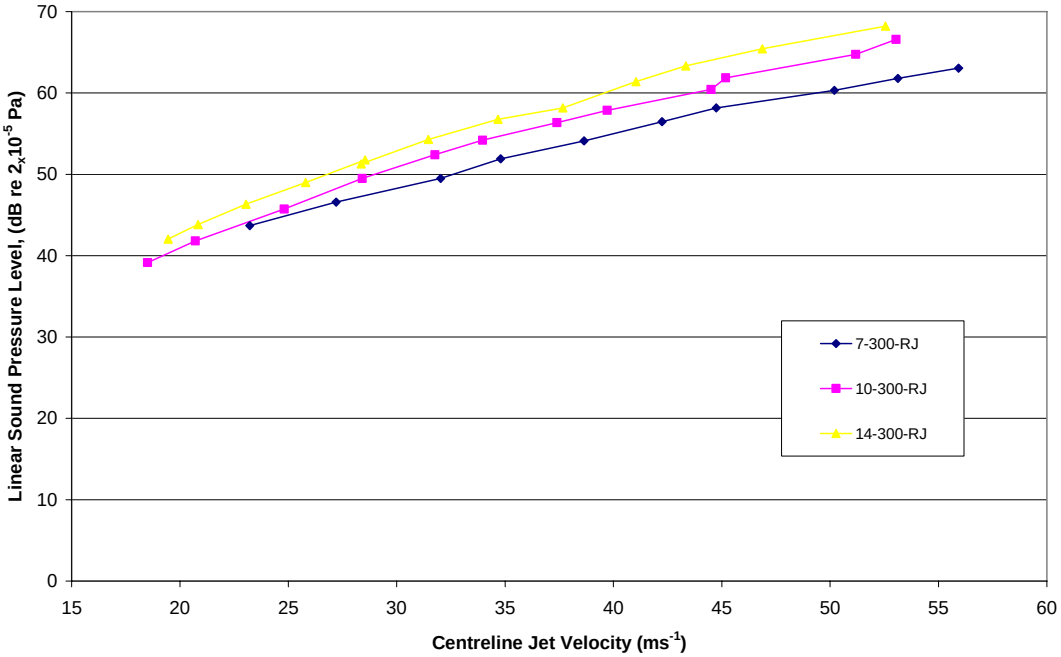

Figure 5.12: Linear SPL comparison for conical diffuser angles of 7˚, 10˚ and 14˚ – with a 300 mm long outlet duct fitted with the round jet outlet grill.

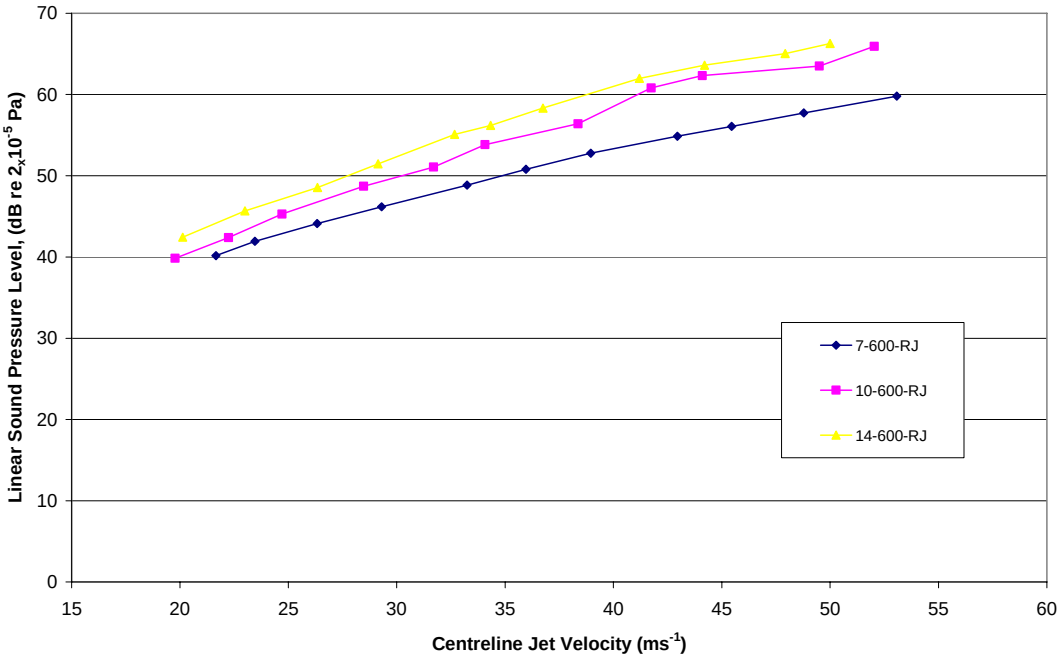

Figure 5.13: Linear SPL comparison for conical diffuser angles of 7˚, 10˚ and 14˚ – with a 600 mm long outlet duct fitted with the round jet outlet grill.

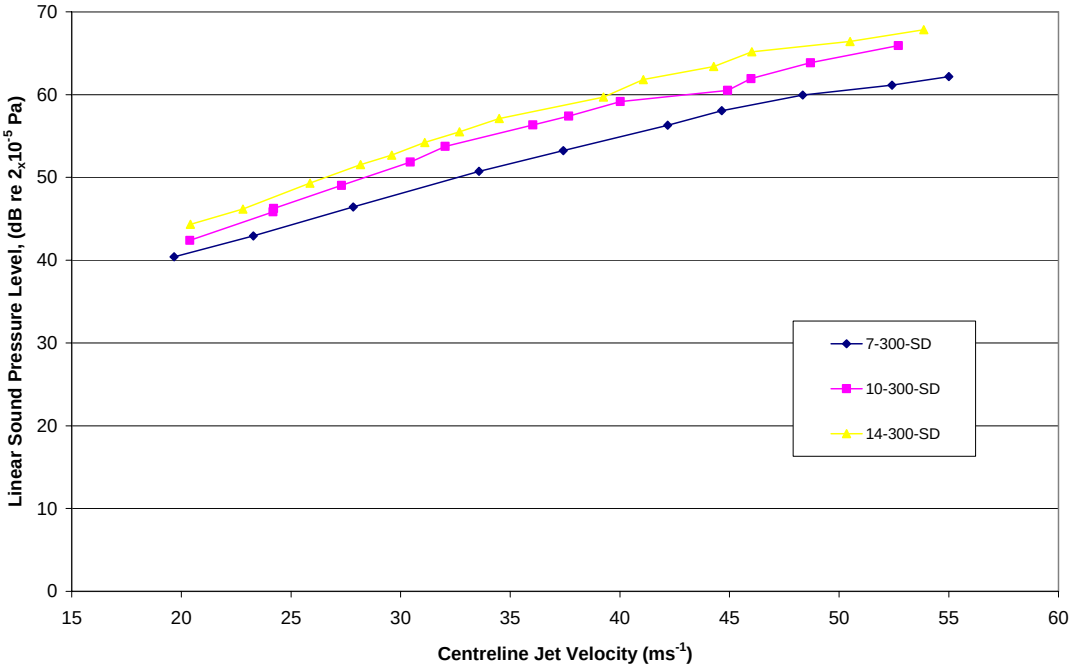

Figure 5.14: Linear SPL comparison for conical diffuser angles of 7˚, 10˚ and 14˚ – with a 300 mm long outlet duct fitted with the square diffuser outlet grill.

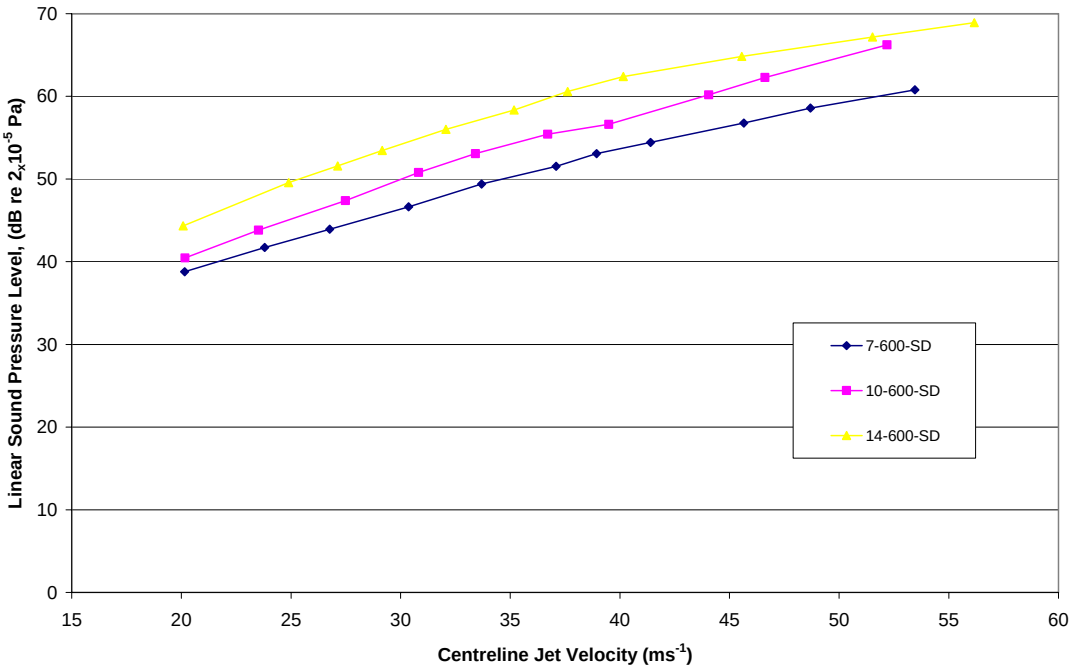

Figure 5.15: Linear SPL comparison for conical diffuser angles of 7˚, 10˚ and 14˚ – with a 600 mm long outlet duct fitted with the square diffuser outlet grill.

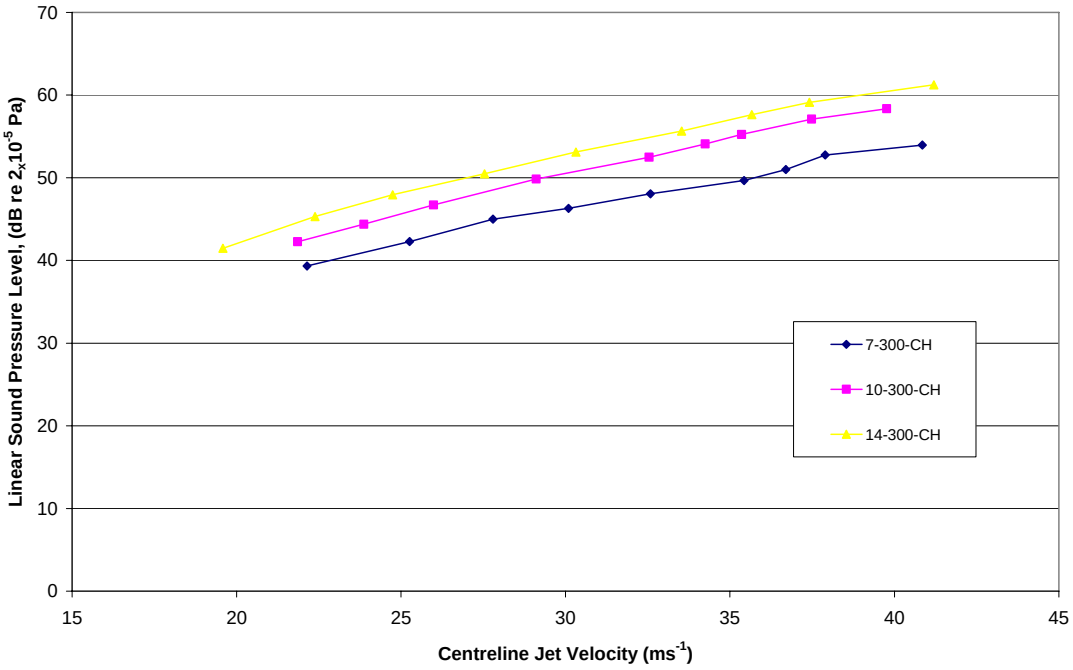

Figure 5.16: Linear SPL comparison for conical diffuser angles of 7˚, 10˚ and 14˚ – with a 300 mm long outlet duct fitted with the cushion head mounted square outlet grill.

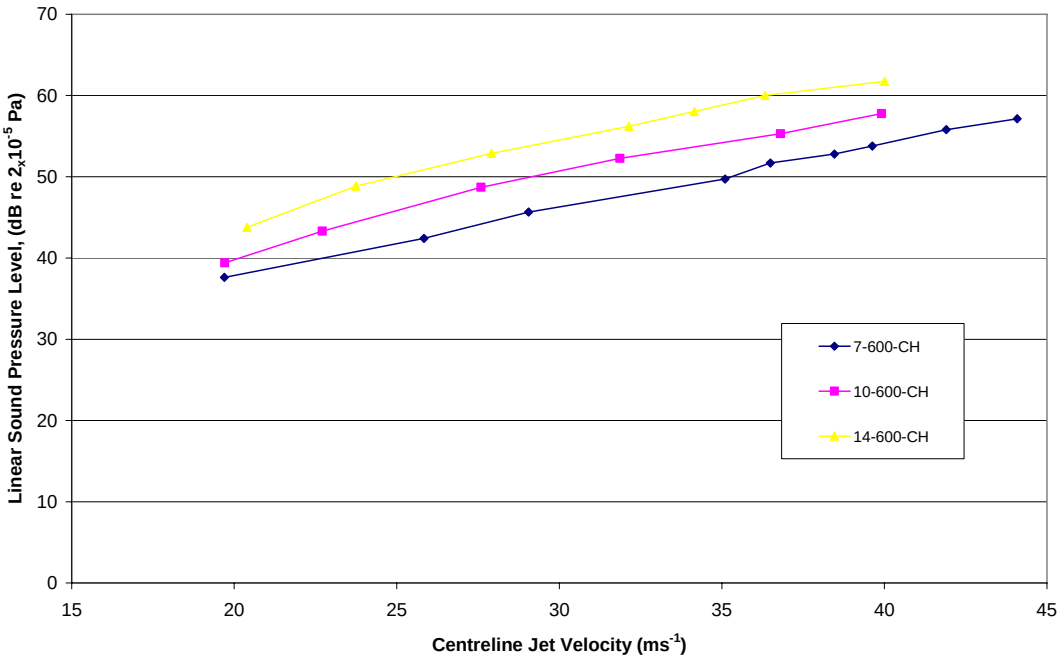

Figure 5.17: Linear SPL comparison for conical diffuser angles of 7˚, 10˚ and 14˚ – with a 600 mm long outlet duct fitted with the cushion head mounted square outlet grill.

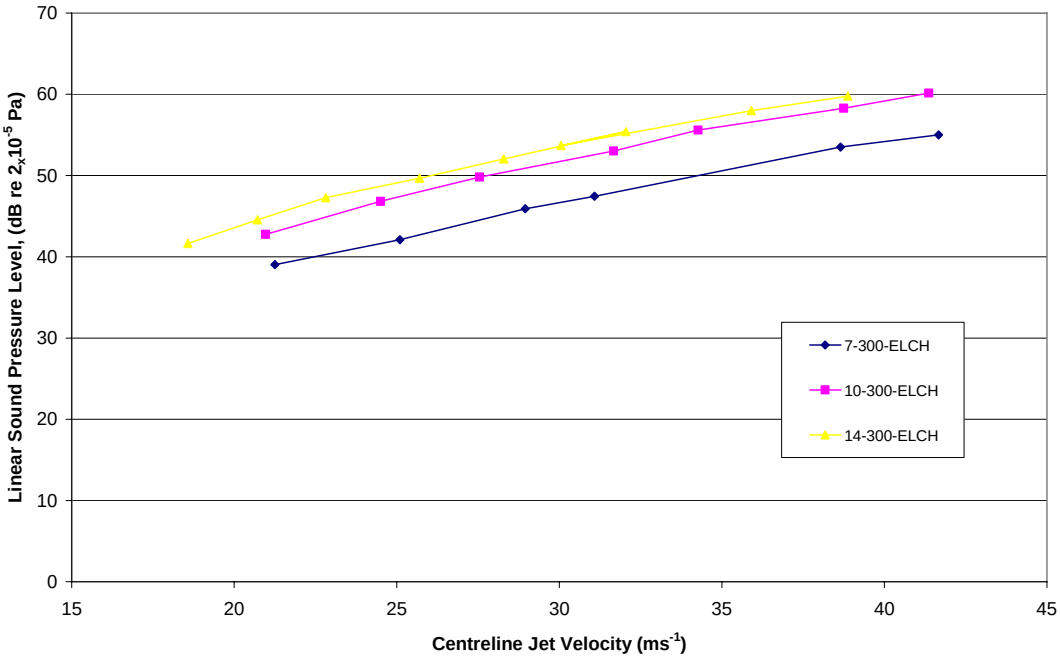

Figure 5.18: Linear SPL comparison for conical diffuser angles of 7˚, 10˚ and 14˚ – with a 300 mm long outlet duct fitted with a 90˚ elbow and the cushion head mounted square outlet grill.

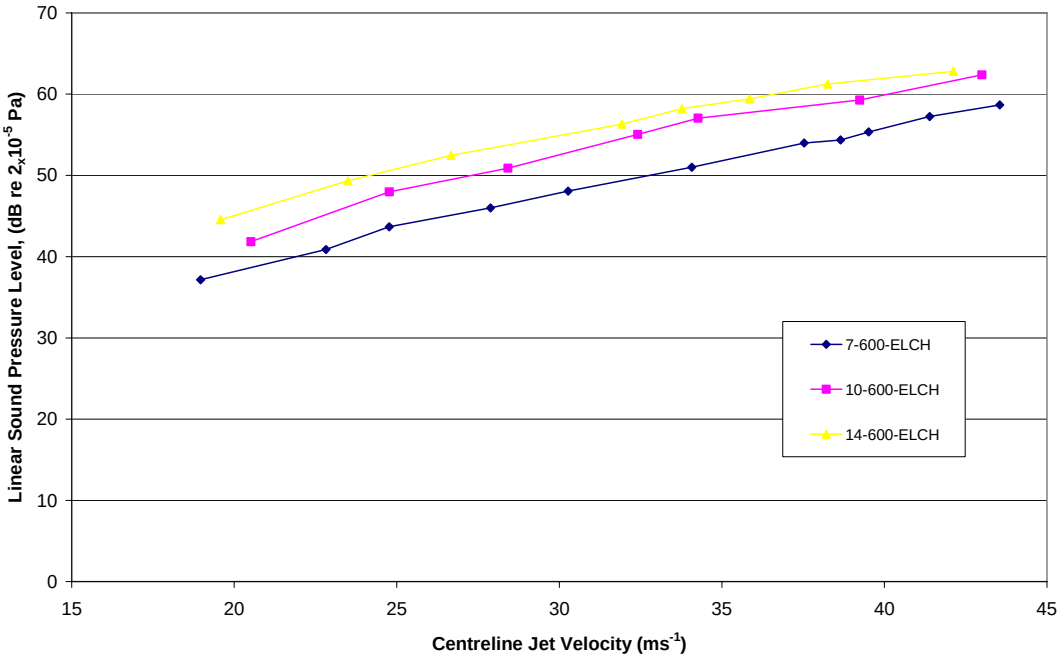

Figure 5.19: Linear SPL comparison for conical diffuser angles of 7˚, 10˚ and 14˚ – with a 600 mm long outlet duct fitted with a 90˚ elbow and the cushion head mounted square outlet grill.

In summary the 7˚ diffuser performed best across all outlet configurations considered, while the performance of the 10˚ diffuser was somewhat more dependent on the jet velocity and the geometry of the downstream outlet duct configuration. The 14˚ diffuser was consistently worse than the other two angles studied. However, where the 300 mm long outlet duct was used some viable results were obtained at jet velocities below 25 ms^{-1}. Therefore in situations where the length of space available in the ceiling cavity is limited the use of a wider angled diffuser of 14˚ may provide a suitable compromise if the air velocity can be lowered to acceptable limits. The use of additional guide vanes inside the conical diffuser section may well enable a wider angle to be used, whilst also preventing the onset of flow separation.

5.5.2 Outlet Termination Grill Variation

As outlined above the selection of the outlet termination grill had a significant impact on the overall acoustic performance of each outlet configuration investigated. To better understand the impact of the outlet grill, cushion heads and the addition of elbows into the outlet duct a comparison was made across a variety of outlet duct lengths and diffuser angles. The first comparison was made for the case of no outlet duct, where the RJ and SD grills were fitted directly onto each of the three conical diffusers discussed previously.

The square diffuser (SD) grill consistently produced a lower SPL than the round jet (RJ) for each of the three diffuser angles investigated, as shown in Figures 5.20, 5.21 and 5.22. In the case of the 7˚ conical diffuser the SD grill configuration produced a SPL 4 to 5 dB lower than the RJ grill that appears to be independent of the jet velocity. The difference between the two outlet grills is reduced slightly to 3 to 4 dB when the 10˚ conical diffuser is used. As with the previous diffuser the relationship appears to be independent of the jet velocity. When the conical diffuser angle is increased further to 14˚ the difference between the two grills is reduced to only 1 to 2 dB and the independence from the jet velocity is maintained. Therefore the square grill in a direct application is the preferred outlet termination option across the entire velocity range of interest to this study. The impact of coupling this grill to the additional outlet ducts must still be evaluated further to confirm the breadth of potential applications.

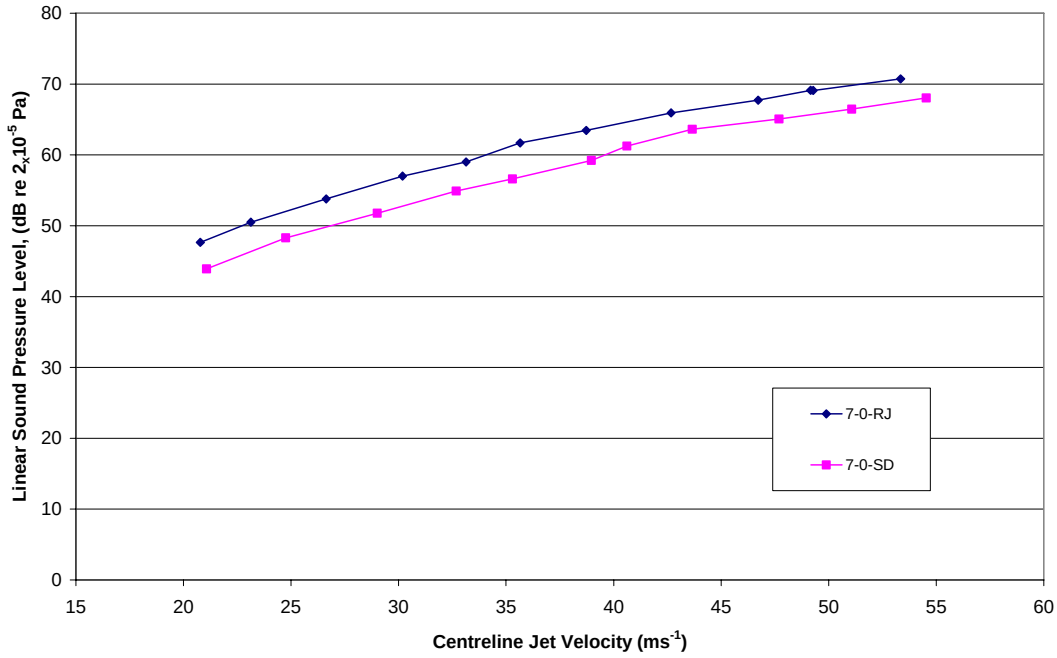

Figure 5.20: Linear SPL comparison between the round jet (RJ) and square (SD) outlet termination grills fitted directly to the 7˚ conical diffuser.

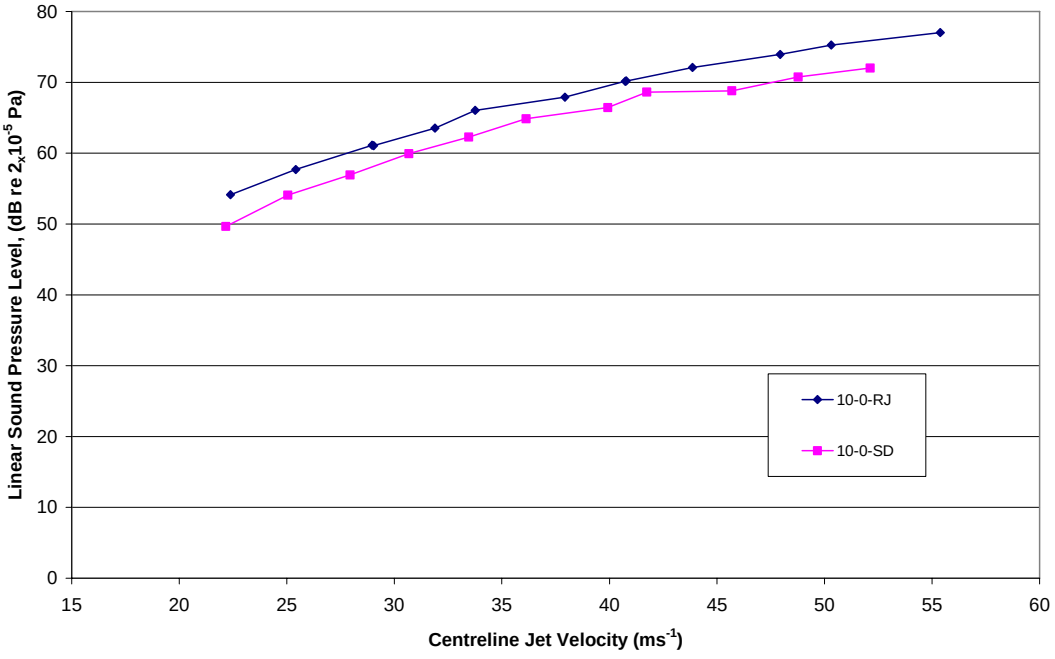

Figure 5.21: Linear SPL comparison between the round jet (RJ) and square (SD) outlet termination grills fitted directly to the 10˚ conical diffuser.

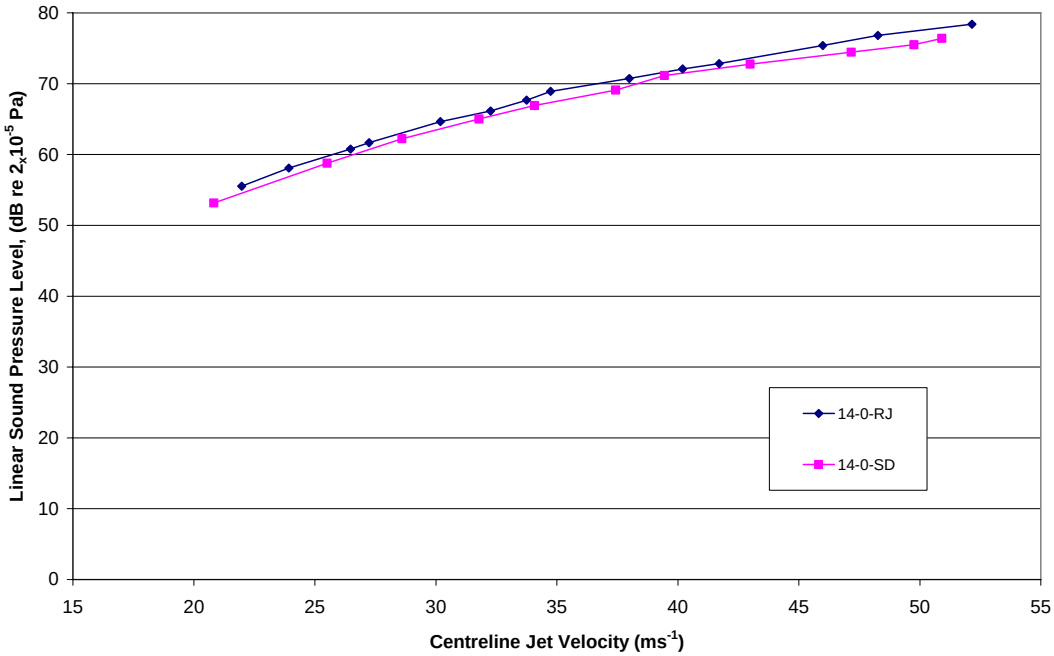

Figure 5.22: Linear SPL comparison between the round jet (RJ) and square (SD) outlet termination grills fitted directly to the 14˚ conical diffuser.

Given the above preference to the SD grill over the RJ grill, additional configurations making use of the SD grill were also investigated. The SD grill was fitted to a rectangular cushion head box, lined with acoustic lagging material (CH termination). The effects of mounting the cushion head box and SD grill (CH) to a 90˚ elbow downstream of the outlet duct and conical diffuser (ELCH) was also investigated. Each of these four outlet termination configurations were also compared back against the baseline of no outlet termination grill.

The first comparison was made based on the 300 mm outlet duct fitted to the 7, 10 and 14˚ conical diffusers, as shown in Figures 5.23, 5.24 and 5.25 respectively. The complex interdependence of multiple variables on the overall linear SPL become evident as each of these results is considered. Firstly the RJ and SD outlets produce a virtually identical SPL curve when fitted to a 300 mm long outlet duct and 7˚ conical diffuser. Furthermore each grill adds minimal additional noise over that produced with no outlet grill for jet velocities up to 30 ms^{-1}, but at velocities above this level there is an increase in the SPL of 3 to 4 dB.

The addition of the cushion head box successfully lowered the overall SPL, particularly at jet velocities below 35 ms^{-1}, where the SPL was lower than the baseline of no outlet grill. A similar result is also achieved when the 90˚ elbow is inserted, however there is no additional attenuation achieved in the case of the 7˚ conical diffuser.

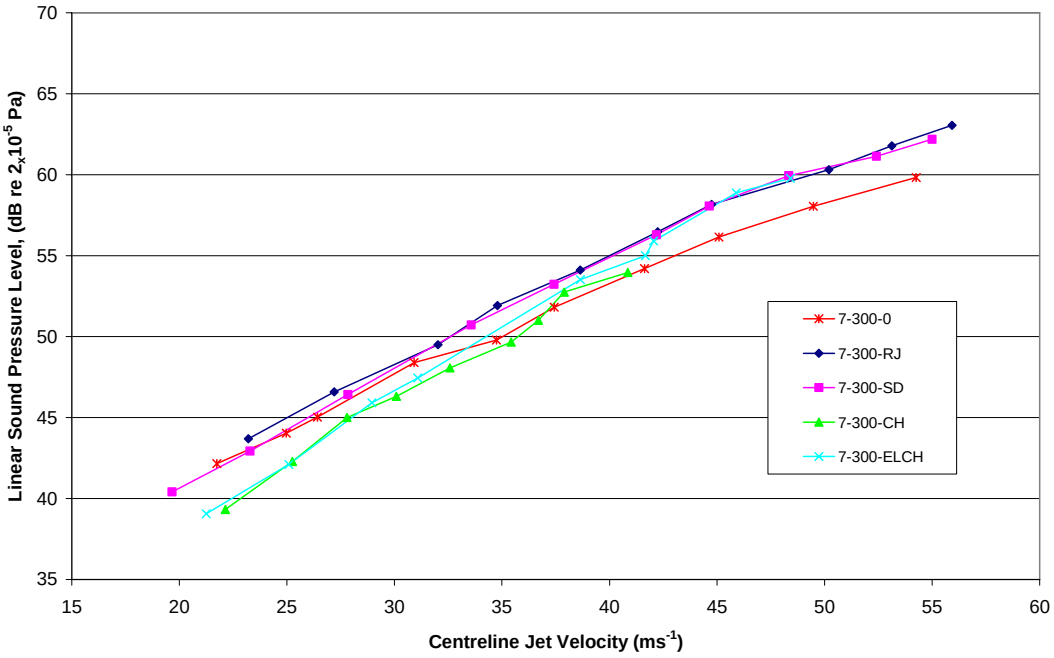

Figure 5.23: Linear SPL comparison between each termination grill configuration fitted to the 7˚ conical diffuser with a 300 mm long outlet duct.

When a conical diffuser angle of 10˚ or 14˚ is used neither the CH or ELCH configuration are able to significantly enhance the acoustic performance of the standard outlet grills. In the case of the 10˚ diffuser none of the configurations considered were able to better the baseline case of no outlet grill, with all cases at least 4 dB above it. Meanwhile when the 14˚ diffuser is used in conjunction with the 300 mm outlet duct the SD outlet grill results in a SPL of 2 to 4 dB lower than the corresponding baseline. As with the 10˚ diffuser cases the cushion head and elbow configurations had a negligible effect on the overall SPL. Of particular note is the indifference between the cushion head with and without the 90˚ elbow.

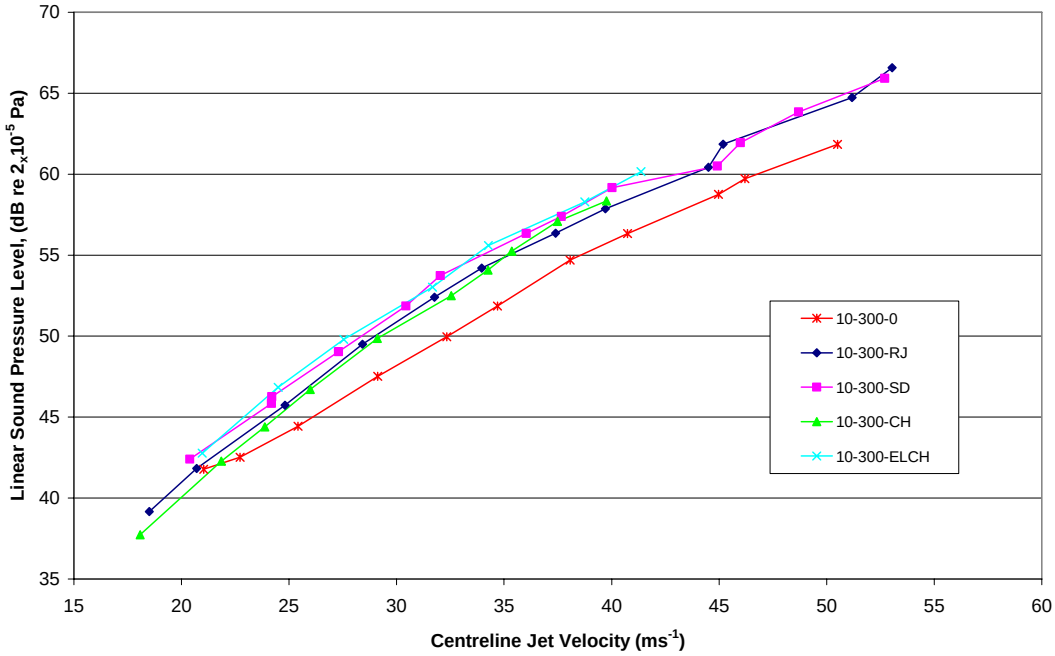

Figure 5.24: Linear SPL comparison between each termination grill configuration fitted to the 10˚ conical diffuser with a 300 mm long outlet duct

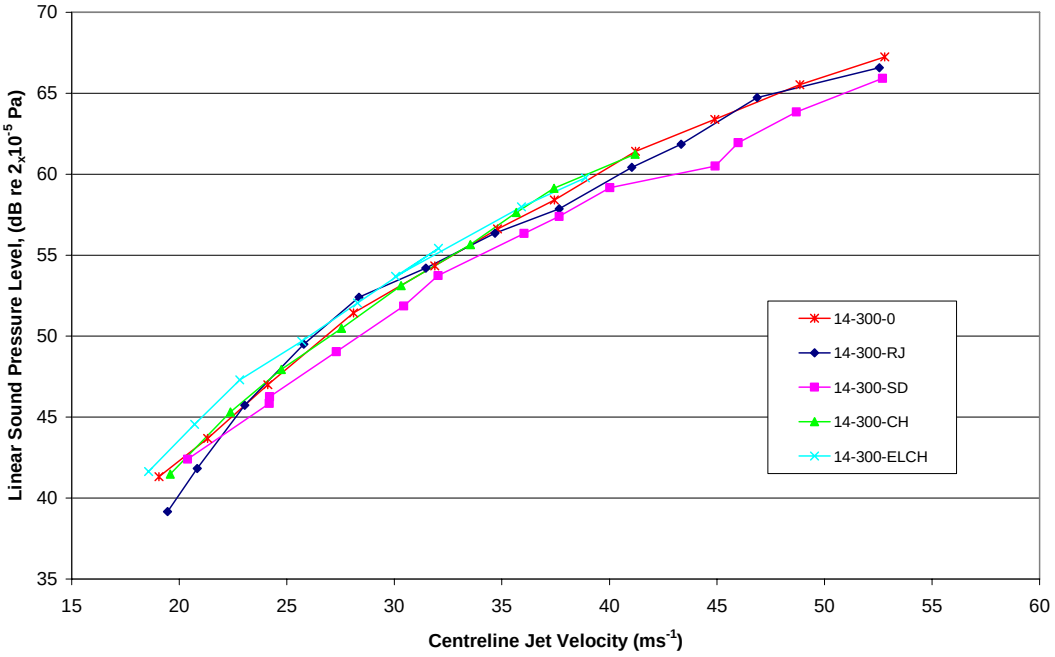

Figure 5.25: Linear SPL comparison between each termination grill configuration fitted to the 14˚ conical diffuser with a 300 mm long outlet duct

The addition of the 300 mm outlet duct had a pronounced effect on the overall acoustic performance of the outlet when compared back against the baseline case of no outlet duct. Therefore it was assumed that the length of the outlet duct had a significant influence on the overall generation and attenuation of the flow generated noise inside the outlet. Based on this hypothesis the above comparison was repeated for an outlet duct length of 600 mm as well.

The SPL for each of the outlet termination grills fitted to a 600 mm outlet duct for the 7˚, 10˚ and 14˚ diffusers are shown in Figures 5.26, 5.27 and 5.28 respectively. Firstly in the case of the 7˚ diffuser the baseline of no outlet grill and the standard RJ and SD grills produce very similar levels of noise. At lower jet velocities of 20 to 30 ms^{-1} the RJ and SD grills have a lower SPL by approximately 1 dB, with the relationship reversed by 1 to 2 dB for velocities above this level. When a 10˚ diffuser is used there is negligible difference between the baseline (no outlet grill) and the SD and RJ grills at velocities up to 35 ms^{-1}. Beyond this level the fluctuations increase, but all three cases remain within 1 to 2 dB of one another. Interestingly when the 14˚ diffuser is used both the SD and RJ outlets produce a consistently lower SPL across the entire velocity range considered. The SD case was 1 to 2 dB lower while the RJ case was 3 to 4 dB lower.

The addition of the cushion head box (CH) proved effective at low jet velocities (20 to 30 ms^{-1}) when used in conjunction with the 7˚ conical diffuser. However when coupled with the 10˚ and 14˚ diffusers there was no significant improvement over the standard SD grill. Interestingly as the jet velocity is increased further the effectiveness of the CH outlet diminishes to the point that is less effective than the SD by itself. The ELCH configuration once again proved to be ineffective, with the total SPL increasing when compared to the other configurations. This effect appears to be independent of the length of the outlet duct. Therefore it would appear that the use of the elbow is not required. A significant point that should also be noted is the increase in the SPL as the conical diffuser angle is increased. For a jet velocity of 20 ms^{-1} the SPL increases from 37.5 dB (7˚) to 40 dB (10˚) and then 42.5 dB (14˚) for the same outlet termination configuration.

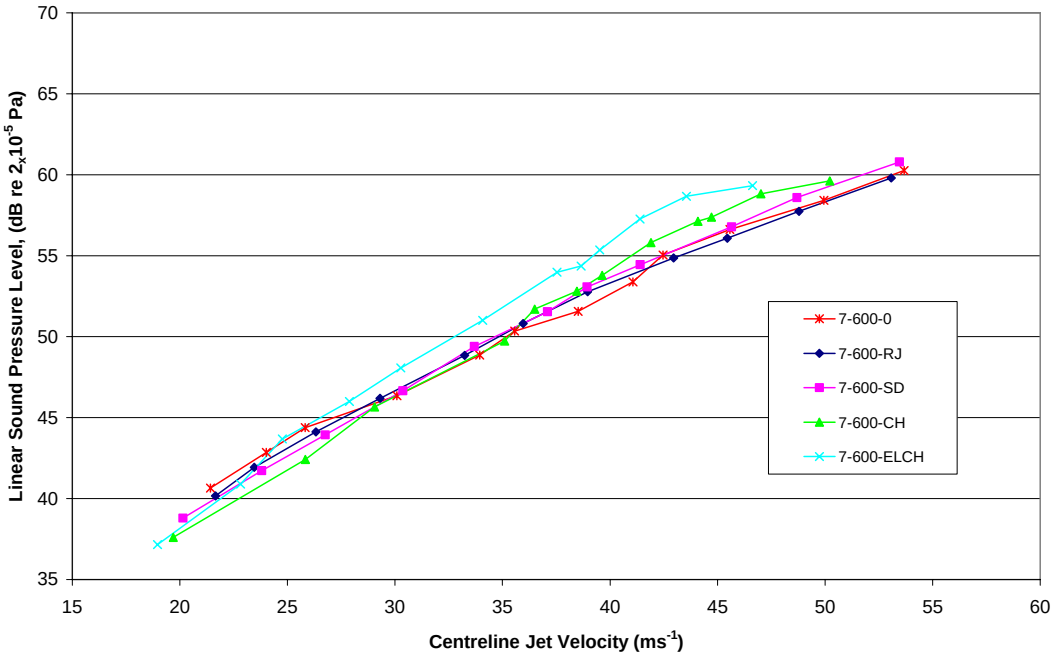

Figure 5.26: Linear SPL comparison between each termination grill configuration fitted to the 7˚ conical diffuser with a 600 mm long outlet duct.

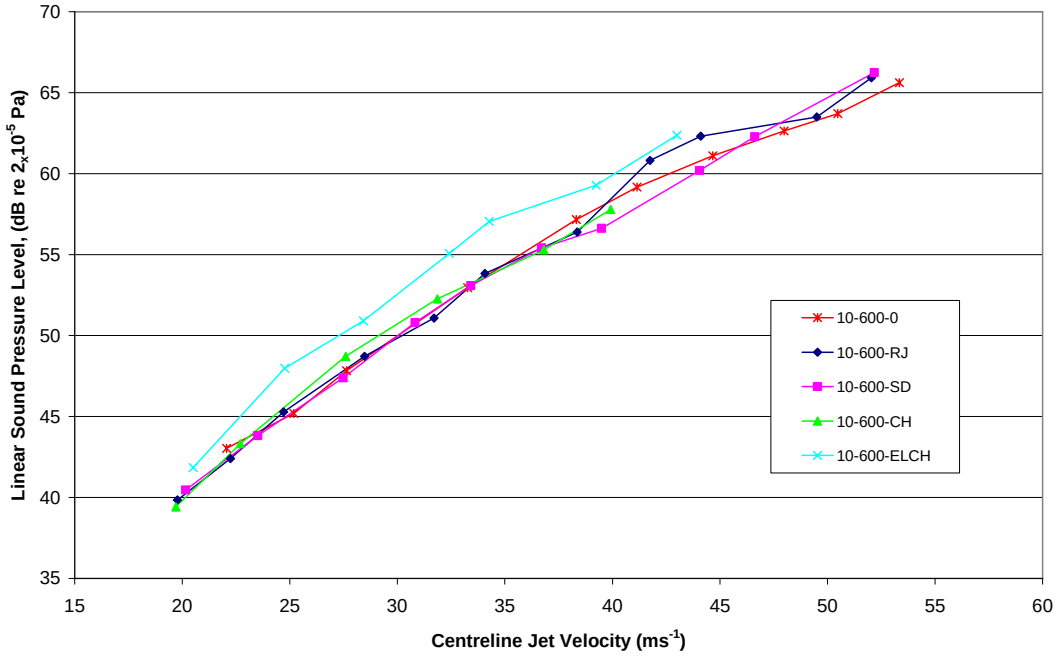

Figure 5.27: Linear SPL comparison between each termination grill configuration fitted to the 10˚ conical diffuser with a 600 mm long outlet duct

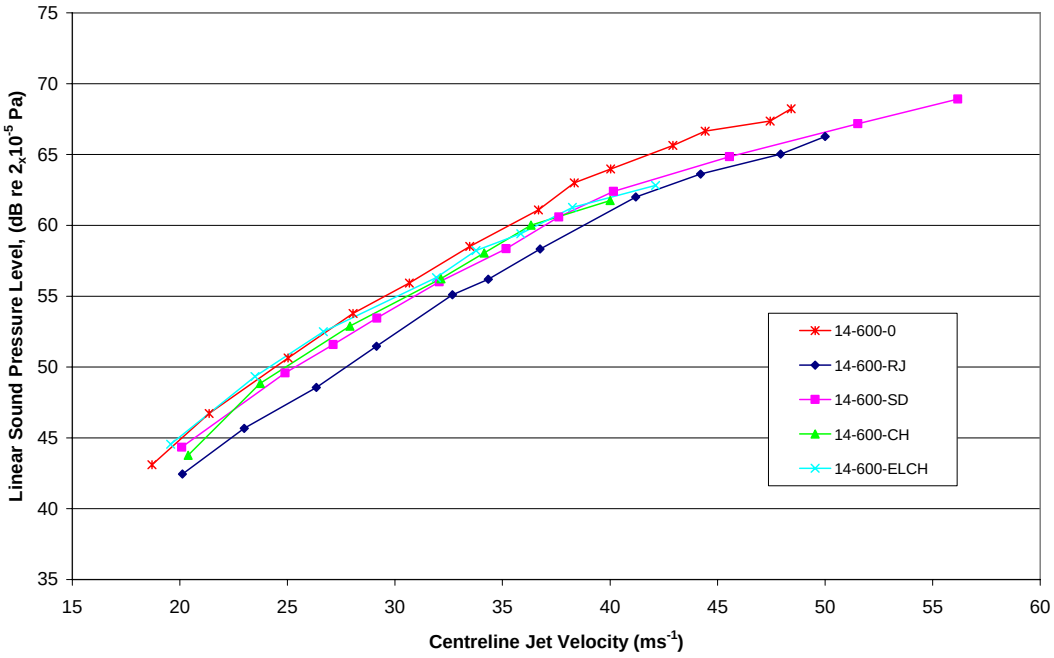

Figure 5.28: Linear SPL comparison between each termination grill configuration fitted to the 14˚ conical diffuser with a 600 mm long outlet duct

On initial inspection the above results could be interpreted as being representative of experimental error or of a weak level of correlation between the SPL and the geometric configuration of the outlet. To evaluate the validity of both of these scenarios the experiments were repeated several times and the same results were achieved with a variation of ± 0.3 dB for the SPL recordings. The variations observed between configurations are in the order of 1 to 5 dB, which is a sizable increase over the level of experimental error encountered. Therefore the variation in acoustic performance has been attributed to the complex interaction between the various geometric properties of each configuration.

The true impact of the outlet duct configuration can be better measured if an A-weighting is applied to the sound pressure level recorded, so as to better account for the different frequency components of the overall acoustic field. The A-weighting provides a more realistic measure of how the acoustic field would appear to an observer, rather than absolute measure of sound pressure.

The A-weighted SPL for each of the outlet termination grills fitted to a 300 mm outlet duct using the 7˚, 10˚ and 14˚ diffusers are shown in Figures 5.29, 5.30 and 5.31 respectively. On an A-weighted basis the standard SD performs marginally better than the RJ grill across the main jet velocity range of interest of 20 to 40 ms^{-1}. Both of these grills actually improve slightly on the open ended outlet duct (with no outlet termination grill). The largest improvement however is achieved with the cushion head (CH) mounted and elbow mounted (ELCH) outlets. There is no significant advantage in adding the 90˚ elbow to the outlet duct, with both of these two cases showing virtually the same A-weighted SPL across a jet velocity range of 20 to 40 ms^{-1}.

These trends are consistent for all three conical diffuser angles used, with a slight increase in the A-weighted SPL as the diffuser angle is increased from 7˚ to 14˚. At the wider diffuser angles there is a small improvement gained with the addition of the 90˚ elbow, however these gains are limited to jet velocities above 30 to 35 ms^{-1}. The difference between the SD and RJ outlets is also increased slightly as the diffuser angle is increased.

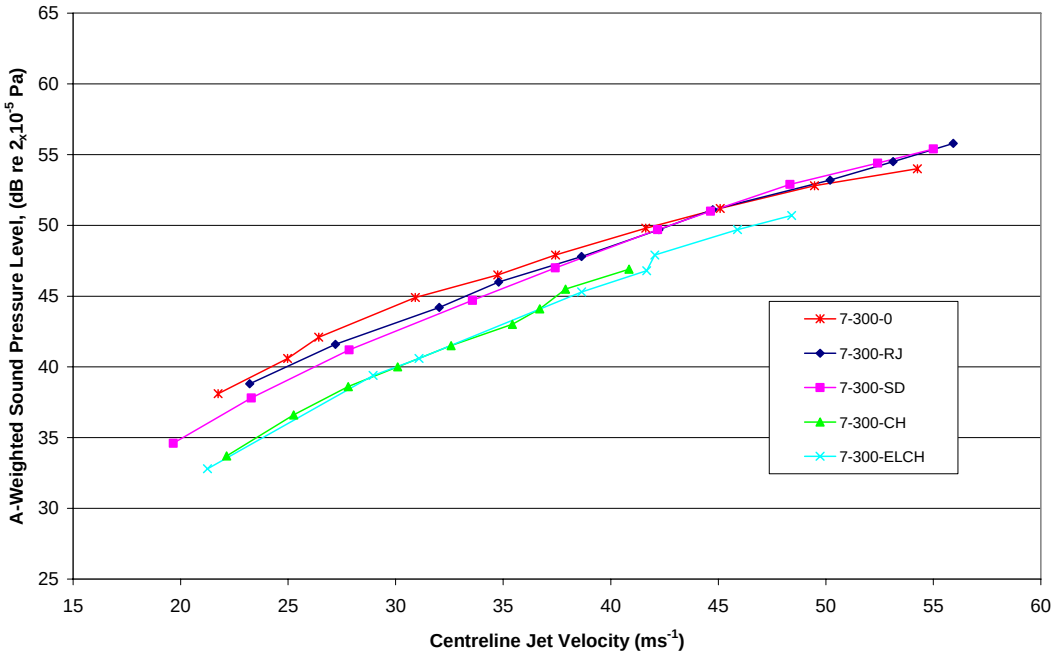

Figure 5.29: A-weighted SPL comparison between each termination grill configuration fitted to the 7˚ conical diffuser with a 300 mm long outlet duct.

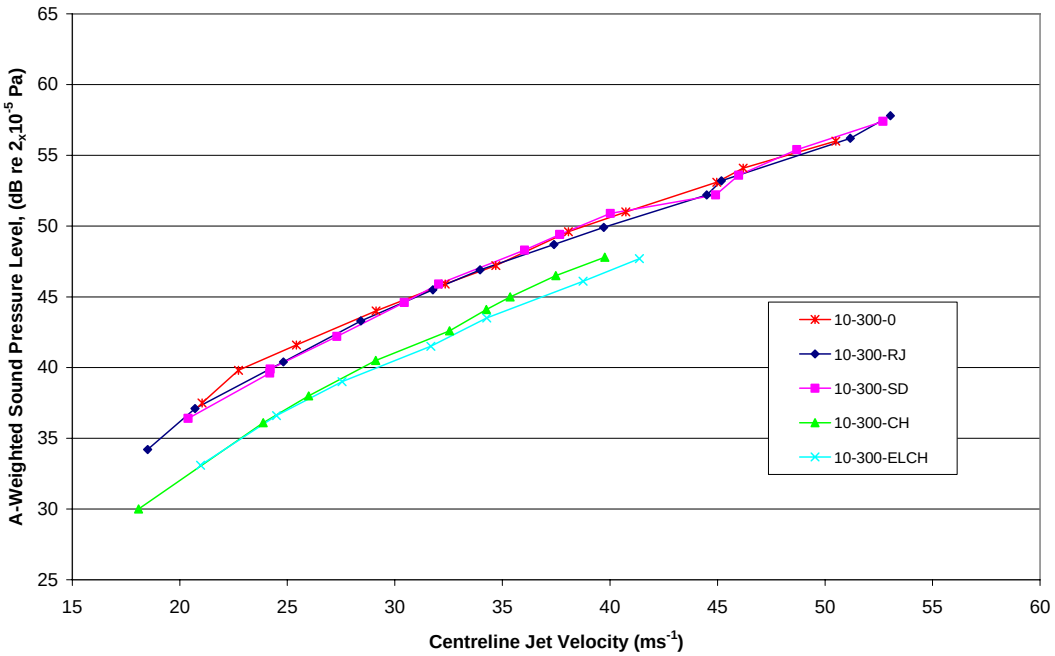

Figure 5.30: A-weighted SPL comparison between each termination grill configuration fitted to the 10˚ conical diffuser with a 300 mm long outlet duct.

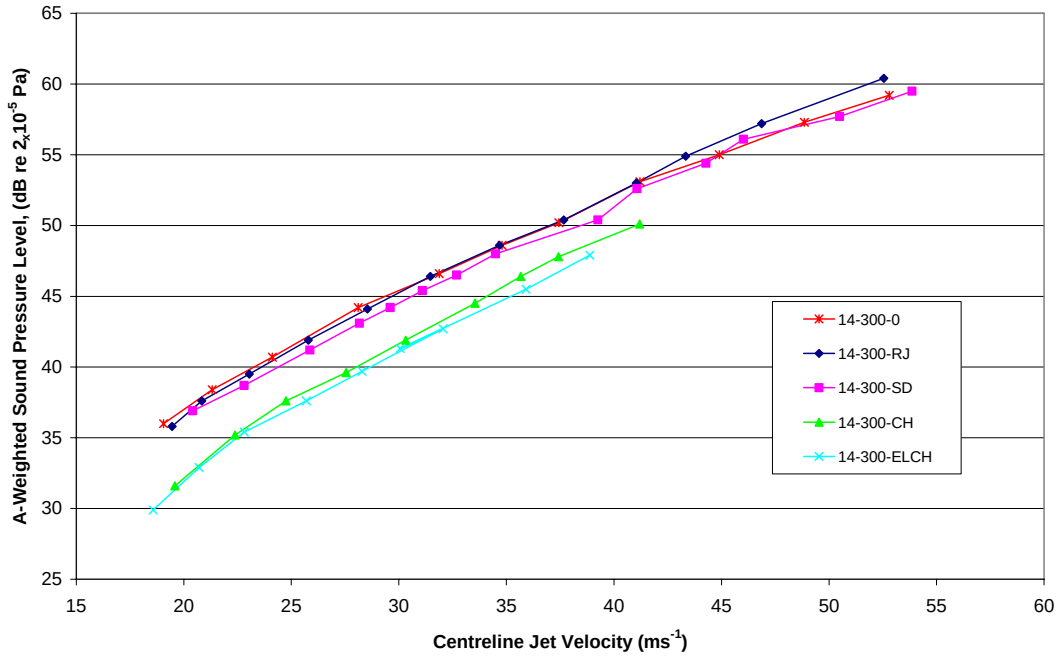

Figure 5.31: A-weighted SPL comparison between each termination grill configuration fitted to the 14˚ conical diffuser with a 300 mm long outlet duct.

The A-weighted SPL analysis used above was repeated for each of the outlet termination grills fitted to a 600 mm outlet duct. The results for the 7˚, 10˚ and 14˚ diffusers are shown in Figures 5.32, 5.33 and 5.34 respectively. As with the 300 mm outlet duct the standard SD performs marginally better than the RJ grill across the main jet velocity range of interest of 20 to 40 ms^{-1}. Once again the largest improvement is achieved with the cushion head (CH) mounted and elbow mounted (ELCH) outlets. Across the jet velocity range of interest (20 to 40 ms^{-1}) there is no significant advantage in adding the 90˚ elbow to the outlet duct, with both of these cases once again showing virtually the same A-weighted SPL.

The increase in the length of the outlet duct makes no significant difference to the minimum A-weighted SPL that is achieved using the cushion head (CH) mounted SD outlet termination grill. The improvement between the baseline case and CH configuration is slightly less for the 600 mm outlet duct, when compared back with the results for the 300 mm outlet duct. In effect this is a reflection of the variation between the two baseline cases more so than any significant difference between the 300 and 600 mm outlet ducts fitted to the CH termination outlet grill.

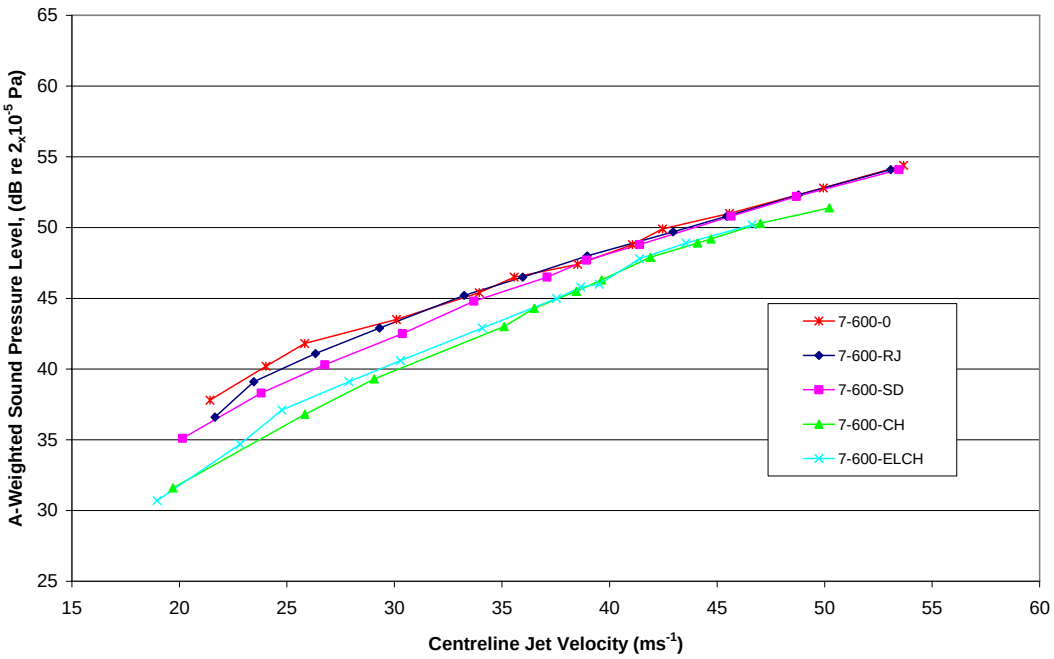

Figure 5.32: A-weighted SPL comparison between each termination grill configuration fitted to the 7˚ conical diffuser with a 600 mm long outlet duct.

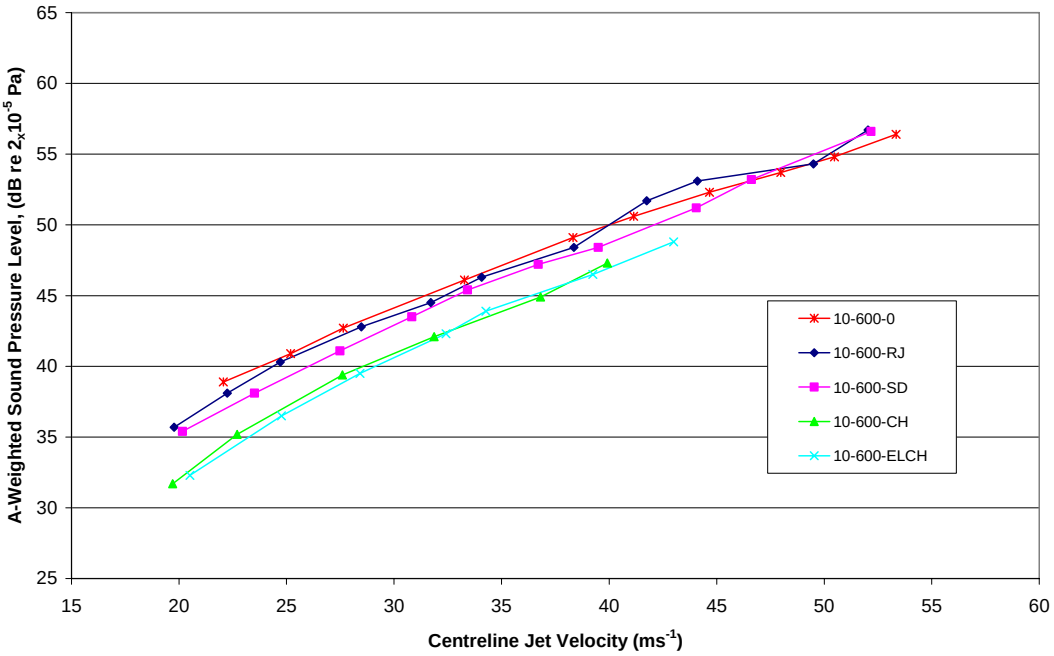

Figure 5.33: A-weighted SPL comparison between each termination grill configuration fitted to the 10˚ conical diffuser with a 600 mm long outlet duct.

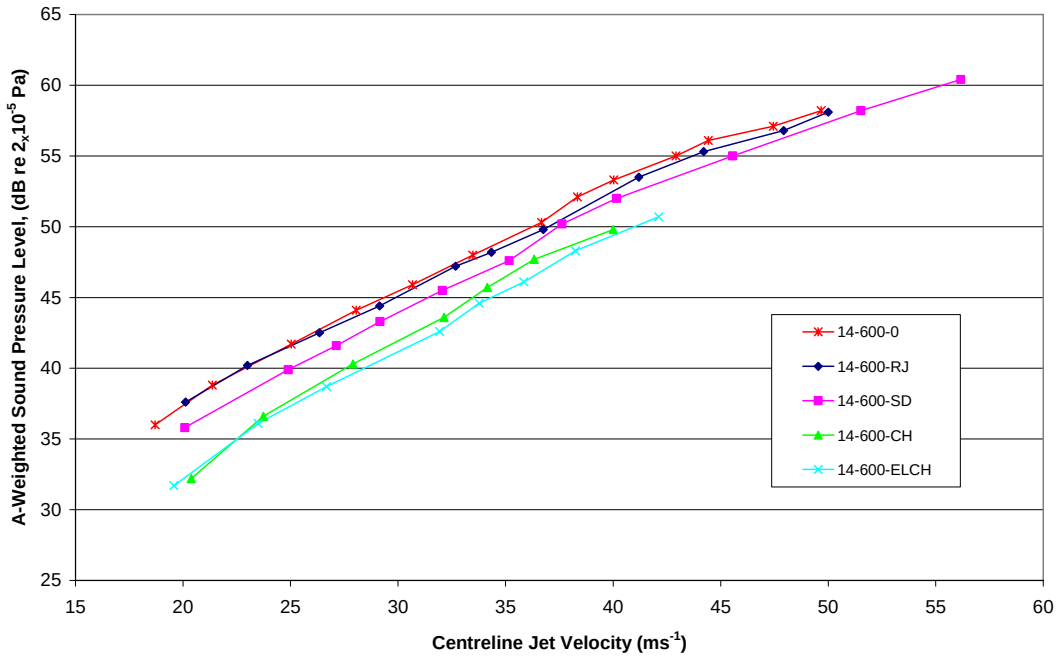

Figure 5.34: A-weighted SPL comparison between each termination grill configuration fitted to the 14˚ conical diffuser with a 600 mm long outlet duct.

5.5.3 Outlet Duct Length Variation

The overall acoustic performance of each of the outlet configurations investigated has been heavily dependent on the length of the outlet duct fitted to each respective conical diffuser and outlet grill. To better understand this relationship a direct comparison between outlet duct lengths will be made for a range of conical diffuser angles and outlet termination grills. The first and most simple comparison involves the variation of the outlet duct length for a constant conical diffuser angle without the added complexity of an outlet grill (the open ended duct case). The secondary effects of then coupling various outlet duct lengths with different termination grills will also be included.

The linear SPL for each of the 7˚, 10˚ and 14˚ conical diffusers, each fitted with an open ended 300, 600 and 900 mm long outlet duct are shown in Figures 5.35, 5.36 and 5.37 respectively. In the case of the 7˚ conical diffuser there is negligible variation between the SPL for the 300 and 600 mm long outlet ducts (open ended). The 900 mm long duct has a SPL up to 4 dB higher, with the effect more pronounced at higher jet velocities.

For the 10˚ conical diffuser the SPL for the 600 and 900 mm long outlet ducts are almost identical across the jet velocity range of interest, while the 300 mm long outlet duct produces a slightly lower SPL (up to 3 dB lower). This difference is less pronounced in the lower jet velocity ranges of 20 to 30 ms^{-1}. The linear SPL for the 10˚ diffuser models is also several dB higher than the same corresponding 7˚ diffuser models.

In the case of the 14˚ diffuser the 300 mm long duct is still the preferred length, however the relative performance of the 600 and 900 mm long ducts is reversed. The 900 mm long duct is 1 to 3 dB lower than the 600 mm long duct and 1 to 2 dB higher than the 300 mm long duct. The gap between the 600 and 900 mm ducts widens at jet velocities above 40 ms^{-1}, but this is beyond the likely range of practical applications. The variation in SPL with outlet duct length is considerably diminished in the 20 to 30 ms^{-1} jet velocity range of interest.

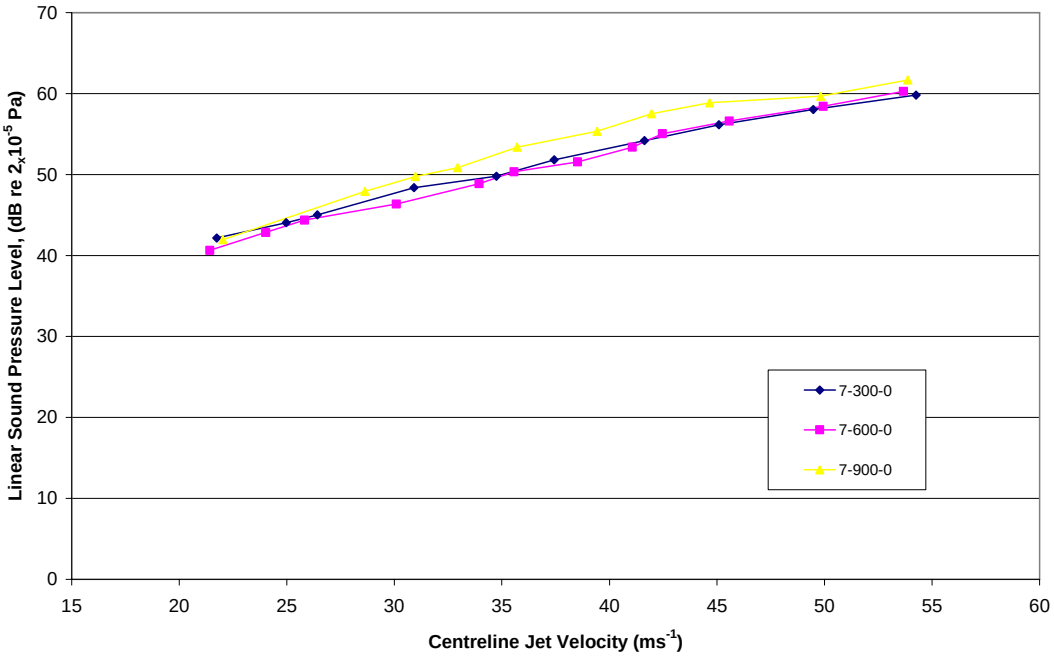

Figure 5.35: Linear SPL comparison for the 7˚ conical diffuser fitted with an open ended 300, 600 and 900 mm long outlet duct.

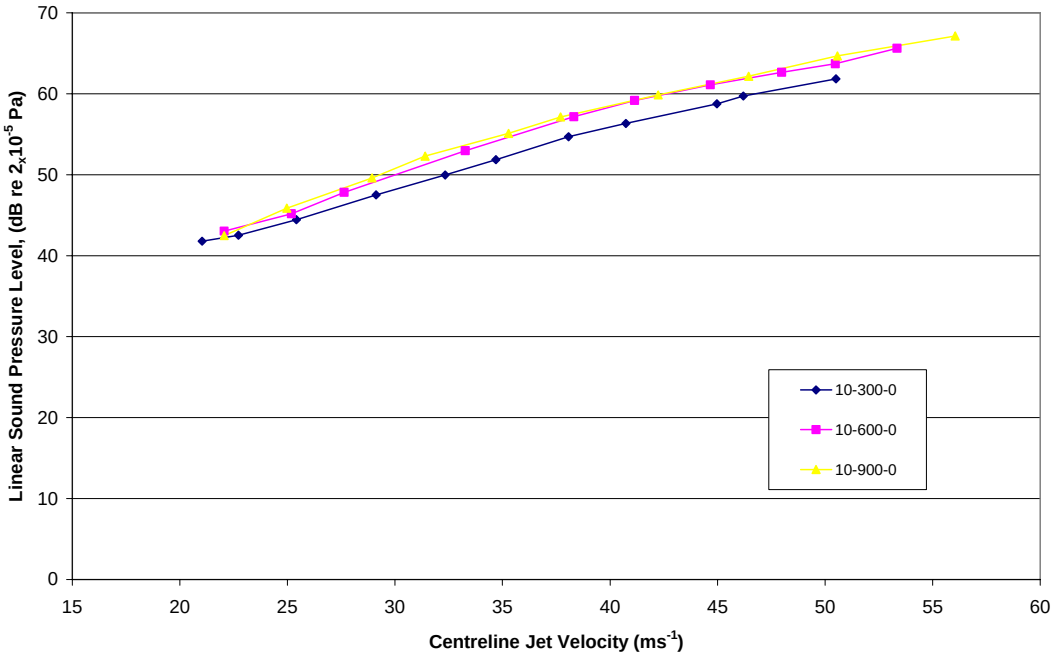

Figure 5.36: Linear SPL comparison for the 10˚ conical diffuser fitted with an open ended 300, 600 and 900 mm long outlet duct.

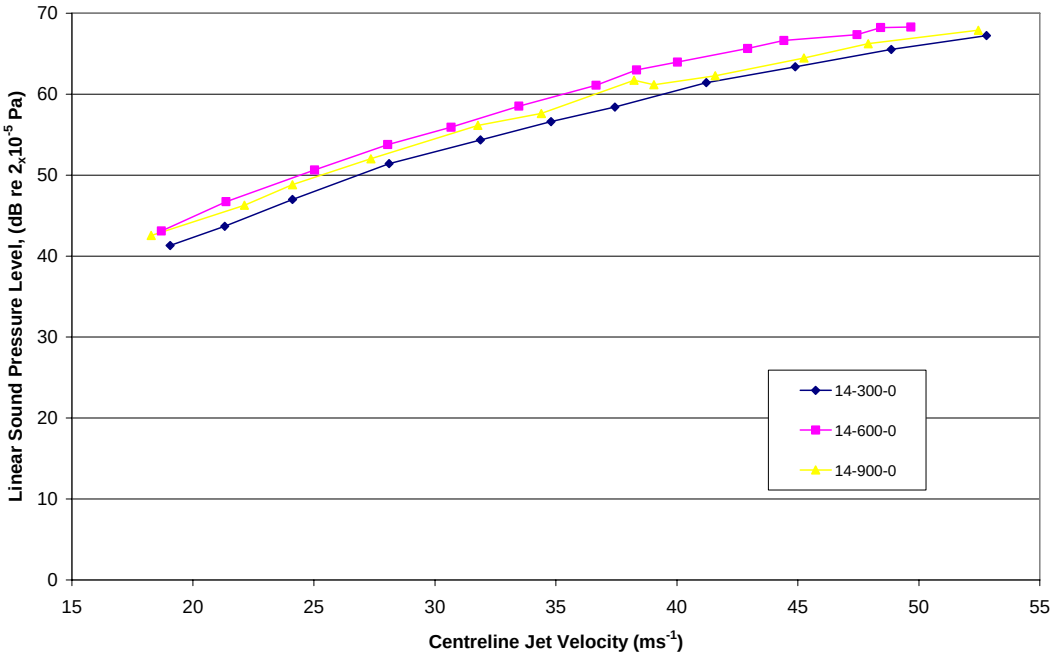

Figure 5.37: Linear SPL comparison for the 14˚ conical diffuser fitted with an open ended 300, 600 and 900 mm long outlet duct.

The impact of the duct length on the SPL has been clearly identified, however the secondary effects resulting from coupling the outlet duct to a termination grill must also be considered. To isolate the effects of the diffuser angle and the selection of the outlet termination grill, comparisons can be made, while keeping each of these variables constant. In the interest of minimising the complexity of the models, the two standard outlet grills (RJ and SD) were selected for this exercise.

The first comparison is made using the RJ grill fitted to the 7˚, 10˚ and 14˚ conical diffuser and an outlet duct length of 0, 300, 600 and 900 mm (shown in Figures 5.38, 5.39 and 5.40 respectively). Two very significant conclusions are immediately visible when looking at these plots. Firstly there is a significant drop (8 to 10 dB) in the SPL with the addition of an outlet duct of any length over fitting the RJ grill directly onto the conical diffuser (0 mm outlet duct). This effect is quite consistent for all three of the diffuser angles considered.

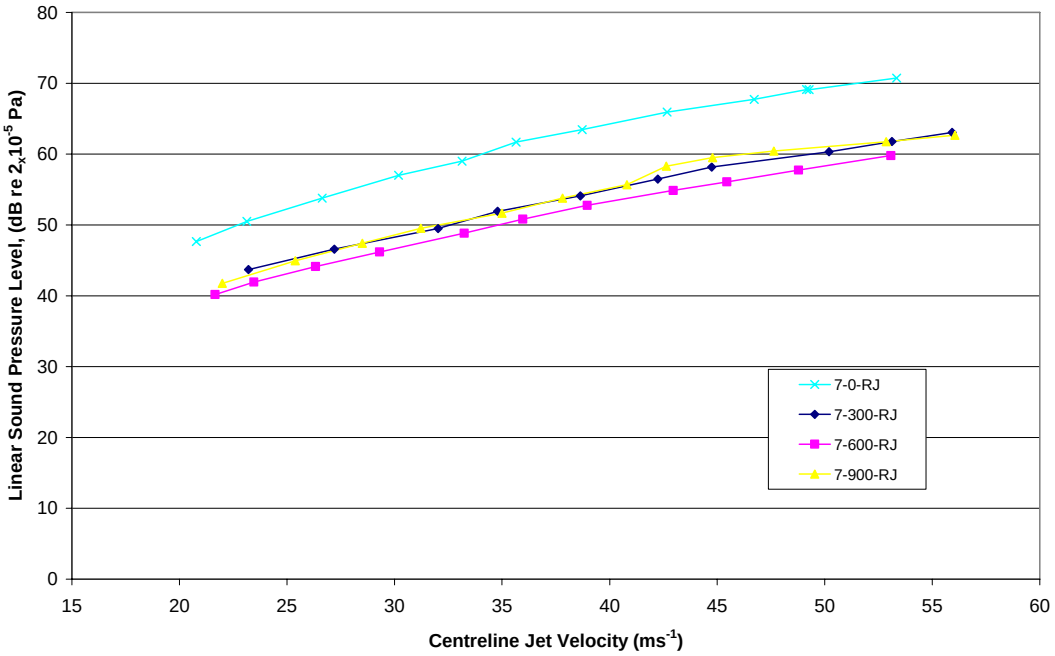

Figure 5.38: Linear SPL comparison for the 7˚ conical diffuser fitted with the round jet (RJ) outlet grill with an extended outlet duct of 0, 300, 600 and 900 mm.

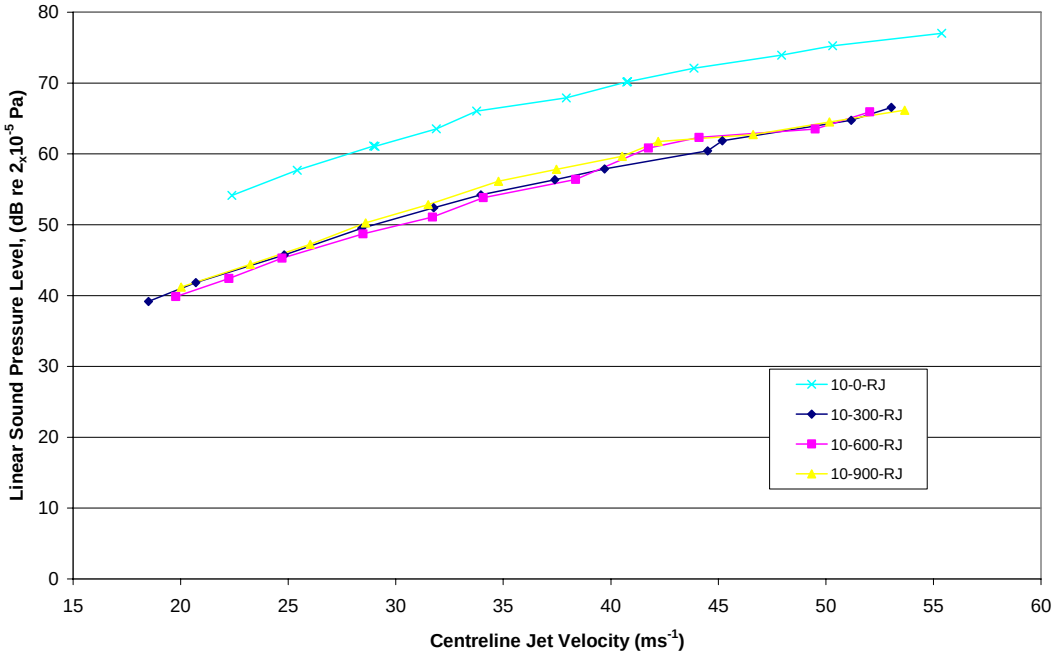

Figure 5.39: Linear SPL comparison for the 10˚ conical diffuser fitted with the round jet (RJ) outlet grill with an extended outlet duct of 0, 300, 600 and 900 mm.

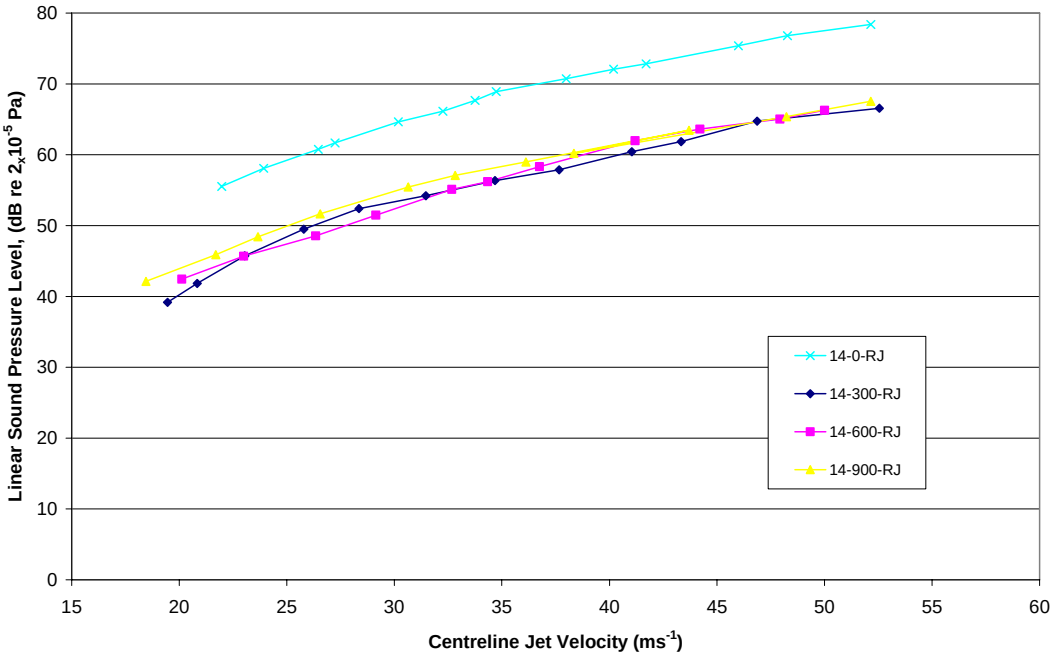

Figure 5.40: Linear SPL comparison for the 14˚ conical diffuser fitted with the round jet (RJ) outlet grill with an extended outlet duct of 0, 300, 600 and 900 mm.

The second observation is the immergence of the 600 mm duct as being the preferred outlet duct length (out of the four lengths investigated) with a better or equal acoustic performance to that of the 300 mm long outlet duct. For all three diffuser angles studied there is no evidence to suggest that a 900 mm long duct should be used. Given that the 300 and 600 mm duct lengths provide equal or better performance there is no need to add additional costs or weight.

The corresponding results for the SD outlet grill are shown in Figures 5.41, 5.42 and 5.43, where very similar trends can be clearly seen. The effect of adding the outlet duct to the conical diffuser is once again very pronounced, although the impact on the 7˚ conical diffuser is slightly less. For all three diffuser angles considered the 600 mm long outlet duct either produced the lowest or equal lowest SPL across the entire jet velocity range of interest.

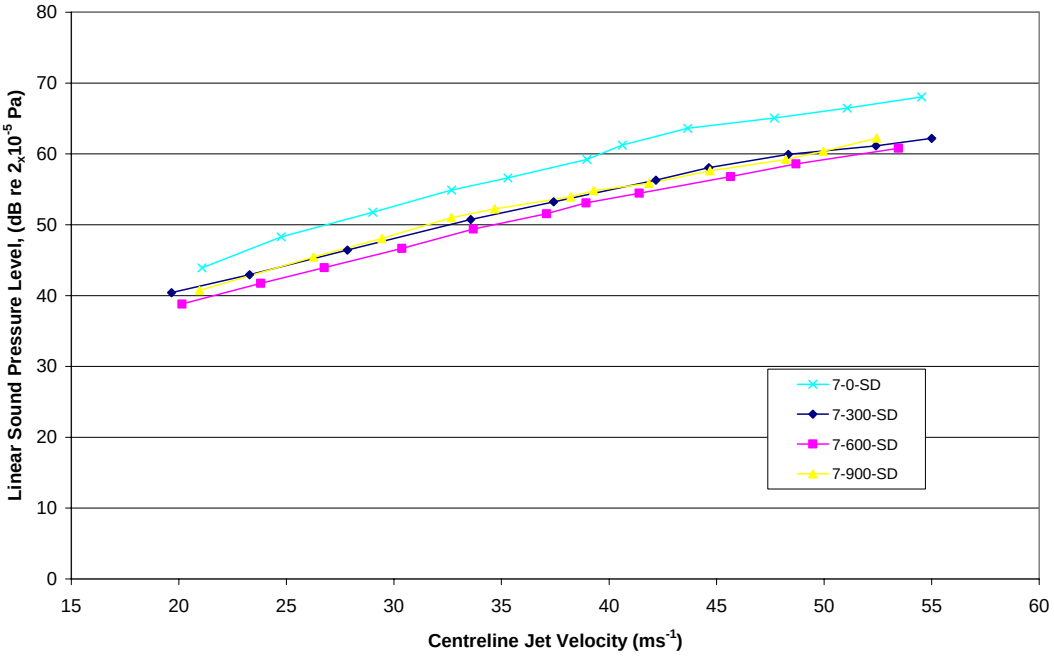

Figure 5.41: Linear SPL comparison for the 7˚ conical diffuser fitted with the square (SD) outlet grill with an extended outlet duct of 0, 300, 600 and 900 mm.

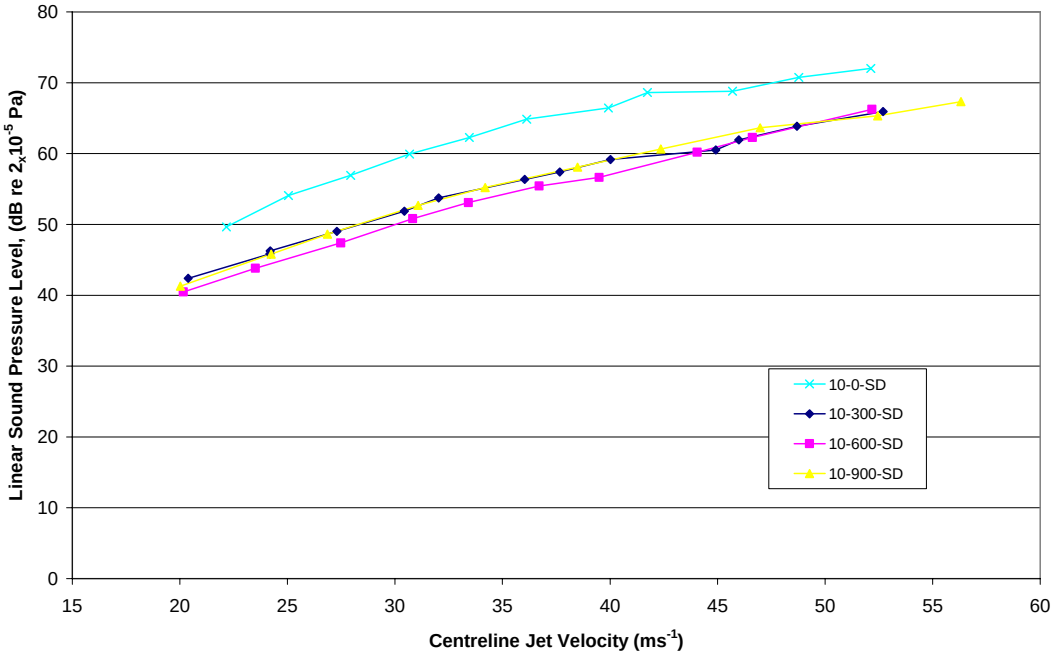

Figure 5.42: Linear SPL comparison for the 10˚ conical diffuser fitted with the square (SD) outlet grill with an extended outlet duct of 0, 300, 600 and 900 mm.

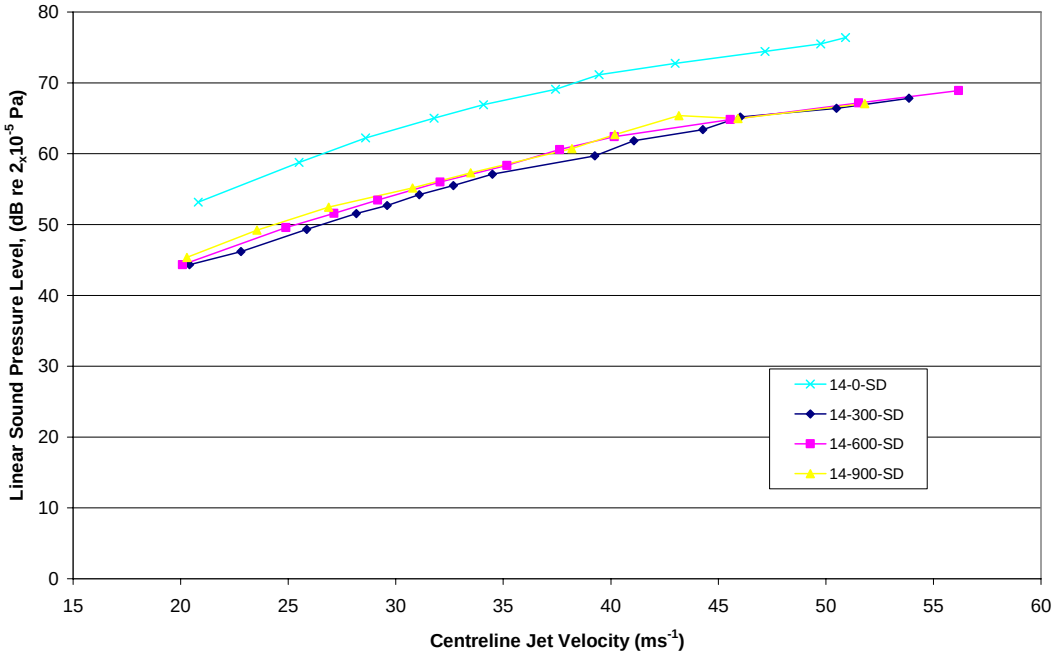

Figure 5.43: Linear SPL comparison for the 14˚ conical diffuser fitted with the square (SD) outlet grill with an extended outlet duct of 0, 300, 600 and 900 mm.

In summary the 7˚conical diffuser provided the lowest SPL, with the 10˚ and 14˚ diffusers leading to a progressive increase across the entire jet velocity band of interest. An outlet duct length of 600 mm was also found to be the preferred length. However, where necessary a shorter duct length of 300 mm may also be used with minimal impact on the acoustic performance of the outlet.

5.6 Total Sound Power Level Analysis

The acoustic properties of the reverberation suite are quite different from those encountered in a standard passenger cabin space on board ocean going fast ferries. Therefore any comparison needs to be made in terms of the sound power; an absolute reference to the total acoustic energy, rather than the sound pressure level which is also dependent on the acoustic properties of the space used. By design the reverberation rooms are very reflective, which supports the establishment of a strong reverberant sound field in addition to the direct sound field created by the HVAC flows. In contrast to this arrangement a typical passenger cabin space is lined with materials that have a relatively high acoustic absorption (carpet, padding and ceiling tiles), which leads to a much weaker reverberant sound field. Therefore the total sound pressure level measured in a passenger space will be somewhat lower than the sound pressure level measured in the reverberation suite. By reporting the results in terms of absolute sound power levels a true understanding of the acoustic energy created by the HVAC flow field can be developed. This can then be used to predict the corresponding sound pressure field for a given set of known acoustic properties of a real passenger cabin application.

Each of the sound power level results has been presented with a log scale for velocity (V) - 10 to 100 ms^{-1} - and a common dB scale of 0 to 80 dB (re 10^{-12} W). This scale has been chosen to allow ready reference to the respective power law relationships governing the sound power level and the velocity of the jet. The dB rise across the x-axis scale can be directly related to the slope of the log (V) line in terms of the total sound power level. This slope can then be used to assess the primary mode of sound generation for each geometric outlet configuration.

5.6.1 Variation of Sound Power Level with Conical Diffuser Angle

The effects of the conical diffuser angle on the sound power level for a selected range of outlet configurations was evaluated, firstly with no outlet termination grill and then with each of the four outlet grill configurations outlined previously. The three initial cases for an opened duct of 300, 600 and 900 mm length are shown in Figures 5.44, 5.45 and 5.46 respectively. For the short outlet duct of 300 mm the 7˚ and 10˚ cases follow a 50logV line with a minor increase in the slope at jet velocities above 35 ms^{-1}. As the outlet duct length is increased to 600 mm the point at which the slope of the sound power line increases occurs at a lower jet velocity of only 25 ms^{-1}, with the increase in slope more pronounced for the 10˚ diffuser. At an outlet duct length of 900 mm the slope of the line for the 10˚ diffuser is more in line with the 14˚ diffuser across the whole velocity range, while a minor inflection point remains for the 7˚ case. The 14˚ diffuser meanwhile follows a consistent 60logV slope across the entire jet velocity range considered for each outlet duct length.

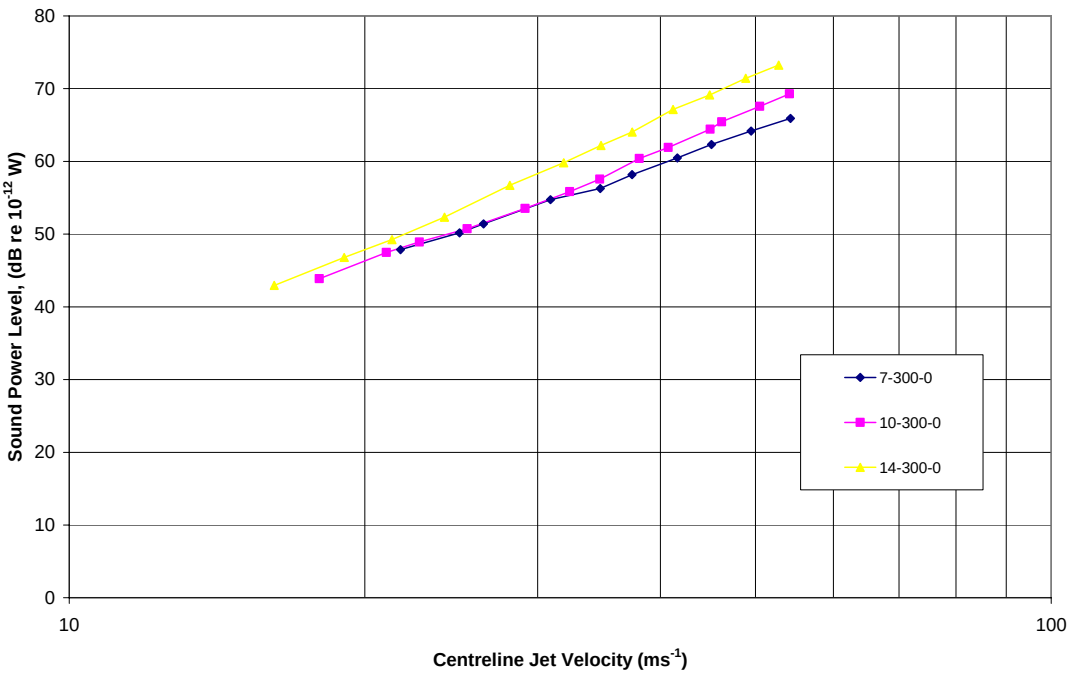

Figure 5.44: Sound power level comparison for conical diffuser angles of 7˚, 10˚ and 14˚ – fitted with an open ended 300 mm long outlet duct.

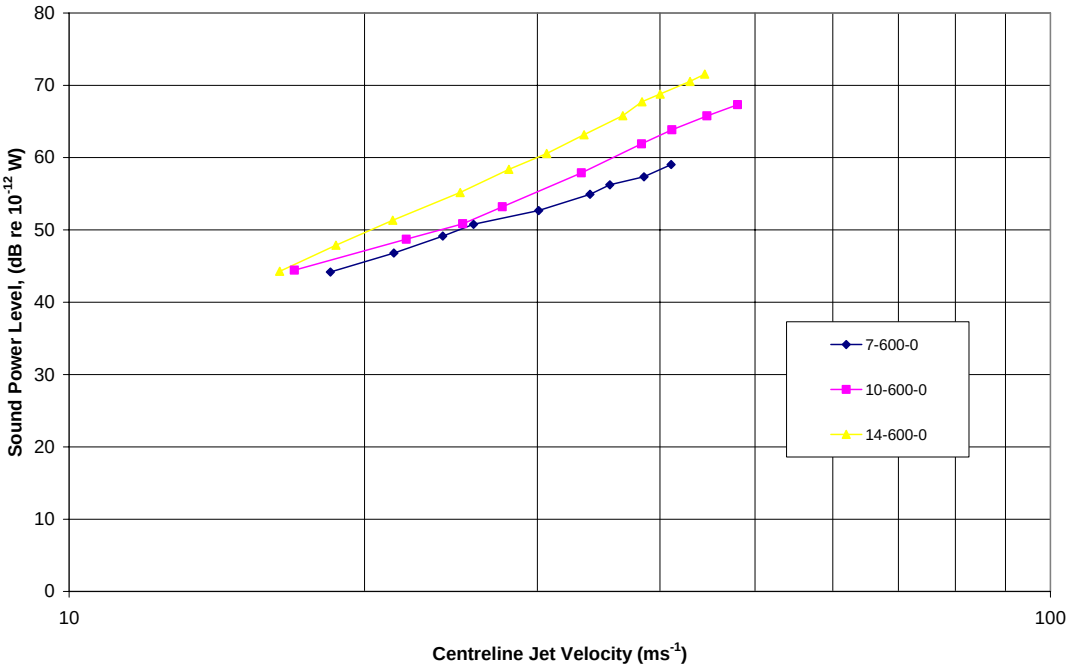

Figure 5.45: Sound power level comparison for conical diffuser angles of 7˚, 10˚ and 14˚ – fitted with an open ended 600 mm long outlet duct.

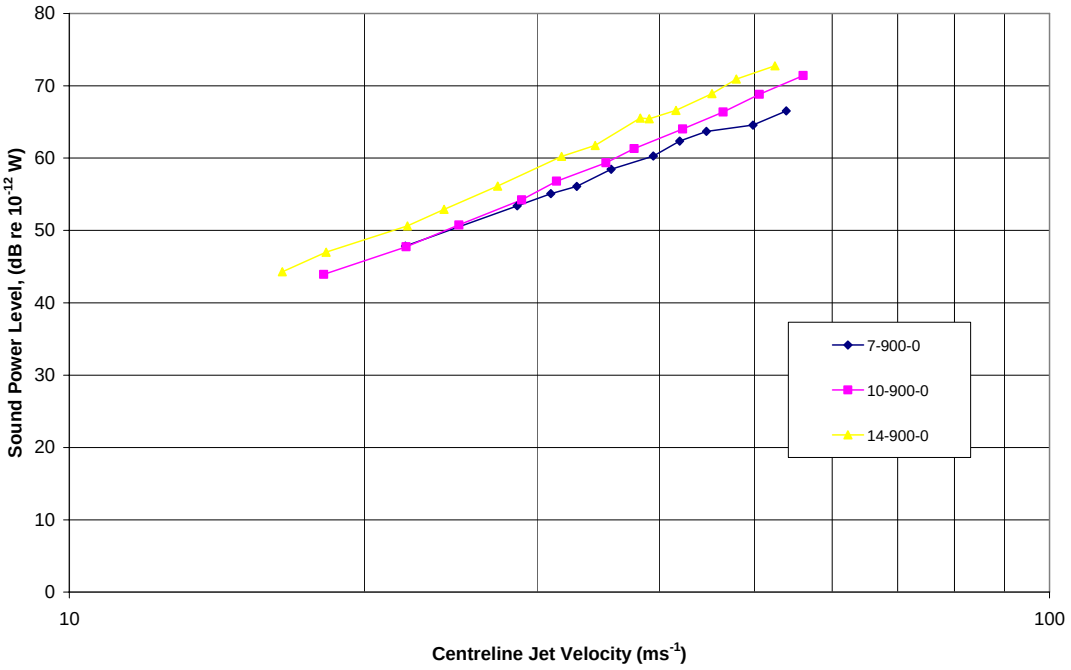

Figure 5.46: Sound power level comparison for conical diffuser angles of 7˚, 10˚ and 14˚ – fitted with an open ended 900 mm long outlet duct.

The impact of adding the four outlet termination grill configurations was investigated, focusing on the key outlet duct lengths of 300 and 600 mm. This decision was made given that the results for the 900 mm outlet duct showed it to be far less effective in reducing the level of flow induced noise. The results for the round jet termination grill (RJ) fitted to the 300 and 600 mm outlet ducts are shown in Figures 5.47 and 5.48 respectively. Figures 5.49 and 5.50 cover the square diffuser grill (SD), and the cushion head mounted SD grill (CH) cases are shown in Figures 5.51 and 5.52. The results for the two cases using the 90˚ elbow (ELCH) fitted into the CH configuration are then shown in Figures 5.53 and 5.54.

For all four outlet termination grill selections the 7˚ diffuser tended to follow a 50logV line while the 10˚ and 14˚ diffuser cases were more closely aligned with a 60logV line. The largest divergence between the two occurred with the RJ outlet fitted to the 600 mm long outlet duct at jet velocities over 40 ms^{-1}. The sound power level for each of the outlet configurations studied was very similar with a minor reduction observed when using a duct length of 600 mm over the shorter length of 300 mm.

The sound power produced by an ideal dipole acoustic source follows a 60logV line, while an ideal quadrupole source will follow an 80logV line. Based on this theory one could attribute the bulk of the 60logV cases being caused by strong dipole sources (surface generated flows) as opposed to quadrupole sources (shear flows). However experimental validation work has found that a true dipole source struggles to get much over the 50logV line due to losses in converting the flow energy into the radiated acoustic field. A similar result is also found with quadrupole sources, where an 80logV line is seldom measured experimentally. The 50logV line found using the 7˚ diffuser suggest a strong presence of wall bounded flow generated noise (little or no flow separation) from dipole sources. The strong 60logV relationship found with the 10˚ and 14˚diffusers can be interpreted as having a significant quadrupole source component, which is therefore indicative of flow separation and shear flow based noise generation. The slight increase in slope as the diffuser angle is increased from 10˚ to 14˚ is also supportive of this conclusion. The upward shift seen in the slope of the sound power level curve above critical jet velocities further reinforces this view.

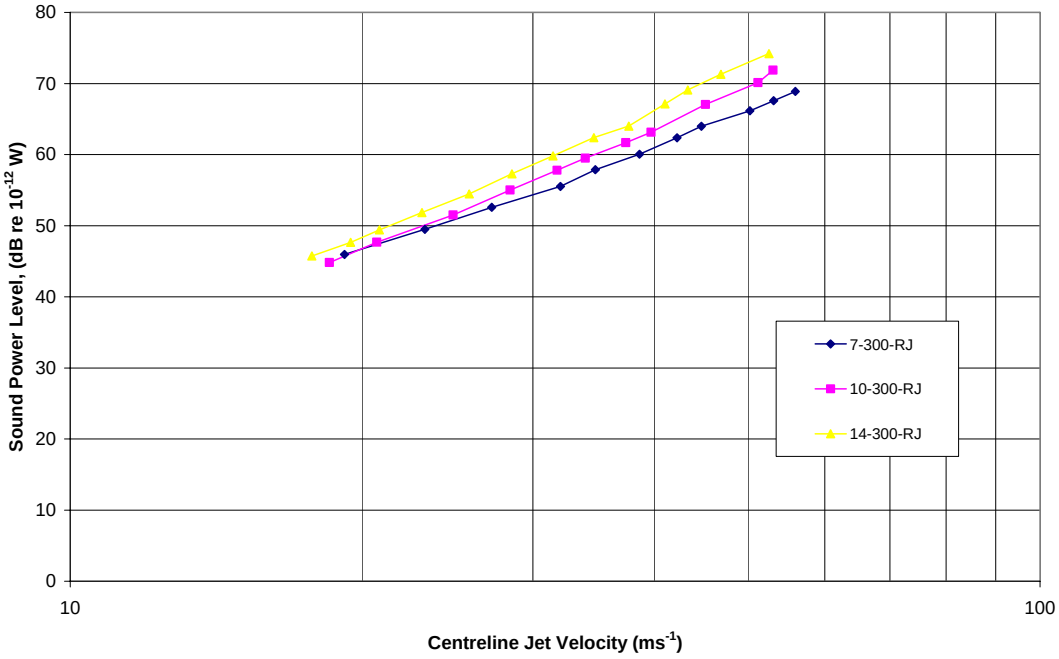

Figure 5.47: Sound power level comparison for conical diffuser angles of 7˚, 10˚ and 14˚ – with a 300 mm long outlet duct fitted with the round jet outlet grill.

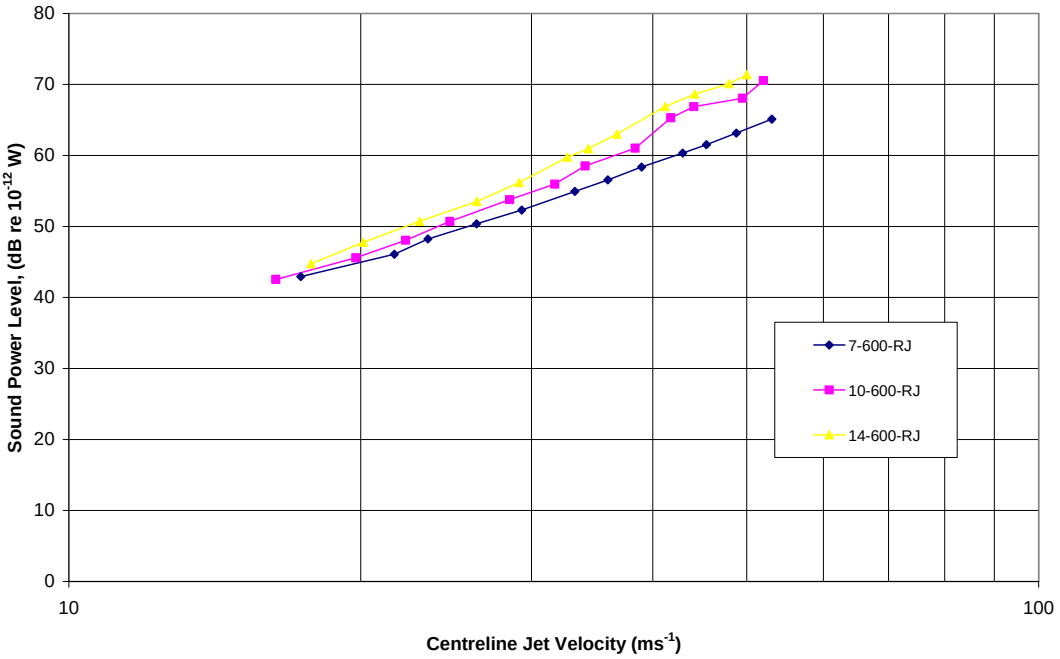

Figure 5.48: Sound power level comparison for conical diffuser angles of 7˚, 10˚ and 14˚ – fitted with a 600 mm long outlet duct fitted with the round jet outlet grill.

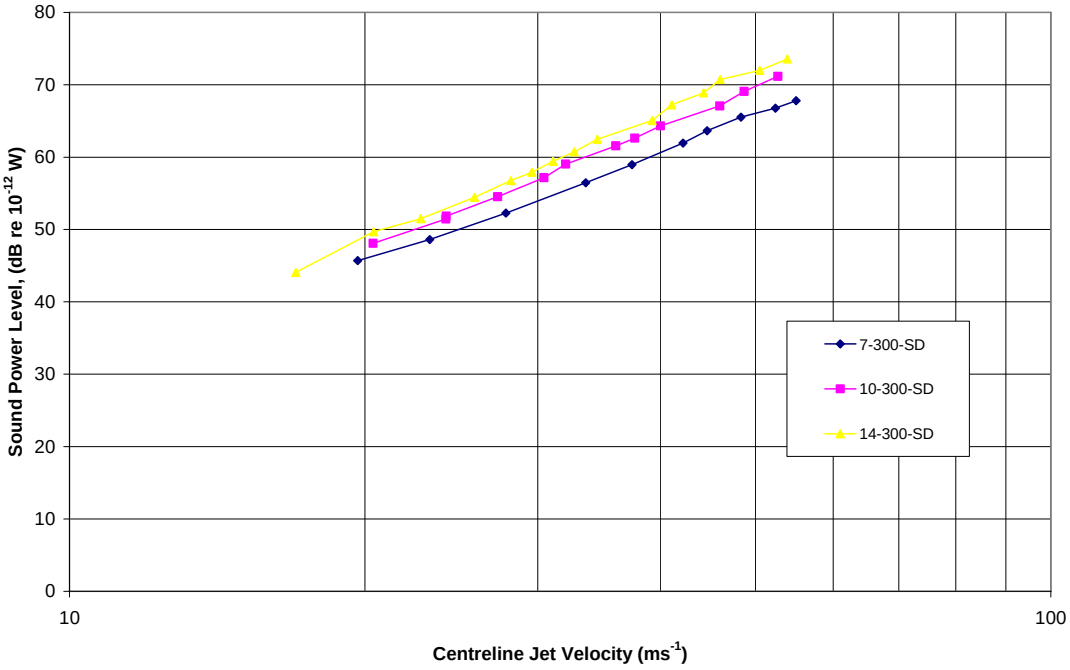

Figure 5.49: Sound power level comparison for conical diffuser angles of 7˚, 10˚ and 14˚ – with a 300 mm long outlet duct fitted with the square diffuser outlet grill.

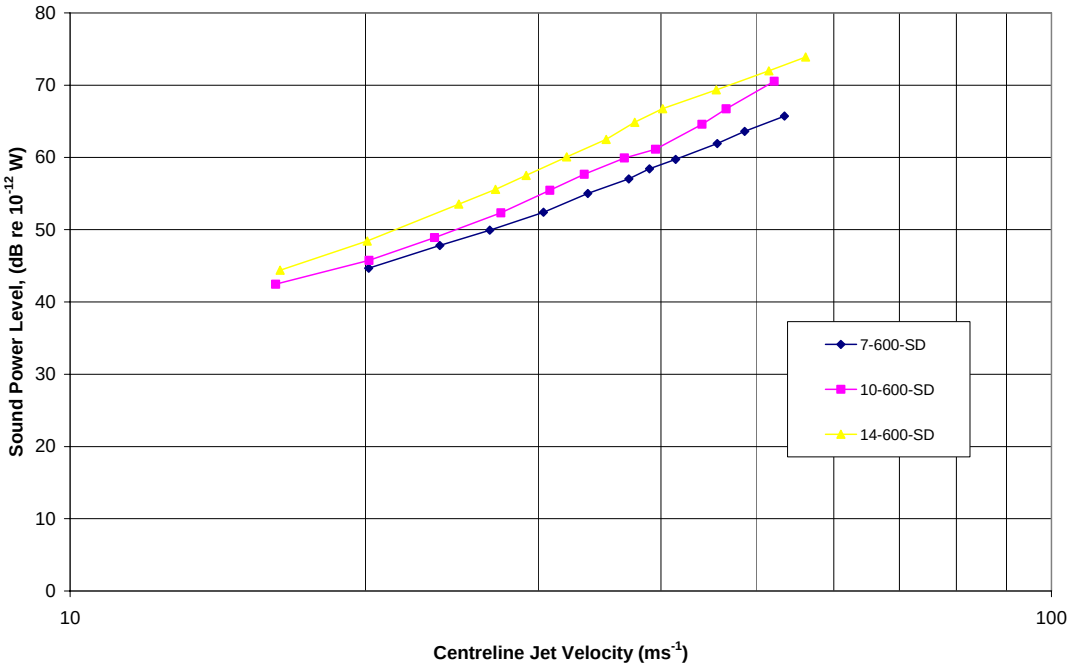

Figure 5.50: Sound power level comparison for conical diffuser angles of 7˚, 10˚ and 14˚ – with a 600 mm long outlet duct fitted with the square diffuser outlet grill.

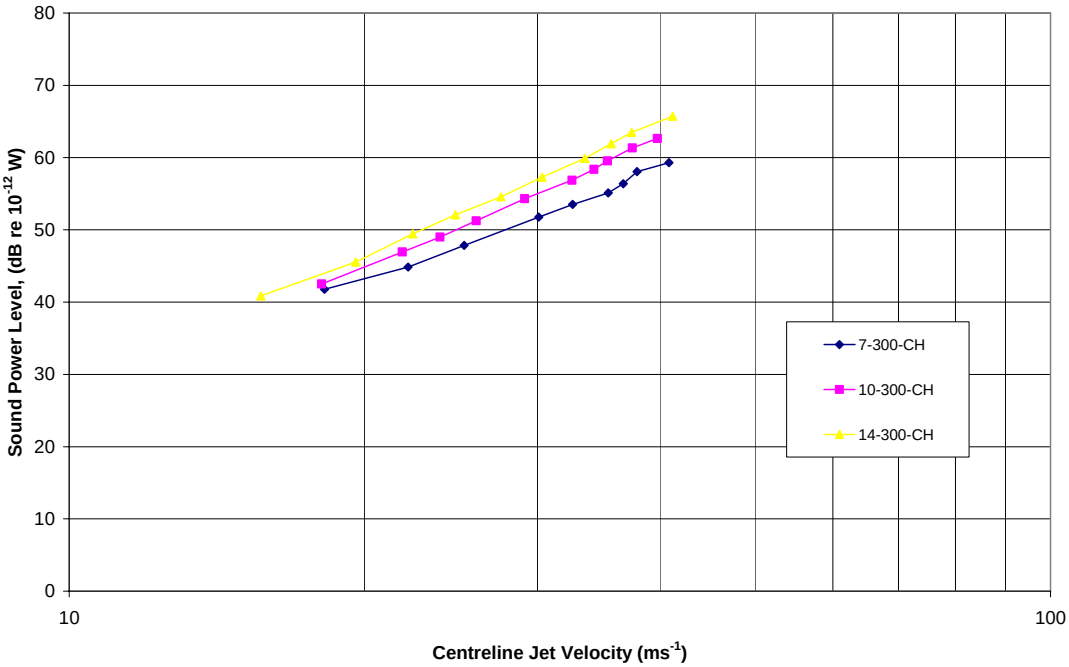

Figure 5.51: Sound power level comparison for conical diffuser angles of 7˚, 10˚ and 14˚ – with a 300 mm long outlet duct fitted with the cushion head mounted SD outlet.

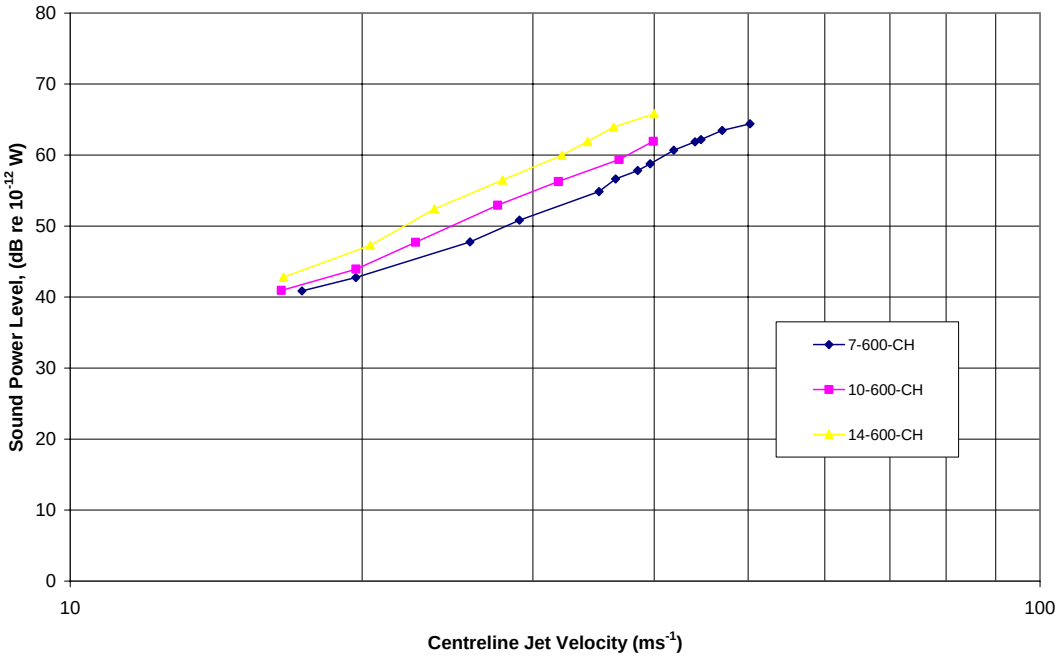

Figure 5.52: Sound power level comparison for conical diffuser angles of 7˚, 10˚ and 14˚ – with a 600 mm long outlet duct fitted with the cushion head mounted SD outlet grill.

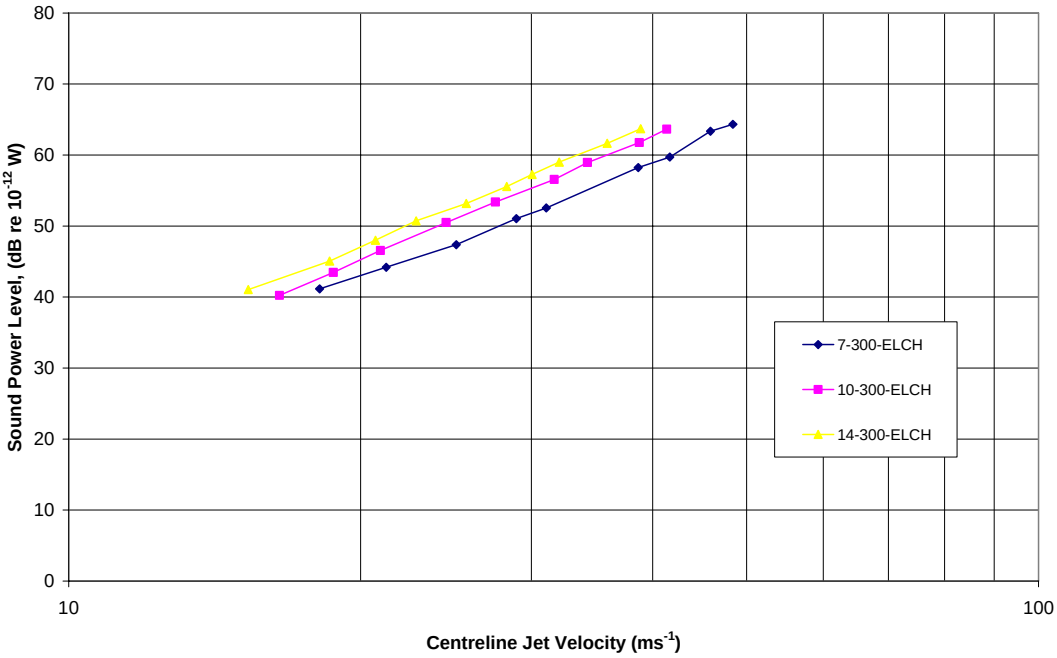

Figure 5.53: Sound power level comparison for conical diffuser angles of 7˚, 10˚ and 14˚ – with a 600 mm long outlet duct fitted with the ELCH outlet grill.

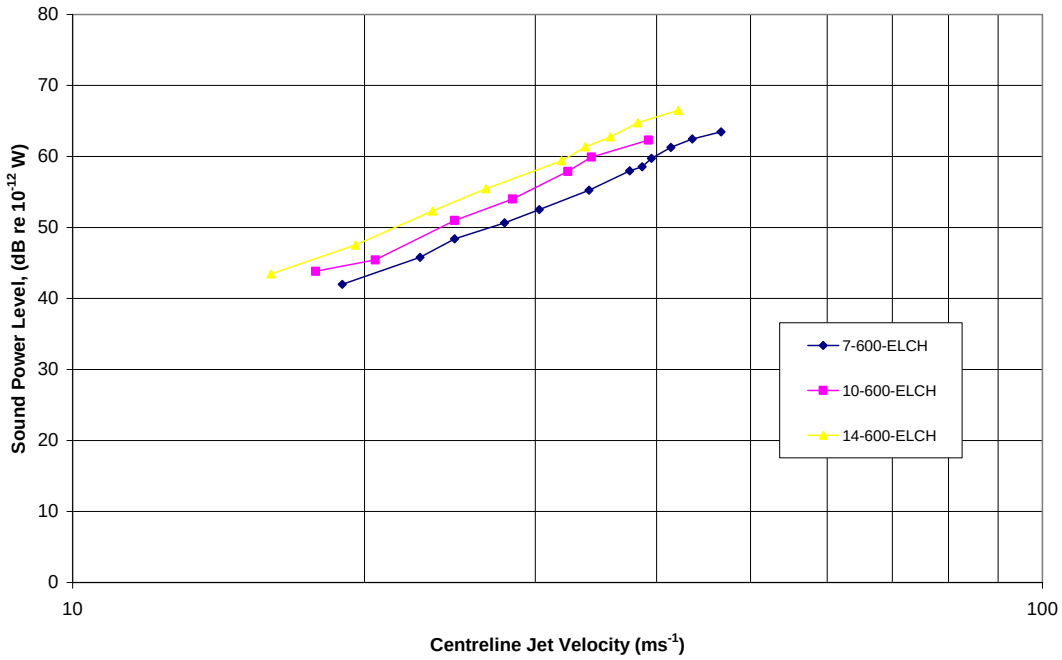

Figure 5.54: Sound power level comparison for conical diffuser angles of 7˚, 10˚ and 14˚ – with a 600 mm long outlet duct fitted with the ELCH outlet grill.

5.6.2 Variation of Sound Power Level with Outlet Termination Configuration

The configuration of the outlet termination grill was found to significantly affect the perceived acoustic performance (in terms of the sound pressure level) of the outlet as a whole. Therefore it is important to complete a further analysis in terms of the absolute sound power generated by each outlet configuration. The first and simplest comparison is made with the round jet and square diffuser grills fitted directly onto each of the 7˚, 10˚ and 14˚ conical diffusers as shown in Figures 5.55, 5.56 and 5.57 respectively. In all three cases the SD grill out performed the RJ grill, with the largest difference of 4 to 5 dB occurring with the 7˚ and 10˚ conical diffusers. The gap between the RJ and SD grill narrowed significantly to only 1 to 2 dB with the 14˚ conical diffuser.

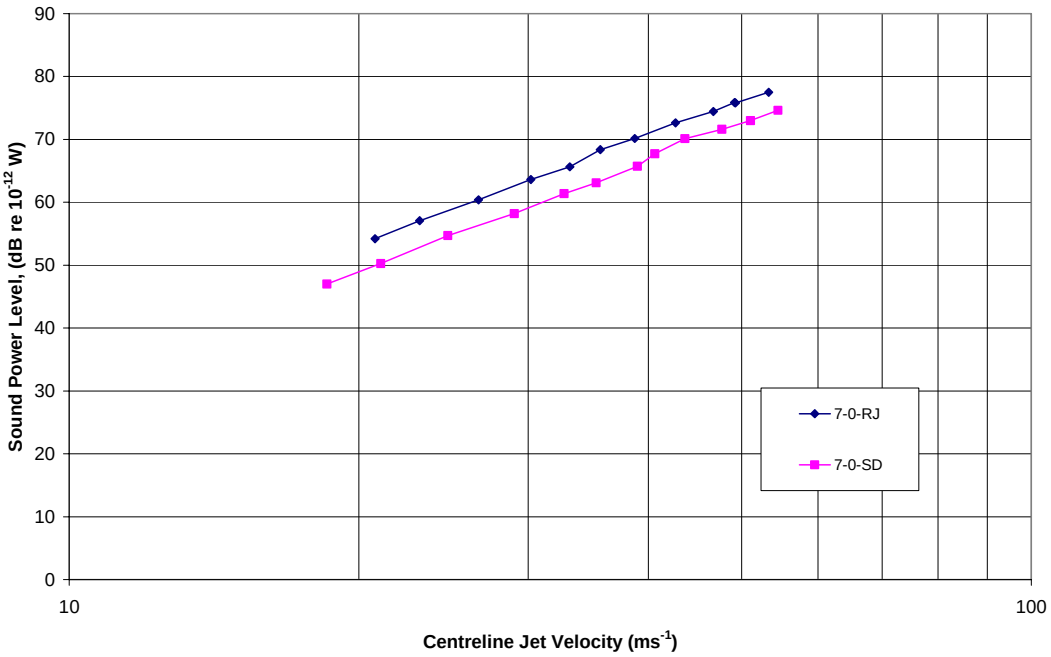

Figure 5.55: Sound power level comparison between the round jet (RJ) and square (SD) outlet termination grills fitted directly to the 7˚ conical diffuser.

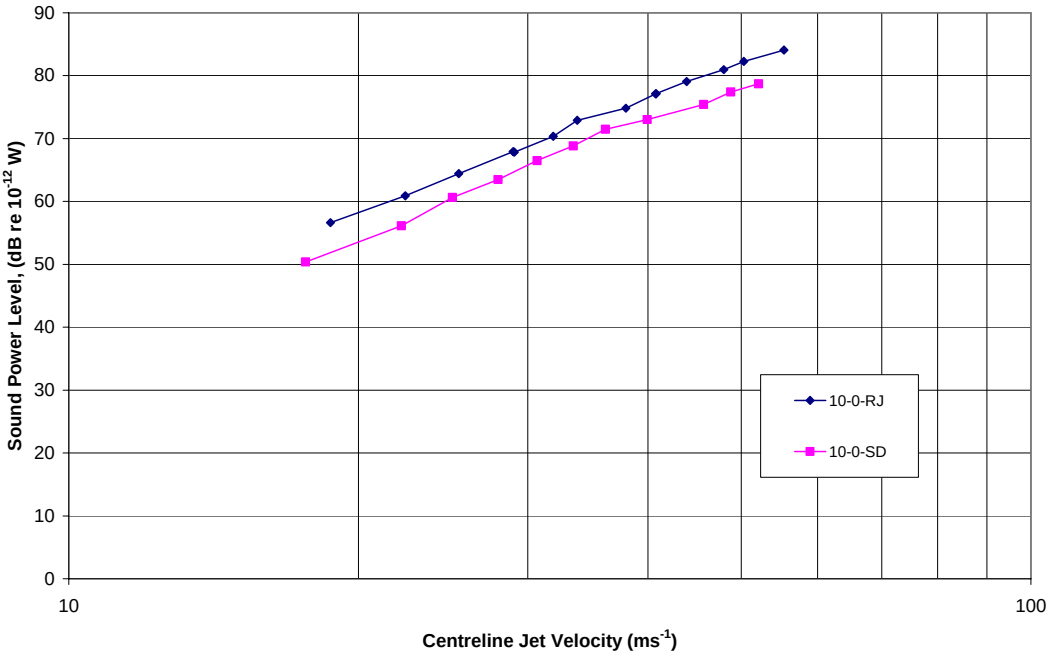

Figure 5.56: Sound power level comparison between the round jet (RJ) and square (SD) outlet termination grills fitted directly to the 10˚ conical diffuser.

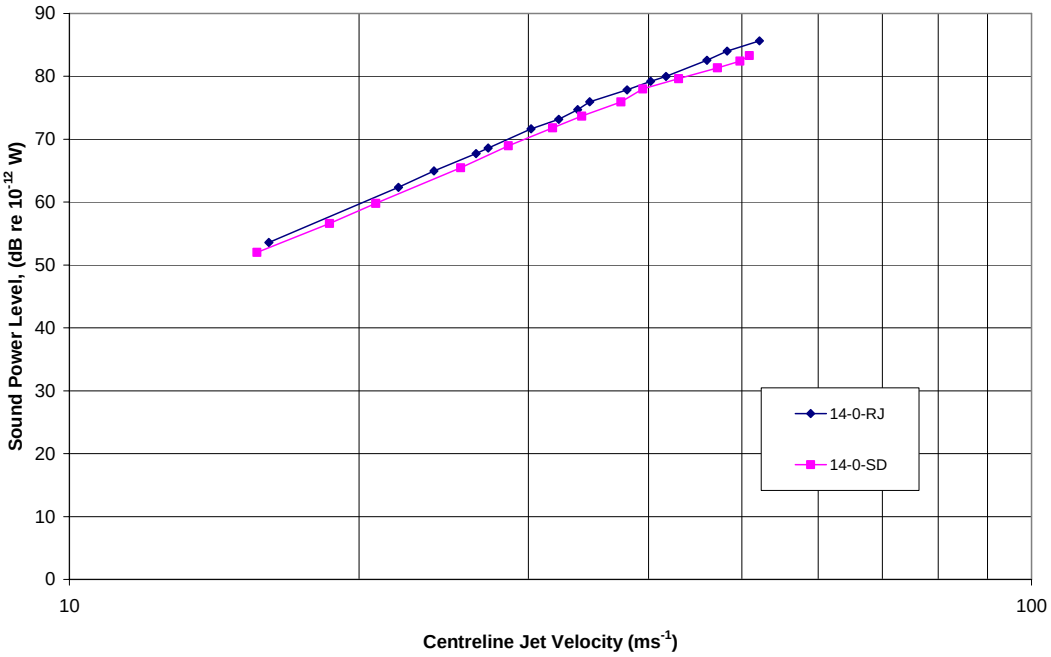

Figure 5.57: Sound power level comparison between the round jet (RJ) and square (SD) outlet termination grills fitted directly to the 14˚ conical diffuser.

The slope of the sound power level curve (against jet velocity) is also higher for the 14˚, at 55 (55logV), compared to only 50 (50logV) for both the 7˚ and 10˚conical diffusers. All three curves have a consistent slope across the velocity range considered of 20 to 50 ms^{-1}. The addition of the outlet grills has however reduced the slope of the curves from the 60logV levels seen in the models with no outlet grills fitted. Therefore it may be concluded that the grills do make some reduction in the level of flow separation and the subsequent generation of quadrupole noise sources.

The effect of each of the outlet grills on the total sound power level, when used in conjunction with an extended outlet duct was investigated, beginning with the 300 mm long outlet duct fitted to each of the conical diffusers. The results for the 7˚, 10˚ and 14˚ conical diffusers are shown in Figures 5.58, 5.59 and 5.60 respectively. For the 7˚ diffuser the CH and ELCH outlet configurations both provided significant improvements in the sound power level, especially in the important 20 to 30 ms^{-1} jet velocity range. The SD and RJ outlet grills are both very similar to the baseline case of no outlet grill in the 20 to 30 ms^{-1} velocity range and worse by 1 to 2 dB at higher jet velocities. The slope of each curve is in the range of 40 to 50 (40logV to 50logV) for the lower jet velocity band of 20 to 30 ms^{-1}, and at jet velocities above this level there is a distinct increase in slope to the 55 to 60 (55logV to 60logV) level. This effect is particularly prominent in the case of the CH and ELCH outlets. The ability of these outlets to disperse the noise inducing turbulence is limited to a maximum jet velocity of the order of 30 ms^{-1}, with diminishing impact thereafter.

For the 10˚ conical diffuser each of the outlet grills perform worse than the baseline case of no outlet, with the exception of the CH and ELCH grills at jet velocities below 25 ms^{-1}. The improvement in the sound power level in this range is only in the order of 1 to 2 dB. The slope of each curve follows a very consistent 60logV line for each of the outlet grills considered.

The 14˚ conical diffuser results showed a similarly consistent slope of 60 (60logV) and the CH and ELCH grills were both 1 to 2 dB lower than both the baseline case and the remaining outlet grills (RJ and SD).

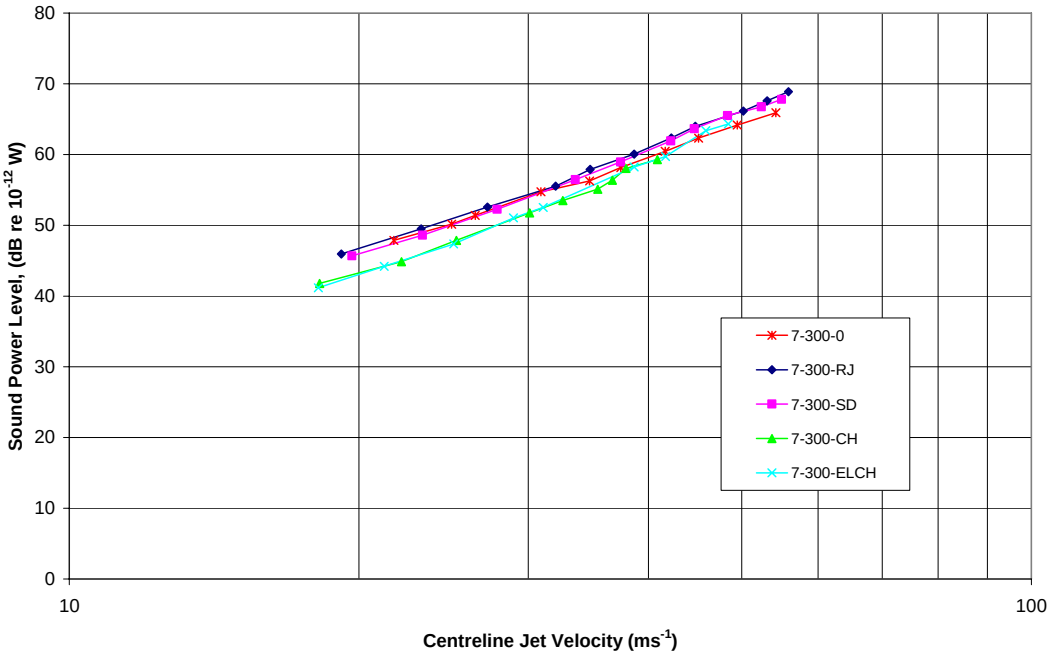

Figure 5.58: Sound power level comparison between each termination grill configuration fitted to the 7˚ conical diffuser with a 300 mm long outlet duct.

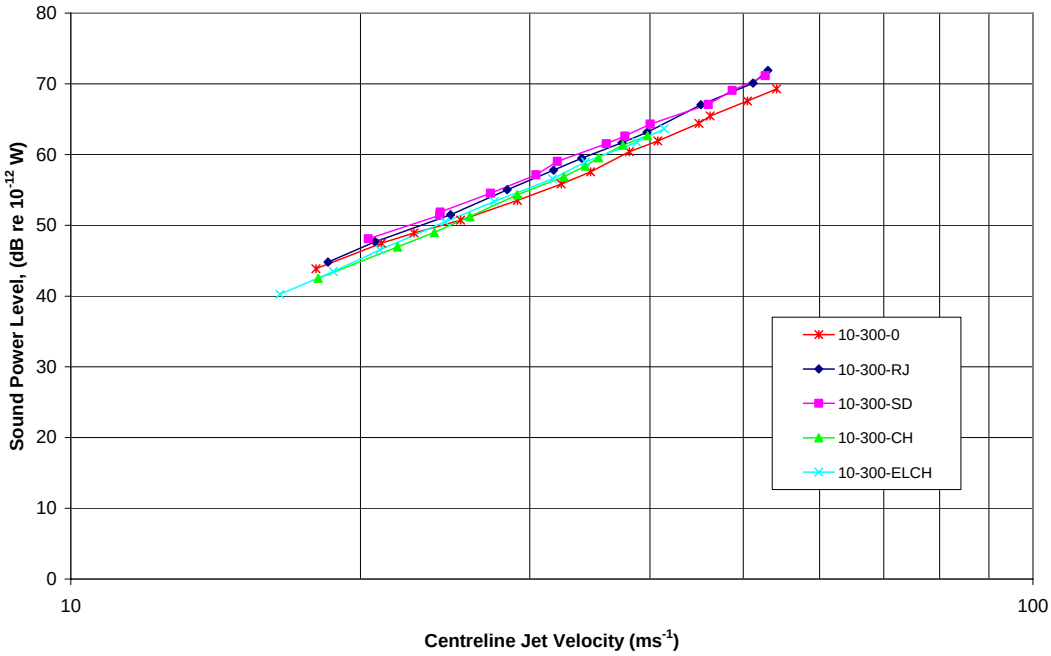

Figure 5.59: Sound power level comparison between each termination grill configuration fitted to the 10˚ conical diffuser with a 300 mm long outlet duct

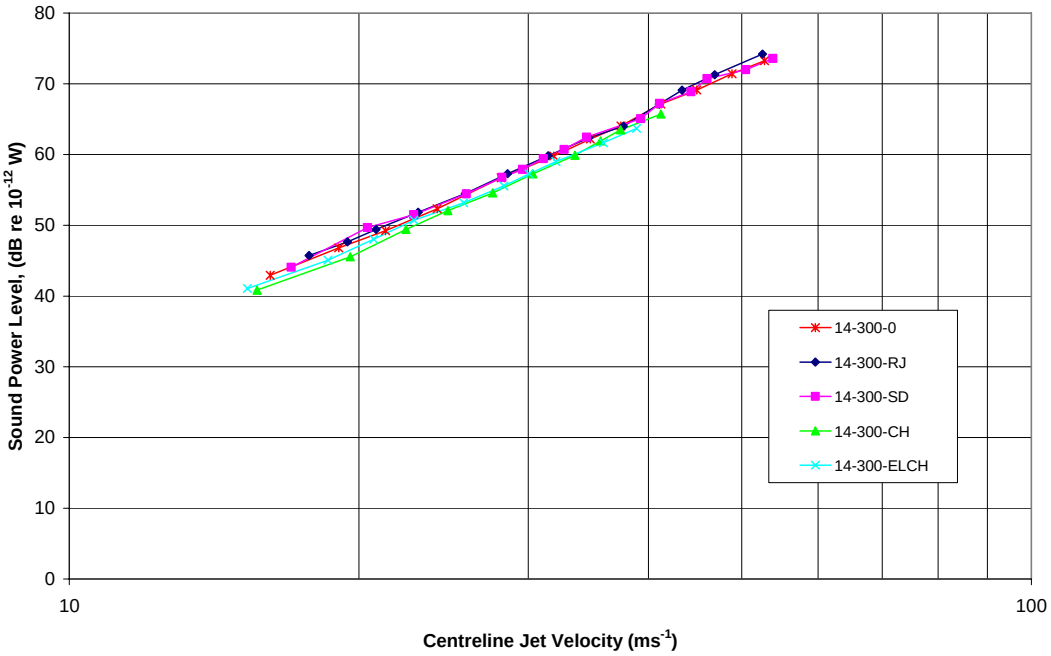

Figure 5.60: Sound power level comparison between each termination grill configuration fitted to the 14˚ conical diffuser with a 300 mm long outlet duct

The same comparison was repeated for an outlet duct length of 600 mm, with the intent to further clarify the preferred outlet duct length and grill selection. The results for the 7˚, 10˚ and 14˚ conical diffusers are shown in Figures 5.61, 5.62 and 5.63 respectively. The results are very similar to the 300 mm outlet duct cases, with CH and ELCH outlets the best performed outlet when coupled with the 7˚ conical diffuser. Once again the slope of the curve for the 7˚ diffuser starts at 40 and increases to 50 above a jet velocity of 30 ms^{-1}. Extending the outlet duct from 300 to 600 mm improved the performance of the 10˚ diffuser, with a reduction in the slope of the curve to only 45 to 50 for jet velocities below 30 ms^{-1}. The results for the 14˚ still show a consistent slope of 60 (60logV), but the extended duct length does improve the performance of each outlet over the baseline case of no outlet. A reduction in the overall sound power level of 2 to 3 dB was achieved for each of the four outlet grill configurations tested across the whole jet velocity range considered.

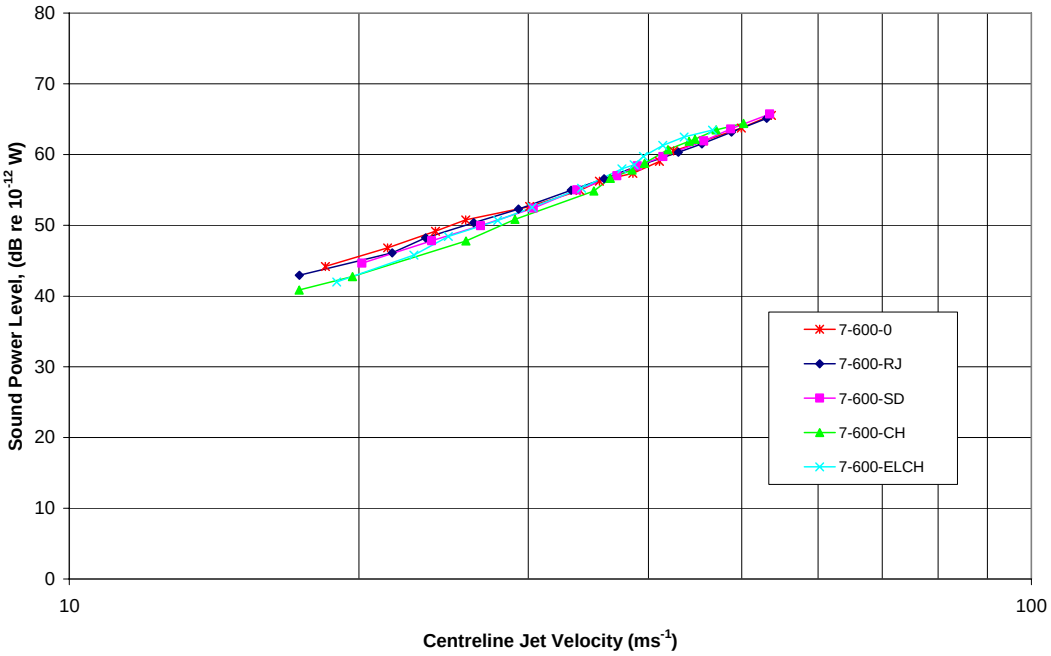

Figure 5.61: Sound power level comparison between each termination grill configuration fitted to the 7˚ conical diffuser with a 600 mm long outlet duct.

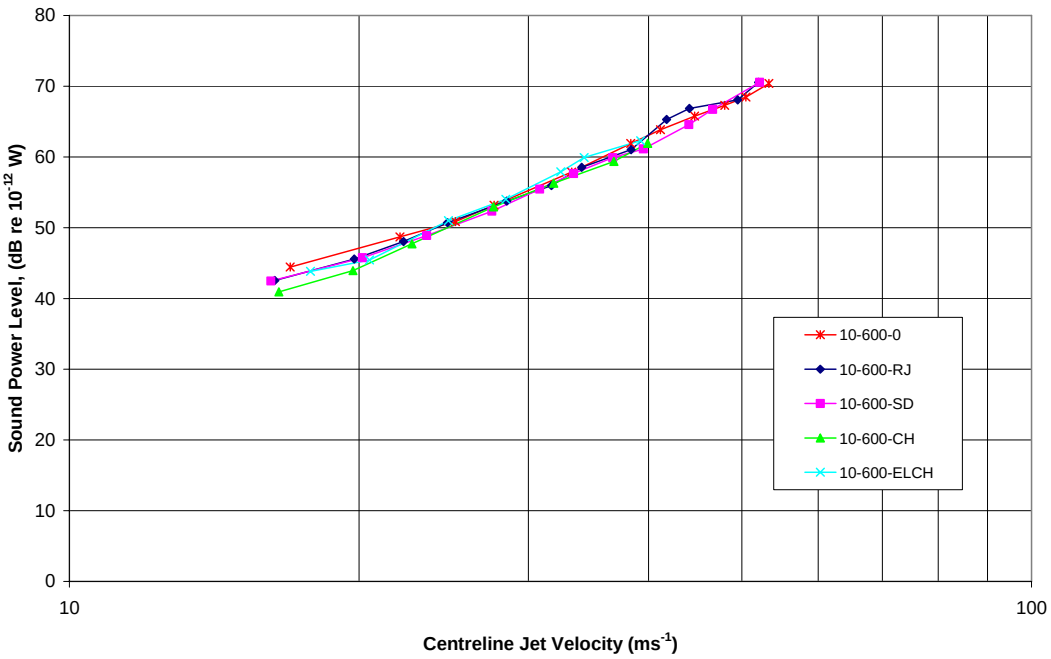

Figure 5.62: Sound power level comparison between each termination grill configuration fitted to the 10˚ conical diffuser with a 600 mm long outlet duct.

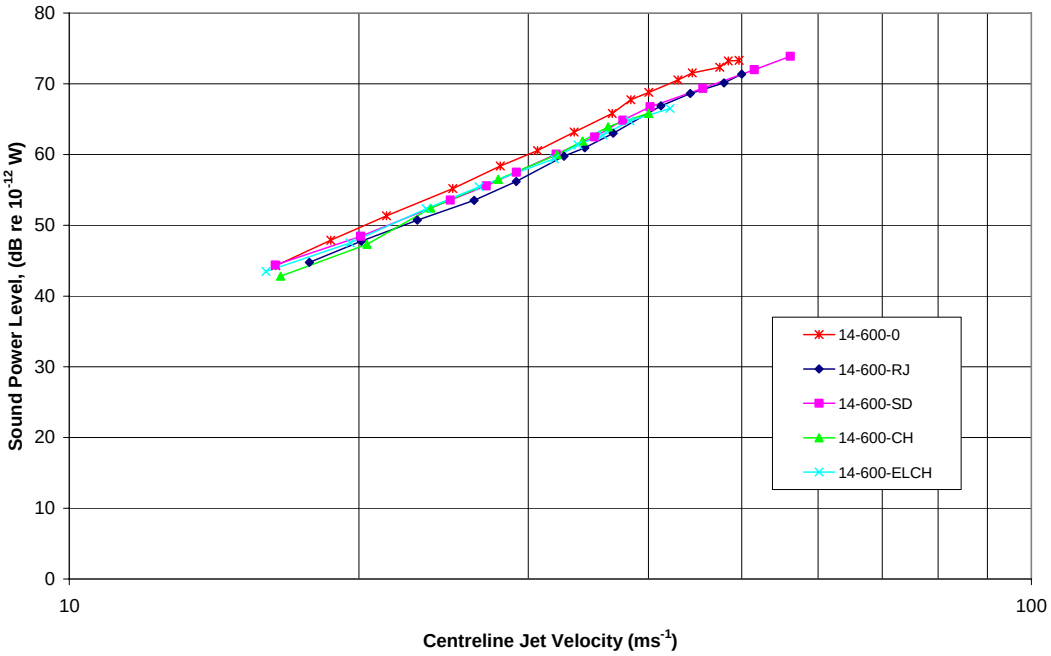

Figure 5.63: Sound power level comparison between each termination grill configuration fitted to the 14˚ conical diffuser with a 600 mm long outlet duct.

5.6.3 Variation of Sound Power Level with Outlet Duct Length

The above results indicate that the outlet duct length has some influence on the overall sound power level produced by a selected outlet for a given inlet jet velocity. To initially isolate the effects of the outlet grill in this analysis the simplified case of fitting open ended outlet ducts to each of the conical diffusers was used. The sound power level was calculated for a duct length of 300, 600 and 900 mm for each of the three conical diffusers with the results shown in Figures 5.64, 5.65 and 5.66 respectively.

All three outlet duct lengths used with the 7˚ conical diffuser produced a very similar sound power level across the jet velocity range considered, with all three curves following a consistent slope of 50 (50logV). There are some minor variations at jet velocities above 30 ms^{-1}, with the 600 mm long duct the preferred selection. At jet velocities below 25 ms^{-1} there is virtually no difference between all three lengths trialled.

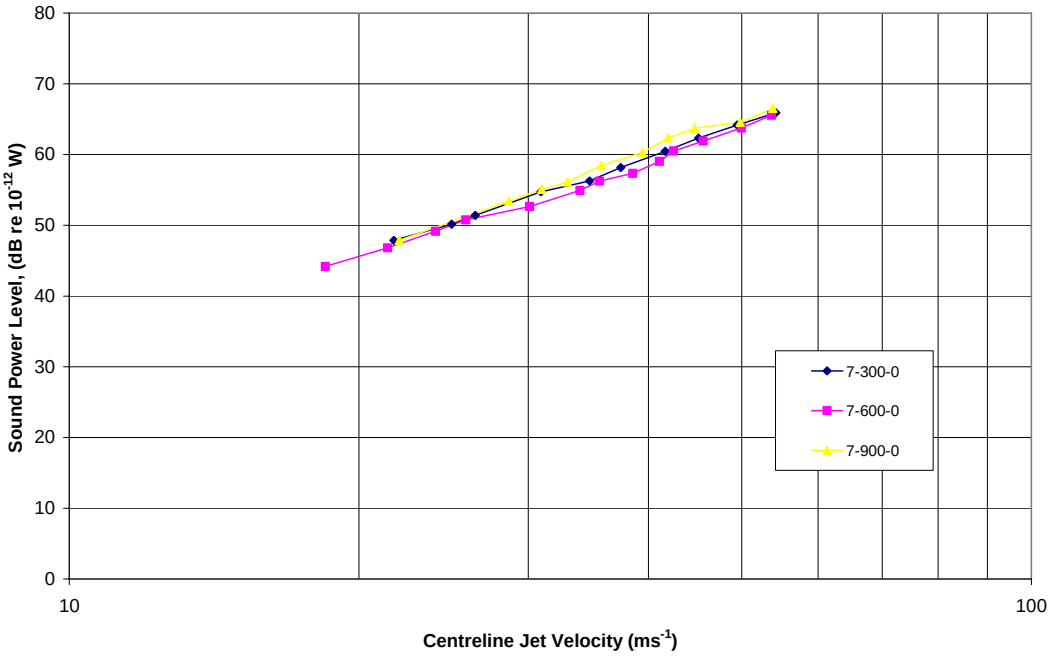

Figure 5.64: Sound power level comparison for the 7˚ conical diffuser fitted with an open ended 300, 600 and 900 mm long outlet duct.

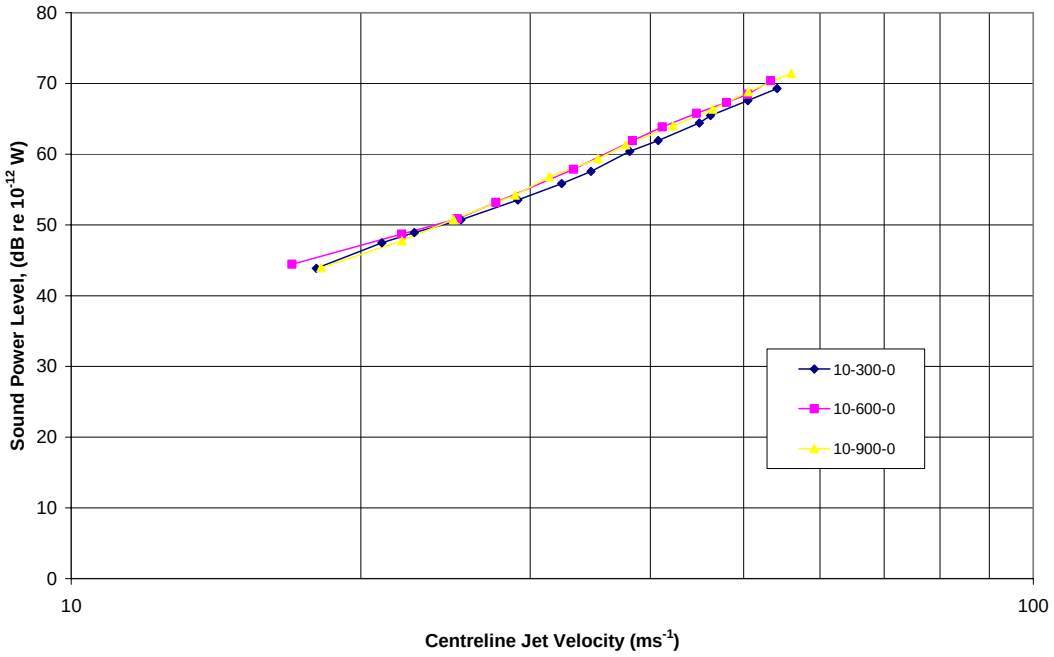

Figure 5.65: Sound power level comparison for the 10˚ conical diffuser fitted with an open ended 300, 600 and 900 mm long outlet duct

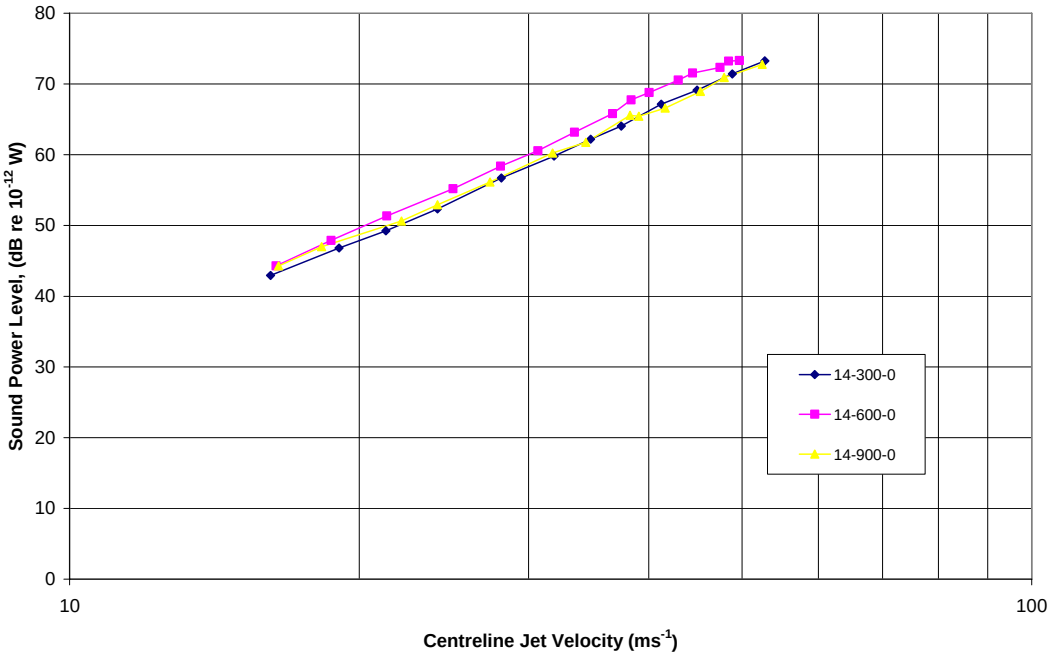

Figure 5.66: Sound power level comparison for the 14˚ conical diffuser fitted with an open ended 300, 600 and 900 mm long outlet duct

In the case of the 10˚ conical diffuser the 300 mm long duct performed marginally better by 1 to 2 dB than the 600 and 900 mm options. The slope of all three curves was around 50 (50logV) for jet velocities below 30 ms^{-1} and this increased to 60 (60logV) at jet velocities above this level. The increase in slope is best illustrated by comparing the sound power level at 50 ms^{-1}, which is 5 dB greater than for the same duct fitted to the 7˚ conical diffuser.

The results for the 14˚ conical diffuser show a further 4 dB increase in the sound power level at the reference jet velocity of 50 ms^{-1}, when compared back to the results for the 10˚ conical diffuser. This increase is also reflected in the increase in the slope of the curves which is a consistent 65 (65logV) across the entire jet velocity range considered. In this instance the 300 mm duct length and 900 mm duct length both perform slightly better than the 600 mm option. This suggests the presence of quadrupole sound sources, which result from flow separation within the primary conical diffuser section. Therefore the 14˚ primary diffuser angle is too large, unless some additional measures are taken to limit the onset of flow separation with the diffuser.

The above cases where an open ended outlet duct is used provides a useful indication of the direct contribution of the outlet duct length to the overall sound power level, however it ignores the important secondary effects of coupling the outlet duct to the outlet termination grill. In a practical HVAC installation some form of outlet grill will be required for aesthetic reasons and to distribute the airflow evenly. Therefore it is important to assess the performance of a more realistic scenario of fitting an outlet termination grill to the same range of outlet duct lengths used above.

The first outlet used was the round jet (RJ) grill, which was fitted to each conical diffuser directly (0 duct length) to provide a baseline case and then each of the 3 duct lengths of 300, 600 and 900 mm. The results for the three conical diffuser angles of 7˚, 10˚ and 14˚ are shown in Figures 5.67, 5.68 and 5.69 respectively. There is the consistent 10 dB reduction in the total sound power level when comparing any outlet duct length back to the baseline of no outlet duct (grill fitted directly onto the primary conical diffuser section) for each of the conical diffusers used. A further improvement of 1 to 2 dB is achieved if the 600 mm duct length is used over the 300 and 900 mm options. The total sound power level at the reference jet velocity of 50 ms^{-1} also increases as the conical diffuser angle is increased from 7˚ to 10˚ and then 14˚. This result mirrors the same increases that were observed for the simple case of no outlet grill outlined previously.

The presence of flow separation within the conical diffuser section is once again highlighted by the variation in the slope of the sound power curves for each of the three conical diffuser angles used. The 7˚ conical diffuser models all had a slope of 40 to 50, with a slight increase seen as the jet velocity increased, while the 10˚ conical diffuser models all had a higher slope of 55 to 60, with the flatter slope observed at jet velocities below 30 ms^{-1}. The 14˚ conical diffuser models however all had a consistent slope in the 60 to 65 range across the whole jet velocity range used.

As the jet velocity increases the gap widens between the baseline case of zero duct length and the 3 duct length options used with 7˚ conical diffuser. This suggests that the outlet duct itself makes a useful contribution to the minimisation of the level of flow induced noise. The size of this contribution increases with the inlet jet velocity.

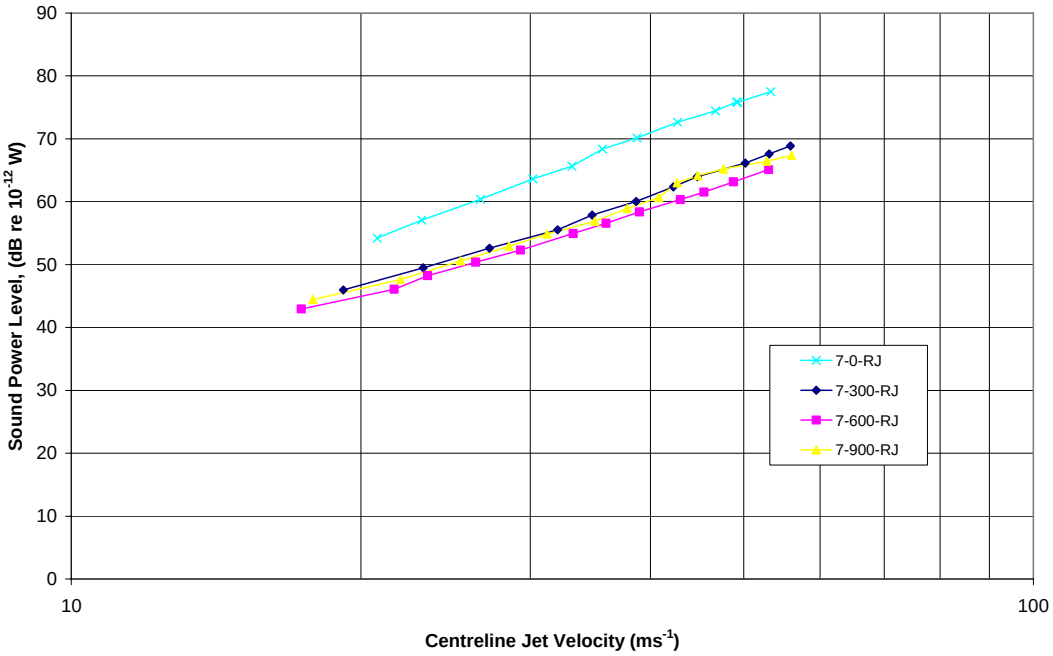

Figure 5.67: Sound power level comparison for the 7˚ conical diffuser fitted with the round jet (RJ) outlet grill with an extended outlet duct of 0, 300, 600 and 900 mm.

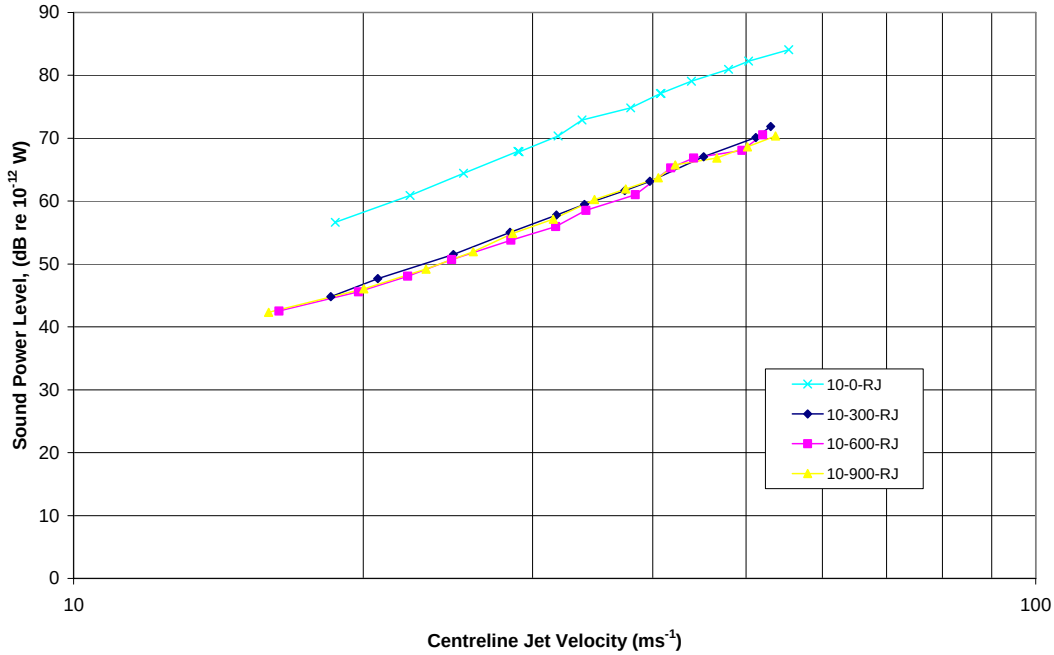

Figure 5.68: Sound power level comparison for the 10˚ conical diffuser fitted with the round jet (RJ) outlet grill with an extended outlet duct of 0, 300, 600 and 900 mm.

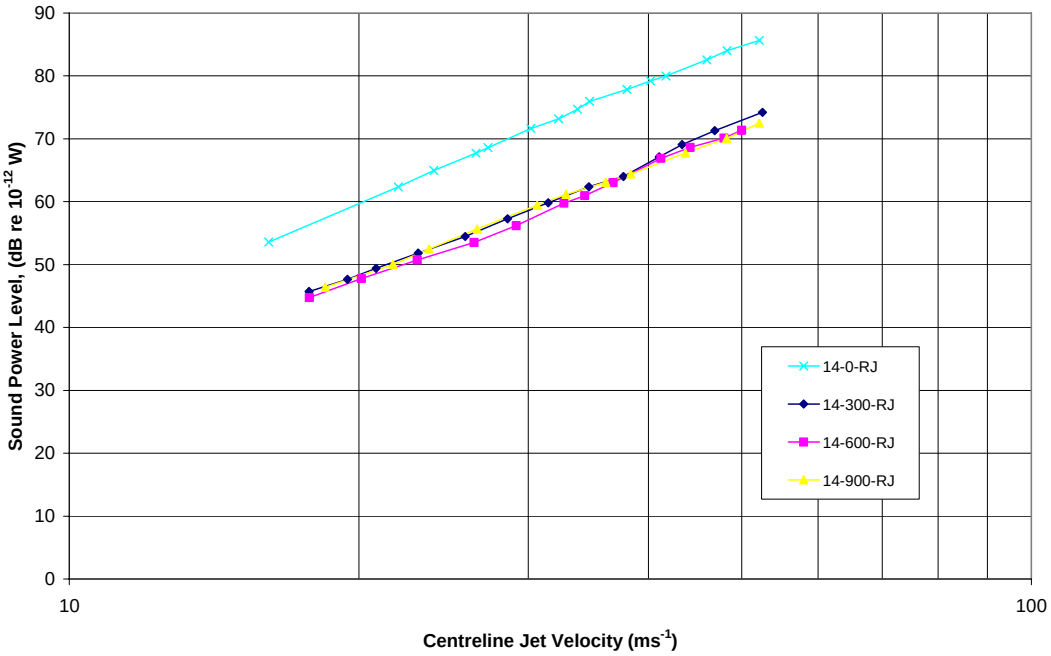

Figure 5.69: Sound power level comparison for the 14˚ conical diffuser fitted with the round jet (RJ) outlet grill with an extended outlet duct of 0, 300, 600 and 900 mm.

The above analysis was repeated for the square diffuser (SD) outlet grill fitted to the 300, 600 and 900 mm outlet ducts for each of the three conical diffusers used. The results for the 7˚, 10˚ and 14˚ diffusers are shown in Figures 5.70, 5.71 and 5.72 respectively. The large reduction in the sound power level for each conical diffuser when comparing the baseline of no outlet duct length to the three lengths tested was once again present. However, the size of the reduction was also partially determined by the angle of the conical diffuser used. For the 7˚ conical diffuser the reduction was only 3 to 4 dB at a jet velocity of 20 ms^{-1}, increasing to a reduction of 8 to 10 dB at a jet velocity of 50 ms^{-1}. Meanwhile the 8 to 10 dB reduction achieved with the 10˚ conical diffuser was much more consistent across the entire velocity range that was tested. The size of this reduction increased further to 10 to 12 dB across the selected velocity range for the 14˚ conical diffuser.

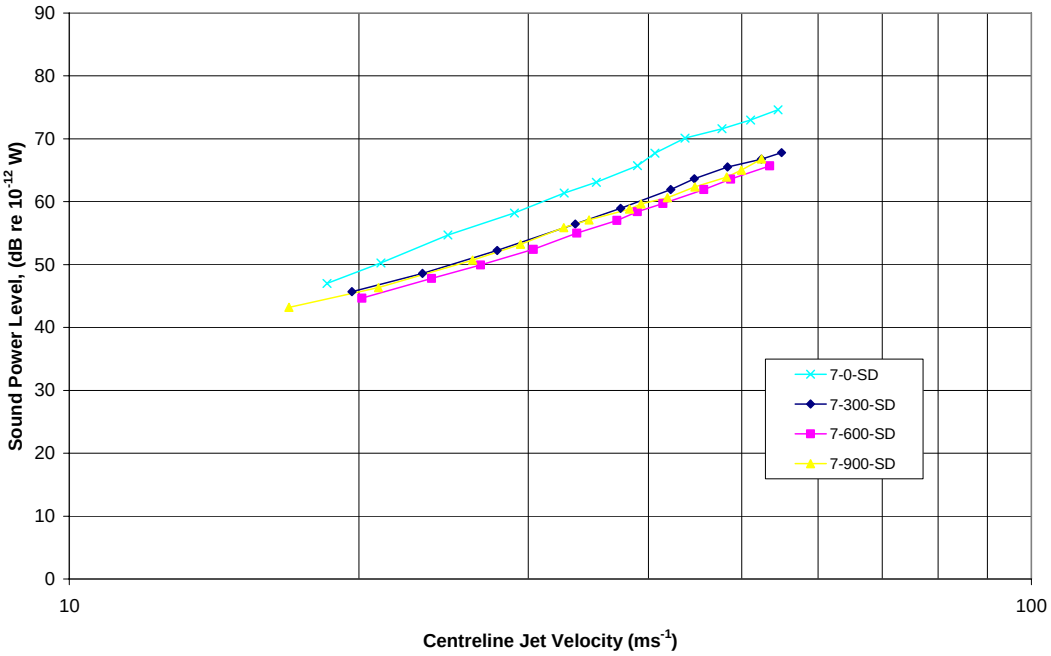

Figure 5.70: Sound power level comparison for the 7˚ conical diffuser fitted with the square (SD) outlet grill with an extended outlet duct of 0, 300, 600 and 900 mm.

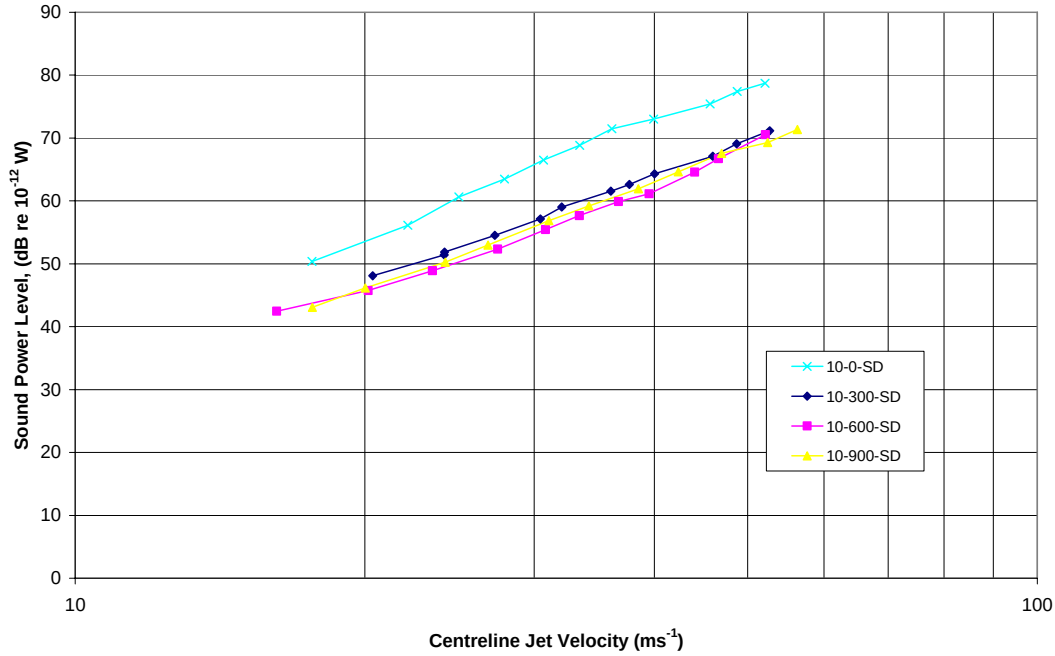

Figure 5.71: Sound power level comparison for the 10˚ conical diffuser fitted with the square (SD) outlet grill with an extended outlet duct of 0, 300, 600 and 900 mm.

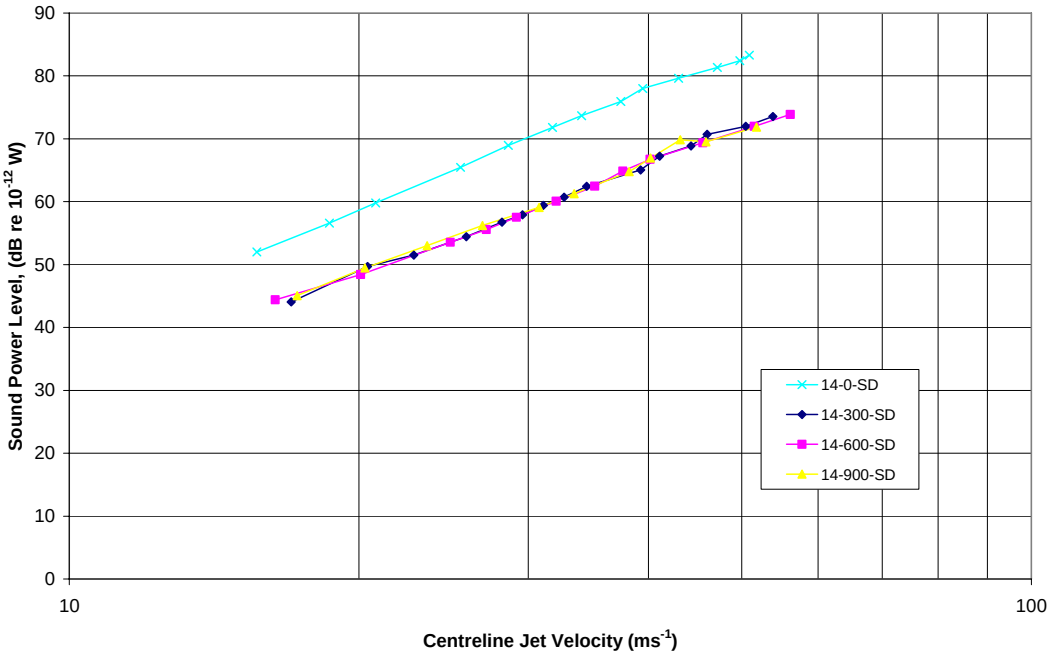

Figure 5.72: Sound power level comparison for the 14˚ conical diffuser fitted with the square (SD) outlet grill with an extended outlet duct of 0, 300, 600 and 900 mm.

Once again the total sound power level at the reference jet velocity of 50 ms^{-1} is increased from 65 to 69 and then 72 dB as the conical diffuser angle is increased from 7˚ to 10˚ and then 14˚ respectively. This result is consistent with both the baseline case of no outlet grill and the RJ outlet grill. Therefore it is likely that this trend is strongly driven by an increase in the level of flow separation caused by the increases in conical diffuser angle.

The widening of the gap between the baseline case of zero duct length and the 3 duct length options used with the 7˚ conical diffuser observed with the RJ grill was once again repeated with the SD outlet grill. Interestingly the gap was much narrower with the SD outlet. At the lower jet velocities there is little flow separation and therefore the need to have an extended outlet duct to allow some settling of the flow is not critical to the acoustic performance of the outlet. A similar narrowing of the gap was also observed with the 10˚ conical diffuser, but on a much smaller scale.

The influence of flow separation on these results is further reinforced by the variation in the slope of the sound power curves for each of the three conical diffuser angles used. As with the RJ outlet grill the 7˚ conical diffuser models all had a slope of 40 to 50, with a slight increase seen as the jet velocity increased. The 10˚ conical diffuser models also mirrored the RJ outlet results with a slope of 50 to 60, with the flatter slope observed at jet velocities below 30 ms^{-1}. The 600 mm long outlet model however deviated from the previous results with a flatter slope at the lower jet velocities and a much steeper slope of 65 to 70 at jet velocities above 45 ms^{-1}. The 14˚ conical diffuser models once again had a consistent slope in the 60 to 65 range across the whole jet velocity range used.

5.7 ⅓ Octave Sound Power Level Analysis

Many of the total sound power level results presented herein have been very similar for the different geometric outlet configurations considered. However, when these results are A-weighted the values tend to diverge quite significantly, due to large variations in the low frequency components of the sound power spectra for each of the outlet configurations tested. To better understand the nature of the sound spectra for each configuration the measured ⅓ octave sound pressure levels have been used to calculate the equivalent ⅓ octave sound power levels, using the reverberation properties of the receiver room. Selected results at reference jet velocities of 20, 30, 40 and 50 ms^{-1} have been used to provide a means of analysing the impact of the selected geometric variables governing the configuration of the HVAC outlet.

This analysis can be separated into three sections, covering the conical diffuser angle, outlet duct length and the outlet termination grill configuration. In each separate series of results the data will be compared at multiple jet velocity settings whilst keeping the other two variables constant. Results for multiple combinations are presented to better cover the secondary effects caused by the combination of selected duct variables.

5.7.1 Variation with Conical Diffuser Angle

The first comparison is made using no outlet termination grill so as to eliminate the influence of the outlet grill on the flow induced noise spectra. The ⅓ octave sound power levels (SWL) for the open ended 300 mm outlet duct fitted to each of the three conical diffusers are shown for a jet velocity of 20, 30, 40 and 50 ms^{-1} in Figures 5.73 to 5.76. Three main conclusions can be drawn for each of these Figures. Firstly, the size of the peak band at each jet velocity increases with the diffuser angle, with an increase of nearly 10 dB between the 7˚ and 14˚ diffusers. Interestingly the 10˚ diffuser is only marginally worse than the 7˚ one. The second observation is that the frequency at which the peak occurs is also higher for the 14˚ conical diffuser when compared with the other diffusers. The high frequency SWL meanwhile increases at a significantly slower rate, with an eventual flattening of the spectra at higher jet velocities.

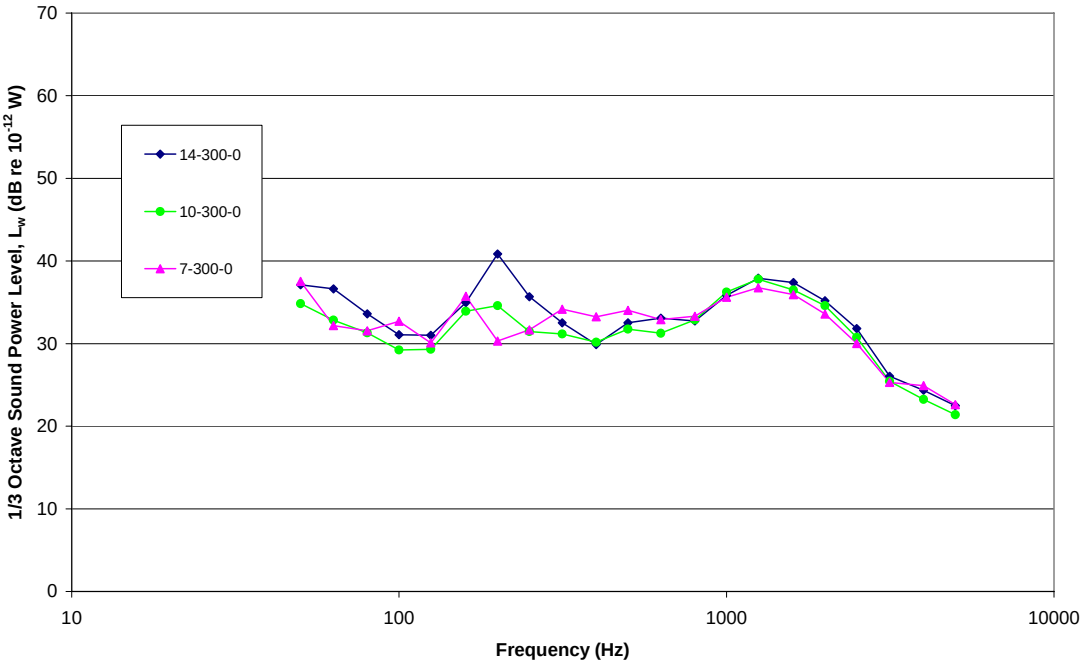

Figure 5.73: ⅓ Octave sound power level comparison for conical diffuser angles of 7˚, 10˚ and 14˚ – fitted with an open ended 300 mm long outlet duct at 20 ms^{-1}.

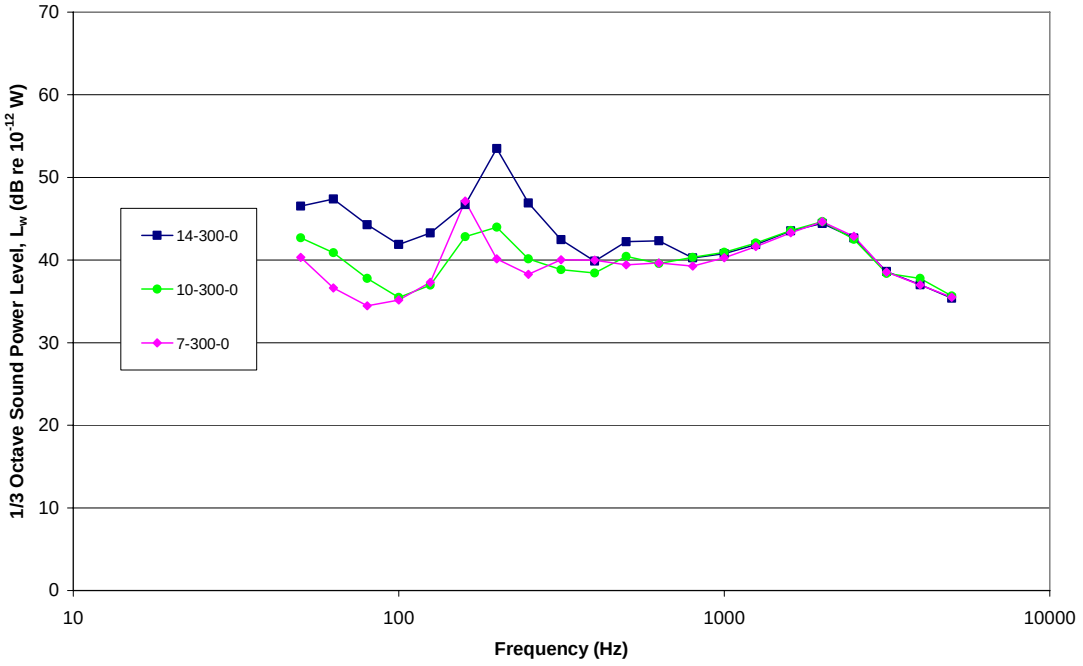

Figure 5.74: ⅓ Octave sound power level comparison for conical diffuser angles of 7˚, 10˚ and 14˚ – fitted with an open ended 300 mm long outlet duct at 30 ms^{-1}.

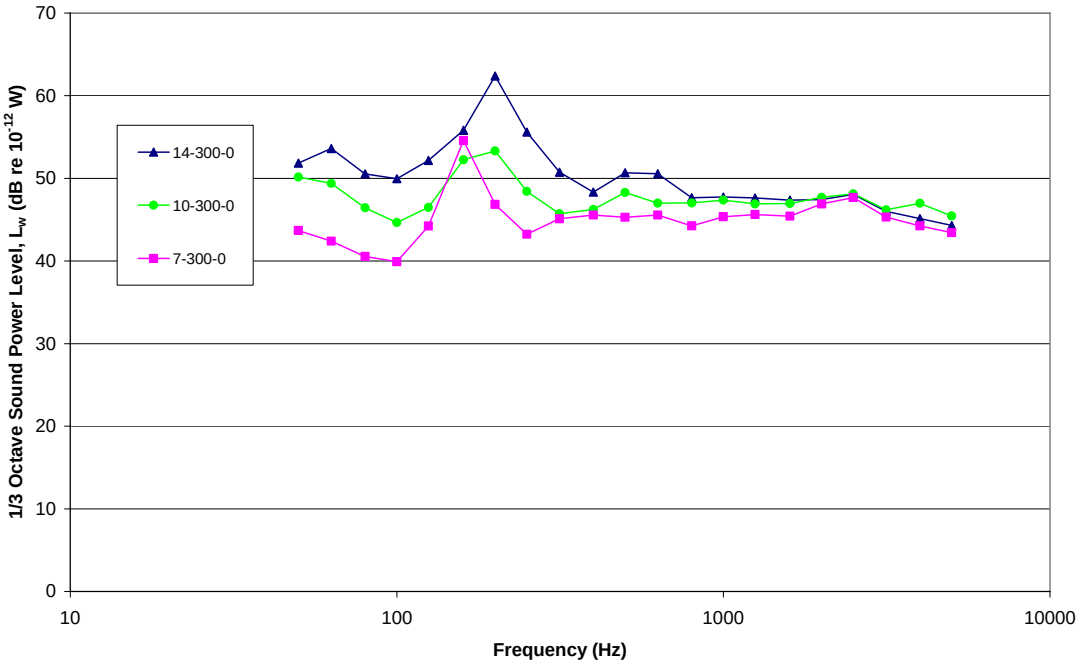

Figure 5.75: ⅓ Octave sound power level comparison for conical diffuser angles of 7˚, 10˚ and 14˚ – fitted with an open ended 300 mm long outlet duct at 40 ms^{-1}.

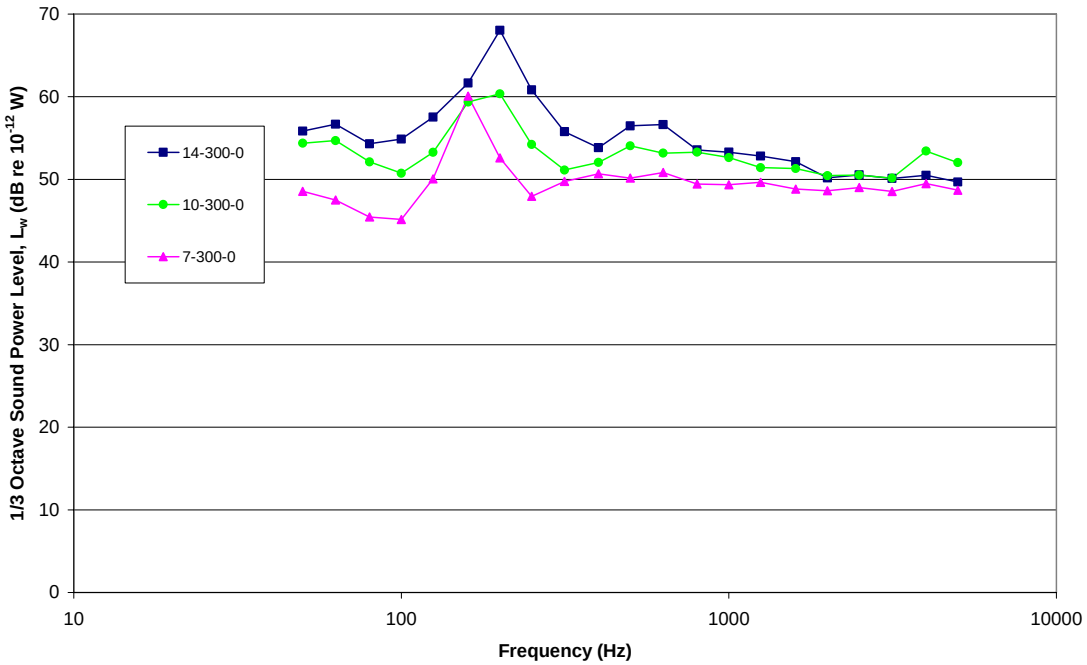

Figure 5.76: ⅓ Octave sound power level comparison for conical diffuser angles of 7˚, 10˚ and 14˚ – fitted with an open ended 300 mm long outlet duct at 50 ms^{-1}.

Although the outlet duct length is fixed at 300 mm the steeper diffuser angles leads to a shortened primary diffuser and therefore a shorter overall length. The fundamental frequency of the flow induced noise associated with the expansion of the jet inside the conical diffuser is directly related to the velocity, duct diameter and the duct length. Therefore any increase in the duct length, with the diameter and velocity kept constant will lead to an increase in the fundamental frequency of sound generated.

Following this result the open ended 600 mm outlet duct was also investigated under the same jet velocities and outlet conditions. The ⅓ octave sound power levels for each of the conical diffuser angles at jet velocities of 20, 30, 40, and 50 ms^{-1} are shown in Figures 5.77 to 5.80. Increasing the length of the outlet duct makes two changes to the sound spectra observed for the shorter 300 mm long outlet duct. Firstly the location of the peak is shifted to a lower frequency band, 125 Hz compared with 160 Hz. Unlike the 300 mm duct cases this peak occurs in the same frequency band for all three conical diffuser angles. As the total duct length is increased the effect of the variation in the length of the conical diffuser becomes less significant.

The second difference between the 300 and 600 mm duct models is the development of a secondary peak in the 315 Hz band when the 600 mm outlet duct is used. This peak is more pronounced with the 14˚ conical diffuser and is also much sharper. The secondary peaks for the 7˚ and 10˚ diffusers are progressively lower and flatter. The high frequency peak in the 1 to 2 kHz bands that is present in both cases does not increase significantly as the jet velocity is increased to 40 and 50 ms^{-1}, with it eventually becoming flat. There is also little variation in the sound power level in the higher frequency bands as the conical diffuser angle changes from 7˚ to 14˚.

The migration of the peak sound power level through the frequency domain as the outlet duct configuration is changed suggests that the outlet geometry can be tuned to maximise the acoustic attenuation obtained.

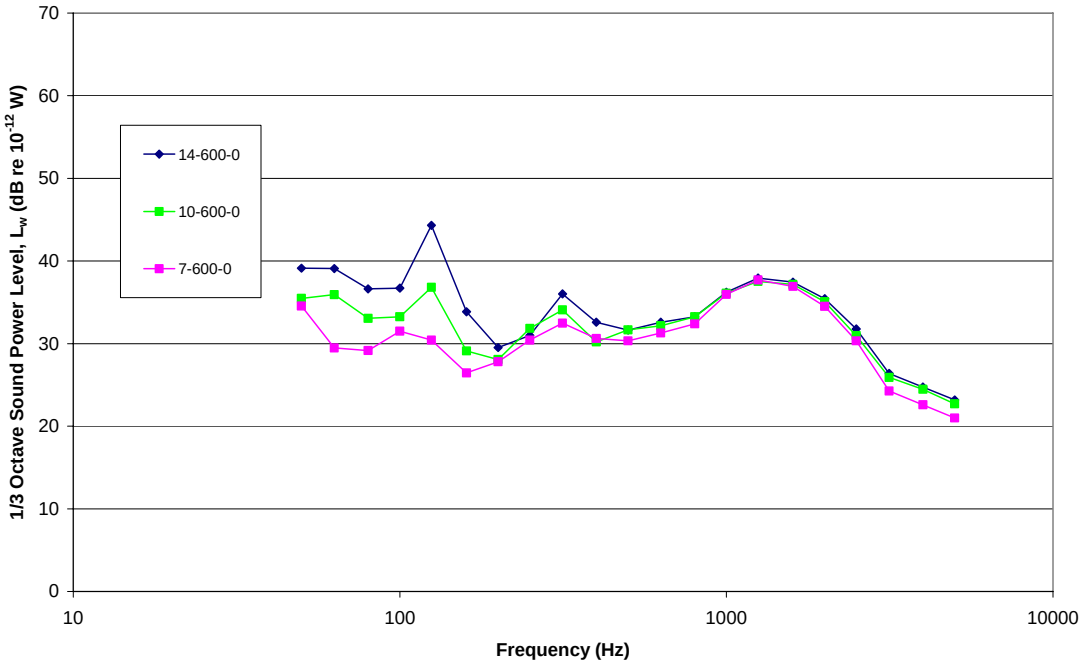

Figure 5.77: ⅓ Octave sound power level comparison for conical diffuser angles of 7˚, 10˚ and 14˚ – fitted with an open ended 600 mm long outlet duct at 20 ms^{-1}.

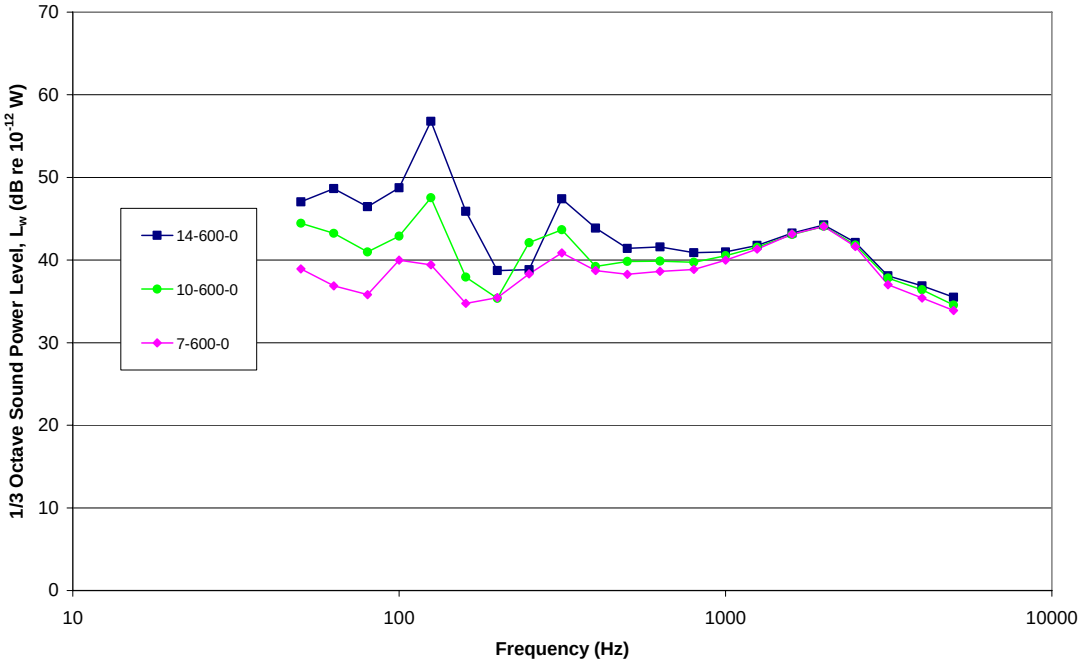

Figure 5.78: ⅓ Octave sound power level comparison for conical diffuser angles of 7˚, 10˚ and 14˚ – fitted with an open ended 600 mm long outlet duct at 30 ms^{-1}.

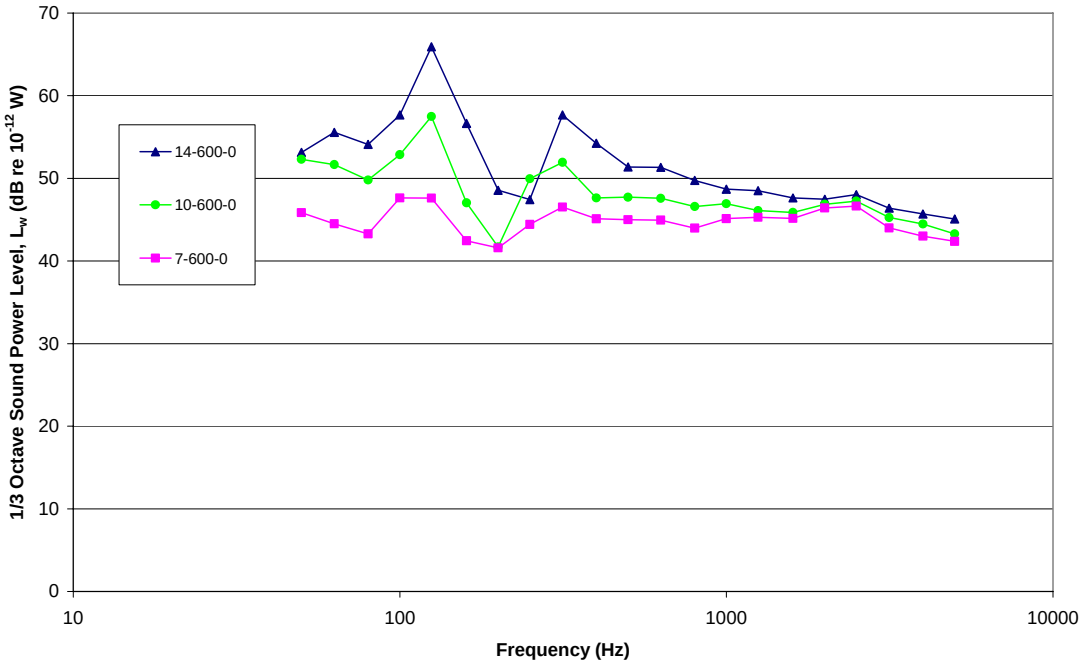

Figure 5.79: ⅓ Octave sound power level comparison for conical diffuser angles of 7˚, 10˚ and 14˚ – fitted with an open ended 600 mm long outlet duct at 40 ms^{-1}.

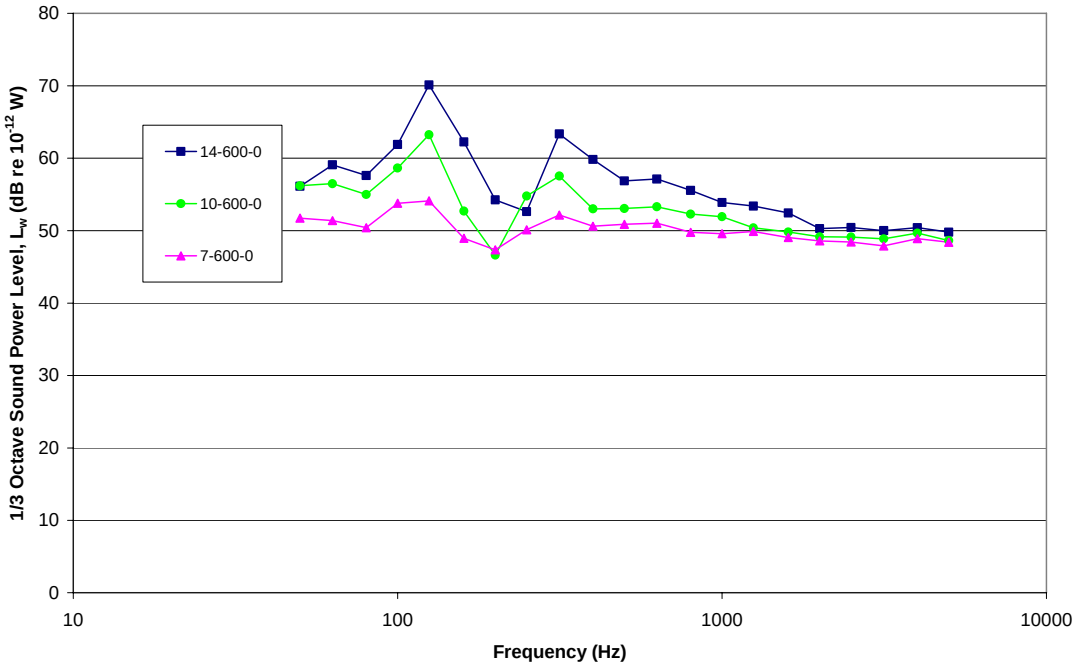

Figure 5.80: ⅓ Octave sound power level comparison for conical diffuser angles of 7˚, 10˚ and 14˚ – fitted with an open ended 600 mm long outlet duct at 50 ms^{-1}.

The ⅓ octave sound power levels for the open ended 900 mm outlet duct for jet velocities of 20, 30, 40 and 50 ms^{-1} are shown in Figures 5.81 to 5.84. The high frequency components of the sound power spectra are virtually identical for all three outlet duct lengths of 300, 600 and 900 mm. The primary peak moves into an even lower frequency band (80 to 100 Hz) and also becomes considerably flatter. The size of the secondary peak is also diminished somewhat and is now also located in a lower frequency band at 250 Hz. In the case of the 14˚ conical diffuser there is also a tertiary peak present in the 400 Hz band that is consistently lower than the first two peaks. Neither of the 7˚ and 10˚ diffusers produce a third peak in the 400 Hz band and even the size of the secondary peak is severely diminished.

Using the 7˚ diffuser significantly reduces the net level of acoustic power generated by the expanding jet, particularly when compared with the corresponding results for the 14˚ diffuser. All of this reduction in acoustic power occurs in the lower frequency bands below 500 Hz, with significant reductions seen in the 100 to 400 Hz bands. At a high jet velocity of 50 ms^{-1} there are some savings in the upper frequency bands, but these are still only in the order of 3 to 5 dB.

To better understand the secondary effects of coupling the selected outlet duct lengths to a realistic outlet termination grill the SD outlet was fitted to the 300 mm outlet duct length and each of the three conical diffusers. The ⅓ octave sound power level for each of these models at jet velocities of 20, 30, 40 and 50 ms^{-1} are presented in Figures 5.85 to 5.88. Adding the outlet grill has two major effects on the sound power spectra for each of the conical diffusers. Firstly the high frequency spectra become more distinctly separated, with the 7˚ diffuser 2 to 5 dB lower than the 10˚ and 14˚ models. The flatness of the high frequency spectra is maintained, however the gap between the 7˚ and 14˚ diffusers increases with the jet velocity.

The second major change relates to the size and shape of the primary low frequency peak in the 125 and 160 Hz bands. For the 7˚ diffuser the peak is significantly lower and flatter, being spread across 2 to 3 frequency bands. The peaks for the 10˚ and 14˚ diffusers meanwhile are significantly higher and sharper across all four jet velocities considered. The net result is a significant increase in the total sound power generated.

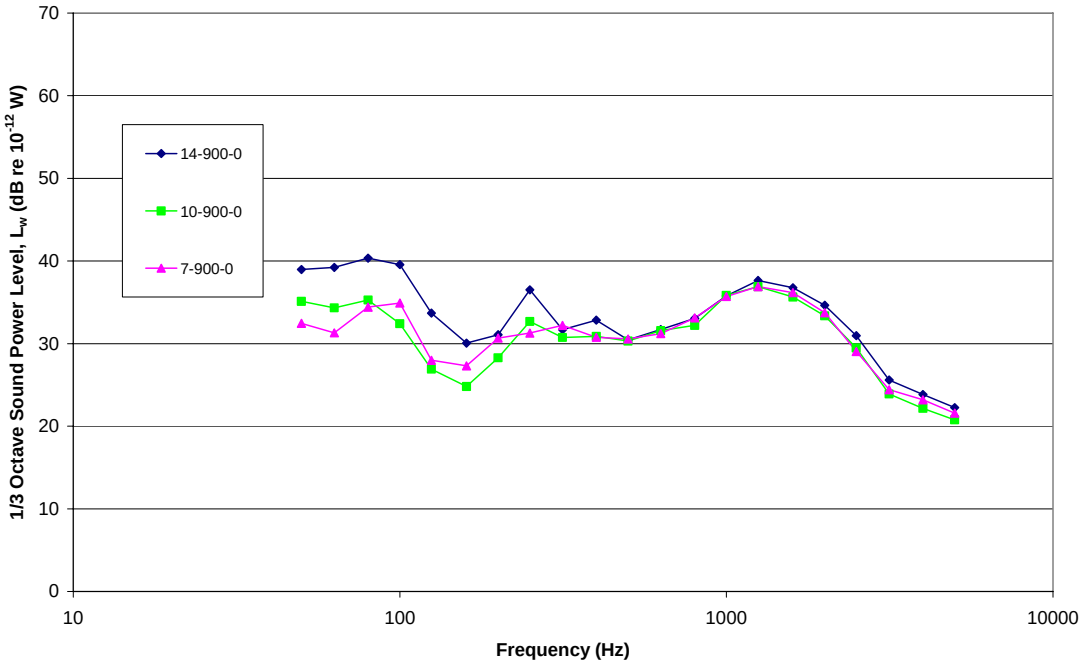

Figure 5.81: ⅓ Octave sound power level comparison for conical diffuser angles of 7˚, 10˚ and 14˚ – fitted with an open ended 900 mm long outlet duct at 20 ms^{-1}.

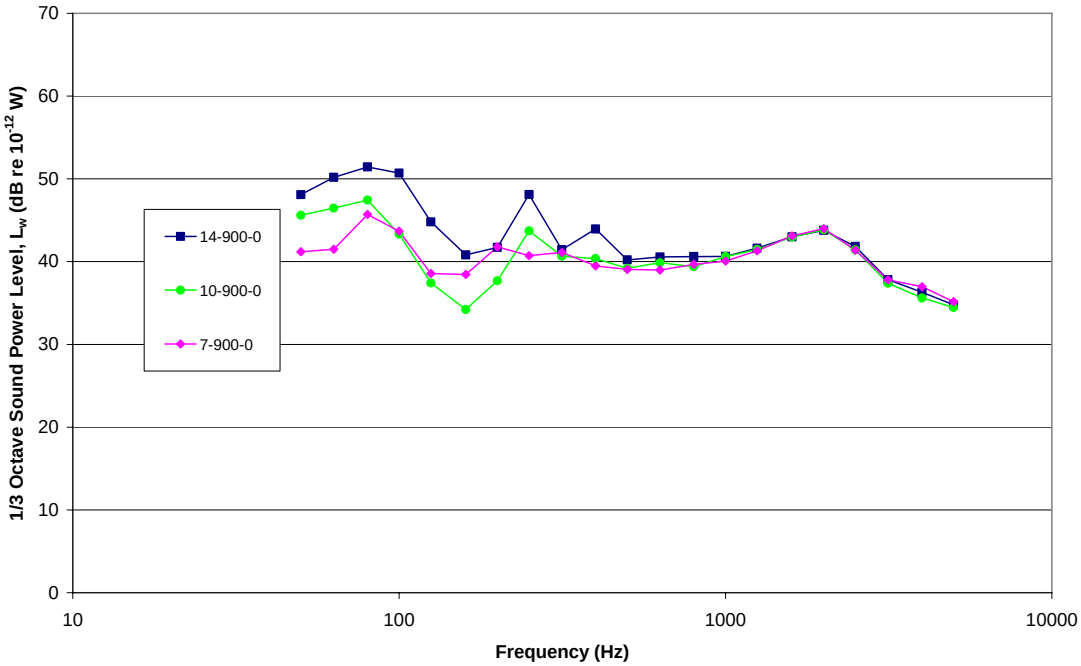

Figure 5.82: ⅓ Octave sound power level comparison for conical diffuser angles of 7˚, 10˚ and 14˚ – fitted with an open ended 900 mm long outlet duct at 30 ms^{-1}.

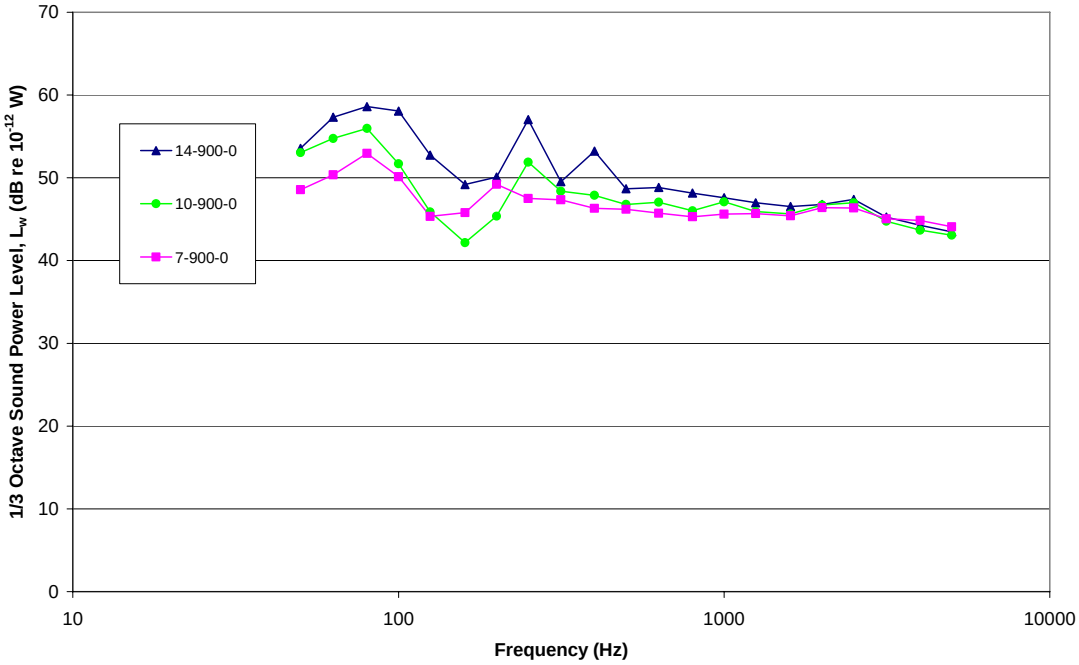

Figure 5.83: ⅓ Octave sound power level comparison for conical diffuser angles of 7˚, 10˚ and 14˚ – fitted with an open ended 900 mm long outlet duct at 40 ms^{-1}.

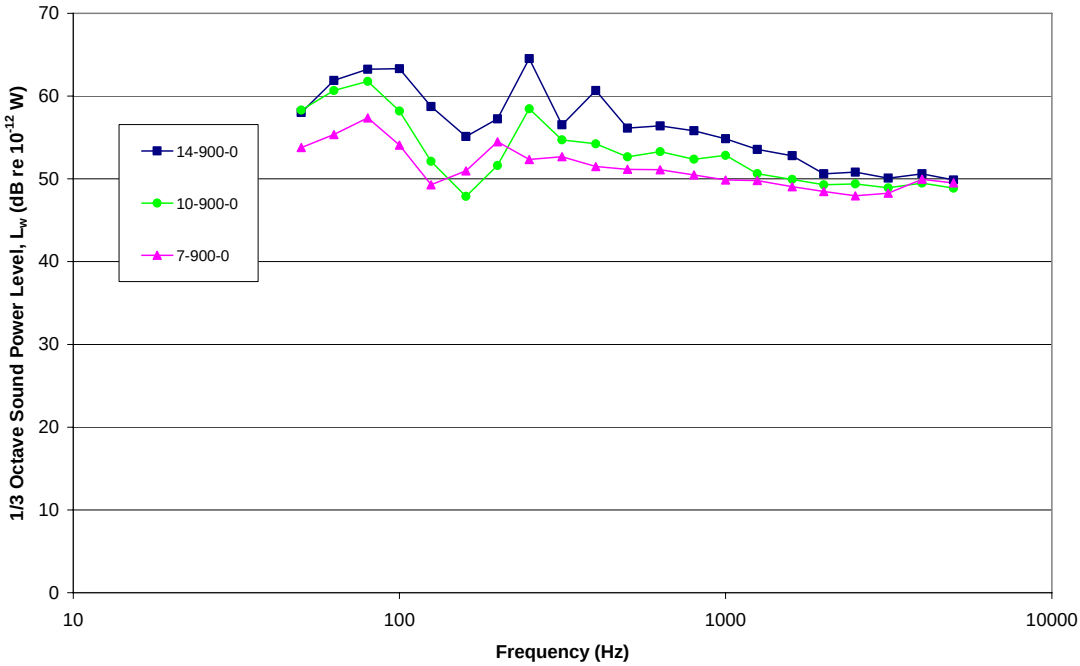

Figure 5.84: ⅓ Octave sound power level comparison for conical diffuser angles of 7˚, 10˚ and 14˚ – fitted with an open ended 900 mm long outlet duct at 50 ms^{-1}.

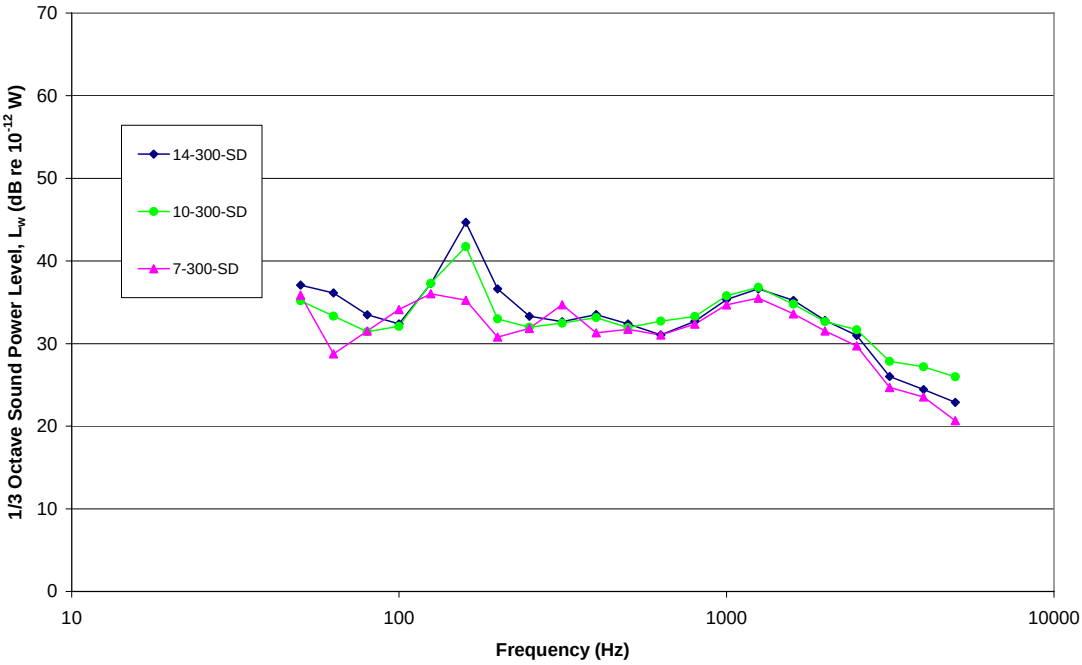

Figure 5.85: ⅓ Octave sound power level comparison for conical diffuser angles of 7˚, 10˚ and 14˚ – fitted with a 300-SD outlet duct at 20 ms^{-1}.

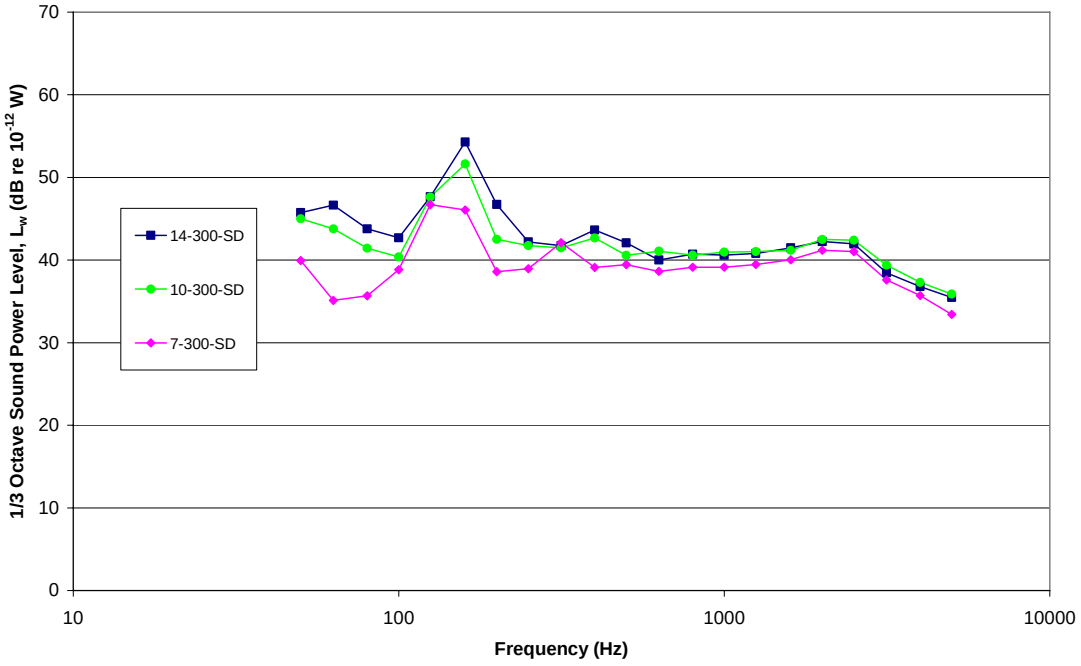

Figure 5.86: ⅓ Octave sound power level comparison for conical diffuser angles of 7˚, 10˚ and 14˚ – fitted with a 300-SD outlet duct at 30 ms^{-1}.

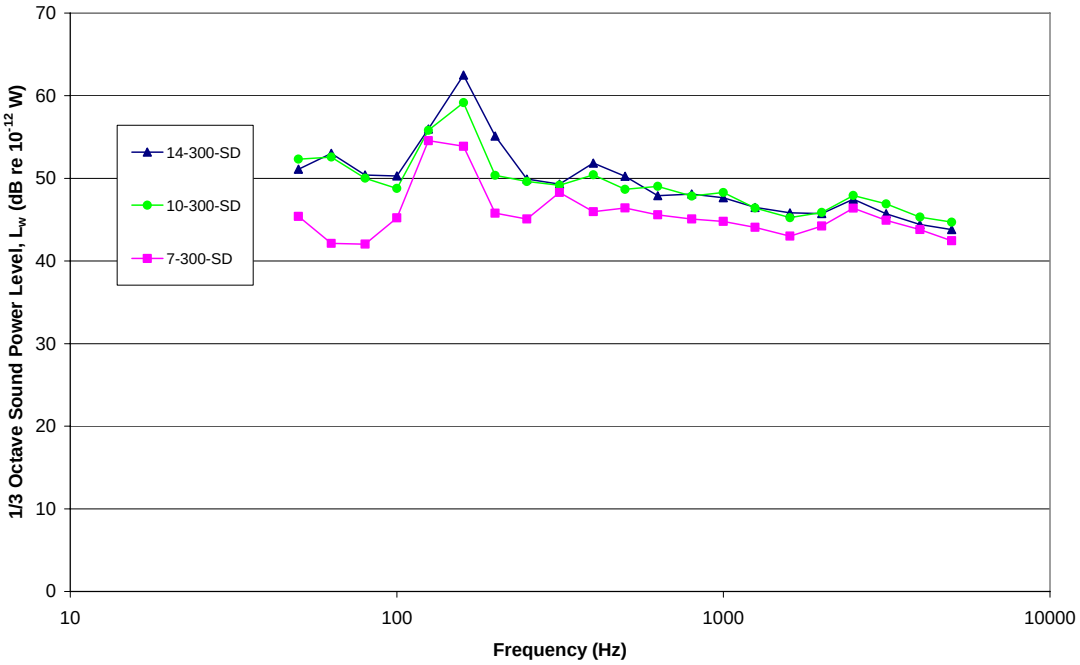

Figure 5.87: ⅓ Octave sound power level comparison for conical diffuser angles of 7˚, 10˚ and 14˚ – fitted with a 300-SD outlet duct at 40 ms^{-1}.

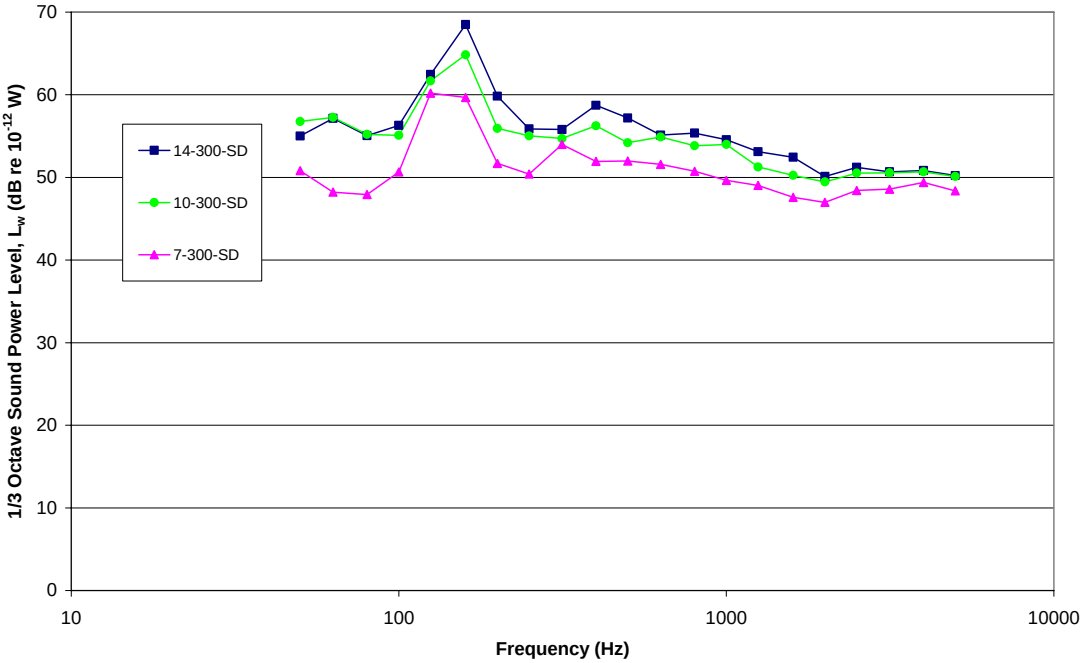

Figure 5.88: ⅓ Octave sound power level comparison for conical diffuser angles of 7˚, 10˚ and 14˚ – fitted with a 300-SD outlet duct at 50 ms^{-1}.

To investigate if the improvement from adding the SD outlet grill could also be achieved with a longer outlet duct; the above analysis was extended to include the 600 mm outlet duct. The ⅓ octave sound power levels for each of the conical diffusers fitted to the 600 mm outlet duct and SD outlet with a jet velocity of 20, 30, 40 and 50 ms^{-1} are shown in Figures 5.89 to 5.92. At each of the jet velocities tested, the peak sound power level is lower when compared with the corresponding test using the open ended 600 mm outlet duct. The peaks are also much flatter than the open ended duct cases, with more of the acoustic energy transferred into the lower frequency bands. This effect is quite beneficial on an A-weighted sound power basis as the perceived level is lower for the same level of sound in a lower frequency band. Clearly this is only acceptable within certain limits as too much low frequency noise can also be problematic and very difficult to treat.

The absolute difference in sound power level between each of the conical diffuser angles is of the same order of magnitude to the variation found with the open ended outlet ducts. The high frequency components of the spectra are reduced slightly with the addition of the SD outlet grill, particularly at the lower jet velocities of 20 and 30 ms^{-1}. In all cases the 7˚ conical diffuser is clearly the best option for minimising the sound power level spectra with either a 300 or 600 mm outlet duct.

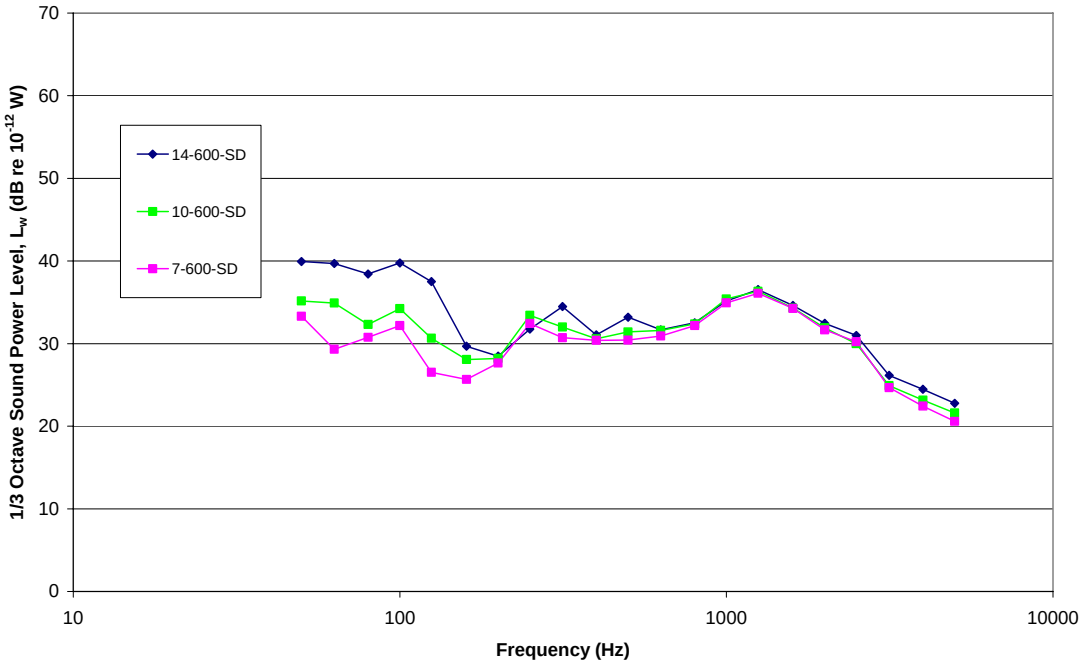

Figure 5.89: ⅓ Octave sound power level comparison for conical diffuser angles of 7˚, 10˚ and 14˚ – fitted with a 600-SD outlet duct at 20 ms^{-1}.

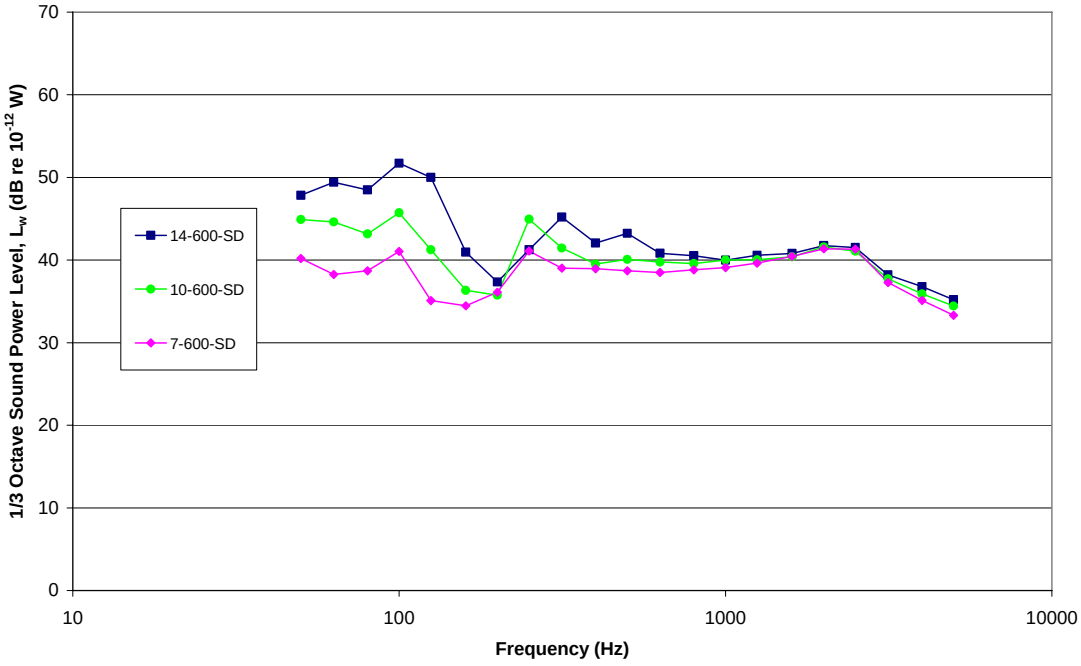

Figure 5.90: ⅓ Octave sound power level comparison for conical diffuser angles of 7˚, 10˚ and 14˚ – fitted with a 600-SD outlet duct at 30 ms^{-1}.

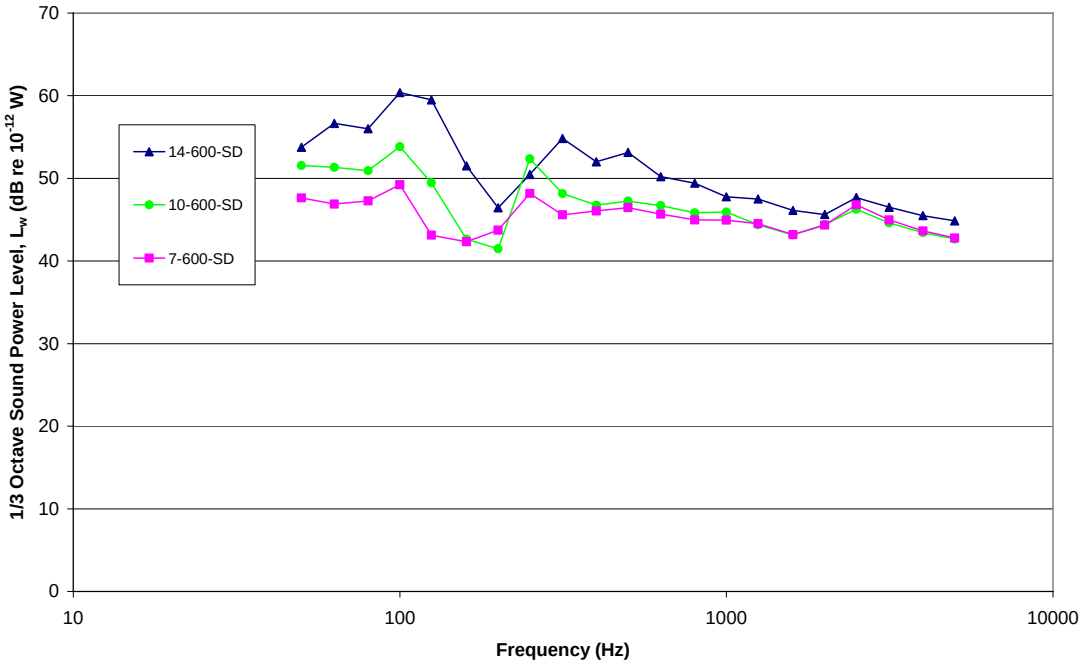

Figure 5.91: ⅓ Octave sound power level comparison for conical diffuser angles of 7˚, 10˚ and 14˚ – fitted with a 600-SD outlet duct at 40 ms^{-1}.

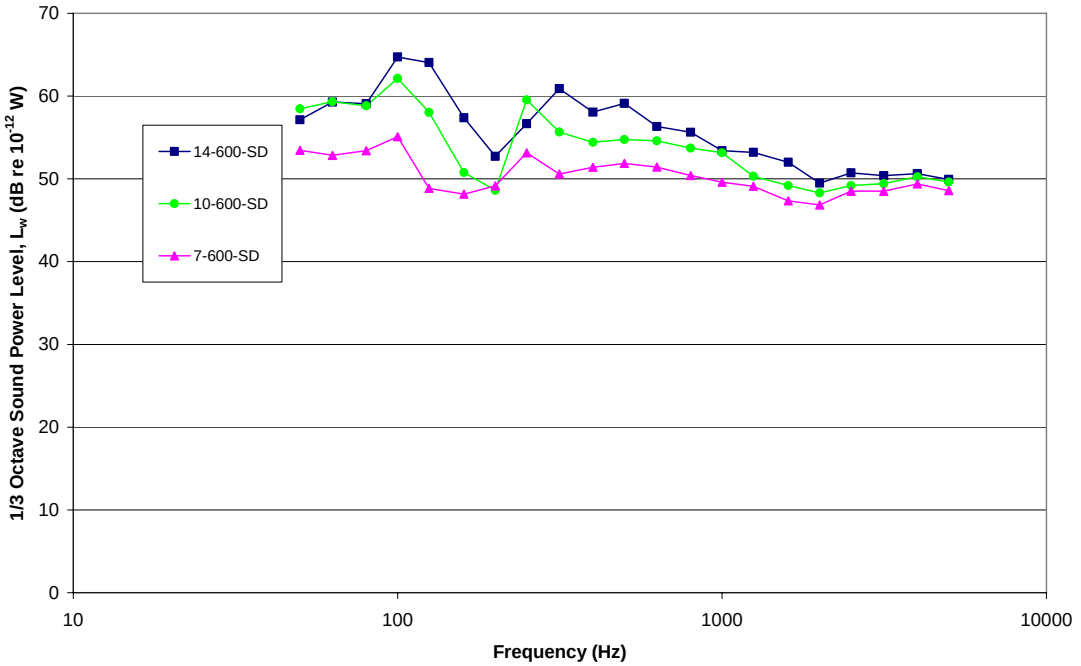

Figure 5.92: ⅓ Octave sound power level comparison for conical diffuser angles of 7˚, 10˚ and 14˚ – fitted with a 600-SD outlet duct at 50 ms^{-1}.

5.7.2 Variation with Outlet Duct Length

The outlet duct length was found to have a significant effect on the shape of the sound power spectra for each of the outlet configurations investigated thus far. To better understand this effect 300, 600 and 900 mm open ended ducts were fitted to each of the three conical diffusers. The ⅓ octave sound power spectra for the 7˚ conical diffuser fitted to each of the open ended outlet ducts at jet velocities of 20, 30, 40 and 50 ms^{-1} are shown in Figures 5.93 to 5.96. At all four jet velocities the 600 mm outlet duct provided the best acoustic performance with a relatively flat sound power spectra. The 300 mm duct produced a peak in the 160 Hz band that progressively got bigger as the jet velocity was increased. At a jet velocity of 50 ms^{-1} the peak was 10 dB higher than the next highest peak.

The 900 mm duct produced a smaller peak that was also much flatter and was located in the 80 to 100 Hz bands. Having the peak located in these frequency bands leads to a lower A-weighted sound power level for the same level of acoustic energy and therefore more closely aligned with the needs of the HVAC design engineer. Despite this advantage the 600 mm duct is still the preferred length as the overall sound power spectra is flatter still, resulting in a lower overall acoustic power level. Incidentally, the length of the outlet duct used had little impact on the sound power level in the higher frequency bands above 500 Hz.

The above tests were repeated for the 10˚ conical diffuser, using the same open ended outlet ducts and the same jet velocity range of 20, 30, 40 and 50 ms^{-1}. The respective ⅓ octave sound power levels for each of these tests are shown in Figures 5.97 to 5.100. As with the 7˚ diffuser cases already discussed the high frequency sound power spectra are essentially independent of the outlet duct length. The lower frequency bands below 500 Hz however are heavily influenced by slight changes in the length of the outlet ducts and the length of the conical diffuser itself. The shape of the low frequency spectra for the 10˚ diffuser varies significantly with similar peak sound power levels across all three outlet duct lengths, but located in differing frequency bands for each duct length.

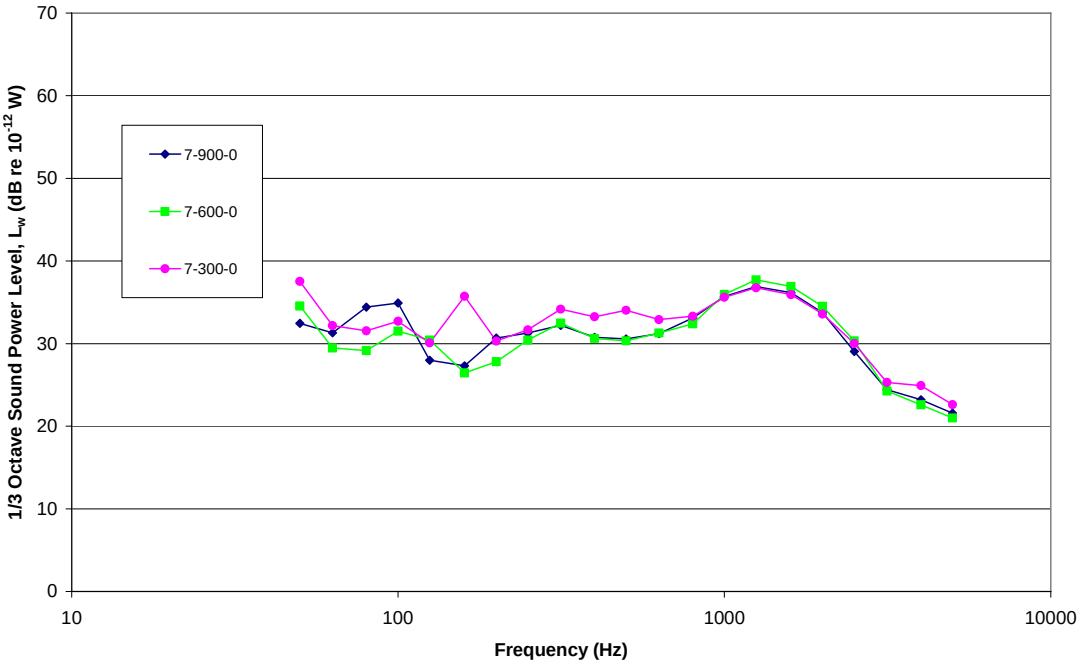

Figure 5.93: ⅓ Octave sound power level comparison for the 7˚ conical diffuser – fitted with a 300, 600 and 900 mm open ended outlet duct at 20 ms^{-1}.

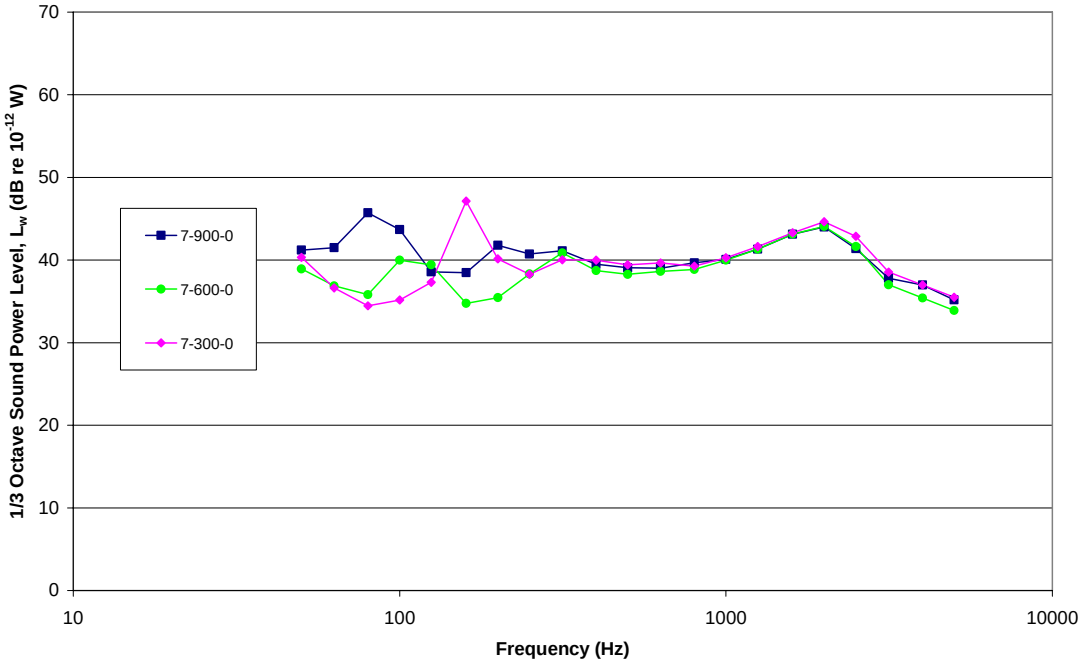

Figure 5.94: ⅓ Octave sound power level comparison for the 7˚ conical diffuser – fitted with a 300, 600 and 900 mm open ended outlet duct at 30 ms^{-1}.

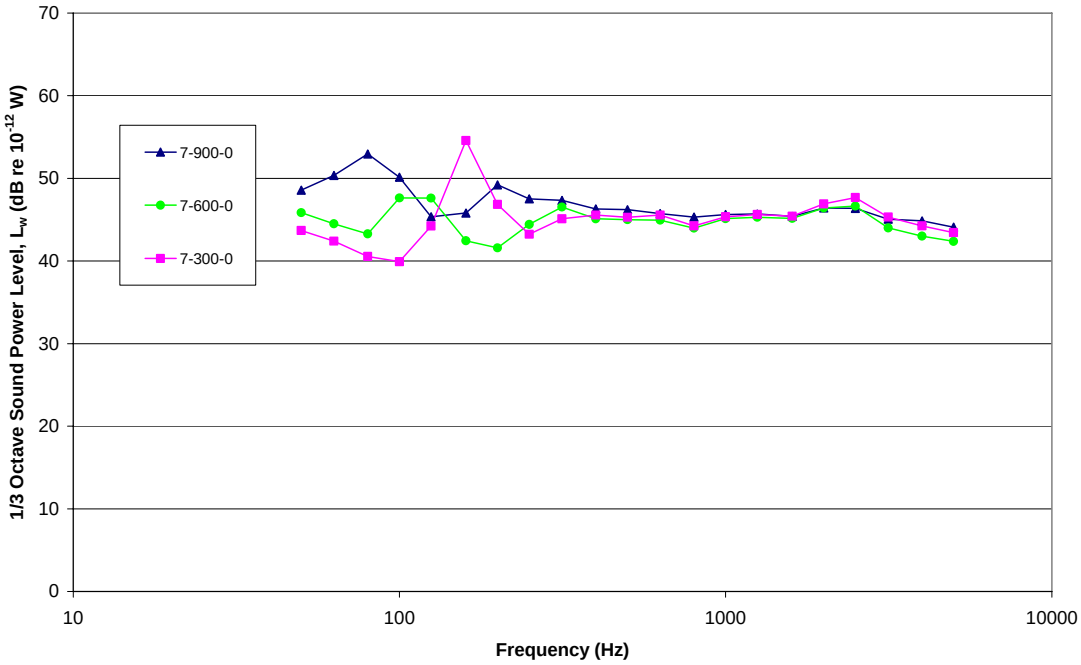

Figure 5.95: ⅓ Octave sound power level comparison for the 7˚ conical diffuser – fitted with a 300, 600 and 900 mm open ended outlet duct at 40 ms^{-1}.

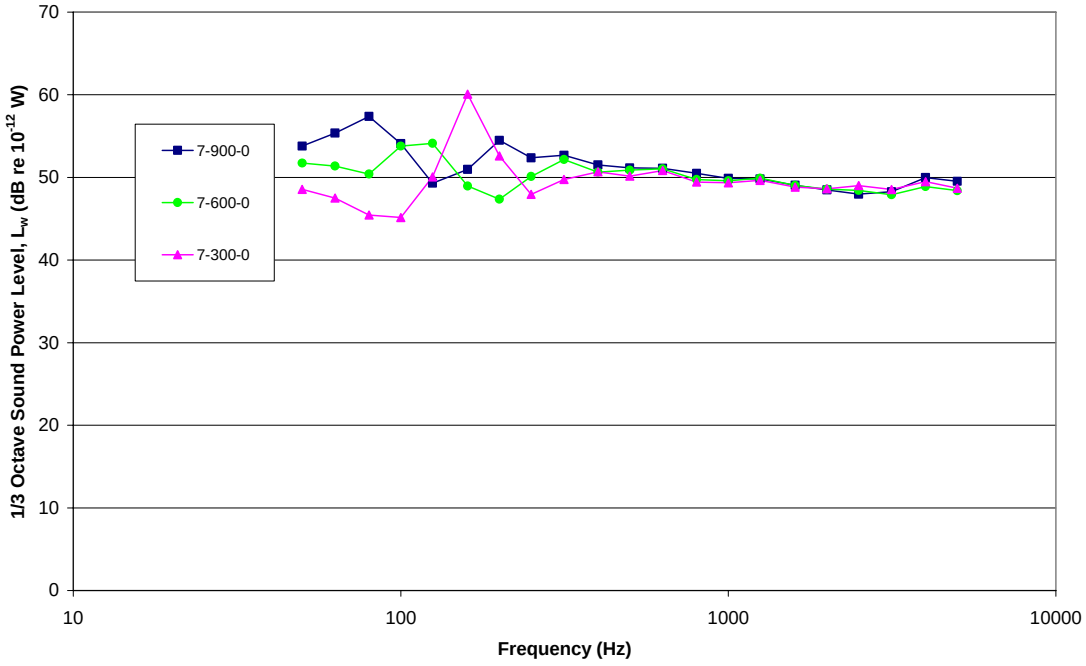

Figure 5.96: ⅓ Octave sound power level comparison for the 7˚ conical diffuser – fitted with a 300, 600 and 900 mm open ended outlet duct at 50 ms^{-1}.

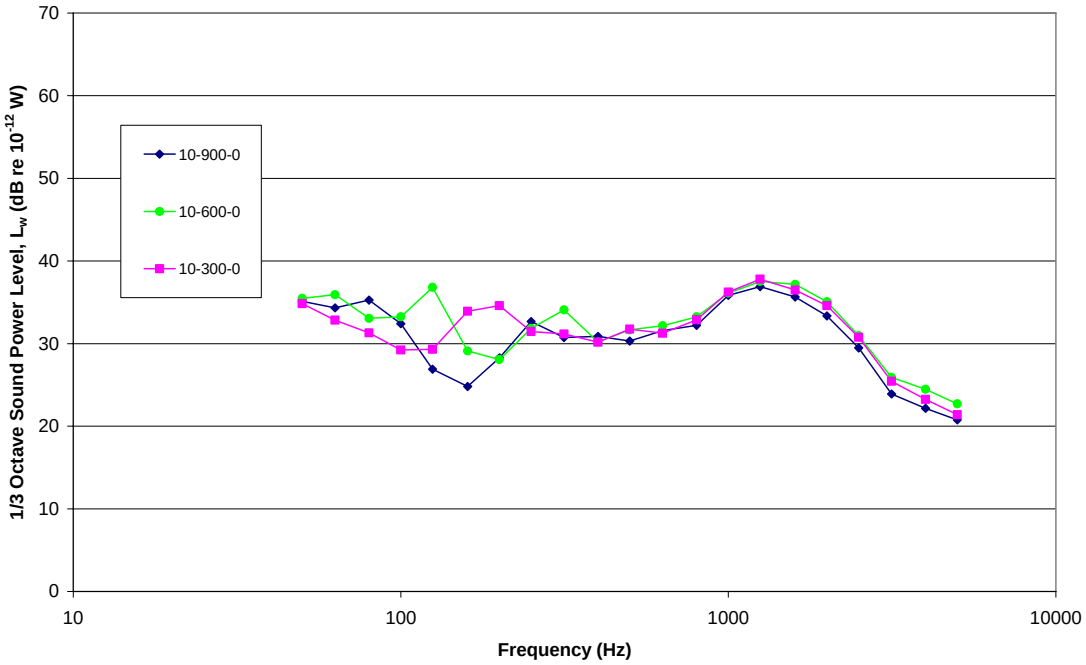

Figure 5.97: ⅓ Octave sound power level comparison for the 10˚ conical diffuser – fitted with a 300, 600 and 900 mm open ended outlet duct at 20 ms^{-1}.

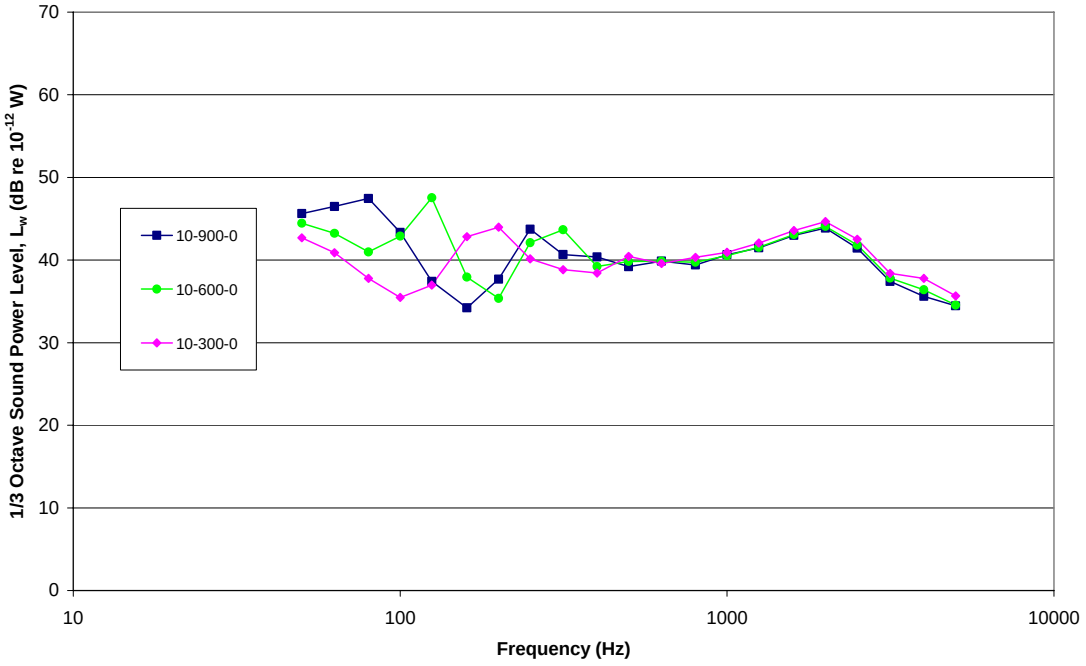

Figure 5.98: ⅓ Octave sound power level comparison for the 10˚ conical diffuser – fitted with a 300, 600 and 900 mm open ended outlet duct at 30 ms^{-1}.

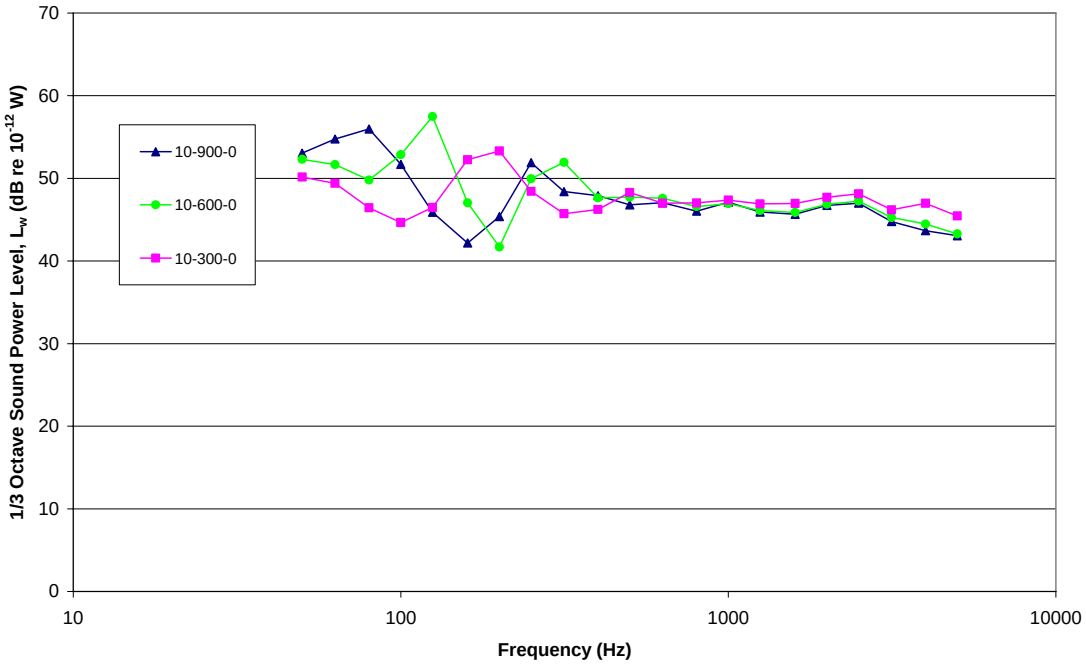

Figure 5.99: ⅓ Octave sound power level comparison for the 10˚ conical diffuser – fitted with a 300, 600 and 900 mm open ended outlet duct at 40 ms^{-1}.

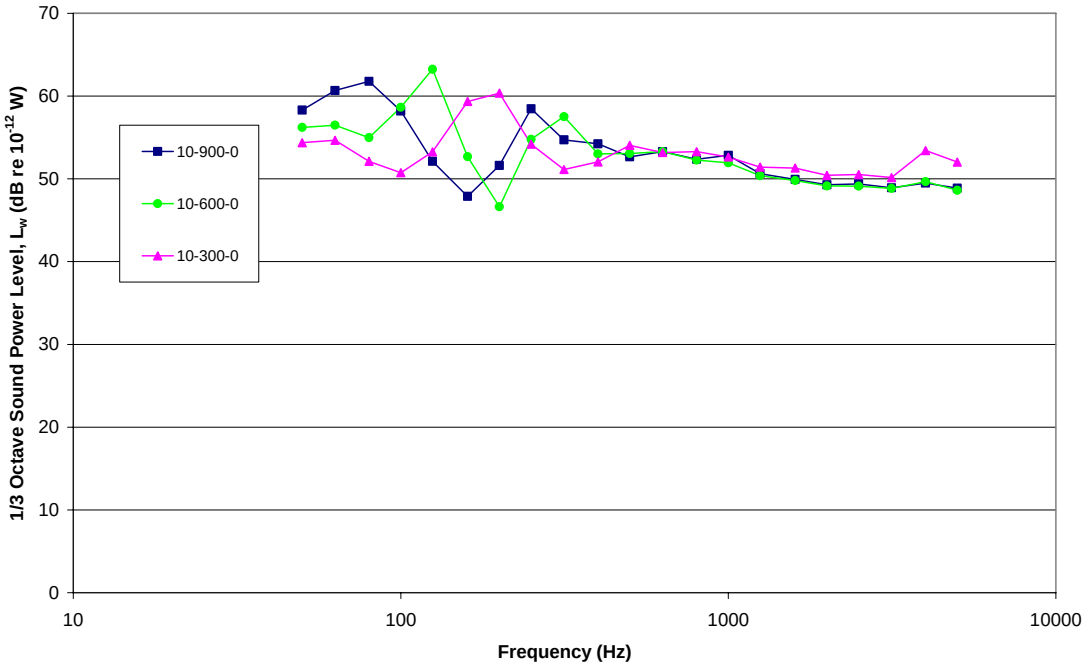

Figure 5.100: ⅓ Octave sound power level comparison for the 10˚ conical diffuser – fitted with a 300, 600 and 900 mm open ended outlet duct at 50 ms^{-1}.

For the 10˚ conical diffuser the 900 mm duct produces a peak sound power in the 80 Hz band and minimum sound power in the 160 Hz band for all four jet velocities used. In comparison the peak and minimum sound power levels for the 600 mm duct are located in the 125 and 200 Hz bands respectively. Meanwhile the peak and minimum sound power levels for the 300 mm outlet duct are located in the 250 and 100 Hz bands respectively. This trend is consistent across each of the four jet velocities used. The magnitude of the fluctuations between the peak and minimum sound power levels increase as the jet velocity rises. The high frequency components of each of the sound power spectra at frequencies above 500 Hz again appear unaffected by changes in the outlet duct length.

The duct length analysis was extended further to also include the 14˚ conical diffuser fitted with the same open ended outlet duct lengths of 300, 600 and 900 mm. The ⅓ octave sound power levels for each of the three outlet ducts at the four reference jet velocities of 20, 30, 40 and 50 ms^{-1} are shown in Figures 5.101 to 5.104. The high frequency components of the sound power spectra above 500 Hz are once again completely independent of any change in the length of the outlet duct. Interestingly this independence also appears to extend to the conical diffuser angle as well. On the other hand however the shape and magnitude of the low frequency components are heavily dependent on the length of the outlet duct. The ⅓ octave frequency band location of the peak and minimum sound power levels for each of the three outlet duct lengths are exactly identical to those identified previously for the 10˚ conical diffuser.

The most significant difference between the 10˚ diffuser cases and the corresponding results for the 14˚ conical diffuser is the sizable increase in the magnitude of the fluctuations in the sound power spectra. At a jet velocity of 30 ms^{-1} there is a variation of 12 dB for the 10˚ diffuser compared with an 18 dB fluctuation for the 14˚ diffuser. The sound power levels in each of the low frequency ⅓ octave bands are also significantly higher for the 14˚ diffuser when compared back to the corresponding results using the 10˚ diffuser.

In summary the length of the outlet duct becomes a critical design variable that can be used to tune the frequency response and attenuation of the overall HVAC outlet.

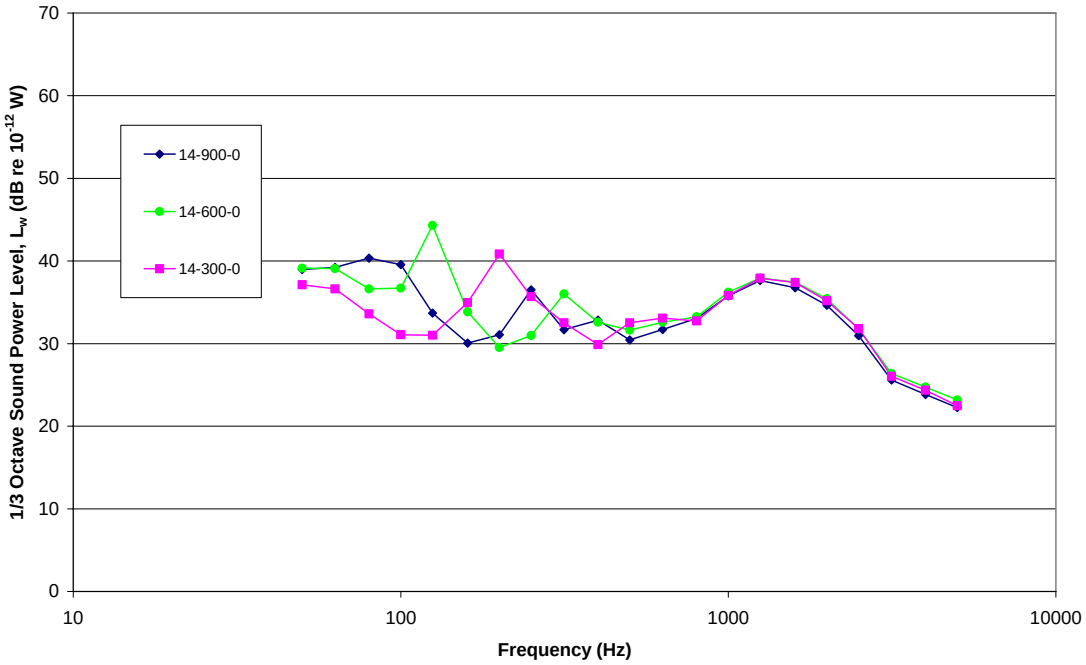

Figure 5.101: ⅓ Octave sound power level comparison for the 14˚ conical diffuser – fitted with a 300, 600 and 900 mm open ended outlet duct at 20 ms^{-1}.

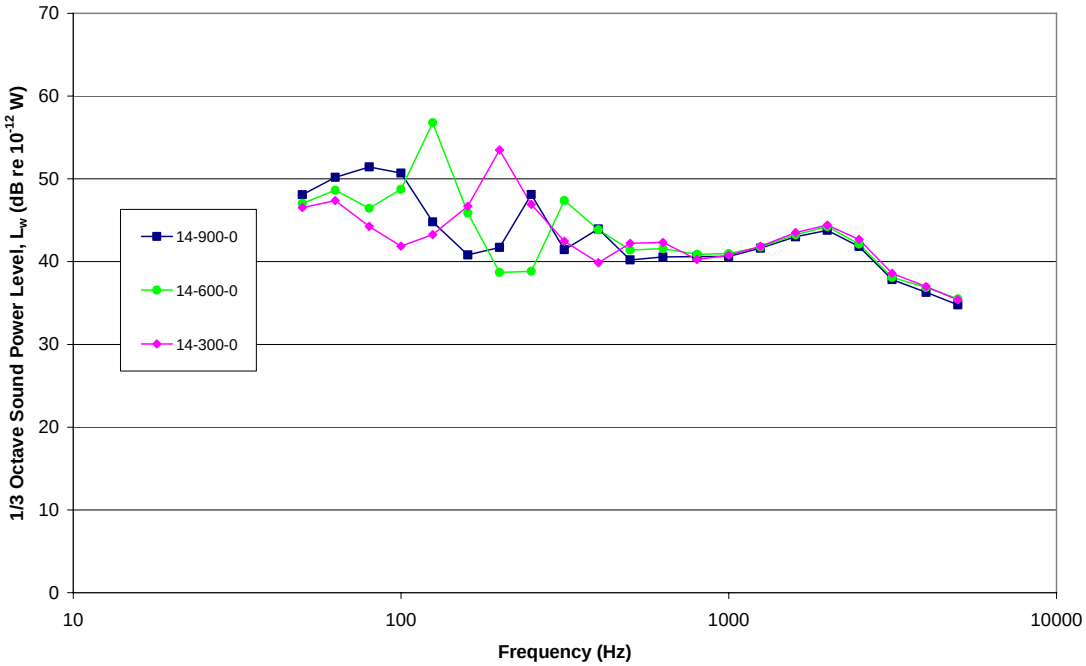

Figure 5.102: ⅓ Octave sound power level comparison for the 14˚ conical diffuser – fitted with a 300, 600 and 900 mm open ended outlet duct at 30 ms^{-1}.

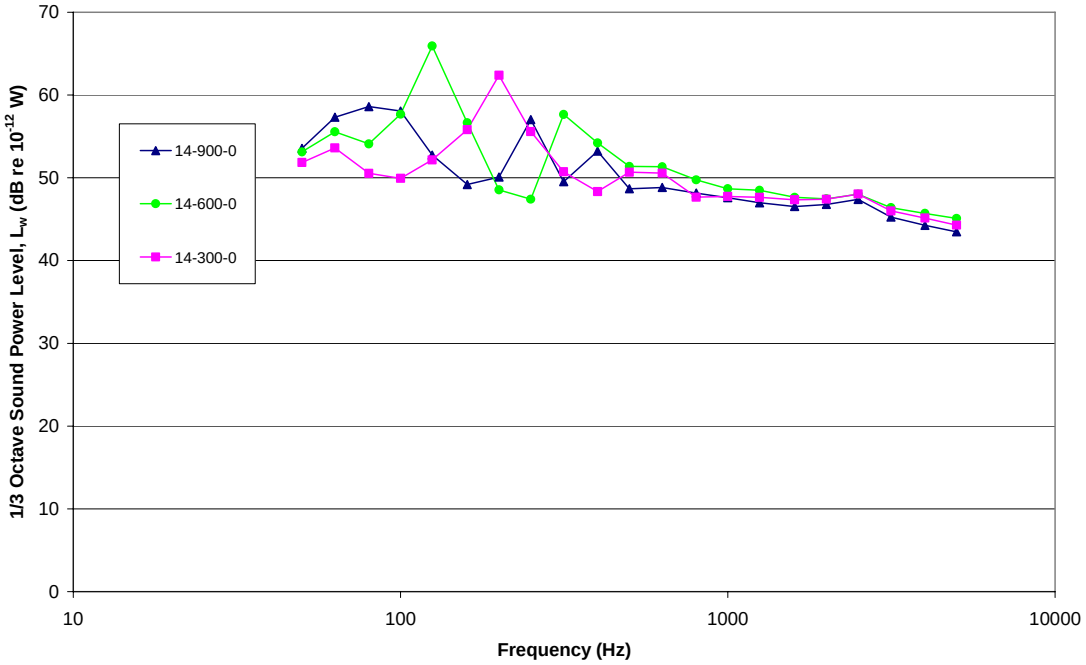

Figure 5.103: ⅓ Octave sound power level comparison for the 14˚ conical diffuser – fitted with a 300, 600 and 900 mm open ended outlet duct at 40 ms^{-1}.

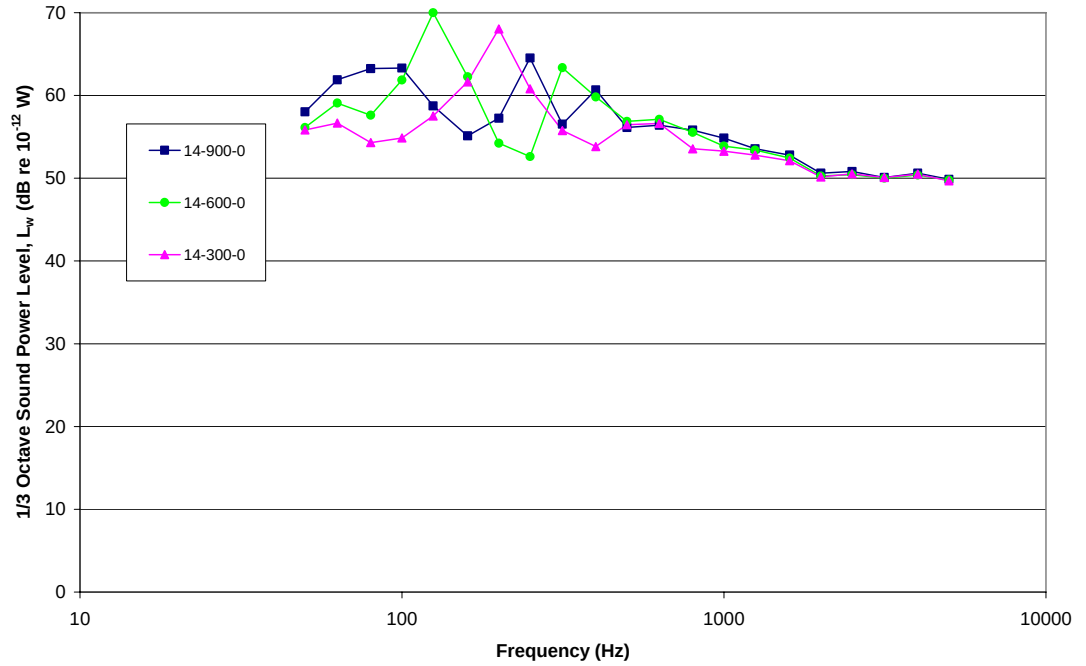

Figure 5.104: ⅓ Octave sound power level comparison for the 14˚ conical diffuser – fitted with a 300, 600 and 900 mm open ended outlet duct at 50 ms^{-1}.

5.7.3 Variation with Outlet Termination Grill Configuration

Neither the outlet duct length nor the conical diffuser angle had any significant effect on the high frequency components of the sound power spectra generated by the expansion of the high velocity jet. Both of these two variables do however have a significant influence on the shape of the low frequency spectra. A series of tests were conducted to compare the effects of fitting different outlet termination grills to the same conical diffuser and outlet duct length to identify the contribution made by the outlet fittings themselves. As the previous results have indicated that the preferred outlet duct length is either 300 or 600 mm the 900 mm duct was not used in these tests. Even though the 14˚ diffuser was found to be less effective than the 7˚ and 10˚ options it has been retained as a part of this analysis. The justification for this decision is based on the potential scenario where space limitations may dictate the use of this diffuser angle, despite the shortcomings acoustically.

A total of 6 individual cases have been selected using each of the three conical diffusers paired with both the 300 and 600 mm outlet ducts. All four potential outlet configurations (RJ, SD, CH and ELCH) have been used along with the additional baseline of no outlet grill (open ended duct).

The ⅓ octave sound power spectra for the 7˚ conical diffuser fitted with the 300 mm outlet duct and each of 5 outlet conditions are shown in Figures 5.105 to 5.107 for jet velocities of 20, 30 and 40 ms^{-1} respectively. Two very important observations can be made from these initial results. Firstly, the selection of the outlet duct configuration has a major impact on the shape of the low frequency sound power spectra across all three jet velocities considered. Of all of the options the cushion head mounted square diffuser with (ELCH) and without (CH) the 90˚ elbow provide the greatest level of noise attenuation. The baseline case of no outlet grill and the two simple grills (RJ and SD) all produce narrow band peaks in the low frequency spectra. The CH and ELCH outlets on the other hand have much flatter low frequency spectra.

The high frequency performance of the CH and ELCH configurations is also dramatically better than the other three cases used. This demonstrates the basis by which the A-weighted total sound pressure levels for these cases were considerably lower than the other options trialled. The SD and RJ outlets have a slightly improved high frequency response over the baseline case of no outlet grill, however this is only in the order of 2 to 3 dB. The CH and ELCH outlet options in comparison provide an improvement of up to 10 dB. Perhaps the most significant result is the high level of attenuation achieved by these two outlets at a jet velocity of 20 and 30 ms^{-1}. This is particularly encouraging given the likelihood that the preferred velocity that would be used in most fast ferry applications falls within this range.

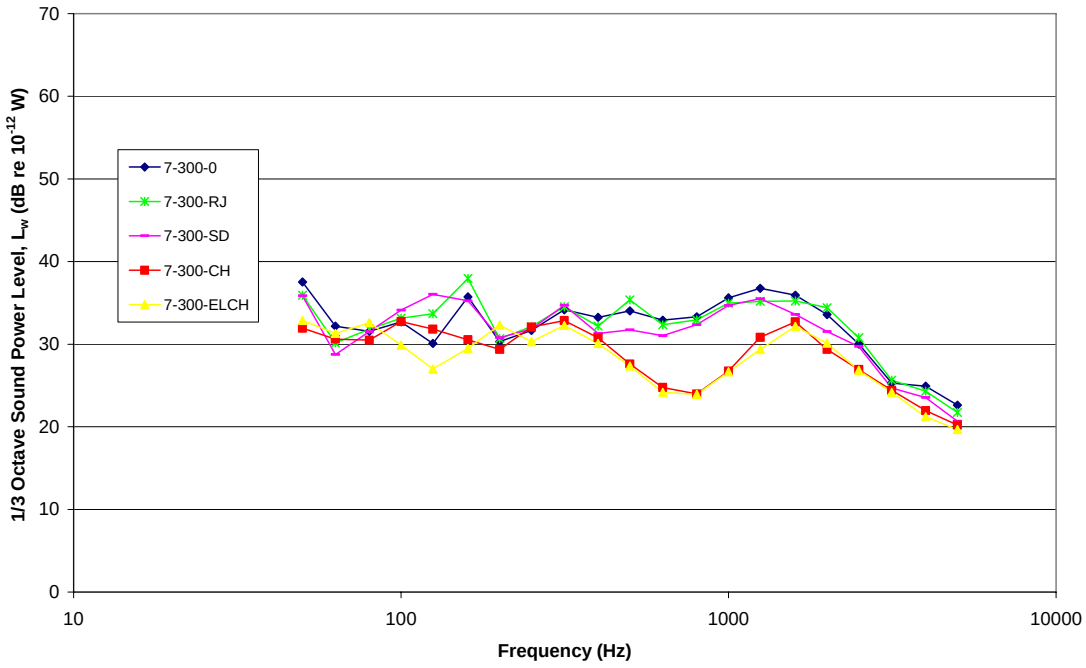

Figure 5.105: ⅓ Octave sound power level comparison between each termination outlet fitted to the 7˚ conical diffuser with a 300 mm long outlet duct at 20 ms^{-1}.

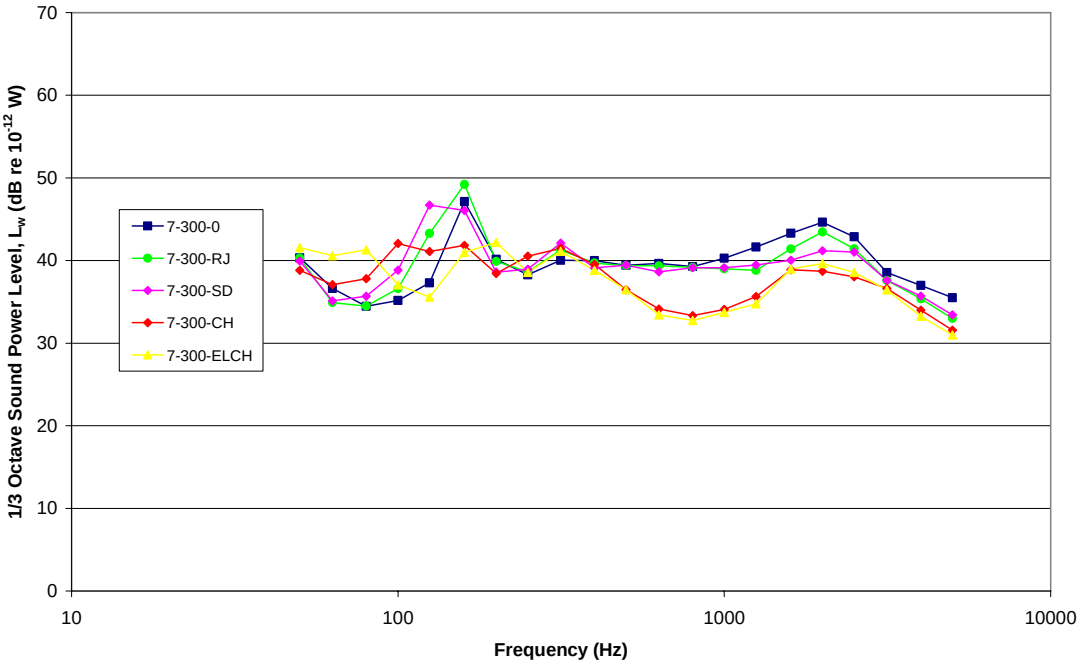

Figure 5.106: ⅓ Octave sound power level comparison between each termination outlet fitted to the 7˚ conical diffuser with a 300 mm long outlet duct at 30 ms^{-1}.

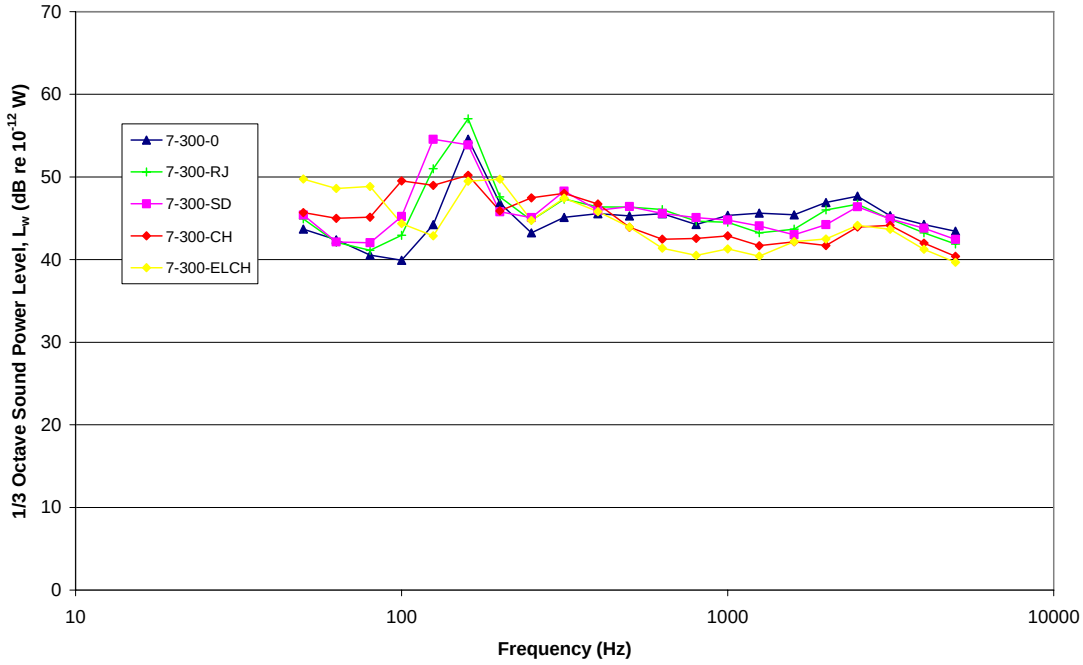

Figure 5.107: ⅓ Octave sound power level comparison between each termination outlet fitted to the 7˚ conical diffuser with a 300 mm long outlet duct at 40 ms^{-1}.

The ⅓ octave sound power spectra for the 10˚ conical diffuser fitted with the 300 mm outlet duct and each of the 5 outlet conditions are shown in Figures 5.108 to 5.110 for jet velocities of 20, 30 and 40 ms^{-1} respectively. As with the 7˚ conical diffuser models both the RJ and SD outlets produce a very sharp low frequency peak in the 160 Hz ⅓ octave band. Both of these peaks are produced at each of the three jet velocities used and the size of the peaks is twice that of the baseline case using no outlet grill. The high frequency spectra for each of these cases are also closely matched to the baseline case.

The CH and ELCH outlets are both again the preferred outlet options, with a flatter low frequency spectra and a lower sound power level across the important high frequency bands. The plain cushion head outlet (CH) has a higher sound power level compared with the ELCH outlet across the 100 to 160 Hz bands and a slightly higher sound power level across the high frequency bands. This variation is most pronounced at a jet velocity of 20 ms^{-1}, with the high frequency performance almost on a par at a jet velocity of 30 and 40 ms^{-1}.

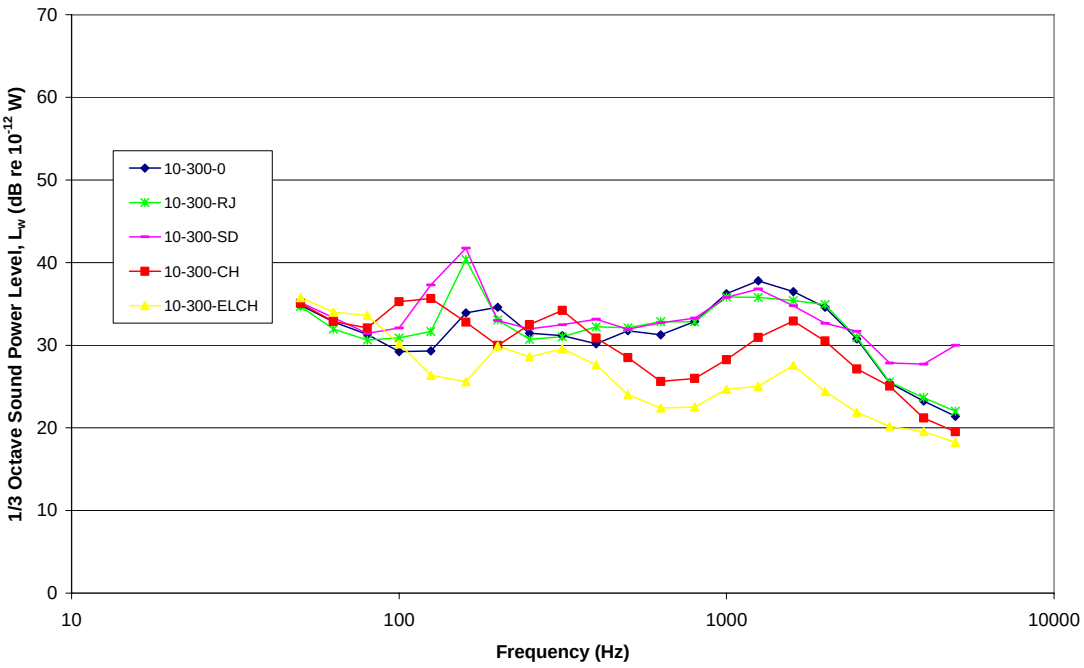

Figure 5.108: ⅓ Octave sound power level comparison between each termination outlet fitted to the 10˚ conical diffuser with a 300 mm long outlet duct at 20 ms^{-1}.

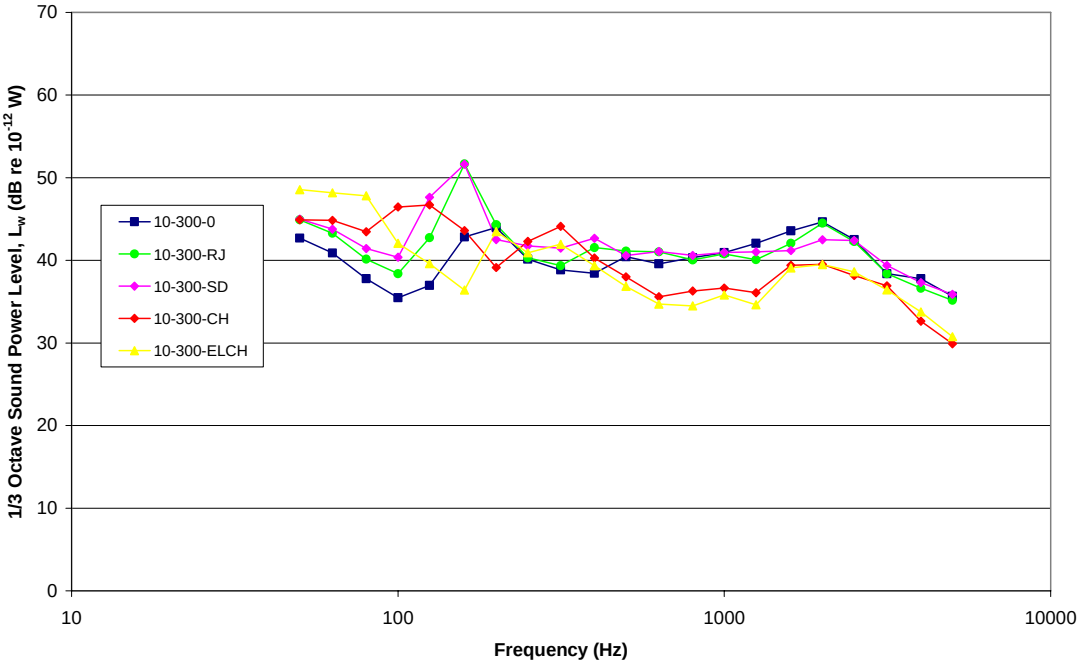

Figure 5.109: ⅓ Octave sound power level comparison between each termination outlet fitted to the 10˚ conical diffuser with a 300 mm long outlet duct at 30 ms^{-1}.

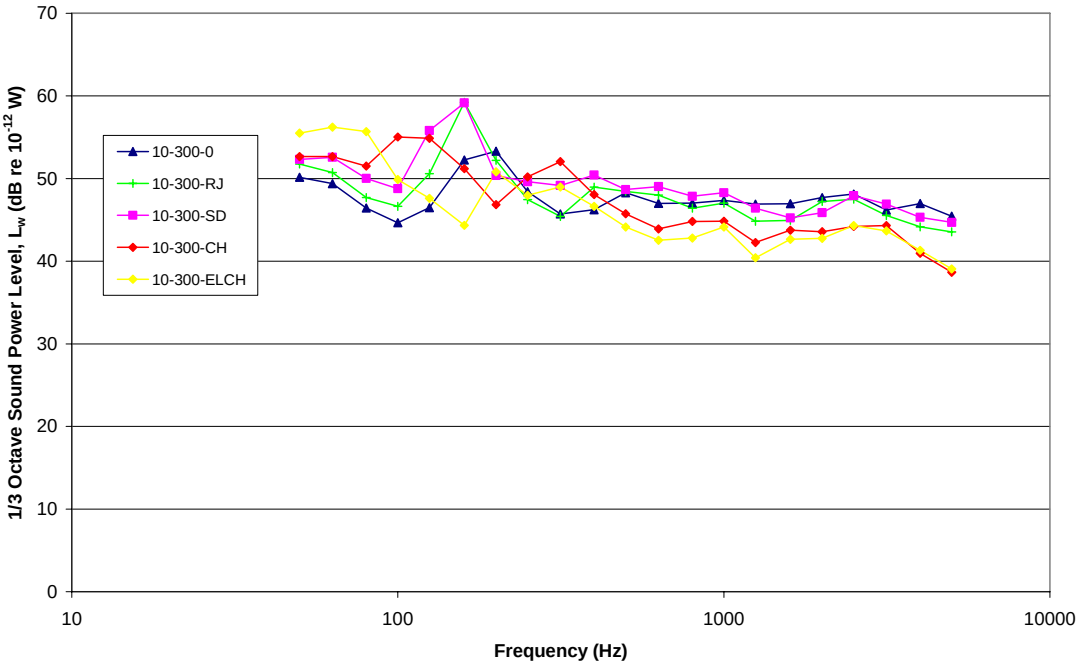

Figure 5.110: ⅓ Octave sound power level comparison between each termination outlet fitted to the 10˚ conical diffuser with a 300 mm long outlet duct at 40 ms^{-1}.

The ⅓ octave sound power spectra for the 14˚ conical diffuser fitted with the 300 mm outlet duct and each of the 5 outlet conditions are shown in Figures 5.111 to 5.113 for jet velocities of 20, 30 and 40 ms^{-1} respectively. Once again the RJ and SD outlets produce a very sharp low frequency peak in the 160 Hz ⅓ octave band, while the baseline case of no outlet grill produces a well defined peak about the 200 Hz band. The peak caused by the RJ outlet is slightly broader than for the SD outlet but at the same order of magnitude. Therefore the total acoustic power associated with the RJ peak is greater than the SD and baseline peaks, both of which occur across a narrow frequency band. On an A-weighted basis the SD curve is a slight improvement, however there is little improvement in the high frequency end of the spectrum. Once again the high frequency spectra for each of these cases are also closely matched to the baseline case.

The CH and ELCH outlets are the preferred outlet options, with superior acoustic performance across both the low and high frequency spectrum. Unlike the 10˚ diffuser models there is no significant difference between the two options. The improvement over the baseline and the remaining two outlet options is once again most prominent with a jet velocity of 20 ms^{-1}.

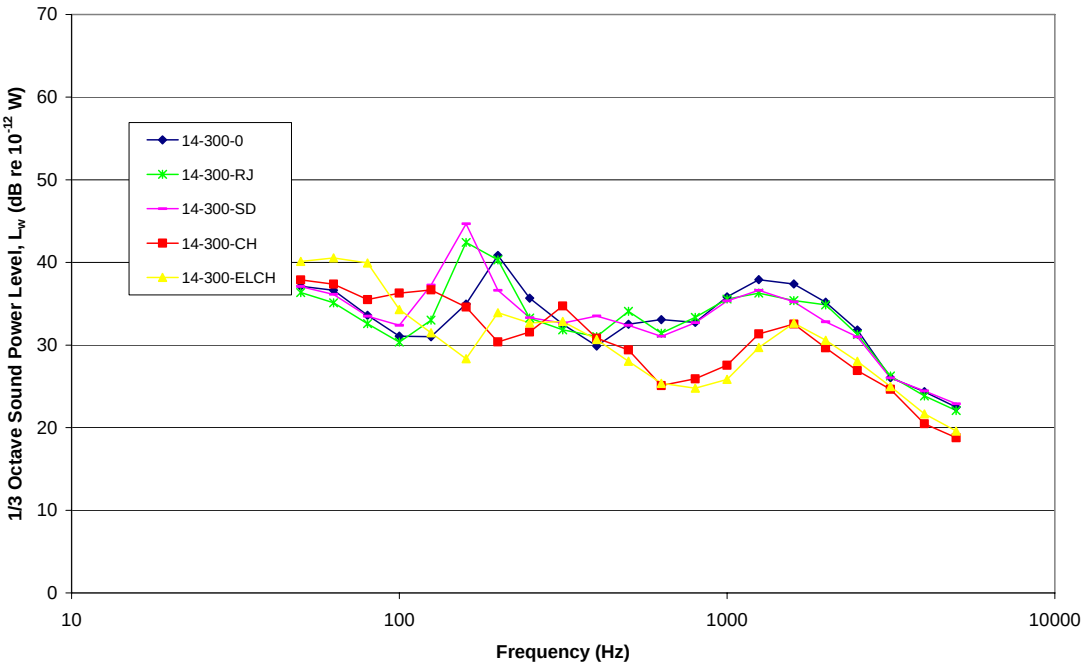

Figure 5.111: ⅓ Octave sound power level comparison between each termination outlet fitted to the 14˚ conical diffuser with a 300 mm long outlet duct at 20 ms^{-1}.

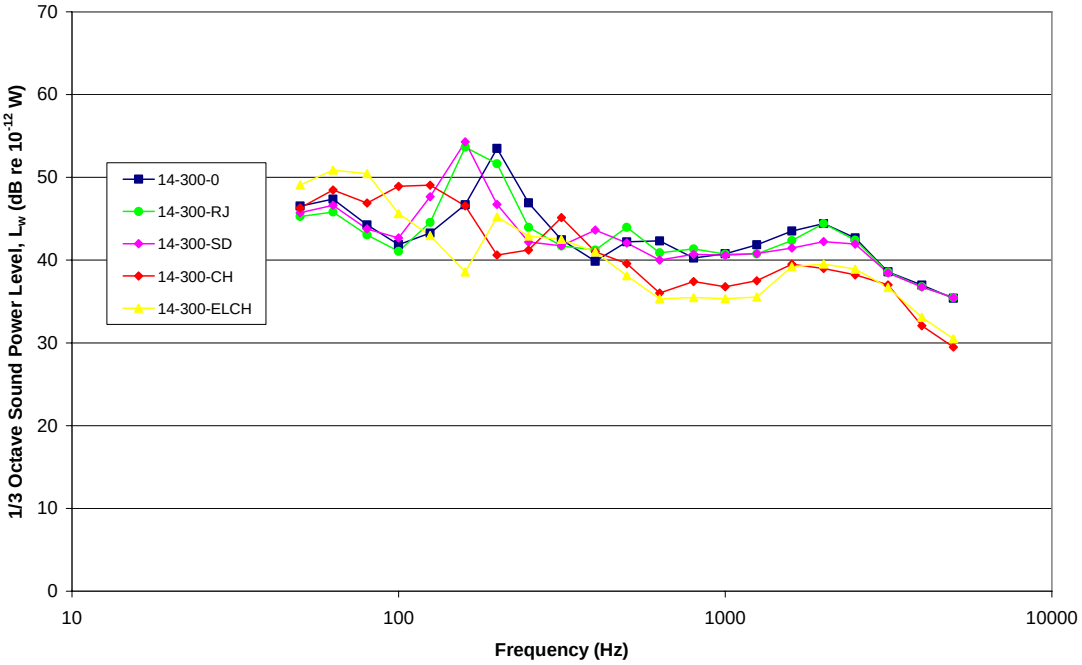

Figure 5.112: ⅓ Octave sound power level comparison between each termination outlet fitted to the 14˚ conical diffuser with a 300 mm long outlet duct at 30 ms^{-1}.

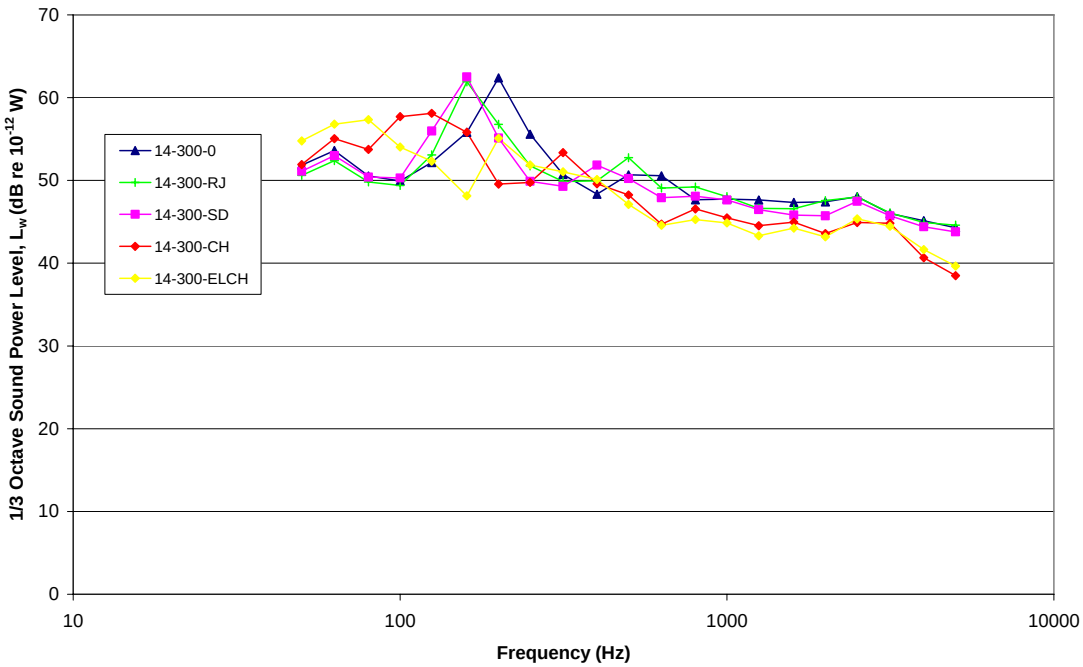

Figure 5.113: ⅓ Octave sound power level comparison between each termination outlet fitted to the 14˚ conical diffuser with a 300 mm long outlet duct at 40 ms^{-1}.

The 300 mm outlet duct provided some promising results, however the presence of the sharp peaks in the low frequency bands are cause for some concern. Knowing that the length of the outlet duct can make significant improvements in the low frequency sound spectra the above analysis was repeated with the 300 mm duct replaced by the 600 mm outlet duct. The ⅓ octave sound power spectra for the 7˚ conical diffuser fitted to each of the 5 outlet conditions are shown in Figures 5.114 to 5.116 for jet velocities of 20, 30 and 40 ms^{-1} respectively.

The use of the 600 mm outlet duct had a major impact on the shape of the low frequency sound power spectrum for each of the 5 outlet conditions. The low frequency sound power levels were all maintained at acceptable levels, with the worst performer being the ELCH outlet. Of the five configurations the ELCH case produced a 50 percent greater variation in the low frequency sound power level when compared with the other four outlets at a jet velocity of 40 ms^{-1}. The performance of the CH and ELCH outlets in the high frequency bands closely match the results using the 300 mm outlet duct. Therefore the preferred outlet option appears to be the CH outlet with a jet velocity of 20 to 30 ms^{-1}.

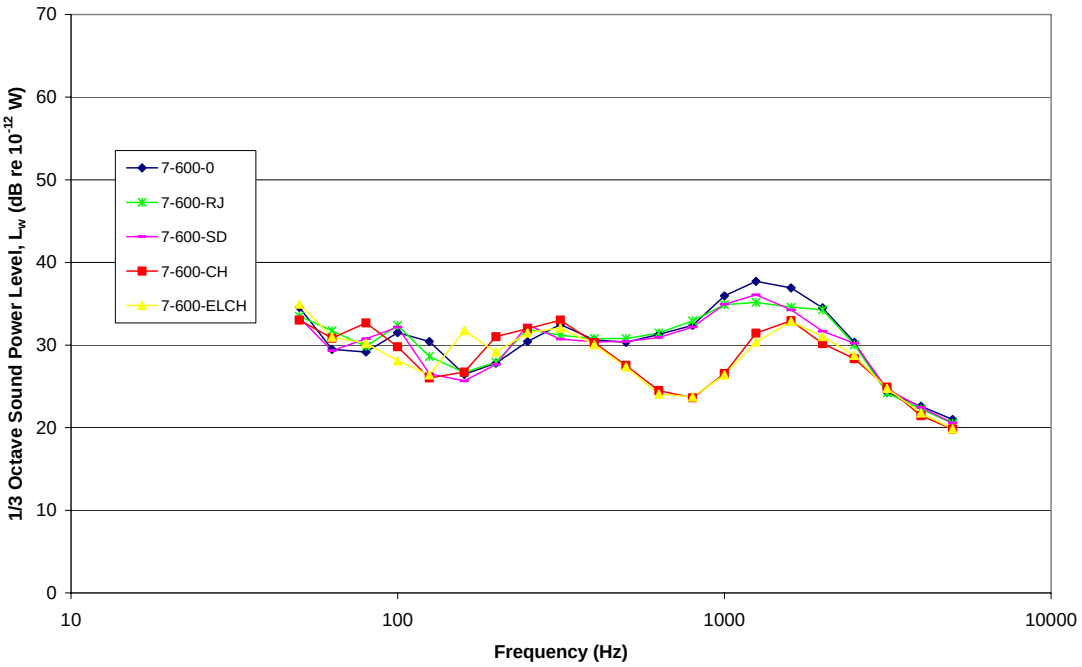

Figure 5.114: ⅓ Octave sound power level comparison between each termination outlet fitted to the 7˚ conical diffuser with a 600 mm long outlet duct at 20 ms^{-1}.

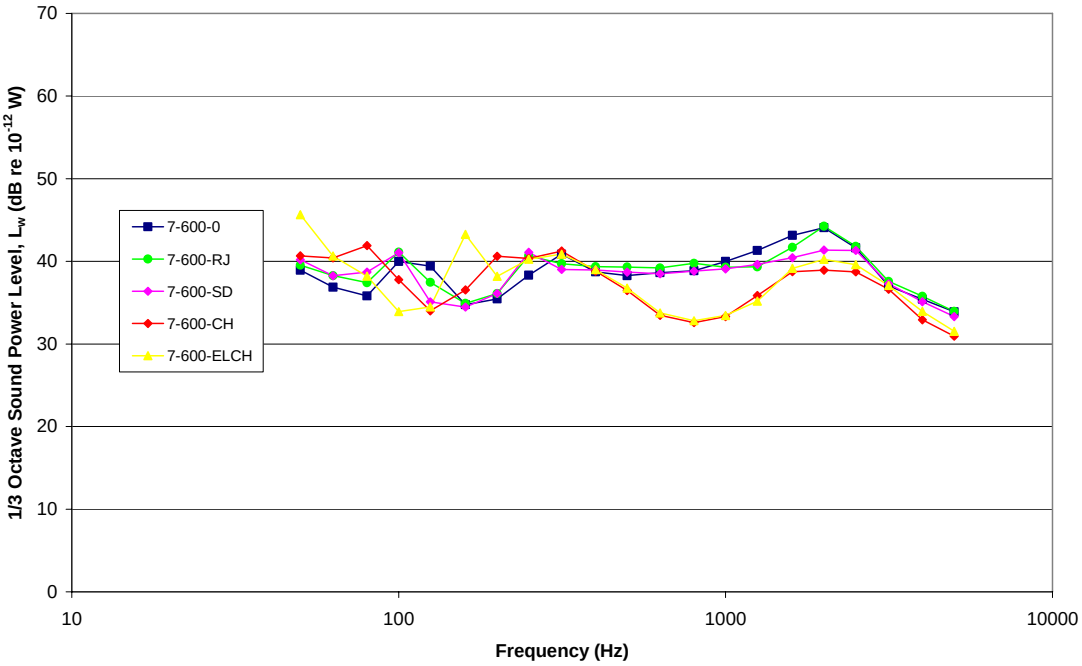

Figure 5.115: ⅓ Octave sound power level comparison between each termination outlet fitted to the 7˚ conical diffuser with a 600 mm long outlet duct at 30 ms^{-1}.

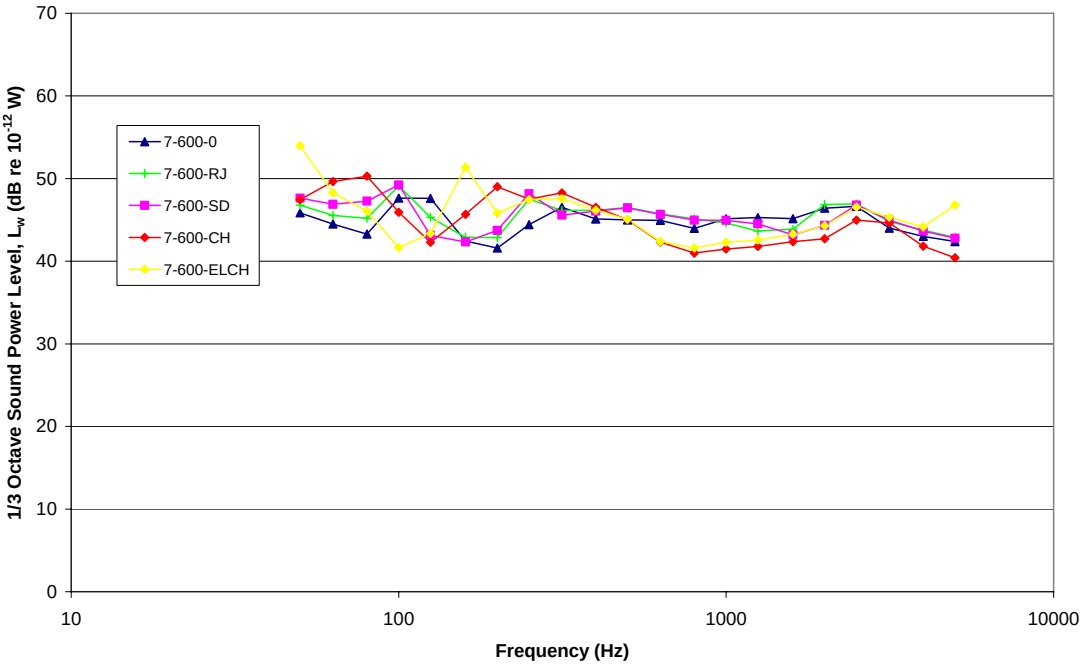

Figure 5.116: ⅓ Octave sound power level comparison between each termination outlet fitted to the 7˚ conical diffuser with a 600 mm long outlet duct at 40 ms^{-1}.

The ⅓ octave sound power spectra for the 10˚ conical diffuser fitted to the 600 mm outlet duct and each of the 5 outlet conditions are shown in Figures 5.117 to 5.119 for jet velocities of 20, 30 and 40 ms^{-1} respectively. There is a small low frequency peak in the 125 Hz ⅓ octave band that is produced by the baseline case of no outlet grill. Each of the four outlet grills out performs this baseline across the whole frequency range of interest. As with the 7˚ conical diffuser fitted to the 600 mm outlet duct the low frequency spectra is well controlled, with the only concern being the ELCH outlet in the 50 and 63 Hz bands.

The high frequency performance of the CH and ELCH is once again far better than the RJ and SD outlet configurations. The SD outlet is marginally better than the RJ outlet across some of the high frequency bands; however this level of improvement is not as effective as the 6 to 10 dB of additional attenuation achieved by the CH and ELCH outlets. Given the minor concerns with the ELCH outlet in the 50 and 63 Hz bands the CH configuration is again the preferred option.

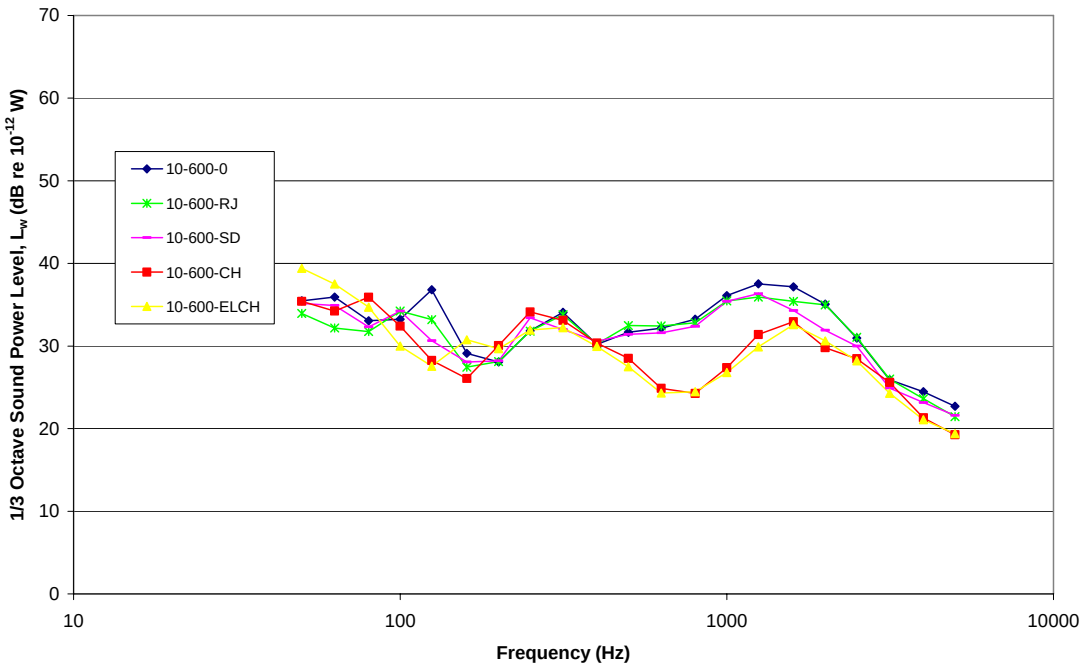

Figure 5.117: ⅓ Octave sound power level comparison between each termination outlet fitted to the 10˚ conical diffuser with a 600 mm long outlet duct at 20 ms^{-1}.

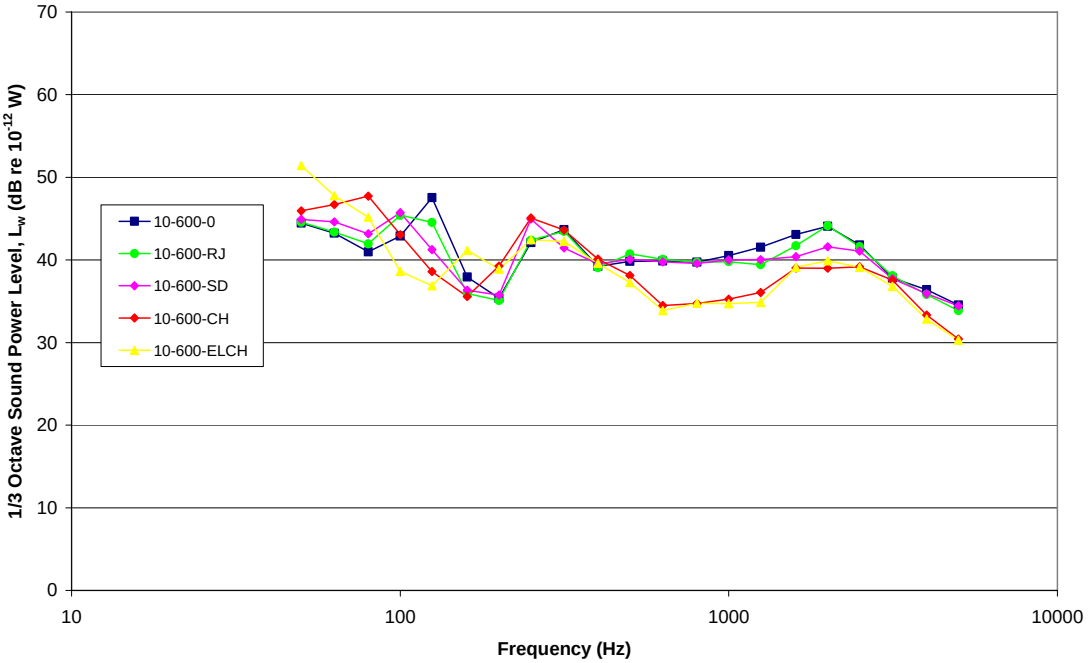

Figure 5.118: ⅓ Octave sound power level comparison between each termination outlet fitted to the 10˚ conical diffuser with a 600 mm long outlet duct at 30 ms^{-1}.

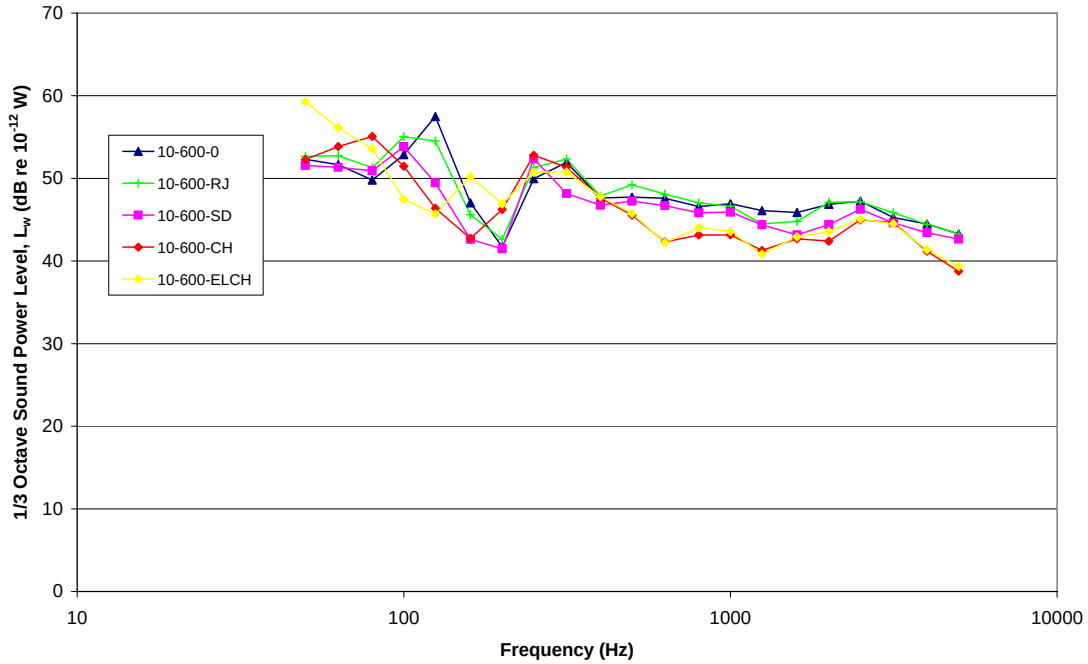

Figure 5.119: ⅓ Octave sound power level comparison between each termination outlet fitted to the 10˚ conical diffuser with a 600 mm long outlet duct at 40 ms^{-1}.

The ⅓ octave sound power spectra for the 14˚ conical diffuser fitted to the 600 mm outlet duct and each of the 5 outlet conditions are shown in Figures 5.120 to 5.122 for jet velocities of 20, 30 and 40 ms^{-1} respectively. The baseline case of no outlet grill produces a primary low frequency peak in the 125 Hz ⅓ octave band and a smaller secondary peak in the 315 Hz ⅓ octave band. As with the 7˚ and 10˚ conical diffusers the low frequency spectrum is well controlled when fitted to the 600 mm outlet duct. Above 100 Hz there is little variation in the low frequency performance of all four outlet duct configurations.

As with all of the previous outlet models the high frequency performance of the CH and ELCH outlets exceeds that of the RJ and SD configurations. The SD outlet is once again marginally better than the RJ outlet, but well above the CH and ELCH options. The improvement gains made by the CH and ELCH outlets are once again most prominent at jet velocities of 20 and 30 ms^{-1}.

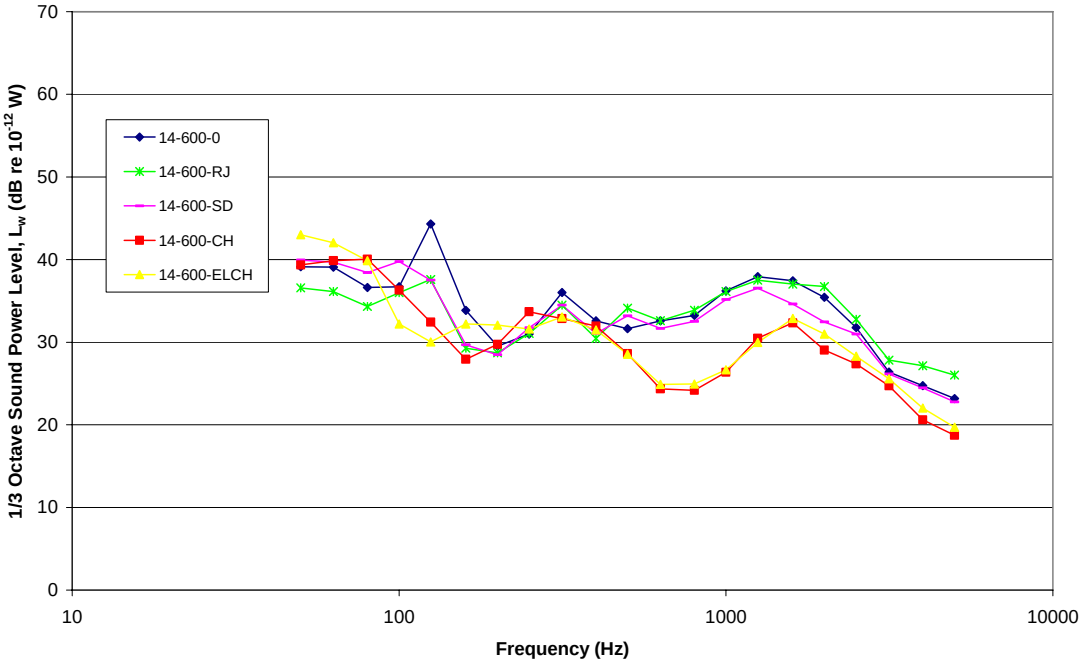

Figure 5.120: ⅓ Octave sound power level comparison between each termination outlet fitted to the 14˚ conical diffuser with a 600 mm long outlet duct at 20 ms^{-1}.

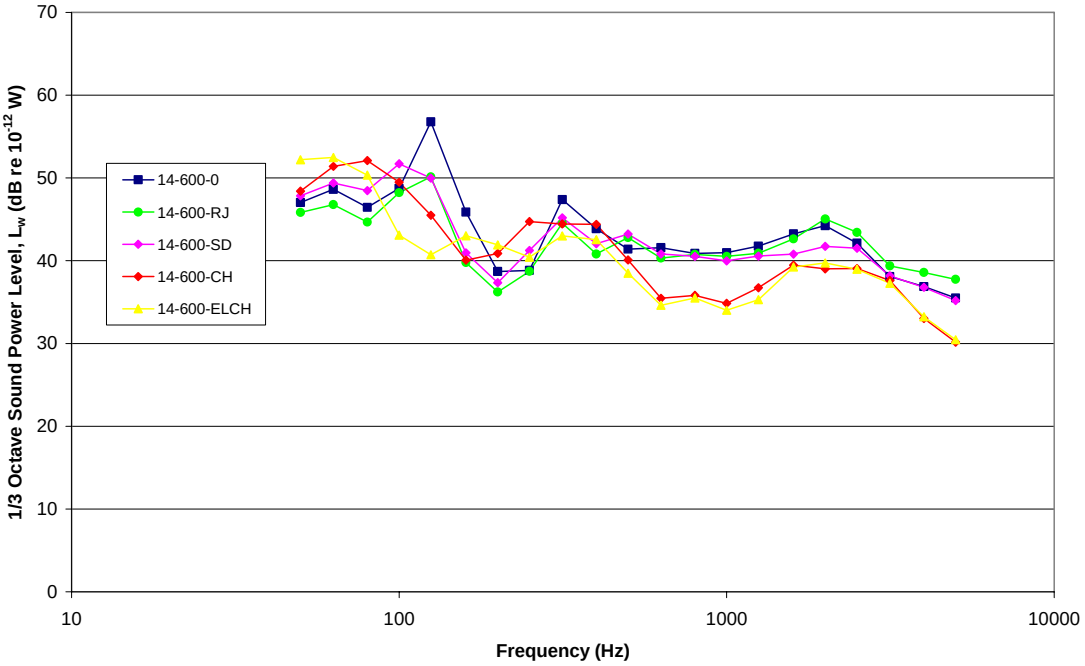

Figure 5.121: ⅓ Octave sound power level comparison between each termination outlet fitted to the 14˚ conical diffuser with a 600 mm long outlet duct at 30 ms^{-1}.

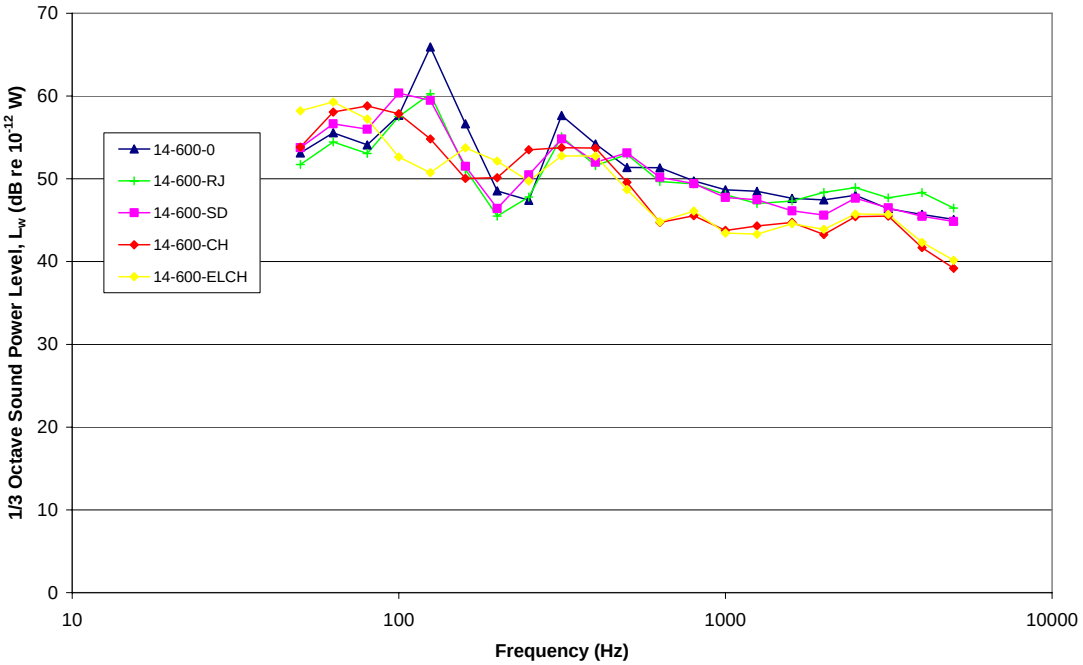

Figure 5.122: ⅓ Octave sound power level comparison between each termination outlet fitted to the 14˚ conical diffuser with a 600 mm long outlet duct at 40 ms^{-1}.

The acoustic lagging material used inside the cushion head box used in both the CH and ELCH outlets clearly has a direct impact on the high frequency sound power levels. The lining inside the cushion head box was only 12 mm thick and there is the option of using thicker material in the future. Increasing the thickness of this material and potentially increasing the area covered by it could add significantly to the attenuation currently identified. Low frequency sound can be controlled effectively through tuning the outlet duct length and the type of outlet grill used (reactive methods). Meanwhile the high frequency sound levels can be effectively minimised by lining header boxes with the correct acoustic lagging material (passive methods).

Underlying all of these strategies it is also important to select the right conical diffuser angle to minimise the onset of flow separation and the subsequent increased levels of noise. The above noise treatment strategies will have a limited capacity to lower the ambient sound power levels, beyond which little can be done. The best noise treatment strategy remains the limiting of the initial acoustic sources rather than containment, reflection or dissipation.

Chapter 6

Numerical Model Development - CFD

The prediction of flow generated noise through the use of a numerical model can significantly reduce the need for extensive experimental investigations and provide a valuable design tool for identifying optimum duct designs. Predicting the corresponding noise levels for potential duct systems can also reduce the possibility of exceeding the desired design specifications and the resulting added costs of rework. The potential risk of having the delivery schedule of a vessel delayed can far outweigh the cost of initial numerical modelling to ensure that the required design specifications will be satisfied. The key elements of a successful numerical model are to firstly predict the flow inside the duct network accurately and secondly predict the resulting noise levels inside the passenger cabin.

A CFD based numerical model was developed to predict the flow generated noise (sound power) for a given jet velocity and outlet configuration. The ultimate purpose of the numerical model is to provide a design tool for predicting the noise generated by proposed high velocity HVAC duct systems. A two-step uncoupled modelling process is used to firstly determine the turbulent flow field and secondly the associated sound pressure levels downstream from the diffuser outlet. By using an uncoupled analysis the modelling process is simplified and the overall computational cost reduced.

The primary purpose of the CFD models used in this work is to provide a suitable transient turbulent flow field for use in predicting the flow generated noise associated with decelerating high velocity airflow inside a HVAC duct. The model also provides a secondary flow analysis for a range of diffuser angles, lengths and duct outlet configurations. This proved useful in identifying the fundamental flow regimes generating the sound measured in the corresponding experimental studies. Rather than solve an entire duct system the purpose of the models developed in this study was to identify the mechanisms driving the generation of turbulence in the flow through the

diffuser outlet and the resulting generation of sound. The transient three dimensional flow field is solved using a LES turbulence model. The sound pressure field is then calculated using a far field acoustic analogy based post processor.

6.1 Model Formulation and Assumptions

The primary purpose of the CFD flow model was to generate the time varying velocity and pressure fields required for input into the acoustic post processor. Given the simple case of an axis-symmetric circular jet the flow model could be simplified down to a two dimensional problem with significant computational savings. However, any model based on this assumption would not account for circumferential fluctuations in both pressure and flow velocity. Although these fluctuating quantities will have a statistical average of zero over time, at any given instance this will not necessarily be the case. Based on these assumptions a fully three dimensional model was selected for the flow field analysis.

The underlying requirement of the model was an accurate simulation of the three dimensional transient pressure and velocity fields. Several turbulence models were considered for generating this data, with the primary selection criteria being the accuracy of the turbulence model and the respective computational cost involved. The three main transient turbulence models considered were RANS, LES and DNS. Of these three models the LES turbulence model was selected as the best compromise between accuracy of the turbulence scales in the model and the computational resources available.

In time future analyses may be able to make use of a full DNS model in line with increasing computational resource availability. It is the author's view however that the reality of this eventuating is less likely given the trend of increasing model complexity matching the advancement in computational power. The development of the LES based models will also provide a useful tool for more commercially based simulations which will ultimately drive the demand for these simulation tools.

The turbulent flow phenomenon observed within the various outlet diffusers investigated herein were quite complex due to the interaction between the primary and secondary expansion of the high velocity jet. The primary expansion occurred inside the conical diffuser with a subsequent secondary expansion as the airflow entered the free space of the simulated passenger cabin. The interaction of these expansion zones produces a complex transient non-isotropic turbulence flow regime. As a means of simplifying the initial modelling process the simple case of a circular jet entering the cabin space directly was considered. This model allowed the overall numerical modelling technique to be developed and refined without the added complexities of accounting for the interaction between the multiple expansion zones within the flow domain.

The straight circular jet model was also used to determine the size of the external flow domain used to simulate the passenger cabin space. The external flow domain was sized by balancing the tradeoff between the size of the computational flow domain and limitations in computational resources. The basic geometry of the simple circular jet model is shown in Figure 6.1. A single jet diameter of 50 mm was used to match the experimental work already covered in Chapters 4 and 5.

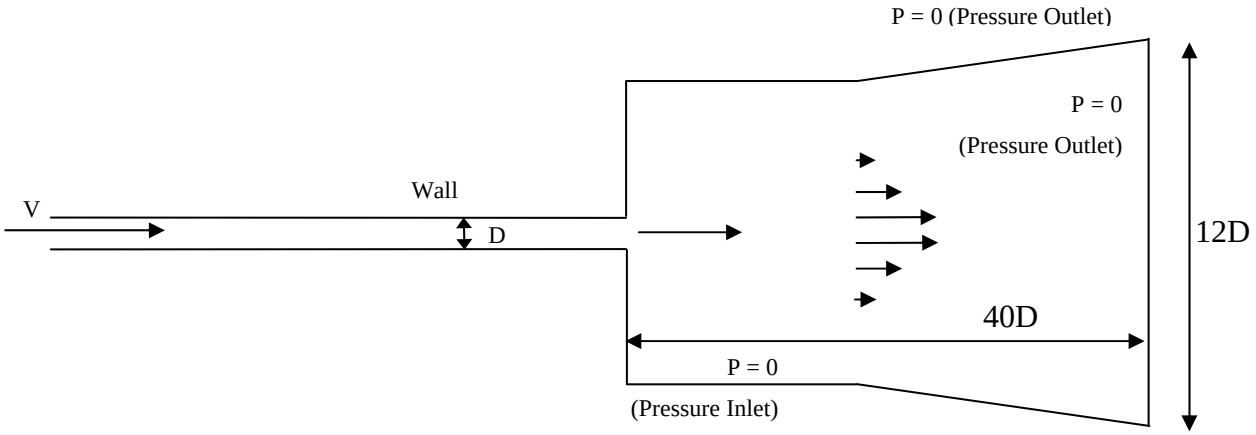

Figure 6.1: Sectional view of the circular jet and the surrounding flow domain

The flow domain consisted of an inlet section of 50 mm pipe with a wall boundary condition and an extended external flow domain around the end of the 50 mm inlet pipe. Two different outlet regimes were considered, one with a wall surrounding the outlet of the pipe and the other with the pipe discharging into free space. As the

results presented in the forthcoming chapters will illustrate there was negligible difference in the exhaust jet flow field and the associated sound power spectra generated.

The numerical model of the conical diffuser models all utilised an open outlet domain surrounding the exit from the enclosed duct section. The free space outlet domain was used so as to match the experimental conditions encountered inside the reverberation rooms used for sound power measurements. Although this outlet condition doesn't match the end application onboard a passenger ferry, a sound power analysis enables a direct correlation to be made, where the acoustic properties of the respective environments can be accounted for.

Figure 6.2 shows the cross section of the three-dimensional geometry of the 50 mm diameter jet, 7˚ conical diffuser and the surrounding outlet flow domain. The conical diffuser is connected to a 150 mm diameter outlet pipe which in turn is surrounded by an external flow domain with a radial extension of 12 jet diameters. The upstream domain extends 3 jet diameters while the downstream domain extends 36 jet diameters. A more detailed model would incorporate an outlet domain of far greater length and girth with a larger upstream extension. Computational limitations have led to this compromise due to the extensive solution time required to numerically simulate the flow generated noise.

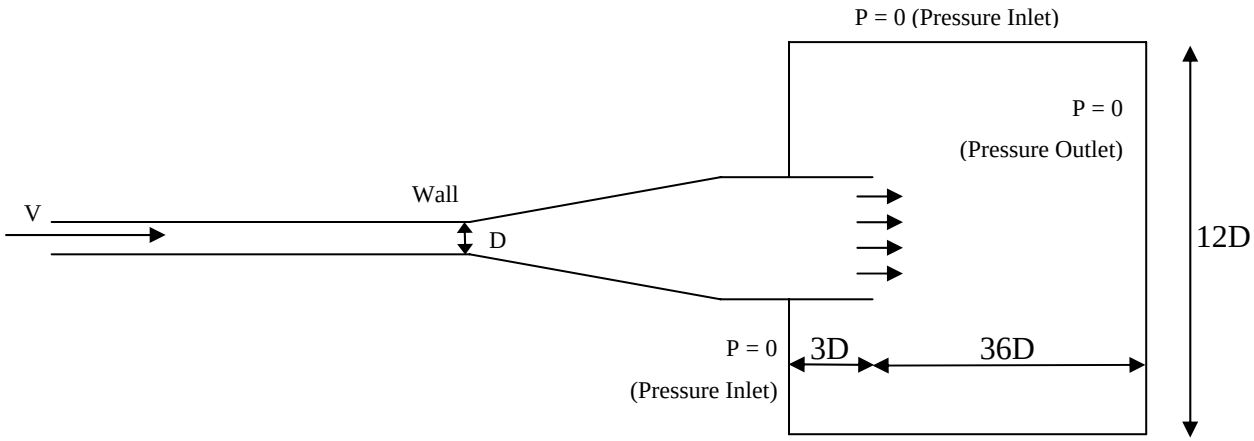

Figure 6.2: Sectional view of the 7˚ conical diffuser and the surrounding flow domain

The numerical flow model was created and solved using the commercially available CFD package Fluent 6.2. The segregated unsteady solver with a LES turbulence model was used to simulate the time varying velocity and pressure within the model. The Smagorinsky-Lilly sub-grid scale model was used with a Smagorinsky constant, C_s of 0.08.

The governing equations for the LES model are derived by filtering the time-dependent Navier-Stokes equations, which effectively filters out all eddies on a scale smaller than the filter width or mesh spacing defined in the model. An axial mesh spacing of 2 to 4 mm was used with negligible difference between models. More detailed information on the derivation of these equations can be found in Ferziger [157] and Sagaut [154].

6.2 Boundary Conditions

6.2.1 Jet Inlet

The circular jet of air in the inlet section is assumed to be fully developed turbulent pipe flow. An average mass flux and fully developed turbulent velocity profile are applied at the upstream inlet. The velocity profile was generated using an existing pipe and recycling the velocity profile from the exit of the pipe back to the inlet. By applying this approach in an iterative manner a fully developed velocity profile was generated for each jet velocity considered. The turbulence intensity *(I_T)* at the jet inlet is calculated using empirical correlations for pipe flows [238] and is defined as:

$$I_T = \frac{u'}{u_{avg}} = 0.16\left(\mathrm{Re}_{Dh}\right)^{-1/8} \tag{6.1}$$

where the Reynolds number (Re_{Dh}) is based on the mean jet velocity and the diameter of the jet (50 mm). The turbulence intensity is used to vary the local mass flux in each cell on the jet inlet face. A random number multiplier is used to generate a fluctuating localised mass flux that is scaled to ensure an average mass flux is maintained across the pipe inlet as a whole. This method provides a statistically steady turbulent velocity profile without artificially driving the static pressure at the boundary.

A standard velocity inlet was initially employed with both an incompressible and compressible flow model. The compressible flow model developing small scale instabilities inside the inlet pipe containing the jet. When these instabilities were left unchecked over thousands of iterations (in time) the magnitude increased exponentially, while maintaining a mean value corresponding to the expected flow regime. The frequency of these fluctuations in flow velocity and static pressure directly correlated to the length of the pipe containing the upstream jet, as shown in Figures 6.3 and 6.4 respectively. When the velocity inlet was replaced with the mass flux boundary condition mentioned above the instability in the flow regime was eliminated entirely.

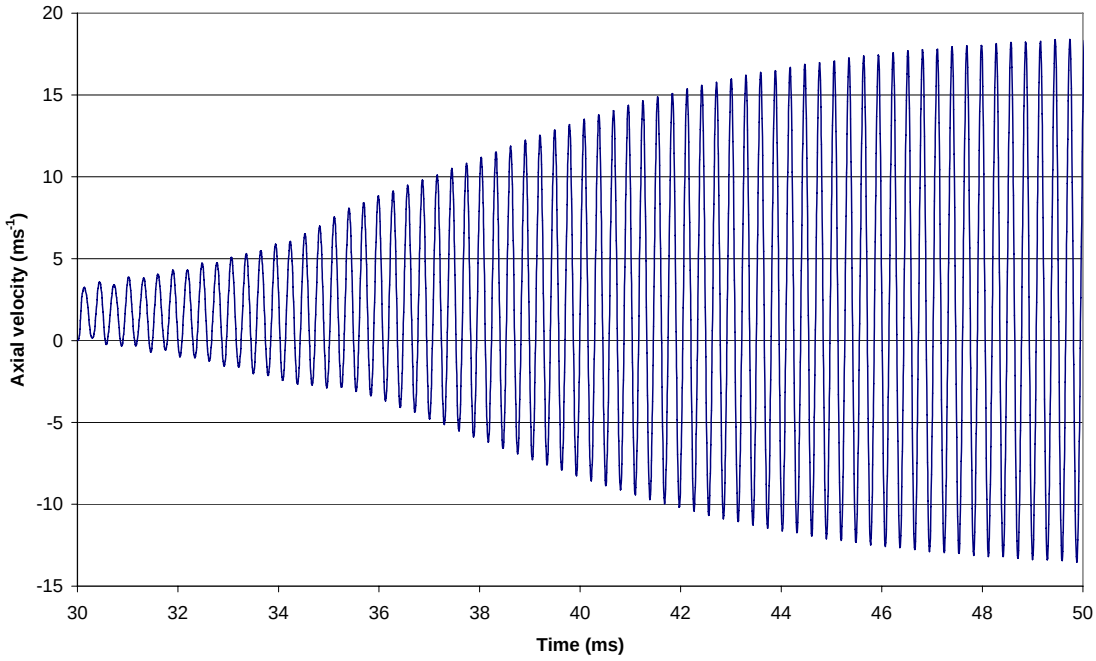

Figure 6.3: Velocity instabilities from a velocity inlet boundary condition used with a compressible flow model.

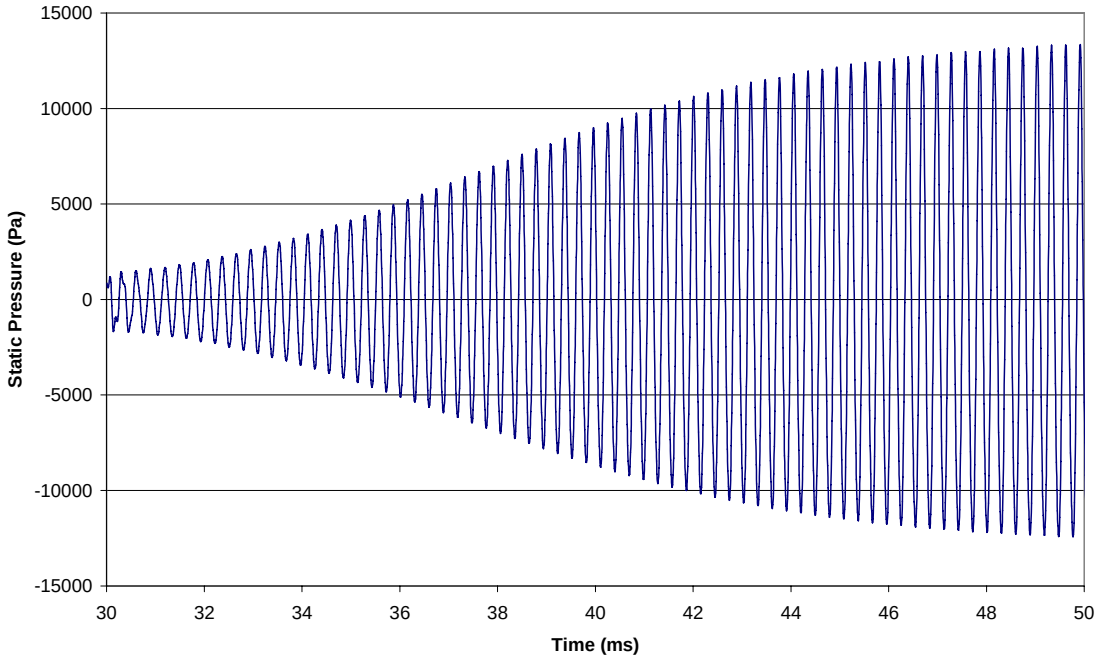

Figure 6.4: Pressure instabilities from a velocity inlet boundary condition used with a compressible flow model.

6.2.2 External Flow Domain

The external flow domain surrounding the outlet of the diffuser contains a combination of pressure inlets and pressure outlets where the local static pressure is set to zero gauge pressure. By ensuring that the boundary of the external flow domain was sufficiently removed from the duct outlet itself the independence of the fluctuating pressure surrounding the outlet of the duct was preserved. The use of an incompressible flow model allowed the overall external flow domain to be much smaller and negated the need for complex non-reflecting boundary conditions.

Initial acoustic analysis suggests that a compressible flow model would be required so as to accurately simulate the localised compression of the air as sound waves radiate from their respective source points. On closer inspection however the actual fluctuations in acoustic pressure and thus the air density are so small in relation to the flows under consideration that the flow is effectively incompressible. By using a far field acoustic analysis in the form of an uncoupled post processor the need for a compressible flow model is based solely on the influence of any sound on the flow regime itself, otherwise known as “self noise”. At the air velocities considered in this study (10 to 50 ms^{-1}) the flow is not significantly influenced by the resulting generated sound pressures.

If a fully integrated computational aero-acoustic model is used, a compressible flow model would be required along with non-reflective boundary conditions. Although this solution method is available the additional computational costs is prohibitive. With such a model the external flow domain would also have to be considerably larger so that all of the acoustic monitoring points (receivers) are located inside the computational flow domain. If the acoustic pressures generated by the flow impacted on the flow regime itself this type of coupled analysis would be required. In all of the cases investigated herein the acoustic particle velocities were several orders of magnitude smaller than the corresponding fluctuating turbulent flow velocities associated with the flow field itself. Therefore a compressible flow model was not absolutely necessary for this particular analysis.

6.2.3 Pipe Walls

The walls of the upstream pipe containing the air jet are assumed to be non-slip and isothermal. Viscous heating was incorporated into the turbulence flow model to ensure accurate simulation of energy dissipation. The application of the fully developed turbulent velocity profile at the inlet of the pipe (outlined above) ensured that the velocity gradients at the pipe walls were correctly established. Applying this profile to the mass flux inlet boundary condition also reduced the length of the upstream inlet pipe used in the numerical model. This minimised the computational cost of the fine mesh used to satisfy the maximum wall $y^+ \approx 1$ requirement of the LES turbulence model.

6.3 CFD Solution Method

6.3.1 Initial Conditions

The initial guess for the unsteady LES model was calculated based on a steady k-ε turbulence model. The steady-state flow model (non-transient) enabled a fast and effective means of establishing a reasonable approximation of the average flow variables of velocity and pressure throughout the flow domain. Starting without a detailed approximation of the flow regime the LES model proved time consuming and cumbersome due to the large transients associated with an incorrect initial flow approximation. Both the centreline jet velocity and the corresponding static pressure increased slightly when switching from the k-ε turbulence model to the LES model. This disparity between the two solutions generated transient fluctuations within the flow domain that dissipated over time. With the use of adaptive time stepping these initial start-up transients in the LES model were eliminated within 30,000 to 40,000 time steps. A further 40,000 to 60,000 time steps were required to generate the statistically steady flow profile required to initiate the recording of the acoustic source data used in the far field acoustic post processor.

Aside from providing a valuable initial guess for the LES model, the k-ε turbulence model also provided a useful design tool for making an initial assessment of the diffuser geometry and corresponding flow profile. Using this basic level of analysis provided a relatively quick indication of the potential for each diffuser configuration investigated. The large number of time steps and the size of the models used to complete a full acoustic analysis results in a relatively high computational cost. This cost must be justified against both technical and budgetary constraints. In a commercial application this approach will lead to significant computational savings by limiting the number of complete acoustic simulations required to develop an optimal design solution.

6.3.2 Discretisation Schemes

Second order discretisation schemes were used for all variables and the Pressure-Implicit with Splitting of Operators (PISO) scheme was used for the pressure-velocity coupling. The initial k-ε turbulence model was solved using the steady solver in Fluent 6.2. The second order upwind discretisation scheme was employed to solve both the momentum and energy equations as well as calculating density (for compressible flow models).

The LES model was then solved using the segregated 2^{nd} order implicit unsteady solver in Fluent 6.2. Central differencing discretisation schemes were employed to solve both the momentum and energy equations, while the 2^{nd} order upwind scheme was used for calculating density (for compressible models only). Initial LES models were run in earlier versions of Fluent 6 using 2^{nd} order upwind discretisation. These models produced artificial dissipation of the turbulence in the flow leading to an under prediction of the flow generated sound pressure levels. This general trend matched similar work published by Montavon et al. [159].

As with the steady k-ε model PISO pressure-velocity coupling was used with second order discretisation of pressure.

6.3.3 Physical Properties

All physical material properties (air at 300 K) were set at constant SI values with the exception of density in the compressible flow models. The ideal gas equation was used to calculate density based on the energy equation thus allowing for a compressible flow simulation. As mentioned previously, an incompressible model was also developed and found to be more robust with a smaller overall computational cost. Viscous heating was also incorporated into the model to improve the stability of the compressible flow calculations and the no slip pipe walls were assumed to be adiabatic.

6.3.4 Mesh Properties

The three dimensional structured mesh was generated in a Cartesian co-ordinate system with the z-axis aligned with the axial centreline of the inlet pipe and subsequent conical diffuser. The cross section of the pipe was separated into 5 individual faces with 4 symmetrical circumferential zones surrounding a central square zone. A cylindrical co-ordinate system with a single face was also considered; however the Cartesian system was selected as it provided a greater flexibility of refining the mesh near the duct walls without compromising the mesh in the centre of the duct. A comparison between the two mesh orientations considered is shown in Figure 6.5.

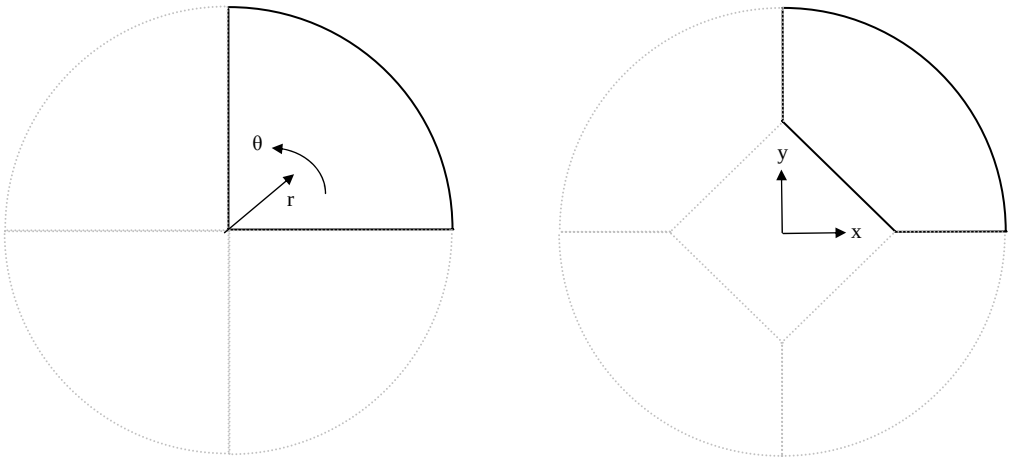

Figure 6.5: Mesh comparison for a ¼ pipe cross section.

The mesh surrounding the central core of the flow domain downstream from the inlet pipe and conical diffusers was constructed using four equal quadrants in a cylindrical orientation concentric to the axial centreline of the inlet pipe. A structured mesh was also used in these regions, with a mesh grading used to maintain acceptable individual cell aspect ratios with increasing radial displacement from the centreline of the flow domain.

Maintaining a structured mesh in the cylindrical co-ordinate system led to high cell aspect ratios and triangular cells along the centreline of the pipe. The simplified geometry also provides limited options for controlling the mesh seeding in both the radial and circumferential directions. An unstructured face mesh was also considered for the purposes of controlling the aspect ratio of the cells across the pipe with limited success. It was found that the structured mesh around the pipe walls provided a superior representation of the velocity gradients for the equivalent number of cells employed. A hybrid mesh coupling a structured boundary layer mesh with an unstructured mesh in the pipe core was also trialled with limited success. The largest obstacle for this type of mesh involved the interface region between the fine structured mesh in the boundary layer region and the adjacent unstructured cells. The final mesh employed was wholly structured, with multiple mesh seeding zones to maximise the computational efficiency of the mesh without compromising the resolution of the boundary layer inside the pipe and diffuser.

Uniform axial mesh spacing was used throughout the inlet pipe section, conical diffuser and outlet duct regions. The same uniform spacing was also used in the local free domain surrounding the outlet of each diffuser configuration, with a gradual grading of the mesh spacing in the outer regions of the external flow domain. This gradual increase in mesh size was chosen to maximise the computational efficiency of each model and to provide an artificial damping of spurious pressure fluctuations associated with the pressure outlet boundary condition. The expansion of the air jet in this region of the model was such that the localised air velocities were considerably reduced enabling a larger mesh spacing to be utilised without increasing the local cell Reynolds number.

6.3.5 Time Stepping Schemes and Sizes

The segregated second order implicit unsteady solver in Fluent 6.2 was used to solve the LES model. Initially an adaptive time stepping regime was used to eliminate the start-up transients associated with the switch from the initial steady state k-ε model to the transient (unsteady) LES model. This approach proved very useful in minimising the solution time required to purge these initial fluctuations from the flow domain. In terms of absolute flow time this start-up period corresponded to 0.5 to 1.0 second, which was covered in 30,000 to 40,000 time steps. Once this initial start-up phase was completed a constant time step was used for the remainder of the analysis. This analysis was completed in two stages. Firstly a statistically steady turbulent flow field was established and secondly the transient flow data required for the acoustic post processor was generated.

A steady time step of 5 to 30 μs was used across a range of mesh sizes to determine the optimum number of cells to resolve the boundary layer and external flow domain accurately yet also minimise the total solution time. Typically each compressible model required 120,000 to 200,000 time steps to reach an approximate statistically steady state after which the noise simulation was initiated. The incompressible models exhibited a more stable transient response and reached a statistically steady solution in approximately half this time. Where possible the model should be run for as long as is computationally feasible to improve the quality of the statistically averaged flow variables upon which the acoustic calculation is made.

A more detailed examination of the time steps chosen is covered in the subsequent section covering the validation and verification of the numerical model.

6.4 Computational Resources Employed

The mesh files used in this analysis were generated in Gambit 6.2, running on AMD dual processor MP1600 to 2800 computers with a Linux operating system located in the CFD research laboratory in the School of Mechanical and Manufacturing Engineering at UNSW. The subsequent CFD simulations were spread across these same computers and the high performance computing facilities operated by AC3, in Redfern, NSW. The initial steady state k-ε simulations were run locally at UNSW with the subsequent LES models run on the parallel computing facilities at AC3. Manually programmed adaptive time stepping routines were used instead of the standard adaptive time stepping routines built into the Fluent 6.1 and 6.2 solvers. This was done to ensure accurate repeatability and control of the time stepping used from one case to the next.

The final stage of the modelling process which called upon the acoustic post processor was run on Pentium 4 single processor workstations running Windows XP. A total of over 1,250,000 processor hours were logged during the preparation of this thesis across a combination of the above computing resources.

6.5 Model Validation and Verification

The AIAA guide for verification and validation of computational fluid dynamics [123] provides a clear definition of model verification and validation. Verification of the model requires that the selected numerical solution is a correct solution to the governing differential equations solved. The critical numerical solution must be independent of the solution process used and be free of any numerical errors. Of primary concern is the independence of the final solution with respect to the discretisation schemes employed and the adequate convergence of each iterative step in the modelling process as outlined by Roache [239]. The verification process was followed to minimise the influence of numerical errors on the final solution obtained.

Validation of the model is focused on ensuring that the real world solution to the problem is matched by the numerical approximation. Experimental measurements can be used to validate the assumptions used in building the numerical modelling such as boundary conditions, physical properties of the fluid and the nature of the flow field behaviour. One such example relevant to this work is the type of turbulence model used and the ability to accurately model the flow field behaviour linked to the generation of flow induced noise. The numerical models used in this thesis were validated against the experimental results previously presented to demonstrate the viability of a CFD based design tool for predicting flow induced sound power levels.

6.5.1 Boundary Conditions

The location of the free boundary surrounding the outlet diffuser and the specification of the upstream pipe inlet were both key areas of interest in the validation of the numerical model. The pressure outlet used in the incompressible models was placed at a distance of 10, 16, 20 and 30 diameters from the diffuser outlet and the changes in the flow field evaluated. This approach was used given that the acoustic simulations were primarily based on the flow variables on the diffuser outlet face and needed to be numerically independent of the virtual boundaries employed. A comparison was made between the velocity profiles across the duct outlet (Figures 6.6a & b).

All four external flow domains resulted in a very similar velocity profile at the outlet of the duct, however upon closer inspection slight variations were found. These variations are best illustrated in terms of the percentage difference between the axial velocity profiles for each of the flow domain lengths (Figure 6.6b). There is no variation between the 1000 and 1500 mm long (20 and 30 diameters) domains, while a maximum error of 0.25 % when this was shortened to 800 mm (16 diameters). The error increased further to 2.35 % when the outlet domain was shortened further to only 500 mm (10 diameters). Based on this result an external flow domain with a length of 16 duct diameters was used. This represented a reasonable compromise in the interest of numerical accuracy and computational efficiency.

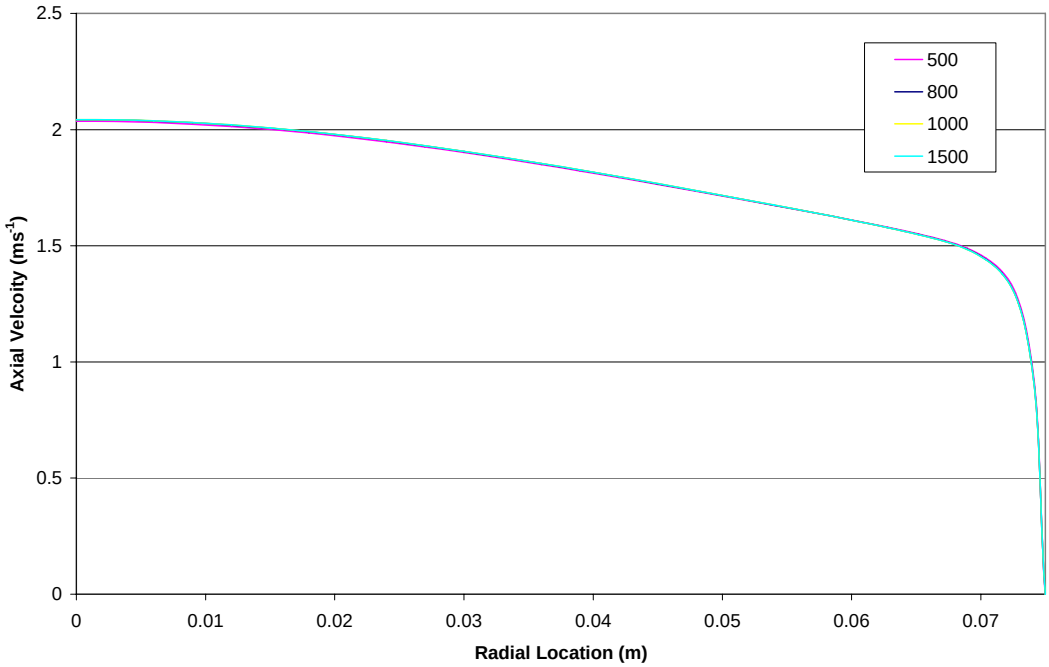

Figure 6.6a: Axial velocity profile at the diffuser outlet for various external flow domain lengths.

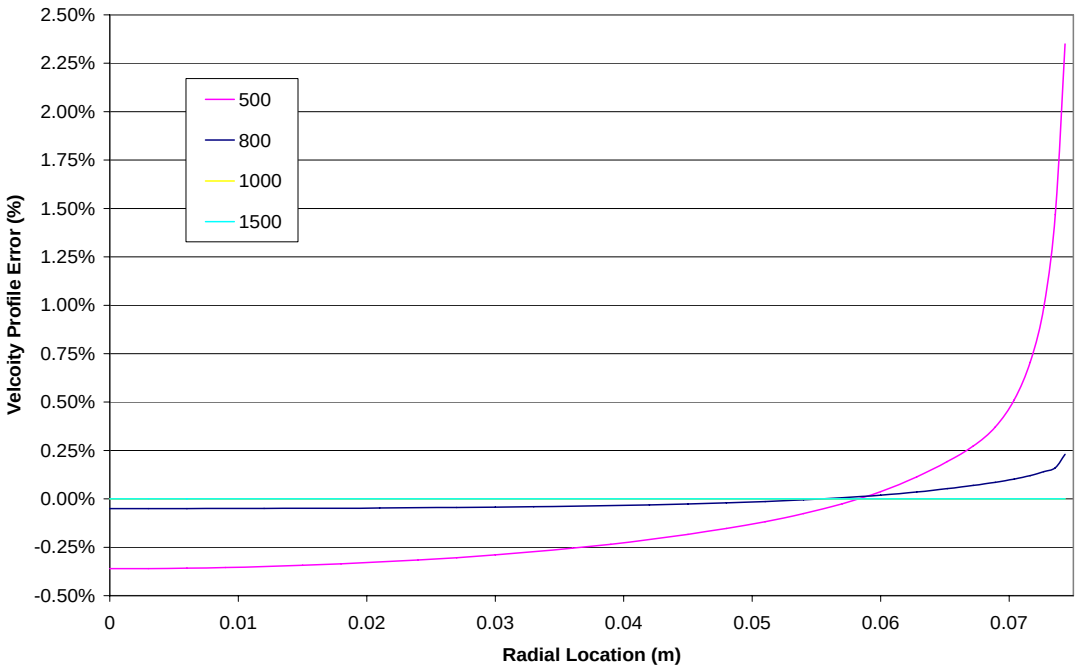

Figure 6.6b: Percentage variation in the axial velocity profile at the diffuser outlet for various external flow domain lengths.

The radial size of the external flow domain was optimised to ensure independence of the velocity profile downstream of the outlet duct and yet also minimise the computational cost. A radial domain size of 150, 300 and 500 mm (3, 6 and 10 diameters) were used. The axial velocity profile across a plane located 300 mm (six diameters) downstream from the outlet was used as a reference for evaluating the mesh independence. The profiles are shown below in Figure 6.7. Quite clearly the 150 mm domain was not large enough, however there was no need to extend it beyond 300 mm (6 diameters). The variation between the 300 and 500 mm cases (6 and 10 diameters) was minimal across the whole spatial plane of interest.

Over the jet velocity range of interest (15 to 45 ms^{-1}) there was no significant variation found on the above result. A radial domain of six jet diameters provides sufficient space to adequately resolve the flow field covering the two stage expansion of the jet. Care should be taken in extrapolating this same conclusion however for jets of significantly higher velocity.

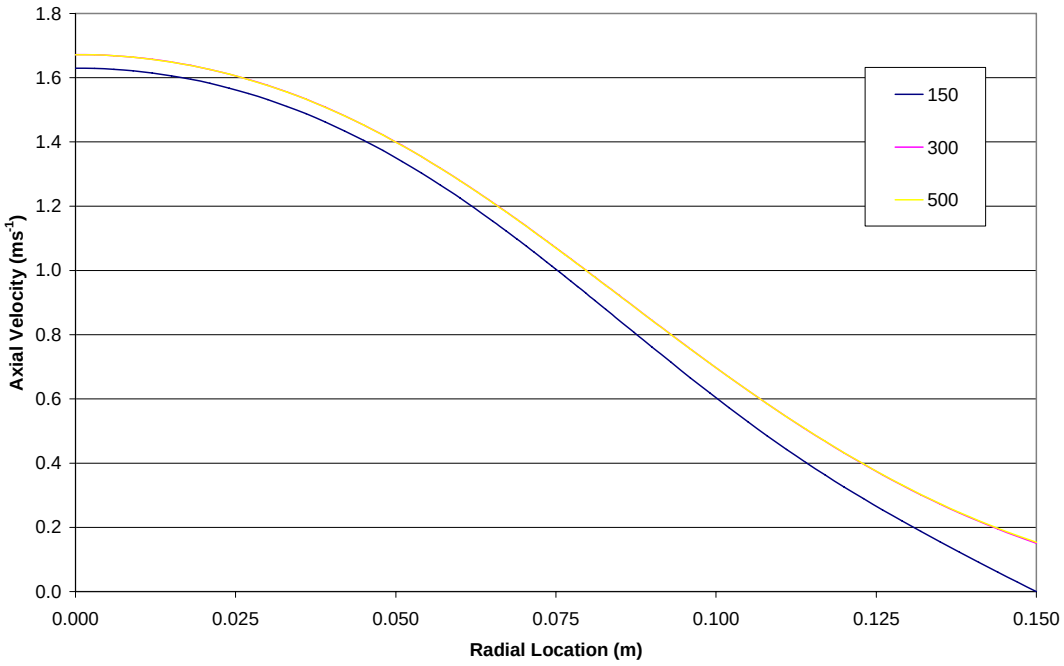

Figure 6.7: Axial velocity profile 300 mm downstream from the duct outlet using an external flow domain radius of 150, 300 and 500 mm (3, 6 and 10 diameters).

The turbulence intensity at the upstream pipe inlet was varied from the ideal fully developed turbulent flow value to determine the sensitivity of the velocity profile inside the pipe to the prescribed inlet turbulence level. Over an inlet length of 20 diameters there was no difference in the velocity profile and turbulence level inside the pipe when this value was varied ± 50 %. The inlet pipe velocity profiles and subsequent outlet velocity profiles from the initial k-ε turbulence model using a turbulence intensity of 2.05, 4.1 and 6.15 percent were evaluated. These same models were then further evaluated using the full transient LES turbulence model as well. In all cases there were no discernable differences between the resultant flow domains in terms of both the velocity and pressure profiles. Given this result the inlet turbulence intensity was increased further up to 10 percent, still resulting in no distinguishable differences in the calculated flow profiles.

6.5.2 Mesh Independence

The independence of the model from the size of mesh used was investigated for a range of axial, radial and circumferential cell sizes. The radial and circumferential mesh sizes were optimised together to ensure a wall y^+ value of around 1 was maintained. A typical graded structured mesh on the 5 individual faces across the pipe section outlined earlier is shown in Figure 6.8. The radial mesh size and grading dictated the mesh size in the boundary layer, while the even mesh spacing of the central core controlled the circumferential mesh spacing. A core spacing of 12, 15, 18, 21 and 24 were trialled, with a radial mesh spacing of 15, 18, 20, 25 and 30. The grading of the radial mesh spacing was critical to balancing the refined mesh inside the boundary layer along the pipe wall, whilst also maintaining a reasonable mesh size and skew ratio towards the central core of the pipe.

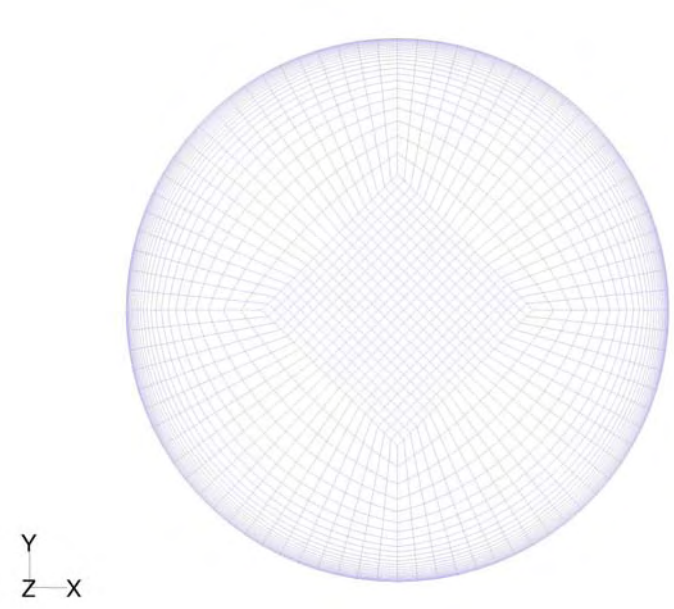

Figure 6.8: The cross section of the inlet pipe and the corresponding mesh used.

The boundary layer mesh inside the pipes was refined so as to ensure a wall $y^+ \approx 1$ and the robustness of the LES model. Further investigation revealed that the model still provided reasonable results when the wall y^+ limit of 1 was exceeded slightly. Again it was found that this limit can be stretched without severely compromising the final solution if necessitated in a commercial application. The effect of reducing the mesh spacing in the boundary layer on the wall y^+ value is shown in Figures 6.9 and 6.10. Twenty-five to thirty cells in the radial axis were required to satisfy the wall $y^+ \approx 1$ condition, which equated to a total of 2025 to 2484 cells across the pipe cross section. The preferred mesh consisted of a circumferential cell count of 18 coupled with a radial cell count of either a 25 or 30 (2124 or 2484 cells respectively). A circumferential cell count of 15 appears to be adequate provided it is used in conjunction with the finer radial mesh using a cell count of 30.

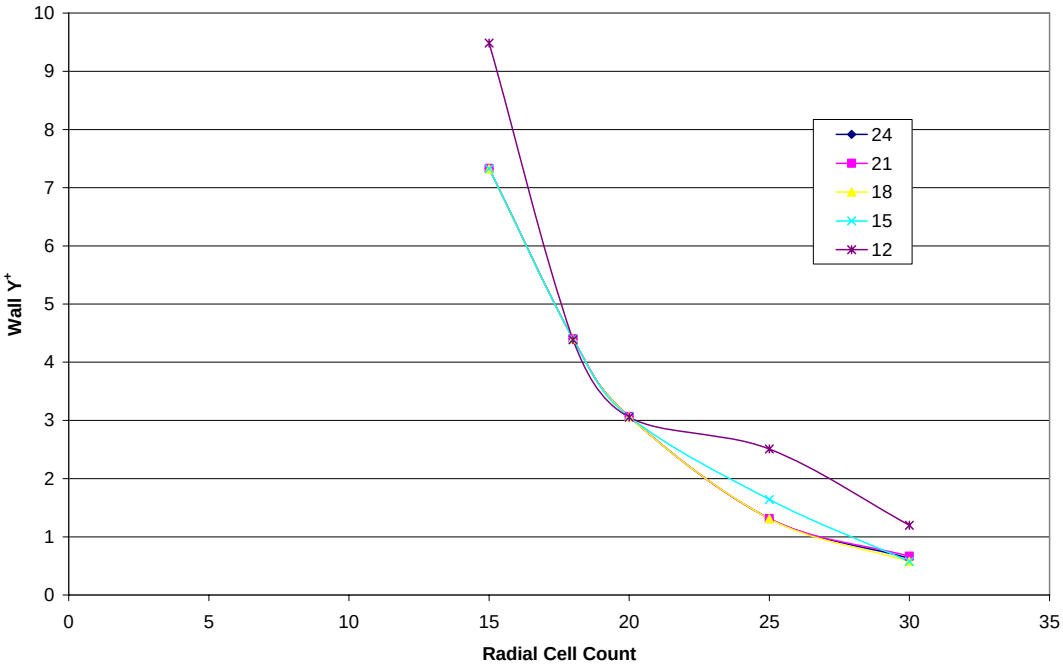

Figure 6.9: Wall y^+ in the inlet pipe section for a range of radial (x axis) and circumferential (legend) mesh counts.

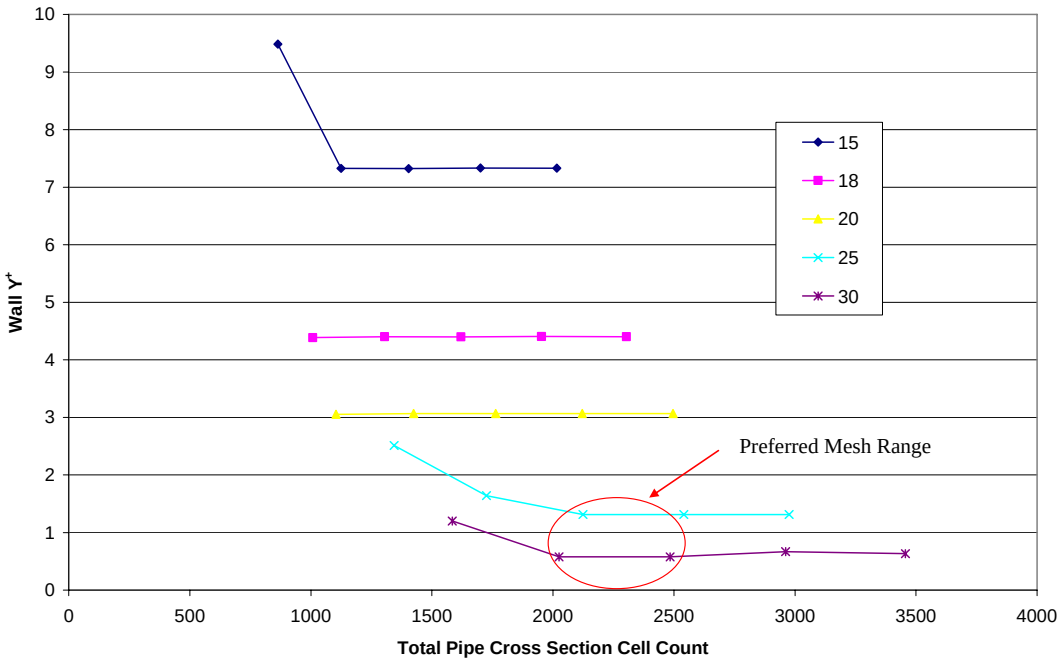

Figure 6.10: Wall y^+ in the inlet pipe section as a function of the total cell count across the cross section of the pipe.

The variation in the internal jet velocity profile for a range of radial mesh sizes can be seen in Figure 6.11. Clearly satisfying the wall y^+ condition also ensures the mesh independence of the velocity profile along the inlet pipe. However, refining the mesh inside the inlet pipe and the subsequent conical diffuser and outlet ducting has an affect on the overall number of cells in the external flow domain. Any increase in the total number of cells used adds significant computational cost and must therefore be carefully balanced against the need for realistic solution time frames. In a commercial application the velocity profile inside the inlet pipe can be compromised to a certain extent in the interest of computational speed. A reduction in the accuracy of the final solution can be offset through a reduction in the solution time involved.

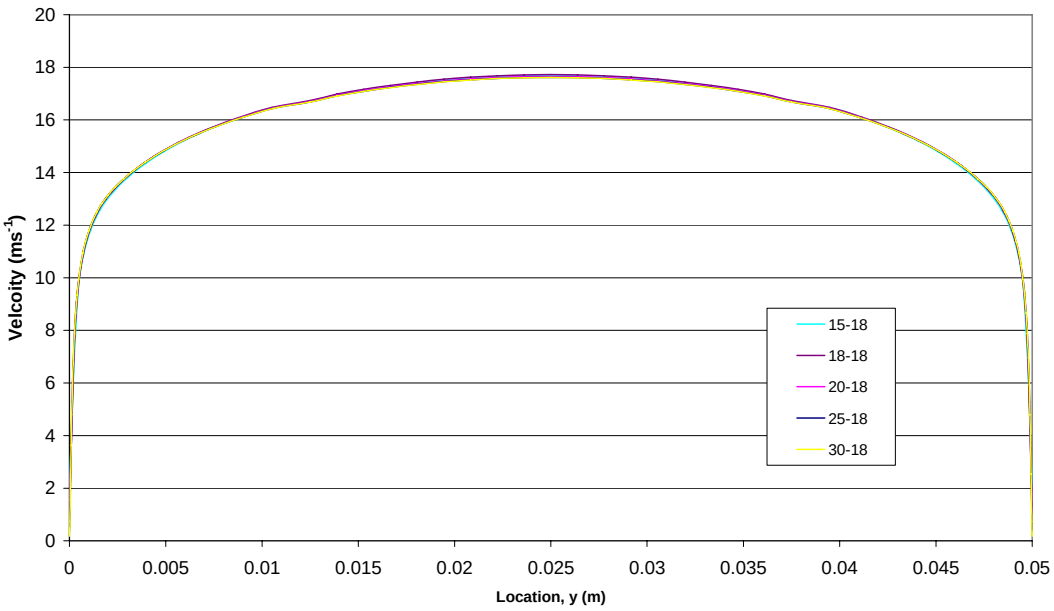

Figure 6.11: Velocity profile inside the inlet pipe for variable radial mesh spacing.

In the interest of maintaining the integrity of this research the results presented hereafter have been based on a non uniform radial mesh cell count of 25 and a total circumferential cell count of 72 (18 x 4). This ensured that the wall y^+ limit of 1 was satisfied. The commercial viability of such models is questionable in light of the relatively high computational costs involved. The most suitable solution method would in fact involve multiple models of a coarser mesh size, with a wall $y^+ > 1$ used to identify the desired model specifications. Once the desired solution is found a refined model can be run in cases where a more accurate solution is required.

Uniform axial mesh spacing was used throughout the upstream inlet pipe, conical diffuser, outlet duct section and the near field external flow domain. Meanwhile, the axial spacing in the outer zones of the external flow domain was gradually increased to maximise computational efficiency. An axial mesh spacing of 2 to 4 mm was used with negligible difference between models. An axial mesh spacing of 5 mm was also investigated with reasonable results obtained. A mesh spacing of this size would be suitable for commercially orientated projects where computational costs could be saved without severely hampering the overall accuracy of the final solution.

The suitability of the axial spacing selected was investigated in detail through evaluating the resolution of the velocity profile across the exit planes of the primary conical diffuser itself and the final duct outlet further downstream. A comparison over the selected range of axial mesh sizes outlined above is shown in Figures 6.12 and 6.13 respectively. In both plots the velocity profiles were consistent across each respective radial cross section for the range of axial mesh spacing used.

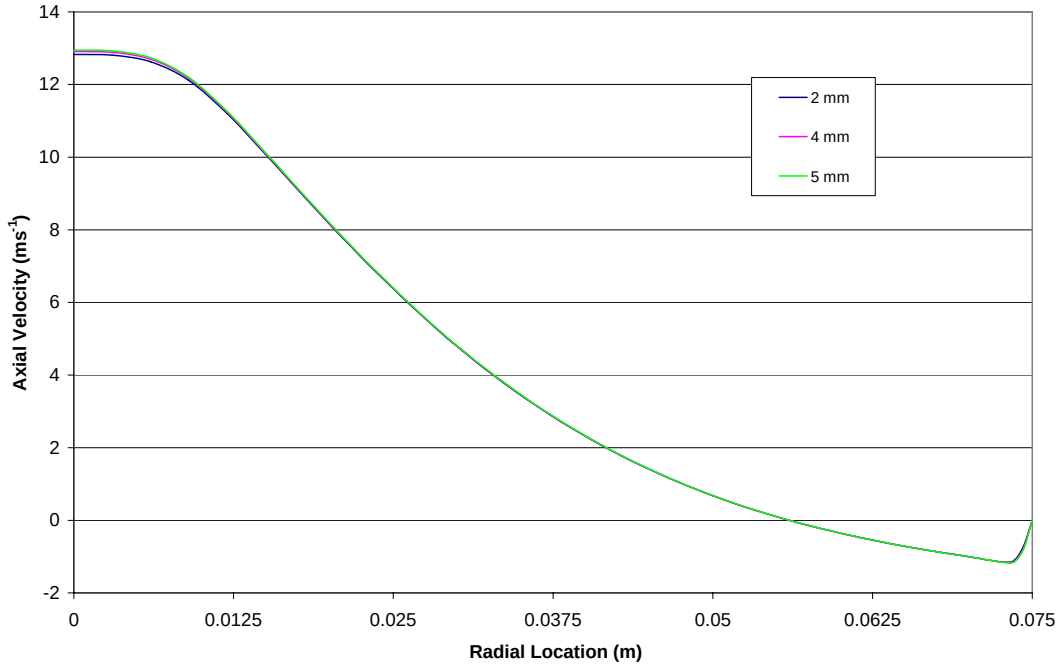

Figure 6.12: Velocity profile across the conical diffuser exit plane with varying axial mesh spacing.

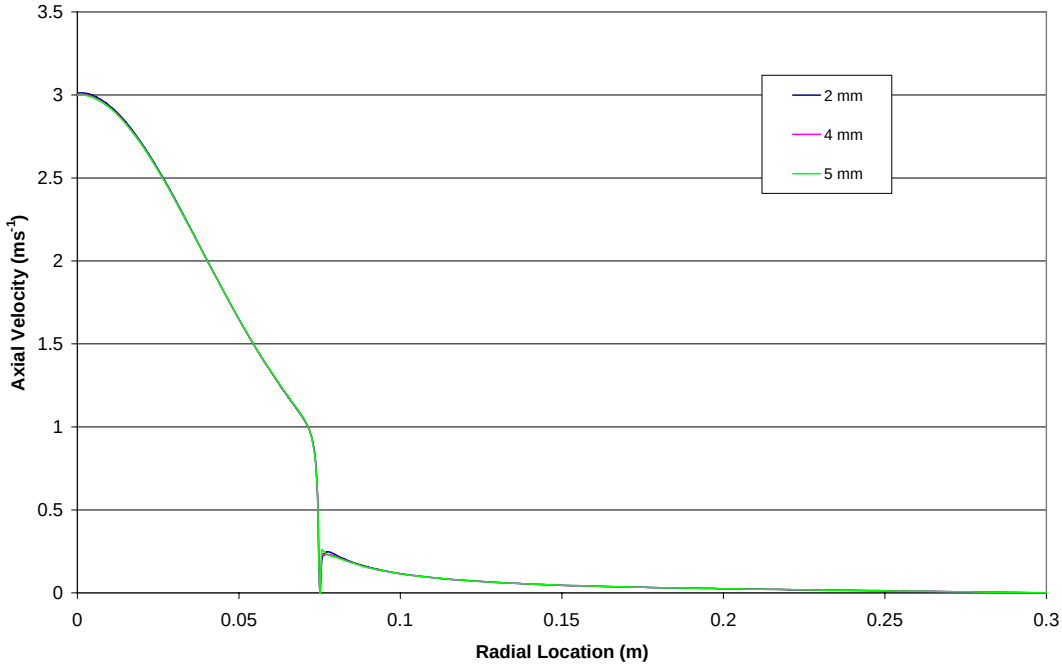

Figure 6.13: Velocity profile across the final outlet exit plane with varying axial mesh spacing.

Using the larger axial spacing leads to an increase in the aspect ratio of the cells located within the boundary layer inside the inlet pipe. The increase in the aspect ratio can be reduced by increasing the size of the cells inside the boundary layer which in turn increases the corresponding wall y^+ values. In the interest of reduced computational cost the accuracy of the final solution can be balanced by using a combination of larger cells inside the boundary layer and allowing a larger maximum aspect ratio. Aspect ratios of 8:1 were found to provide reasonable results due to the directional nature of the flow inside the inlet pipe.

6.5.3 Time Independence

The time step sizes used in the unsteady transient simulations were varied from 1 to 100 μs, with a larger time step possible when the incompressible flow model was used. The initial LES model was started with a time step of 100 μs to allow a rapid transition through the initial start-up phase of the LES solution. Once the flow had settled and the statistically steady turbulent fluctuations established, the time step was progressively reduced down to 10 μs to allow the smaller scale turbulent fluctuations to be fully established within the flow field.

This final time step size was varied between 5 and 30 μs with negligible difference to the final flow field or fluctuating flow variables observed when a time step of 5 to 10 μs was used. A comparison between the pressure and flow velocity at several discrete points within the model for this range of time steps is shown in Figures 6.14 and 6.15 respectively. Over the extended number of time steps used to complete the acoustic analysis the models using the larger time steps were still reasonably close to the results derived using the smaller time steps of 5 and 10 μs.

The variation in the jet velocity appears to be much more random, however when these values are looked at in statistical terms there is in fact very little variation between the three time steps used in this comparison. The mean and the standard deviation of the flow velocity for a time step of 10, 20 and 30 μs are summarised in Table 6.1.

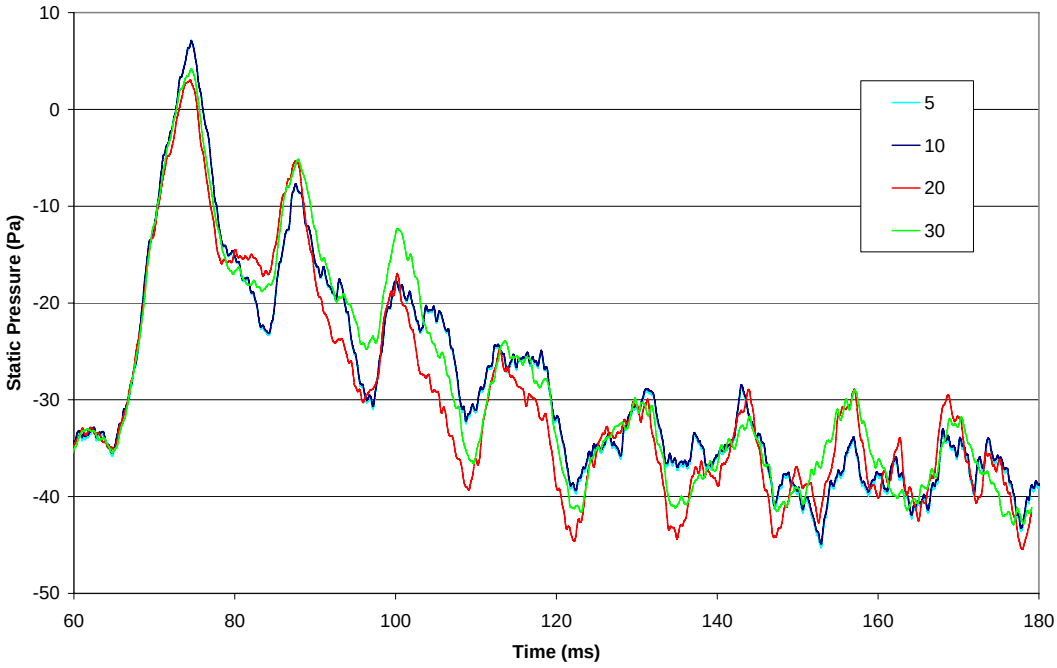

Figure 6.14: Time step comparison for static pressure.

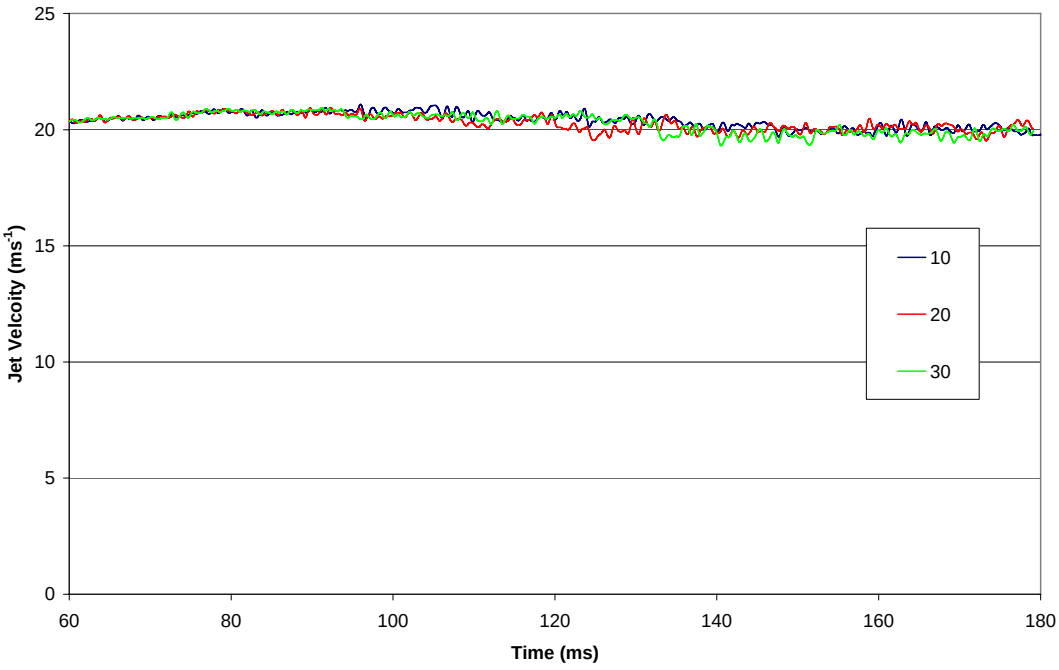

Figure 6.15: Time step comparison for jet velocity.

Table 6.1: Summary of jet velocity flow statistics for time step comparison.

Time Step (μs)	Average Velocity (ms^{-1})	Standard Deviation (ms^{-1})
5	20.41	0.33
10	20.40	0.33
20	20.30	0.33
30	20.29	0.42

From the above results it is clear that the time averaged jet velocity and the level of turbulent fluctuation in the instantaneous value is very stable across the time step range employed. Additional spectral analysis of the time varying data can also be used to reinforce the independence of the solution form the time step used. This is shown clearly in the spectral signature of the flow induced noise calculated form the time varying flow data set. This will be discussed further in Chapter 8.4 (pages 278-279).

As a consequence of this result the final determining factor in selecting the time step size was a function of the desired acoustic sampling frequency. The sampling frequency was determined based on the desired frequency bandwidth for the acoustic simulations. As this data is already sampled (discretised) an anti-aliasing filter would be ineffective, leading to a smaller time step than would otherwise be necessary. A sampling frequency of 100 kHz (time step of 10 μs) was selected, corresponding to a Niquist frequency of 50 kHz – an order of magnitude greater than the maximum frequency band of interest of 5 kHz.

6.5.4 Solution Convergence

The convergence criteria specified for each time step was set at $1x10^{-5}$ for continuity, x, y, z velocities and energy, with approximately 8 iterations per time step required to reach convergence. Relaxing this criterion to $1\ x10^{-4}$ reduced the number of iterations per time step down to 5 with minimal variation in the final solution, while relaxing it further to $1\ x10^{-3}$ reduced the number of iterations per time step to 3. This final reduction resulted in a very gradual drift in the solution away from that obtained with the tighter convergence criterion. As a result the initial convergence criterion of $1\ x10^{-5}$ was used to ensure no drift over the extended time that the acoustic simulations were conducted. In a commercial application a convergence criterion of $1\ x10^{-4}$ would be expected to provide a reasonable solution, particularly given that the length of the acoustic simulation would also be reduced.

6.6 Statistically Steady Flow

The transient turbulent flow domain was monitored to ensure that the flow field was statistically steady prior to initiating the acoustic simulations. The steadiness of the flow was monitored by way of the time varying statistics of the flow field variables including the velocity component vectors and the corresponding static pressure. Both the average and rms fluctuating components of each respective variable were monitored to ensure that the flow was truly statistically steady. As a secondary measure the acoustic simulations were also conducted such that the initial starting point for the acoustic fluctuations could be varied to test the independence of the sample length and location in the time domain. This will be discussed in more detail in subsequent chapters focusing on the acoustic simulations themselves.

Chapter 7

Numerical Results and Discussion - CFD

Initial CFD modelling was based on a 7° conical diffuser fitted with an open ended 300 mm long circular outlet duct, with simulations completed for a jet velocity of 10, 15, 20, 25 and 30 ms^{-1}. Both the compressible and incompressible models gave similar airflow profiles and pressures, with the latter providing significant computational savings as outlined previously. The LES turbulence model effectively modelled the re-circulation zones inside the diffuser and the fluctuating vortex shedding associated with the primary expansion of the air jet.

7.1 Critical Performance Parameters

The CFD models of each outlet diffuser configuration considered were used to identify the optimum angle for the conical diffuser and the preferred length of down stream outlet ducting. Statistically steady LES models were then used to generate acoustic source input data for the far-field acoustic post processor. Each individual model was assessed based on the following key performance parameters:

(a) Mean velocity profile across the duct outlet
(b) Deceleration of the supply air jet
(c) Mean and RMS velocity at the duct outlet
(d) RMS pressure at the duct outlet

The first two of these parameters were assessed using the initial steady k-ε model, and then the subsequent LES model. The RMS velocity and pressure levels across the duct outlet were calculated from the unsteady statistics derived from the statistically steady LES models. Additional point data was also recorded to assess the progressive stability and performance of each model during the iterative solution process.

7.2 Rapid Assessment of Outlet Diffuser Designs

The commercial application of this research will require a rapid and cost effective numerical design tool for assessing the merits of proposed diffuser designs at minimum computational cost. Rather than completing detailed LES CFD models for each proposed design at substantial computational cost (time and money) a simpler and coarser modelling method is required. A steady (in time) k-ε turbulence model can be completed in a fraction of the time taken for each full scale LES model to assess the relative merits of proposed diffuser designs.

In certain applications a simplified two dimensional axis-symmetric model can be used in place of a more computationally intensive three dimensional model; lowering the computational cost further still. The application of this type of model would be limited to simplified diffuser shapes and the placement of secondary diffuser vanes based on a cylindrical co-ordinate structure. The major advantage of this approach is the minimisation of the computational cost of the optimisation of fundamental diffuser shape and structure for implementation into the more detailed three dimensional LES models.

The accuracy of the k-ε turbulence model in predicting the flow related turbulence levels and the formation of recirculation zones within the diffuser is limited; with artificial attenuation of flow disturbances routinely found. This source of error can in part be attributed to the unavailability of a central differencing discretisation scheme in commercial CFD packages such as Fluent when using the k-ε turbulence model. Numerous reports in published literature also demonstrate the tendency of the k-ε turbulence model to under predict the levels of turbulence in cases of non-isotropic turbulence in the flow regime; such as the expansion of an axial jet. Despite these shortcomings the simplified k-ε model still provides a useful approximation of the air flow through a proposed diffuser design with reasonable levels of comparative accuracy.

The steady k-ε flow models were used to assess the mean flow regime through each proposed diffuser design and identify the most suitable configurations for detailed three dimensional modelling using the full LES turbulence model. The primary three assessment criteria were the mean velocity profile at the diffuser outlet, the location and size of any recirculation zones within the flow and the distribution of the turbulence intensity.

The subsequent implementation of the LES models routinely gave rise to an increase in the strength and size of any recirculation zones and the local turbulence levels within the diffuser outlet region. Corresponding increases were also observed in the magnitude of the fluctuations in the local static pressure. The intent of this research is to demonstrate the capability of this simplified modelling approach and to map out the limitations for future reference in actual commercial applications.

7.2.1 Conical Outlet Diffuser

Three conical diffuser angles of 7˚, 10˚ and 14˚ were used (matching the experimental work previously reported), with significant variation in the location and nature of the flow separation observed. The steady k-ε model was used as an initial assessment of the suitability of each respective diffuser angle. The first major variation to consider was the change in the velocity profile at the end of the 300 mm outlet duct fitted to each respective diffuser. A jet velocity range of 15 to 45 ms^{-1}, in increments of 5 ms^{-1}, was used for both this comparison and all subsequent cases that will be discussed. The velocity profiles at the end of a 300 mm long outlet duct (150 mm in diameter) fitted to the exit of each of the three respective conical diffusers are shown in Figures 7.1, 7.2 and 7.3.

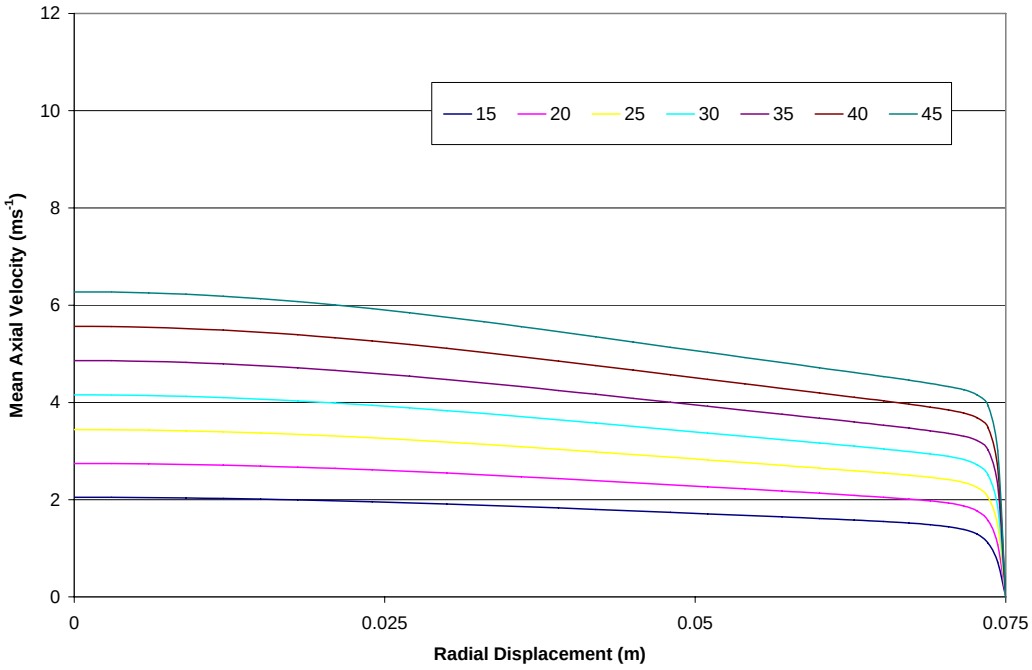

Figure 7.1: Velocity profiles for a 50 mm diameter jet at 15, 20, 25, 30, 40 and 45 ms^{-1}, with a 7˚ conical diffuser fitted with a 300 mm long outlet duct.

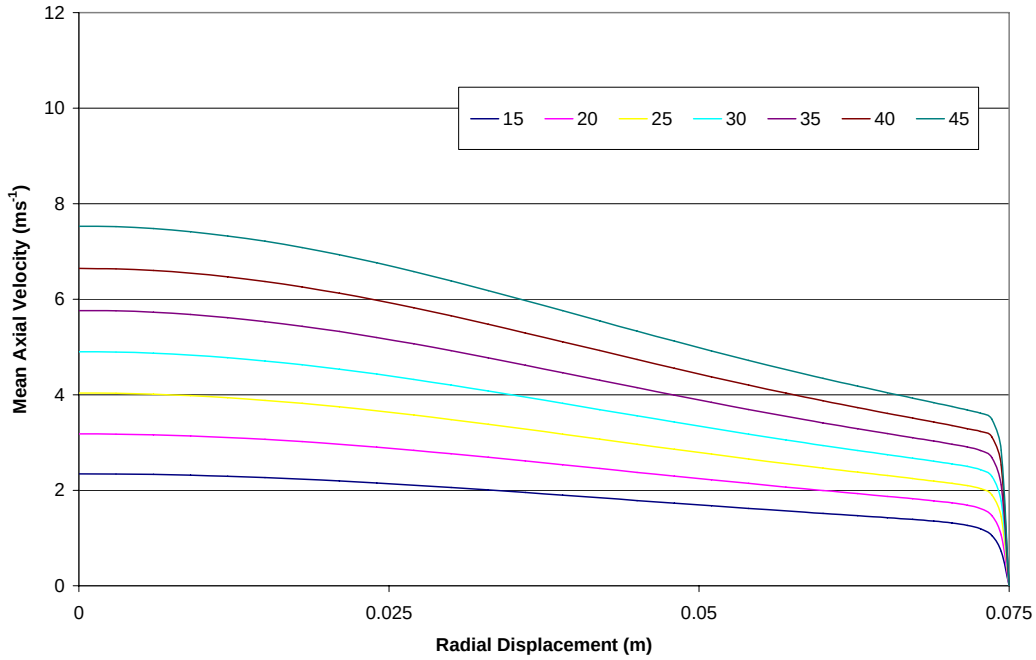

Figure 7.2: Velocity profiles for a 50 mm diameter jet at 15, 20, 25, 30, 40 and 45 ms^{-1}, with a 10˚ conical diffuser fitted with a 300 mm long outlet duct.

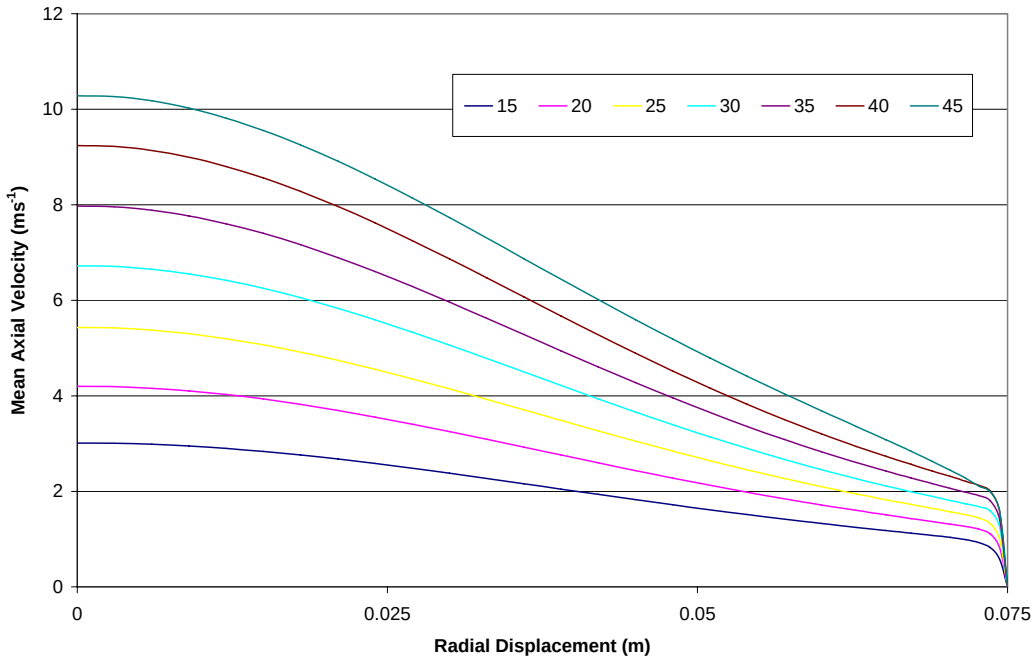

Figure 7.3: Velocity profiles for a 50 mm diameter jet at 15, 20, 25, 30, 40 and 45 ms^{-1}, with a 14˚ conical diffuser fitted with a 300 mm long outlet duct.

The velocity profile for the 7˚ diffuser is relatively flat, with a gradual increase in the bias towards the centre of the outlet duct as the jet velocity is increased. This reduced rate of flow expansion at higher jet velocities is expected in line with the increase in the velocity gradients observed near the wall of the duct. As the diffuser angle is increased to 10˚ the flow becomes more entrained in the centre of the duct and the velocity gradient at the wall is slightly reduced for the same corresponding jet velocities. These effects can be directly linked to the increased levels of flow separation that are observed and the establishment of recirculation regions within the conical diffuser. The 300 mm long outlet duct is too short to allow complete stabilisation of the flow, resulting in the high velocity central core, surrounded by a low velocity stream reattached to the walls of the outlet duct. When the diffuser angle is increased further to 14˚ the above effects are even more pronounced. Clearly a 14˚ diffuser requires a greater outlet duct length if the flat velocity profile produced by the 7˚ diffuser is to be replicated.

The above comparison is better visualised with the use of normalised velocity profiles, where the axial velocity is divided by the average velocity (u_0) that would be observed if the flow was uniformly expanded:

$$u_0 = \overline{u}_{jet} \frac{A_1}{A_2} \qquad (7.1)$$

where the area ratio of the conical diffuser is defined as (A_1/A_2) and $\overline{u}_{jet}$ is the average axial velocity of the incoming jet. By presenting the data in this manner the true effect of both jet velocity and diffuser angle on the outlet velocity profile can be clearly seen. The normalised velocity profiles across the exit plane of the 300 mm long outlet duct (150 mm in diameter) fitted to each of the three respective conical diffusers are shown in Figures 7.4, 7.5 and 7.6. The normalised centreline velocities observed for the 7˚, 10˚ and 14˚ conical diffusers were respectively 1.25, 1.5 and 2. The spread of the curves for each of the conical diffusers also increased with the diffuser angle, with the spread most prominent for the 14˚ diffuser.

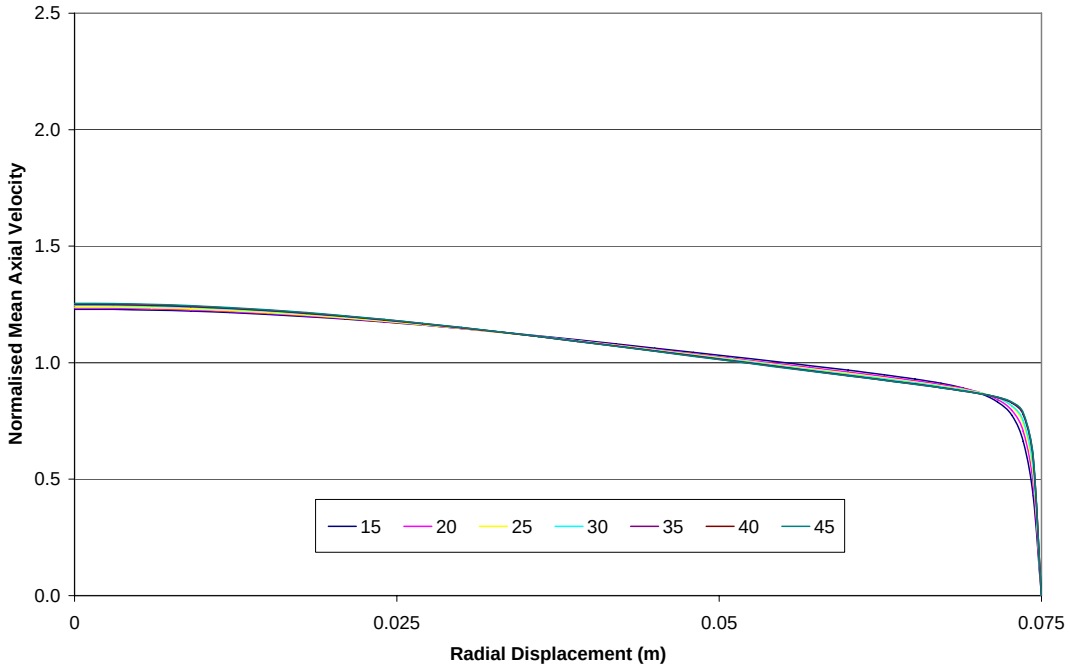

Figure 7.4: Normalised velocity profiles for a 50 mm diameter jet at 15, 20, 25, 30, 40 and 45 ms^{-1}, with a 7˚ conical diffuser fitted with a 300 mm long outlet duct.

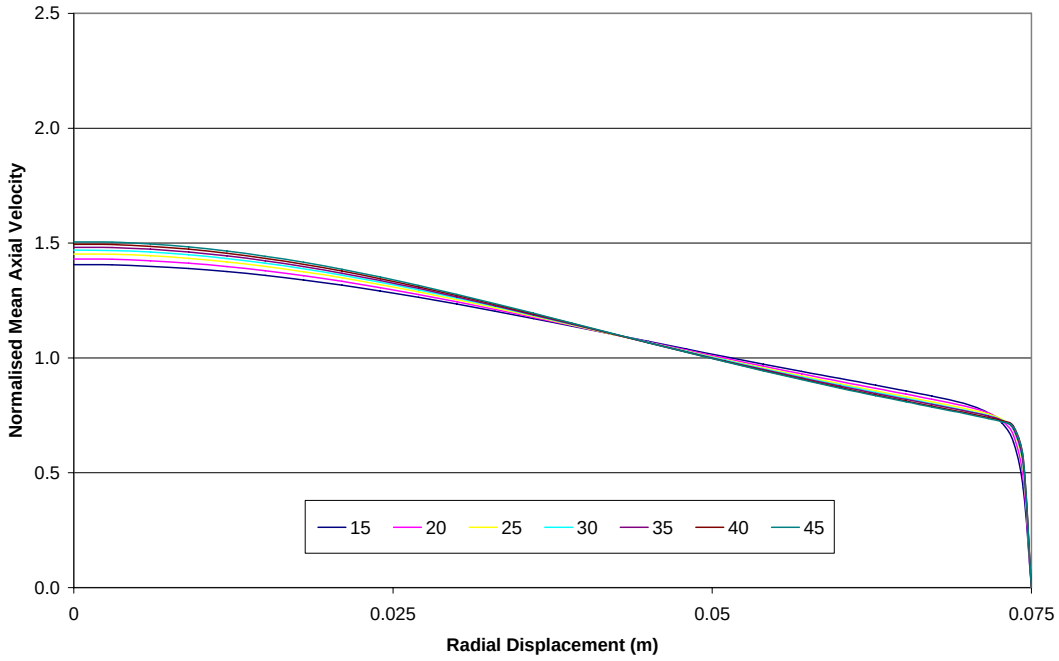

Figure 7.5: Normalised velocity profiles for a 50 mm diameter jet at 15, 20, 25, 30, 40 and 45 ms^{-1}, with a 10˚ conical diffuser fitted with a 300 mm long outlet duct.

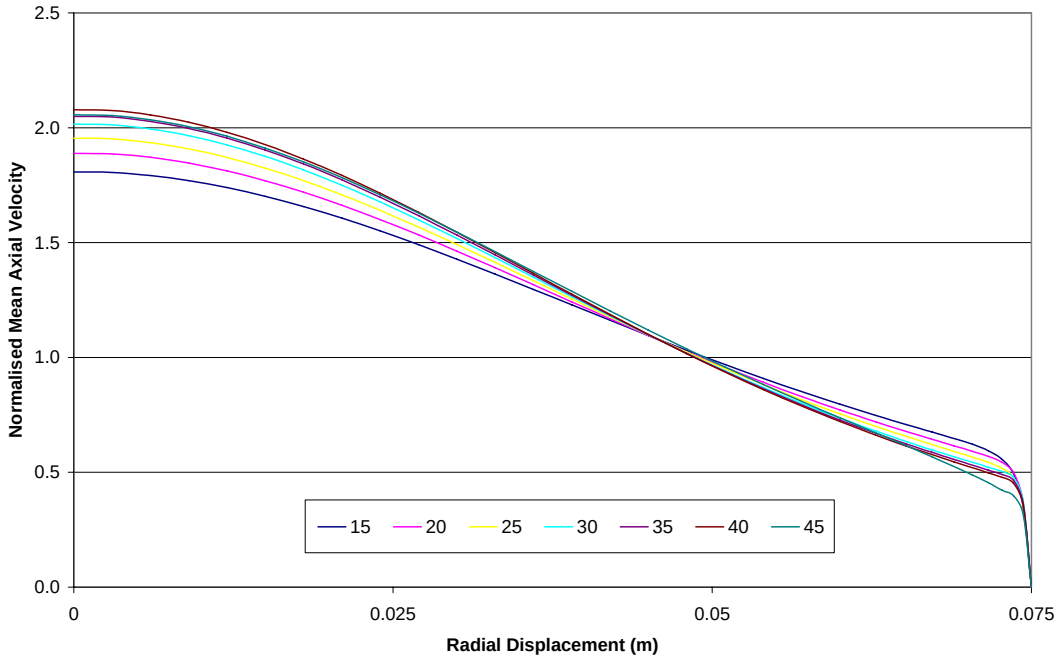

Figure 7.6: Normalised velocity profiles for a 50 mm diameter jet at 15, 20, 25, 30, 40 and 45 ms^{-1}, with a 14˚ conical diffuser fitted with a 300 mm long outlet duct.

The variation in the outlet velocity profile associated with the increase in the conical diffuser angle is more clearly understood by studying the velocity profile across the exit plane of the conical diffuser itself. By measuring the velocity profile upstream of the outlet duct section the impact of the conical diffuser angle and any potential flow separation (and associated recirculation zones) can be isolated for further analysis. The normalised velocity profiles across the diffuser exit plane for the 7˚, 10˚ and 14˚ conical diffusers are shown in Figures 7.7, 7.8 and 7.9 respectively. The results are derived from the model fitted with a 300 mm long outlet duct, however when the corresponding graphs were generated for each of the jet velocities using the 600 and 900 mm long outlet ducts there was no variation in the mean diffuser exit velocity profile.

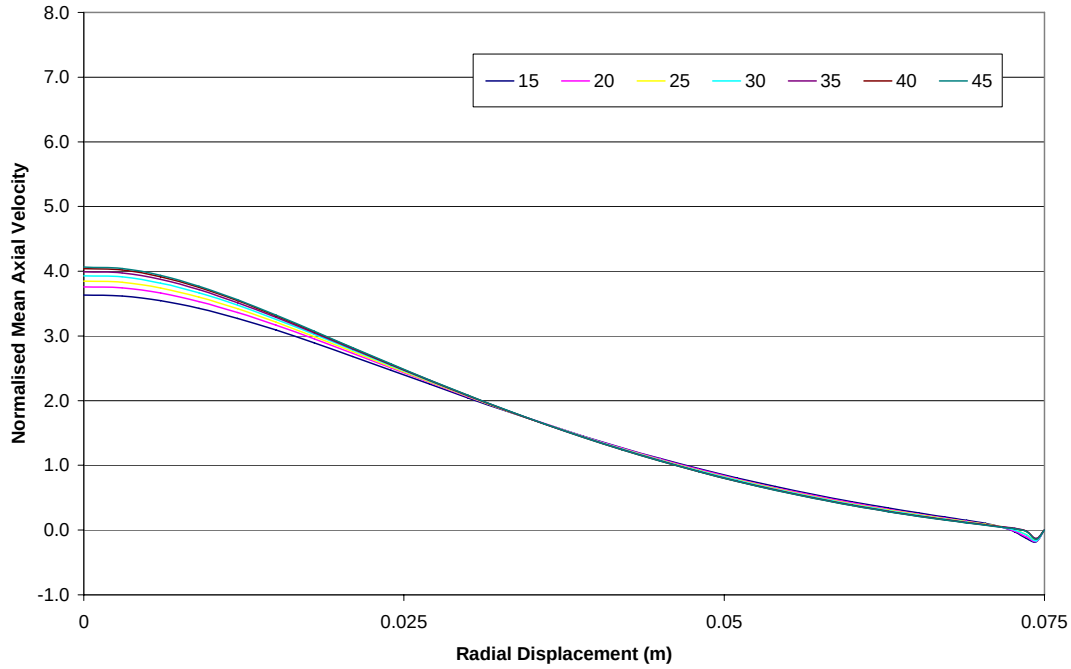

Figure 7.7: Normalised diffuser exit velocity profiles for a 50 mm diameter jet at 15, 20, 25, 30, 40 and 45 ms^{-1}, with a 7° conical diffuser.

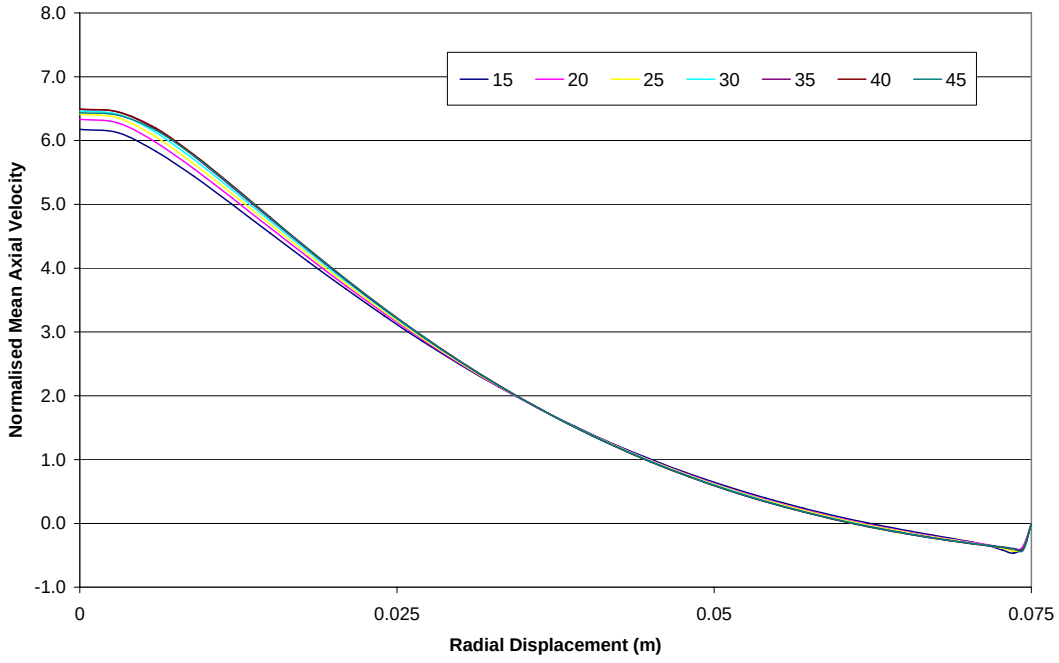

Figure 7.8: Normalised diffuser exit velocity profiles for a 50 mm diameter jet at 15, 20, 25, 30, 40 and 45 ms^{-1}, with a 10° conical diffuser.

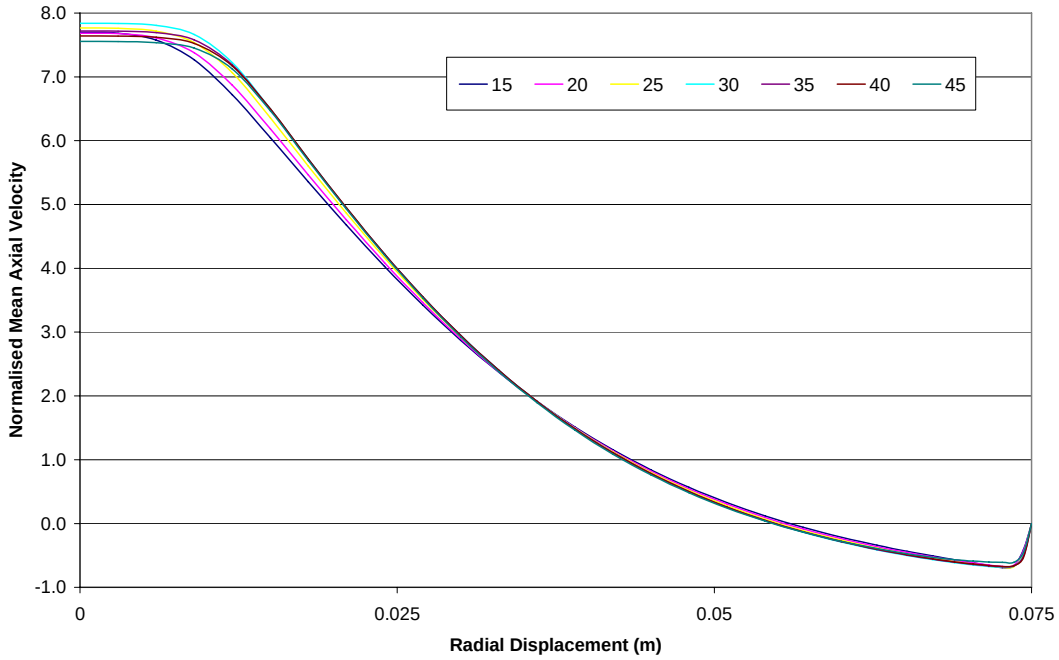

Figure 7.9: Normalised diffuser exit velocity profiles for a 50 mm diameter jet at 15, 20, 25, 30, 40 and 45 ms^{-1}, with a 14˚ conical diffuser.

The 7˚ diffuser provided good deceleration with minimal flow recirculation; whereas the 14˚ diffuser resulted in significant recirculation zones inside the conical diffuser section, and a corresponding increase in the static pressure drop. The 10˚ diffuser proved a useful compromise between the two, providing a reasonable deceleration of the flow, but without an excessive use of valuable ceiling space. (The 10˚ diffuser was 30 percent shorter in length than the equivalent 7˚ design). For all three diffuser angles used a high velocity central core develops at the exit of the conical diffuser, which in part is magnified by the presence of a recirculation zone in the near wall region. The recirculation zone increases in both size and magnitude as the diffuser angle is increased.

In the case of the 14˚ diffuser the peak normalised velocity of 7.8 is only a marginal drop from the average inlet jet velocity of 9. That the final outlet velocity profile peak measured across the exit plane on the outlet duct is only 2 highlights the importance of including the extended outlet duct following the conical diffuser.

7.2.2 Conical Diffuser With Extended Outlet Ducts

Given the effectiveness of the outlet duct in dispersing the high velocity jet core present in the exit plane of the conical diffuser the above analysis was also extended to outlet duct lengths of 600 and 900 mm. Numerical models were developed for each of the conical diffuser angles of 7˚, 10˚ and 14˚. Extending the length of the outlet duct increases the ceiling space required to house the HVAC system, however this added space requirement was allowed on the premise that a more favourable flow and acoustic solution may be found. The potential to increase the attenuation of the flow induced noise and improve the deceleration potential of the diffuser assembly could be offset against the increased space requirements.

The normalised velocity profiles at the outlet duct exit, using an inlet jet velocity of 15 ms^{-1}, were recorded for each of the three lengths of 300, 600 and 900 mm and are shown in Figures 7.10, 7.11 and 7.12 respectively.

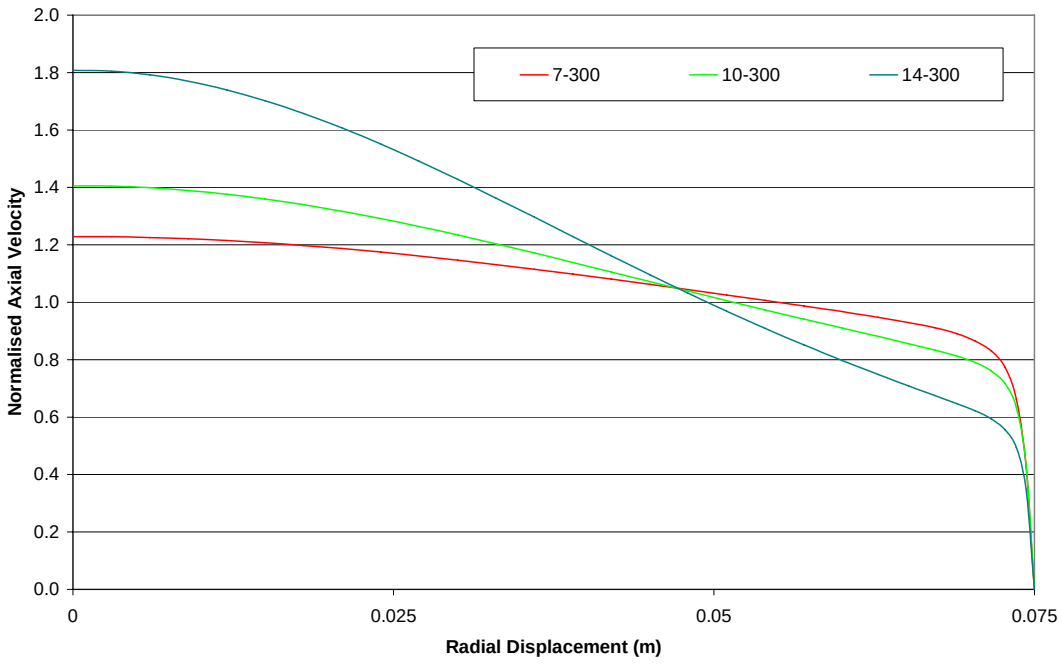

Figure 7.10: Normalised exit plane velocity profiles for a 15 ms^{-1} jet with a 7˚, 10˚ and 14˚ conical diffuser fitted with a 300 mm long outlet duct.

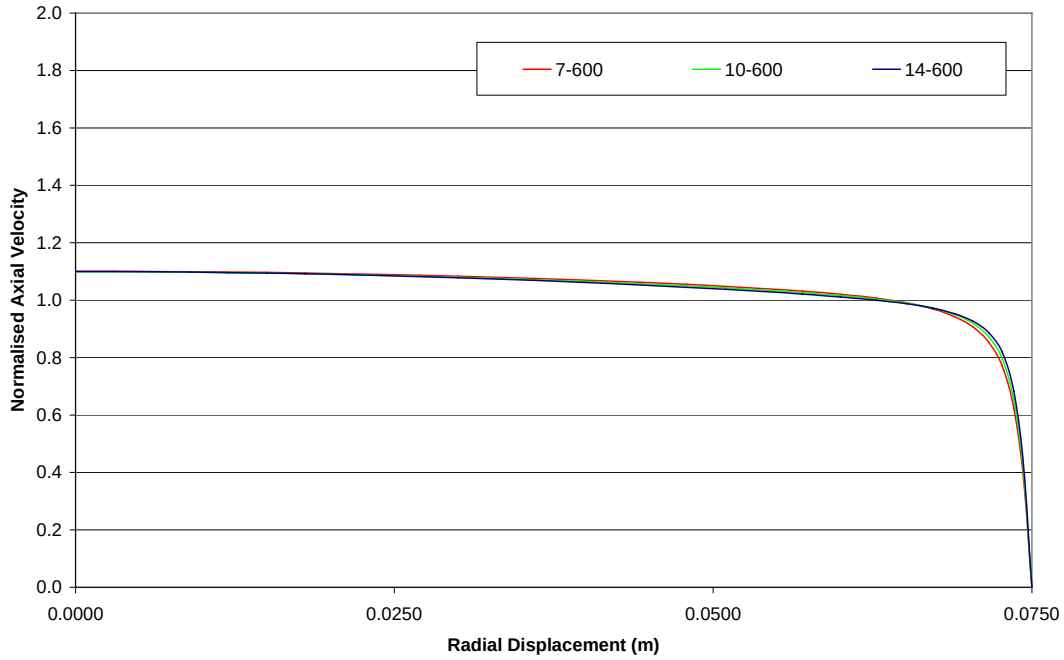

Figure 7.11: Normalised exit plane velocity profiles for a 15 ms^{-1} jet with a 7˚, 10˚ and 14˚ conical diffuser fitted with a 600 mm long outlet duct.

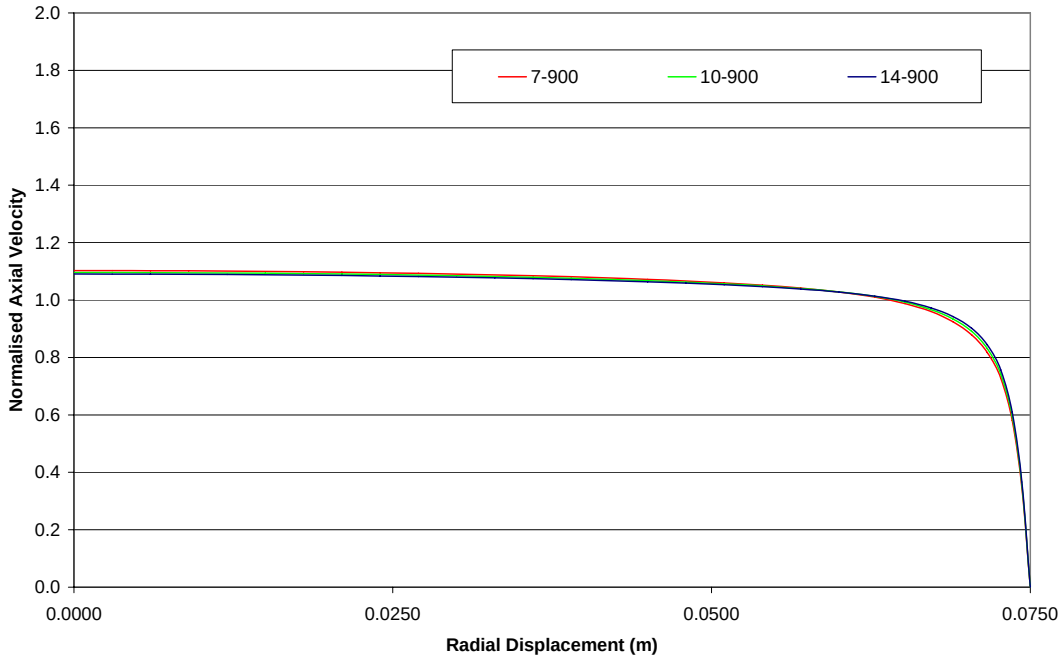

Figure 7.12: Normalised exit plane velocity profiles for a 15 ms^{-1} jet with a 7˚, 10˚ and 14˚ conical diffuser fitted with a 900 mm long outlet duct.

The result for the 300 mm long outlet duct has been included here as a point of reference and to also highlight the velocity profiles for the benchmark inlet jet velocity of 15 ms^{-1}. For this reference case the sharp increase in the centreline velocity as the diffuser angle is increased from 7˚ to 10˚ is clearly seen (an increase of 14.8 %). A further increase of 18.6 % in the centreline velocity is observed as the diffuser angle is changed from 10˚ to 14˚. In stark contrast to this result there is little variation between the three conical diffuser angles once the outlet duct length is extended to both 600 and 900 mm. When this same analysis is applied to the results for higher inlet jet velocities of up to 45 ms^{-1} there is still no significant variation between the outlet velocity profiles for any of the diffuser angles tested with an outlet duct of 600 and 900 mm. Therefore there appears to be no justifiable reason to consider extending the outlet duct length beyond 600 mm. This numerical result is in line with the conclusions drawn from the experimental acoustic tests discussed previously.

There may be scope to reduce the length of the outlet duct below 600 mm, but it will clearly need to be somewhat longer than the 300 mm ducts already tested. The final optimum length of outlet duct used will largely be determined by the individual space limitations and the inlet jet velocities employed. In some circumstances it may also be possible to use a larger diffuser angle (say 10˚ to 14˚) and result in an overall shorter assembly that could be fitted into constrained ceiling cavities. In these instances the acoustic performance of the proposed outlet diffuser and duct section would need to be more carefully investigated. Despite these limitations there is a clear advantage in being able to conduct relatively low cost steady state flow simulations to narrow down the number of outlet diffuser configurations to be fully evaluated using the numerical acoustic model.

The time required to complete each computational solution and the limited access to shared experimental facilities restricted the number of outlet duct lengths and diffuser angles investigated under the time frame available for this work. Statistical averaging from repeated experimental measurements was critical to minimising the experimental error in the acoustic measurements used to validate the numerical acoustic model. The validation of the numerical acoustic model was therefore placed above the need to trial a wide range of duct geometry and outlet grills.

The identification of precise duct geometry for optimum outlet configurations in terms of both flow delivery and noise limits will be case specific and therefore not the primary aim of this work. Additional models can be run for specific design cases as required in future where the computational costs can be weighed against the benefits obtained. The numerical modelling methodologies developed in this work can be applied to each specific design case as required, with the general duct lengths and diffuser angles outlined above providing a useful starting point for individual optimisation.

7.3 Unsteady LES Flow Simulations

Once the optimal outlet diffuser geometry has been identified using steady state flow models, fully transient LES models can then be used to generate the time varying flow field data required to complete a numerical acoustic calculation. The LES models also provide useful guidance as to the true effectiveness of the diffuser and the extended outlet duct in terms of the fluctuating components of both the velocity and pressure flow fields. Most of the flow induced sound is generated from fluctuating pressures from within the flow field. Therefore anything that can minimise or eliminate these sources will be quite effective in reducing the generation and subsequent propagation into a passenger cabin of flow induced noise.

Contour plots of the mean and rms fluctuating axial velocity – as shown in Figures 7.13 and 7.14 respectively - illustrate the effectiveness of the diffuser and extended outlet pipe in retarding and dispersing the air jet. The rms fluctuating Y-axis velocity also follows this same trend as shown in Figure 7.15. The slight irregularities in the shape of these plots are associated with the transient nature of the flow and the length of sample used to calculate the statistics represented. Extending the total flow time used in the model will improve this result somewhat and further improve the quality of the fluctuating pressure data used in the acoustic analysis.

The fluctuating turbulent velocity field is several orders of magnitude greater than the true acoustic particle velocity corresponding to the fluctuating acoustic pressure. This is expected given that the bulk fluid medium is not at rest – a fundamental assumption of acoustic theory. Consequently a far field acoustic analysis has been chosen instead of a direct acoustic calculation using a near field technique. As the flow velocities in this analysis are all under 45 ms^{-1} ($M < 0.13$) the flow is effectively incompressible and as such the added complexity of running a compressible model is avoided.

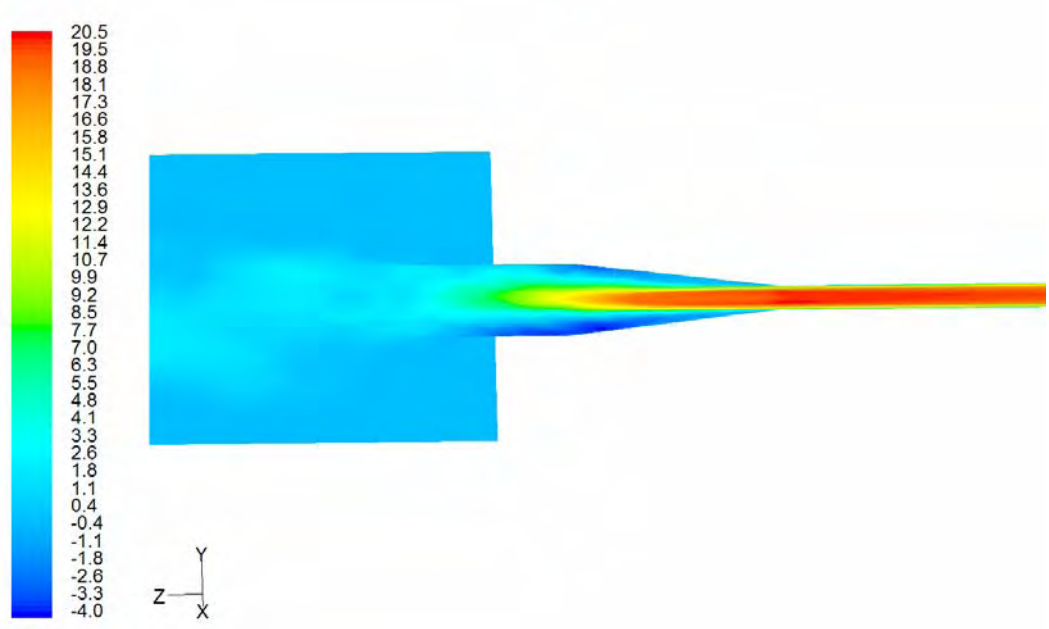

Figure 7.13: Mean axial velocity for 20ms^{-1} jet

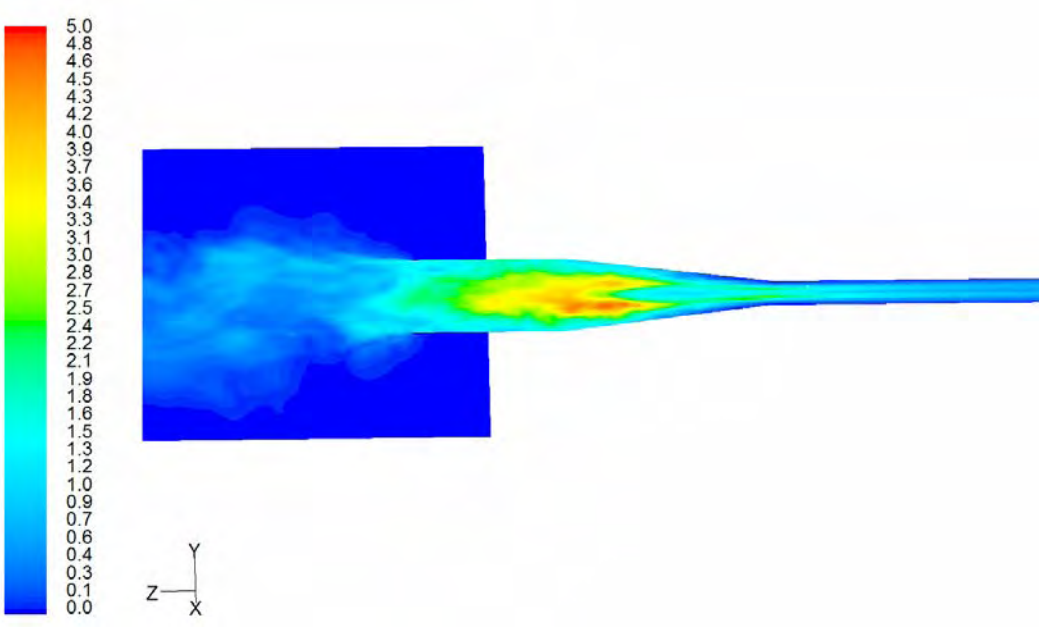

Figure 7.14: RMS axial velocity for 20ms^{-1} jet.

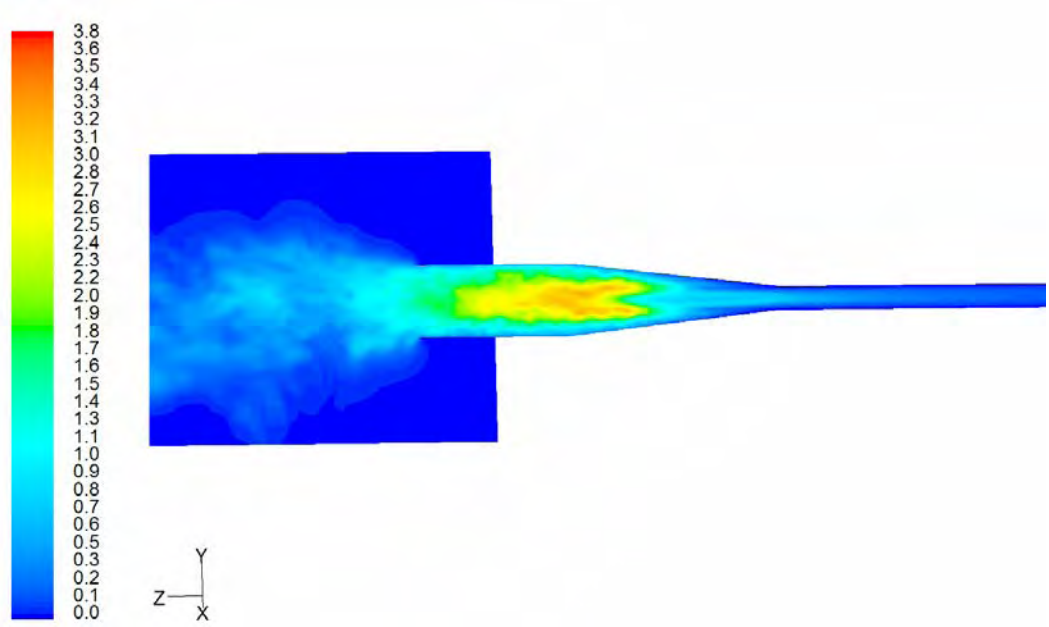

Figure 7.15: RMS Y-axis Velocity for 20ms^{-1} jet.

The effectiveness of each outlet configuration (diffuser angle and outlet duct length) can be more closely scrutinised by comparing the fluctuating velocity and pressure across the outlet exit plane. The mean and rms components of the fluctuating axial velocity across the exit plane and the corresponding rms fluctuating static pressure can be used to make this assessment. The effectiveness of each outlet configuration was found to vary with the inlet jet velocity as well as the diffuser angle and outlet duct length. To isolate the dependency of each of these variables a matrix comparison between the various numerical models was completed in a similar manner to that used for the experimental analysis covered in Chapter 5.

7.3.1 Conical Outlet Diffuser Performance - Jet Velocity Comparison

The experimental results were used to select the following four conical diffuser and outlet duct lengths used in the numerical analysis:

(a) 7-300-0: 7˚ conical diffuser with an open ended 300 mm outlet duct
(b) 10-300-0: 10˚ conical diffuser with an open ended 300 mm outlet duct
(c) 14-300-0: 14˚ conical diffuser with an open ended 300 mm outlet duct
(d) 10-600-0: 10˚ conical diffuser with an open ended 600 mm outlet duct

The first selection (a) was considered the base line reference case, with the following two configurations (b) and (c) used to simulate the direct effect of the conical diffuser angle. The model (d) was used to investigate the impact of extending the outlet duct on the 10˚ diffuser. The corresponding 7˚ model has not been included in this analysis due to the limited variation observed. Likewise the 14˚ diffuser model has been omitted due to the limited improvement achieved when fitted with the longer 600 mm outlet duct.

7.3.1.1. 7-300-0

The mean axial velocity across the duct outlet for the baseline case (7-300-0) is shown in Figure 7.16, for jet velocities of 15, 20 and 25 ms^{-1}. As expected the exit velocity increases with the inlet jet velocity and there is a general flattening of the overall velocity profile. The turbulent nature of the flow field is evident in the slight irregularity in each of the velocity profiles. Normalising the velocity profiles against the jet velocity input and area ratio, as shown in Figure 7.17, provides a better indication of the effectiveness of the diffuser for each of the inlet jet velocities considered. The turbulent velocity profile for the 20 and 25 ms^{-1} cases actually improve the overall performance of the outlet with a peak normalised velocity of only 1.2 to 1.25, compared to the higher value of 1.4 produced at a jet velocity of only 15 ms^{-1}.

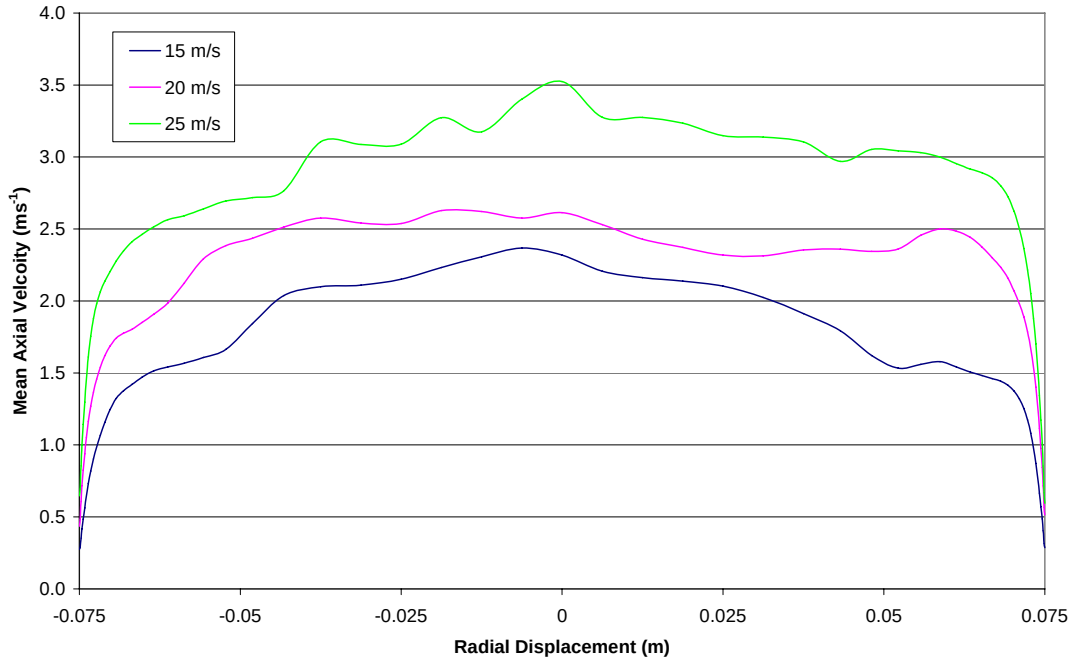

Figure 7.16: Mean axial velocity at the outlet of the 7˚ conical diffuser fitted with a 300 mm long outlet duct.

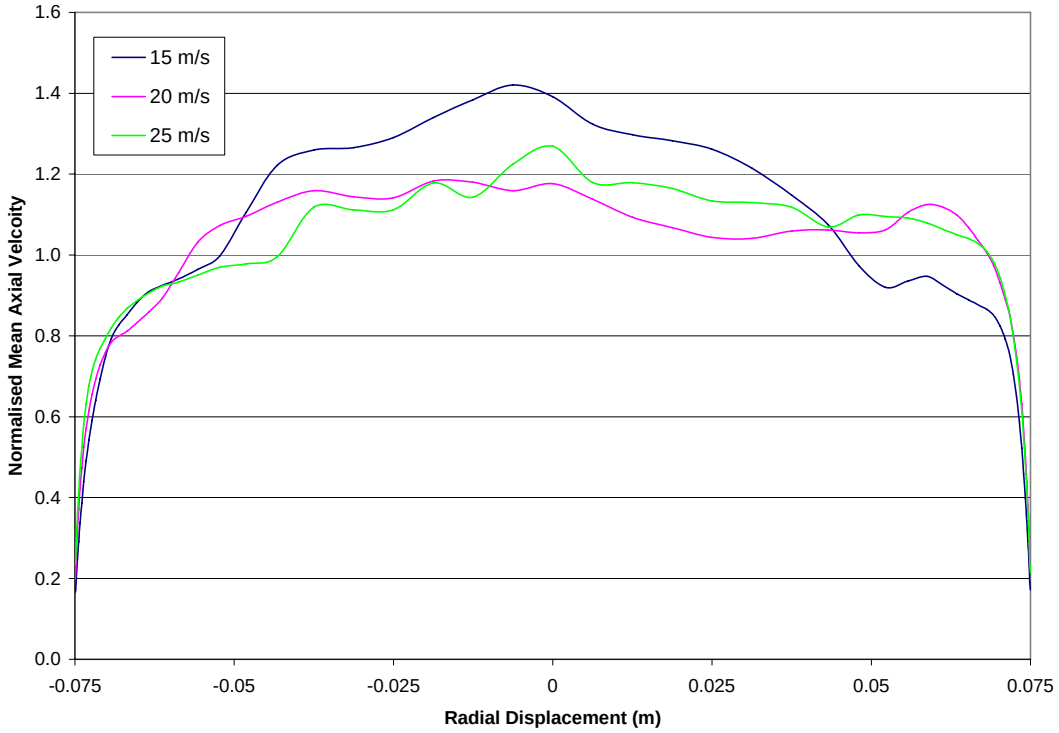

Figure 7.17: Normalised (mean) axial velocity at the outlet of the 7˚ conical diffuser fitted with a 300 mm long outlet duct.

Aside from the general deceleration of the air jet the other major aim of the outlet configuration is the minimisation of the resulting flow induced noise. To this end the fluctuating axial velocity and pressure components must be minimised as much as possible. The rms fluctuating axial velocity components and the rms static pressure at the duct outlet, for the same three jet velocities used above, are shown in Figures 7.18 and 7.19 respectively. The effect of increasing the jet velocity can be clearly seen here with a significant increase in the fluctuating axial velocity observed. Interestingly there is minimal radial variation across the outlet plane, indicative of the effectiveness of the diffuser in adequately dispersing the air jet.

The fluctuating static pressure across the duct outlet, as shown in Figure 7.19 increases significantly as the jet velocity is increased, matching the observations made experimentally in the reverberation suite. The slight concentration in the centre of the duct is to be expected and is most likely a key contributing factor to the directivity observed in the acoustic radiation away from the duct outlet.

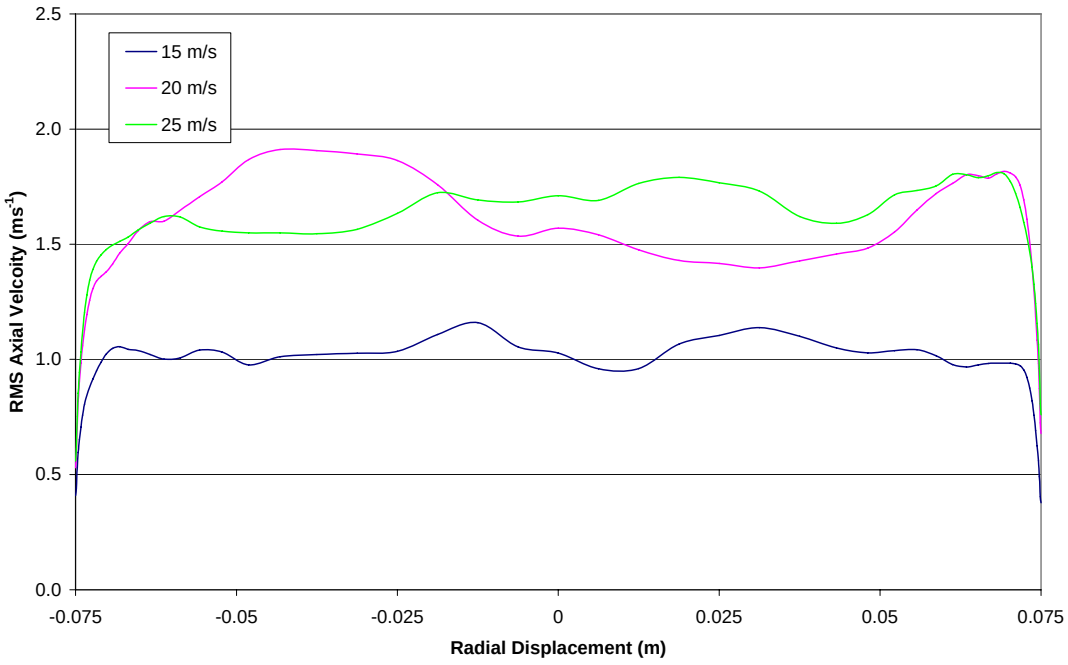

Figure 7.18: RMS axial velocity at the outlet of the 7˚ conical diffuser fitted with a 300 mm long outlet duct.

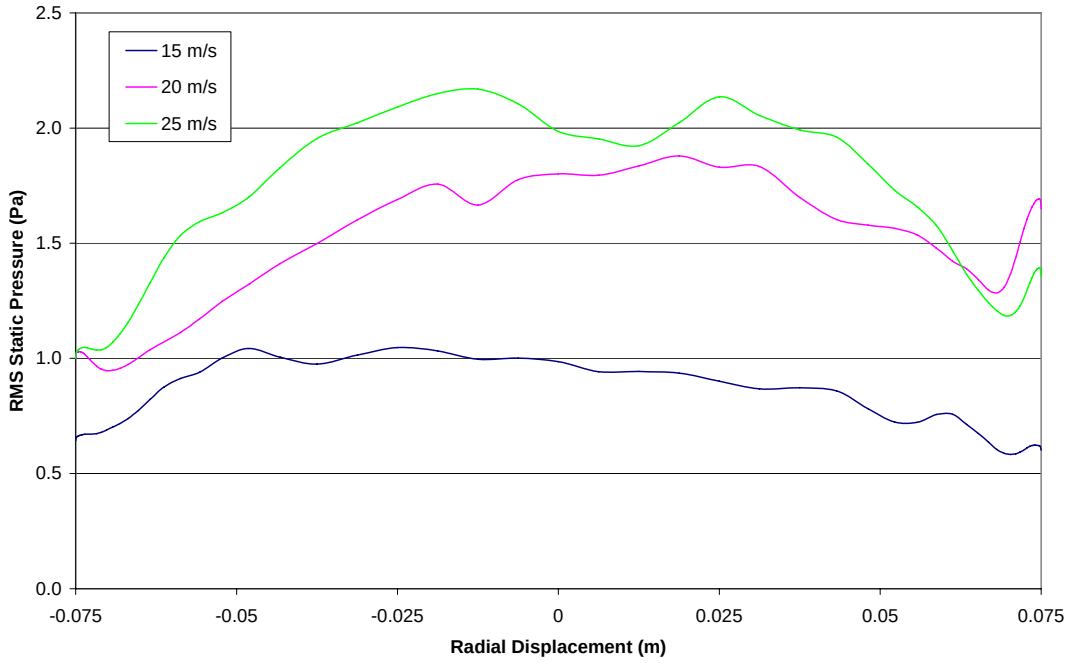

Figure 7.19: RMS static pressure at the outlet of the 7˚ conical diffuser fitted with a 300 mm long outlet duct.

7.3.1.2. 10-300-0

The mean axial velocity across the duct outlet for the 10˚ conical diffuser fitted to the open ended 300 mm long outlet duct is shown in Figure 7.20, for jet velocities of 15, 20 and 25 ms^{-1}. The velocity peak located in the centre of the duct outlet is substantially sharper when compared to the baseline case outlined above. The 15 ms^{-1} jet produces a low velocity region near the duct wall, which becomes less prominent as the jet velocity is increased to 20 and 25 ms^{-1}. Normalising the velocity profiles against the jet velocity input and area ratio, as shown in Figure 7.21, once again provides a better indication of the relative shape of the three velocity profiles. The inability of the 10˚ diffuser to adequately expand the air jet is clearly seen by the central high velocity core observed at the duct outlet. The outlet does however appear to be better suited to the high jet velocities of 20 and 25 ms^{-1}.

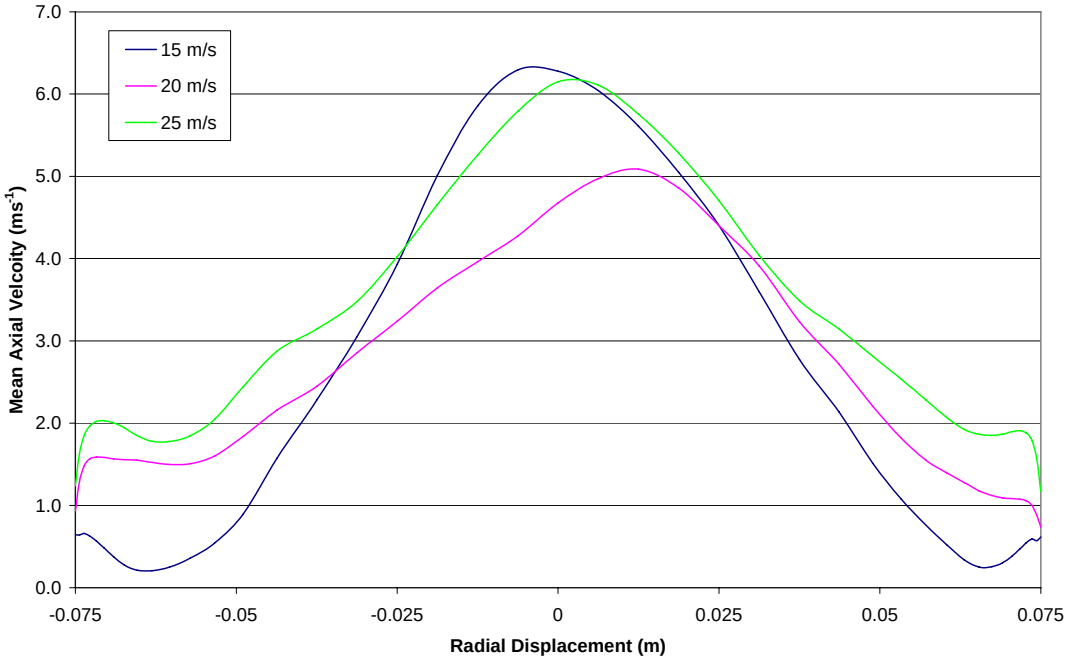

Figure 7.20: Mean axial velocity at the outlet of the 10˚ conical diffuser fitted with a 300 mm long outlet duct.

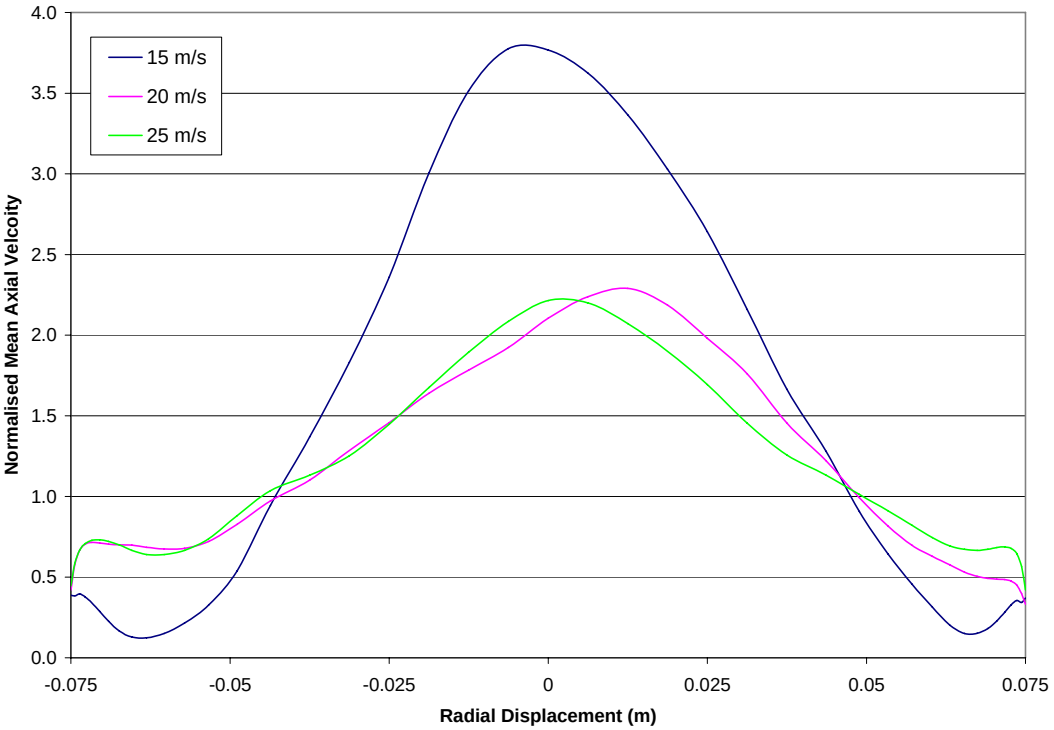

Figure 7.21: Normalised (mean) axial velocity at the outlet of the 10˚ conical diffuser fitted with a 300 mm long outlet duct.

The rms fluctuating axial velocity components and the rms static pressure at the duct outlet, are shown in Figures 7.22 and 7.23 respectively. The relatively high normalised peak velocity observed above with the 15 ms^{-1} jet is offset by the low fluctuating axial velocity component. Interestingly the fluctuating velocity component is more evenly spread across the whole duct outlet, with only a minor increase encountered as the jet velocity is increased to 20 ms^{-1}. Increasing the jet velocity from 20 to 25 ms^{-1} however produces a significant increase in the fluctuating axial velocity observed. The acoustic performance of this outlet is therefore expected to drop off significantly at jet velocities over 20 ms^{-1}.

The fluctuating static pressure across the duct outlet, as shown in Figure 7.23 follows a similar trend to the fluctuating axial velocity, with significant increases at a jet velocity of 25 ms^{-1}. The inability of the diffuser to adequately disperse the flow also becomes more prominent as the jet velocity is increased. This is evidenced by the increasing concentration of the fluctuating flow field in the centre of the outlet duct. The drop off in the acoustic performance of the outlet is strongly linked to the steep increase in the magnitude of the fluctuating flow field.

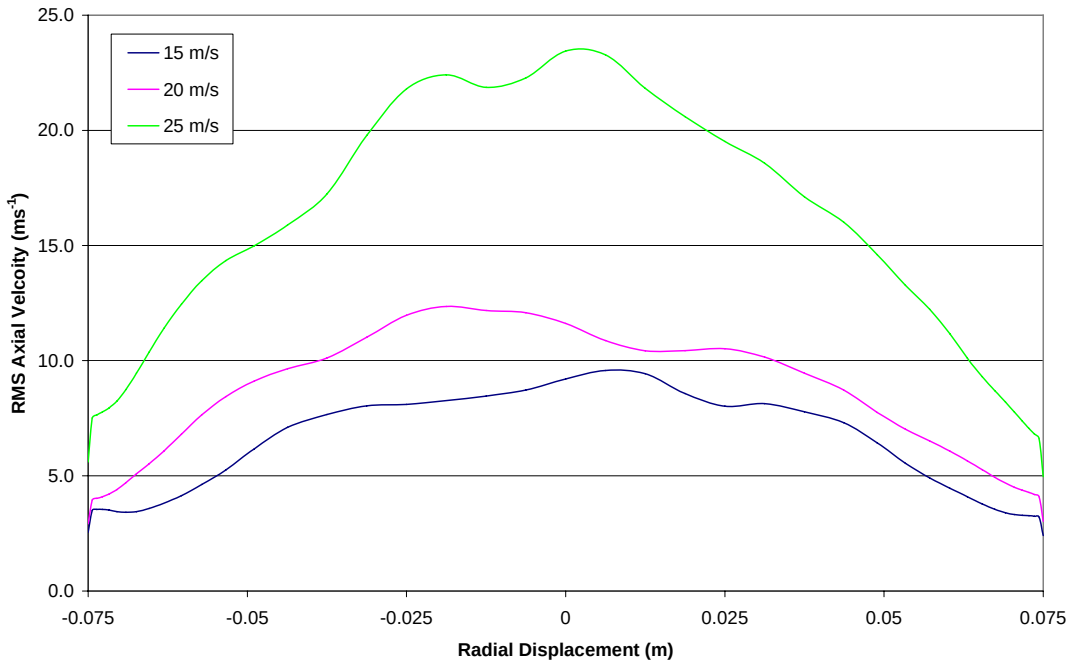

Figure 7.22: RMS axial velocity at the outlet of the 10˚ conical diffuser fitted with a 300 mm long outlet duct.

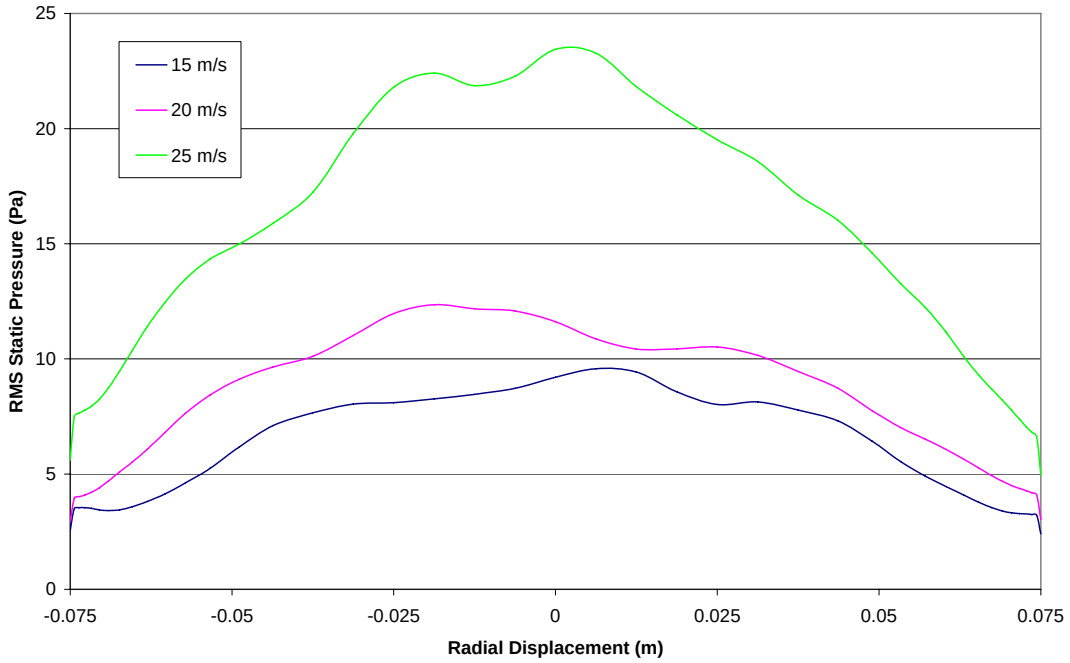

Figure 7.23: RMS static pressure at the outlet of the 10˚ conical diffuser fitted with a 300 mm long outlet duct.

7.3.1.3. 14-300-0

The mean axial velocity across the duct outlet for the 14˚ conical diffuser fitted to the open ended 300 mm long outlet duct is shown in Figure 7.24, for jet velocities of 15, 20 and 25 ms^{-1}. For all three jet velocities there is a prominent high velocity core located in the centre of the outlet duct, indicative of the low level of flow expansion achieved with the 14˚ conical diffuser. The presence of the recirculation zone at the duct outlet for all three jet velocities also reinforces the jet like flow through the core of the expanded outlet. The size of both the recirculation zone and the central jet core tends to increases with the jet velocity. Figure 7.25 shows the normalised velocity profiles at the exit for each jet velocity, with profile relatively independent of the jet velocity itself.

For diffuser angles this large to work effectively additional internal guide vanes would be required. These would dissect the diffuser angle into smaller increments that would then limit the onset of flow separation and subsequent establishment of recirculation zones within the diffuser.

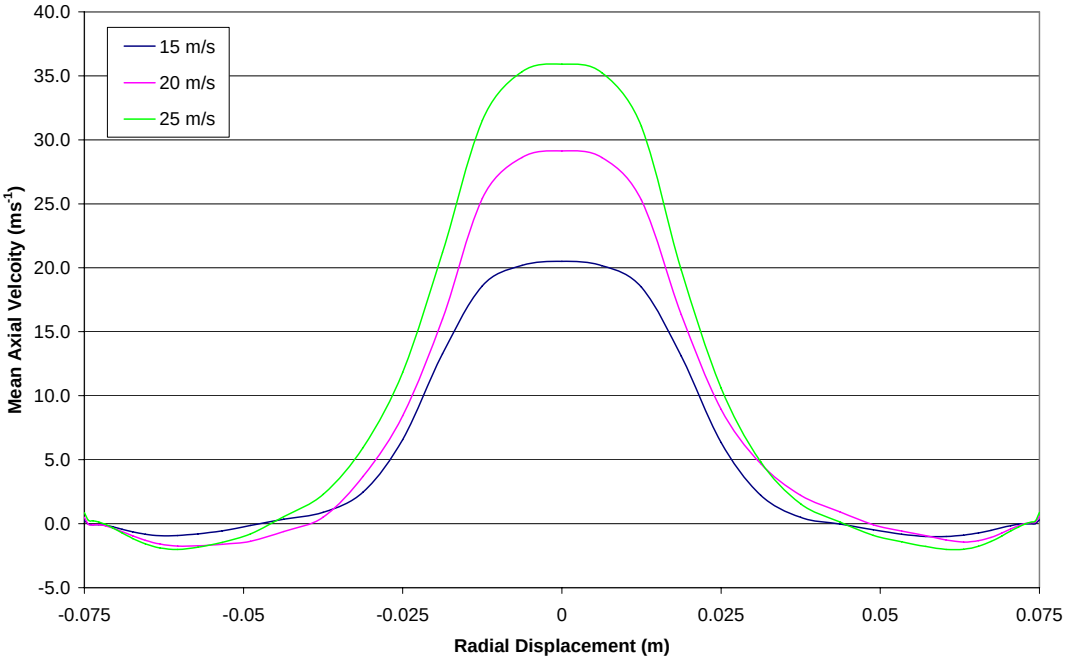

Figure 7.24: Mean axial velocity at the outlet of the 14˚ conical diffuser fitted with a 300 mm long outlet duct.

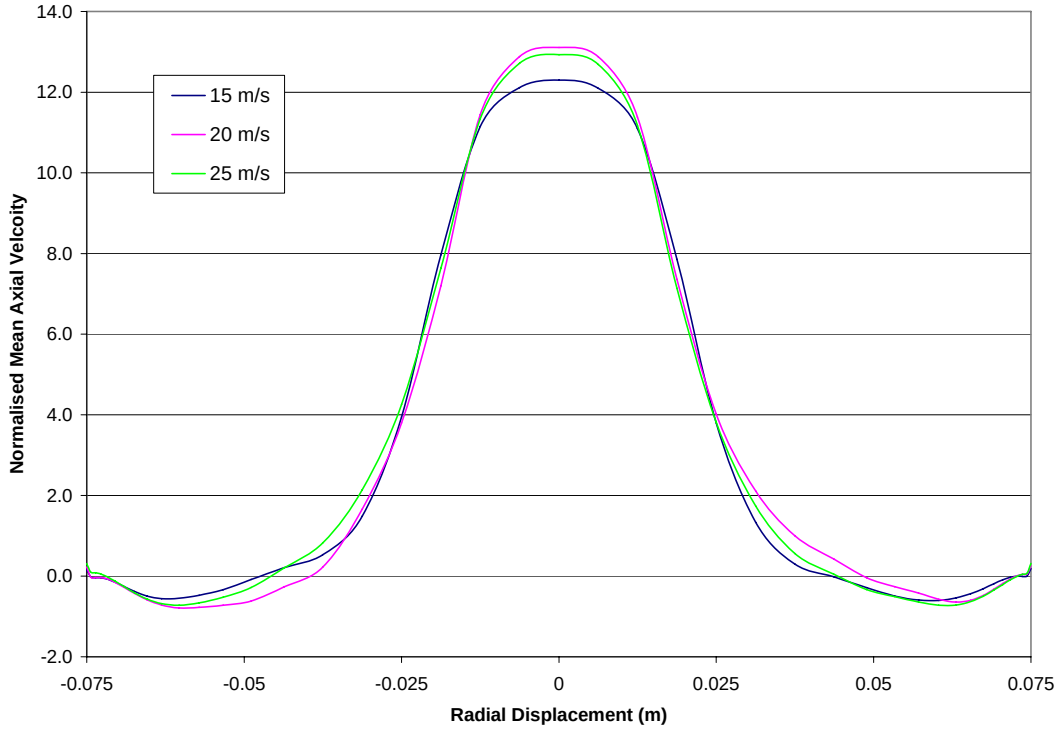

Figure 7.25: Normalised (mean) axial velocity at the outlet of the 14˚ conical diffuser fitted with a 300 mm long outlet duct.

Although the mean velocity profile indicates that the flow is predominantly contained within a central core the fluctuating axial velocity and pressure profiles across the outlet indicate a strong presence of oscillatory fluid motion. The rms fluctuating axial velocity (for a jet velocity of 15, 20 and 25 ms^{-1}) is shown in Figure 7.26. At a jet velocity of 15 ms^{-1} the oscillating axial component is very high in the central core of the duct at 80 % of the inlet velocity. The surrounding duct meanwhile has very low levels of oscillations. As the jet velocity is increased to 20 and 25 ms^{-1} the oscillations in the central core have died down, being replaced with oscillations in the shear layer surrounding the high velocity central core. The increased jet velocity prevents the jet from expanding inside the conical diffuser and outlet duct section, resulting in minimal dispersion of the jet. The oscillations in the shear layer are in part directly caused by the flow separation point, located inside the 14˚ conical diffuser. The acoustic performance of this outlet is therefore expected to be significantly compromised across the whole range of jet velocities considered.

The limited effectiveness of the 14˚ diffuser is further demonstrated by the high fluctuating static pressure observed across the duct outlet, as shown in Figure 7.27. The rms static pressure follows a similar trend to the fluctuating axial velocity, where the main noise sources are located in the shear layer surrounding the high velocity central core. The peak rms pressure readings were consistently located 25 mm out from the duct centreline, directly in line with the shear layer surrounding the jet. The magnitude of the oscillations increases substantially and with a general broadening of the turbulent shear layer as the jet velocity is increased. The inability of this diffuser to adequately expand and decelerate the air jet directly results in the observed ineffective acoustic performance.

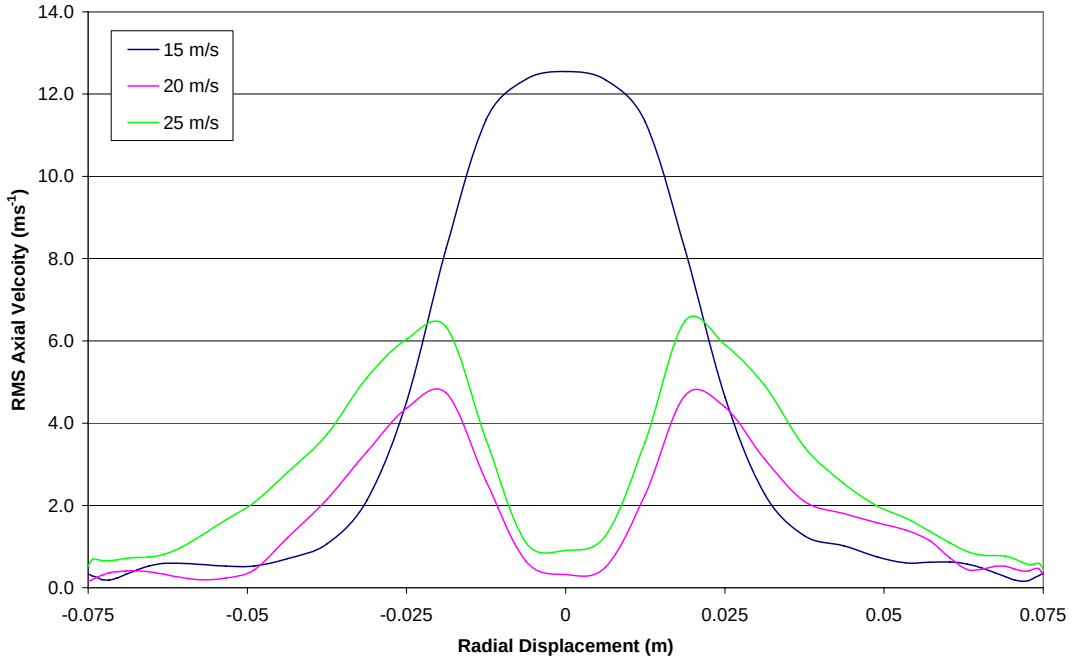

Figure 7.26: RMS axial velocity at the outlet of the 14˚ conical diffuser fitted with a 300 mm long outlet duct.

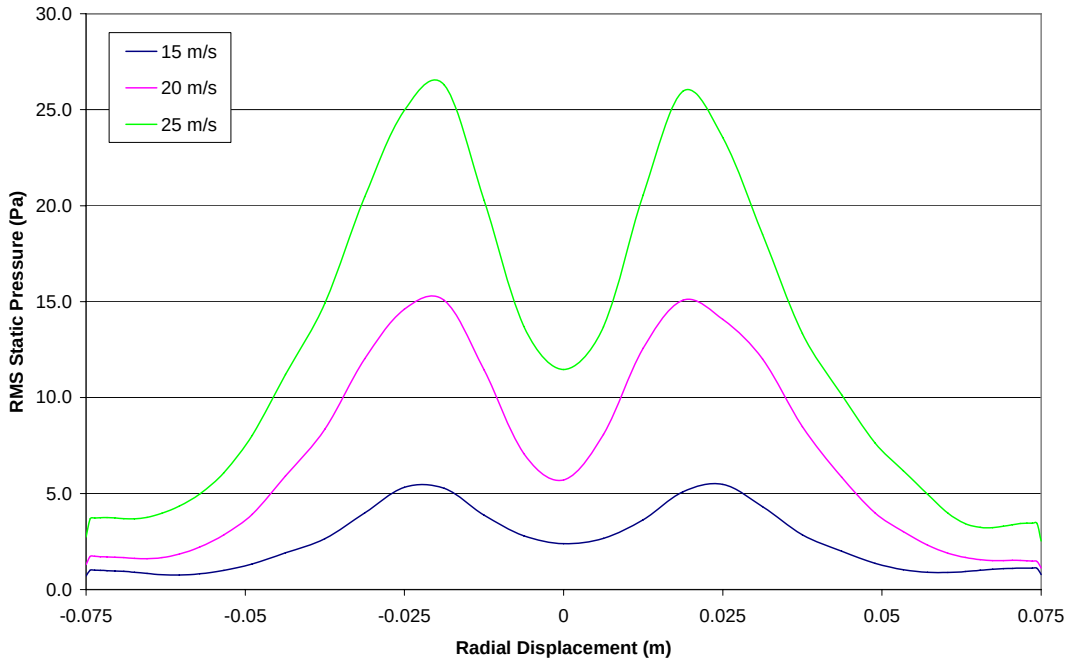

Figure 7.27: RMS static pressure at the outlet of the 14˚ conical diffuser fitted with a 300 mm long outlet duct.

7.3.1.4. 10-600-0

Experimentally the 10˚ conical diffuser when fitted with the 300 mm outlet duct struggled to fully expand the high velocity jet, yet when fitted with the 600 mm duct provided a reasonable level of deceleration of the flow and good acoustic performance. The ability for the CFD model to match this experimental result was deemed a valuable test of the numerical modelling capability and the eventual commercial practicality of such methods in a real design process. Therefore close attention was paid to the velocity profile across the duct outlet for this model.

The mean axial velocity across the duct outlet is shown in Figure 7.28, and the corresponding normalised velocity profile is shown in Figure 7.29. The same jet velocities of 15, 20 and 25 ms^{-1} have been used once more. The velocity profiles for all three jet velocities considered was relatively flat, with some minor localised peaks that can be attributed to localised turbulence effects. The effectiveness of the additional outlet duct length is clearly demonstrated by the normalised velocity profiles, with a steady profile produced for all three jet velocities considered.

The dramatic improvement in the performance of the outlet from the extension of the outlet duct is reinforced by both the fluctuating axial velocity and static pressure profiles that are shown in Figures 7.30 and 7.31 respectively. The fluctuating axial velocity increases with increasing jet velocity, however the magnitude of the oscillations is substantially lower than those observed with the shorted 300 mm outlet duct. With a jet velocity of 15 ms^{-1} the fluctuating axial velocity profile is very flat, with some localised peaks immerging as the jet velocity is increased to 20 and 25 ms^{-1}. The level of variation highlighted here however is minor in comparison to the peaks observed in the two previously outlined configurations (10-300-0 and 14-300-0).

These same trends are reinforced once more in the fluctuating static pressure profiles, with a promising acoustic performance predicted. The magnitude of the pressure oscillations increases with the jet velocity, but with the general profile remaining relatively flat. A minor rise in the oscillations about the centre of the duct does become evident at higher jet velocities (25 ms^{-1}), but within acceptable limits.

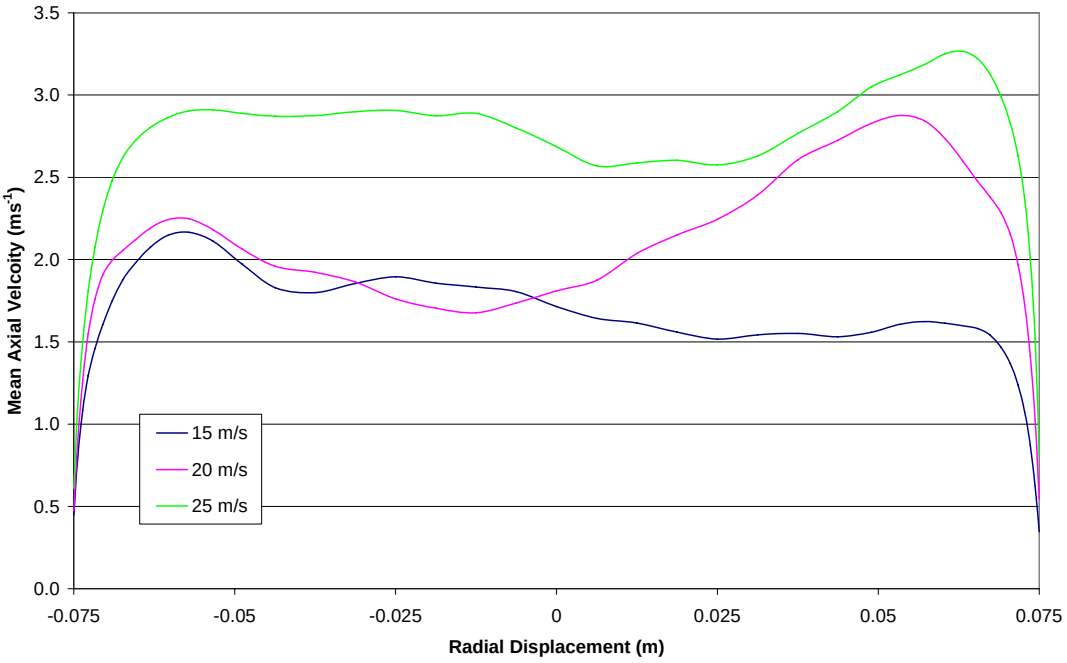

Figure 7.28: Mean axial velocity at the outlet of the 10˚ conical diffuser fitted with a 600 mm long outlet duct.

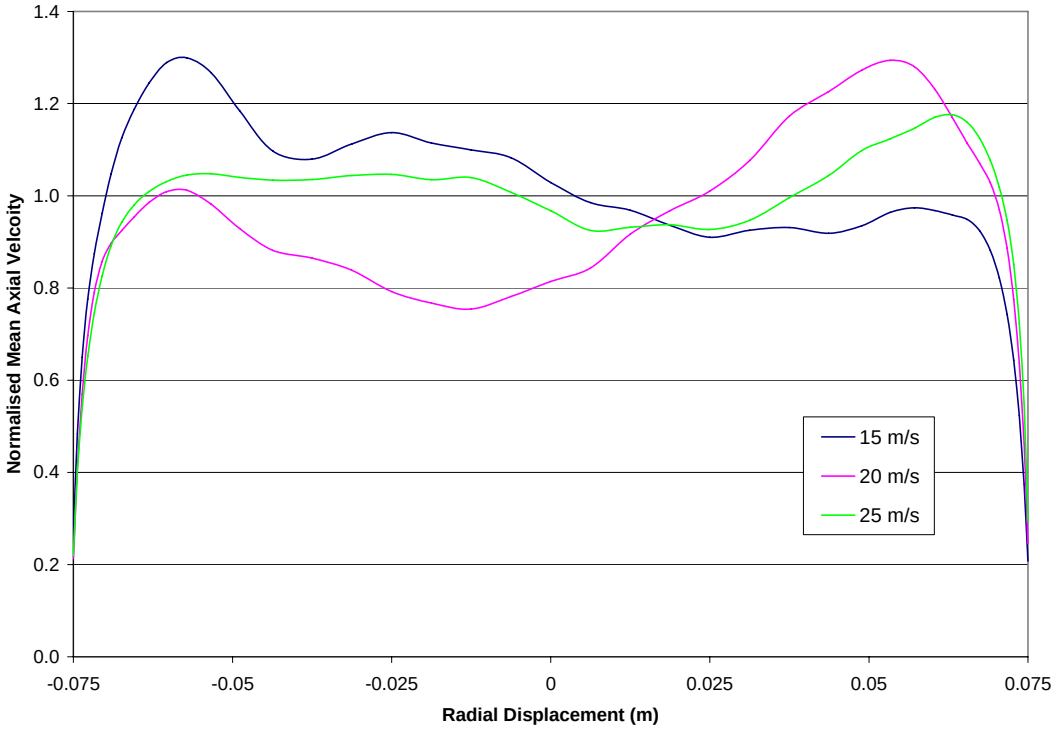

Figure 7.29: Normalised (mean) axial velocity at the outlet of the 10˚ conical diffuser fitted with a 600 mm long outlet duct.

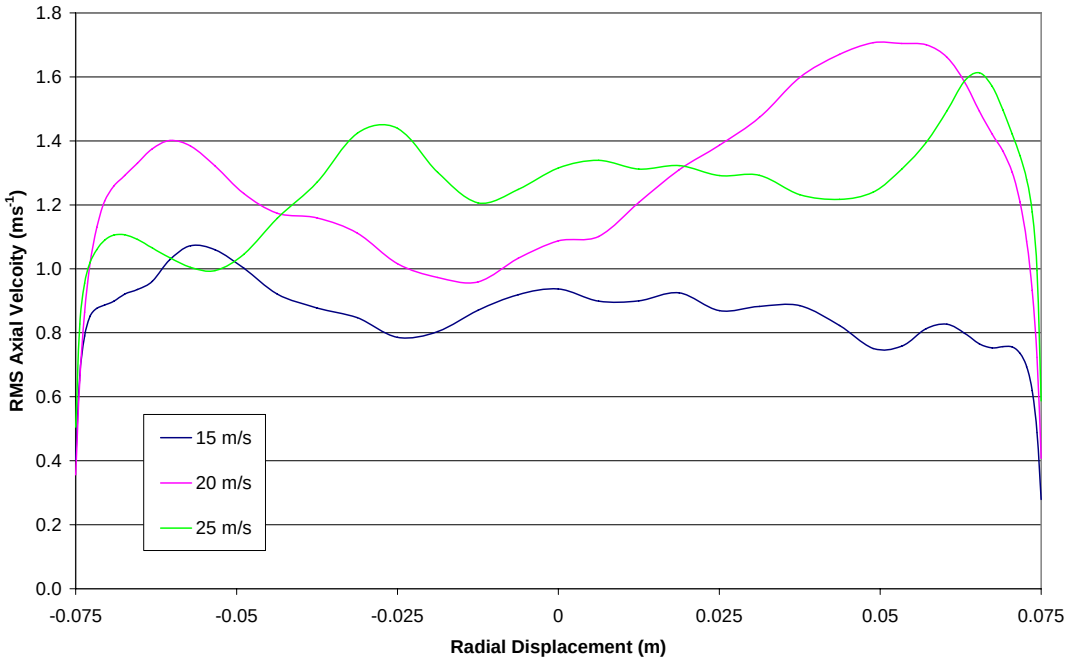

Figure 7.30: RMS axial velocity at the outlet of the 10˚ conical diffuser fitted with a 600 mm long outlet duct.

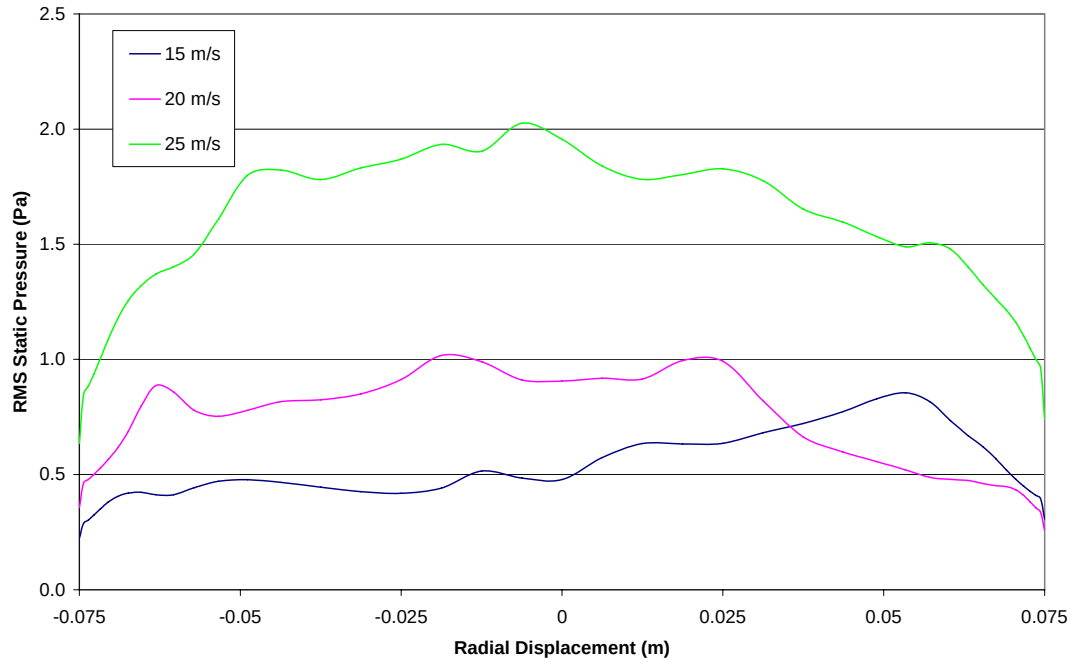

Figure 7.31: RMS static pressure at the outlet of the 10˚ conical diffuser fitted with a 600 mm long outlet duct.

7.3.2 Conical Outlet Diffuser Performance - Diffuser Angle Comparison

To isolate the influence of the conical diffuser angle on the performance of the outlet, comparisons will be made between the three diffuser angles used (7˚, 10˚ and 14˚) when fitted to the 300 mm open ended outlet duct. The shorter outlet duct length has been deliberately chosen to maximise the variation between each diffuser angle and limit the damping effect of the outlet duct itself. Comparisons will be made for each of the three jet velocities of interest - 15, 20 and 25 ms^{-1}.

7.3.2.1. 15 ms^{-1} Jet Velocity

The normalised mean axial velocity across the duct outlet for an inlet jet velocity of 15 ms^{-1} is shown in Figure 7.32, where the impact of increasing the diffuser angle becomes immediately apparent. The 7˚ diffuser provides a very good velocity profile across the full width of the outlet duct with a small boundary layer located in the near wall region. When the diffuser angle is increased to 10˚ the low velocity region near the wall extends one third of the way in towards the centre of the duct. The result of this is a higher peak velocity in the centre of the outlet, indicative of the incomplete expansion of the initial air jet. However this result is quite good when it is compared with the profile produced by the 14˚ diffuser. In this case the near wall low velocity region is reversed as part of a large recirculation zone, which results in an acceleration effect on the jet, leading to normalised exit velocity that is greater than the inlet jet velocity.

The fluctuating axial velocity profile for each conical diffuser angle also reinforces the above conclusions, with considerable increases in the oscillating velocity profile as the conical diffuser angle is increased, as shown in Figure 7.33. The 7˚ diffuser produces a very low and stable oscillating profile, while the 10˚ diffuser produces a higher level of oscillations with a broad peak in the centre of the duct. The failure of the 14˚ diffuser is clearly evident in the sharp peak in the fluctuating axial velocity profile around the centre of the duct. The rms component of the velocity is extremely high at 12.5 ms^{-1}, compared with the original inlet jet velocity of 15 ms^{-1}. Meanwhile the magnitude of the oscillations in the near wall recirculation region is very low, highlighting the inability of this diffuser to adequately expand and diffuse the jet.

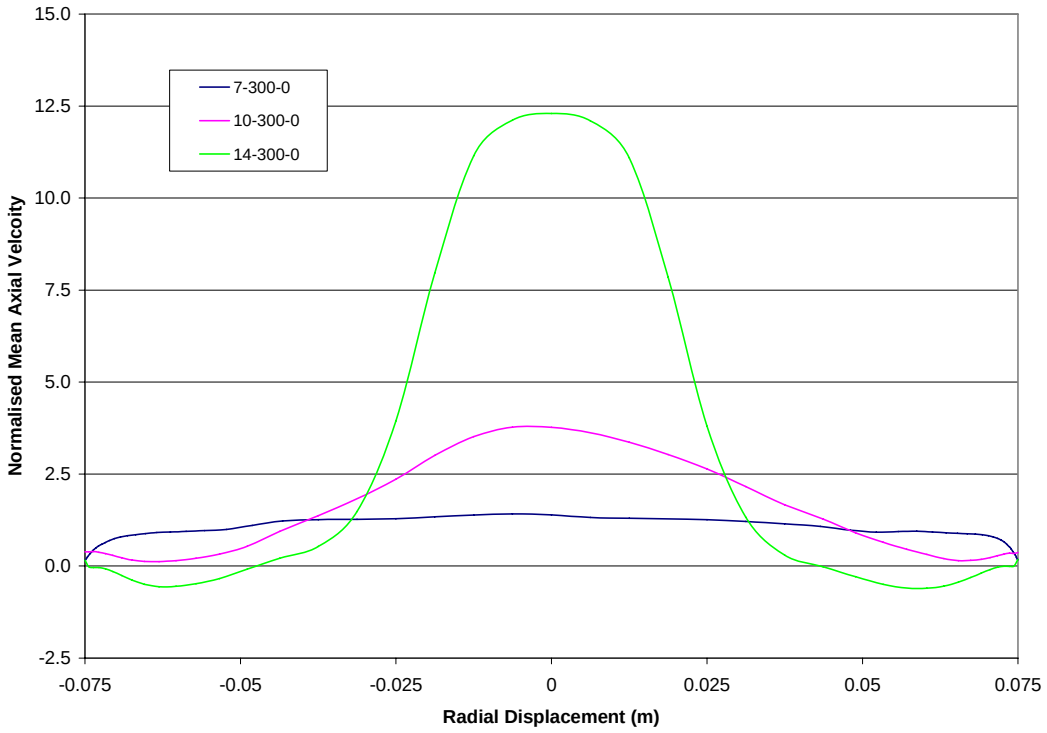

Figure 7.32: Normalised (mean) axial velocity at the outlet of the 7˚, 10˚ and 14˚ conical diffusers fitted with a 300 mm long outlet duct and an inlet jet velocity of 15 ms^{-1}.

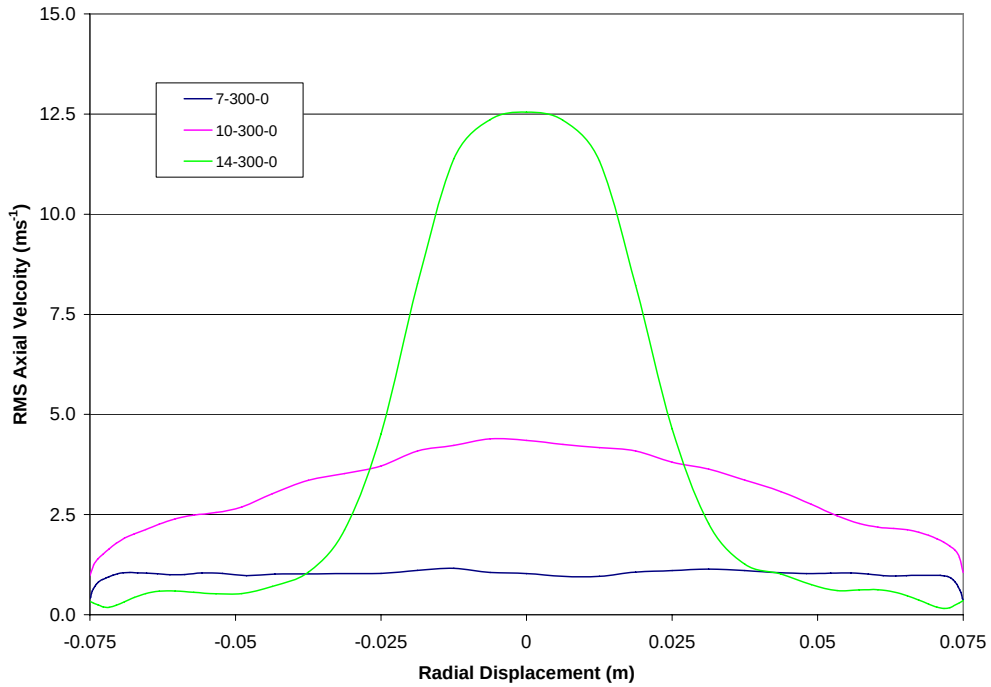

Figure 7.33: RMS axial velocity at the outlet of the 7˚, 10˚ and 14˚ conical diffusers fitted with a 300 mm long outlet duct and an inlet jet velocity of 15 ms^{-1}.

The fluctuating static pressure profile across the outlet for each of the three diffuser angles used, as shown in Figure 7.34, follows a similar trend to that observed in the fluctuating axial velocity profile above. The 7˚ diffuser produces a very flat and uniform fluctuating static pressure across the whole duct outlet, demonstrating the effectiveness of the conical diffuser. The inability of the 10˚ diffuser to fully expand the air jet is highlighted by the much larger magnitude oscillations in the static pressure, with the increase most pronounced in the centre of the duct. These larger fluctuations are linked directly to the instability of the flow in the central core of the outlet.

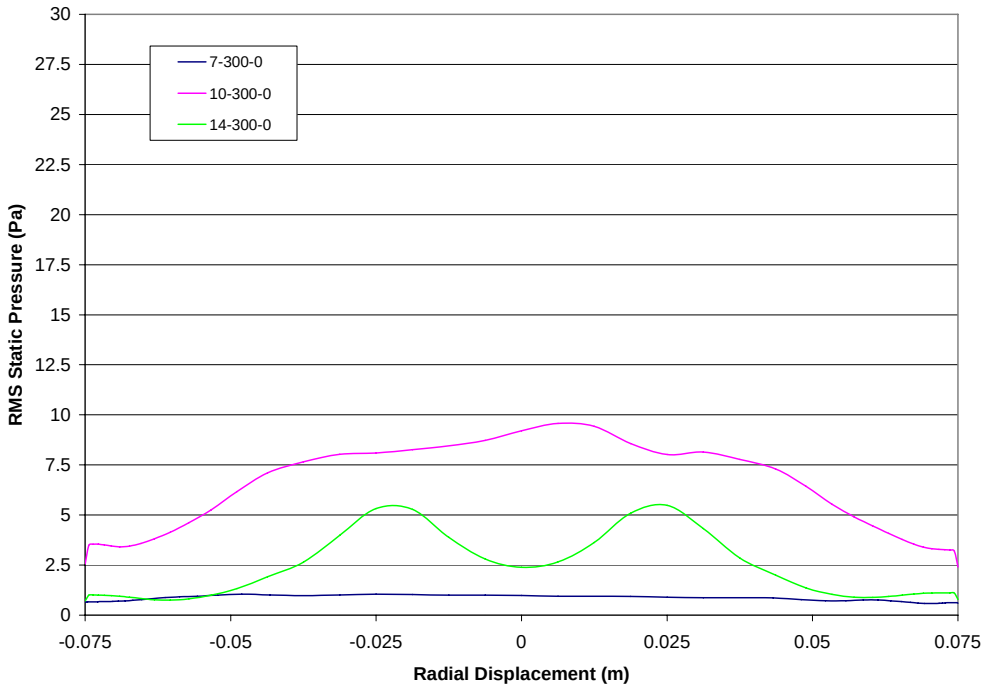

Figure 7.34: RMS static pressure at the outlet of the 7˚, 10˚ and 14˚ conical diffusers fitted with a 300 mm long outlet duct and an inlet jet velocity of 15 ms^{-1}.

The fluctuating static pressure observed at the outlet for the 14˚ diffuser provides an interesting result, where the oscillations are somewhat smaller than those produced by the 10˚ diffuser. This result is misleading in that the lower fluctuations in the static pressure are caused by the jet passing straight through the duct, with minimal expansion of the flow occurring. The acceleration of the jet in the confined space is a direct result of the recirculation zone present inside the diffuser and the outlet duct which all acts to constrict the development of the shear layer that normally surrounds an expanding jet.

The twin peaks in the fluctuating static pressure profile are aligned with the shear layer that is present in the outlet duct, but clearly most of the turbulent expansion of the jet is occurring down stream of the duct exit. In a true HVAC installation this high velocity jet would be impinging on the outlet diffuser grill and would therefore produce significant levels of flow induced noise. Therefore a conical diffuser of 14˚ should be avoided wherever possible.

7.3.2.2. 20 ms^{-1} Jet Velocity

The normalised mean axial velocity across the duct outlet for an inlet jet velocity of 20 ms^{-1} is shown in Figure 7.35, with a very similar performance by each of the three conical diffusers to results for the 15 ms^{-1} inlet jet. Once again the 7˚ diffuser provides a very good velocity profile across the full width of the outlet duct, while the 10˚ diffuser produces an improved normalised velocity profile at the higher inlet velocity. The central peak observed with the 15ms^{-1} jet is considerably lower and the near wall boundary layer region is significantly diminished. The velocity profile produced by the 14˚ diffuser is not significantly affected, with an identical central peak and outer recirculation region to that produced with the 15 ms^{-1} jet.

The fluctuating axial velocity profiles, as shown in Figure 7.36, for both the 7˚ and 10˚ conical diffusers are both relatively flat, with the 10˚ result actually better than the corresponding profile produced by the 15ms^{-1} inlet jet. The fluctuating velocity profile produced by the 14˚ diffuser at the high inlet jet velocity decrease in magnitude significantly, with the single central peak replaced by twin peaks aligned with the shear layer surrounding the central high velocity core.

The true performance of each respective diffuser is most clearly shown by the fluctuating static pressure profiles shown in Figure 7.37. The 7˚ diffuser produces a very low and flat profile, while the 10˚ diffuser produces a substantially higher level of fluctuations, with a concentration about the centre of the duct. The jetting effect produced by the 14˚ diffuser is once more evident, where the fluctuating pressure field is still developing in the shear layer surrounding the constrained jet.

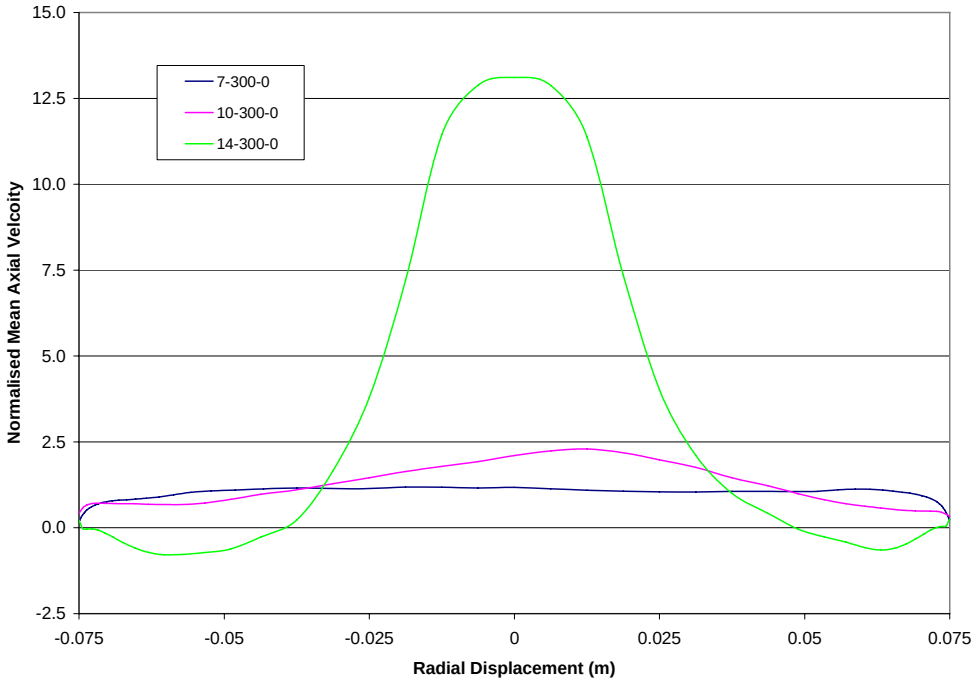

Figure 7.35: Normalised (mean) axial velocity at the outlet of the 7˚, 10˚ and 14˚ conical diffusers fitted with a 300 mm long outlet duct and an inlet jet velocity of 20 ms^{-1}.

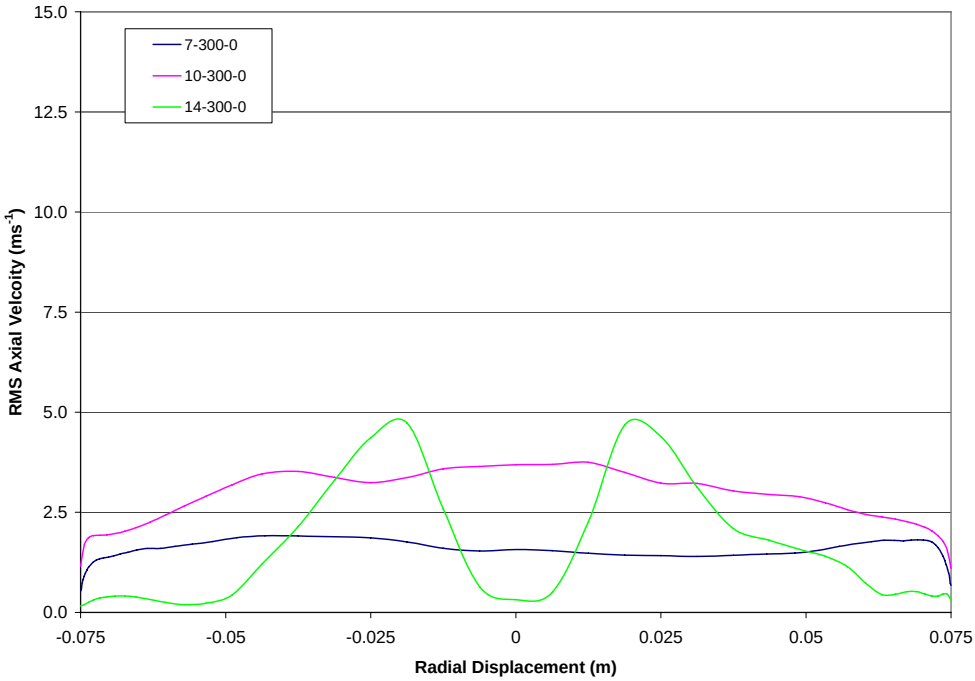

Figure 7.36: RMS axial velocity at the outlet of the 7˚, 10˚ and 14˚ conical diffusers fitted with a 300 mm long outlet duct and an inlet jet velocity of 20 ms^{-1}.

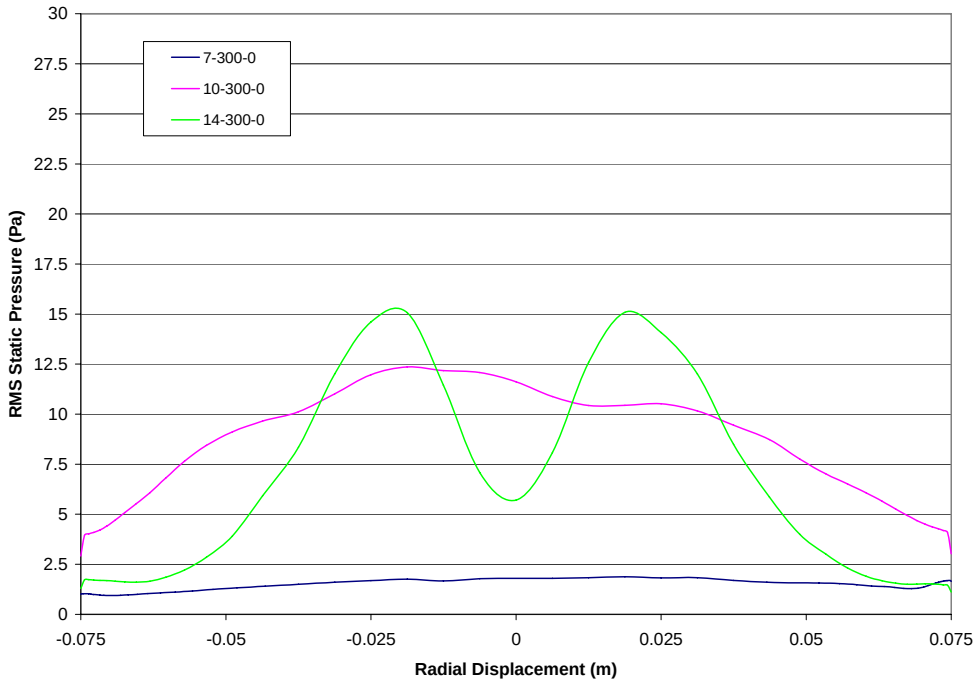

Figure 7.37: RMS static pressure at the outlet of the 7˚, 10˚ and 14˚ conical diffusers fitted with a 300 mm long outlet duct and an inlet jet velocity of 20 ms^{-1}.

7.3.2.3. 25 ms^{-1} Jet Velocity

The normalised mean axial velocity across the duct outlet for an inlet jet velocity of 25 ms^{-1} is shown in Figure 7.38, with a very similar performance by each of the three conical diffusers to results for the 15 and 20 ms^{-1} inlet jets. Both the 7˚ and 10˚ diffusers produce a flat velocity profile across the width of the outlet, with only a minor central peak observed in the 10˚ case. The velocity profile produced by 14˚ diffuser is once again seriously compromised, with the same central peak and outer recirculation regions present. The fluctuating axial velocity profiles, as shown in Figure 7.39, for both the 7˚ and 10˚ conical diffusers are once again relatively flat, but with the gap between the 7˚ and 10˚ increasing compared to the results for the 20 ms^{-1} inlet jet. For the 14˚ diffuser the twin peaks in the fluctuating velocity profile aligned with the shear layer surrounding the central high velocity core are once again present, but with a higher magnitude. The increase in magnitude for both the 10˚ and 14˚ diffusers is to be expected.

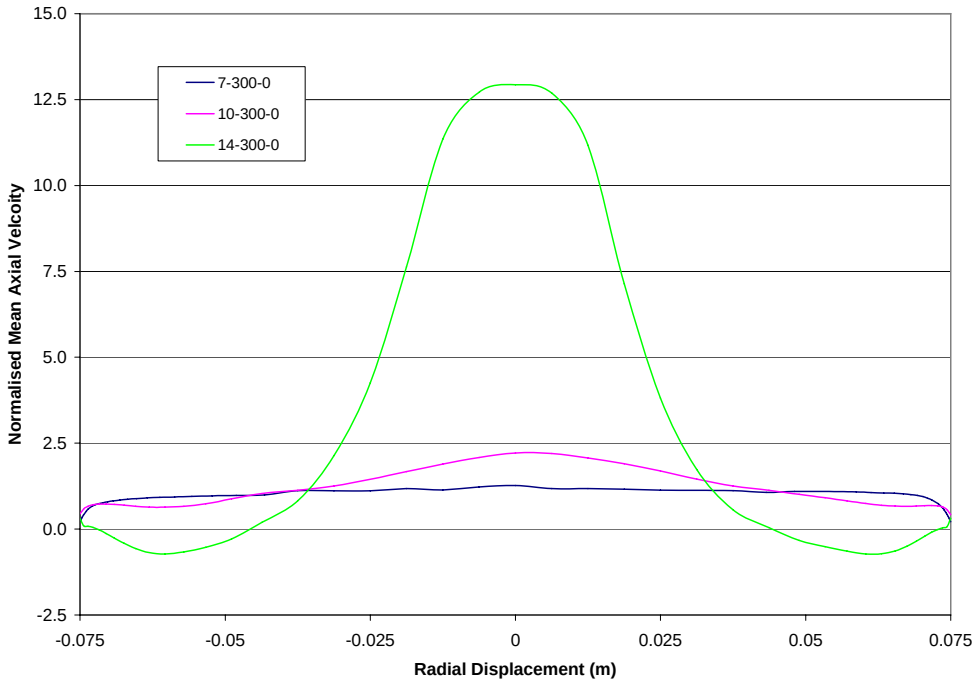

Figure 7.38: Normalised (mean) axial velocity at the outlet of the 7˚, 10˚ and 14˚ conical diffusers fitted with a 300 mm long outlet duct and an inlet jet velocity of 25 ms^{-1}.

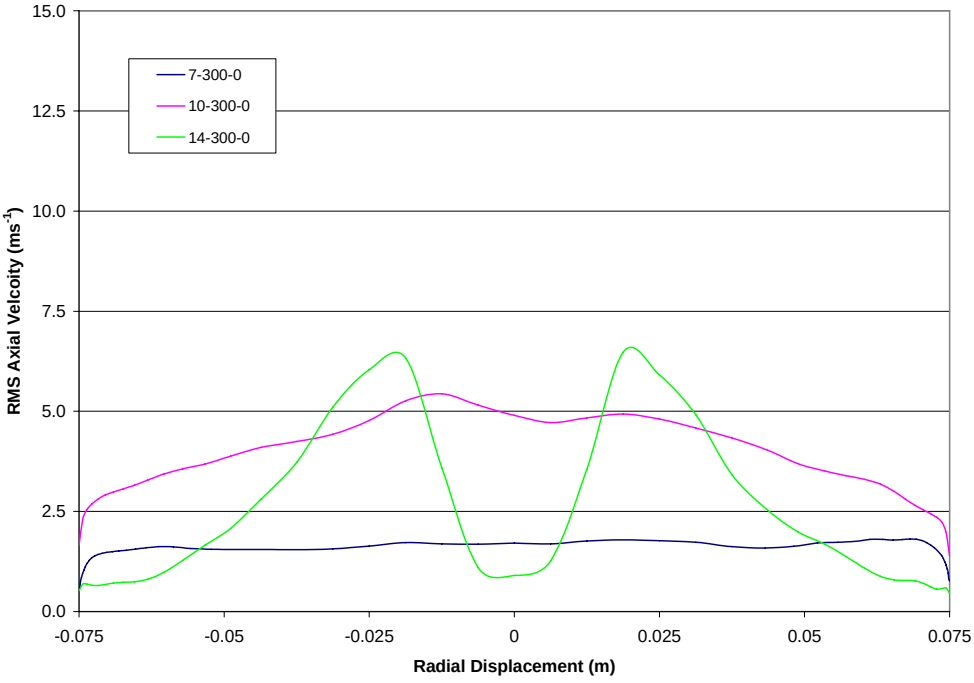

Figure 7.39: RMS axial velocity at the outlet of the 7˚, 10˚ and 14˚ conical diffusers fitted with a 300 mm long outlet duct and an inlet jet velocity of 25 ms^{-1}.

The widening performance gap between the 7˚ and 10˚ diffusers is best highlighted by comparing the fluctuating static pressure profiles for each respective diffuser, as shown in Figure 7.40. The 7˚ diffuser produces the same consistent low and flat profile, while the 10˚ and 14˚ diffusers both produce pressure fluctuations over an order of magnitude greater. The pressure oscillations across the outlet fitted to the 10˚ diffuser has a strong peak in the centre of the duct which can be linked back to the incomplete dispersion of the inlet jet. The jetting effect produced by the 14˚ diffuser is again present, however the magnitude of the pressure fluctuations in the centre of the outlet are also increased.

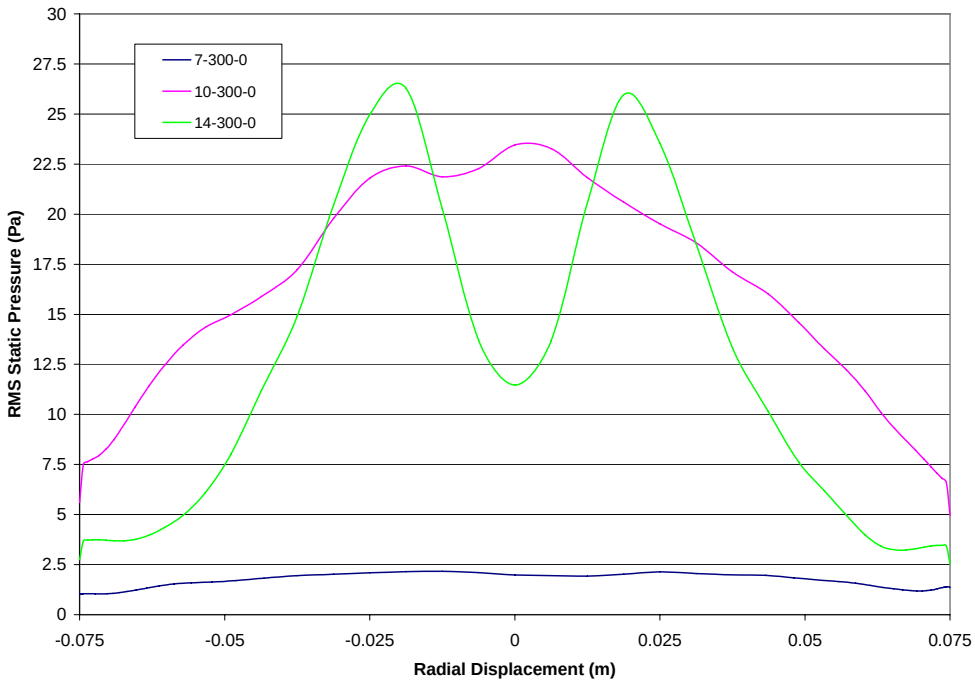

Figure 7.40: RMS static pressure at the outlet of the 7˚, 10˚ and 14˚ conical diffusers fitted with a 300 mm long outlet duct and an inlet jet velocity of 25 ms^{-1}.

Without allowing for the use of extended outlet ducts the 7˚ conical diffuser is the preferred design option, with the 10˚ diffuser showing some potential, but only if additional flow control mechanisms are employed. The 14˚ diffuser should however be avoided wherever possible.

7.3.3 Conical Outlet Diffuser Performance - Duct Length Comparison

The experimental investigation (reported in Chapter 5) found that the performance of the 10˚ diffuser could be significantly improved by extending the standard outlet duct length from 300 to 600 mm. This result must be matched by the numerical flow model if it is to become a viable design tool. The impact of fitting the 600 mm outlet duct to the 14˚ conical diffuser was also investigated as a test of the versatility of the numerical model. Extending the duct further to 900 mm did not result in any further significant improvement and therefore will not be considered here.

Results will be presented for the 10˚ diffuser with an inlet jet velocity of 15, 20 and 25 ms^{-1} and for the 14˚ diffuser with an inlet jet velocity of 15 ms^{-1}. The baseline reference case of the 7˚ diffuser fitted with the 300 mm outlet duct has also been included with each comparison to provide a fixed reference frame for the given inlet jet velocity.

7.3.3.1. 10˚ Conical Diffuser with a 15 ms^{-1} Jet Velocity

Fitting the 600 mm long outlet duct to the 10˚ diffuser allows the outlet axial velocity profile to stabilise evenly, producing a slightly flatter profile than that observed with the standard 7˚ diffuser. The normalised mean axial velocity profiles, as shown in Figure 7.41, provide a clear indication of the effectiveness of extending the outlet duct length to 600 mm. The centralised velocity peak produced by the 300 mm outlet duct is completely dispersed in the extended outlet duct region. This effect is further reinforced by the plot of the fluctuating axial velocity profile across the duct outlet, as shown in Figure 7.42. The higher rms axial velocity profile produced by the 10˚ diffuser fitted to the 300 mm outlet duct is significantly reduced by extending the outlet duct.

The fluctuating static pressure across the duct outlet is similarly reduced by the increase in duct length from 300 to 600 mm, as shown in Figure 7.43. This corresponds to the experimentally measured improvement in the acoustic performance of the 600 mm outlet duct over the 300 mm duct when fitted to the 10˚ conical diffuser. Clearly significant gains can be made by increasing the outlet duct length to 600 mm.

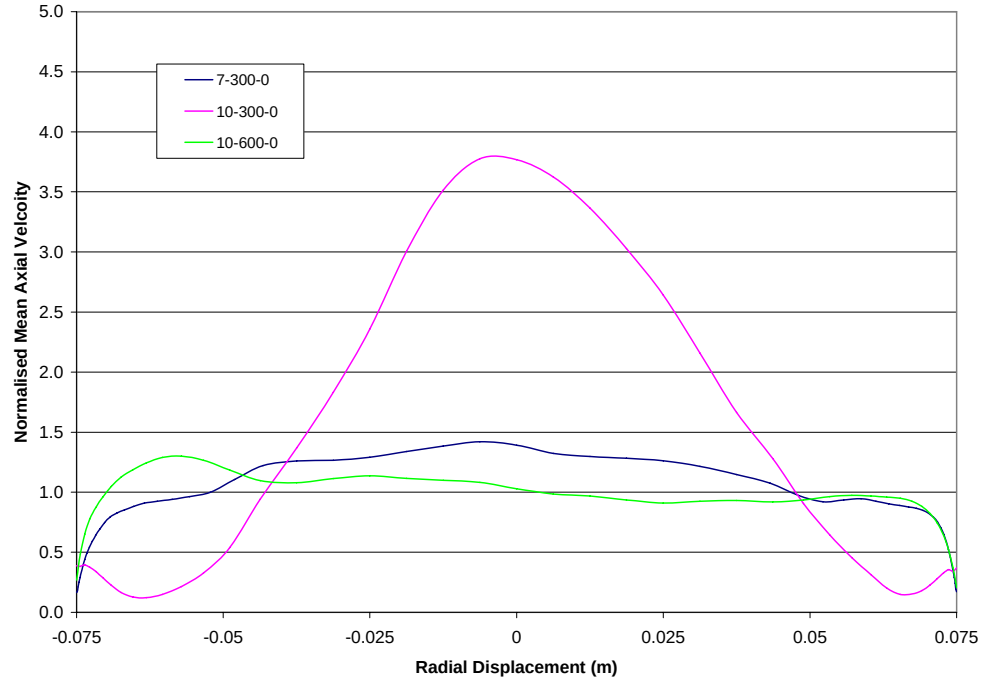

Figure 7.41: Normalised (mean) axial velocity at the outlet of the 10˚ conical diffuser fitted with a 300 and 600 mm long outlet duct and an inlet jet velocity of 15 ms^{-1}.

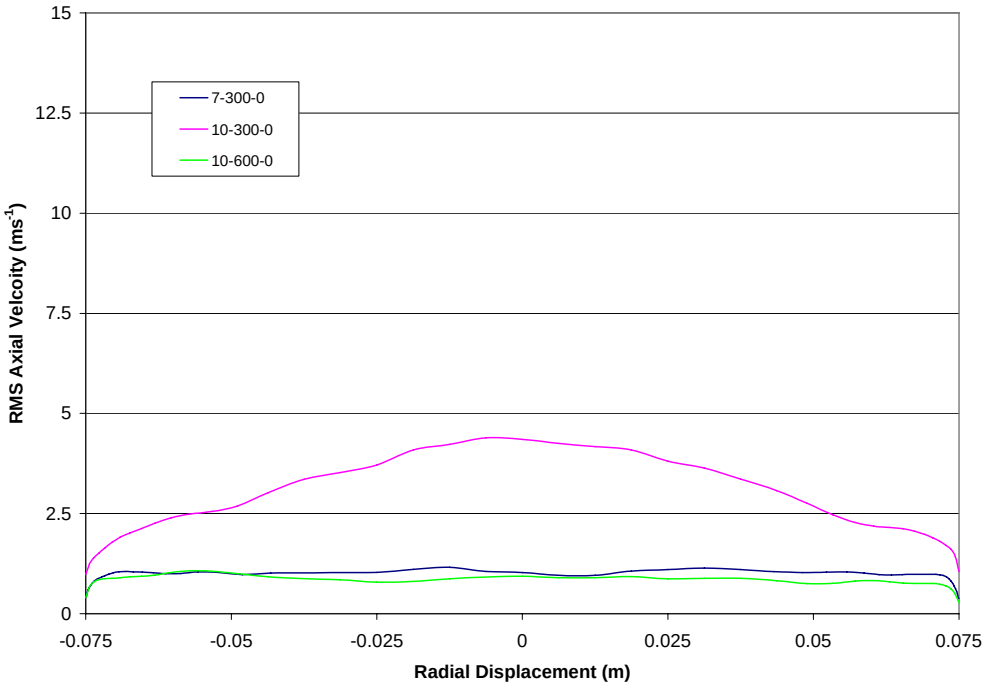

Figure 7.42: RMS axial velocity at the outlet of the 10˚ conical diffuser fitted with a 300 and 600 mm long outlet duct and an inlet jet velocity of 15 ms^{-1}.

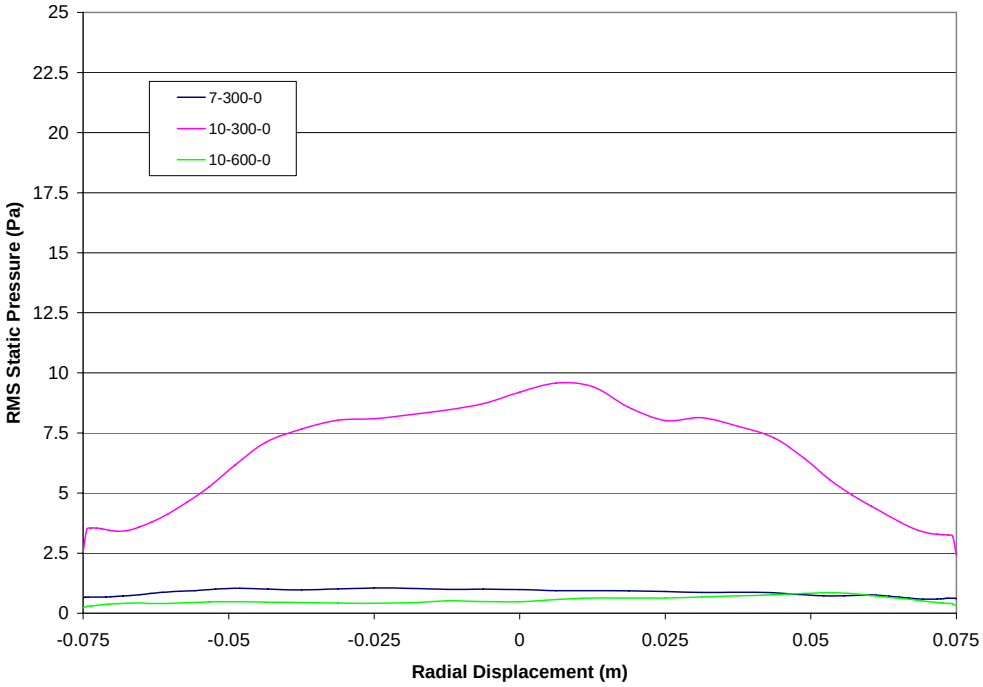

Figure 7.43: RMS static pressure at the outlet of the 10˚ conical diffuser fitted with a 300 and 600 mm long outlet duct and an inlet jet velocity of 15 ms^{-1}.

7.3.3.2. 10˚ Conical Diffuser with a 20 ms^{-1} Jet Velocity

The improvement in the normalised axial velocity profile from the increase in the outlet duct length to 600 mm is repeated at the higher inlet jet velocity of 20 ms^{-1}, as indicated in Figure 7.44. Once again the central peak in the outlet velocity profile is eliminated by the outlet duct extension such that the result from the baseline case of the 7˚ diffuser fitted to the 300 mm outlet duct is closely replicated. The same level of improvement is also observed in the fluctuating axial velocity across the outlet and is shown in Figure 7.45.

The significance of this result is best typified by the fluctuating static pressure field across the duct outlet, which is shown in Figure 7.46. The extension of the outlet duct has resulted in an impressive 5 to 6 fold reduction in the magnitude of the calculated pressure fluctuations. This would translate into a significant reduction in the resulting flow induced noise levels. Identifying these types of design improvements is a valuable outcome from a commercial design tool perspective.

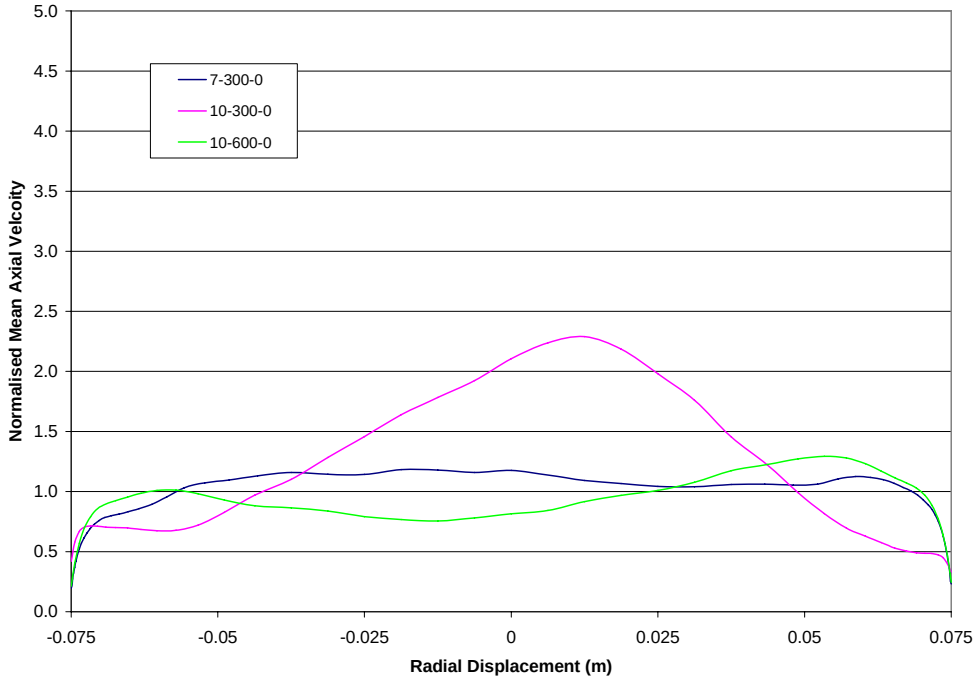

Figure 7.44: Normalised (mean) axial velocity at the outlet of the 10˚ conical diffuser fitted with a 300 and 600 mm long outlet duct and an inlet jet velocity of 20 ms^{-1}.

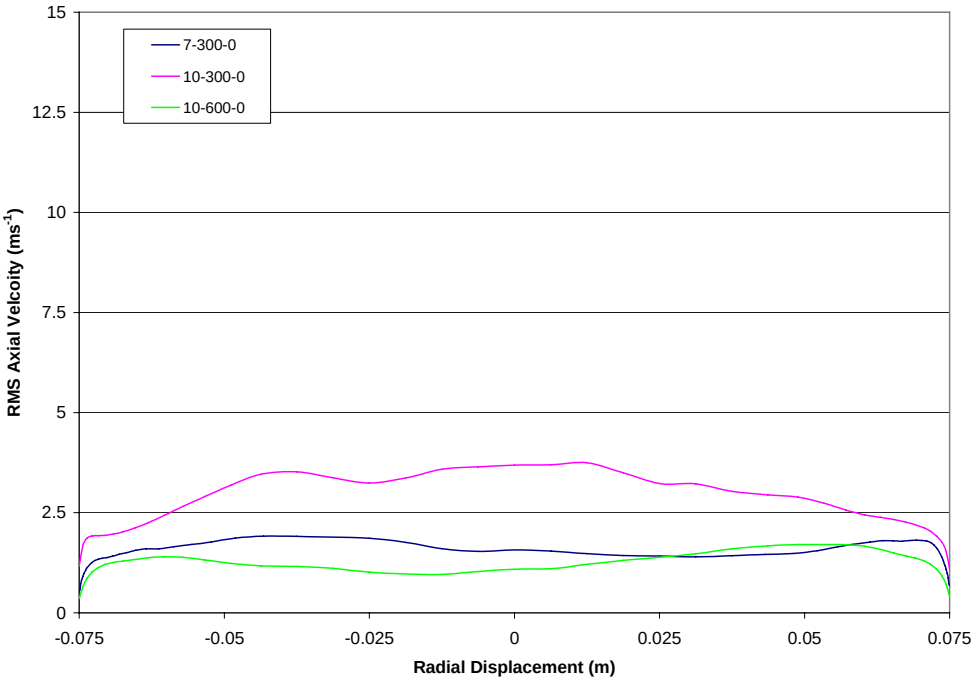

Figure 7.45: RMS axial velocity at the outlet of the 10˚ conical diffuser fitted with a 300 and 600 mm long outlet duct and an inlet jet velocity of 20 ms^{-1}.

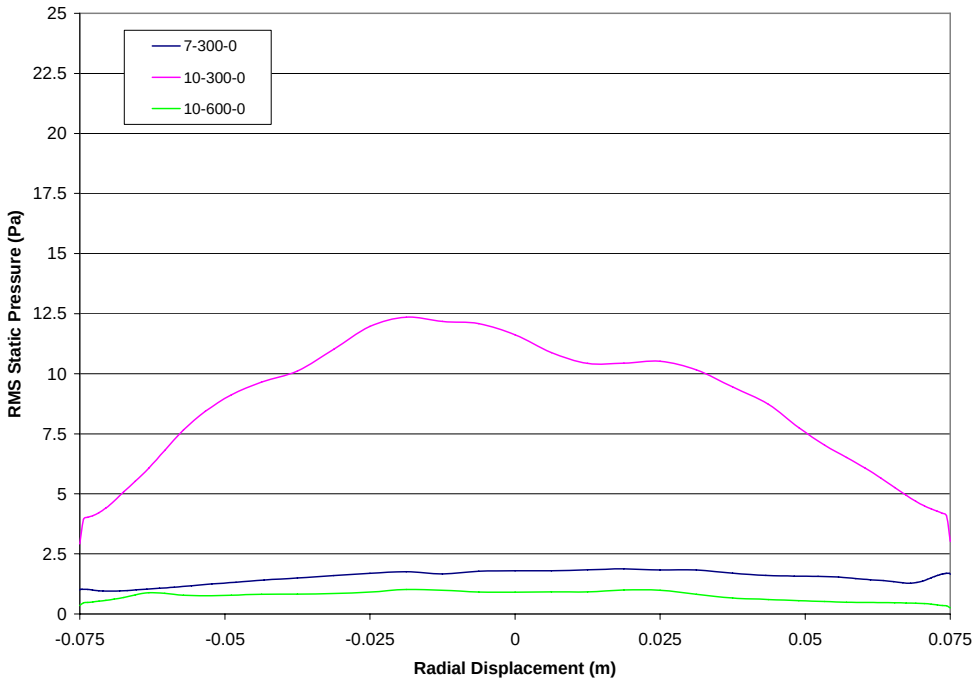

Figure 7.46: RMS static pressure at the outlet of the 10˚ conical diffuser fitted with a 300 and 600 mm long outlet duct and an inlet jet velocity of 20 ms^{-1}.

7.3.3.3. 10˚ Conical Diffuser with a 25 ms^{-1} Jet Velocity

The level of improvement from the extension of the outlet duct to 600 mm tends to increase with the inlet jet velocity; with an even more pronounced improvement seen with the 25 ms^{-1} jet. Both the normalised mean axial velocity (shown in Figure 7.47) and the rms axial velocity profiles (shown in Figure 7.48) across the duct outlet show consistent improvement, with a total flattening of each profile. The dispersion of the inlet jet is complete and importantly the level of turbulence in the flow across the outlet exit plane is diminished.

The most significant change however comes in the full order of magnitude reduction in the level of static pressure oscillations across the outlet duct as shown in Figure 7.49. At the higher inlet jet velocities there is a slight peak observed in the centre of the duct, yet the peak rms static pressure fluctuation of over 22 Pa is reduced to less than 2.5 Pa. The 600 mm outlet duct is therefore well suited to the 10˚ outlet diffuser.

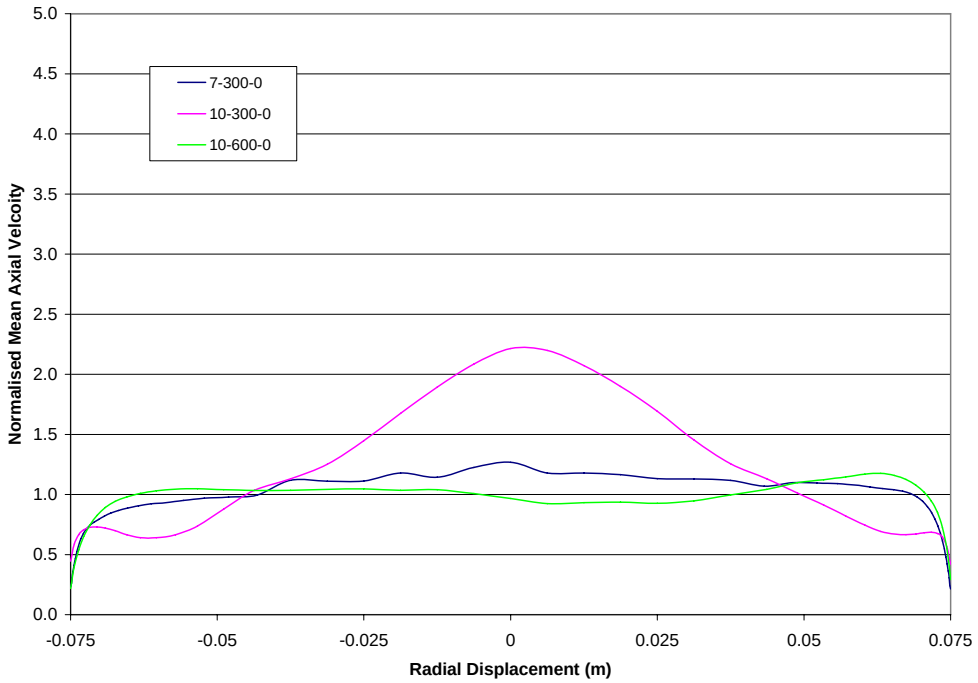

Figure 7.47: Normalised (mean) axial velocity at the outlet of the 10˚ conical diffuser fitted with a 300 and 600 mm long outlet duct and an inlet jet velocity of 25 ms^{-1}.

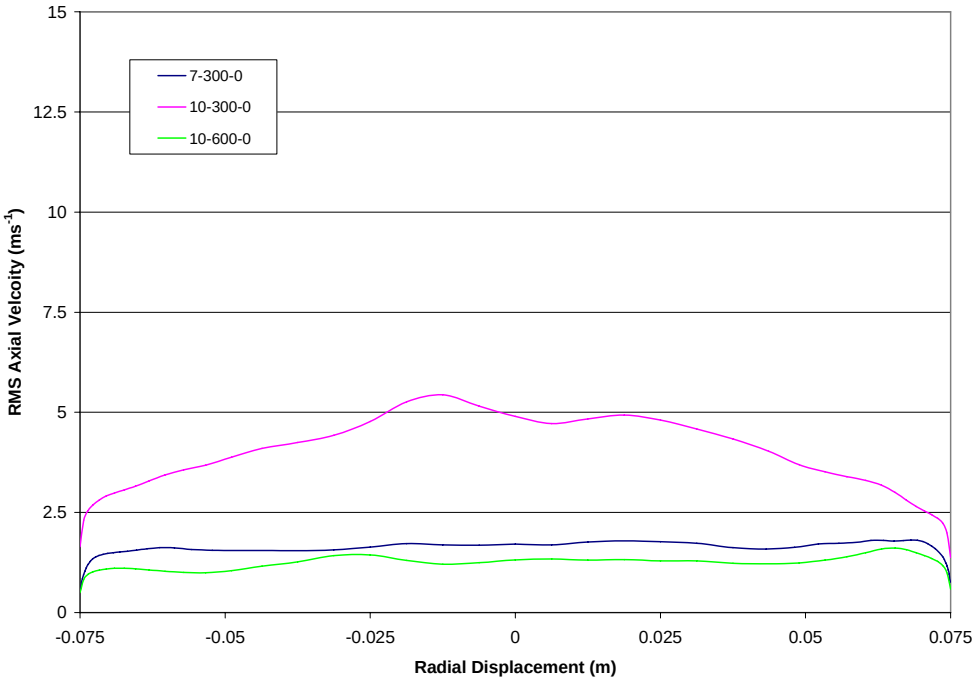

Figure 7.48: RMS axial velocity at the outlet of the 10˚ conical diffuser fitted with a 300 and 600 mm long outlet duct and an inlet jet velocity of 25 ms^{-1}.

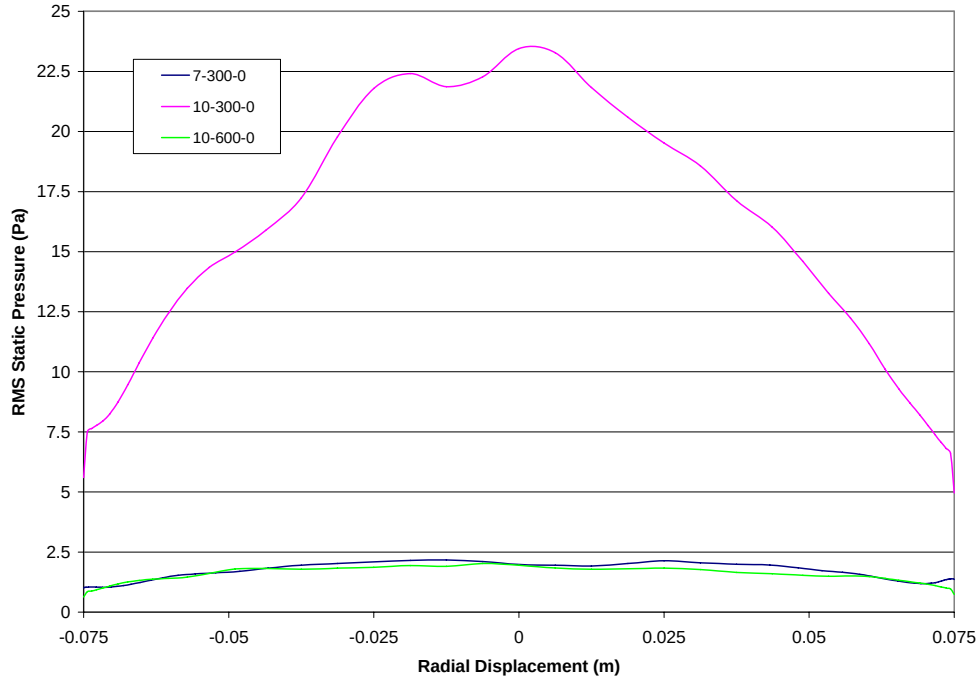

Figure 7.49: RMS static pressure at the outlet of the 10˚ conical diffuser fitted with a 300 and 600 mm long outlet duct and an inlet jet velocity of 25 ms^{-1}.

7.3.3.4. 14˚ Conical Diffuser with a 15 ms^{-1} Jet Velocity

Following the success of the extended 600 mm outlet duct with the 10˚ diffuser a similar analysis was completed with the 14˚ diffuser to investigate the potential to improve on the poor performance achieved with the 300 mm outlet duct. The first consideration was the normalised mean axial velocity profile across the duct outlet and the need to reduce the jetting effect found with the shorter outlet duct. The size of the velocity peak is halved by extending the outlet duct and the size of the recirculation zones in the near wall regions is also significantly reduced, as shown in Figure 7.50. It should be noted however that the jet itself is not fully dispersed and additional guide vanes would need to be employed to prevent the establishment of the near wall zones of low velocity and/or flow recirculation. The improvement that comes from reducing the strength of the central high velocity core is highlighted by the significant reduction in the fluctuating axial velocity across the outlet, as indicated in Figure 7.51. The peak fluctuations are replaced by a more broad fluctuation across the whole outlet at a significantly lower magnitude.

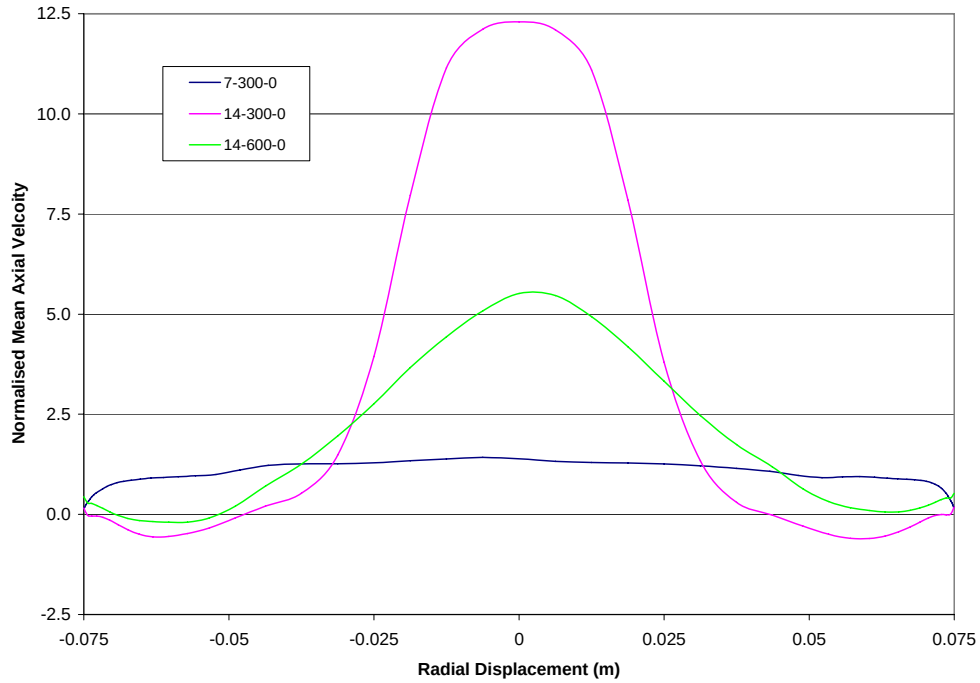

Figure 7.50: Normalised (mean) axial velocity at the outlet of the 14˚ conical diffuser fitted with a 300 and 600 mm long outlet duct and an inlet jet velocity of 15 ms^{-1}.

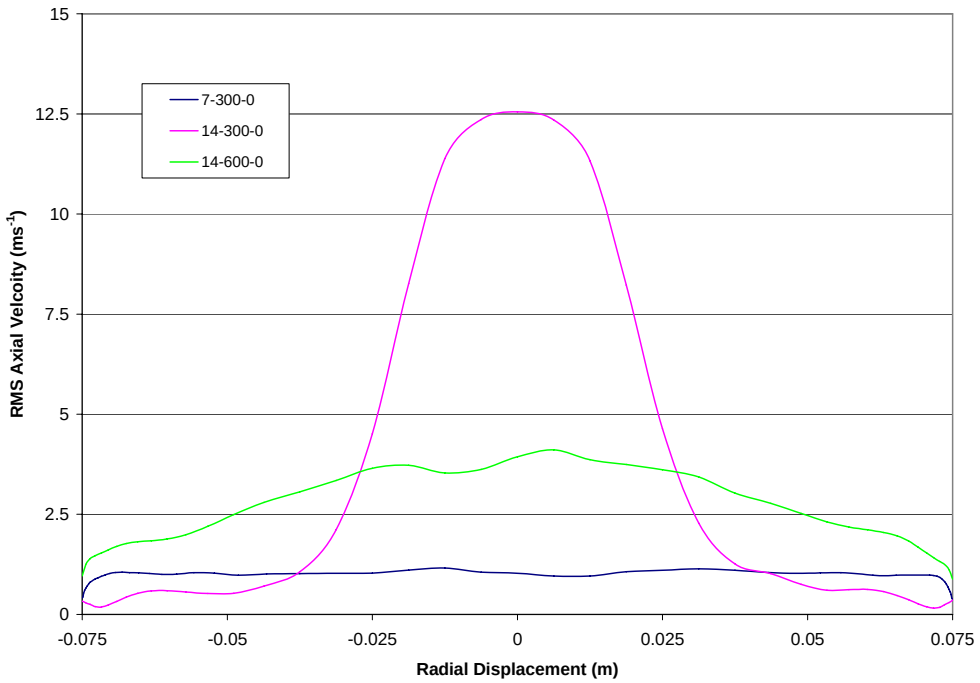

Figure 7.51: RMS axial velocity at the outlet of the 14˚ conical diffuser fitted with a 300 and 600 mm long outlet duct and an inlet jet velocity of 15 ms^{-1}.

The level of turbulence across the outlet is not completely controlled by the extension of the outlet duct to 600 mm, with a reasonable gap between the 14˚ diffuser and the baseline reference case based on the 7˚ diffuser. Even with the extended outlet duct the level of fluctuation in the axial velocity is up to 3 times greater than the reference case. The fluctuating static pressure across the outlet, as shown in Figure 7.52, reinforces this conclusion with a significant increase in the magnitude of oscillations produced by the extended outlet duct. This can be a little deceptive in that there is a significant level of turbulence located in the flow field down stream from the duct outlet where the constrained high velocity core present in the duct outlet is dispersed.

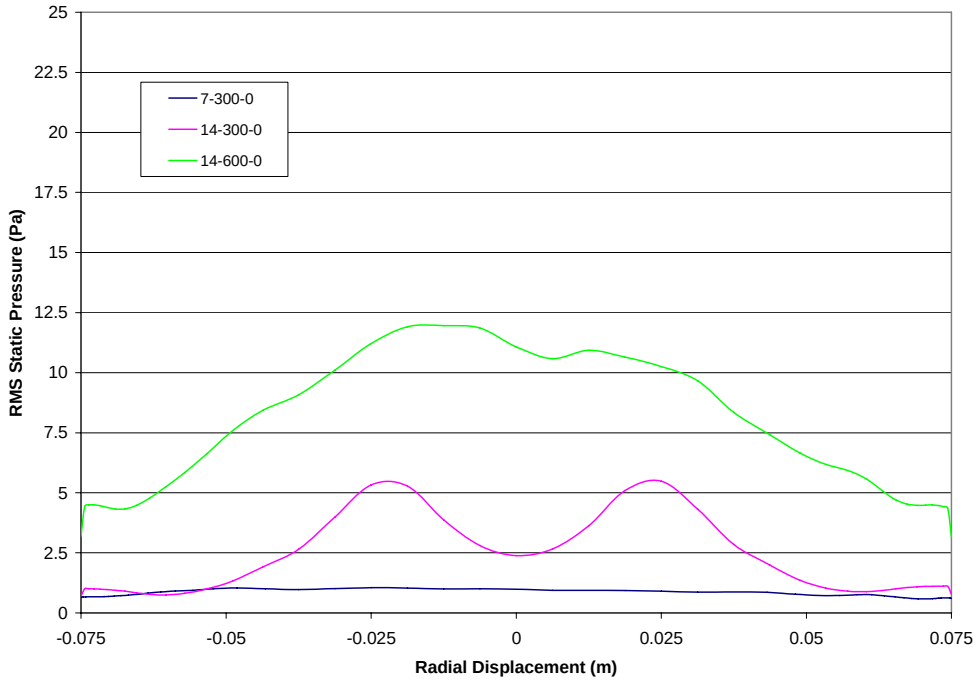

Figure 7.52: RMS static pressure at the outlet of the 14˚ conical diffuser fitted with a 300 and 600 mm long outlet duct and an inlet jet velocity of 15 ms^{-1}.

The total length of the reference case configuration is 710 mm, compared to the 800 mm required for the 14˚ diffuser fitted to the 600 mm outlet duct. Therefore there is no justification to use the wider diffuser angle in the current configuration. This conclusion may be different however, if the performance of the 14˚ diffuser can be improved with the addition of flow control guide vanes inside the conical diffuser section.

The above analysis provides a clear indication of the effect of both the conical diffuser and the outlet duct on the fluctuating components in the flow domain. The fluctuating velocity associated with the expanding jet is predominantly contained within the diffuser and outlet duct sections. The extension of these fluctuations beyond the exit plane of the outlet duct for the wider diffuser angles indicates that a longer outlet duct length should be used. Alternately flow control guide vanes could be fitted inside the conical diffuser to reduce the effective diffuser angle.

Both the axial and radial fluctuating velocity components are concentrated in the initial portion of the outlet duct downstream from the conical diffuser. This reinforces the earlier observation that the conical diffuser alone is not sufficient to control the expanding air jet. Extending the outlet duct does not provide the most efficient means of controlling the generation of turbulence and the subsequent flow induced noise, especially in a space constrained environment. The inclusion of guide vanes inside the conical diffuser sections and even possibly shorter outlet duct sections should be explored in the future. This solution has the potential to allow the use of even shorter outlet duct lengths and even greater diffuser angles.

The application of CFD modelling to the optimisation of flow expansion devices has been found to be very useful and has the potential to make significant improvements in the overall design process used in commercial applications. By completing fundamental flow analyses the amount of time and computational resources required to complete detailed acoustic models can be minimised. If a limited quantity of numerical simulations is required the long term economic viability of the numerical design process can be significantly enhanced.

The limited number of duct configurations used in this work has not conclusively identified the “optimum” design, yet the ability of the numerical models to iteratively identify preferred geometry selections is clearly demonstrated. Additional iterations can be run to ensure that the true optimum design is identified, however this will always need to be balanced against the computational costs incurred. The level of detail and accuracy targeted can be based on the specific needs of each individual case in question.

Chapter 8

Numerical Model Development - Acoustics

The numerical solutions generated using the previously outlined CFD model provide the time varying velocity and pressure data used to simulate the acoustic sources generated by the expansion of the high velocity air jet. The primary purpose of this acoustic model is the prediction of the flow generated noise for a variety of outlet duct configurations for a range of air distribution velocities. The ability to predict the acoustic performance of an air duct diffuser design under a variety of operating conditions will be a valuable design tool. Simple outlet duct configurations were used in the development of this model as a means of developing the correct modelling techniques using direct comparison to controlled experimental results. As available computing power increases and the efficiency of LES based CFD models develop the practical extension of this approach will become applicable to more complex duct geometries and outlet grills.

8.1 Model Formulation and Assumptions

The Ffowcs-Williams Hawkings (FWH) formulation of Lighthill's acoustic analogy is used to calculate the associated far field sound pressure level. This method enables the flow domain to be solved independently around the region of interest (noise sources), with the acoustic analysis completed using a post processor application. Under these conditions the required acoustic receivers may be located outside the original flow domain. This integral based approach is available as a post processor in Fluent 6.1 and 6.2 and has been used for the work presented herein. The Fluent formulation does not include the volume integral, which is a valid simplification for the relatively low mach number flows encountered in this work.

The same result could be achieved with a computational aero-acoustics (CAA) approach if sufficient computational resources were available. However the integration of the acoustic model with a common commercial CFD code allows for greater flexibility in the development of the desired HVAC design tool.

Current CFD based acoustic models have been limited to external flows around bluff bodies due to the limitations of Lighthill's analogy. Solution algorithms have been developed to apply this analogy, but these are limited to the prediction of sound propagating toward free space or an unbounded field. This limitation has restricted the application of this method to internal duct flows and enclosed spaces. By locating the source surface at the outlet of the jet (in free space) – coincident with the exit plane of the outlet pipe - this limitation is satisfied (as shown in Figure 8.1). With this approach the source surface captures the pressure and flow oscillations driving the quadrupole sources associated with the shear layers in the jet plume and the dipole sources located upstream inside the duct system. This assumption holds as long as the flow field remains incompressible. The incompressible flow field enables the fluctuating flow field variables to propagate downstream and therefore be captured at the source surface – located at the outlet.

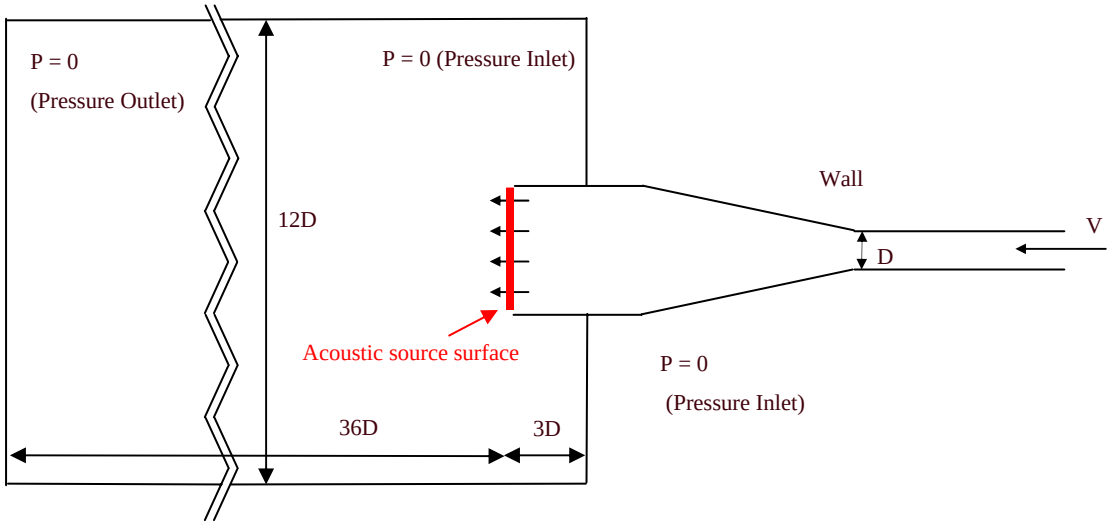

Figure 8.1: Schematic diagram of the computational flow domain showing the location of the acoustic source surface.

As the flow field becomes increasingly compressible the need for the volume integral terms becomes more critical due to the increased coupling between the oscillating flow and acoustic fields superimposed over one another. As the flow velocity encountered in this work does not reach these levels the added computational complexity can be legitimately avoided, without compromising the accuracy of the final solution obtained.

A radial hemisphere of receiver locations can also be defined around this source surface and a free field sound pressure calculation can be made. By assuming a free field (no enclosed room) the sound pressures can be used to calculate the total sound power radiated by the jet, assuming that the diameter of the duct outlet is significantly smaller than the radial placement of the acoustic receiver locations. The numerical model has a free field boundary condition and as such the free field contains no reverberant field or acoustic reflections.

The experimental measurements were recorded in a reverberation room, and as such the measured sound pressure levels can be converted into an equivalent sound power level based on the known physical dimensions and acoustic properties of the room. In effect the contribution form the reverberant sound field is isolated and thus enables a fair and true comparison between the “ideal” numerical model and the practical limitations associated with the experimentally recorded values.

The numerical method (based on free field theory) is only valid if the acoustic pressure and velocity are in phase and the (virtual) receiver locations are located in a medium with a characteristic acoustic impedance of ρc, where ρ is the air density and c is the speed of sound. Modelling the jet exhausting to free space instead of a closed room satisfies the above assumptions.

Once the sound pressure level (L_p) at a given receiver location is known the rms acoustic pressure (p_{rms}) can be calculated:

$$L_p = 20\log_{10}\left(\frac{p_{rms}}{p_{ref}}\right) \tag{8.1}$$

where p_{ref} is reference pressure of $2e^{-5}$ Pa. The acoustic intensity (I_A) is defined as the sound power per unit area (Wm^{-2}) and for a free field can be calculated using the acoustic particle velocity (u) and acoustic pressure (p):

$$I_A = u_{rms}\, p_{rms} = \frac{p_{rms}^2}{\rho c} \tag{8.2}$$

The sound power (W) is then calculated based on the product of the acoustic intensity and corresponding surface area of the hemisphere defined by the receiver locations with respect to the source surface.

8.2 Boundary Conditions

The flow induced noise sources are derived from the fluctuating velocity and pressure data generated using the LES CFD model. The surface used in the acoustic source calculation was coincident with the respective exit face of the outlet ducts considered, as shown in red in Figure 8.1 above. This assumption allowed for all of the receiver locations surrounding the outlet of the duct to be in direct line with the source surface. This eliminates any reflective or unrealistic propagation paths that would violate the underlying assumptions of the far-field acoustic analogy proposed by Lighthill.

The receiver locations were defined in a spherical arc surrounding the outlet of each respective outlet duct with a constant radius measured from the centre of the outlet face. The radial spacing of the receiver locations was varied from 2.5 to 5 m and the corresponding sound pressure levels were used to calculate the equivalent sound power level. The sound pressure level dropped off with increasing radial spacing from the centre of the outlet duct exit plane, however when these values are converted to an equivalent sound power level there was negligible variation across the radial spacing range used. The maximum variation in the sound power level was ± 0.2 dB.

8.3 Far Field Analysis

The numerical simulation of flow induced noise is heavily dependent on the strength of the CFD model used to generate the fluctuating flow field variables used in the application of the far-field acoustic analogy. The type of turbulence model and the numerical discretisation schemes employed can strongly affect the level of turbulence in the flow and the subsequent sound power level prediction.

8.3.1 Sources of Flow Induced Noise

The numerical acoustic model includes the contributions from both the dipole and quadrupole sources within the flow field. The total sound power generated by a dipole source increases with the 6^{th} power of velocity, while the sound power generated by a quadrupole source increases with the 8^{th} power of velocity. These laws have proved to be true for pure sound source applications however experimental evidence (as outlined in Chapter 5) suggest that there are additional effects that reduce the extent to which the sound power generated by the flow is actually increased for a given increase in jet velocity. One potential explanation for this discrepancy was the interaction of the complex flow field observed in the conical diffuser and downstream outlet duct acting to dissipate a portion of the energy associated with the turbulent flow regime.

8.3.2 Model Limitations

The proposed numerical acoustic model was envisaged to account for this variation through including an accurate simulation of interaction between the outlet geometry and the transient turbulent flow field. Given that the acoustic source surface is located coincident with the outlet duct exit plane only half of the total sound power is actually radiated into the open space surrounding the outlet. The remaining acoustic energy is actually radiated back up stream inside the supply duct. The levels of acoustic reflection and transmission at the numerous cross sectional area changes within the duct system itself have not been allowed for as part of this analysis. This could potentially be incorporated into the total simulation if a fully compressible flow model was employed, however the computational cost of generating a solution would significantly increase.

The impact of the acoustic field on the flow field has been assumed to be insignificant and as such no attempt has been made to calculate this contribution. The literature cited in Chapter 3 and personal anecdotal experience suggests that this is a legitimate assumption, with minimal impact on the overall accuracy of the model.

Given that an incompressible flow model has been used, a near field analysis using data directly from the flow domain to calculate the radiated sound power level can not be completed with any level of confidence. Whereas the far field calculations can be completed independently of the flow field simulation provided that the acoustic source data is generated from a statistically steady flow domain. Therefore the stability of the numerical flow field was monitored closely to ensure adequate stability prior to recording data for use in acoustic calculations.

8.4 Model Validation and Verification

As with the CFD based models the numerical model was validated against experimental data and verified to ensure independence from the model's boundary conditions in terms of frequency, flow time and space.

8.4.1 Frequency Analysis

The far field acoustic analogy effectively calculates the radiated acoustic fluctuations at the selected receiver locations for a given acoustic source strength. As the acoustic source is fluctuating in both magnitude and direction (in time) the resulting acoustic signals calculated for each receiver location also fluctuate accordingly. The raw data file for each receiver location consists of an acoustic pressure that varies in time at discrete time intervals which are determined by the size of the computational time step employed. The sampling frequency used to collect the data for the acoustic source surface therefore directly dictates the resolution in time of the discrete acoustic pressures for each receiver location. Although the time step used in the CFD simulation dictates the maximum discrete frequency of the final acoustic calculation a coarser resolution is possible by increasing the period of the acoustic simulation with respect to the original CFD model.

Incidentally the time step required to adequately resolve the LES CFD model resulted in a maximum sampling frequency of 100 kHz, and therefore a Nyquist frequency of 50 kHz. The frequency range of interest for this work of 0.1 to 5 kHz is well within this limit and hence little concern was held for needing to use an even finer time step. As the flow simulation was being run independently of the needs of the acoustic simulation, acoustic source data was saved at each time step. The computational time required to complete the acoustic simulation following the conclusion of the CFD solution process was minimal in comparison and therefore little benefit was derived from reducing the sampling frequency.

Given that the end goal of this research was to identify appropriate design tools for use in a commercial application the effect of reducing the sampling frequency was conducted to establish the acceptable limits that could be applied. A comparison between a sampling frequency of 20, 50 and 100 kHz is shown in Figure 8.2 below. The main impact of the lower sampling frequency is a slight drop off in the high frequency bands and therefore the acoustic model is solved at every CFD time step (100 kHz).

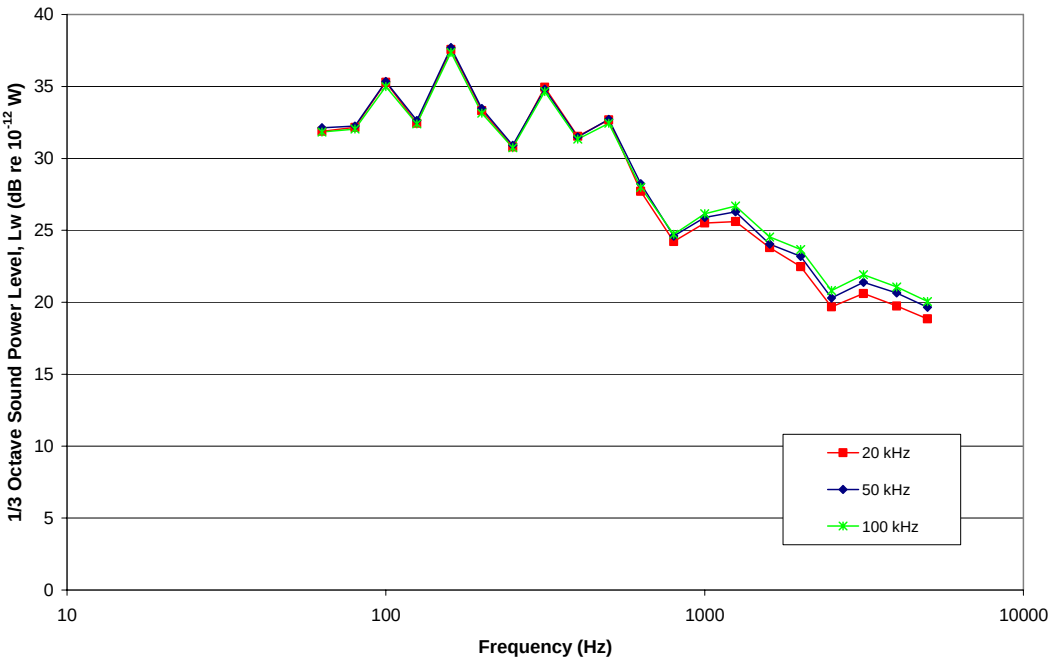

Figure 8.2: Predicted sound power level comparison between a sampling frequency of 20, 50 and 100 kHz

8.4.2 Sample Length Independence

The length of the data stream used to calculate the far field acoustic pressures is determined by the number of samples and the sampling frequency. As the flow field is transient in nature and only steady in a statistical sense, it is important to capture enough data to allow for a good approximation of the overall acoustic pressure spectra. There are also finite limits that must be met in order to complete an acceptable Fast Fourier transform (FFT) of the acoustic pressure data in order to generate the sound power spectra in the frequency domain. The effect of the sample length on the numerical model was investigated for a sampling frequency of 100 kHz. Sample lengths of 62.5, 100 and 120 ms were used. A comparison between the resulting sound power level for each of these cases is shown in Figure 8.3. Increasing the length of the sample especially improved the low frequency resolution of the sound power spectra, with a slight improvement in accuracy when compared to the experimental results outlined previously. Hence, a minimum sample length of 100 to 120 ms is recommended.

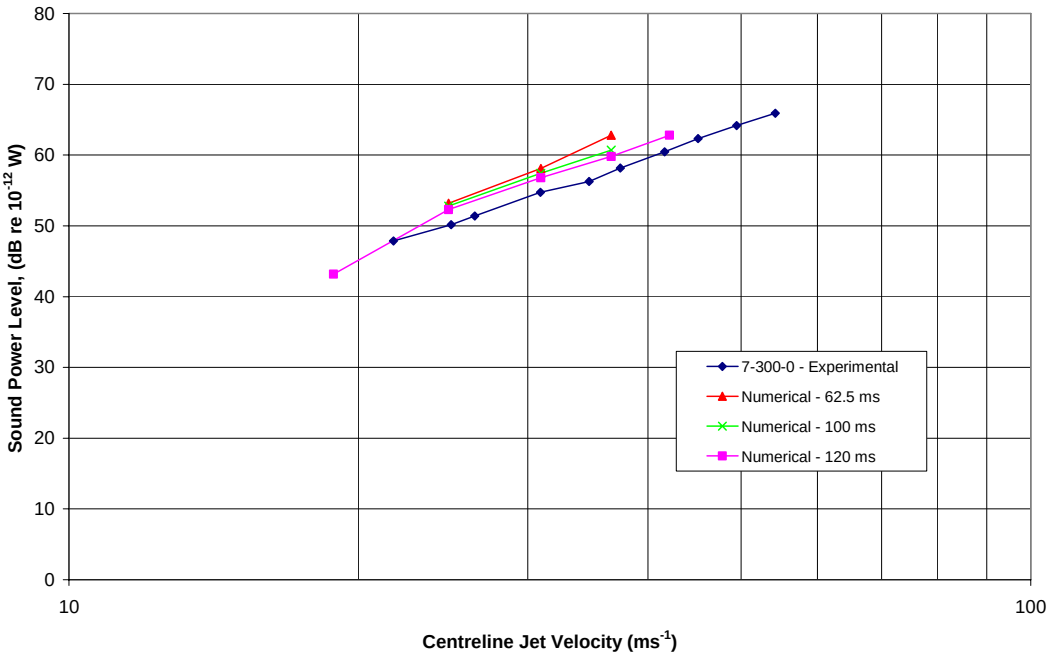

Figure 8.3: Predicted sound power level comparison with a sampling frequency of 100 kHz and a sample length of 62.5, 100 and 120 ms.

8.4.3 Source and Receiver Locations

The radial displacement of receiver locations with respect to the acoustic source surface (duct outlet) was varied between 2.5 and 5 m and the resulting calculated sound power levels compared. The sound pressure level dropped off in proportion to the square of the radial displacement. This was an expected result, given that the acoustic energy intensity drops off in direct proportion to the surface area of the sphere containing the receiver locations. The sound power level however which is a direct measure of the total radiated acoustic energy level is effectively independent of radial displacements used. A comparison between the sound power spectra for the 2.5 and 5 m cases reveal a minor variation of ± 0.6 dB. A variation of this order is of little significance and it is therefore reasonable to assume that the numerical acoustic model is adequately independent of the specific location of the receiver points in relation to the acoustic source surface. Clearly the receiver locations must still be located such that there is a direct line of radiation between each receiver point and the acoustic source surface.

8.4.4 Comparison to Experimental Results

A comparison between the numerical model and experimental results will be made in the following chapter. Selected outlet diffuser configurations have been chosen for the purpose of this research. The more complex geometry of the outlet diffuser grills and duct elbows have been omitted from this analysis due to computational limitations. The available resources were carefully balanced against the computational time required to complete the work to the desired level of accuracy. As computational resources become more cost effective and the required numerical models are further improved this work will be realistically achievable in the coming years.

Chapter 9

Numerical Results and Discussions - Acoustics

The statistically steady turbulent LES model was used to generate a time history of the pressure fluctuations on the acoustic source surface located at the duct outlet. Acoustic receiver points were positioned in a 180° arc surrounding the outlet at a fixed radial displacement. The Ffowcs-Williams and Hawkings (FWH) formulation of the Lighthill's far-field analogy was fully implemented and used to integrate the acoustic source data from the duct outlet and calculate the instantaneous acoustic pressures at each of the fixed acoustic receiver locations. Repeating this analysis for each of the selected time steps in the data file created an acoustic pressure data file for each unique receiver location based in the time domain. Each of these data files form the basis of the acoustic analysis performed for the selected outlet configurations.

Given that the actual calculation of the individual acoustic pressure files for each receiver location is an imbedded algorithm within the commercial CFD code Fluent, no further explanation will be included in this text. Further information relating to how this calculation is formulated can be found in the Fluent 6.1 and 6.2 documentation files available with the software. This work will focus on the derived methodology used to convert the discrete acoustic pressure data into usable sound pressure and sound power levels and the subsequent frequency analysis of these signals.

9.1 Critical Performance Parameters

Several acoustic measures may be used to assess the absolute and relative performance of each outlet diffuser configuration; however care must be taken to ensure that the limitations of each method used is both clearly understood and accounted for. For the purposes of this work the following three parameters have been used.

1. Sound Pressure Level
2. Acoustic Intensity
3. Sound Power Level

Each of these parameters have been used in both absolute values and on a frequency band basis, using both octave and ⅓ octave bands. Each of these parameters has applications to the assessment of the performance of the various outlet diffuser configurations investigated herein. It is important to understand where absolute comparisons can be drawn and where comparisons are limited to a relative measure only.

9.1.1 Sound Pressure Level

The sound pressure levels at each of the receiver locations provide a good indication of the effectiveness of the outlet diffuser; however this is based on an anechoic external boundary. Any passenger cabin is going to have a reasonable level of acoustic absorption from carpet, seats and people but this will not be 100 %. Therefore there will be an additional reverberant component in any real installation. Based on this assumption the free field sound pressure levels calculated using the far field acoustic analogy will be less than those observed in any given passenger cabin space.

Absolute measurement of sound pressure levels in the cabin space for the purpose of assessing conformance to room noise criteria standards is not possible without also allowing for the reverberation effects of the cabin space. Despite this shortcoming the sound pressure level can still provide an immediate and direct means of making relative comparisons between different outlet duct configurations without the completion of complex acoustic intensity and sound power level calculations.

The acoustic signature of each configuration can also be assessed using the sound pressure level reference frame in both octave and ⅓ octave frequency bands. The level of reverberation within the passenger cabin space will change slightly across the frequency bands of interest and therefore the spectra shape may alter slightly between the sound pressure and sound power levels. However, the sound pressure level spectra will still provide a useful guide in terms of the relative performance of the outlet diffuser and immediate feedback on the effectiveness of efforts used to tune specific acoustic attenuation characteristics.

9.1.2 Acoustic Intensity

The acoustic intensity is derived directly from the sound pressure level and as such the uses and limitations pertaining to the sound pressure level also apply to the calculated acoustic intensity. The primary use of the acoustic intensity is to facilitate the conversion of the sound pressure level data into an absolute measure of the acoustic energy radiated form the duct outlet in the form of a sound power level.

9.1.3 Sound Power Level

The sound power level provides an absolute measurement of the total acoustic energy radiating from the outlet duct. When dissected into octave and ⅓ octave frequency band sound power levels an absolute assessment of the acoustic performance can be completed. The acoustic properties of a given passenger space will be known on an octave and ⅓ octave frequency band basis and therefore definitive predictions of the final sound power level inside the passenger space can be derived. With this information the expected sound pressure levels inside the passenger cabin can then be predicted as a precursor to determining the room noise criteria rating.

Given that this calculation process is non-trivial, one would expect to only pursue this course of action once the design of the outlet duct configuration has been refined using relative sound pressure level comparisons outlined above.

9.2 Far-Field Acoustic Simulation Results

Once the acoustic model was validated against the results for the free axial jet, models for selected outlet diffuser configurations were developed to evaluate the versatility of the model. To maximise the return on the relatively high computational cost of running the full LES model and the subsequent acoustic analysis the preliminary CFD results were used to narrow down the diffuser angle and outlet duct length to those with greatest potential. The analysis was separated into two stages with the first looking at a fixed conical diffuser angle of 7˚ with an outlet duct length of 300 and 600 mm. A duct length of 900 mm was omitted based on the experimental results as was the trivial case of no outlet duct length.

A secondary analysis was also completed for the 10˚ and 14˚ conical diffusers fitted with the 600 mm long outlet duct. The 900 mm long outlet duct models were not simulated due to a limitation of computational resources. This decision was based on the experimental results combined with the preliminary CFD results for these configurations. Each of the six selected outlet diffuser models were simulated at multiple jet velocities so as to generate a reasonable sound power - jet velocity curve for comparison with the corresponding experimental results.

9.2.1 Conical Outlet Diffuser

An initial sound pressure calculation was made using a data file covering a real flow time of 100 ms. The sound pressure levels were calculated at a radius of 2.5 m from the jet outlet at angular increments of 15°. The acoustic intensity around a 180° arc surrounding the outlet exit plane is shown in Figure 9.1. This intensity corresponds to a total sound power level (L_w) of 44.3dB (re $1e^{-12}$ W). If the radius of the receiver locations is doubled to 5 m the calculated total sound power level is 43.9 dB – an acceptable level of variation. There is a slight concentration of acoustic intensity in the core of the jet in the region within ± 30° from the jet centreline.

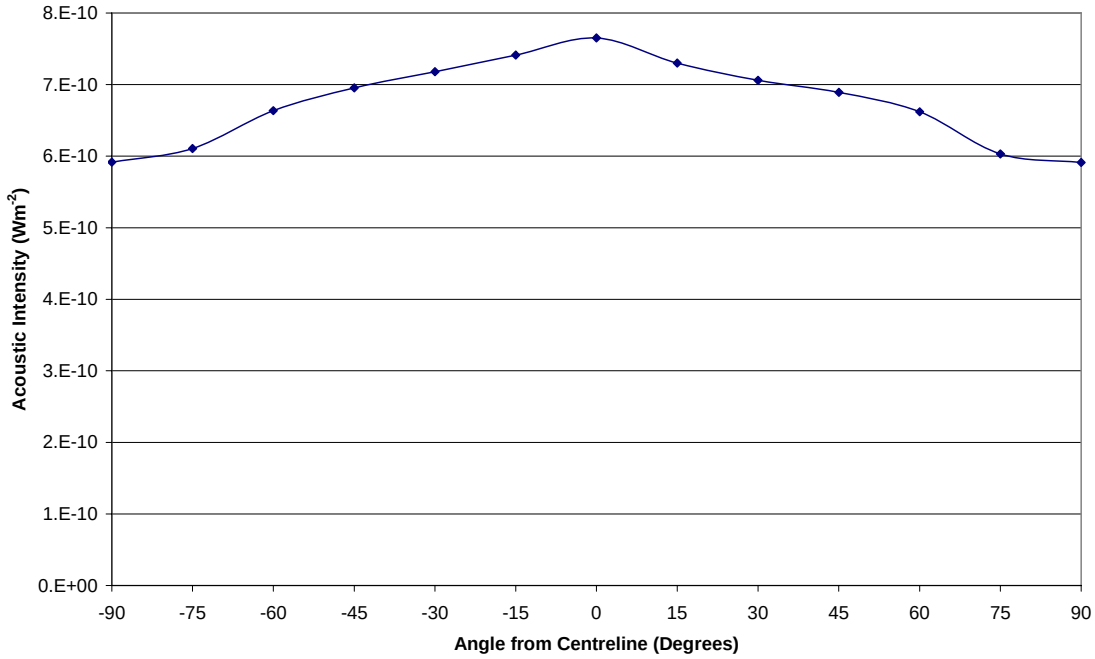

Figure 9.1: Acoustic intensity for 20 ms^{-1} jet.

This result is not unexpected given the directionality of the jet at the outlet. The slight skewness of the above plot is representative of the transient nature of the turbulent flow field and statistical variation of the acoustic field. Increasing the sample length improves the accuracy of the predicted acoustic field but must also be balanced against the increased computational cost. Even allowing for some error in the acoustic predictions the relative magnitudes will be a key indicator of the effectiveness of different duct outlet configurations under investigation.

The experimental sound power levels, along with the numerical predictions for the same outlet configuration (7-300-0) are shown in Figure 9.2. The predicted sound power level appears to be a very good estimate of the true sound power that is generated. The numerical model tends to slightly over predict the total sound power level by approximately 2 dB, with the exception of the lowest jet velocity considered (18 ms^{-1}). The discrepancy here is perhaps best explained by the increasing influence of background noise levels at the lower jet velocity settings. Increasing the jet velocity leads to a progressive rise in the flow induced sound power level and a corresponding diminishing influence from the background noise.

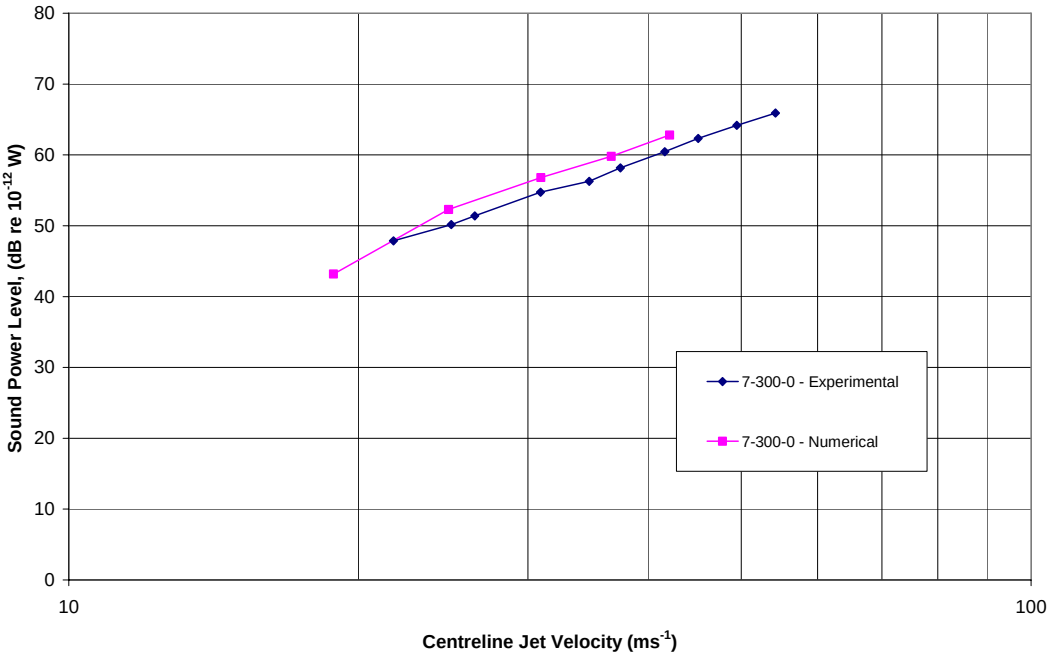

Figure 9.2: Sound power level comparison for the 7˚ conical diffuser fitted with a 300 mm long outlet duct.

Following the successful comparison between the numerical and experimental results for the 7˚ conical diffuser, corresponding models were run using a conical diffuser angle of 10˚ and 14˚. Both of these models initially used the same outlet duct length of 300 mm. The total sound power level comparison between each respective model and the corresponding experimental results are shown in Figures 9.3 and 9.4. The primary jet velocity range of interest was 20 to 40 ms^{-1}. In both cases the results were very positive with the numerically predicted sound power level consistently 2 to 3 dB higher than the experimentally recorded values. At jet velocities below 20 ms^{-1} this variation is reversed with the experimental results slightly higher by 1 to 2 dB. This result closely follows the observations made previously using the model for the 7˚ conical diffuser. The most likely explanation for this common variation is the influence of background noise levels that are not accounted for in the numerical simulation.

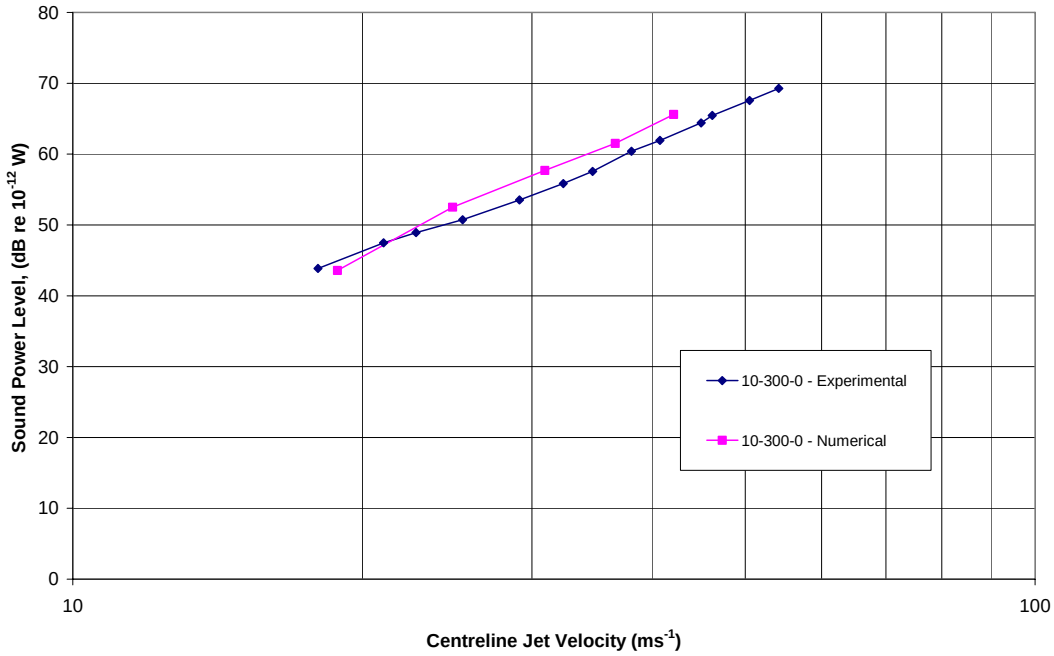

Figure 9.3: Sound power level comparison for the 10˚ conical diffuser fitted with a 300 mm long outlet duct.

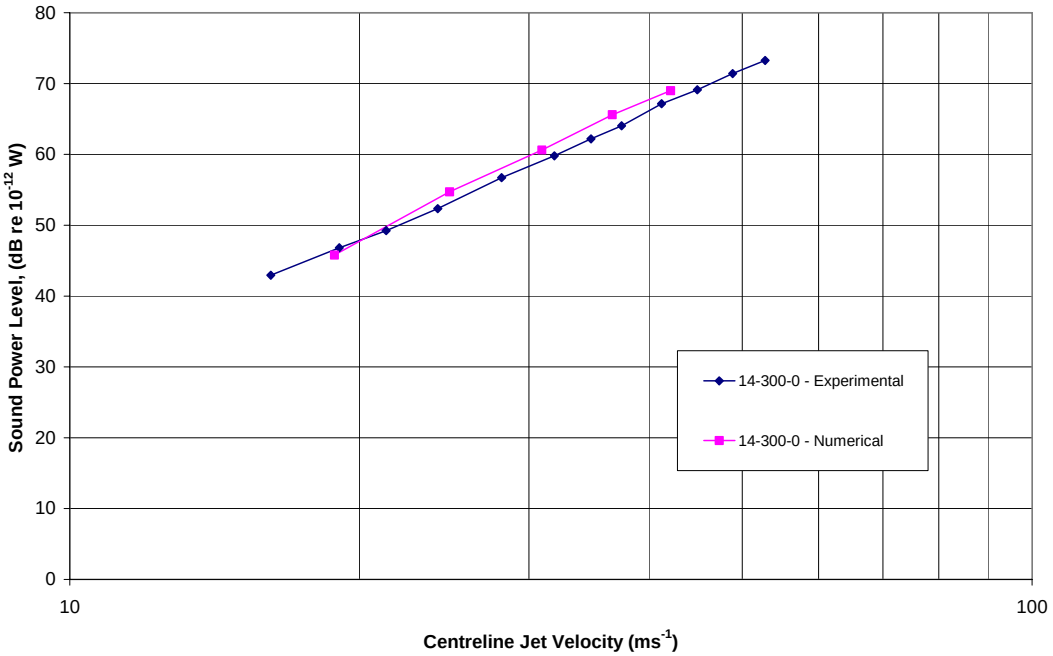

Figure 9.4: Sound power level comparison for the 14˚ conical diffuser fitted with a 300 mm long outlet duct.

From an acoustic design perspective a variation of 2 dB is quite acceptable, particularly in the early design phase of a project, where the need for costly experimental investigations can be avoided. The numerical model provides a reasonable level of accuracy in the prediction of the overall sound power level, otherwise considered as the level of flow induced acoustic energy. Importantly the slope of the sound power - velocity curve measured experimentally is closely matched by the numerical model. The slope of this curve is strongly driven by the relative strength of the dipole and quadrupole acoustic sources generating the noise. Therefore the above results can also be interpreted as a demonstration of the ability of the numerical model to correctly incorporate the mix of acoustic sources generated by each respective flow field.

9.2.2 Conical Diffuser With Extended Outlet Ducts

Following the success of the baseline numerical models using the 300 mm outlet duct fitted to each of the three selected conical diffusers additional models were prepared with the outlet duct extended to 600 mm.

The total sound power level across the jet velocity range of interest for the 7˚, 10˚ and 14˚ conical diffusers are shown in Figures 9.5, 9.6 and 9.7 respectively. The 2 to 3 dB variation between the numerical and experimental results observed previously was manifested once again, with the exception of jet velocities below 20 ms^{-1}. The influence of the background noise levels in the lower velocity range (below 20 ms^{-1}) appears to be slightly more pronounced with these results, when compared to the corresponding results for the 300 mm outlet duct. This can largely be attributed to the lower levels of noise generated when the longer outlet duct is employed. The lower levels of sound generation would lead to a higher impact from any consistent background noise sources. The slope of each sound power - velocity curve is also well represented in each of the three models considered.

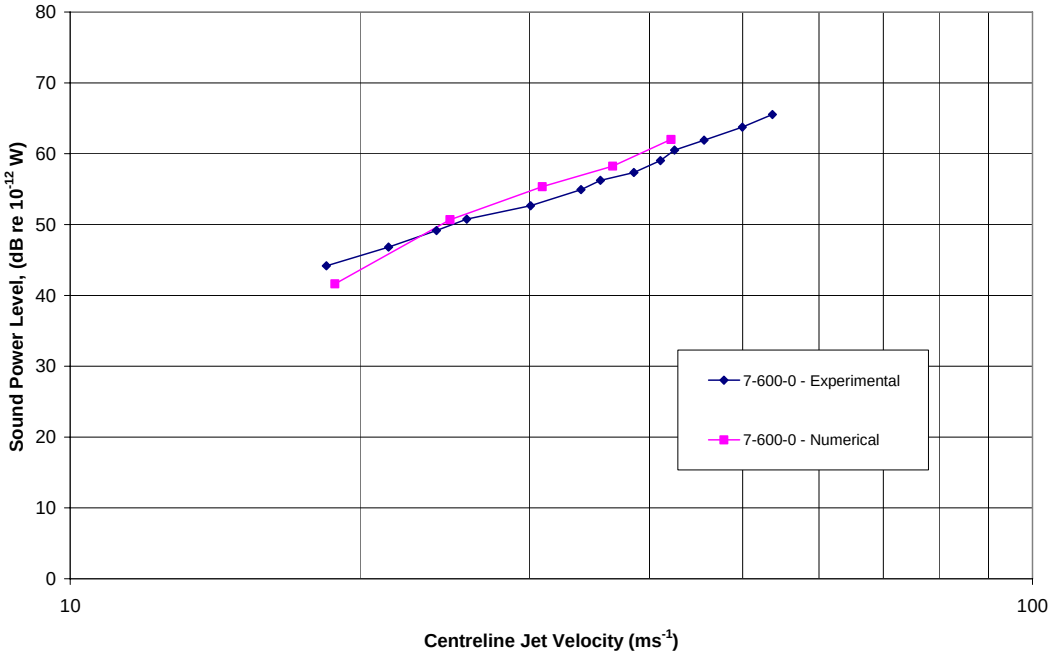

Figure 9.5: Sound power level comparison for the 7˚ conical diffuser fitted with a 600 mm long outlet duct.

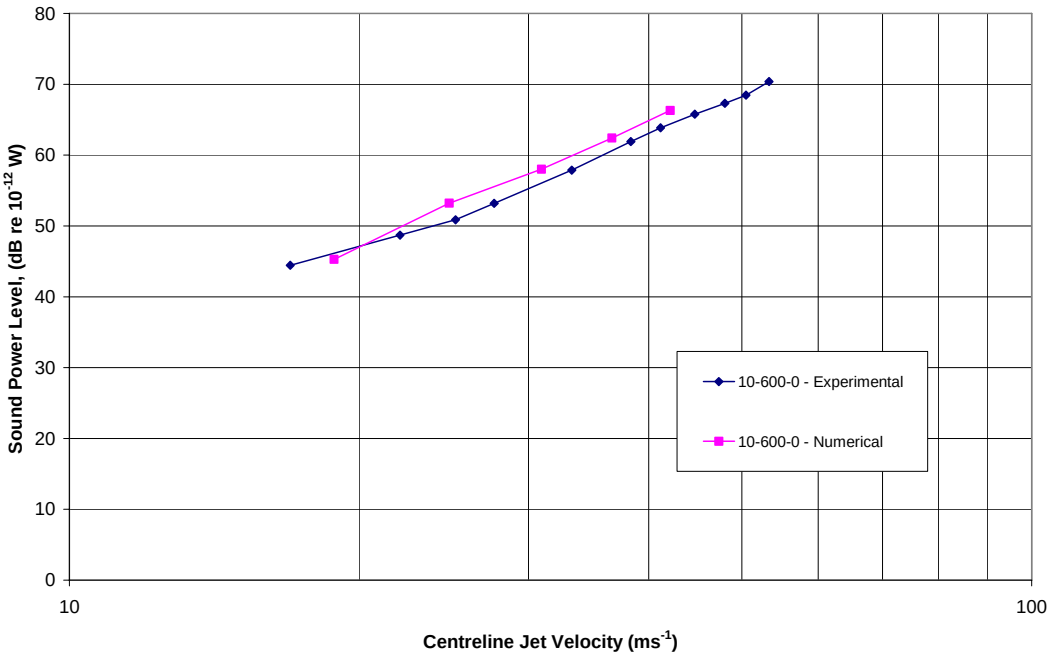

Figure 9.6: Sound power level comparison for the 10˚ conical diffuser fitted with a 600 mm long outlet duct.

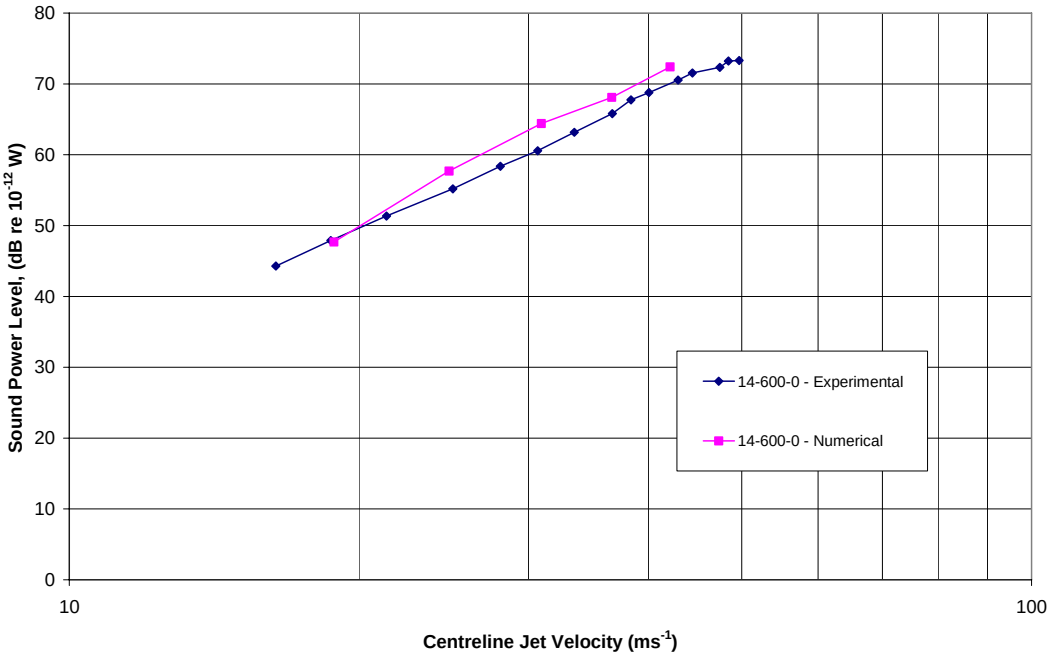

Figure 9.7: Sound power level comparison for the 14˚ conical diffuser fitted with a 600 mm long outlet duct.

9.3 ⅓ Octave Sound Power Level Analysis

The acoustic design specification for ocean going fast ferries is based on an A-weighted sound pressure level scale and therefore the frequency composition of any noise generation becomes significant. The total sound power level can be used to back calculate an equivalent sound pressure level in the cabin space, based on the expected acoustic properties (volume, surface area and acoustic absorption) of the passenger cabin space. However, to allow this predicted sound pressure level to be A-weighted correctly it is important that the acoustic spectral composition is adequately represented. To this end a ⅓ octave band frequency analysis of the numerically predicted sound power level was completed.

The ⅓ octave band sound power levels generated by the 7˚ conical diffuser, fitted with the 300 mm long outlet duct, are shown in Figures 9.8 and 9.9 below, with a jet velocity of 20 and 40 ms^{-1} respectively. The corresponding experimentally measured sound power spectra have also been included for both cases.

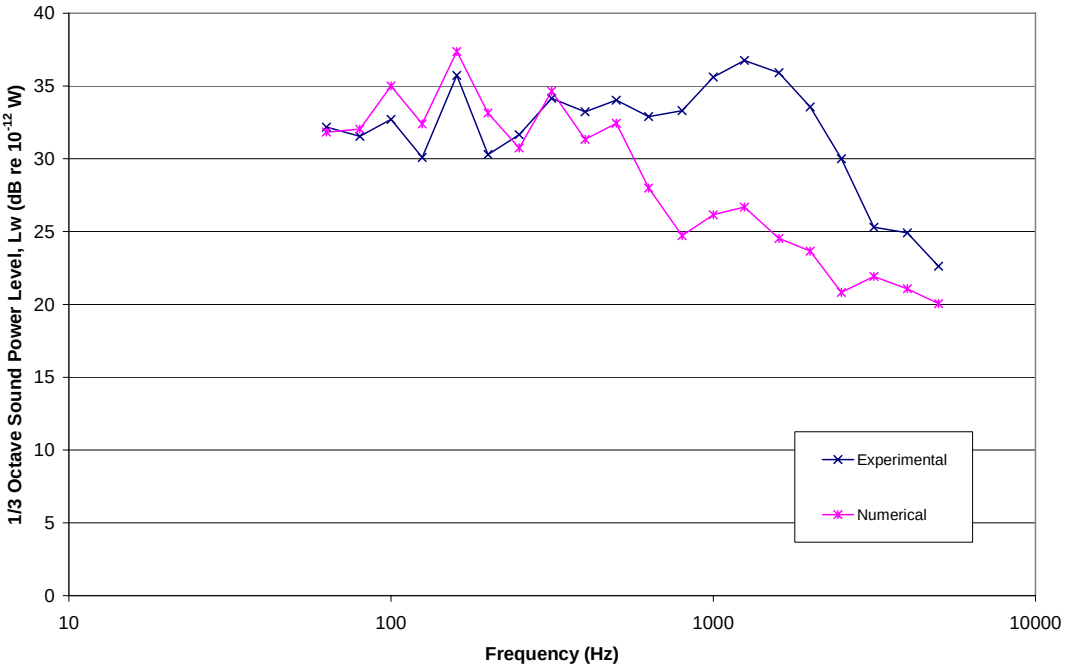

Figure 9.8: ⅓ Octave sound power level comparison for the 7˚ conical diffuser fitted with a 300 mm long outlet duct and a jet velocity of 20 ms^{-1}.

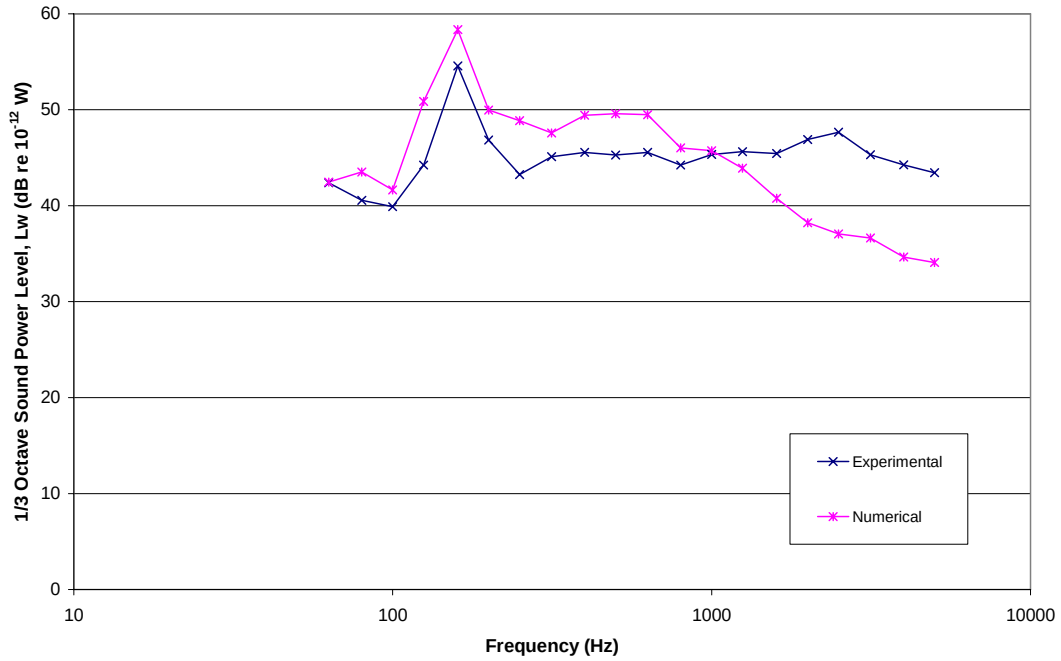

Figure 9.9: ⅓ Octave sound power level comparison for the 7˚ conical diffuser fitted with a 300 mm long outlet duct and a jet velocity of 40 ms^{-1}.

For the 20 ms^{-1} jet the numerically predicted sound power spectra differ slightly from the experimentally measured spectra. The main peaks in the low frequency bands (below 500 Hz) are closely aligned, with the numerically predicted values typically 2 to 3 dB higher than the corresponding experimental values. In the case of the mid to high frequency bands (above 500 Hz) the numerical predictions are somewhat less than the corresponding experimentally measured levels. The variation in the high frequency bands of around 10 dB is of some concern, however it is expected that a considerable part of this noise is a result of background noise levels contaminating the experimentally measured sound power levels. On a positive note, the peak of these spectra still appears in the same frequency band and the total sound power level predicted by the numerical model is 2.0 dB lower than the experimental measurement.

When the jet velocity is increased to 40 ms^{-1} the impact of the background noise levels is diminished, resulting in an improved correlation between the numerically predicted and experimentally measured sound power spectra. As with the 20 ms^{-1} jet velocity case the low frequency spectra predicted by the numerical model is 2 to 4 dB higher than the corresponding experimental values. The general shape of the spectra and the location of the peak sound power level are closely matched between the numerical and experimental results.

In the mid to high frequency bands above 500 Hz the experimental results are still around 5 dB higher than those predicted from the numerical model. Overall the general shape of the numerically predicted spectra is more closely aligned with that measured experimentally in the reverberation suite at the high jet velocity of 40 ms^{-1}. This improved result is largely attributed to the diminished impact of external noise sources - both background and flanking - effects. The overall sound power level predicted from the numerical model was 2.3 dB greater than that measured experimentally.

9.4 Applications of the Acoustic Model

9.4.1 Diffuser Outlet Assessment

Although not perfectly aligned, the numerical sound power spectra provided a reasonable approximation of the true sound power spectra generated for the outlet diffuser configurations considered. The ability of the model to accurately mimic the high frequency spectra is of some minor concern; however the overall performance of the modelling process represents a significant step forward in the ability to simulate the acoustic performance of potential high velocity outlet diffuser designs.

Importantly the model was able to closely predict the spectral shape in the low frequency bands, which are the most crucial frequency ranges of interest in this particular application. The experimental component of this research provided a clear indication that the configuration of the conical diffuser, outlet duct length and outlet grill selection can be tuned to maximise acoustic performance. The majority of this tuning is focused in the frequency bands below 500 Hz and as such the ability of the numerical model to closely match the experimental results across these frequencies represents a significant result.

The acoustic performance in the upper frequency bands above the 500 Hz is far more responsive to additional attenuation material installed in the header box fitted between the outlet duct and the selected outlet grill. From a design point of view most high frequency attenuation needs can be catered for with the addition of extra acoustic lagging material. The low frequency performance of this attenuation methodology is severely limited and therefore alternative means must be pursued, such as the acoustic tuning methodology made viable by the application of the numerical simulation tools outlined herein.

9.4.2 HVAC Design Tool Potential

Considerable work is still required to develop this modelling approach to the point that a commercially viable design process is feasible. Current limitations on computational resources are progressively being reduced and in time this limitation will be progressively eroded. With careful attention to detail simplified CFD models can be used to rapidly identify optimum outlet diffuser configurations that can then be more closely refined using the more rigorous LES and numerical acoustic simulations outlined in this thesis.

In time, improvements in computational resource capabilities will make the addition of porous media (acoustic lagging) and actual simulation of the outlet grill economically viable. In the interim more work can be completed in further exploring the limitations of the far field acoustic analogy and how the placement of the acoustic source surface(s) can be used to best effect.

Chapter 10

Commercial Application of Research Results, General Recommendations and Conclusions

The primary aim of this research as outlined in Chapter One was to investigate the feasibility of installing high velocity HVAC systems on board ocean going fast ferries. Numerous technical challenges must be overcome if such a system is to be installed in an operational capacity, some of which go beyond the scope of this thesis. Increasing the distribution velocity inside the HVAC ducting would require specialised air handling equipment, air treatment plants and associated in-duct noise treatment. However none of this work can be justified unless the high velocity conditioned air can be adequately expanded in a controlled manner prior to entering the passenger cabin spaces. The velocity of the air as it enters the cabin must be tightly controlled along with any associated flow induced noise if the required passenger comfort specifications are to be met.

This research has successfully demonstrated that air distribution velocities of 20 to 30 ms^{-1} can be adequately expanded in a controlled manner with the use of a two stage expansion whilst simultaneously restricting the associated flow induced noise. Under existing passenger cabin noise specifications applicable to ocean going fast ferries there is considerable scope to increase the distribution velocity above the current levels of 5 to 7 ms^{-1} without excessive design work. Significant duct size reductions of over 50 to 75 percent can be achieved with careful design of the outlet diffusers employed.

In the event of more stringent passenger comfort specifications being implemented there is still room for significant increases in the distribution velocity and therefore reduction in the size of the installed HVAC ducts. However this would require a greater level of acoustic and flow analysis to ensure optimum system performance. In this circumstance the current design practices would require extensive revision as well.

The eventual commercialisation of this research is contingent on the successful navigation of the remaining technical hurdles outlined above. However successful completion of this research along with the potential savings of reduced deck to deck height, installation costs and ongoing operating costs can be used to justify this future work. The numerical modelling capabilities developed as part of this research also provide a useful tool for the commercial design of such a system as the opportunities develop. There are a number of limitations on the current capabilities and several areas in need of further investigation which will be discussed herein.

10.1 Optimum Outlet Diffuser Geometry

This research has focused on the development of a two stage diffuser for the purpose of expanding a high velocity air jet prior to the subsequent dispersion into a passenger cabin space. The primary expansion of the jet of air was achieved with the use of a conical diffuser, with diffuser angles of 7˚, 10˚ and 14˚ investigated. The conical diffuser section was followed by an outlet duct length of 300, 600 and 900 mm used. Several outlet grills and header box configurations were also trialled as part of this analysis. The actual selection of the diffuser angle and outlet duct length for any given application is not limited to these discrete values, with comprehensive project specific analysis strongly recommended.

The optimum outlet diffuser geometry for any given application will depend on the specific constraints involved; however some general conclusions can be drawn from the results reported in this thesis. A conical diffuser angle of 7˚ was preferred, with an outlet duct of 300 and 600 mm providing very similar results. In the event that space limitations dictate the use of a larger diffuser angle a limit of 10˚ is recommended. In this instance an outlet duct length of 600 mm will provide a similar acoustic performance to a 7˚ conical diffuser. Extreme space constraints that dictate the use of an even greater diffuser angle (such as 14˚) will call for additional acoustic treatment in the header box connected to the outlet diffuser grill. The length of the outlet duct joining the primary and secondary diffusers should also be carefully tuned to ensure maximum low frequency attenuation of the higher levels of flow induced noise that will be produced.

10.2 Guide Vane Placement

The onset of flow separation inside wider angle conical diffusers can be at least partially averted with the installation of multiple guide vanes inside the diffuser. Careful alignment of the vanes can result in an effective diffuser angle of less than the preferred 7˚, and therefore a significant reduction in flow separation. This is one very good example of how simple CFD based flow models can be used for application specific design investigations, prior to the eventual acoustic simulation of the outlet. Potential guide vane placements can be simulated relatively quickly and the resulting flow fields compared.

One of the common flaws in the existing design methodology employed by Austal ships is the lack of guide vane use across their HVAC ducting systems, predominantly driven by the need to reduce the weight of the installed system. This research has demonstrated that the installation of such guide vanes will significantly reduce the onset of flow separation around duct corners and fittings and therefore the noise levels observed in the passenger cabin. Given the relatively high A-weighted sound pressure level specification of 65 dB (A) for the passenger cabin spaces, the need to reduce the cabin noise levels is no doubt poorly regarded. However the use of guide vanes in the duct corners and fittings would in fact enable a much higher distribution velocity and therefore a significant reduction in the required duct size. The possible gains from the simple application of guide vanes would be substantial and could be implemented almost immediately. The commercial gains from such actions could then be used to fund the work required to implement an even higher distribution velocity.

10.3 Optimum Use Of Acoustic Lagging Material

The best performing outlet configuration tested as part of this research was the square diffuser (SD) fitted to the cushion head (CH) box, which was lined with 12 mm of acoustic lagging material. The lagging material was found to provide considerable high frequency attenuation upstream of the outlet grill feeding the passenger cabin. Additional attenuation can be achieved with the use of thicker lagging material; however the low frequency performance is only marginally affected if at all.

Acoustic lagging material can also be used upstream of the passenger cabin outlets to treat duct related flow induced noise and any fan noise which is radiated down the duct. Where thermal insulation of the air distribution ducts is also required a combined acoustic lagging and thermal barrier should be employed. However one major drawback of using this lagging material is the added weight introduced to the system. For this reason reactive attenuation should be preferentially used wherever possible. Reactive attenuators can also be tuned to the specific needs of the system, but do potentially add to the line pressure drop incurred and therefore the associated running costs of the system.

10.4 Air Distribution Velocity Limits

The primary motivating driver for this research is the need to reduce the size of the air distribution ducts needed to operate a centralised HVAC system on board ocean going fast ferries. Within the design constraints of operating costs, noise levels and general system operability, this need can ultimately be simplified down to maximising the air distribution velocity. The potential air distribution velocities that could be utilised are summarised in Table 10.1 below, along with the associated duct area reduction and deck to deck height reduction.

Table 10.1: Potential distribution velocity increases and deck height reductions.

	Air Velocity	Area Reduction	Deck Height Reduction
Current	5 - 7 ms^{-1}	-	-
Guide Vanes	10 - 12 ms^{-1}	50 %	30 %
High Velocity	20 - 30 ms^{-1}	75 - 80 %	50 - 60 %

As outlined previously, the immediate application of basic guide vane technology can potentially result in the doubling of the existing air distribution velocity used without exceeding the prescribed passenger comfort levels. This would result in a 30 % reduction in the ceiling height required to house the HVAC services, provided a duct aspect ratio of one is maintained.

The implementation of a high velocity air distribution system with an air velocity of 20 to 30 ms^{-1} will result in an area reduction of 75 to 80 % or a height reduction of 50 to 60 % (assuming a duct aspect ratio of one). This level of reduction would clearly be contingent on the required acoustic attenuation and flow expansion needs also being satisfied by the outlet diffusers employed.

While the service ceiling height reduction listed here is based on a duct aspect ratio of one, there is the potential for the net space saving to be far greater with the use of multiple ducts. The additional cost of the extra ducts can be offset against any additional height savings and/or any reduction in the duct pressure drop resulting from the use of the extra duct(s). Multiple ducts can be used to good effect in offsetting the total increase in air distribution velocity and therefore the required flow expansion and acoustic attenuation treatments. Where there is little to be gained from further reducing the height of the ducts, the installation of multiple ducts can still be used to reduce the air distribution velocity and the corresponding pressure drop across the ducts.

10.5 Applications of the CFD Model

The application of CFD modelling in general to the design of HVAC systems for ocean going fast ferries can be separated into two distinct categories. The first and simplest to implement commercially involves the simulation of system air flows and pressure balancing. In many respects this type of work is already in use in a limited capacity within the wider HVAC industry as outlined in the ASHRAE handbooks [5, 9]. The cost of this type of work is somewhat prohibitive to most general HVAC applications, however there does exist a limited number of niche projects where the potential savings justify the added design costs incurred. The research covered in this thesis leads the author to strongly believe that such savings are clearly applicable to the HVAC systems currently installed on the ocean going fast ferries manufactured by Austal Ships.

The second application of CFD based modelling is the far more detailed and costly analysis of high velocity air distribution systems, including the numerical simulation of flow induced noise and the subsequent attenuation strategies. This work would be aimed at minimising the space required for the HVAC system on board ocean going fast ferries. There is also the wider scope to apply these methodologies to other niche applications where the added operating costs associated with a high velocity HVAC system are justified due to other direct or indirect application specific design constraints.

10.5.1 HVAC Design Tool Potential - Airflow Visualisation and Optimisation

There is considerable scope to increase the air distribution velocity within the HVAC systems currently employed, and to move to what would generally be considered a medium velocity system (10 to 12 ms^{-1}). This type of system would not need the same level of detailed acoustic simulation associated with the design of an equivalent high velocity system. General improvements to individual duct designs, especially around corners, side branch intersections and other such regions of high turbulence can be simulated using relatively low cost steady state simulations. The approximate solutions that are derived from the use of steady state RANS turbulence models enable sufficient levels of accuracy to assess the relative merits of multiple duct configurations.

The placement, sizing and optimisation of guide vanes can also largely be simulated using these relatively simple steady state models. The computational cost of this type of analysis is such that it would be immediately commercially viable for a company such as Austal Ships to implement. The level of potential material, installation and resulting structural cost savings would be more than offset by the added design costs. The added weight of the guide vanes would also be offset against weight savings elsewhere in the vessel.

Admittedly the installation of guide vanes inside the relevant duct sections does introduce an added manufacturing expense; however this would at least be offset against the reduced cost arising from the installation of smaller duct sections. In most instances the guide vanes would be prefabricated in conjunction with the HVAC ducts themselves prior to the installation of the HVAC system on board the vessel. Therefore limited additional assembly costs would be incurred by Austal Ships.

This type of CFD model will also enable better optimisation of the duct geometry in terms of the overall pressure drop across the distribution duct work. By completing this work numerically as part of the design process the duct shape can be optimised prior to the vessel design being locked in and costly rework avoided. Correct flow balancing may well reduce the need to employ dampers to balance the pressure across the duct system and therefore reduce the net pressure drop supplied by the supply fan. The time required to commission the HVAC system may therefore also be reduced.

The general conclusion that can be drawn from each of these options is the clear technical improvement that can be made over the current methodologies employed by Austal Ships. There are immediate opportunities that can be exploited to generate an immediate return to the company through incremental evolutionary improvements to the HVAC design process. The added CFD based capacity that can be developed using this type of initiative could then have the potential to be leveraged to initiate more advanced CFD analyses into the future.

10.5.2 Unsteady Turbulence Models - Flow Field Optimisation

The design and development of a customised high velocity HVAC system will require a considerable level of detailed analysis of the resulting transient turbulent flow fields and the associated flow induced noise. The use of unsteady transient turbulence models, such as the LES models used in this research consume a significantly greater computational resource when compared with the simpler RANS models outlined above. Notwithstanding the added cost, this research has been able to successfully demonstrate that significant increases in the air distribution velocity can be achieved, provided the right flow control strategies are employed.

The detailed CFD modelling of proposed designs can allow multiple system designs to be investigated, without expensive experimental evaluation. Steady state RANS models can still be used to iterate down to the preferred design specification, which can then be fine tuned with the more computationally expensive LES model. These modelling solutions will become more economically viable over time in line with the progressive decline in the cost of computational resources.

10.6 Numerical Modelling of Flow Induced Noise

10.6.1 Computational Limitations

The numerical cost of the LES turbulence based CFD model will continue to be a major obstacle to the wider applications without significant increases in computing power efficiencies. Alternative simplified models based on DES turbulence models may provide a viable alternative if appropriate mesh controls can be implemented. With this type of model the length scales of the resolved eddies are directly dependent on the size of the mesh used. There is therefore the potential to compromise the integrity of any numerical solution to complex flow geometries and material properties. New Scale Adaptive Simulation (SAS) turbulence models may well lead to a long term viable compromise to this modelling compromise. As this is a recent technology development in the sphere of commercial CFD codes, further assessment will be required to fully assess the true viability of numerical simulations based on a SAS turbulence model.

The SAS model is designed to resolve the flow field based on prescribed turbulence length scales and not just the prescribed mesh, leading to a mesh independent simulation of the turbulent eddies within the flow field. The SAS model reverts to a standard RANS based turbulence model in areas of the flow domain with low turbulence levels; leading to significant computational savings in terms of both direct solution time and more relaxed meshing criteria.

A cautionary note must be made in relation to the accuracy of any model based on the SAS assumptions outlined above. There was a strong presence of dipole based noise sources in the flow generated noise observed in the case studies presented herein. Noise sources of this type are predominantly based on the shear flow around solid surfaces such as walls and obstacles in the flow path, while shear layers surrounding an expanding jet of air produce predominantly quadrupole sound sources. With this result in mind, a SAS based model would require detailed investigation into the relationship between the prescribed turbulence length scales used and the corresponding predicted sound pressure levels. The potential computational cost savings associated with a positive outcome from this work provide a strong case for further research in this area.

10.6.2 Acoustic Model Limitations

The fundamental assumption of Lighthill's far field acoustic analogy is that the acoustic receivers are located in a free field medium that is at rest. As such no attempt is made to incorporate the effects of self noise, where the flow field is itself impacted by the induced acoustic field. Given the relatively low mach number flows covered by this work and what would be normally considered in a high velocity HVAC system this is a reasonable assumption. Care should be taken however in applying this same methodology to higher velocity jets. Increasing the jet velocity would also call for the use of a fully compressible CFD model.

The acoustic receiver points used to generate the far field sound power levels must also be located such that they are in direct line with the acoustic source surface. There is no compensation for any reverberation effects and therefore any simulation that includes solid surfaces adjacent to the acoustic source surface(s) that may interfere with the propagation path of the acoustic waves would produce a questionable result. The acoustic source surface and the corresponding receiver point locations must be carefully chosen to ensure an accurate representation of the flow induced sound field.

The numerical acoustic model developed as part of this research was found to provide a good overall prediction of the total sound power level in the far field and a reasonable approximation of the ⅓ octave sound power level spectra. Care should however be taken when interpreting the high frequency components of the ⅓ octave spectra. The model tends to over predict the sound power level in the low frequency bands below 500 Hz, whilst also under predicting the high frequency components. There is potential to extend this research to further refine this process and improve the accuracy of the ⅓ octave sound spectra, however this will no doubt require the commitment of substantial computational resources. Potential areas of interest include the type of CFD turbulence model, the mesh spacing across the acoustic source surface and the sampling of the acoustic source data.

An accuracy of 2 to 3 dB is quite acceptable for the design of a HVAC system, especially given that no such design tool has been available to date.

10.6.3 Potential Applications

The acoustic modelling methodology developed as part of this research can be used to assess the acoustic performance of a proposed outlet diffuser design to ensure that correctly tuned duct sizes and lengths are selected. This work can be completed in a two step process with the primary conical diffuser and outlet duct tuned numerically without the presence of the outlet grill. Once the primary diffuser has been tuned the secondary effects of the outlet grill can be modelled based on the velocity profile from the earlier models. Care would need to be taken in ensuring that the acoustic source surfaces were placed correctly along with appropriately placed acoustic receiver locations.

There is the potential to also explore non HVAC related applications where internal flow exits into an external flow domain, provided that the relevant acoustic model assumptions can be satisfied. These applications would have to be limited to low mach number flows where incompressible flow models can be employed. No internal reverberation effects or the propagation of upstream flow related noise could be adequately simulated in this process. A separate acoustic model would be required to

calculate the far field sound field from such sources, allowing for propagation and attenuation effects that would be encountered. This result could then potentially be combined with the far-field prediction of the flow induced noise to develop an approximation of the combined acoustic field. Such work would require extensive investigation and proper validation with experimentally verifiable results.

10.7 Summary and Conclusion

Experimental tests have been conducted to prove the viability of a high velocity HVAC duct system in meeting the airflow requirements whilst also maintaining acceptable passenger cabin noise levels on board ocean going fast ferries. The existing air distribution velocities of 5 to 7 ms^{-1} can be immediately increased to 10 to 12 ms^{-1}, without any major impact or design changes. The only requirement of such a system would be the introduction of appropriately sized guide vanes to limit the onset of flow separation and the associated noise generation.

With the use of appropriately designed two stage outlet diffusers, an air distribution velocity of 20 to 30 ms^{-1} can be used without exceeding current passenger comfort thresholds. The experimental research presented herein demonstrates that the sound power levels radiating from these customised outlets can meet the current acoustic and airflow specifications dictated by the passenger comfort standards.

A numerical modelling methodology capable of predicting the flow induced noise generated by airflow exiting a ventilation duct has been successfully developed and validated against a range of experimental results. The computational cost of this model is probably beyond the current economic benefits that could be derived from it commercially. However, ongoing advances in computational capabilities coupled with sharp increases in energy costs will ensure that the viability of such design solutions will become a reality at some stage. In the interim clever use of simplified CFD models can be used to identify optimum system designs that can then be cost effectively simulated at an improved cost-benefit ratio.

The application of general CFD design techniques can also be used to make significant improvements to existing HVAC designs on both new and existing installations. In particular the placement and sizing of guide vanes can be optimised with the use of CFD models without the need for expensive experimental investigations or rework. In niche applications such as the ocean going fast ferry market there are far greater savings potential then would otherwise be found in standard HVAC applications. It is strongly recommended that this form of analysis is integrated into the HVAC design process employed by Austal Ships so as to realise these gains.

Chapter 11

References

1. Xue, H., S.K. Chou, and X.Q. Zhong, *Thermal environment in a confined space of high-rise building with split air conditioning system.* Building and Environment, 2004. **39**(7): p. 817.
2. Lighthill, M.J., *On sound generated aerodynamically: I: General Theory.* Proceedings of the Royal Society London, Series A, 1952. **211**: p. 564-581.
3. Lighthill, M.J., *Sound generated aerodynamically.* Proceedings of the Royal Society London, Series A, 1962. **267**: p. 147-173.
4. Strock, C. and R. Koral, *Handbook of air conditioning, heating and ventilating*. 2nd Edition ed. 1965, New York: Industrial Press.
5. ASHRAE, *Chapetr 34: Duct Design*, in *ASHRAE Fundamentals Handbook*. 2001, ASHRAE.
6. Habjan, J., *Medium pressure duct sizing and design.* Heating, Piping and Air Conditioning, 1984. **56**(12): p. 95-100.
7. Mason, M., *Duct design: Considerations in the design of air conditioning ductwork system.* Australian Refrigeration, Air Conditioning and Heating, 1989. **43**(3): p. 36-49.
8. ASHRAE, *Chapetr 46: Sound and Vibration Control*, in *ASHRAE Applications Handbook*. 1999, ASHRAE.
9. ASHRAE, *Chapter 10: Ships*, in *ASHRAE Applications Handbook*. 1999, ASHRAE.
10. Soylemez, M.S., *On the optimum channel sizing for HVAC systems.* Energy Conversion and Management, 2001. **42**(7): p. 791.
11. Lu, L., Cai, W., Soh, Y. C., Xie, L., *Global optimization for overall HVAC systems--Part I problem formulation and analysis.* Energy Conversion and Management, 2005. **46**(7-8): p. 999.
12. Lu, L., Cai, W., Soh, Y. C., Xie, L., *Global optimization for overall HVAC systems--Part II problem solution and simulations.* Energy Conversion and Management, 2005. **46**(7-8): p. 1015.
13. Lu, L., Cai, W., Soh, Y. C., Xie, L., *HVAC system optimization--in-building section.* Energy and Buildings, 2005. 37(1): p. 11.
14. Scheuer, C., G.A. Keoleian, and P. Reppe, *Life cycle energy and environmental performance of a new university building: modelling challenges and design implications.* Energy and Buildings, 2003. **35**(10): p. 1049.
15. ASHRAE, *Chapter 17: Air Diffusing Equipment*, in *ASHRAE Systems and Equipment Handbook*. 2000, ASHRAE.
16. Int-Hout, D., *Air distribution for large spaces.* ASHRAE Journal, 1999. **41**(4): p. 57-64.
17. Pierce, W.M., Janczewski, J.N., Roethlisberger, B., Janczewski, M.G., *Air quality on commercial aircraft.* ASHRAE Journal, 1999. 41(9): p. 26-34.
18. Janczewski, J.N., *IAQ on passenger planes.* ASHRAE Journal, 1999. **41**(9): p. 18-22.

19. Tokarev, V.I., O.I. Zaporozhets, and V.M. Vorotyntsev, *Sound generation by airborne air conditioning systems: Theory and analysis.* Applied Acoustics, 1998. **55**(2): p. 145-162.
20. Warner, D.W., Humbad, N.G., Alzahabi, B., Porada, R.A., *Design considerations for flow noise in automotive air handling systems*. in *ASME IMECE*. 1999. Nashville, TN, November 1999: ASME.
21. Botros, M.B., Hanna, D.F., Nava, T., Lai, M., A new design feature to improve the sound and efficiency of automotove HVAC centrifugal blower systems. in ASME IMECE. 1999. Nashville, TN, November 1999.: ASME.
22. Trent, R.W., *Air conditioning in submarines.* ASHRAE Journal, 2001. **43**(1): p. 20-23.
23. Yankaskas, K. *Successful airborne noise control: Attention to detail*. in *Noise-Con 96*. 1996. Seattle, Washington.
24. ASHRAE, *Chapter 7: Sound and Vibration*, in *ASHRAE Fundamentals Handbook*. 2001, ASHRAE.
25. ASHRAE, *Chapter 33: HVAC compuattional fluid dynamics*, in *ASHRAE Fundamentals Handbook*. 2001, ASHRAE.
26. Mcquiston, F.C., J.D. Parker, and J.D. Spitler, *Heating, Ventilating and Air Conditioning*. 5th Edition ed. 2000: John Wiley & Sons.
27. Idelchik, I.E., *Handbook of Hydraulic Resistance*. 3rd Edition ed. 1994: CRC Press.
28. Bies, D.A. and C.H. Hansen, *Engineering Noise Control*. 1997: E & FN Spon.
29. Beranek, L.L., *Revised criteria for noise in buildings.* Noise Control, 1957. **1:19**.
30. Beranek, L.L., *Application of NCB noise criterion curves.* Noise Control Engineering Journal, 1989. **33**(2): p. 45-56.
31. Beranek, L.L., *Balanced Noise-Criterion (NCB) curves.* Journal of the Acoustical Society of America, 1989. **86**(2): p. 650-664.
32. Kingsbury, H.F., *Review and revision of room noise criteria.* Noise Control Engineering Journal, 1995. **43**(3): p. 65-72.
33. Blazier, W.E., *Sound quality considerations in rating noise from heating, ventilating and air conditioning (HVAC) systems in buildings.* Noise Control Engineering Journal, 1995. **43**(3): p. 53-63.
34. Bradley, J.S., *Annoyance caused by constant-amplitude and amplitude-modulated sounds containing rumble.* Noise Control Engineering Journal, 1994. **42**(6): p. 203-208.
35. Blazier, W.E., *Revised noise criteria for applicationto the acoustical design of HVAC systems.* Noise Control Engineering Journal, 1981. **16**(2): p. 64-73.
36. Blazier, W.E., *RC Mark II: A refined procedure for rating the noise of heating, venmtilating and air conditioning (HVAC) systems in buildings.* Noise Control Engineering Journal, 1997. **45**(6): p. 243-250.
37. Schomer, P.D., *Proposed revisions to room noise criteria.* Noise Control Engineering Journal, 2000. **48**(3): p. 85-96.
38. Armstrong, T., *Personal discussion on HVAC acoustic testing methods for ocean going fast ferries.* 2002.
39. Goujard, B., A. Sakout, and V. Valeau, *Acoustic comfort on board ships: An evaluation based on a questionnaire.* Applied Acoustics, 2005. **66**(9): p. 1063.
40. Hardy, A.E.J., *Measurement and assessment of noise within passenger trains.* Journal of Sound and Vibration, 2000. **231**(3): p. 819-829.

41. Hogstrom, C., *Sound quality of air conditioning systems in trains*. 1999, MSc Thesis**,** Royal Institute of Technology, Sweden
42. Choi, S., Lee, C., Kim, J., Cho, J. *Interior noise of a Korean high-speed train in tunnels*. in *Proceedings of Acoustics 2004*. 2004. Gold Coast, Australia, p. 415-419.
43. Tamura, Y., T. Kawada, and Y. Sasazawa, *Effect of Ship noise on sleep.* Journal of Sound and Vibration, 1997. **205**(4): p. 417-425.
44. Byrne, K. and J. Challen, *Course Notes: Fundamentals of Noise*. 1997: School of Mechanical and Manufacturing Engineering, UNSW.
45. Lighthill, J., *Waves in fluids*. 2001: Cambridge University Press.
46. Marretta, R.A., et al., *A procedure for the evaluation of installed propellor noise.* Journal of Sound and Vibration, 2001. **244**(4): p. 697.
47. Lucas, M.J., et al., *Handbook of the acoustic characteristics of turbomachinery cavities*. 1997: ASME Press.
48. Bogey, C. and C. Bailly, *A family of low dispersive and low dissipative explicit schemes for flow and noise computations.* Journal of Computational Physics, 2004. **194**(1): p. 194.
49. Bridges, J. and F. Hussain, *Effects of nozzle body on jet noise.* Journal of Sound and Vibration, 1995. **188**(3): p. 407.
50. Watson, W.R. and O.O. Storassli, *Application of NASA general-purpose solver to large-scale computations in aeroacoustics.* Advances in Engineering Software, 2000. **31**: p. 555-561.
51. Dobrzynski, W., B. Gehlhar, and H. Buchholz, *Model and full scale high lift wing wind tunnel experiments dedicated to airframe noise reduction.* Aerospace Science Technology, 2001. **5**: p. 27-33.
52. Campos, L.M.B.C., *On the spectra of aerodynamic noise and aeroacoustic fatigue.* Progress in Aerospace Sciences, 1997. **33**(5-6): p. 353.
53. Hu, F.Q., M.Y. Hussaini, and J.L. Manthey, *Low-Dissipation and Low-Dispersion Runge-Kutta Schemes for Computational Acoustics.* Journal of Computational Physics, 1996. **124**(1): p. 177.
54. Dumbser, M. and C.-D. Munz, *ADER discontinuous Galerkin schemes for aeroacoustics.* Comptes Rendus Mecanique, 2005. **333**(9): p. 683.
55. Dyson, R.W. and J.W. Goodrich, *Automated approach to very high order aeroacoustic computations.* AIAA, 2001. **39**(3): p. 396-406.
56. Lin, S. and J. Hu, *Parametric study of weighted essentially nonoscillatory schemes for computational aeroacoustics.* AIAA, 2001. **39**(3): p. 371-379.
57. Tam, C.K.W. and J.C. Webb, *Dispersion-Relation-Preserving finite difference schemes for computational acoustics.* Journal of Computational Physics, 1993. **107**: p. 262-281.
58. Lele, S.K., *Compact finite difference schemes with spectral-like resolution.* Journal of Computational Physics, 1992. **103**: p. 16-42.
59. Kim, J.W. and D.J. Lee, *Optimized compact finite difference schemes with maximum resolution.* AIAA, 1996. **34**: p. 887-893.
60. Tam, C.K.W., *Computational aeroacoustics: Issues and methods.* AIAA, 1995. **33**(10): p. 1788-1796.
61. Zhauang, M. and R.F. Chen, *Optimized upwind dispersion-relation-preserving finite difference scheme for computational aeroacoustics.* AIAA, 1998. **36**(11): p. 2146-2148.

62. Ono, K., Himeno, R., Shiozawa, H., Wakamatsu, J., *An analysis of A-pillar wind noise using finite difference method with an overlaid grid system.* JSAE Review, 1997. 18(2): p. 187-188.
63. Kravchenko, A.G. and P.Moin, *B-spline methods and zonal grids for numerical simulations of turbulent flow*. 1998, Standford University.
64. Morinishi, Y., S. Tamano, and K. Nakabayashi, *A DNS algorithm using B-spline collocation method for compressible turbulent channel flow.* Journal of Fluids, 2003. **32**: p. 751-776.
65. Widjaja, R., Ooi, A., Chen, L., Manasseh, R., *Computational aeroacoustics using the B-spline collocation method.* Comptes Rendus Mecanique, 2005. 333(9): p. 726.
66. Alkishriwi, N., Meinke, M., Schroder, W., *A large-eddy simulation method for low Mach number flows using preconditioning and multigrid.* Computers & Fluids, 2006, 35 (10): p. 1126-1136.
67. Baysal, O., G. Yen, and K. Fouladi, *Navier-Stokes computations of cavity aeroacoustics with suppression devices.* Journal of Vibartion and Acoustics, 1994. **116**: p. 105-112.
68. Colonius, T. and S.K. Lele, *Computational aeroacoustics: progress on nonlinear problems of sound generation.* Progress in Aerospace Sciences, 2004. **40**(6): p. 345.
69. Djambazov, G., C. Lai, and K. Pericleous, *Development of numerical techniques for near-field aeroacoustic computations.* International Journal for Numerical Methods in Fluids, 1999. **29**(6): p. 719-731.
70. Fedorchenko, A.T., *On some fundamental flaws in present aeroacoustic theory.* Journal of Sound and Vibration, 2000. **232**(4): p. 719-782.
71. Francescantonio, P.D. and D. Casalino, *Green's function discretization scheme for sound propagation in nonuniform flows.* AIAA, 1999. **37**(10): p. 1161-1172.
72. Hixon, R., S.H. Shih, and R.R. Mankbadi, *Evaluation of boundary conditions for computational aeroacoustics.* AIAA, 1995. **33**(11): p. 2006-2012.
73. Hou, Y. and K. Mahesh, *A robust, colocated, implicit algorithm for direct numerical simulation of compressible, turbulent flows.* Journal of Computational Physics, 2005. **205**(1): p. 205.
74. Hwang, C.J. and J.Y. Kuo, *Adaptive finite volume upwind approaches for aeroacoustic computations.* AIAA, 1997. **35**(8): p. 1286-1293.
75. Kessler, M. and S. Wagner, *Source-time dominant aeroacoustics.* Computers & Fluids, 2004. **33**(5-6): p. 791.
76. Khavaran, A. and J. Bridges, *Modelling of fine-scale turbulence mixing noise.* Journal of Sound and Vibration, 2005. **279**(3-5): p. 1131.
77. Morris, P.J., et al., *A Parallel Three-Dimensional Computational Aeroacoustics Method Using Nonlinear Disturbance Equations.* Journal of Computational Physics, 1997. **133**(1): p. 56.
78. Guenanff, R. and M. Terracol, *Study of stabilization methods for computational aeroacoustics.* Comptes Rendus Mecanique, 2005. **333**(9): p. 694.
79. Ozdemir, H., R. Hagmeijer, and H.W.M. Hoeijmakers, *Verification of higher-order discontinuous Galerkin method for hexahedral elements.* Comptes Rendus Mecanique, 2005. **333**(9): p. 719.
80. Delorme, P., Mazet, P., Peyret, C., Ventribout, Y., *Computational aeroacoustics applications based on a discontinuous Galerkin method.* Comptes Rendus Mecanique, 2005. 333(9): p. 676.

81. Longatte, E. and P. Laffon, *Computation of acoustic propagation in two-dimensional sheared flows.* AIAA, 2000. **38**(3): p. 389-394.
82. Nordstrom, J. and J. Gong, *A stable and efficient hybrid method for aeroacoustic sound generation and propagation.* Comptes Rendus Mecanique, 2005. **333**(9): p. 713.
83. Munz, C.-D., R. Fortenbach, and M. Dumbser, *Multiple-scale modelling of acoustic sources in low Mach-number flow.* Comptes Rendus Mecanique, 2005. **333**(9): p. 706.
84. Ewert, R. and W. Schroder, *Acoustic perturbation equations based on flow decomposition via source filtering.* Journal of Computational Physics, 2003. **188**(2): p. 365.
85. Ewert, R. and W. Schroder, *On the simulation of trailing edge noise with a hybrid LES/APE method.* Journal of Sound and Vibration, 2004. **270**(3): p. 509.
86. Bogey, C. and C. Bailly, *Computation of a high Reynolds number jet and its radiated noise using large eddy simulation based on explicit filtering.* Computers & Fluids, 2006, **35** (10): p. 1344-1358.
87. Marsden, O., X. Gloerfelt, and C. Bailly, *Direct noise computation of adaptive control applied to a cavity flow.* Comptes Rendus Mecanique, 2003. **331**(6): p. 423.
88. Lilley, G.M., *The radiated noise from isotropic turbulence with applications to the theory of jet noise.* Journal of Sound and Vibration, 1996. **190**(3): p. 463.
89. Proudman, I., *The generation of noise by isotropic turbulence.* Proceedings of the Royal Society London, Series A, 1952. **214**: p. 119-132.
90. Curle, N., *The influence of solid boundaries on aerodynamic sound.* Proceedings of the Royal Society London, Series A, 1955. **231**: p. 505-514.
91. Bies, D.A., *An experimental investigation of Curle's theory of aerodynamic noise generation by a stationary body in a turbulent air stream.* Journal of Sound and Vibration, 2004. **278**(3): p. 581.
92. Kim, H.J., S. Lee, and N. Fujisawa, *Computation of unsteady flow and aerodynamic noise of NACA0018 airfoil using large-eddy simulation.* International Journal of Heat and Fluid Flow, 2006, **27** (2): p. 229-242.
93. Kato, C., Yamade, Y., Wang, H., Guo, Y., Miyazawa, M., Takaishi, T., Yoshimura, S., Takano, Y., *Numerical prediction of sound generated from flows with a low Mach number.* Computers & Fluids, 2007, **36** (1): p. 53-68.
94. Ask, J. and L. Davidson, *An acoustic analogy applied to the laminar upstream flow over an open 2D cavity.* Comptes Rendus Mecanique, 2005. **333**(9): p. 660.
95. Ffowcs-Williams, J.E. and D.L. Hawkings, *Sound generated by turbulence and surfaces in arbitrary motion.* Philsophical Transactions of the Royal Society Series A, 1969. **264**: p. 321-342.
96. Dowling, A.P. and J.E. Ffowcs-Williams, *Sound And Sources Of Sound*: Ellis Horwood.
97. Shur, M.L., Spalart, P. R., Strelets, M. K., Travin, A. K., *Towards the prediction of noise from jet engines.* International Journal of Heat and Fluid Flow, 2003. 24(4): p. 551.
98. Ffowcs-Williams, J.E., *Aeroacoustics.* The Aeronautical Journal, 1996. **100**(1000): p. 531-537.
99. Ashcroft, G.B., K. Takeda, and X. Zhang, *A numerical investigation of the noise radiated by a turbulent flow over a cavity.* Journal of Sound and Vibration, 2003. **265**(1): p. 43.

100. Casper, J. and F. Farassat, *Broadband trailing edge noise predictions in the time domain.* Journal of Sound and Vibration, 2004. **271**(1-2): p. 159.
101. Gloerfelt, X., C. Bailly, and D. Juve, *Direct computation of the noise radiated by a subsonic cavity flow and application of integral methods.* Journal of Sound and Vibration, 2003. **266**(1): p. 119.
102. Maaloum, A., S. Kouidri, and R. Rey, *Aeroacoustic performance evaluation of axial flow fans based on the unsteady pressure field on the blade surface.* Applied Acoustics, 2004. **65**(4): p. 367.
103. Polacsek, C. and F. Desbois-Lavergne, *Fan interaction noise reduction using a wake generator: experiments and computational aeroacoustics.* Journal of Sound and Vibration, 2003. **265**(4): p. 725.
104. Rahier, G., Prieur, J., Vuillot, F., Lupoglazoff, N., Biancherin, A., *Investigation of integral surface formulations for acoustic post-processing of unsteady aerodynamic jet simulations.* Aerospace Science and Technology, 2004. 8(6): p. 453.
105. Singer, B.A., Brentner, K. S., Lockard, D. P., Lilley, G. M., *Simulation of acoustic scattering from a trailing edge.* Journal of Sound and Vibration, 2000. 230(3): p. 541.
106. Sun, H., H. Shin, and S. Lee, *Analysis and optimization of aerodynamic noise in a centrifugal compressor.* Journal of Sound and Vibration, 2006. **289**(4-5): p. 999.
107. Takeda, K., X. Zhang, and P.A. Nelson, *Computational aeroacoustic simulations of leading-edge slat flow.* Journal of Sound and Vibration, 2004. **270**(3): p. 559.
108. Tucker, P.G., *Novel MILES computations for jet flows and noise.* International Journal of Heat and Fluid Flow, 2004. **25**(4): p. 625.
109. Brentner, K.S., *An efficient and robust method for predicting helicopter high-speed implusive noise.* Journal of Sound and Vibration, 1997. **203**(1): p. 87.
110. Brentner, K.S. and F. Farassat, *Modelling aerodynamically generated sound of helicopter rotors.* Progress in Aerospace Sciences, 2003. **39**(2-3): p. 83.
111. Cesnik, C.E.S., Opoku, D. G., Nitzsche, F., Cheng, T., Active twist rotor blade modelling using particle-wake aerodynamics and geometrically exact beam structural dynamics. Journal of Fluids and Structures, 2004. 19(5): p. 651.
112. Ianniello, S., *Aeroacoustic analysis of high tip-speed rotating blades.* Aerospace Science and Technology, 2001. **5**(3): p. 179.
113. di Francescantonio, P., *A new boundary integral formulation for the prediction of sound radiation.* Journal of Sound and Vibration, 1997. **202**(4): p. 491.
114. Seol, H., et al., *Prediction of non-cavitating underwater propellor noise.* Journal of Sound and Vibration, 2002. **257**(1): p. 131.
115. Yin, J.P., S.R. Ahmed, and W. Dobrzynski, *New acoustic and aerodynamic phenomena due to non-uniform rotation of propellors.* Journal of Sound and Vibration, 1999. **225**(1): p. 171.
116. Casalino, D. and M. Jacob, *Prediction of aerodynamic sound from circular rods via spanwise statistical modelling.* Journal of Sound and Vibration, 2003. **262**(4): p. 815.
117. Chen, X.X., Zhang, X., Morfey, C. L., Nelson, P. A., *A numerical method for computation of sound radiation from an unflanged duct.* Journal of Sound and Vibration, 2004. 270(3): p. 573.

118. Casalino, D., *An advanced time approach for acoustic analogy predictions.* Journal of Sound and Vibration, 2003. **261**(4): p. 583.
119. Farassat, F. and M.K. Myers, *Further comments on the paper by Zinoviev and Bies, "On acoustic radiation by a rigid object in a fluid flow".* Journal of Sound and Vibration, 2006. **290**(1-2): p. 538.
120. Lockard, D.P., *An efficient, two-dimensional implementation of the Ffowcs Williams and Hawkings equation.* Journal of Sound and Vibration, 2000. **229**(4): p. 897.
121. Prieur, J. and G. Rahier, *Aeroacoustic integral methods, formulation and efficient numerical implementation.* Aerospace Science and Technology, 2001. **5**(7): p. 457.
122. Zinoviev, A. and D.A. Bies, *On acoustic radiation by a rigid object in a fluid flow.* Journal of Sound and Vibration, 2004. **269**(3-5): p. 535.
123. AIAA, *Guide for the verification and validation of computational fluid dynamic simulations.* AIAA, 1998. **AIAA-G-077-1998**.
124. Farassat, F., *Acoustic radiation from rotating blades--the Kirchhoff method in aeroacoustics.* Journal of Sound and Vibration, 2001. **239**(4): p. 785.
125. Goldstein, M.E., *Aeroacoustics*. 1976, New York: McGraw Hill.
126. Lee, S., et al., *Prediction of rotor high-speed impulsive noise with a combined CFD-Kirchhoff method.* Journal of Sound and Vibration, 1997. **207**(4): p. 453.
127. Sides, J., K. Pahlke, and M. Costes, *Numerical simulation of flows around helicopters at DLR and ONERA.* Aerospace Science and Technology, 2001. **5**(1): p. 35.
128. Strawn, R.C. and R. Biswas, *Numerical simulations of helicopter aerodynamics and acoustics.* Journal of Computational and Applied Mathematics, 1996. **66**(1-2): p. 471.
129. Andersson, N., L.-E. Eriksson, and L. Davidson, *Investigation of an isothermal Mach 0.75 jet and its radiated sound using large-eddy simulation and Kirchhoff surface integration.* International Journal of Heat and Fluid Flow, 2005. **26**(3): p. 393.
130. Jeon, W.-H. and D.-J. Lee, *A numerical study on the flow and sound fields of centrifugal impeller located near a wedge.* Journal of Sound and Vibration, 2003. **266**(4): p. 785.
131. Rumsey, C.L., Biedron, R. T., Farassat, F., Spence, P. L., *Ducted-fan engine acoustic predictions using a navier-stokes code.* Journal of Sound and Vibration, 1998. 213(4): p. 643.
132. Yoon, T.S., Lee, S.,Hwang, J. H., Lee, D. H., P*rediction and validation on the sonic boom by a high-speed train entering a tunnel.* Journal of Sound and Vibration, 2001. 247(2): p. 195.
133. Lyrintzis, A.S., *Review: The use of Kirchhoff's method in computational aeroacoustics.* Journal of Fluids Engioneering, 1994. **116**: p. 665-676.
134. Antes, H. and J. Baaran, *Noise radiation from moving surfaces.* Engineering Analysis with Boundary Elements, 2001. **25**(9): p. 725.
135. Dowling, A.P. and T.P. Hynes, *Sound generation by turbulence.* European Journal of Mechanics - B/Fluids, 2004. **23**(3): p. 491.
136. Hardin, J.C. and D.S. Pope, *An acoustic/vortical splitting technique for computational aeroacoustics.* Theoretical and Computational Fluid Dynamics, 1994. **6**: p. 323-340.

137. Ekaterinaris, J.A., *New formulation of Hardin-Pope equations for aeroacoustics.* AIAA, 1999. **37**(9): p. 1033-1039.
138. Grace, S.M., C.K. Curtis, and A.D. Pierce. *Acoustic Computations Using Incompressible Invscid CFD Results as Input*. in *ASME IMECE*. 1999. Nashville, TN, November 1999: ASME.
139. Su, M., X. Zhang, and Z. Yao, *Numerical simulation of sound field in axisymmetric jet of incompressible fluid.* Communications in Nonlinear Science and Numerical Simulation, 1997. **2**(3): p. 140.
140. Dayanandan, S. and M. Damodaran. *Computation of ventilation aerodynamics in Singapore's new underground expressway tunnel*. in *2003 ASME INternational Mechanical Engineering Congress*. 2003. Washington, D.C.
141. Gori, F. and E. Nino. *Fluid dynamics measurements and flow visualisations of a free slot jet of air*. in *2003 ASME INternational Mechanical Engineering Congress*. 2003. washington, D.C.
142. Gori, F. and I. Petracci. *Fluid dynamics measurements and numerical simulations around a circular cylinder impinged by a submerged slot jet of air*. in *2003 ASME INternational Mechanical Engineering Congress*. 2003. Washington, D.C.
143. Hall, J.W., Ewing, D., Xu, Z., Hangan, H., the dynamics of the large scale turbulent structures in the impinging round jet. in 2003 ASME INternational Mechanical Engineering Congress. 2003. Washington, D.C.
144. Page, G.J., et al. *A CFD coupled acoustics approach for coaxial jet noise*. in *9th AIAA/CEAS Aeroacoustics Conference and Exhibit*. 2003. Hilton Head, South Carolina.
145. Senthooran, S., D.-D. Lee, and S. Parameswaran, *A computational model to calculate the flow-induced pressure fluctuations on buildings.* Journal of Wind Engineering and Industrial Aerodynamics, 2004. **92**(13): p. 1131.
146. Bailly, C., C. Bogey, and X. Gloerfelt, *Some useful hybrid approaches for predicting aerodynamic noise.* Comptes Rendus Mecanique, 2005. **333**(9): p. 666.
147. Versteeg, H.K. and W. Malalasekera, *An introduction to computational fluid dynamics*. 1995: Prentice Hall.
148. Shao, L. and S.B. Riffat, *Accuracy of CFD for predicting pressure losses in HVAC duct fittings.* Applied Energy, 1995. **51**(3): p. 233.
149. Koskela, H., *Momentum source model for CFD-simulation of nozzle duct air diffuser.* Energy and Buildings, 2004. **36**(10): p. 1011.
150. Wilcox, D.C., *Turbulence Modelling for CFD*. 1998: DCW Industries.
151. Addad, Y., Laurence, D., Talotte, C., Jacob, M. C., *Large eddy simulation of a forward-backward facing step for acoustic source identification.* International Journal of Heat and Fluid Flow, 2003. 24(4): p. 562.
152. Lee, J.S., X. Xu, and R.H. Pletcher. *LES of compressible turbulent annular pipe flow with rotating wall*. in *2003 ASME INternational Mechanical Engineering Congress*. 2003. Washington, D.C.
153. Moin, P., *Advances in large eddy simulation methodology for complex flows.* Heat and Fluid Flow, 2002. **23**: p. 710-720.
154. Sagaut, P., *Lareg Eddy Simulation for Incompressible flows*. 2nd Edition ed. 1998: Springer.

155. Roux, S., et al., *Studies of mean and unsteady flow in a swirled combustor using experiments, acoustic analysis, and large eddy simulations.* Combustion and Flame, 2005. **141**(1-2): p. 40.
156. Yan, H. and M. Su, *Application and comparison of two SGS models in large eddy simulation of free turbulent jet flow.* Communications in Nonlinear Science and Numerical Simulation, 1999. **4**(1): p. 12.
157. Ferziger, J.H., *Computational methods for fluid dynamics*. 2nd Edition ed. 2000: Springer.
158. Slimon, S. *Computation of internal separated flows using a zonal detached eddy simulation approach*. in *2003 ASME INternational Mechanical Engineering Congress*. 2003. Washington, D.C.
159. Montavon, C., Jones, I., Bosch, D.T., Szepessy, S., Henrikson, R., *ALESSIA: Best practice guide: LES and acoustics*. 2002, AEA technology Engineering Software.
160. Neale, J.R., Middelberg, J.M., Leong, S.S., Barber, T.J., Byrne, K.P., Leonardi, E. *Silencing high velocity ducts in ocean going fast ferries*. in *Proceedings of Acoustics 2004*. 2004. Gold Coast, Australia, p. 581-586.
161. Fisher, M.J., G.A. Preston, and W.D. Bryce, *A modelling of the noise from simple coaxial jets, Part I: With unheated primary flow.* Journal of Sound and Vibration, 1998. **209**(3): p. 385.
162. Fisher, M.J., G.A. Preston, and C.J. Mead, *A modelling of the noise from simple coaxial jets, Part II: With heated primary flow.* Journal of Sound and Vibration, 1998. **209**(3): p. 405.
163. Self, R.H., *Jet noise prediction using the Lighthill acoustic analogy.* Journal of Sound and Vibration, 2004. **275**(3-5): p. 757.
164. Tang, S.K. and N.W.M. Ko, *On sound generated from the interation of two inviscid coaxial vortex rings moving in the same direction.* Journal of Sound and Vibration, 1995. **187**(2): p. 287.
165. Smith, C. and P.W. Carpenter, *The effect of solid surfaces on turbulent jet noise.* Journal of Sound and Vibration, 1995. **185**(3): p. 397.
166. Taherzadeh, S. and K.M. Li, *On the tubulent jet noise near an impedance surface.* Journal of Sound and Vibration, 1997. **208**(3): p. 491.
167. Boersma, B.J., *Numerical simulation of the noise generated by a low Mach number, low Reynolds number jet.* Fluid Dynamics Research, 2004. **35**(6): p. 425.
168. Bogey, C. and C. Bailly, *Downstream subsonic jet noise: link with vortical structures intruding into the jet core.* Comptes Rendus Mecanique, 2002. **330**(8): p. 527.
169. Jiang, X., E.J. Avital, and K.H. Luo, *Direct computation and aeroacoustic modelling of a subsonic axisymmetric jet.* Journal of Sound and Vibration, 2004. **270**(3): p. 525.
170. Jordan, P. and Y. Gervais, *Modelling self- and shear-noise mechanisms in inhomogeneous, anisotropic turbulence.* Journal of Sound and Vibration, 2005. **279**(3-5): p. 529.
171. Picard, C. and J. Delville, *Pressure velocity coupling in a subsonic round jet.* International Journal of Heat and Fluid Flow, 2000. **21**(3): p. 359.
172. Fleury, V., C. Bailly, and D. Juve, *Shear-layer acoustic radiation in an excited subsonic jet: experimental study.* Comptes Rendus Mecanique, 2005. **333**(10): p. 746.

173. Fleury, V., C. Bailly, and D. Juve, *Shear-layer acoustic radiation in an excited subsonic jet: models for vortex pairing and superdirective noise.* Comptes Rendus Mecanique, 2005. **333**(10): p. 754.
174. Guj, G., et al., *Acoustic identification of coherrent structures in a turbulent jet.* Journal of Sound and Vibration, 2003. **259**(5): p. 1037.
175. Morfey, C.L. and P.F. Joseph, *Shear layer refraction corrections for off-axis sources in a jet flow.* Journal of Sound and Vibration, 2001. **239**(4): p. 819.
176. Verma, S.B. and E. Rathakrishnan, *An experimental study on the noise characteristics of notched circular-slot jets.* Journal of Sound and Vibration, 1999. **226**(2): p. 383.
177. Verma, S.B. and E. Rathakrishnan, *Influence of aspect-ratio on the mixing and acoustic characteristics of plain and modified elliptic slot jets.* Aerospace Science and Technology, 2003. **7**(6): p. 451.
178. Munjal, M.L., *Acoustics of Ducts and Mufflers*. 1987, New York: John Wiley.
179. Morse, P.M., *Vibration and Sound*. 2nd ed. 1948, New York: McGraw Hill.
180. Middelberg, J.M., Barber, T.J., Leong, S.S., Byrne, K.P., Leonardi, E. *Computational fluid dynamics analysis of the acoustic performance of various simple expansion chamber mufflers*. in *Proceedings of Acoustics 2004*. 2004. Gold Coast, Australia, p. 123-127.
181. Delaney, M.E. and E.N. Bazley, *Acoustical characteristics of fibrous absorbent materials.* Applied Acoustics, 1970. **3**.
182. Ramakrishnan, R. and W.R. Watson, *Design curves for circular and annular duct silencers.* Noise Control Engineering Journal, 1991. **36**: p. 107-120.
183. Ramakrishnan, R. and W.R. watson, *Design curves for rectangular splitter silencers.* Applied Acoustics, 1992. **35**: p. 1-24.
184. Astley, R.J. and A. Cummings, *A finite element scheme for attenuation in ducts lined with porous material: comparison with experiment.* Journal of Sound and Vibration, 1987. **116**: p. 239-263.
185. Mehdizadeh, O.Z. and M. Paraschivoiu, *A three-dimensional finite element approach for predicting the transmission loss in mufflers and silencers with no mean flow.* Applied Acoustics, 2006. **66**(8): p. 902.
186. Dickey, N.S., A. Selamet, and J.M. Novak, *Multi-pass perforated tube silencers: A computational approach.* Journal of Sound and Vibration, 1998. **211**(3): p. 435.
187. Tsuji, T., T. Tsuchiya, and Y. Kagawa, *Finite element and boundary element modelling fro the acoustic wave transmission in mean flow.* Journal of Sound and Vibration, 2002. **255**(5): p. 849.
188. Tanaka, M., Y. Yamada, and M. Shirotori, *Boundary element method applied to simulation of active noise control in ducts.* JSME Series III, 1992. **35**(3): p. 387392.
189. Wu, T.W., P. Zhang, and C.Y.R. Cheng, *Boundary element analysis of mufflers with an improved method for deriving the four-pole parameters.* Journal of Sound and Vibration, 1998. **217**(4): p. 767.
190. Aly, M.E., *Effect of bulk-reacting liners on sound wave propagation in annular variable area ducts.* Applied Acoustics, 2000. **61**(1): p. 27.
191. Bies, D.A., C.H. Hansen, and G.E. Bridges, *Sound attenuation in rectangular and circular cross-section ducts with flow and bulk reacting liner.* Journal of Sound and Vibration, 1991. **146**: p. 47-80.

192. Kakoty, S.K. and V.K. Roy, *Bulk reaction modelling of ducts with and without mean flow.* Journal of the Acoustical Society of America, 2002. **112**: p. 75-83.
193. Kirby, R., *Transmission loss predictions for dissipative silencers of arbitrary cross section in the presence of mean flow.* Journal of the Acoustical Society of America, 2003. **114**: p. 200-209.
194. Kirby, R. and J.B. Lawrie, *A point collocation approach to modelling large dissipative silencers.* Journal of Sound and Vibration, 2005. **286**(1-2): p. 313.
195. Mechel, F.P., *Numerical results to the theory of baffle-type silencers.* Acoustica, 1990. **72**: p. 7-20.
196. Mechel, F.P., *Theory of baffle-type silencers.* Acoustica, 1990. **70**: p. 93-111.
197. Munjal, M.L., *Analysis and design of pod silencers.* Journal of Sound and Vibration, 2003. **262**(3): p. 497.
198. Panigrahi, S.N. and M.L. Munjal, *Comparison of various methods for analyzing lined circular ducts.* Journal of Sound and Vibration, 2005. **285**(4-5): p. 905.
199. Shenoda, F.B., *An effective acoustic lining for broad rectangular air ducts.* Indian Journal of Technology, 1986. **24**: p. 682-686.
200. Reichert, R.S. and S. Biringen, *Time-domain simulation of acoustic propagation in a lined duct.* Applied Acoustics, 2001. **62**(9): p. 1049.
201. Munjal, M.L., *Plane wave analysis of side inlet/outlet chamber mufflers with mean flow.* Applied Acoustics, 1997. **52**(2): p. 165.
202. Munjal, M.L., *Analysis and design of mufflers - An overview of research at the Indian Institute of Science.* Journal of Sound and Vibration, 1998. **211**(3): p. 425.
203. Munjal, M.L., *Prediction of the break-out noise of the cylindrical sandwich plate muffler shells.* Applied Acoustics, 1998. **53**(1-3): p. 153.
204. Munjal, M.L., *An error inherent in the use of the two-microphone method for gas pulsation measurement in a reflective environment.* Journal of Sound and Vibration, 2001. **242**(3): p. 539.
205. Munjal, M.L. *Automotive noise - The Indian scene*. in *Acoustics 2004*. 2004. Gold Coast, Australia.
206. Munjal, M.L., B.K. Behera, and P.T. Thawani, *Transfer Matrix Model for the Reverse-flow, three-duct, Open End Perforated Element Muffler.* Applied Acoustics, 1998. **54**(3): p. 229.
207. Sastry, J.S. and M.L. Munjal, *Response of a multi-layered infinite cylinder to a plane wave excitation by means of transfer matricies.* Journal of Sound and Vibration, 1998. **209**(1): p. 99.
208. Sastry, J.S. and M.L. Munjal, *Response of a multi-layered infinite cylinder to two-dimensional pressure excitation by means of transfer matricies.* Journal of Sound and Vibration, 1998. **209**(1): p. 123.
209. Kar, T. and M.L. Munjal, *Generalized analysis of a muffler with any number of interacting ducts.* Journal of Sound and Vibration, 2005. **285**(3): p. 585.
210. Sathyanarayana, Y. and M.L. Munjal, *A hybrid approach for aeroacoustic analysis of the engine exhaust system.* Applied Acoustics, 2000. **60**(4): p. 425.
211. Boij, S. and B. Nilsson, *Reflection of sound at area expansions in a flow duct.* Journal of Sound and Vibration, 2003. **260**(3): p. 477.
212. Boij, S. and B. Nilsson, *Scattering and absorption of sound at flow duct expansions.* Journal of Sound and Vibration, 2006. **289**(3): p. 577.
213. Dokumaci, E., *Sound transmission in mufflers with multiple perforated co-axial pipes.* Journal of Sound and Vibration, 2001. **247**(3): p. 379.

214. Dokumaci, E., *Effect of sheared grazing mean flow on acoustic transmission in perforated pipe mufflers.* Journal of Sound and Vibration, 2005. **283**(3-5): p. 645.
215. Endo, M., Y. Futagami, and J. Iwamoto, *Relation between the flow pattern downstream of duct and the noise.* JSAE Review, 2000. **21**(1): p. 125.
216. Davies, P.O.A.L., *Aeroacoustics and time varying systems.* Journal of Sound and Vibration, 1996. **190**(3): p. 345.
217. Ver, I.L., *Review of the attenuation of sound in straight lined and unlined ductwork of rectangular cross section.* ASHRAE Transactions, 1978. **84**: p. 122-149.
218. Cummings, A., I.J. Chang, and R.J. Astley, *Sound transmission at low frequencies through the walls of distorted circular ducts.* Journal of Sound and Vibration, 1984. **97**(2): p. 261-286.
219. Nayfeh, A.H. and O.A. Kandil, *Propagation of waves in cylindrical hard-walled ducts with generally weak undulations.* AIAA, 1978. **16**(10): p. 1041-1045.
220. Cerami, V.J., *HVAC equipment and noise.* Heating, Piping and Air Conditioning, 1996. **68**(3): p. 49-60.
221. Ebbing, C.E. and W.E. Blazier, *Using manufacturers'acoustical data.* ASHRAE Transactions, 1997. **103**(2): p. 18-22.
222. Smith, M.J. and M. Airah, *Trouble shooting noise and vibration in the HVAC industry.* Australian Refrigeration, Air Conditioning and Heating, 1989. **43**(10): p. 38-51.
223. Schaffer, M.E., *A practical guide to noise and vibration control for HVAC systems*. 1991, Atlanta: ASHRAE.
224. Watson, J.H., *System noise control - A current review.* Australian Refrigeration, Air Conditioning and Heating, 1986. **40**(11): p. 30-33.
225. Jeng, M., et al. *Control of the HVAC system noise emission: A case study*. in *Noise-Con 96*. 1996. Sealttle, Washington.
226. Dean, R.H., *Removing the roar: In-duct noise treatment.* Heating, Piping and Air Conditioning, 1975. **47**(2): p. 28-35, 58.
227. Wise, S.S., S.D. Goodman, and S.H. Dineen, *Active control of low-frequency HVAC fan noise in building systems.* ASHRAE Transactions, 1993. **99**(2): p. 1037-1043.
228. Canavet, G., *Active sound absorption in an air conditioning duct.* Journal of Sound and Vibration, 1978. **58**(3): p. 333-345.
229. Dutt, D.N. and B.S. Ramakrishna, *An experimental study of controlling the sound distribution in tube by using auxillary driving sources.* Journal of Sound and Vibration, 1978. **60**(2): p. 267-271.
230. Pelton, H.K., S. Wise, and W.S. Sims, *Active HVAC noise control systems provide acoustical comfort.* Sound and Vibration, 1994. **28**(7): p. 14-18.
231. Carmona, J.C. and V.M. Alvarado, *Active noise control of a duct using robust control theory.* IEEE Transactions on Control Systems Technmology, 2000. **8**(6): p. 930-938.
232. Powell, C.A. and B.M. Sullivan, *Subjective response to propellor airplane interior sounds modified by hypothetical active noise control systems.* Noise Control Engineering Journal, 2001. **49**(3): p. 125-136.
233. Wright, S.E. and B. Vuksanovic, *Active control of environmental noise.* Journal of Sound and Vibration, 1996. **190**(3): p. 565-585.

234. Vorlander, M., *Recent progress in room acoustical computer simulations.* Building Acoustics, 1997. **4**(4): p. 229-245.
235. Maluski, S. and H. Bougdah, *Predicted and measured low frequency response of small rooms.* Building Acoustics, 1997. **4**(2): p. 73-85.
236. Wentzel, R.E. and P. Saha, *Sound Transmission Loss Prediction of Double-Wall Barrier Assemblies.* Sound and Vibration, July, 1997: p. 18-27.
237. Fuchs, H.V., X. Zha, and M. Pommerer, *Qualifying freefield and reverberation rooms for frequencies below 100 Hz.* Applied Acoustics, 2000. **59**: p. 303-322.
238. Durran, D.R., *Numerical methods for wave equations in geophysical fluid dynamics*. 1999: Springer.
239. Roache, P.J., *Fundamentals of Computational Fluid Dynamics*. 1998, Albuquerque, New Mexico: Hermosa Publishers.

Publications

Neale, J.R., et al. *Silencing high velocity ducts in ocean going fast ferries*. in *Acoustics 2004*. 2004. Gold Coast, Australia.

Neale, J.R., et al. *Noise treatment strategies for high velocity HVAC ducts in ocean going fast ferries.* in IMECE2004. 2004. Anaheim, California, USA.

Appendix A: Outlet Diffuser Grill Geometry

All fittings referenced here were sourced from Bradflo Australia: www.bradflo.com.au

Round Grill:

160 mm diameter inlet
305 mm external diameter.

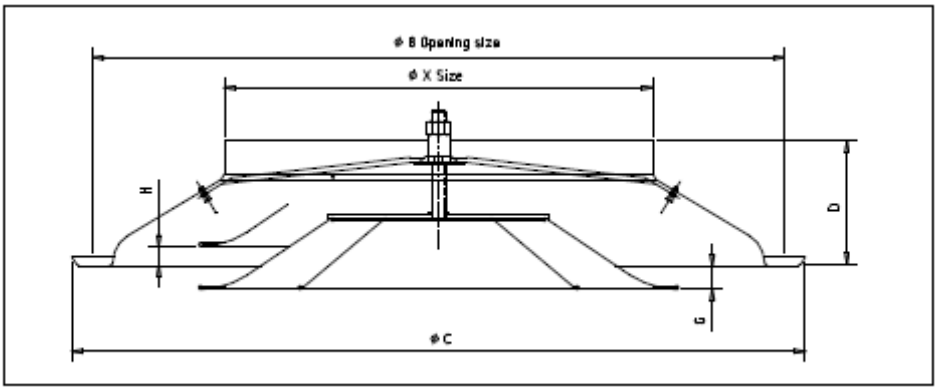

X Size	Dia. B	Dia. C	D	G	H
125	270	305	90	13	10
160	270	305	80	13	10
200	330	378	92	14	13
250	420	477	107	17	16
315	530	591	126	20	20
400	630	703	138	24	24
500	780	845	150	30	30

Square 4-way Outlet Grill:

150 mm square inlet
258 mm square external face - Type 4

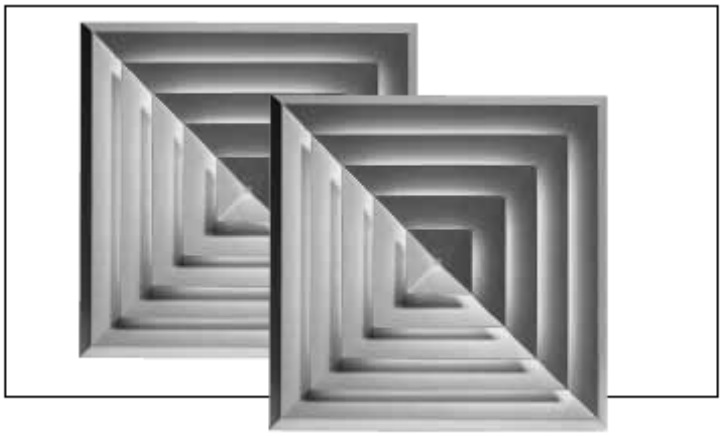

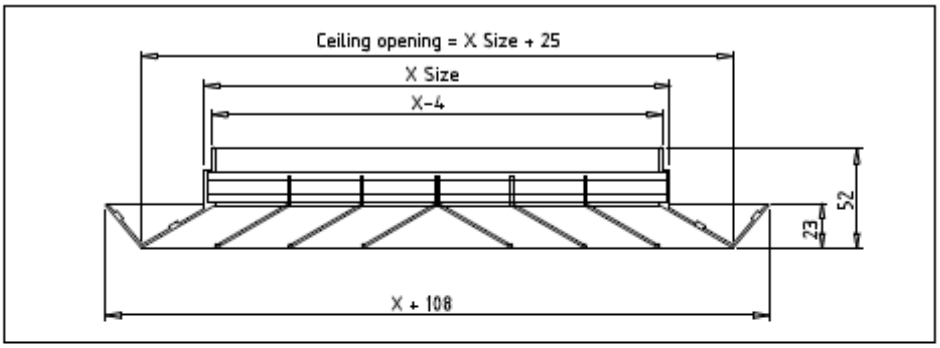

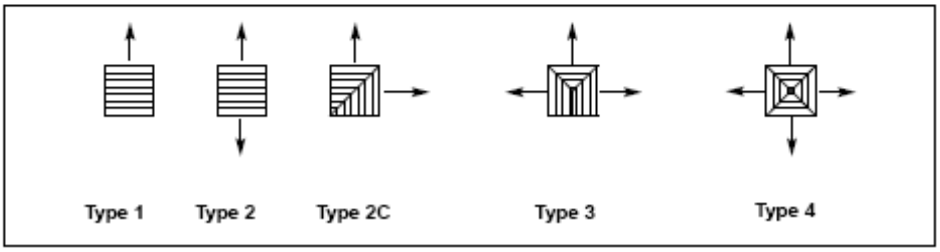

Cushion Head Box:

150 mm diameter spigot (X = 150 mm)
150 mm square cross section
150 mm deep
13 mm black polyester insulation

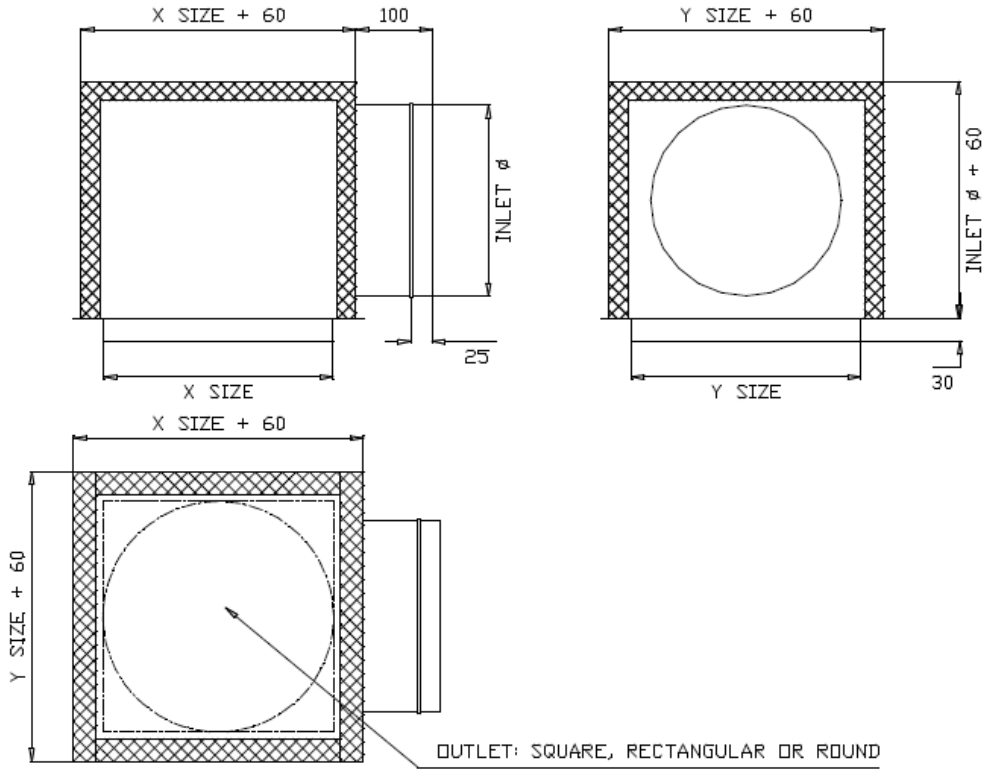

Appendix B: Reverberation Suite Risk Assessment and Standard Operating Procedure

SCHOOL OF MECHANICAL AND MANUFACTURING ENGINEERING

THE UNIVERSITY OF NEW SOUTH WALES

Risk Assessment

Reference No.OVE290803-290803

e.g. HAR061100-101200 (name-date-revision)

Laboratory Reverberation Room

Activity Sound Level Measurements

Frequency 1 per week

Duration 5 hours

Comments

Note:

If possible more than one person should carry out the assessment.

Write none for each heading if no hazard.

Add lines to the Tables as required, add name/s of assessor/s and approver, print and sign.

Material Safety Data Sheets (MSDS) must be obtained and consulted for any chemical hazard.

Original to be given to Laboratory Manager, copies held by relevant persons.

A Standard Operating Procedure (SOP) must be derived from this assessment and all persons carrying out the activity must be familiar with and abide by the SOP and Risk Assessment.

Students must have signed a Student Laboratory Activity Approval form before carrying out this activity.

* S=Severity, L=Likelihood, R=Rating, see attached sheet for definitions.

Hazard Type	R/C	R=Risk C=Control	S*	L*	R*
Mechanical e.g. Sharp objects Rotating equipment Hot/cold material Lifting Ergonomics Compressed gas Compressed gas storage	R	Back or neck injury closing large aperture doors	!!!	-	3
	C	Only use chain blocks to open or close doors	!!!		>6
	R	Back or neck injury removing or replacing door plugs	!!!	-	3
	C	A lifting tool exists to safely remove or replace plugs this must be used together with a chain block and lifting sling. Removing or replacing plugs is not to be undertaken without the permission and assistance of the OIC of the reverb room	!!!		>6
	R				
	C				

Hazard Type	R/C	R=Risk C=Control	S*	L*	R*
Electrical e.g. Shock Burns Overloading	R				
	C				
	R				
	C				

Hazard Type	R/C	R=Risk C=Control	S*	L*	R*
Chemical e.g. Gas Liquid Powder Storage Disposal Emergency procedures	R				
	C				
	R				
	C				
	R				
	C				

Hazard Type	R/C	R=Risk C=Control	S*	L*	R*
Environmental e.g. Vibration/noise Slipping Tripping Temperatures Gas/vapour/dust Radiation	R	Trip hazard on floor of room	!!	-	4
	C	Caution signs at entrance, good housekeeping ,good lighting	!!	--	5
	R	Hearing damage from exposure to high sound levels	!!!	-	3
	C	Sound source not to be run unless doors are closed	!!!		>6
	R				
	C				

Hazard Type	R/C	R=Risk C=Control	S*	L*	R*
Fire e.g. Explosion Fuels Strong oxidisers Ignition sources Housekeeping Disposal Storage Emergency procedures	R				
	C				
	R				
	C				
	R				
	C				
	R				
	C				

Assessment carried out by R. Overhall

Signature/s

Approved by

Signature: Date :

Rating Assessment Table

	++ very likely could happen any time	+ likely could happen somtime	- unlikely could happen but very rarely	-- very unlikely could happen but probably never will
!!!! kill or cause permanent disability	1	1	2	3
!!! long term illness or serious injury	1	2	3	4
!! medical attention and several days off work	2	3	4	5
! first aid needed	3	4	5	6

SCHOOL OF MECHANICAL AND MANUFACTURING ENGINEERING

THE UNIVERSITY OF NEW SOUTH WALES

STANDARD OPERATING PROCEDURE (SOP)

LABORATORY - Reveberation Room
ACTIVITY - Sound Level Measurements

Risk Assessment Reference No. OVE 290803-290803

Note: This SOP must be updated if the risk assessment is revised.

Date 08/09/03

1. Ensure floor area of control room and reverberation rooms are free from trip hazards.
2. Ensure that all of the installed lighting is working properly.
3. When entering reverberation rooms ensure sound source is disabled
4. Aperture doors are only to be opened or closed by use of a chainblock
5. Door plugs are only to be replaced or removed using the plug lifting jig, chain block and lifting sling. The lab OIC must be informed before moving the door plugs.

Compiled by…R. Overhall……

Signature

Approved by……..

Signature

Date:- 9/9/03

Appendix C: Research Compressor Risk Assessment and Standard Operating Procedure

SCHOOL OF MECHANICAL AND MANUFACTURING ENGINEERING

THE UNIVERSITY OF NEW SOUTH WALES

Risk Assessment (RA)

Reference No. FLY-150604-170305

e.g. HAR061100-101200 (name-date-revision)

Laboratory L107

Activity Centac centrifugal compressor

Frequency Weekly

Duration 7hours

Note:

If possible more than one person should carry out the assessment.

Write none for each heading if no hazard.

Add lines to the Tables as required, add name/s of assessor/s and approver, print and sign.

Material Safety Data Sheets (MSDS) must be obtained and consulted for any chemical hazard.

Original to be given to Laboratory Manager, copies held by relevant persons.

A Standard Operating Procedure (SOP) must be derived from this assessment and all persons carrying out the activity must be familiar with and abide by the SOP and Risk Assessment.

Students must have signed a Student Laboratory Activity Approval form (known as RISK CONTROL) before carrying out this activity.

* C=Consequence, P=Probability, R=Rating, (AS4360 adopted by UNSW, see attached sheets for definitions and guidelines)

Hazard Type	R/C	R=Risk C=Control	C*	P*	R*
	R	If set pressure is above test rig test maximum safe pressure, the test rig may fail.	5	C	E
	C	Check set pressure is below the maximum safe pressure of the test rig before starting. Place a sign stating danger, do not change settings or stop compressor. Include the operators name, contact details and date.	1	E	L

Hazard Type	R/C	R=Risk C=Control	C*	P*	R*
Mechanical e.g. Sharp objects Rotating equipment Hot/cold material Lifting Ergonomics Compressed gas Compressed gas storage	R	If the set pressure is above 895kpa over pressurization of the laboratory pressure vessels may occur.	5	C	E
	C	Check maximum pressure setting is below 895kPa.	1	E	L
	R	Bearing failure due to quick shutdown	2	C	M
	C	Shutdown by pressing unload on key pad first then press stop after 20 seconds, wait until display panel indicates ready before turning compressor off. Only use the emergency stop button in an emergency.	2	E	L
	R	Bearing failure due to overheating, lack of cooling water.	2	C	M
	C	Turn on booster pump Check cooling water pressure gauge reads at least 100kPa	2	E	L
	R	Mechanical overload of compressor due to isolation valves shut	5	C	E
	C	Check and open all isolation valves on compressor	1	E	L
	R	Noise	2	B	H
	C	Use ear protection	1	E	L
	R	Compressed air line in another lab is open to atmosphere or has low pressure rig attached causing rig failure or hazard.	5	C	E
	C	Check all isolation valves to labs are closed and only open valve to test rig being used. Close isolation valves to each lab after use.	1	E	L

Hazard Type	R/C	R=Risk C=Control	C*	P*	R*
Electrical e.g. Shock Burns Overloading	R	Electric shock from internal wiring	5	D	E
	C	All covers to be in place and secured before operation	1	E	L
	R				
	C				

Hazard Type	R/C	R=Risk C=Control	C*	P*	R*
Chemical e.g. Gas Liquid Powder Storage Disposal Emergency procedures	R				
	C				
	R				
	C				
	R				
	C				

Hazard Type	R/C	R=Risk C=Control	C*	P*	R*
Environmental e.g. Vibration/noise Slipping Tripping Temperatures Gas/vapour/dust Radiation	R				
	C				
	R				
	C				
	R				
	C				

Hazard Type	R/C	R=Risk C=Control	C*	P*	R*
Fire e.g. Explosion Fuels Strong oxidisers Ignition sources Housekeeping Disposal Storage Emergency procedures	R				
	C				
	R				
	C				
	R				
	C				
	R				
	C				

Hazard Type	R/C	R=Risk C=Control	C*	P*	R*
Other	R				
	C				
	R				
	C				

Assessment carried out by

Signature/s

Approved by

Signature

Table 1 - Consequence

Level	Descriptor	Examples of Description
1	Insignificant	No injuries. Minor delays. Little financial loss. $0 - $4,999*
2	Minor	First aid required. Small spill/gas release easily contained within work area. Nil environmental impact. Financial loss $5,000 - $49,999*
3	Moderate	Medical treatment required. Large spill/gas release contained on campus with help of emergency services. Nil environmental impact. Financial loss $50,000 - $99,999*
4	Major	Extensive or multiple injuries. Hospitalisation required. Permanent severe health effects. Spill/gas release spreads outside campus area. Minimal environmental impact. Financial loss $100,000 - $250,000*
5	Catastrophic	Death of one or more people. Toxic substance or toxic gas release spreads outside campus area. Release of genetically modified organism (s) (GMO). Major environmental impact. Financial loss greater than $250,000*

* Financial loss includes direct and indirect costs, eg impact of loss of research data.

Table 2 - Probability

Level	Descriptor	Examples of Description
A	Almost certain	Task/process performed weekly or more often. The event is expected to occur in most circumstances. Common or repetitive occurrence at UNSW. Constant exposure to hazard. Very high probability of damage.
B	Likely	Task/process performed weekly to monthly. The event will probably occur in most circumstances. Known history of occurrence at UNSW. Frequent exposure to hazard. High probability of damage.
C	Possible	Task/process performed monthly to yearly. The event could occur at some time. History of single occurrence at UNSW. Regular or occasional exposure to hazard. Moderate probability of damage.
D	Unlikely	Task/process performed yearly to 5 yearly. The event is not likely to occur. Known occurrence in industry. Infrequent exposure to hazard. Low probability of damage.
E	Rare	Task/process performed 5 yearly or less often. The event may occur only in exceptional circumstances. No reported occurrence globally. Rare exposure to hazard. Very low probability of damage. Requires multiple system failures.

Table 3 – Risk Rating

Probability	Consequence				
	Insignificant 1	Minor 2	Moderate 3	Major 4	Catastrophic 5
A (Almost certain)	H	H	E	E	E
B (Likely)	M	H	H	E	E
C (Possible)	L	M	H	E	E
D (Unlikely)	L	L	M	H	E
E (Rare)	L	L	M	H	H

Recommended Action Guide:

Abbrev	Action Level	Descriptor
E	Extreme	The proposed task or process activity MUST NOT proceed. The supervisor must review the task or process design and risk controls. In the case of an existing hazard that is identified, controls must be put in place immediately.
H	High	Urgent action is required to eliminate or reduce the risk. The supervisor must be made aware of the hazard. However, the supervisor may give special permission for staff to undertake some high risk activities provided that specific training has been given and an adequate review of the task has been undertaken. This includes providing risk controls identified in Legislation, Australian Standards, Codes of Practice etc.* A detailed Safe Work Method Statement is required. *
M	Moderate	Action to eliminate or reduce the risk is required within a specified period. The supervisor should approve all moderate risk task or process activities. A Safe Work Method statement is required
L	Low	Manage by routine procedures. Action should be taken to eliminate or reduce the risk if practicable.

*Note: These regulatory documents identify specific requirements/controls that must be implemented to reduce the risk of an individual undertaking the task to a level that the regulatory body identifies as being acceptable.

SCHOOL OF MECHANICAL AND MANUFACTURING ENGINEERING

THE UNIVERSITY OF NEW SOUTH WALES

STANDARD OPERATING PROCEDURE (SOP)

LABORATORY - L107
ACTIVITY - Centac centrifugal compressor

Risk Assessment Reference No. FLY-150604-170305

Note: This SOP must be updated if the risk assessment is revised.

Date 17/03/05

General Safety Issues

A sign stating 'DANGER do not change settings or stop compressor' should be placed over the control panel when in operation. The date, operators name and contact details should be included on the sign.

The set pressure must be set below 895kpa.

The set pressure must be set below the test rigs maximum safe pressure

Ear protection to be worn when compressor is operating.

All panels and covers must be fixed in place before operating.

Compressor start procedure

1. Open (turn anti clockwise) isolation valve to lab being used
2. Check that isolation valves to other labs are closed (turn clockwise)
3. Open air valve from building air supply.
4. Turn on cooling water booster pump.
5. Check cooling water pressure gauge reads at least 100kPa
6. Check main air isolation valves are open
7. Check MAN-AUTO switch is set to MAN
8. Turn AUX SUPPLY switch to ON position
9. Use navigation key pad to select SYSTEM folder
10. Press ENTER key pad to highlight pressure set point
11. Press UP and DOWN key pads to change pressure set point (must be less than 895kpa)
12. Press ENTER key pad to exit

13. Press RESET key pad
14. Wait for Ready indication on panel
15. Press START key pad
16. Press LOAD key pad
17. Place danger sign over control panel

Compressor shut down procedure

1. Press UNLOAD key pad
2. Wait 20 seconds
3. Press STOP key pad
4. Allow compressor to coast for 30 minutes
5. Turn AUX SUPPLY switch to OFF position
6. Close air valve from building air supply.
7. Turn off cooling water booster pump.
8. Remove danger sign
9. Close (turn clockwise) isolation valves to each lab

Compiled by……

Signature

Approved by……..

Signature